Click here for papers

The 25th International North Sea Flow Measurement Workshop

Exhibitors 2007

At the time of printing, the following companies have confirmed their intention to exhibit at the workshop

ABBON

IKM Products AS

P2 Energy Solutions

ADVANTICA

KROHNE
achieve more

roxar
MAXIMUM RESERVOIR PERFORMANCE

CAMERON

mpm

SICK | MAIHAK

elster Instromet

NMi Nederlands Meetinstituut

Pietro Fiorentini®

Endress+Hauser
People for Process Automation

norsk analyse a·s

Weatherford®

solartron ISA

FMC Technologies

CANADA PIPELINE ACCESSORIES

nel
technology for life

FRAMO ENGINEERING AS

ODS
klöckner & co multi metal distribution

LMC last_mile_communication

CLAMPON

SIEMENS

Index

Fluid Quality

Key Note
The Importance of Discerning the Impact of New Measurement Technology
David J. Fish, Senior Vice President, Welker Engineering Company, USA

1 A Method for Remote In-Line Calibration of Water in Oil Meters
Dag A. Fløio, StatoilHydro, Norway

2 Traceable Calibration of Liquid Densitometers
Norman F Glen - TUV NEL Ltd and Douglas Griffin – DTI, UK

Multiphase Measurement

3 Tomography Powered Multiphase- and We Gas Flow Meter, Providing Fiscal Accuracy
Arnstein Wee, MpM, Norway, Hans Berentsen, Vidar Rune Midttveit and Håkon Mostue, StatoilHydro, Hans Olav Hide, MpM, Norway

4 Calibration and Verification of Multiphase Meters for Allocation Metering of the Urd Field
Knut Skårdalsmo and Erik Aabro, StatoilHydro, Norway

5 Fluid Composition Analysis by Multiple Gamma-ray Beam and Modality Measurements
Geir Anton Johansen, University of Bergen,
Stein-Arild Tjugum Roxar Flow Measurement, Norway

6 Wet Gas Measurement Using Sonar-based Flow Meters and Piping Pressure Loss Gradients
Daniel Gysling, CiDRA Corporation, Nicolas Morlino, BP, USA,
Douglas Loose, CiDRA Corp, UK

Multiphase continued

7 A Prototype Wet-Gas and Multiphase Flow Meter
Espen S. Johansen,, Weatherford/eP Solutions, USA.
Andrew R. W. Hall, BP Exploration, UK.
Ö. Haldun Ünalmis,Weatherford/eP Solutions, USA.

8 A Discussion on Wet Gas Flow Parameter Definitions
Andrew Hall, BP, Douglas Griffin, Petroleum Inspectorate, DTI
Richard Steven, Colorado Engineering Experiment Station, Inc.

9 Wet Gas Performance of Differential Pressure Flow Meters
Russell Evans,Stephen Ifft,
Emerson Process Management, Rosemount Division
David Hodges, TUV NEL Ltd.

Gas Measurement

10 A New V-Cone Wet Gas Meter
Richard Steven, Colorado Engineering Experiment, USA

11 Pressure and Temperature Effects for Ormen Lange Ultrasonic Gas Flow Meters
Per Lunde and Kjell-Eivind Frøysa, Christian Michelsen Research AS, Norway, Trond Folkestad, Norsk Hydro ASA, Bergen, Norway.

12 Impact of Regulator Noise on Ultrasonic Flow Meters in Natural Gas
Adriz Krajcin, Martin Uhrig,E.ON Ruhrgas AG
Toralf Dietz, Volker Herrmann, SICK MAIHAK GmbH

13 Euroloop: Metrological Concepts for Efficient Calibrations and Primary Realization of Accurate Reference Values in Flow
Mijndert van der Beek, NMi Van Swinden Laboratory B.V.

14 Uncertainty Modelling for Instruments Systems and Plants - An essential Guide to Optimising Performance
Justin Walter METCO Services Limited

Heavy Oil Measurement

15 Erosion in a Venturi Meter with Laminar and Turbulent Flow
Steven J. Svedeman and Robert A. Hart, Southwest Research Institute, Gordon J. Stobie, ConocoPhillips

16 Experience with Ultrasonic Meters on High Viscosity Oil
Øyvind Nesse, StatoilHydro ASA, Norway

17 A New Approach to MPFM Performance Assessment in Heavy Oil
Martin Basil, SOLV Limit, UK, Gordon Stobie, ConocoPhillips,
Richard Sharp Scandpower Petroleum Technology, USA

LNG Measurement

18 LNG Allocation Metering Using 8-Path Ultrasonic Meters
Gregor Brown, Terry Cousins and Don Augenstein, Caldon Ultrasonics, Cameron Measurement Systems, UK

19 An Ultrasonic Flowmeter for Custody Transfer Measurement of LNG: A Challenge for Design and Calibration
Jankees Hogendoorn and André Boer,
Krohne-Altometer, The Netherlands

20 Hammerfest LNG Plant – Fiscal metering system
Erik Forgaard Andreasse,StatoilHydro, Norway

Environmental Measurement Issues

21 Flare Metering with Optics– From Blue-Sky Technology to the Real World
Chip Letton, Letton Group, USA, Gordon Stobie, ConocoPhillips, UK
Ivan Melnyk, Photon Control, Canada,
Jody Parker, ConocoPhillips, Canada

22 Uncertainty Analysis of Emissions from the Statoil Mongstad Oil Refinery
Kjell-Eivind Frøysa, CMR, Norway, Anne Lise Hopland Vågenes,
Bernhard Sørli and Helge Jørgenvik, StatoiHydro, Norway

23 Measurement of Produced Water Discharges – Regulatory Requirements and Recent Progress
Alick MacGillvray, Ming Yang, Richard Paton, TUV NEL, UK

Poster/Alternate

The relevance of two different Path Layouts for Diagnostic Purposes in one Ultrasonic Meter
Toralf Dietz, Volker Herrmann, John Lansing, SICK MAIHAK GmbH, Germany

Test of a 1 Inch Roxar Watercut Meter on light Condensate with very Low Water Content
Georg Johnsen and Rune Martinussen, Roxar, Norway

THE IMPORTANCE OF DISCERNING

THE IMPACT OF NEW MEASUREMENT TECHNOLOGY

David J. Fish
Senior Vice President
Welker Engineering Company

Presented at

The 25th Annual North Sea
Flow Measurement Workshop

October 16 – 19, 2007

Oslo, Norway

THE IMPORTANCE OF DISCERNING THE IMPACT OF NEW MEASUREMENT TECHNOLGY

David J. Fish
Senior Vice President
Welker Engineering Company

Introduction

With the current demand for improved technologies in the area of fluid measurement, the rush to the market place is raising as many questions as it is answering. In the last 25 years, the natural gas pipeline industry has transitioned from the supplier of clean, dry gas to the mover of billable gas energy; clean and dry or dirty and wet. The LNG market has impacted the operations of the typical gas supply systems worldwide. The demand for more and more crude oil has put pressure on old measurement designs to become increasingly flexible to a variety of crude oil deliveries. Designing and creating improved products for the measurement of volume and quality has provided new challenges as the marketing and transportation of oil and natural gas has changed. This paper will focus on the natural gas sector, however, the lessons can be transferred to the entire industry.

Perhaps the single major issue that has created an interest in ascertaining the total picture of the natural gas pipeline system is "wet gas." The definition of "wet gas" as gas with more than 7 lbs. water per million cubic feet is almost history. Wet gas metering is redefining how we talk about wet gas. There is a white paper written by Dr. Parviz Mehdizadeh that describes wet gas. Wet gas, in that multiphase white paper, is defined as "gas, which contains some liquid. The amount of liquid can vary from a small amount of water or hydrocarbon to a substantial amount of water or hydrocarbon." Today's measurement issues are different from the past, but they are here to stay. We must either return to the insistence and requirement of a clean, dry gas pipeline system (separators, processing plants, dehydration systems, etc) or acknowledge the realities of the present. One of the biggest challenges is the multiphase system. Liquids cause corrosion, pulsation, freezing problems and basic maintenance issues that create concerns for a natural gas pipeline system. Their presence must be addressed with an awareness of what that means to our industry.

This paper is presented with the desire to focus on the lessons learned from the past, review a few of the new technologies that we have at present and to consider the challenges that lie ahead. It is the author's desire to stimulate dialogue about the ultimate goal of measurement quality equipment for the industry as it operates in the real world today. In order to promote discussions, there has to be an awareness of the issues that

impact the pursuit of new procedures or technology. The concerns of the natural gas measurement industry are real and legitimate concerns. However, in the race to find answers, we should not fail to keep in mind the lessons that we have learned and have documented to be true in the past. If we are mindful of those lessons, it will allow us to appreciate the current advancements and accept how we arrived at them. As we look for answers in the new world of gas pipeline measurement, we should not purge the data base of knowledge just to solve one aspect of the problem. We must incorporate that knowledge into the pursuit of future advancements. Technology can provide solutions to these new challenges but as we provide advancements in measurement, we must be cautious to not retreat from lessons that we have learned in the past.

In the last two to three years, a term has become very commonplace in our industry. A few years back the term was not to be found on the cover of an industry magazine. Today, it appears on the cover as many as 10 times during a 12 issue year. That term or phrase is **"Pipeline Integrity"** and its meaning is legion. To one person, it means billable quality and to another it means structural soundness and to yet another it means operational stability. But we all agree, it means and encompasses a lot more today than it did 10 years ago. Today, it means everything that is right or everything that could go wrong in the transportation of oil, natural gas and petrochemical products. Because of the changing parameters of our industry, the impact of what we do and how we do it, has taken on a new dimension.

Let's look briefly at a few of the areas that are affected by these changes.

Volumetric Measurement

Volume measurement has undergone a major change with the advent of Ultrasonic Metering (USM). Issues that caused alarm with an orifice plate in the line have all but disappeared. Liquid slugs that slam into meter stations and deform orifice plates are now allowed to pass through relatively unnoticed, past non-intrusive meter heads. Faster flow rates and improved flow information have been widely achieved throughout the industry and a tolerance for a harsher environment has been established. Such is the benefit of this new technology.

However, with the liberties of a less restrictive environment comes the concern of not knowing what has passed through the station and down the pipeline. This is not to say that liquids and the like never existed before, but with all the maintenance issues and equipment that was required to handle those liquids correctly, came the knowledge that they were there. Today, there is a potential to forget about their presence until it surfaces as a costly problem.

Therefore, while we have seen great improvement with the advent of the USM, we cannot suddenly forget the lessons of the past and assume that the USM is the solution to the need for any form of liquid identification. While liquids do not destroy a USM as they might do with an orifice plate, they still need to be identified and their presence acknowledged.

With the introduction of USM technology, there has been an increase of volume in the pipeline because of the removal of the orifice plate, allowing for higher flow rates and faster velocities. With higher velocities comes the realization of the need to check designs of equipment that insert into the line. Previous flow rates were slow enough to cause little concern, but with higher flowing velocities in the pipeline, wake frequencies, bending moments and shear calculations become concerns that demand our attention. Engineering departments need to look at physical stresses in a new light. Old knowledge cannot be forgotten with new advancements.

Quality

The level of interest in effective and accurate gas sampling techniques is currently at a very high priority within the natural gas industry. With the recent dramatic increase in natural gas prices, exploration interests, profitability, deregulation and consolidation of the work force, recoverable revenue must be found and reported. At large volume delivery points, a 3-5 BTU error in energy determination can cost companies tens of thousands of dollars within a very short time period. Accurate sampling techniques must be implemented with equal interest as that which is given to accurate volume measurement. MMBTU is the total of volume and energy. Sampling is the energy determination delivery system for this equation, and the results have a dramatic influence on the volume measurement totals and the bottom line profitability for the company.

With the combination of USM and higher demands, our natural gas pipelines are seeing changes within the pipeline, relative to quality. Liquids are present for a number of reasons. One dramatic reason is simply the cost of natural gas. Producers are trying to meet the demand and sell their product. In so doing, gas processing is being streamlined or reduced. Liquids are being passed along in the interest of providing energy. Another reason for the increased presence of liquids is a change in system operations. Today, we pull from our storage domes harder and faster than ever before. This tends to increase the presence of liquids in the system. Deeper wells and colder pipelines in deepwater production is yet another source of liquids. Reduced maintenance, more flexible contracts and a host of operational considerations are in play.

In the past 35 years, sampling systems have been refined to meet more exacting requirements of the industry and sampling standards have been revised to reflect the latest reliable knowledge and techniques. The equipment available today is truly “state of the art.” Samplers, cylinders, probe regulators, protective filtration systems, separators, membranes, protective shut in devices for analyzers, insulated and heated enclosures and the like are available from a number of known manufacturers. Historically, natural gas was sampled as natural gas. Most equipment used in the gas industry is not designed to account for and handle liquids. Liquids have typically been removed and handled as a liquid product. Today however, that is not always the case in a new multiphase world. The quality of the pipeline product cannot be represented as accurate if the method of taking a sample incorporates a technology or procedure that is designed to reject or isolate liquids that are present. Using a separator, coalescing filter or a membrane

designed to reject the intrusion of liquids, is not providing the complete answer for the pipeline measurement department. If liquids never show up in the sample, but continue to be found in headers, river crossings and drips, then something in the procedure or technology is not allowing for a truly representative analysis to be attained. All of our sampling standards – ISO 10715, API 14.1, GPA 2166, etc. – call for a representative sample of the flowing stream. We must capture a representative sample regardless of the effort. Then, a technology or procedure for correctly and accurately handling the combined sample must be developed. That is the challenge. Not ignoring, rejecting or masking the liquids! We figured out how to do that long ago. That is no longer sufficient.

It is noteworthy that the current and updated gas sampling standards all make the clear statement that they are to be used in gas streams that are clean, dry, non-saturated and above the hydrocarbon dew point of the flowing gas stream. Therefore, lessons learned in the programs need to be presented accurately and honestly. While there are indeed few issues with taking a sample of 1012 BTU gas at 80° F, it is not likely a good practice to infer from that data that there are few issues to be seen with 1348 BTU gas at 58° F. While it is true that a probe is not required in a laboratory test of nearly pure methane, it might be considered questionable to extrapolate that to a 10 year old 8 inch meter run installation in North Dakota with1246 BTU gas and only a bottom tapping and a valve for a sample point. While we continue as an industry to find new answers, we must not forget the lessons learned over the last 45 years.

If we state that we have taken a representative sample from a flowing stream, then it must represent ALL of the components present in that stream; not simply all the gas phase components of the stream. In the quest for full knowledge of our system, we must know all of the components of the gas stream. Not all of the components act the same, flow at the same speed or stay equally dispersed across the inside diameter of the pipeline. It is not as simple as sampling a dry gas stream. That is the challenge involved in sampling today's wet gas system.

And, it bears repeating over and over again. Most flow equations receive the specific gravity portion of the formula from the analysis of the gas sample. If the analysis is deprived of the total picture, how can the volumetric answers be relied upon as representative of the total system? The error is compounded and the integrity of the system is compromised.

Allocation

In today's world, the natural gas and crude oil industry is in a continual battle to provide energy to the consumer as quickly and efficiently as possible. In times past, individual companies explored, produced, processed and delivered their own product. Today, especially with the cost of offshore production, the picture has changed. Several companies may participate on one platform. Other systems may have multiple individual producers, but they will all use the same pipelines to reach the shore. Gathering fields may have mixed partners and processing facilities. All of this is exciting and helps the

end user with a steady supply of energy, but the difficulty comes on the business side. Companies are trying to make money and meet shareholder expectations. They want a fair allocation of the end result. Bluntly, you want to be paid equitably for the energy that you put into the system. Since much of the production goes into a common pipeline, there is a need for determination of volume and quality before it is processed and ready for normal measurement systems. Business integrity demands a method of determining the total content of the pipeline in a production phase, not just a processed phase.

Corrosion

Corrosion is an aspect of the total pipeline operation and integrity question that must receive data relative to the whole picture. If the corrosion department is not informed of the total contents of the pipeline, then how are they to take the appropriate steps to protect and preserve the structural soundness of the pipeline system? If corrosive elements are present, but are overlooked by a procedure or technology that masks their presence, the issue of pipeline integrity and structural soundness will not be addressed. If we cannot ascertain all the information from a single source, then we need to state that clearly and provide guidance on the direction for attaining the missing information. There are sensors and methods to detect contaminants in the flowing stream. Those options must be used if we are to be able to maintain the total package of "Pipeline and Operational Integrity." And there is new technology yet to be developed that can see the complete package. None the less, we cannot forget the lessons that we have learned and the principles that we currently know to be true.

Where are we?

There is excellent technology available in the industry. We have samplers and cylinders that allow us to maintain pipeline conditions and get a representative sample to the lab. We have the latest in flow measurement equipment that allows for higher degrees of accuracy than ever before. We have convenient systems for the removal of collected raw liquids from river crossings, ring mains and other natural low points, while not interrupting the pipeline operation. We have equipment for the detection of corrosion and methods for reducing corrosive environments in the pipeline system. We have new designs for sampling LNG. We have improved the technology for attaining a representative aliquot of high vapor pressure crude's. We have advancements in processing and production that continually improve the total issue of pipeline integrity. We have sophisticated odorant injection systems that maintain safe levels of odorant based on constant input of gathered data. We have procedures and standards that supply correct techniques and guidance on how to prepare, handle and transport samples and train technicians in that process. We have the latest in standards that direct the industry in flow measurement devices and calculations. We have superior monitoring protocols for the protection of the crude oil, light liquid and natural gas infrastructure.
All these elements continue to improve the industry and the quest for the very best overall operation and delivery system for the consumer. Simply stated, we have experienced great improvement in measurement in the last 25 years.

We now need to look closely at procedures and technologies to pool this vast cornucopia of knowledge and refine it to meet the needs of a changing industry. Do we have the right equipment but the wrong procedure? Do we have the right understanding but an outdated procedure? Do we have the correct concept but the wrong equipment? Or, do we have everything we need, but just not in the right order yet?

For many years the industry has talked about the 4 main ingredients to a successful measurement program:

- The reliability of the equipment and instrumentation used
- The specified policies and practices followed while performing the task
- The quality of the training and performance of the technician
- The proper recording and documentation of the transactions based on a quantifiable standard.

We can now add a fifth major consideration to a superior measurement program:

- Awareness of the total changing environment in which you work, including the evolving system, the changing technology and the revision and introduction of new standards.

Conclusion

Admittedly, much of the basis for this paper and its content is the result of the fact that we now see gas pipelines with more liquid content than before. Many are in fact, multiphase pipelines. Similar challenges are clearly understood by the crude oil and liquids segments of the industry. At times, we are led to believe that our leaders of the past never faced or thought of this issue. This is why the author reflects in this paper about not forgetting the lessons of the past. Here is an interesting paragraph from a paper presented at the University of Oklahoma, to the International School of Hydrocarbon Measurement in 1982. A full quarter of a century ago!

> "The ability to "tame" liquids when they appear in the gas sample streams or cylinders is now at hand with the availability of high quality new equipment. The capability of determining the heating value of the gas at any pressure and temperature condition can be determined with reasonable accuracy by conditioning the sample as it is directed to the measuring instrument. However, there is a need to more precisely define a "liquid" in our contracts and state how to account for the heating value of the fluid when liquid is present as an aerosol or otherwise. Should the Btu be determined on the gas at flowing conditions, or should it be determined at a greatly reduced pressure and elevated temperature? Should a pressure and temperature be selected for determining the Btu that would correspond with the average annual ground temperature and average annual pipeline pressure? These and other points must be resolved before any determined effort can be instituted to standardize Btu determination procedure on aerosol gasses."

And we are still working on that question today. It is all a part of this issue. We can no longer look for only one solution to one problem. We have to know what the impact of that technology is to the rest of the operation. All of it!

What is the full impact? Do you know?

REFERENCES

"Practical Considerations of Gas Sampling and Gas Sampling Systems", D. J. Fish, Pipeline and Gas Journal, July 1997

"Analyzing Heating Value", T. F. Welker, Pipe Line Industry, October 1990

"Wet Gas through Two Phase Complete Measurement", Daniel J. Rudroff, Draft presentation to Texas A & M University, 2003

"Methods, Equipment & Installation of Composite Hydrocarbon Sampling Systems", D. J. Fish, Presented at Belgian Institute for Regulation and Automation, Brussels, Belgium, 1993

"Techniques of Gas Sampling", Charles F. Drake, Presented at the International School of Hydrocarbon Measurement, Norman, Oklahoma, May, 1982

"Selection and Installation of Hydrocarbon Sampling Systems", D. A. Dobbs & D. J. Fish, Presented at Australian International Oil & Gas Conference, Melbourne, Australia, 1991

Personal Interviews of the Author with Industry Measurement Specialists from 8 major Natural Gas Producing, Transmission and Distribution companies, worldwide.

Various Standards of AGA, GPA, API, ASTM and ISO

djf/Oct. 2007

DHF@STATOILHYDRO.COM

Dag Flølo

A method for remote in-line calibration of water fraction meters

A method for remote in-line calibration of water fraction meters

Dag Flølo
Discipline advisor
Fiscal metering and allocation;
StatoilHydro

Abstract

A new method has been developed which is suitable for remote in-line calibration of water fraction meters. The method utilizes settling of water in a vertical line under no-flow conditions.

As water is allowed to settle in a hydrocarbon liquid, a repeatable, low, amount of water will remain solved in the hydrocarbon liquid. This amount of water can be determined, and the water in oil meter can be zero-point calibrated at this point. The method is suitable for installations where water cut meters are installed in a vertical pipe section, and where no flow conditions can be provided manually or happens in occasional shut downs without depressurization.

Current methods for calibration require entering a well-defined test fluid or air into the meter and/or that representative samples are taken and analyzed in a laboratory. This is especially challenging with unstable hydrocarbon liquid or low-density condensates. Current methods also require the presence of competent personnel at the site.

This new method is suitable for remote operation, and only requires available trend curves and remote access to the metering system / water fraction meter. The new method for inline calibration represents relatively large cost reduction and reduction of HES risks relative current methods. It is expected that the uncertainty of the method can be within fiscal requirements (0.05 [vol %]) for well-known fluids.

1. Introduction

The method described herein was developed to overcome significant problems with performing a satisfactory calibration of a water fraction meter installed downstream an inlet separator at a metering station used for allocation metering.

The process conditions at the metering station were the following:

- Pressure: 100 [Barg]
- Temperature: 30 [DegC]
- Density: 600 [kg/m3]

The following make in-line calibration of the water fraction meters challenging, as it makes it real difficult do take a representative sample and analyze it at standard conditions using Karl Fisher analysis:

- The condensate is not stable. When a sample is depressurized a large amount of the liquid will change to gas phase.
- Due to large difference in density and low viscosity water separates real fast from the condensate.

Further the water fraction meter is installed inline with no possibility to remove the meter or to fill the meter with a reference fluid without shutting down production.

2. The Challenge

The Handbook of water fraction metering presents the main causes that might bring a water fraction meter out of calibration. Ref.: Handbook of water fraction metering revision 2. Section 9. Calibration.

> *Calibration may generally be required to determine (and – in the case of adjustment – to compensate for) the effect on the measured % Water of any of the following three main elements:*
>
> *1. Mechanical wear and ageing of components*
>
> *2. Contamination of sensor section by scaling, asphaltenes etc.*
>
> *3. Changes in fluid composition due to non-hydrocarbon components*
>
> *. . . This handbook also seeks to make the calibration and adjustment of the WFM independent of conventional sampling and analysis (cf. Section 9.1.2).*

The method of the handbook basically prescribes the following steps for getting and maintaining a calibrated meter.

> *• Primary calibration (performing adjustment and recording footprint)*
>
> *• Reproducibility check (verifying meter against footprint)*
> *(Ref: Section9 Calibration)*

Primary calibration:

> *The purpose of the primary calibration is to:*
>
> *• Record the footprint of the WFM with a repeatable reference material*
>
> *• Establish the error of the measured WLR on a stabilised field oil sample*
>
> *• Perform adjustment of the WFM with a stabilised field oil sample*
>
> *(Ref: Section 9.1 Primary calibration)*

Reproducibility check:

> *The purpose of the reproducibility check is to verify that the most recent primary calibration (adjustment) of the WFM is still valid. Such verification is achieved through reproduction of the WFM footprint in the field, and comparing this with the footprint from the primary calibration certificate.*
>
> *(Ref: Section 9.2 Reproducibility check)*

The main challenge with following the Handbook in this case is that the meter is installed inline with no possibilities to fill the meter with a reference fluid without shutting down production, opening the flow line and filling the reference fluid into the meter.

Further a stabilized field oil sample will have significantly different density than the unstable fluid at operating conditions. A change of density by 1 [kg/m3] will alter the measurement by 0.027 [vol%]. Ref. RFM WCM Installation and operating instructions section 3.2.3. The zero point of the water fraction meter would therefore be significantly affected by this change in density. However this could be compensated for.

The prescribed procedure also requires a detailed procedure, planning, and coordination of personnel, documentation, competent personnel onshore and offshore. All in all the process becomes laborious, expensive and the risk of failing becomes significant. In this case it would also involve building of scaffolding and HES risk related to opening the flow line.

The method to perform inline calibration by taking a representative sample, analyze it in the laboratory and adjusting the meter accordingly is not achievable as the condensate is far from stabilized, and water settle real fast making it very difficult to inject a representative sample into the Karl Fisher apparatus.

3. The operating principle of the water fraction meter

The meter used in this case was a full bore microwave water fraction meter made by ROXAR.

The operating principle of this meter is described in the Installation and operating instructions. Ref. RFM WCM Installation and operating instructions section 3.1.1

3.1.1 Operating principle

1. The Meter is factory calibrated with vacuum (air) frequency of sensor
2. A discrete sweep over the measurement range from high to low frequencies is done by transmitting a frequency on one antenna while measuring power on the other.
3. A curve fit on the resulting peak power measured is done to achieve highest accuracy
4. Temperature, pressure and mixture density (Optional) is input to the meter
5. Water and oil basic configuration data is converted to line conditions and the respective dielectric constants are calculated using a Roxar patented method
6. The mixture dielectric constant is calculated from measured frequency
7. The water cut is calculated using the Bruggemann equation

$$WC = 1 - \frac{\varepsilon_{mix} - \varepsilon_{water}}{\varepsilon_{oil} - \varepsilon_{water}} \cdot \sqrt[3]{\frac{\varepsilon_{oil}}{\varepsilon_{mix}}}$$

The uncertainty obtained solely by entering dry density at operating conditions is specified by the manufacturer to be:

Fixed density method
- ±(0,3 % + 5 % of reading)
- Max. 1 % absolute
- Effect of oil density variations: ± 0,027 % abs. per 1 kg/m³

However it will require calibration to verify that this uncertainty is maintained in operation.

The uncertainty can be further reduced down to the uncertainty of the reference method by performing inline calibration. Inline calibration is performed by taking a sample, analyzing the sample in a laboratory and adjusting the meter reading to the laboratory result. If combined with a density meter the effect of oil density variations can be eliminated.

4. The metering station used for the tests

The metering station is placed downstream of the Skirne / Byggve inlet separator at Heimdal. The separator is operated at 100 [Barg] and approximately 30 [DegC]. The metering station is measuring condensate at approximately 605 [kg/m3] from the separator.

The condensate metering station is equipped with a densitometer, an ultrasonic flow meter, and a full bore inline water fraction meter. The density meter and the water fraction meter are installed on a vertical part of the flow line. The ultrasonic meter is installed in a horizontal part of the flow line.

These instruments are connected to a fiscal supervisory system. The system is accessible from intranet or internet (Virtual Private Network).

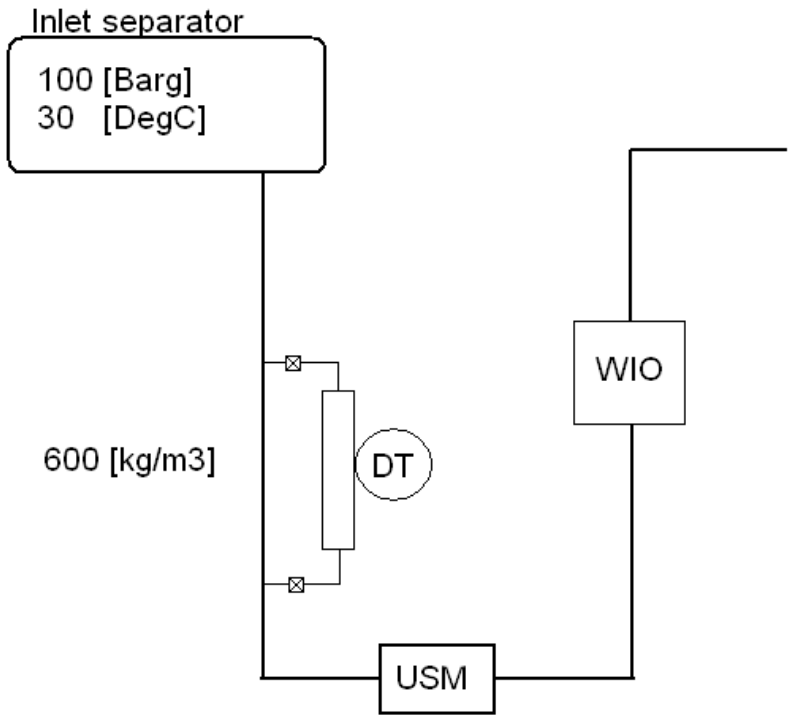

Figure 1. Principle sketch over the metering station.

5. Hypothesis

The following two hypotheses were formed as basis for the new method for calibration.

Hypothesis: When water is allowed to settle in a hydrocarbon liquid a repeatable, low amount of water will remain solved in the hydrocarbon liquid (in this case condensate). The water fraction meter can then be calibrated at this point.

> *Hypothesis 1:*
>
> *Expected repeatability of remaining water in condensate when water is allowed to settle out: better than 0.05 [%]*
>
> *Hypothesis 2:*
>
> *Theory about liquid liquid equilibrium of water and hydrocarbons will predict that the expected water fraction remaining in the condensate when water is allowed to settle out is less than 0.2 [%].*

6. Tests

It turned out that occasionally the process was shut down without depressurization of the flow line. By investigating the trend curves it turned out that the measured water fraction rapidly fell and stabilized. As the pressure fell by 2.5 [Barg] gas bubbles will form. It is anticipated that the gas bubbles will rapidly rise through the vertical section. Further it is anticipated that the change of density following this formation of gas will be negligible.

The water fraction meter was first calibrated to show 0.00 [%] at a no flow condition without depressurization at 2006/03/11 21:16. Before calibration water was allowed to settle for approximately 2 hours.

The first test was performed at 2006/04/03 09:35. The following figure is a trend curve from the metering system showing a no flow condition without depressurization. Figure 2 represents a test of hypothesis1:

> *Hypothesis 1:*
>
> *Expected repeatability of remaining water in condensate when water is allowed to settle out: better than 0.05 [%]*

Figure 2.Trend curves from a no flow condition without depressurization.

Red	*Volume flow rate (USM nr. 1)*
Yellow	*Measured Density at process conditions*
Green	*Calculated net condensate density*
Blue	*Measured water fraction from water in oil meter*
Magenta	*Pressure*
Orange	*Line temperature*
Turquoise	*Volume flow rate (USM nr. 2)*
White	*Calculated volume flow rate at standard conditions.*

As can be seen from the figure, water rapidly settles out, and water fraction stabilizes at 0.01 [%]. Figure 2 therefore gives support for hypothesis 1.

A similar test was performed 2006/06/26 23:34 with measured water fraction at no flow condition equal to 0.01 [%]. This gives strong support both for the stability of the water fraction meter and hypothesis 1. It even indicates that the hypothesis is conservative, and that an even better repeatability is achieved for this condensate.

Another test was performed by using trend curves to check calculated net condensate density against measured density on a pressurized sample at an onshore accredited laboratory.

In the onshore laboratory, the density is measured by heating and applying pressure on the cylinder until it reach process temperature and pressure. The density is than measured at process pressure and temperature by using appropriate equipment the sample cylinder is

kept still to allow water to settle out. The objective of the measurement is to measure net condensate density.

Intertek West Lab report reference: 2006-03308
The sample was taken: 20.06.2006, 21:00 hrs.
The reported density from Intertek West Lab is 605.3 [kg/m3]
Trend curve from the metering system shows a calculated net condensate density of 605.4 [kg/m3] at the time where the sample was taken.

The difference of 0.1 [kg/m3] in density account for a difference in water fraction of approximately 0.025 [vol%], if all the density difference is explained by difference in water fraction. Again this gives strong support for hypothesis 1.

Unfortunately, none of these tests are suitable for testing hypothesis 2 as the remaining water fraction in condensate in theory could be repeatable and still be higher than 0.2 [%]:

> *Hypothesis nr 2:*
> *Theory about liquid liquid equilibrium of water and hydrocarbons will predict that the expected water fraction remaining in the condensate when water is allowed to settle out is Less than 0.2 [%].*

An internet and article search was performed by the author in order to look for experimental data / theoretical results about the liquid-liquid equilibrium of water and hydrocarbons. The solubility of water in 50 different hydrocarbons at 20 [DegC] are presented in the article: "Nonlinear Dependence of the Solubility of Water in Hydrocarbons on the Molar Volume of the Hydrocarbon." [3]. Experimental results referred to in this article for the water fraction at equilibrium, range from approximately 0.005 [%] to approximately 0.05 [%] for Benzene. The article seems to give support hypothesis nr. 2, however the article does not provide data for multi component hydrocarbons nor does it provide data for solubility at higher temperatures.

The article "Liquid-liquid equilibria of water-hydrocarbon systems from cubic equations of state" [4] turned out to be disappointing regarding hypothesis nr. 2. In section "3.2 Multi component systems" it is stated that "Few multi-component data are available for liquid-liquid equilibria of water-hydrocarbon systems." As few data are available it will be hard to verify that theoretical calculation of the liquid-liquid equilibrium of our condensate is precise within required uncertainty. It is also pointed out that the solubility of water will increase with increasing temperatures. Further the calculation of the liquid-liquid equilibrium seems to be quite laborious.

Even though Hypothesis 2 still seems to be reasonable, the author has still not found sufficiently support for hypothesis nr.2 by general theory / experimental data. This leaves us with the only possibility to measure the amount of water in solution with the condensate to provide a traceable calibration of a water fraction meter. However, when it comes to representative sampling and analysis it will be much easier to determine the amount of water in solution with condensate than it is to determine a larger amount of water mixed with condensate.

As the densitometer can be isolated from the flow the original idea was to isolate the densitometer, allow water to settle out from the condensate and then measure the density of condensate without water. The metering station continuously calculates the net density of condensate by compensating for the water fraction. This calculated net density is then expected to be equal to the measured net density. Calibration of the water fraction meter could than be performed by adjusting meter reading until the calculated net condensate density equalled the measured net condensate density. This is an indirect method which probably also could be used for calibration of the water fraction meter. The uncertainty of this method would be somewhat higher than direct calibration of the water fraction meter at no flow conditions.

7. Conclusions

A new method for remote inline calibration of water fraction meters has been established. A vertical installed water fraction meter, measuring water in condensate, can be calibrated from remote by using trend curves and occasional no flow conditions without depressurization.

The performed tests give strong support to hypothesis 1:

> *Hypothesis 1:*
>
> *Expected repeatability of remaining water in condensate when water is allowed to settle out: better than 0.05 [%]*

The performed tests even indicate that the repeatability can be as low as 0.02 [%].

Hypothesis number 2 still seems to be reasonable, but is still not sufficiently supported to replace laboratory measurement of water fraction by Karl Fisher analysis:

> *Hypothesis 2:*
> *Theory about liquid liquid equilibrium of water and hydrocarbons will predict that the expected water fraction remaining in the condensate when water is allowed to settle out is Less than 0.2 [%].*

The amount of water in solution with condensate has to be determined by analysis. However it seems far easier to measure the amount of water which remains in solution with condensate than it is to perform representative sampling and analysis of the two immiscible liquids at higher water fractions.

When a representative sample is shipped onshore the analysis can most likely be performed by a laboratory onshore, as the amount of water in solution with condensate seems to be repeatable within 0.02 [%].

8. Method for remote inline calibration of water fraction meters

Large reductions of costs and HES risks can be achieved by adapting this new method for calibration. However the method requires that no flow conditions without depressurisation either occur naturally or can be created. Further the repeatability of water in solution with the hydrocarbon liquid will have to be checked.
The method is described by the following:

9. Establish the liquid liquid equilibrium of water in hydrocarbon by letting water settle out and measure the amount of water in solution with the hydrocarbon liquid by Karl Fisher or equivalent method.
9. Verify acceptable repeatability.
9. Use trend curves to find a no-flow condition without depressurisation.
9. Use trend curves to establish meter reading when water has been allowed to settle out.
9. Adjust meter reading of water in equilibrium with the hydrocarbon liquid by the difference to the Karl Fisher result.

9. Implications for design of future metering stations

New metering stations should be designed for this method by:

1. Installing water fraction meters vertically
2. Ensuring remote access to the metering system.
3. Ensuring remote access to the water fraction meter.
4. Ensuring that shut downs with no flow conditions and without depressurization will occur.
5. If shut downs without depressurisation will not occur naturally, valve arrangement should be designed so that no flow conditions can be created without shutting down production.
6. Calibration interval can be prolonged by duplicating water fraction meters and using condition based maintenance.

Automatic systems for calibration can possibly be made by:

1. Duplication of water fraction meters in a master meter configuration.
2. Using automatic operated valves to regularly create a no flow condition without depressurisation.
3. Automatically calibrate one of the two meters by the method.
4. Raise alarm if deviation between the meters exceeds a preset limit.

5. References

[1] Handbook of water fraction metering Revision 2. www.nfogm.no
[2] Water fraction meter user manual: RFM WCM Installation and operating instructions
[3] Liquid-liquid equlibria of water-hydrocarbon systems from cubic equations of state; NASRIFAR Kh. ; MOSHFEGHIAN M.
[4] Nonlinear Dependence of the Solubility of Water in Hydrocarbons on the Molar Volume of the Hydrocarbon; Paul Ruelle and Ulrich W. Kesselring.

25th International North Sea Flow Measurement Workshop
16th – 19th October 2007

Traceable Calibration of Liquid Densitometers

Norman Glen, TUV NEL Ltd
Douglas Griffin, Department for Business, Enterprise and Regulatory Reform

1 INTRODUCTION

Density measurement is a key element of both mass and volume flowrate measurement in the oil industry and as such is fundamental to the commercial operation of facilities. The most widely implemented approach for mass flow measurement is to use a volumetric flowmeter and a densitometer. All flowmeters require periodic calibration and traceability within the UK is provided through the Flow Programme. All commercial densitometers also require periodic calibration. In 2004 the Aberdeen-based Energy Resources Development Unit of DTI's Energy Group identified a need for research into practical methods for in-situ calibration of densitometers, as well as a greater understanding of the effects on densitometer performance of variations in product density, pressure and temperature.

This is particularly important as more and more operators are involved in smaller field developments tied back to other operators' platforms, feeding third-party pipeline infrastructures. In addition, as more HTHP fields come on stream, more densitometers will be operating at temperatures and pressures significantly different from those currently used as the reference conditions for calibration.

TUV NEL, the custodians of the UK Fluid Density Standards, are leading a Joint Industry Project (JIP) aimed at providing the oil and gas industry with confidence in densitometer performance, by developing a calibration procedure which links traceably to National Standards. Fourteen operators, a densitometer manufacturer and the UK oil and gas regulator (part of the Department for Business, Enterprise and Regulatory Reform) have joined the project.

The key task of the JIP is the detailed characterisation of densitometers in well-controlled conditions, making use of accurately-characterised transfer standard fluids that cover the density and viscosity ranges which are encountered across the full temperature and pressure range of operation of UK offshore oil facilities.

This paper describes the technical approach being used and presents initial results.

2 BACKGROUND

The most widely implemented approach for mass flow measurement is to use a volumetric flowmeter and a densitometer. In this case, the uncertainty in mass flow measurement is dependent equally on the uncertainty in volumetric flowmeter measurement and in densitometer measurement. The calculation of volume flow rate however also requires a knowledge of the density since it is necessary to reduce the measurements of volume throughput to standard conditions. It can therefore be seen that density measurement, volumetric and mass flow measurement are of equal importance.

The essential requirements of a density measurement system are that:-

- Calibrations should only be carried out using instruments that form part of a calibration chain traceable to national standards.

- Densitometers should be checked and calibrated regularly at temperatures and pressures corresponding to actual operational conditions.

All commercial densitometers, for use on gases or liquids, operate on an oscillatory principle and as such are not independent of other fluid properties. However, the theory of such methods is not rigorously established and even with careful design it is not possible to uncouple fully the effects of density from the other physical properties of the calibration fluids. To maximise the accuracy attainable with such densitometers, it is necessary to calibrate them against reference fluids with similar physical characteristics (such as speed of sound and viscosity).

It has been accepted industry practice to quote a calibration at only a single reference temperature (generally 20°C) and apply correction factors to account for the influence of temperature and pressure on both the calculated density and its uncertainty. However, recent work has raised a number of issues with regard to the whole calibration process, in particular when a densitometer is operated at a temperature different from the reference temperature. This has significant implications for fields operating in common transportation systems, where the mass allocations are based on densitometer readings.

3 OSCILLATORY DENSITOMETER THEORY

All commercial liquid density transducers operate on the same general principle. The manufacturers generally model the instruments as a simple spring mass oscillator system comprising the vibrating test section and the fluid contained in it, totally disregarding hydrodynamic effects. As the liquid density changes it in turn changes the total vibrating mass, which is then detected by a change in the resonant frequency. For a simple system, the resonant frequency f is given by:

$$f = \frac{1}{2\pi}\sqrt{\frac{K}{M}} \tag{1}$$

where K is the stiffness and M is the mass of the element (M_1) plus the mass of the fluid (M_2).

If K, M and V_f (the volume of fluid in the test section) are constant then equation 1 can be written in terms of density ρ as

$$\rho = K_0 + \frac{K_2}{f^2} \tag{2}$$

where $K_0 = -M_1/V_f$ and $K_2 = K/4\pi^2 V_f$, or, in terms of oscillation period τ,

$$\rho = K_0 + K_2\tau^2 \ . \tag{3}$$

In recognition that equation 1 is only a first approximation to the actual behaviour of an oscillating tube filled with liquid [1], equation 3 is normally modified by the inclusion of a linear term K_1, giving an empirical expression of the form

$$\rho = K_0 + K_1\tau + K_2\tau^2 \ . \tag{4}$$

At any given temperature t and pressure p the three constants in equation 4 can be determined by calibrating the device with three fluids of known density. To ensure the highest accuracy this should be undertaken across the full operational temperature and pressure range, thus requiring a knowledge of the density of each calibration fluid at the corresponding conditions. Accepted practice however has been to calibrate at one reference temperature (normally 20°C) at atmospheric pressure to determine the coefficients at those conditions and then apply correction terms to account for the effects of operation at other temperatures and elevated pressure. The correction terms are of the form

$$\rho_t = \rho_0\{1 + K_a(t - t_0)\} + K_b(t - t_0) \tag{5}$$

where ρ_0 is the density at the reference calibration temperature t_0 and

$$\rho_{t,P} = \rho_T\left\{1 + K_c(p - p_0) + K_d(p - p_0)^2\right\} + \left\{K_e(p - p_0) + K_f(p - p_0)^2\right\} . \tag{6}$$

At the time of manufacture, the coefficients in equations 5 and 6 are determined for each instrument and these temperature and pressure coefficients are provided for use by the operator. For example, Emerson Process Management calibrate each Solartron 7835 densitometer using three fluids to cover the full operating density range of the instrument (300 to 1100kgm^{-3}). Each instrument is calibrated at 20°C and 60°C, followed by a separate pressure calibration at pressures which cover the specified pressure range of the instrument.

Whilst the procedures used by manufacturers to obtain instrument coefficients at the time of manufacture ensure that these coefficients are as accurate as possible, this will not necessarily be the case following recalibration, unless similar procedures are followed. Within the UK the majority of industrial densitometers are recalibrated by third-party calibration laboratories. Current practice is to calibrate each instrument in a test rig using three fluids at atmospheric pressure and a reference pressure. In practice this means that the range of pressures and temperatures at which the instruments are

normally calibrated is limited to near ambient conditions but many densitometers, particularly those used in offshore applications, operate under high pressure, high temperature conditions.

The density of each test fluid is typically measured by two in-line transfer standard densitometers that are periodically calibrated using fluids of accurately known density. From at least 1986 accepted practice was to check the temperature coefficients (K_a and K_b in equation 5) of the transfer standard densitometers using air and then apply corrections for use with other calibration fluids and assume that no systematic bias was introduced. However, a note issued by the Licensing and Consents Unit of DTI's Energy Group in 2004 [2] summarising a review carried out by industry, found that there was a small but systematic 'offset error' when a densitometer is operated at a temperature different from the reference temperature. The offset error was corrected in 2004 by the use of revised temperature coefficients.

Although the magnitude of the particular offset error identified by the manufacturer and reported by DTI seemed small, 0.014kg m^{-3} K^{-1}, a number of UK Continental Shelf fields operate with measuring stations at temperatures approaching 100°C. For a field producing 50,000 barrels per day the mis-measurement at the platform would be of the order of 25,000 barrels per annum. A similar effect will occur at the on-shore terminal. If the oil from a number of fields has been fed in to a common pipeline the allocation to each field is based on the 'measured' mass fed in by each. Clearly the actual mis-allocations will depend on the temperatures of each off-shore measuring station, the flow rates and the temperature of the on-shore measurements but could easily run to 10s of thousands of barrels per annum for each field. The mismeasurement on condensate fields will be greater than that for oilfields, as the relative error in density measurement is greater for lower-density product; in addition, condensate production tends to be at relatively high temperatures. Taken over the whole of the UK production, mis-allocation errors arising from this effect alone could run to several million pounds per annum and possibly hundreds of millions over a 20 year period.

In addition to this specific point, the review raised a number of issues with regard to the whole calibration process and the calculation methodology. TUV NEL have been aware for many years of the influence of other fluid properties (primarily viscosity and speed of sound) on the operation of oscillatory densitometers and sponsored work to investigate these effects [3,4]. For liquids, this clearly demonstrated the coupling between density and viscosity: it is possible to optimise a vibrating element to respond to either density or viscosity as a first-order effect but the other property is always present as a second-order effect. Accurate characterisation, and calibration, of oscillatory densitometers therefore requires knowledge of the effects of temperature and pressure on a number of fluid properties across the full operational range of the device. Furthermore, a complete characterisation of a vibrating tube densitometer would also require to investigate additional effects including fluid velocity, torque loading, mounting misalignment etc.

4 TECHNICAL APPROACH

As part of previous Flow Programmes, DTI funded the establishment of density standard facilities at TUV NEL [5]. These consist of two primary standard densitometers, one each for liquids and gases. In addition, a facility for the calibration of liquid densitometers (insertion and in-line devices) was also developed.

The original concept for the TUV NEL Industrial Densitometer Calibration Facility for the calibration of liquid densitometers envisaged that the facility would be directly linked to the TUV NEL Primary Standard Densitometer for liquids. Whilst this has the merit that the fluid in the densitometer under calibration is the same as that in the Primary Standard Densitometer and at identical conditions, thus minimising the uncertainty in the fluid density, it has a number of practical drawbacks. In particular, the time required for the Primary Standard Densitometer to reach equilibrium and make a measurement is substantially longer than the time required in the Industrial Densitometer Calibration Facility. In addition, the task of cleaning the Primary Standard Densitometer is time-consuming, particularly if it has been filled with difficult fluids such as heavy oils.

In view of these considerations, a better approach is to use stable, accurately characterised transfer standard fluids. As noted in Section 3, there is a coupling between fluid density and viscosity in an oscillatory densitometer and hence the chosen fluids must cover the density and viscosity ranges which are encountered across the full temperature and pressure range of operation of UK offshore oil facilities.

To be considered for use as true transfer standard fluids, fluids must either be single components or stable mixtures of known composition. Such fluids have the advantage that once their PVT behaviour has been established (using the TUV NEL Primary Standard Densitometer) they can then be used in any other (transfer) facility without further characterisation, thus providing much closer traceability to primary standards.

4.1 The TUV NEL Primary Standard Liquid Densitometer

The TUV NEL Primary Standard Liquid Densitometer is based on the buoyancy method using the Archimedes' principle This involves measuring the weight of an object of known mass and volume in the test fluid at the conditions of measurement. The weight, W, of an object of mass m and volume V in a fluid is given to a first approximation by the equation:

$$W/g = m - V\rho \tag{7}$$

from which the density, ρ, of the fluid can be expressed as:

$$\rho = \left[(W/g) - m\right]/V \ . \tag{8}$$

The operating range of the densitometer is from -40 to 150°C across the pressure range from 0.1 to 30MPa.

4.1.1 Magnetic-Suspension Coupling System

The standard object is not coupled directly to the microbalance. Instead, as shown in see Figure 1, the microbalance is indirectly connected by a magnetic-suspension coupling to the standard object which is located within the measurement chamber. The coupling comprises an electromagnet, a permanent magnet, a sensor core and coil and a device for coupling and decoupling the standard object. The electromagnet, which is hooked to the underside of the balance pan, maintains the permanent magnet and its attachments within the measurement chamber in a freely suspended state. Control is effected by an electronic unit with position feedback obtained from the sensor coil and core. Using this technique the measuring or buoyancy force on the permanent magnet and its attachments, including the standard object, are transmitted without contact and with negligible error through the walls of the test chamber to the microbalance at ambient conditions.

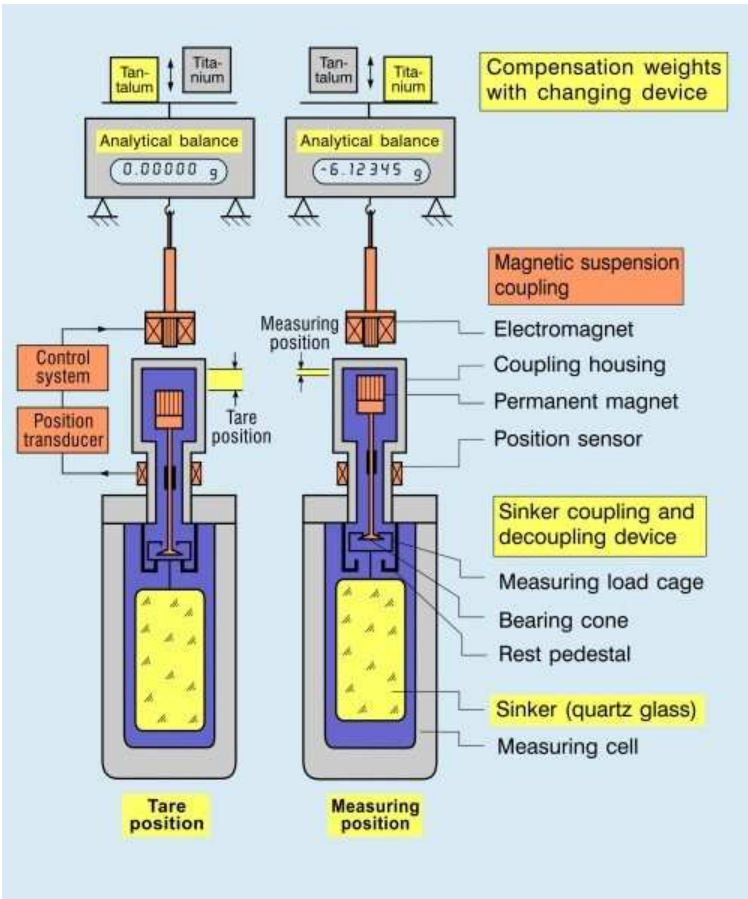

Figure 1 Magnetic-suspension coupling
(a) tare position, (b) measuring position

The electronic control unit contains two separate PID controllers: the first, to raise and lower the permanent magnet and its attachments in a controlled way between its rest position and either the 'measuring' or 'zero-point' position; and the second, a fast response system, to effect stable position control at the required 'measuring' or 'zero-point' position. In the 'measuring' condition, as indicated in Figure 1b, the standard

object is directly coupled to the permanent magnet and buoyancy forces act on all of the freely suspended components. In the 'zero-point' position, which is a few millimetres below the 'measuring' position, only the permanent magnet (Figure 1a), the position sensor and part of the load decoupling device are freely suspended. Here the small cage or carrier to which the standard object is attached is seated on an internal support. In this so-called 'zero-position' the balance can be tared and calibrated at all times even during a sequence of measurements. The difference in balance readings between the 'zero-point' and 'measuring' positions determines the buoyancy forces acting on the standard object and its carrier. The volume of the latter is less than 0.4% of that of the standard object.

Only force measurements are involved in the density determination, both in the calibration of the standard objects and in the measurement process. The accuracy and repeatability of the magnetic-suspension coupling is readily confirmed by weighing standard masses alternately on the balance pan and hung from the coupling.

The densitometer utilises a single sinker: a gold-plated solid cylinder of fused quartz with a volume, V, of some 24 cm^3. This sinker is coupled by a thin stainless steel rod to a simple mechanical linking mechanism then to a microbalance via other thin rods and an electronically controlled magnetic-suspension coupling. This coupling, as outlined in the previous section, transmits the load from the sinker inside the pressure vessel to the microbalance at ambient conditions without any direct contact. To measure the density, the sinker is alternatively coupled to, and detached from, the simple mechanical coupling and the resulting differential force, the buoyancy-force ΔF, is measured with a microbalance (resolution ~10 μg). From these force measurements, the density of the liquid at the temperature and pressure of measurement can be obtained from an equation of the form:

$$\rho = \left(\Delta F / g\right) / V_{t,p} \tag{9}$$

For liquids the buoyancy forces are considerable, of the order of 25 to 45% of the weight of the sinker, and the uncertainties in force measurement are negligibly small. The sinker is gold-plated to eliminate electrostatic forces and since the test liquid fills the densitometer completely the force measurements are free from the effects of surface tension.

The major uncertainty associated with this method of measurement arises from the determination of the volumes of the sinker and the small stainless steel carrier. The volumes are obtained by careful weighing in air and in pure water at around 20°C and ambient pressure. The relative uncertainty in the combined sinker and carrier volume at the reference conditions is assessed at less than 30 ppm. Taken together with the uncertainties resulting from the thermal expansion and the compression of the sinker, force determination, and temperature and pressure measurement, this leads to a total uncertainty in fluid density of 0.015% across the full operating range of the densitometer.

4.1.2 Dilation of Sinker

The volumes of the principal components of the densitometer are subject to dilation with both temperature and pressure. The volume of the sinker at absolute temperature t and pressure p can be obtained accurately from its known volume at the specified reference conditions, V_{ref}, from the expression:

$$V_{t,p} = V_{ref}\left[1 + 3\varepsilon_t\left(t - t_{ref}\right)\right]\left[1 - \kappa_t\left(p - p_{ref}\right)\right] \tag{10}$$

where $\boxtimes_t$ the thermal expansion, and
♲_t the isothermal compressibility,

are functions of temperature for each of the individual sinker materials. The maximum total uncertainty in the dilation of the fused silica artifact due to the combined effects of temperature and pressure is estimated to be within 57 ppm over the operational range of the densitometer. The maximum effective contribution to the uncertainty in the calculation of liquid density arising from the dilation of the suspension cage and hook of the single-sinker densitometer is around 1 ppm.

4.1.3 Supporting Systems

The densitometer is hung from a horizontally levelled platform mounted on a robust aluminium alloy structure. The microbalance is mounted above the platform and the upper part of the suspension coupling is enclosed in a transparent housing which is fed from a dry-air source with a dew-point of -80°C. The latter prevents condensation of atmospheric moisture on the upper connecting rods and electromagnets when the densitometer is used at sub-ambient temperatures. The magnetic-suspension coupling, its housing and the densitometer are contained in an oil-filled bath positioned beneath the platform. The bath consists of two dewar vessels mounted concentrically and has provision, in the annular space between each dewar, for both heating and cooling. Good circulation of the bath fluid is provided by magnetically-driven screw impellers mounted in the base of the outer dewar vessel. The control temperature of the bath is monitored by a 25 ohm standard platinum-resistance thermometer positioned some distance above the screw-impeller. The thermometer is monitored through a data acquisition system by a control computer and the power inputs to the heating/cooling circuits are adjusted using PID control software. The temperature of the densitometer is measured using four 25 ohm standard platinum-resistance thermometers attached to the body of the densitometer.

The temperature stability of the bath is within ±1 mK over its entire operating range and the absolute temperature can be set by the computer to within a few millikelvins of the desired conditions. The total uncertainty in the temperature of the working fluid in the densitometers is estimated to be 4 mK.

The densitometer is provided with a circuit for filling and evacuation. A gas-operated pressure balance of the highest metrology class is used to provide reference gauge pressures accurate to within 5 parts in 10^5. Atmospheric pressure is measured by means of a calibrated digital barometer accurate to within 20 Pa.

The pressure of the test fluid in the densitometer is obtained with reference to the pressure of nitrogen in the gas-operated balance through a mercury manometer separator. The uncertainty in the measurement of differential pressure is within 100 Pa.

As shown in Figure 2 and equations 11 to 13, the absolute pressure of the test fluid in the densitometer is obtained from the atmospheric pressure, gas-operated pressure balance and mercury manometer separator, corrected for temperature effects and pressure heads in the connecting lines as necessary. The uncertainty in the calculated total pressure is assessed as 7 10^{-5} p ± 100 Pa.

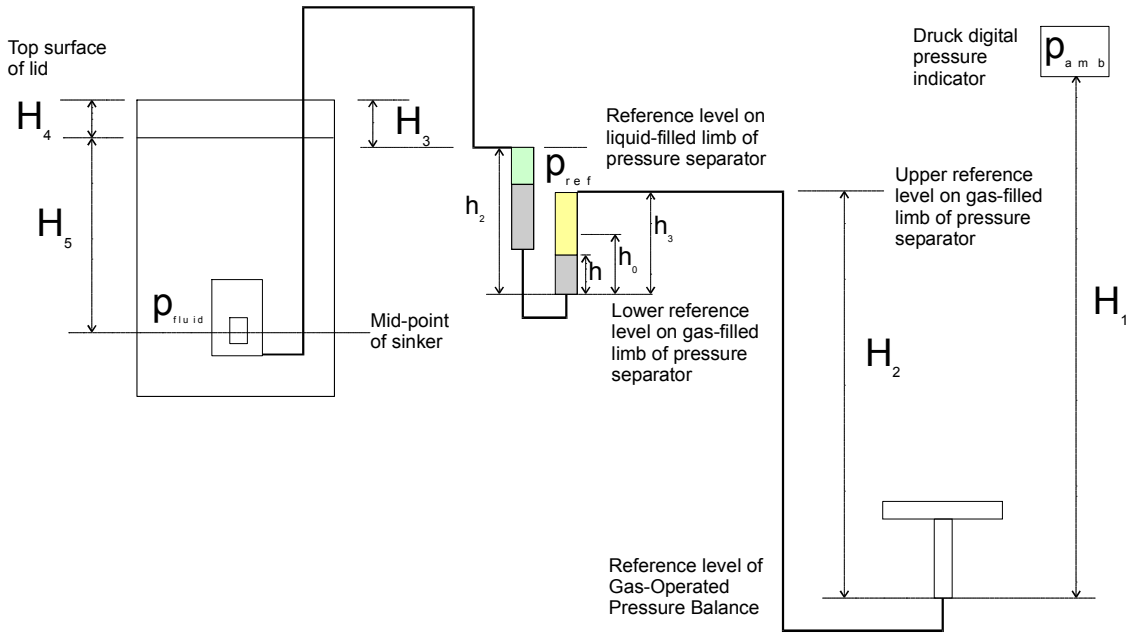

Figure 2 Schematic of pressure circuit for primary standard liquid densitometer

$$\begin{aligned} p_{ref} &= \left\{p_{amb,pri} + g \cdot \rho_{air}\left(p_{amb,pri}, t_{amb,pri}\right) \cdot H_1\right\} \\ &+ \left\{p_{stand} + g \cdot \rho_{N_2}\left(p_{stand}, t_{amb,pri}\right) \cdot H_2\right\} \end{aligned} \tag{11}$$

$$\begin{aligned} p_{fluid} &= p_{ref} + dp_{sep} + \left\{g \cdot \rho_{fluid}\left(p_{ref}, t_{amb,pri}\right) \cdot H_3\right. \\ &\left. + g \cdot \rho_{fluid}\left(p_{ref}, t_{lid}\right) \cdot H_4 + g \cdot \rho_{fluid}\left(p_{ref}, t_{bath}\right) \cdot H_5\right\} \end{aligned} \tag{12}$$

$$\begin{aligned} dp_{sep} &= g \cdot \left\{\rho_{N_2}\left(p_{ref}, t_{amb,pri}\right) \cdot \left(h_3 - h\right) + 2 \cdot \rho_{Hg}\left(t_{amb,pri}\right) \cdot \left(h - h_0\right)\right. \\ &\left. + \rho_{fluid}\left(p_{ref}, t_{amb,pri}\right) \cdot \left(2 \cdot h_0 - h - h_2\right)\right\} \end{aligned} \tag{13}$$

4.1.4 Densitometer Performance

As part of an international intercomparison exercise carried out in 1999 [6], the TUV NEL Primary Standard Liquid Densitometer was used to measure the density of a sample of ultra-pure toluene. As discussed in Section 4.3, one of the fluids chosen as a transfer standard was toluene, allowing a comparison with the previous data. Figures 3 and 4 show examples of the stability of weighing the sinker at various conditions for the 1999 and 2007 measurements respectively.

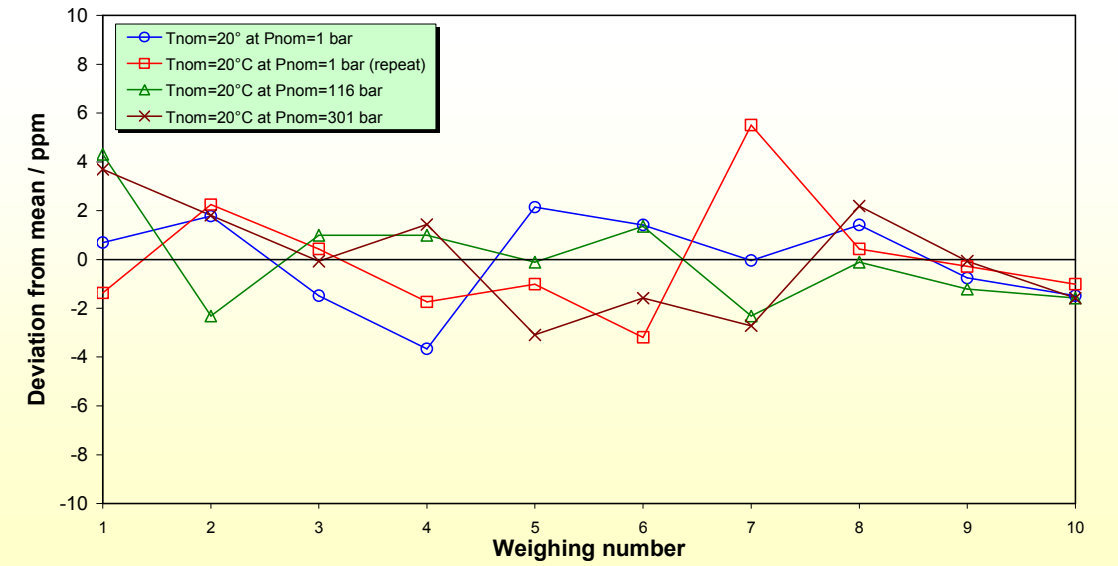

Figure 3 Example of weighing stability, toluene sample, 1999

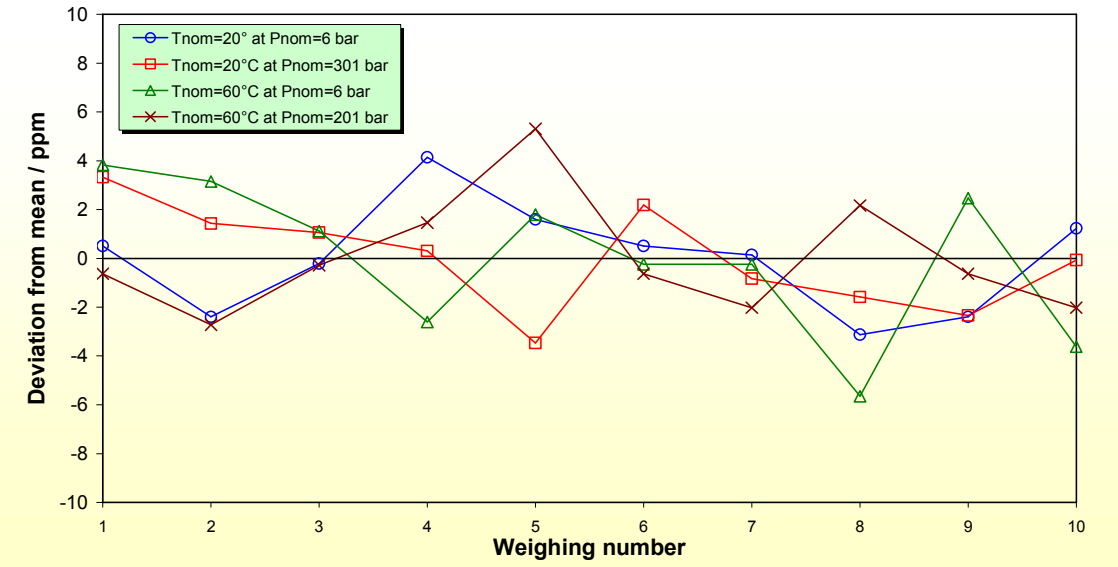

Figure 4 Example of weighing stability, toluene sample, 2007

These data confirm that the magnetic suspension coupling and weighing system is operating as expected and is capable of determining the weight of the sinker in the fluid to within a few parts per million.

The data from the measurements made in 1999 were fitted to an equation of the form

$$\rho_{t,p} = 1000 \sum_{i=1}^{13} a(i) \theta^{m(i)} \pi^{n(i)} \tag{14}$$

where θ is the reduced temperature, $\theta = t / 100$ for t in degrees Celsius on ITS90,

π is the reduced pressure, $\pi = p / 30$ for p in MPa,

a(i) are coefficients and

m(i) and *n(i)* are exponents.

Equation 14 represents the 1999 TUV NEL data set to within minimum and maximum deviations of –8 and +10 parts per million respectively. The total uncertainty in the measured values of density was assessed as 0.01 % at a 95 % confidence level, leading to the values calculated from equation 14 having an uncertainty not exceeding 0.012% across the temperature range from 0 to 80°C at pressures up to 30MPa.

Table 1 shows the data obtained for toluene from the current measurement programme up to 80°C and values at corresponding temperatures and pressures calculated from equation 14. Whilst the agreement between the two data sets is within their combined uncertainty, it is clear from Figure 5 that there is both an absolute difference and a temperature dependence to the difference. The origins of these effects are still being investigated.

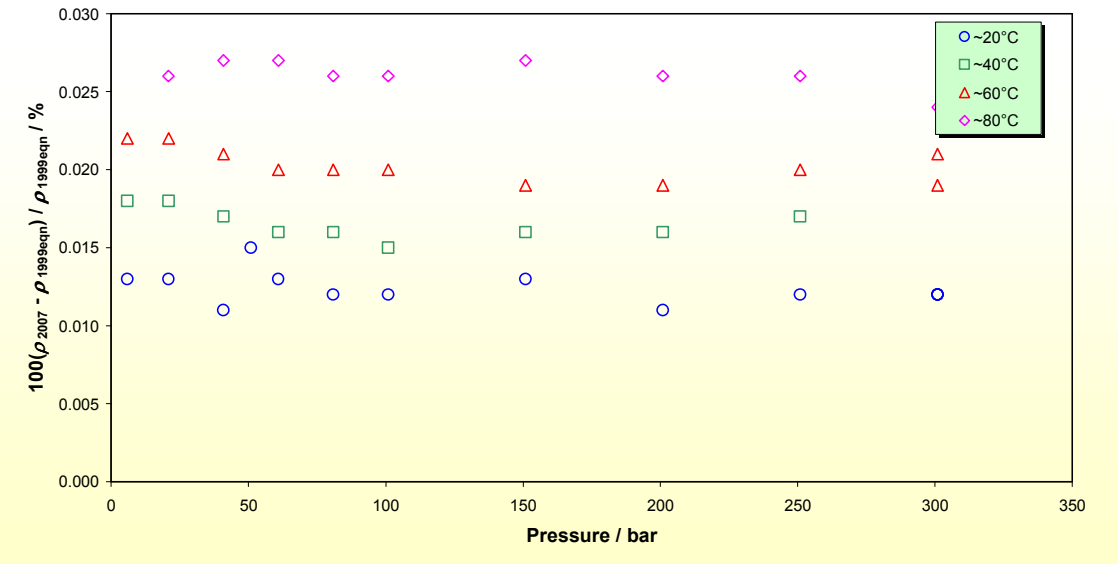

Figure 5 Comparison of 1999 and 2007 toluene density measurements

Table 1
Comparison of 1999 and 2007 toluene density measurements

t °C	p MPa	ρ_{2007} kgm^{-3}	ρ_{1999} kgm^{-3}	$100(\rho_{2007}-\rho_{1999})/\rho_{1999}$ %
19.993	0.5821	867.302	867.189	0.013
19.994	2.0821	868.438	868.327	0.013
29.991	5.0897	861.628	861.496	0.015
19.996	4.0815	869.920	869.820	0.011
19.992	6.0817	871.409	871.295	0.013
19.994	8.0823	872.844	872.741	0.012
19.991	10.0842	874.272	874.170	0.012
20.005	15.0859	877.744	877.629	0.013
19.993	20.0873	881.087	880.986	0.011
19.994	25.0892	884.328	884.221	0.012
19.994	30.0909	887.462	887.358	0.012
19.992	30.0930	887.469	887.361	0.012
19.992	30.0929	887.471	887.361	0.012
19.995	30.0926	887.469	887.358	0.012
39.990	0.5880	848.731	848.576	0.018
39.990	2.0884	850.016	849.864	0.018
39.990	4.0893	851.698	851.553	0.017
39.989	6.0880	853.351	853.210	0.016
39.990	8.0892	854.977	854.837	0.016
39.990	10.0895	856.566	856.433	0.015
39.990	15.0909	860.444	860.306	0.016
39.991	20.0919	864.156	864.019	0.016
39.990	25.0935	867.738	867.593	0.017
59.990	0.5889	829.858	829.676	0.022
59.990	2.0885	831.321	831.140	0.022
59.990	4.0889	833.232	833.055	0.021
59.990	6.0888	835.098	834.928	0.020
59.990	8.0889	836.927	836.763	0.020
59.990	10.0891	838.725	838.559	0.020
59.991	15.0898	843.060	842.895	0.019
59.988	20.0905	847.195	847.032	0.019
59.992	25.0916	851.150	850.984	0.020
59.991	30.0924	854.964	854.785	0.021
59.992	30.0927	854.949	854.785	0.019

Table 1 (continued)

t °C	p MPa	ρ_{2007} kgm^{-3}	ρ_{1999} kgm^{-3}	$100(\rho_{2007}-\rho_{1999})/\rho_{1999}$ %
79.994	2.0879	812.259	812.046	0.026
79.994	4.0875	814.439	814.222	0.027
79.993	6.0878	816.571	816.349	0.027
79.995	8.0877	818.633	818.422	0.026
79.991	10.0875	820.662	820.453	0.026
79.995	15.0878	825.542	825.322	0.027
79.997	20.0891	830.155	829.938	0.026
79.998	25.0892	834.544	834.326	0.026
79.996	30.0898	838.721	838.520	0.024

4.2 The TUV NEL Industrial Densitometer Calibration Facility

The TUV NEL Industrial Densitometer Calibration Facility consists of a thermostated enclosure capable of containing a densitometer, as shown in Figure 6. In conjunction with a pressurising system, this enables the temperature and pressure of the fluid in the densitometer to be set and maintained at any set-point across the range from 10 to 110°C at pressures between 0.1 and 20 MPa and the period output signal from the densitometer to be measured.

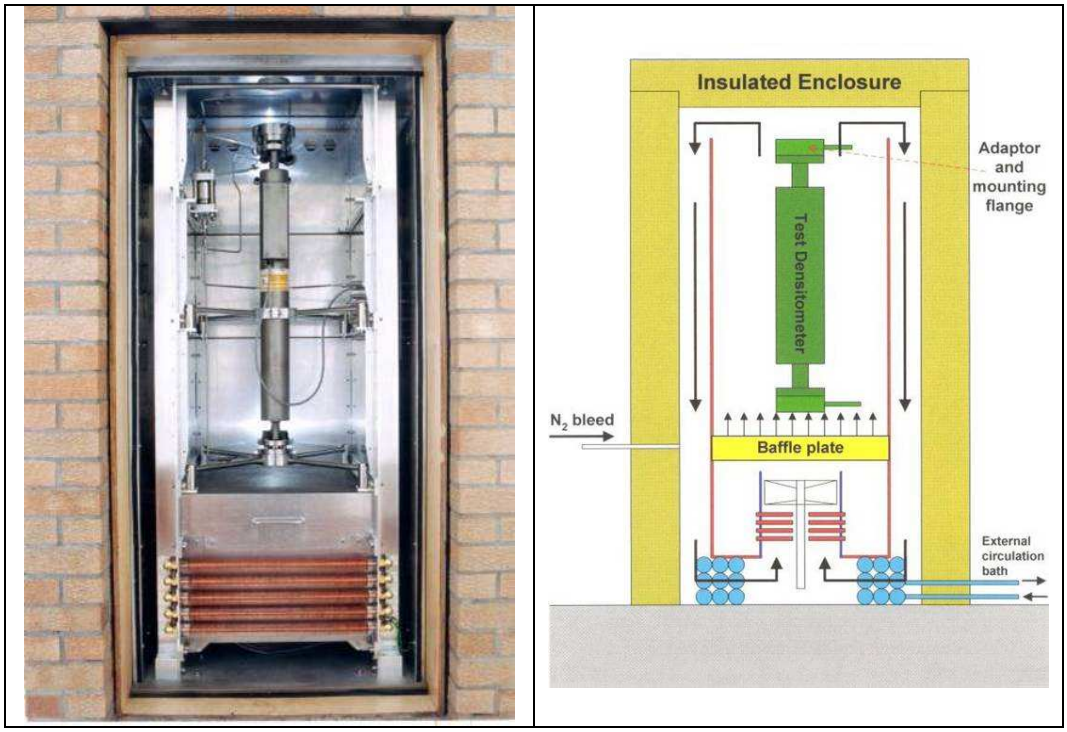

Figure 6 The TUV NEL Industrial Densitometer Calibration Facility

4.2.1 Temperature and Pressure Control

Temperature control is provided by an insulated enclosure plus heating and cooling circuits. A series of coils in the base of the enclosure are connected to an external circulation bath capable of maintaining the temperature of the coils between -80 and 20°C. This provides a constant background temperature against which the heating circuit operates. The control temperature of the enclosure is monitored by a 25 ohm standard platinum-resistance thermometer positioned close to the mid-point of the enclosure. The thermometer is monitored by a control computer similar to that used in the Primary Liquid Standard Densitometer and the power inputs to the heating/cooling circuits are adjusted using PID control software. The temperature of the densitometer under test is measured using two 25 ohm standard platinum-resistance thermometers attached to the body of the densitometer.

The temperature stability of the enclosure is within ±5 mK over its entire operating range and the absolute temperature can be set by the computer to within a few millikelvins of the desired conditions. The total uncertainty in the temperature of the working fluid in the densitometers is estimated to be 4 mK.

An external pressurising circuit generates and controls the pressure of the fluid in the densitometer under test. A computer-controlled pump supplies hydraulic fluid to a piston in cylinder interface to the test fluid. The feedback signal for the control system is provided by a Quartzdyne pressure transducer on the test fluid side of the piston in cylinder interface.

A gas-operated pressure balance of the highest metrology class, located in the Primary Standards Densitometer Laboratory, is used to provide reference gauge pressures accurate to within 5 parts in 10^5. Atmospheric pressure is measured by means of the calibrated digital barometer used for the Primary Liquid Standard Densitometer, providing values accurate to within 20 Pa.

The pressure of the test fluid in the densitometer under test is obtained with reference to the pressure of nitrogen in the gas-operated balance through a Yokogawa differential pressure transducer. The transducer was calibrated across a range of differential pressures from -5000 to 5000 Pa at static pressures from 2.5 to 15 MPa and a function derived to calculate differential pressure from the output voltage. The uncertainty in the measurement of differential pressure is within 50 Pa.

As shown in Figure 7 and equations 15 to 18, the absolute pressure of the test fluid in the densitometer is obtained from the atmospheric pressure, gas-operated pressure balance and Yokogawa differential pressure transducer, corrected for temperature effects and pressure heads in the connecting lines as necessary. The uncertainty in the calculated total pressure is assessed as $7\ 10^{-5}\ p \pm 100$ Pa.

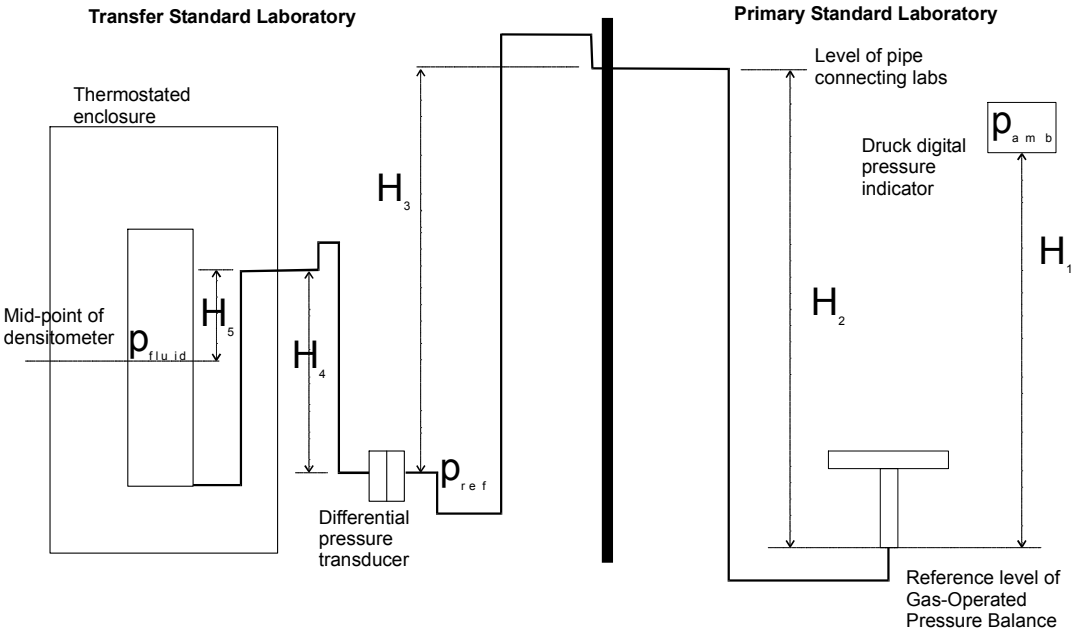

Figure 7 Schematic of pressure circuit for industrial densitometer calibration facility

$$\begin{aligned} p_{ref} &= \left\{p_{amb,pri} + g \cdot \rho_{air}\left(p_{amb,pri}, t_{amb,pri}\right) \cdot H_1\right\} \\ &+ \left\{p_{stand} + g \cdot \rho_{N_2}\left(p_{stand}, t_{amb,pri}\right) \cdot H_2\right\} \\ &+ \left\{g \cdot \rho_{N_2}\left(p_{stand}, t_{amb,sec}\right) \cdot H_3\right\} \end{aligned} \tag{15}$$

$$\begin{aligned} p_{fluid} &= p_{ref} + dp_{sep} + \left\{g \cdot \rho_{fluid}\left(p_{ref}, t_{amb,\sec}\right) \cdot H_4 \right. \\ &\left. + g \cdot \rho_{fluid}\left(p_{ref}, t_{dens}\right) \cdot H_5\right\} \end{aligned} \tag{16}$$

$$dp_{sep} = \left\{a_0 + a_1 \cdot v_{Yok}\right\} + \left\{b_1 \cdot p_{ref} + b_2 \cdot p_{ref}^2 + b_3 \cdot p_{ref}^3\right\} \tag{17}$$

4.2.2 Calibration Facility Performance

Once the system has stabilised at a set temperature and pressure, the temperature of the densitometer, the pressure of the fluid within the densitometer and the period output signal from the densitometer are measured. The time take to complete one measurement cycle is of the order of one minute. A minimum of two measurement cycles are made at each set point. Table 2 provides an indication of the stability and repeatability of the temperature and pressure control achieved at the densitometer within the thermostated enclosure. These results relate to a new densitometer (Solartron 7835) supplied by the manufacturer (Emerson Process Management) and filled with a sample of the same toluene used in the Primary Standard Liquid Densitometer.

Table 2
Temperature and pressure stability in Industrial Densitometer Calibration Facility

Date	$t_{den,NEL}$ °C	p_{fluid} bar	ρ_{nel} kgm^{-3}	τ_{den} µs	ρ_{den} kgm^{-3}
27/10/2006 15:20	19.792	41.028	869.79	1358.974	870.59
27/10/2006 16:18	19.793	41.026	869.79	1358.977	870.60
19/01/2007 15:00	19.778	40.978	869.76	1358.942	870.49
19/01/2007 15:06	19.778	40.978	869.76	1358.940	870.48
13/11/2006 14:44	59.480	81.053	836.87	1352.288	838.19
13/11/2006 14:50	59.484	81.053	836.87	1352.289	838.19
26/01/2007 11:55	59.492	81.053	836.86	1352.279	838.15
26/01/2007 12:04	59.490	81.052	836.86	1352.279	838.15

4.3 Transfer Standard Fluids

As noted previously, to be considered for use as true transfer standard fluids, fluids must either be single components or stable mixtures of known composition. Furthermore, for this application, they must also cover the range of other fluid properties that will influence the operation of an oscillatory densitometer across its full operational range. For an oscillatory device, the most important secondary property will be fluid viscosity. A survey was therefore undertaken of the project's industrial sponsors to determine the temperature, pressure, density and viscosity ranges over which their densitometers operate. The results are summarised in Table 3.

Table 3
Densitometer operating conditions

Parameter	Full range	Most common range
Temperature / °C	8 - 105	20 - 80
Pressure / MPa	0.5 - 14.0	0.5 - 5.0
Density / kgm^{-3}	530 - 1180	700 - 850
Viscosity / mPa s	0.3 - 40	2 - 8

Whilst it would be ideal to cover the full operational range, in practice it would be very difficult to find suitable fluids. By agreement with the project sponsors, it was therefore decided to concentrate on the most common range, allowing the use of four fluids, as shown in Figure 8. In addition to providing coverage of the key parameters, the fluids must be readily available in sufficiently high purity at reasonable cost. Iso-octane (2,2,4-trimethylpentane), toluene, and di-(2-ethylhexyl) sebacate meet these criteria, covering the low density / low viscosity, high density / low viscosity and high density / high viscosity conditions respectively. However, to a first approximation, fluid density and viscosity are correlated, making it difficult to find a low density / high viscosity

fluid. Although 9-n-octylheptadecane would cover a significant part of the range (particularly at elevated temperatures), it is not readily available in sufficient purity at reasonable cost and so an alternative fluid is being sought.

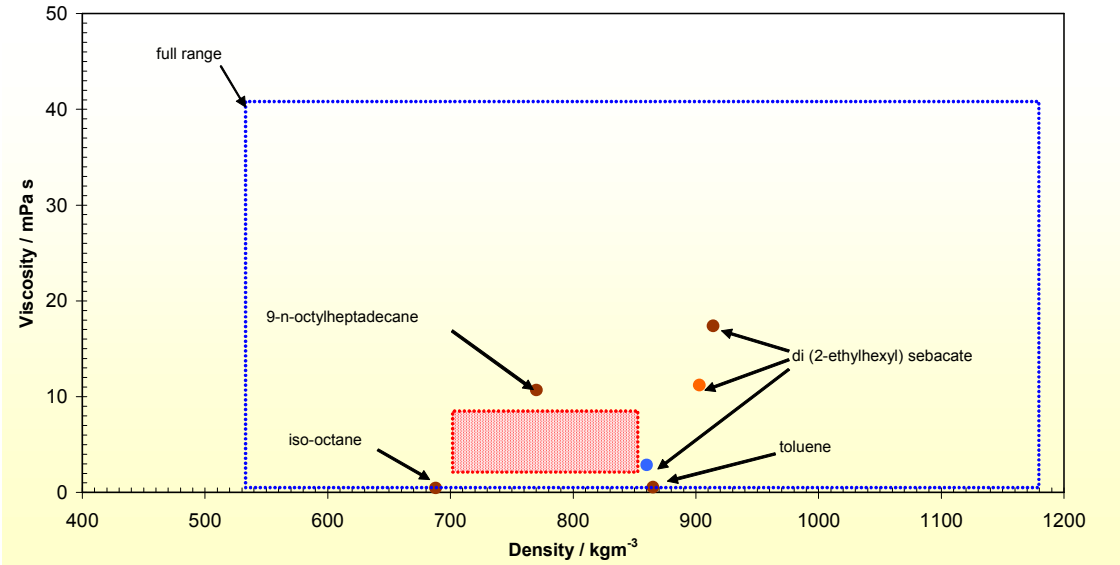

Figure 8 Transfer standard fluids

5 RESULTS

Measurements on the first transfer standard fluid, toluene, have been completed in the Primary Standard Liquid Densitometer and the results are summarised in Table 1. The fluid sample measured, CHROMASOLV® Plus, for HPLC, was obtained from Sigma-Aldrich and used as received. The stated minimum purity of the sample (by gas liquid chromatography) was 99.90%, with a maximum water content of 0.02% (by titration). The measurements cover the temperature range from 20 to 100°C at pressures from 0.1 to 30 MPa.

Measurements with the three transfer standard fluids already identified have been completed with the Emerson Process Management-supplied Solartron 7835 densitometer in the Industrial Densitometer Calibration Facility across the temperature range from 20 to 100°C at pressures from 0.1 to 100 MPa. In addition to toluene, the other two fluids were Sigma-Aldrich anhydrous 2,2,4-trimethylpentane (stated minimum purity 99.75% by gas liquid chromatography, maximum water content 0.003% by titration) and Sigma-Aldrich Fluka Bis(2-ethylhexyl) sebacate (stated minimum purity 97.0% by gas liquid chromatography).

6 DISCUSSION

The initial results obtained for the density of a sample of toluene measured in the Primary Standard Liquid Densitometer agree within the combined uncertainty with data obtained previously for a sample of toluene of similar purity.

The measurement principle used in the Primary Standard Liquid Densitometer, Archimedes' Principle, is as close to a primary method as can be obtained for density, a derived unit. All the measurements required to determine the density are fully traceable to primary standard measurements and the quoted uncertainty of 0.015% is derived from the component uncertainties in each of those measurements, thus providing traceability to National Standards.

As noted in Section 4.1.4, Whilst the agreement between the two data sets is within their combined uncertainty, it is clear from Figure 5 that there is both an absolute difference and a temperature dependence to the difference. The origins of these effects are still being investigated.

Initial results for the Emerson Process Management-supplied Solartron 7835 densitometer in the Industrial Densitometer Calibration Facility appeared to show systematic deviations between the values calculated from the measured period outputs and values calculated at corresponding conditions for the transfer standard fluids.

The coefficients used for the densitometer (the K_a to K_f in equations 5 and 6) were those originally supplied by the manufacturer. In work undertaken by them on pressure effects, entirely independently of but in parallel with this project, they have now issued a revised calculation procedure and new pressure coefficients. Whilst this brings the results from the industrial densitometer in to line with the values calculated for toluene, no further conclusions can be drawn until the measurement programme is complete for all the transfer standard fluids.

ACKNOWLEDGEMENTS

Modifications to the TUV NEL facilities were carried out as part of the 2002-2005 Flow Programme. The support of BERR and DIUS (formerly the UK Department of Trade and Industry) is acknowledged. The financial and technical support of the JIP members (BG Group, BP, Chevron Texaco, CNR International, Conoco Phillips, Emerson Process Management, Exxon Mobil, Hess UK Ltd, Maersk Oil, Marathon Oil UK Ltd, Nexen Petroleum UK Ltd, Paladin Resources, Shell Exploration and Production, Talisman Energy UK Ltd and Total E&P UK) is also acknowledged.

7 REFERENCES

[1] Glen, N. F. Viscosity coefficient measurement at elevated pressure. PhD Thesis. University of Glasgow, Glasgow, 1985.

[2] Griffin, D. Solartron Mobrey Densitometer Calibration Issue. DTI Energy Group, Licensing and Consents Unit, Aberdeen, 2004.

[3] Retsina, T. Design of a vibrating rod densitometer for liquids at high pressure. PhD Thesis, Imperial College, London, 1987.

[4] Padrel de Oliveira, C. M. B. Viscosity of liquid hydrocarbons at high pressure. PhD Thesis, Imperial College, London, 1991.

[5] Watson, J. T. R., Ferguson, D. and Ryan, G. National standard facilities for the density of liquids and gases at elevated pressures. Paper presented at the Density Seminar held in the James Watt Conference Centre, NEL, on 24 October, 1994, in conjunction with the North Sea Flow Measurement Workshop, 1994.

[6] Watson, J.T.R. Intercomparison of density facilities. Flow Centre Report No 057/2000 produced for the NMSPU; National Engineering Laboratory, East Kilbride, Glasgow, March 2000.

North Sea Flow Measurement Workshop

16-19 October 2007

Tomography powered multiphase and wetgas meter providing measurements used for fiscal metering

By

Arnstein Wee[1], Hans Berentsen [2], Vidar Rune Midttveit [2],
Håkon Moestue[3] and Hans Olav Hide[1]

INTRODUCTION

Multiphase meters were initially developed by several companies during the 1990's and operating companies have gained about 10 – 15 years of operational experience by using them. The meters are offering significant benefits in several applications such as

- Allocation Metering
- Well Testing and Reservoir Management
- E-field implementation
- Field developments without new platforms

While the benefits are great and the potential savings are large, the concept of multiphase metering has not yet emerged to the extent one should expect. This is mainly caused by the fact that multiphase measurements are complex, and far more difficult than what was earlier believed. An appreciable number of the meters deployed may not have performed to user expectations to measurement accuracy and - perhaps more important - reproducibility and operational stability. Also, some meters have not been able to perform satisfactory when the operational conditions have changed from initial/design conditions.

This paper presents the basis for the development of the MPM HighPerformance Flowmeter, and describes the steps taken to arrive at an instrument that's capable of providing measurements to be used for fiscal metering, for both multiphase and wetgas conditions.

[1] Multi Phase Meters AS
[2] StatoilHydro ASA
[3] Hydro (until 1.10.2007)

ACKNOWLEDGEMENT

The development of the High Performance Flowmeter by MPM has been supported technically and financially by the six oil companies; ENI, ConocoPhillips, Hydro, Shell, Statoil, and Total.

Their involvement in the project as technical advisors and though active participation in the Steering Committee has been of great value, and enabled the development and qualification projects be completed over a relatively short time period.

CHALLENGING APPLICATIONS

Understanding, describing and modeling the local conditions inside a pipe, where unknown constituents of water, oil and gas are flowing at unknown velocities, is very challenging. Measuring the flow rates of the three constituents at an acceptable uncertainty is may be even more difficult.

Measuring the multiphase flow rates is very important of several reasons.

- Firstly, the amounts of hydrocarbon must be measured precisely to allocate the production (and revenue) to the different partners.
- Secondly, the measurements are important to be able to monitor and thereby maximize production from the well and the reservoir, to enhance the recovery and increasing the revenue.
- Thirdly, it will help avoiding operational problems. To give an example; for several fields measuring the water fraction to mitigate hydrate formation is of importance, as is the possibility to detect formation water break-through in particular wells. and
- Finally it is used to minimize environmental issues by contributing to reducing and optimizing the use of chemicals and inhibitors.

The operating conditions and challenges for wetgas and multiphase metering are quite different, which has led to the development and manufacture of different meters by some vendors. For this reason, the operators have had to select in advance of production start-up, which type of meter to install. In many cases, this might pose a large problem; the production of a particular well is often not well-known in advance of start-up, and the behavior of a well may very well change over its lifetime. In such case, the performance of the installed meter might be very poor, and the Operator might be required to replace the multiphase meter with a wetgas one.

A typical oil well may start producing without any water coming with the oil. As the well matures, water normally starts breaking through, and the Water Liquid Range (WLR) may increase to as high as 90-95% before the well is shut in. At the same time, the GVF might increase, both as a result of the pressure in the well being decreased, but also as a

result of gas lift or other related techniques. From being initially in the range of 50 to 60%, the GVF may increase to 90 to 95 % and even above. Figure 1 shows typical well development patterns, where the developments in GVF and WLR are illustrated. Similar examples may be found in the presentation by Lex Scheers /ref 1/.

The particular case where the gas fraction of a multiphase flow is in the high 90 percent level (typically 96 to 99+ % of gas) is denoted WetGas. Measuring the tiny amounts of liquid flowing with the gas, at a satisfactory accuracy is extremely challenging. Even more difficult is it to correctly being able to split the tiny amount of liquid into water and hydrocarbons. On top of this, operators would like to know what is the salinity of the produced water.

In Figure 2 is sketched out the perceived measurement uncertainty for existing multiphase meters. The x-axis represents the GVF, while the Y-axis describes the measurement uncertainty of the hydrocarbons. As is seen, the uncertainty is in line with that obtained with a test separator for GVF's below 50 %. For higher GVF's, the uncertainty increases to unacceptable levels. The figure is of course illustrative only, but the main message is very clear.

The need for high performance meters has been expressed by the oil companies since quite many years back. One example was the paper by Andy Jamieson at the NSFMW in 1999 /ref2/. Statoil has voiced similar needs, for instance in a paper by Eirk Aabro /ref3/.

The above reasons and several years operational experiences with the existing products have made the major oil companies support the development of new concepts and methodologies.

CLOSING THE GAPS

MPM started more than four years ago addressing these challenges, and decided after careful considerations to do an attempt to closing the above mentioned gaps, and to provide a new type of instrument.

Being a very challenging task, MPM sought support for its work from the oil industry. MPM considered it extremely important to aligning the project goals and results with the needs of the industry, and established a Joint Industry Project (JIP), with a Steering Committee comprising some of the most experienced and skilled measurement people from the oil companies.

MPM further decided to build a very advanced flow laboratory, which today comprises five different flow loops. These are tailored to different tasks, and offer a unique set of tools for performing the enormous amount of tests that have been done. The test facilities also function as a training centre.

An international co-operation model was established, with participants from many different universities, laboratories, specialist companies and suppliers.

The JIP partners helped defining the overall goals of the MPM High Performance Flowmeter, as follows:

1. High operational stability
2. Unique sensitivity and reproducibility
3. Improved measurement uncertainty
4. Easy field configuration and operation

To achieve the above, MPM realized that a completely new technology basis was required. In addition, all aspects needed to be addressed with special focus on the following issues:

- The measurement errors due to the presence of annular gas concentration, as is in vertical flow, had to be eliminated. An example of this effect is shown in Figure 5. Whereas the actual GVF is 36%, the gamma meter will measure 55%, since the result is based on the shaded area only (i.e. the beam of the gamma meter) and not the full pipe area. MPM decided that rather than trying to mixing the flow, the MPM meter should be made capable of providing the right result, independent of the flow regime and the presence of annular gas concentrations.
- Extremely fast measurements must be obtained to correctly capture rapid fluctuations in the flow (slugs, etc). In multiphase flow conditions, a multiphase meter's sampling frequency must be several Hz., to enable it to track the naturally found and fast changing flowing conditions.
- Very accurate watercut measurements must be made at high watercuts and at high GVF's (as liquid fraction becomes smaller) to measure flow rates of oil more precisely.
- One single meter should be capable of covering both multiphase and wetgas applications, since replacing meters in an operating asset is very costly and implies operational risks. This is particularly important for subsea meters.
- The conductivity of the produced water should be measured, rather than be required as a user input. An error in water conductivity may imply large measurement errors, and how would the operator know the water conductivity for wells that are commingled? Again, this is particularly important for subsea meters.

MPM HIGHPERFORMANCE FLOWMETER

The High Performance Meter from MPM represents an important technological step in multiphase metering and instrumentation. It will facilitate the in-line allocation metering of produced hydrocarbons and allow for low-cost offshore tie-backs and subsea metering.

The Meter is built with all parts in one unit with minimum need for final assembly on site. The electronics are designed and built to survive in severe and violent conditions and the transmitters are fixed to the sensor body. The MPM Meter is shown in Figure 3.

The MPM meter is using tomography and the patented 3D Broadband™ method (5 patents) in combination with a Venturi and other sensors to obtain unparalleled performance in multiphase and wetgas flowing regimes. With its dual mode functionality and capability to measure water salinity, the MPM Meter bridges existing measurement gaps in conventional multiphase and wetgas meters. The main physical components of the MPM Meter are shown in Figure 4. The special features of the Meter are, however, software based.

The Meter performs measurements over the full Gas Volume Fraction (GVF) range, and covers watercuts from 0 to 100%. One of the Meters really unique properties is the ability to measure the watercut equally well at high watercuts (water continuous flow) and lower watercuts (oil continuous). As a consequence, the MPM Meter performs reliable oil flow rate measurements even at high watercuts and high GVFs. This has until now been the perceived a weakness by the users of all of the multiphase meters on the market.

MPM has recently finalized the development and qualification program for the subsea version of the MPM Meter. In a special made test rig, the subsea meter was tested at operating pressures of up to 1000 bars while, at the same time, the temperatures varied from from -50 to + 250 °C. The Subsea meter can be delivered for use in water depths of 3500 meters maximum.

MPM METER MEASUREMENT PRINCIPLES

Multi sensor system

The MPM Meter encompasses several sensors for different measurements, which are combined in a multi-modal tomographic measurement system.

The flow first passes through a Venturi, which is used to measure the total mass flow rate. MPM has developed special Venturi models in close co-operation and on license from its partners. The Venturi is also used to create radial symmetrical flow conditions in the 3D Broadband™ section downstream the Venturi.

The MPM Meter utilizes a special gamma densitometer solution, as well as temperature and pressure transmitters.

3D Broadband™

The 3D Broadband™ technology is used to establish a three dimensional picture of what's flowing inside the pipe. The basis for the technology is often referred to as 'process tomography' which has many parallels to tomographs used in medical applications.

In the oilfield, the challenges are however different than in a hospital. Firstly, the meter is measuring fluids and gases under high temperature and pressure. Secondly, the multiphase mixture can be mowing at velocities of more than 30 meters per second inside of the pipe, and the amounts of gas, water and oil are normally unstable and changes all the time.

The 3D Broadband™ system is a high-speed radio- frequency (RF) based technique for measuring the watercut, the composition and the liquid/gas distribution within the pipe cross section. By combining this information with the measurements from the Venturi, accurate flow rates of oil, water and gas can be calculated.

The MPM Meter is extremely fast. Averaging of measured raw data is very limited, to avid errors due to non-linearities in the flow. The result is measurements at an unparalleled performance in multiphase and wetgas flowing regimes. With its dual mode functionality, which means that both multiphase and wetgas applications are addressed with the same hardware, and its capability to measure water salinity, the MPM Meter bridges existing measurement gaps in conventional multiphase and wetgas meters.

Capturing rapid fluctuations in the flow rate

The MPM Meter performs RF measurements in many different planes. At each plane, measurements are done at many frequencies over a broad frequency range, and combined with gamma ray absorption measurements. Each measurement frequency in each direction forms a unique and independent equation resulting in many thousand equations per second for accurate determination of the multiphase cross sectional composition and distribution. The principle is illustrated in Figure 6.

Flow changes in the longitudinal axis are captured precisely by doing many measurements every second, which also enables flow characteristics like slug intervals & lengths to be monitored, as illustrated in Figure 7.

Dual Mode Operation

The MPM Meter is designed to perform accurate flow rate measurements on all types of wells, throughout their entire life. The MPM Meter can address both multiphase– and wetgas applications; at oil-, gas- and water continuous flow regimes.

In the multiphase composition chart in Figure 1 are displayed some typical well trajectories, (A, B and C) which indicate the need to have a meter that can handle both wetgas- and multiphase flow.

In Wetgas mode the MPM Meter's sensitivity is used to obtain extremely accurate water fraction measurements. In MultiPhase Mode, the Meter performs high speed measurements to detect and compensate for variations and changes in the flow regime.

Oil & water continuous flow

The MPM Meter is able to perform accurate measurements of the WLR (watercut) with both oil and water continuous liquid emulsions.

In Figure 8 are presented results from a large number of two-phase (oil, water) tests, covering water salinities from 0 to 20%, which were performed to verify the performance of the watercut measurement. The WLR was varied over the full range from 0 to 100%.

For WLR's in the range 30-55% the emulsion is either oil or water continuous depending on the flow conditions. As seen from the graph, the measurement performance has been demonstrated to be equally good in both oil- and water continuous flow conditions, and even in the transition region between oil and water continuous liquid emulsion.

RESULTS FROM QUALIFICATION TESTING

The MPM Meter has gone through a comprehensive qualification process, after several years of intensive development work.

The MPM Meter used in the qualification testing was a 3" device built to requirements and specifications for Gullfaks A (GFA). The Meter was delivered from MPM after completing the Factory Acceptance Test (FAT).

The first external test was performed at K-lab /Kårstø during fall of 2006, where the Meter was exposed to high pressure conditions. During tests at K-lab, a large series of tests points were completed, covering both wetgas and multiphase conditions.

Subsequently the meter was shipped directly to GFA for testing and permanent installation. The testing covered a variety of wells and flowing conditions, in series with a reliable test separator. In Figure 9 is shown the different phases of the qualification process.

The different sites provided a large variety of test conditions, both in terms of fluids used, pressures and temperatures, and other aspects. As seen in Figure 10, a large part of the tests were conducted for conditions normally considered very difficult, with high GVF's and high WLR's.

All tests were performed and supervised by Statoil on the behalf of the six JIP companies. It is especially pointed out that no modification was done to the MPM meter during the whole qualification program.

Field configuration

The field configuration performed at K-lab and Gullfaks A followed the standard procedure, consisting of

- A single point calibration in air at commissioning (Nov 06)
- Water Density and Water Conductivity measured online by MPM Meter
- Oil and Gas Density calculated by online PVT package in FMC flow computer
  - Two different well composition used for all wells
    - One composition for high GOR wells
    - One composition for low GOR wells

The MPM Meter's sensitivity to the configuration parameters (oil and gas density) is exemplified in Figure 11, based on results in the MPM Flow Laboratory.

Operational Stability

During testing and use in the field the MPM Meter has demonstrated high operational stability, with no hardware or software problems on the Meter side.

The in-built self diagnostics functionality provides a means for the user to verify the performance, and to validate the field configuration data.

Accuracy – Reference system

The reference systems used during the testing of the MPM Meter are believed to be of a high standard.

At K-Lab, the reference system is of a very high and proven standard. Stabilisation time was what had to be considered with care, especially for those tests involving very small increments of a small fraction. The time to achieve stable flow conditions at the point where the MPM meter was located (15 m downstream of the mixing point), had to be managed and monitored.

At GFA, the reference system is good, in particular following a few upgrades which had to be implemented for the second round of testing (from December 06 to Jan 07).

In Figure 12 is shown the data flow at Gullfaks A, between the MPM Meter and the Platforms Flow Computer.

Sensitivity

The MPM meter is extremely sensitive to small changes in the composition. At K-Lab, a special test set-.up was configured, with highly reliable reference instrumentation, to verify this feature.

During the tests, gas was flowing at a constant rate of 300 m3/h, while tiny amounts of water only was injected just upstream the MPM Meter in three steps. The amounts of water, and the corresponding fraction of total flow is as follows:

	M3/h	water fraction
Step 1	0,008	0,0026 %
Step 2	0,043	0,0143 %
Step 3	0,086	0,0287 %

The results are presented in Figure 13. As is seen from the graph, the MPM Meter proved capable of detecting a change in water fraction of less than 0.0025% water.

Measurement uncertainty

The measurement uncertainty of the MPM Meter was within the specifications for all the different test campaigns.

In the following are presented examples and a summary of the results obtained. Reference is made to Figure 10, and it should be noted that tests cover a wide variety of operating conditions. Most of the tests points are made at flowing conditions that normally are perceived very challenging. In particular, they cover GVF from 0 % to 99,9%, and WLR's from 0 to 95 %. Most of the wells at GFA have WLR's above 50%.

In Figure 14 are shown comparisons of flow rates of oil, water and gas, for the MPM Meter versus the reference system, for tests simulating GFA wells, performed in the MPM Flow Laboratory.

Figure 15 presents a screen-print of a tests at K-lab, for GVF of 99,7 % and a WLR of 30%. While the gas rate was around 300 m3/h, the oil rate was 0,6 m3/h and the water rate was less than 0,3 m3/h. As is seen in the Figure, there are only very small differences between the reference and the MPM Meter measurements.

The same good match between the meter and the reference is seen in Figure 16. In this chart, the GVF is 98 %, and the WLR is around 5%.

Quite different flow conditions were experienced at K-Lab when the GVF was reduced to 93 %. As is seen in Figure 17, there was quite a lot of rapid slugging at the point where the Meter was installed. This was as expected, since the Meter was installed 15 meters downstream of the mixing point. While the Meter was installed in a vertical position, the

piping leading up to its location consisted of a horizontal 8" pipe. The measured values were, however, very much in line with those of the reference system.

In Figure 18 are shown comparisons of flow rates of oil and gas, for the MPM Meter versus the reference system for all test points. As is seen, the delta in oil rate was within 4 to 10 % for the full range of GVF's and WLR's. For gas rates, the corresponding delta was within 3 to 5 % when the pressure was above 10 bars.

In Figure 19 are shown similar deltas, but in this case on an accumulated basis. This is representative for the Meter performance, if used to measure the accumulated production from a series of wells. An example could be when commingling and tying back several subsea wells to a host platform. As is seen from the Figure, the deltas between the MPM Meter and the reference measurements are in less than 1,5 % for all the three sites, for flow rates of both oil and gas.

Repeatability

The repeatability of the MPM Meter has proved to be beyond the level which is quantifiable with the available reference instrumentation in a field location. It was concluded that for oil and gas rates, the reproducibility was within tenths of a percent.

In Figure 20 is shown an example of the Meter's stability and repeatability. It shows the measured WLR (increasing from 73 to 74 %) for a given well at GFA for a number of tests covering a time period of two months, both for the MPM Metter and the reference.

In Figure 21 is shown the liquid flow rate for the same well and the same test periods. The drop in flow rate, for the two December points, was at first not easy to understand, since no change was made to the test set-up. As is seen in Figure 13, nor was any change observed for the WLR. After carefully analyzing the logs of the reference system and the Meter, it was found that the change was caused by a leaking valve located between the test and the production manifolds. What had happened was that the pressure setting of the production header was lowered by 2,5 bars, while the test manifold pressure was kept constant. Consequently, a portion of the liquids went over to the production header. After fixing the valve, results for the Meter and the reference were back to normal.

Water Salinity Measurement

The MPM Meter is capable of measuring the conductivity of the produced water at actual conditions. The measured conductivity is converted to conductivity at 25 °C and used to calculate the measured water salinity and water density. During the conversion, it is assumed that the salt is constituted of NaCl, or as specified by the user.

The salinity measurement can be implemented as an automatic function, and no field configuration at all is required.

The graph in Figure 22 is prepared based on the results of the qualification testing at K-lab and GFA. It shows the measured water conductivity by the MPM Meter compared to the water conductivity of the reference water sample.

As is seen in the graph, all the conductivity measurements are within the target band of ± 2 mS/cm.The reproducibility of the water conductivity measurement was demonstrated to be within ± 0.5 mS/cm for all the wells in the reproducibility tests at GFA and within ± 0.25 mS/cm for 60% of the tests.

SUMMARY AND CONCLUSIONS

The MPM High Performance Flow Meter has been developed and thoroughly tested and qualified in a JIP with six oil companies.

The qualification testing has demonstrated the four overall goals of the JIP Project to be achieved; it is an instrument with high operational stability; with high sensitivity; which is very accurate; and which is easy to configure and to use.

The overall conclusions drawn by the Field Operator (Statoil) are:

- The MPM Meter's performance is such that it is capable to replace the existing test separator, and for some wells, the MPM Meter provided more reliable measurements than the existing test separator.
- The MPM Meter can be used to increase the production capacity of the Gullfaks A platform (significant NPV increase).
- Testing of wells at Gullfaks A can be done in 0.5 hour compared to typical 4 hours with the existing test separator.

During the qualification testing, installation and commissioning was done in a few hours. The Meter was started-up and the signal interface came quickly in place. The MPM meter has demonstrated superb operational stability, with 100 % uptime since commissioning. The Meter performance has been verified to be within specifications, and the repeatability of the MPM Meter was demonstrated to be extremely good, by testing the same wells at several times. The field testing concluded that the self calibration modus is imperative at high WLR's and changing water properties.

A very important conclusion was that the meter proved flexible to operate at different operating conditions, and it was demonstrated that the Meter can go directly from the MPM lab to the field whilst maintaining its specified performance.

Figure 23 summarizes the performance of the MPM Meter relating to measurement uncertainty, compared to conventional products with respect to measurement uncertainty and operating range. It can be concluded that the MPM Meter represents a leap-change

in multiphase and wetgas metering. Providing high accuracy over a large operating range, it enables in-line allocation metering of produced hydrocarbons at a standard acceptable for fiscal allocation metering.

The qualification of the subsea version of the MPM Meter is recently completed. This will be covered in a later presentation

REFERENCES

/1/ *Challenges at High Accuracy MultiPhase and WetGas Measurements*, by Lex Scheers and Arnstein Wee, MMR Galveston US, 27 April 07

/2/ *High performance multiphase metering - a personal perspective,* Mr A.W. Jamieson, Shell U.K. Exploration and Production, Norflow seminar, 9th June 1999

/3/ *Status på våtgass/flerfasemålere i drift*, by Eirik Aabro, Temadag NFOGM, 23 mars 2006.

Figure 1: Typical oil well trajectory in 3-phase Flow Chart

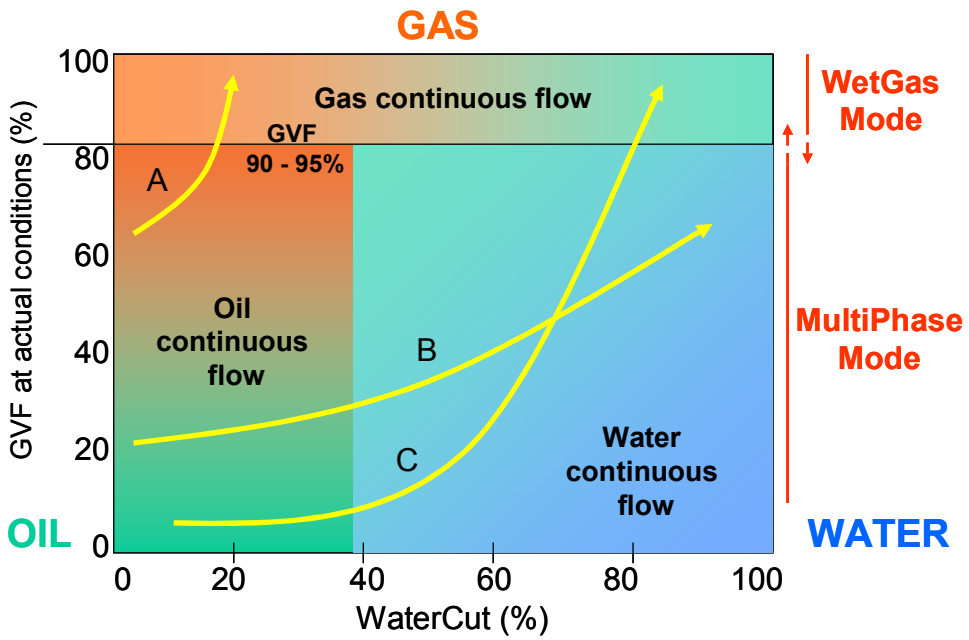

Figure 2: Perceived measurement uncertainty – conventional meters

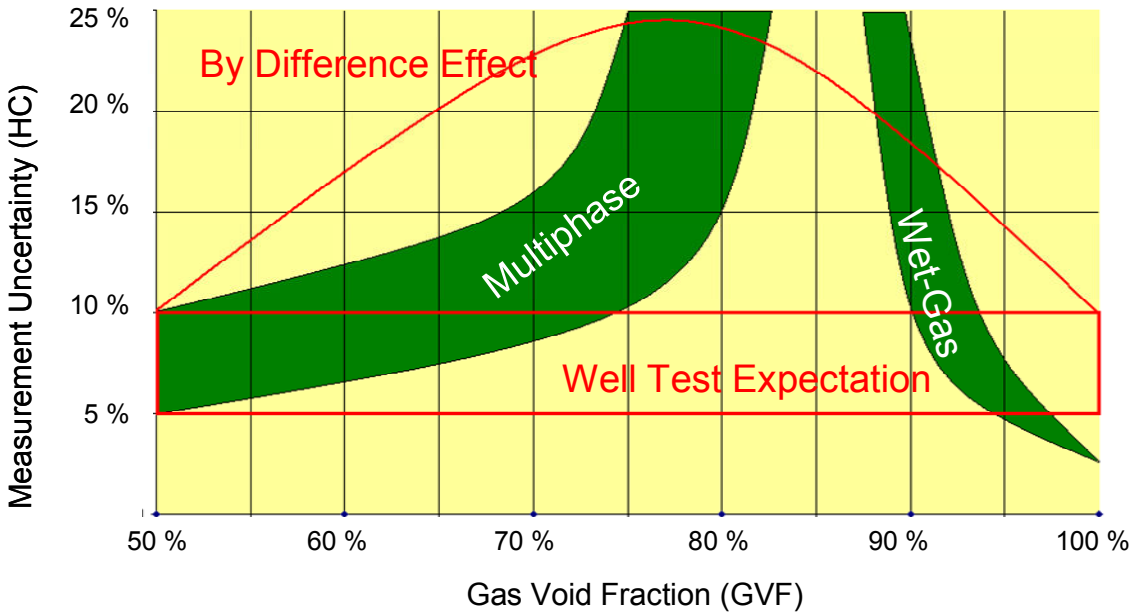

Figure 3: MPM HighPerformance Flowmeeter

Figure 4: MPM Meter – Main components

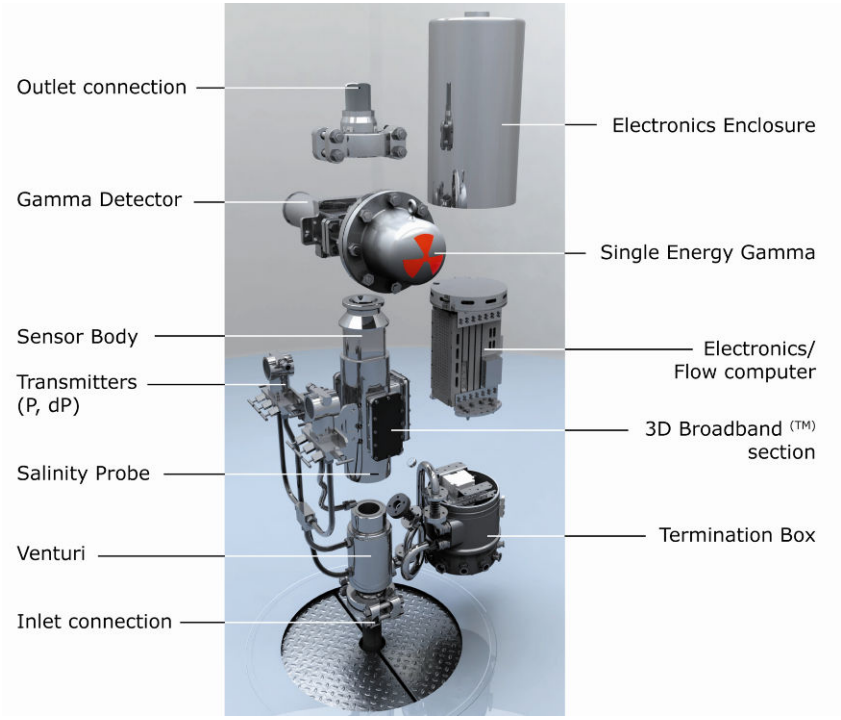

Figure 5: Effects of annual gas concentration

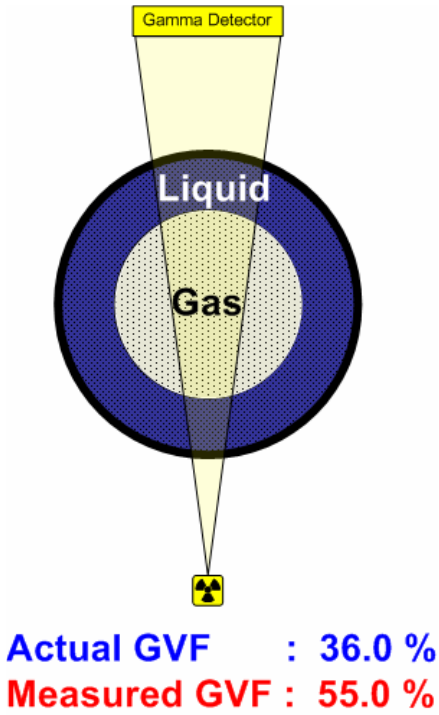

Figure 6: Establishing a 3D picture of the cross section

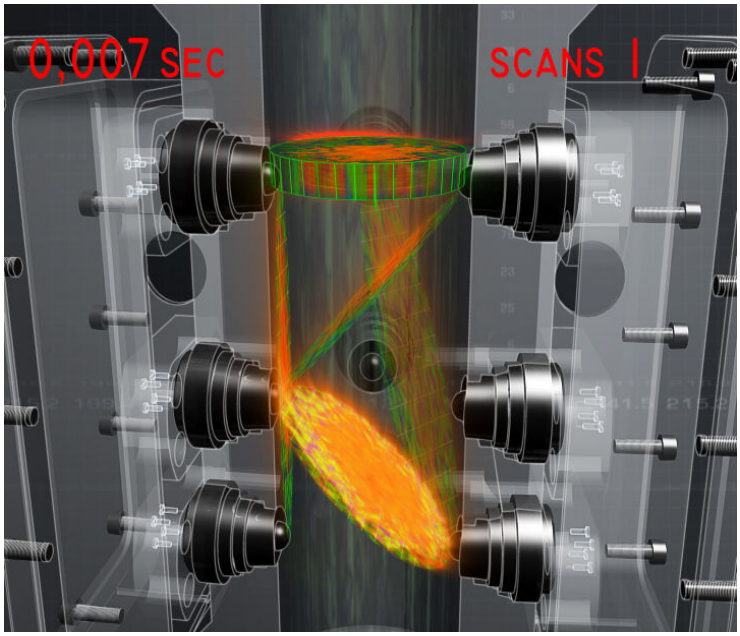

Figure 7: Capturing longitudinal flow variations

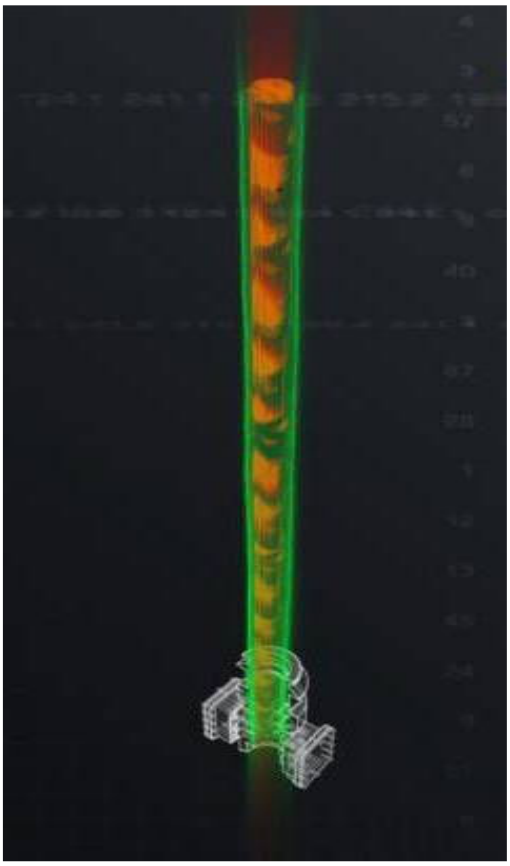

Figure 8: Results from test of WLR accuracy

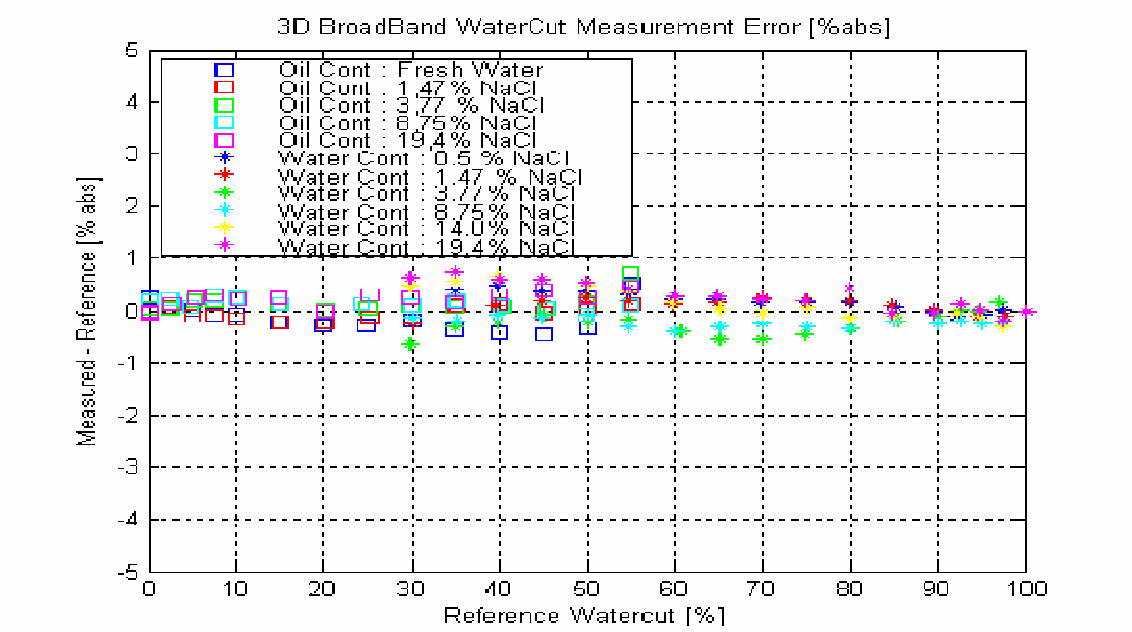

Figure 9: Qualification Test Program

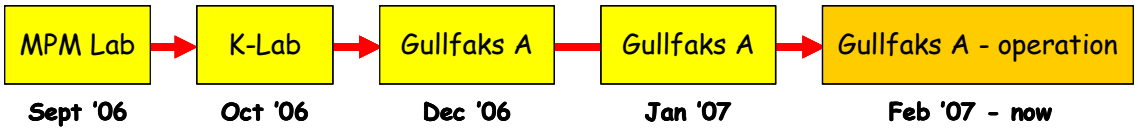

- All tests performed using the same unit
  - 3" MPM Meter
  - Made as per Gullfaks Specifications
- Field test program conducted by Statoil

Figure 10: Overview of qualification test conditions

	MPM Flow Lab FAT Sept '06	K-Lab Test Oct '06	Gullfaks A Dec '06	Gullfaks A Jan '07	Gullfaks A March '07
GVF	0 - 99,9 %	25 - 99,9 %	40 - 96 %	20 - 95 %	10 - 85 %
WLR	0 - 95 %	0 - 70 %	2 - 78 %	2 - 85 %	25 - 93 %
Pressure	< 10 bar	120 bar	60 bar	60 bar	60 bar
Oil	Exxol D 140 830 kg/m3	Condensate 620 kg/m3	Crude 780 - 840 kg/m3	Crude 780 - 840 kg/m3	Crude 780 - 840 kg/m3

Note: Reference system improvements at GFA from Dec '06 to Jan '07
Meter taken into permanent use in Feb '07 – for well testing

Figure 11: Sensitivity to changes in configuration data

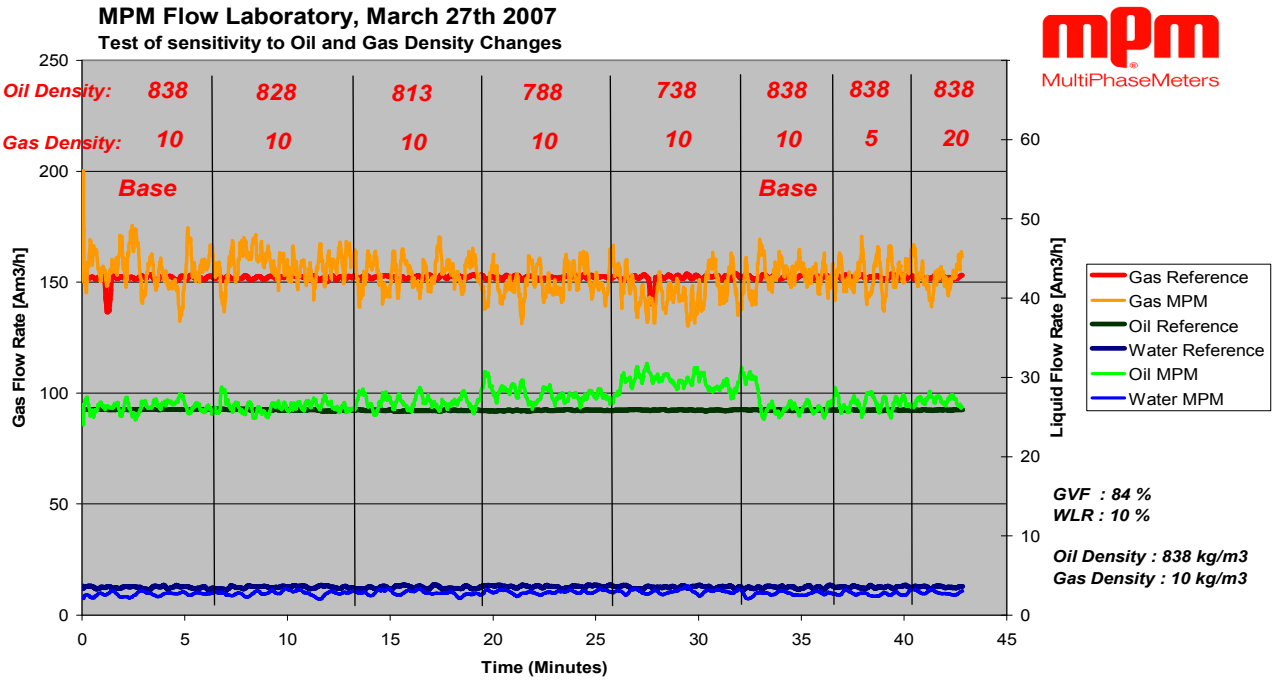

Figure 12: MPM Meter installation at Gullfaks A

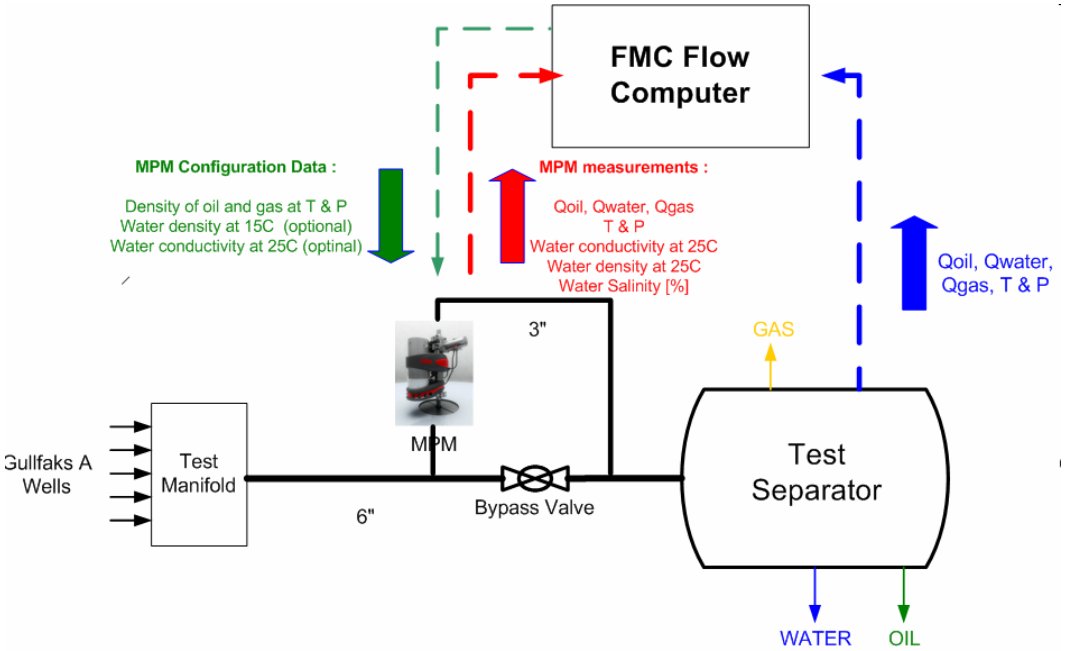

Figure 13: Sensitivity to injection of tiny water amounts in wetgas flow

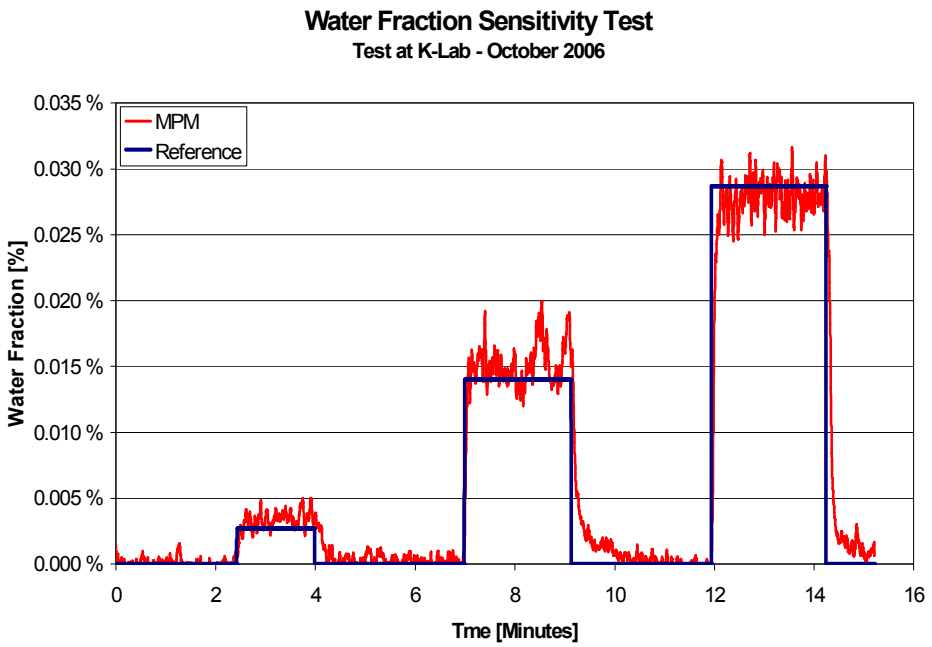

Figure 14: Flow test of Gullfaks A "wells" - MPM Flow Laboratory

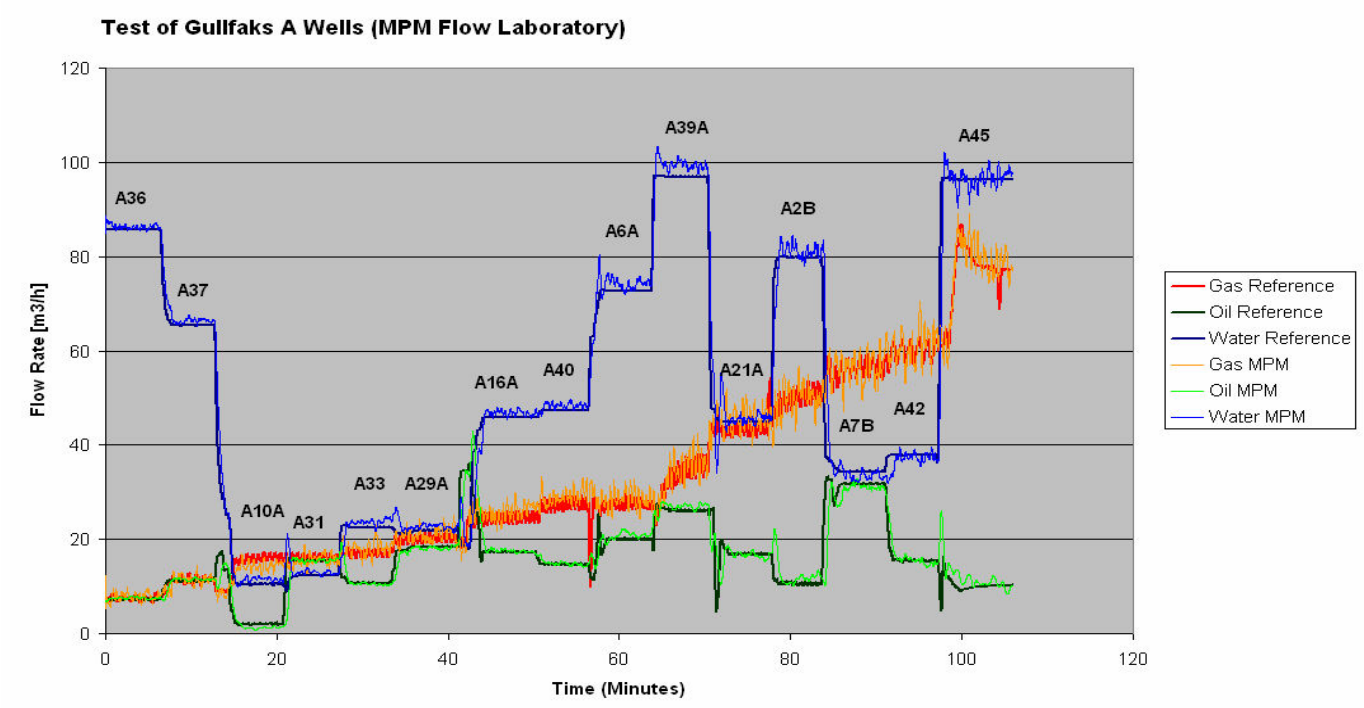

Figure 15: Qualification Testing - Wetgas

K-Lab test
Wetgas Mode GVF 99,7%, WLR 30 %

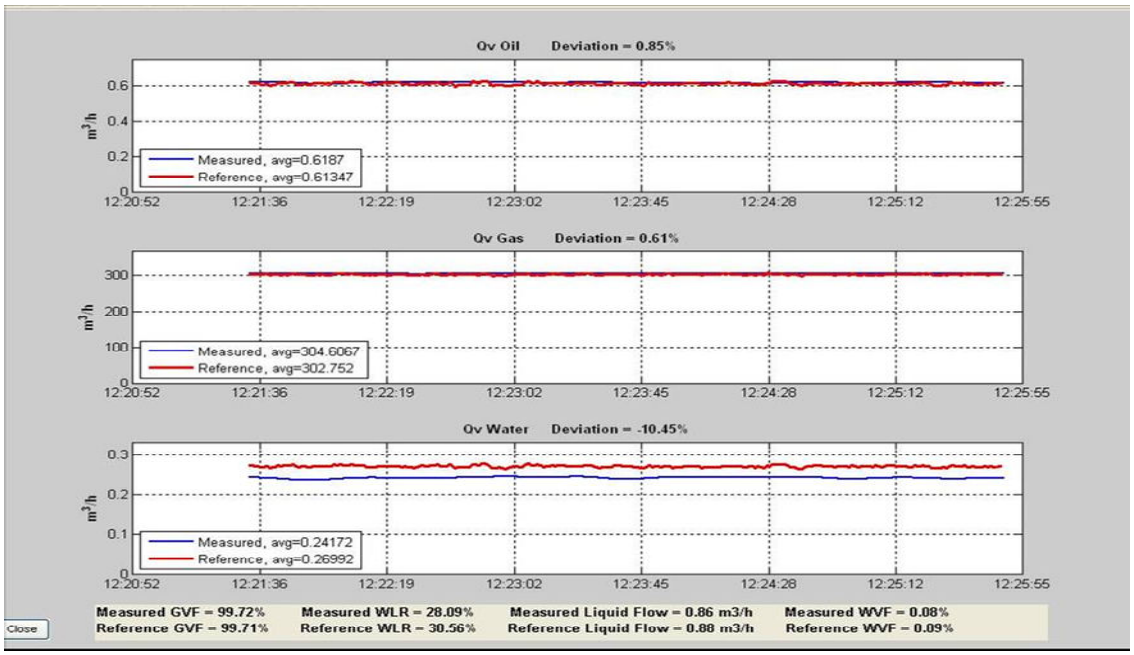

Figure 16: Qualification Testing - Wetgas

K-Lab test
Wetgas Mode GVF 98%, WLR 5 %

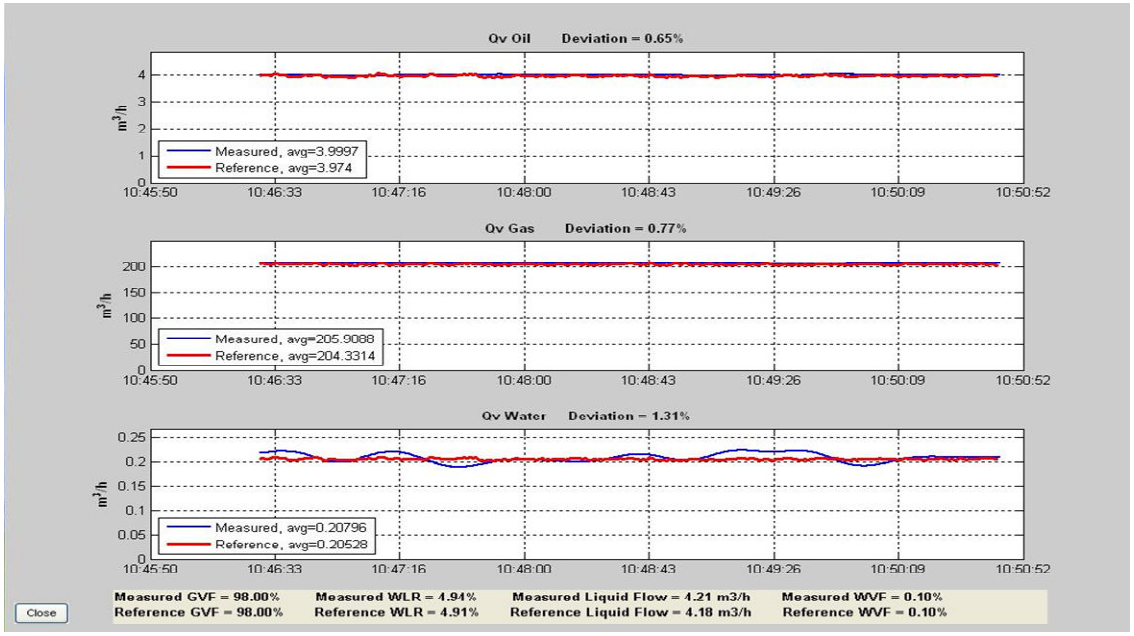

Figure 17|: Qualification Testing – MultiPhase

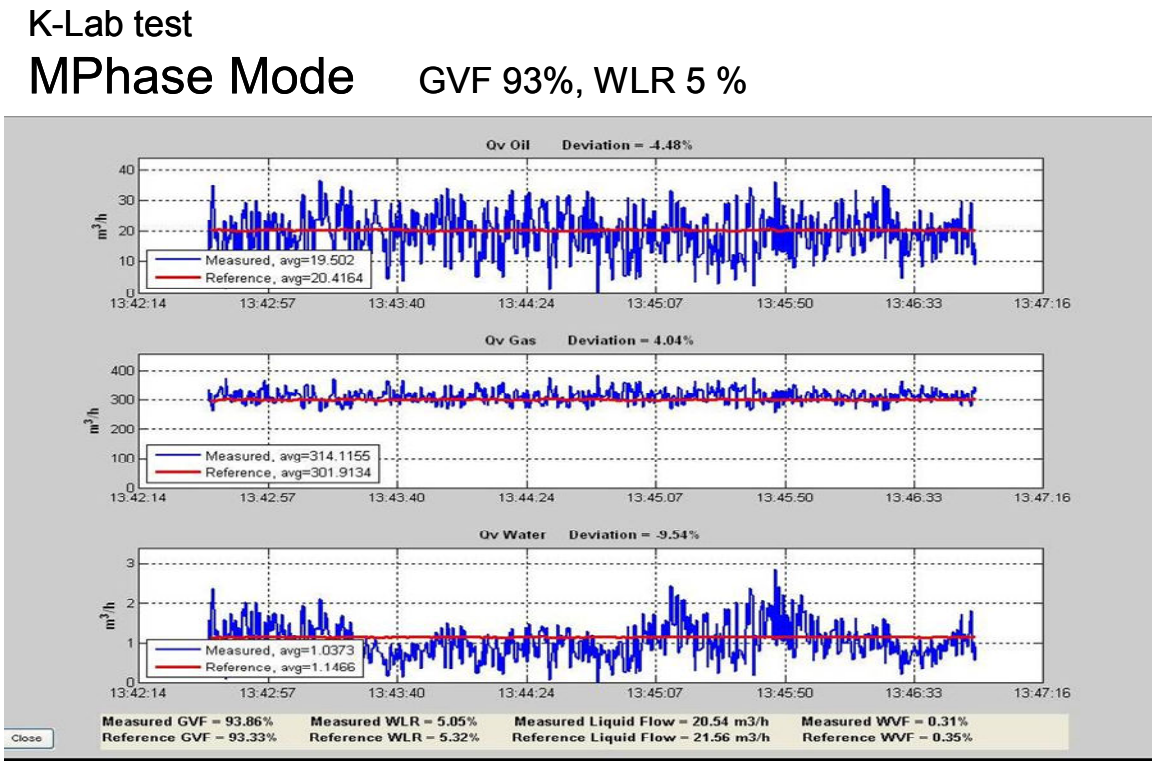

Figure 18: Summary – Qualification program – individual tests

	Individual wells / test points			
	MPM Lab	K-Lab	Gullfaks Dec	Gullfaks Jan
Oil Flow rate	± 5 to 10 %	± 4 to 10 %	± 8 %	± 6 %
Gas Flow rate	± 6 %	± 5 %	± 8 %	± 3 %

Notes:
- Accross full range of GVF and WLR
- Difference includes measurement uncertainty of reference and MPM meter, as well as other potential errors
- 90 % confidence level

Figure 19: Summary – Qualification program - Cumulative

	Cumulative rates - all wells / tests combined			
	MPM Lab	K-Lab	Gullfaks Dec	Gullfaks Jan
Oil Flow rate	+ 1,1 %	+ 0,1 %	+ 3,4 %	+ 1,4 %
Gas Flow rate	+ 1,4 %	+ 1,3 %	+ 1,4 %	+ 0,1 %

Note: (1)
- Accross full range of GVF and WLR
- Difference includes measurement uncertainty of reference and MPM meter, as well as other potential errors
- 90 % confidence level

Figure 20: Tests of operational stability and reproducibility at Gullfaks A

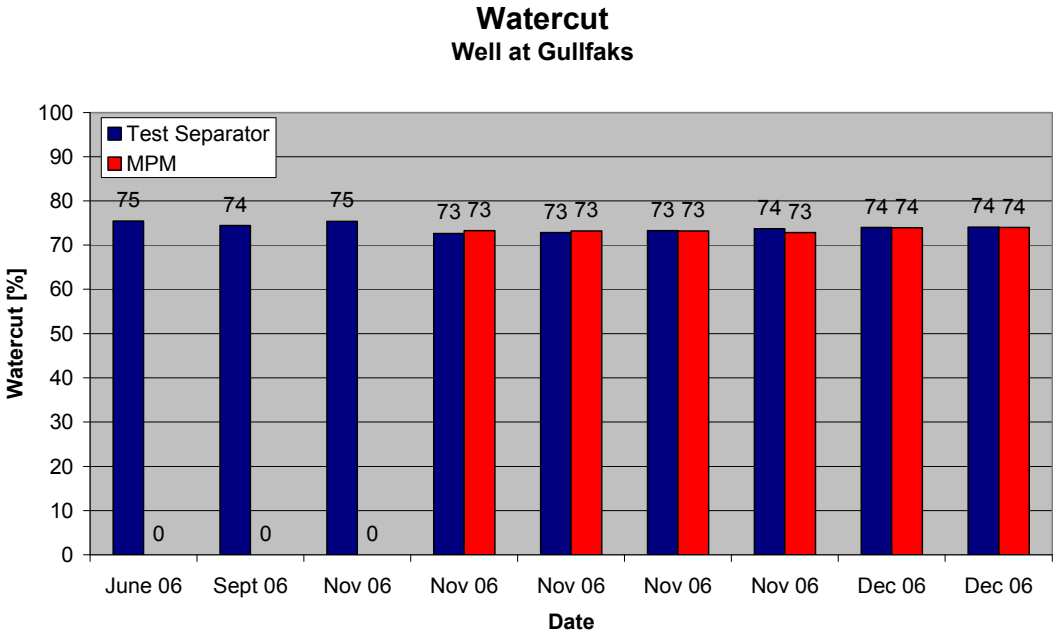

Figure 21: Repeatability tests at Gullfaks A

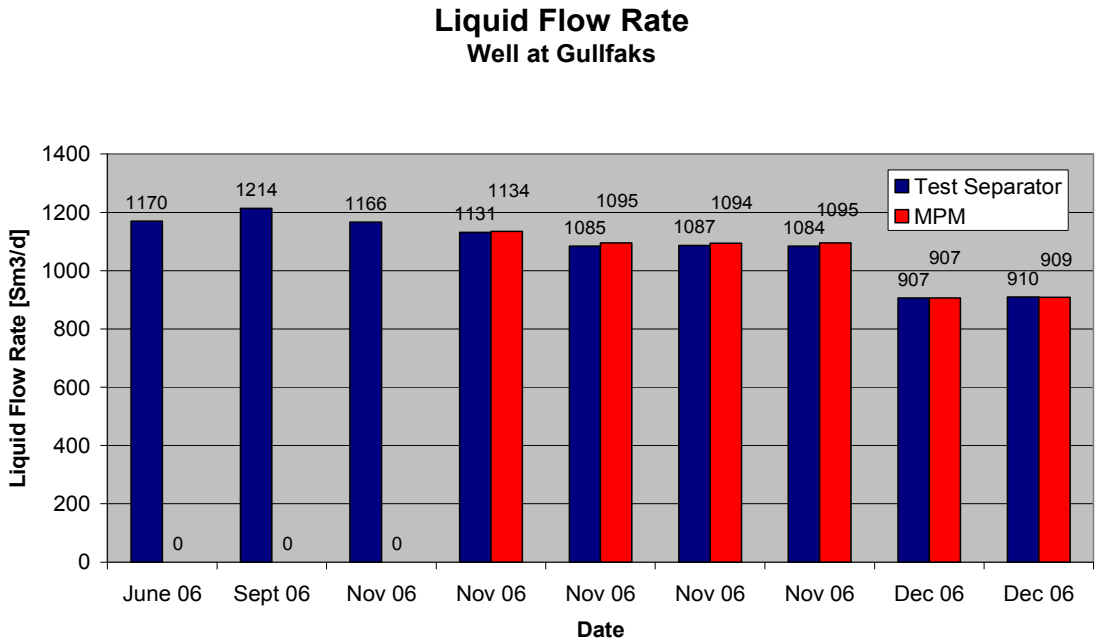

Figure 22: Verification of water salinity measurement method

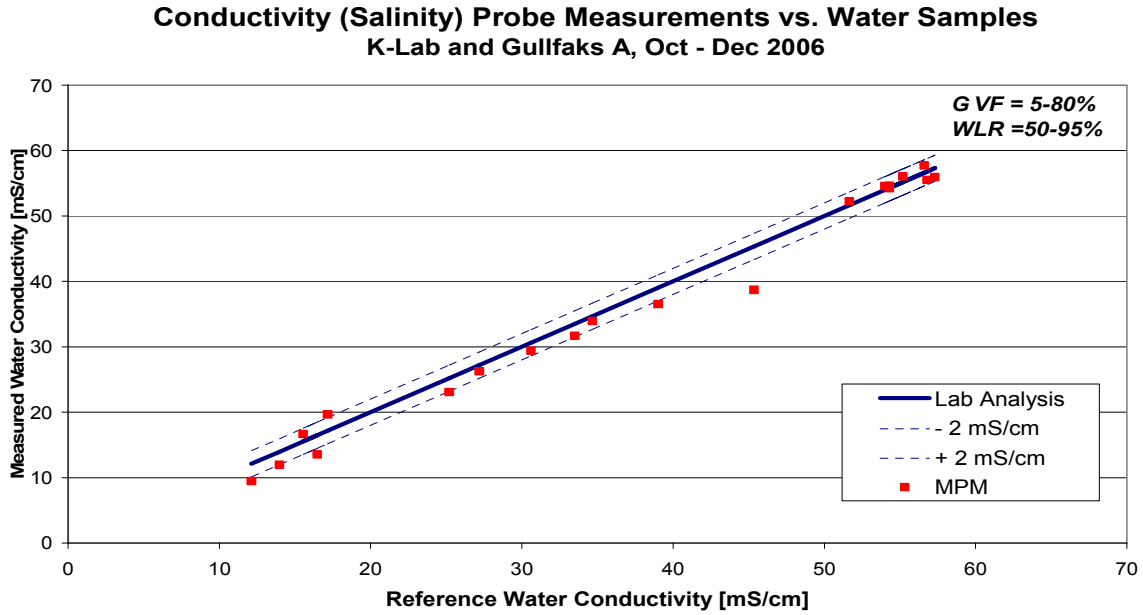

Figure 23: MPM's contributions to closing the gaps.

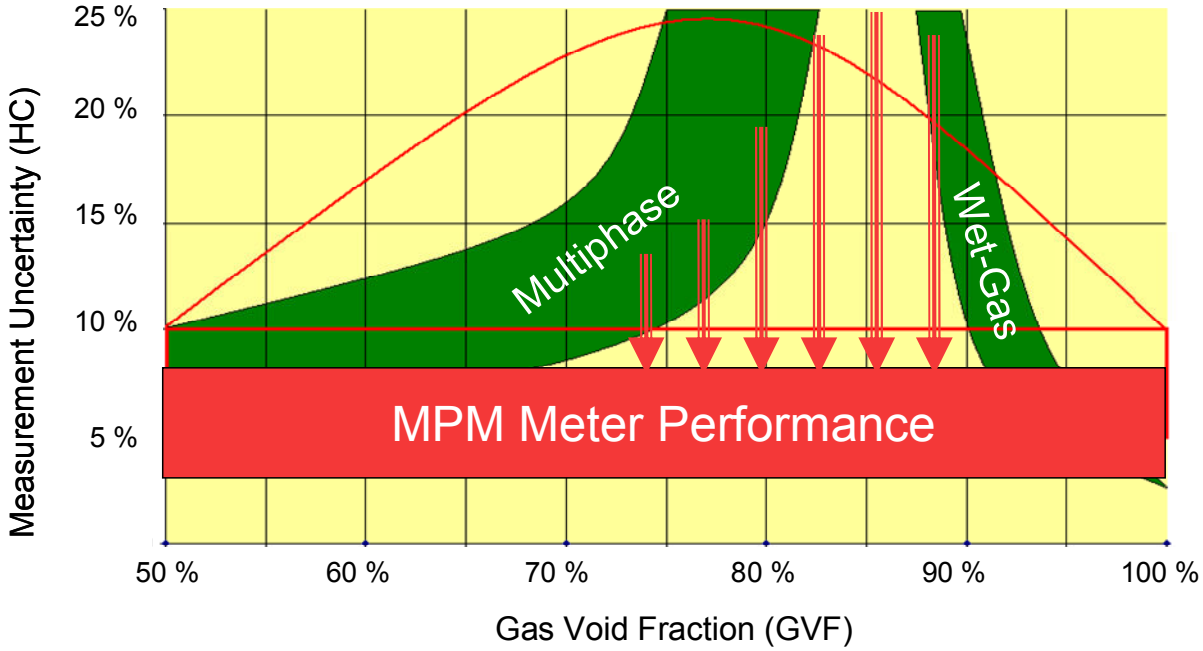

Calibration and Verification of Multiphase Meters for Allocation Metering of the Urd Field

Knut Skårdalsmo and Erik Aabro, SatoilHydro, Norway

1. INTRODUCTION

This paper presents the history and current status of multiphase metering of the production from the five sub sea wells of the Urd field. The Urd field is a satellite field to the Norne FPSO and the Urd stream is processed onboard Norne. The production from the Urd field was started in November 2005.

The Urd field consists of two sub sea templates, "Svale" and Stær", and the distance to the Norne FPSO is respectively nine and five kilometres. Each of the five production wells is equipped with a multiphase meter and the total Urd stream is measured in a topside multiphase meter at Norne. Furthermore it is possible to route the Urd stream through a test separator with state of the art metering equipment.

The oil from the "Svale" skid has high density and viscosity whereas the oil from the "Stær" is lighter and quite similar to the oil from the Norne field.

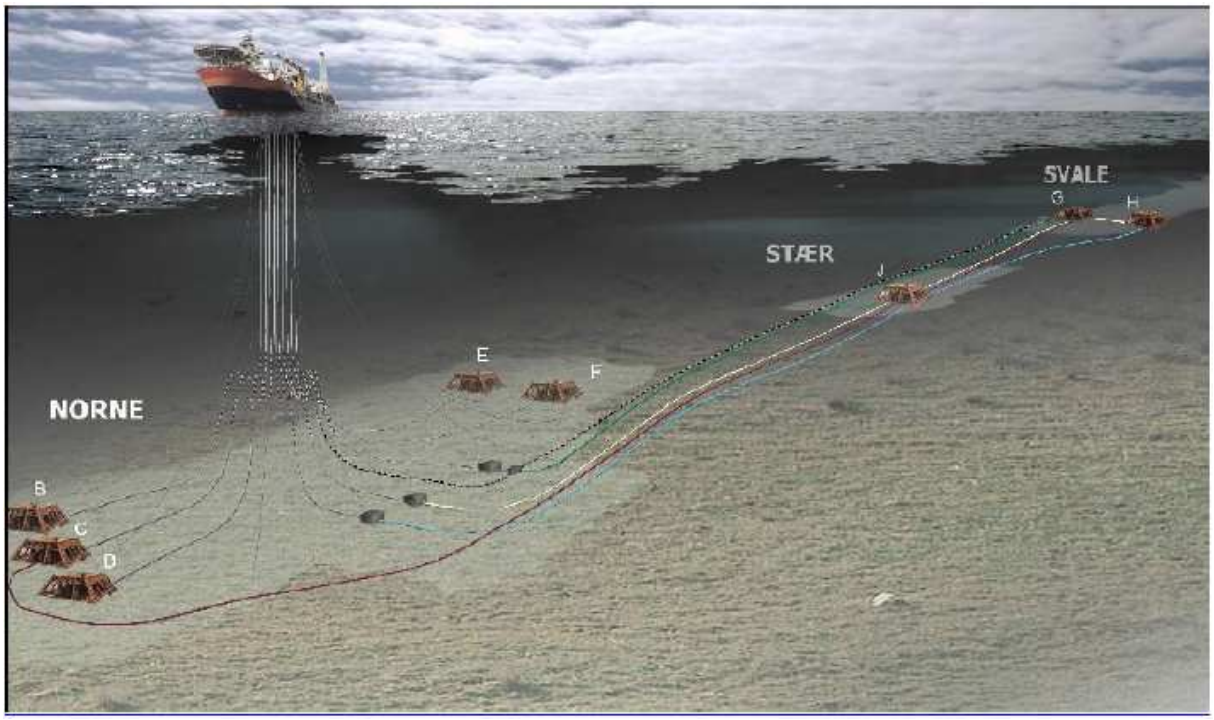

2. URD CALIBRATION PHILOSOPHY

Due to the fact that all of the three measuring points (sub sea, topside and test separator) will have different operating conditions it was agreed upon that the main comparison should be in total hydrocarbon mass. From the sub sea meters only the measured flow rates at line conditions are used for further calculations.

3. METERING EQUIPMENT

Test Separator
The Norne test separator has the following instrumentation:

- Gas metering: V-cone, split range using 8”- and 16” meters
- Oil metering: 5-path ultrasonic (Krohne Altosonic V) Foure Herman turbine meter as back up
- Water-in-oil; Water Cut Meter (Roxar)
- Oil Density; Densitometer (Solartron)
- Water metering Electromagnetic (Krohne)

Sub sea MPFM
One MPFM on each production well, all of the same size, 52 mm venturi diameter.

Top side MPFM
One MPFM placed on the turret on the Norne FPSO, 12” venturi diameter.

Metering computers
The Urd metering system including the test separator is connected via separate flow computers to a supervisory system for further data analysis and where also the PVT calculations are performed.

Sketch of the Urd / Norne top side metering and production system

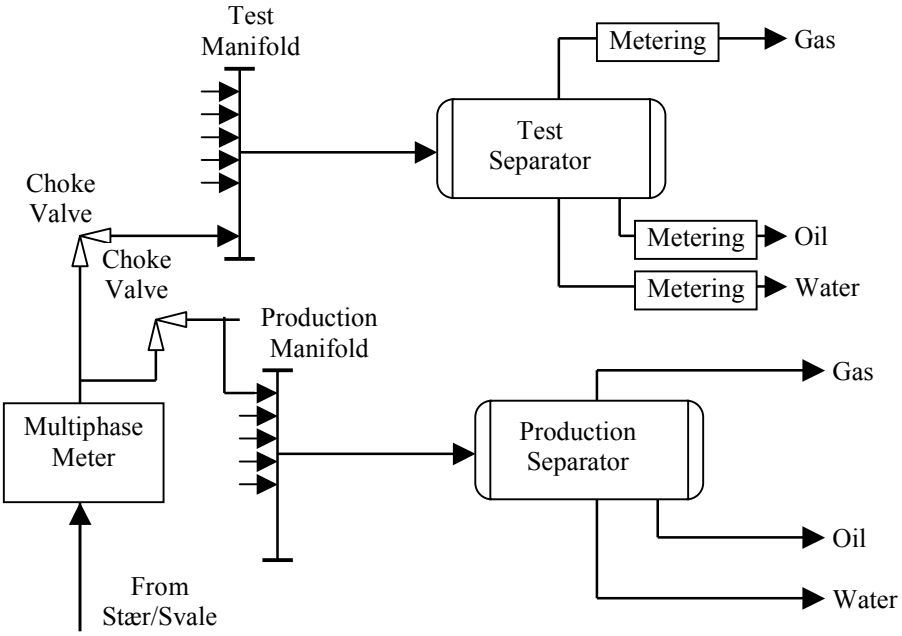

Normally the Urd production is routed to the production separator. The composition of the fluid arriving top side is determined by the flow measured by the sub sea MPFMs.

4. URD FLUID PROPERTIES

As previously described the Urd field consists of the Stær and Svale templates and the fluid properties are quite different.

Sample Field Well Formation		**Crude oil Svale 6608/10-6 MDT Lower Åre**	**Crude oil Stær 6608/10-8 MDT Tilje**	**Crude oil Norne 6608/10-3 DST 1 Åre**
Statoil Fluid Ref no.		2000-205	2002-300	94.110
Biodegraded		Yes	No	No
Weight % C_{10+} fraction		98.95	90.29	89.02
Weight % C_{20+} fraction		70.71	55.08	52.00
Molecular weight oil (g/mole)		315	237	228
Molecular weight C_{10+} (g/mole)		323	273	282
Molecular weight C_{20+} (g/mole)		428	403	415
Density oil (g/cc)		0.915	0,865	0.861
Density C_{10+} (g/cc)		0.918	0.877	0.876
Density C_{20+} (g/cc)		0.935	0.896	0.898
Wax content (wt%)	Not purified	2.8	5.7	10.0
	Purified	1.7	5.0	7.8
Pentane insolubles (wt%)	Precipitated 1 X	0.29	0,54	0.19
	Precipitated 2 X	0.17	0,10	0.08
Total acid number, mg KOH/g		0.67	0.05	0.03
Sulphur (wt%)		0.33	0.19	0.18
Pour point (°C)	Maximum	<-38	+22	+20
	Minimum	<-38	+16	+10
WAT by microscopy. (°C) WAT by NIR (°C)		<25 -	40.9 42.6	38.5 -
Wax dissolution temp. (°C)		-	53	47
Viscosity (cp) (shear rate 100 s-1)	80 °C	7.51	2.31	2.33
	50 °C	20.0	4.21	3.88
	20 °C	90.0	43.7	32.4
	10 °C	182	242	172
	5 °C	280	-	326
	0 °C	405	557	500

5. TEST RESULTS

The first proper flow test was performed with two Stær – and one Svale wells in operation. The reason for this was that Norne had problems separating the Svale fluid and this was the only Urd mix that could be properly separated and hence giving proper measurements downstream the test separator. In all the following result tables the MPFMs performance are compared to the test separator. It should be noted that no calibrations or tuning has been done to the sub sea MPFM during the period of operation.

There are of course more tests performed than the three tests described in this paper, but the included tests are very typical for the meters. For all the tests the stable period exceeds 6 hours and the Urd production has been run stable for at least 12 hours prior to the test period.

The average GVF is approximately 80 in all tests.

Test #1, june 2006

Metering	Sub Sea	Topside
Total HC Mass	0,4 %	14,0 %
Water (Mass)	-16,8%	-41,5 %

In March 2007 it was planned to perform a calibration of the topside MPFM, but due to problems with the supervisory system it was not possible to perform a complete calibration. It was however discovered quite heavy slugging thorough the topside MPFM with the dp varying from 200 – 600 mbar and 40 cycles in 15 minutes.

The next successful (?) test was performed in May 2007 after some attempts to calibrate/tune the topside MPFM had been undertaken and this time the entire Urd production was measured. It should be noted that the flow signals from the sub sea MPFM indicate quite heavy slugging in at least one of the wells giving dp-readings from zero to approx. 600 mbar.

Test #2, May 2007

Metering	Sub Sea	Topside
Total HC Mass	3,2 %	17,8 %
Water (Mass)	-15,5 %	-26,1 %

After some further attempts to tune the topside MPFM another test was performed in September 2007.

Test #3, September 2007

Metering	Sub Sea	Topside
Total HC Mass	-3,5 %	6,2 %
Water	-11,5 %	6,2 %

6. CONCLUSIONS AND LESSONS LEARNED SO FAR

It is likely to believe that slugging has a detrimental influence on the performance of the MPFMs and according to the StatoilHydro experts on slug control the observed slugging must be regarded as a “normal” flow situation for the Urd production stream. However the performance guarantee given by the manufacturer does not take this into consideration. The topside MPFM was installed in order to be the main allocation meter but so far only the sub sea MPFMs have been used for this purpose. Due to the large size of the top side MPFM it was not possible to conduct flow tests (FAT) on the meter prior to installation and based on the lessons learned so far we may conclude that is was a very brave decision to install an untested MPFM.

Although it seems like we still have quite a way to go before the top side MPFM can be used as the main allocation meter StatoilHydro will continue to challenge the manufacturer in order to get acceptable performance of the meter.

Regarding the sub sea MPFMs some work need to be done in order to evaluate the performance of each of the meters. We do however believe that the main cause for the deviation from the test separator is the slug flow in one of the wells. The deviation in water production rate may also to some extent be explained by the long production line from Urd to the Norne FPSO, i.e. water accumulation in the flow line and subsequent water slugs arriving topside.

FLUID COMPOSITION ANALYSIS BY MULTIPLE GAMMA-RAY BEAM AND MODALITY MEASUREMENTS

Geir Anton Johansen[1,3] and Stein-Arild Tjugum[2,3]

[1] University of Bergen, Department of Physics and Technology
Allégaten 55, N-5007 Bergen, Norway
geir.johansen@ift.uib.no

[2] Roxar Flow Measurement
PO Box 2364 Solheimsviken, N-5824 Bergen, Norway
stein-arild.tjugum@roxar.com

[3] The Michelsen Centre for Industrial Measurement Science and Technology
P.O.Box 6031, N-5892 Bergen, Norway

ABSTRACT

The feasibility of using multiple gamma-ray beams to identify the type of flow regime has been demonstrated. One gamma-source with principal emission at 60 keV is used because this relatively low energy enables efficient collimation and thereby shaping of the beams, as well as compact detectors. One detector is placed diametrically opposite the source whereas the second and eventually the third are positioned to the sides so that these beams are close to the pipe wall. The principle is then straight forward to compare the measured intensities of these detectors through that identify the instantaneous cross sectional gas-liquid distribution. By counting the intensity short time slots and (< 100 ms), rapid regime variations are revealed.

Varying water salinity is another challenge for most multiphase flow meters because it affects volume fraction calculations based on gamma-ray, electrical conductance and other measurements. There have been a few approaches to solve this without relaying on off line calibration. One of these utilizes the difference in the composition of the gamma-ray attenuation coefficient at different energies. The method presented here take advantage of the same effect, but though simultaneous measurements of transmitted and scattered gamma-rays from a $^{241-}$Am source. It has been shown that the gas volume fraction then can be determined independent of changes in the water salinity. Once again the challenge is to minimize the effects of changes in the flow regime.

1. INTRODUCTION

Measurement of multiphase pipe flow of gas, oil and water is not at all trivial and in spite of considerable achievements over the past two decades, important challenges remain 1. These are related to reducing measurement uncertainties arising from variations in the flow regime, improving long term stability and developing new means for calibration, adjustment and verification of the multiphase flow meters. This work focuses on the first two issues using gamma-ray attenuation and scattering methods.

Multiphase flow meters operate by combining instantaneous velocity and cross sectional fraction measurements of the flow components. The major source of flow regime induced errors is temporal variations in the distribution of gas and liquid in the measurement cross section of the pipe. The oil/ water distribution is less critical because these components are closer in density - which also implies that they are less likely to be separated. Although flow velocity measurements in some cases may be somewhat affected by temporal variations in the gas/ liquid distribution, the major problem is the component volume fraction measurement principles. Not surprisingly, measurements of the gas volume fraction (GVF) are most susceptible; however, significant errors may also be present in some measurements of the water in liquid ratio (WLR- also known as water cut). This is because the sensitivity of single global measurements is inhomogeneous over the pipe cross section. In this work we attempt to reduce these errors by identifying temporal variations in the flow regime and making the necessary corrections. Gamma-ray attenuation is the most frequently applied principle for GVF measurements and was therefore obvious to investigate the use of multiple gamma-ray beams (MGB). The feasibility of this approach has been proven 2.

Varying water salinity is another challenge for most multiphase flow meters because it affects volume fraction calculations based on gamma-ray attenuation, electrical conductance and other measurements. One approach to solve this without relaying on off line calibration utilizes the difference in the composition of the gamma-ray attenuation coefficient at different energies 3. The dual modality method (DMD) method in this work take advantage of the same effect, but though measuring the scatter response with a separate detector in addition to the total attenuation by traditional transmission measurement. It has been shown that the gas volume fraction then can be determined independent of changes in the water salinity [4]. Once again the challenge is to minimize the effects of changes in the flow regime, particularly of the scatter measurements.

2. THE DMD AND MBG PRINCIPLES

2.1 Choice of Radioisotope

The most frequently used radioisotope for GVF measurements in pipe flows is ^{137}Cs with 662 keV gamma-ray emission. It has a relatively long half life (30 years) and a pure emission spectrum with sufficiently high energy to enable clamp-on installation on pipes. The latter is less important for multiphase flow meters which need to be installed in-line anyway. For successful implementation of the MGB and DMD principles it is a requirement to use an isotope with lower emission energy for several reasons:

- The DMD principle requires sufficiently low energy for photoelectric absorption to make a significant contribution to the total attenuation in the fluid in addition to Compton scatter, see Figure 1. This will be further explained in the next section.
- The MBG principle depends on efficient beam collimation and this can be achieved with much less material (thickness) at low energies.
- It is possible to use smaller and more compact detectors which in combination with less collimation and shielding thickness make it possible to embed both source and detectors in the pipe wall in the final design.

Lower radiation energy also has the advantage of far less radiation dose to the environment 5. The first of these conditions suggest that a gamma-ray energy of about 50 keV would be ideal. Energies lower than this would put severe restrictions on the material, wall thickness and diameter of the pipe. Based on these considerations and the available radioisotopes, ^{241}Am was selected as source. For all practical purposes this has a pure emission spectrum with principal energy at 59.5 keV and also a long half-life (432 years).

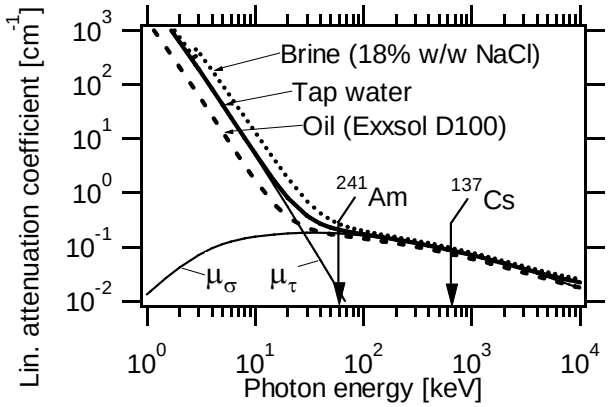

Figure 1. The linear gamma-ray attenuation coefficient of oil, water and brine as a function of energy. Its contributions from Compton scattering (μ_σ) and photoelectric absorption (μ_τ) are shown for tap water. The emission lines of ^{241}Am (60 keV) and ^{241}Am (662 keV) are also shown.

2.2 Dual Modality Densitometry for Salinity Measurements

The foundation of the dual modality principle is that Compton scattering is roughly proportional to the density of the fluid ($\mu_\sigma \sim \rho$), whereas the photoelectric absorption coefficient is strongly dependent on its atomic composition ($\mu_\tau \sim Z^4$ to Z^5) 5. This makes the latter very sensitive to salt elements such as chlorine because of their higher atomic numbers (Z). To enable measurements of these two components, two detectors are used as illustrated in Figure 2.

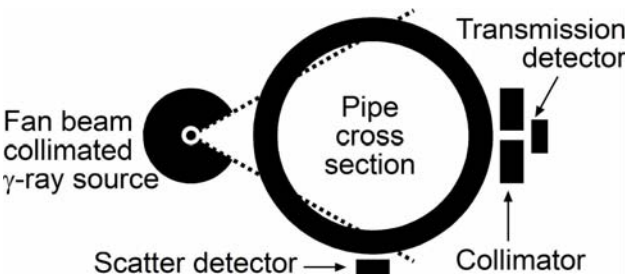

Figure 2. The DMD measurement geometry using one transmission detector and one scatter detector 4.

The total attenuation measured by the transmission detector will have contributions from both photoelectric absorption and Compton scatter. The response is expressed by Lambert-Beer's exponential decay law provided a fairly strict detector collimation is applied to avoid forward

scatter contribution (build-up). The scatter detector is positioned outside the direct view from the source and will thus not detect any directly transmitted radiation at all. Its response will solely be measurement of radiation originating from Compton scatter in the pipe cross section. The transmission detector thus provides a measurement of both the photoelectric and Compton scatter coefficients, whereas the scatter detector mainly provides a measurement of the Compton coefficient. The response in the latter will also have a small contribution from photoelectric absorption through the attenuation of scattered radiation between the measurement cross section and the scatter detector.

Several semi-empirical models have been developed for the response in the scatter detector 6. They all use the proportionality of the scatter response to the number of scatter events generated over the pipe diameter (d) or active volume:

$$I_s \sim \frac{\mu_\sigma}{\mu}\left[1-\exp(-\mu(1-GVF)d)\right] \tag{1}$$

Here μ and μ_σ are the total and Compton linear attenuation coefficients of the fluid, respectively. In addition corrections must be made for attenuation of the incident beam before it reaches the active volume, and for that of the scattered radiation. Since the scatter emission is isotropic and the geometrical factor of the scatter detector is small, it is advantageous to have Compton dominant attenuation in the fluid, but yet some contribution from photoelectric absorption to monitor the salinity. As can be seen from Figure 1, this is fulfilled at 60 keV.

Accurate semi-empirical models of the scatter response are just the first step in calculating the water salinity in addition to the *GVF*. It turns out that that it is more efficient to correct for changes in the water salinity directly by using a simple empirical relationship between the measured transmitted (I_T) and scattered (I_S) intensities:

$$R = \frac{I_S}{I_T^n} \tag{2}$$

Several experiments with different geometries confirm that this ratio varies with the *GVF*, but not with the water salinity. In other words it provides salinity independent *GVF* calculation. The exponent is in most cases $n \approx 0.55$, but is slightly dependent on the measurement geometry. Its value is found from calibration measurements. The results of the first pilot project, which was carried out with static fluid at controlled conditions, are shown in Figure 3. A limited number of experiments with oil (Exxsol D100) indicate that the slope of the calibration curve varies with the WLR (water liquid ratio). So, as otherwise in calculation of the flow parameters in multiphase flow metering, iterative methods must be applied to solve the set of transcendental equations. These, and later results call for more extensive experiments with a larger variety *GVF* and *WLR* combinations at different salinity. Another issue also revealed in the pilot project is that the salinity independence of the empirical expression in Equation 2 fails for annular type of flow regimes. So this is yet another example on a multiphase measurement principle that requires knowledge about the flow pattern.

2.3 Flow Regime Identification using Multiple Gamma-Ray Beams

Most of today's multiphase flow meters relay on T-bend vertical installation to achieve some degree of fluid homogeneity in the measurement cross section. But even at moderate *GVFs* slug flow with annular type of flow pattern is quickly established causing traditional gamma-ray densitometers to overestimate the *GVF*. This is compensated for using models taking into account the difference in *GVF* inside the beam to that of the full cross section. However, the flow regime depends on a range of factors making it difficult to use general models to correct the GVF.

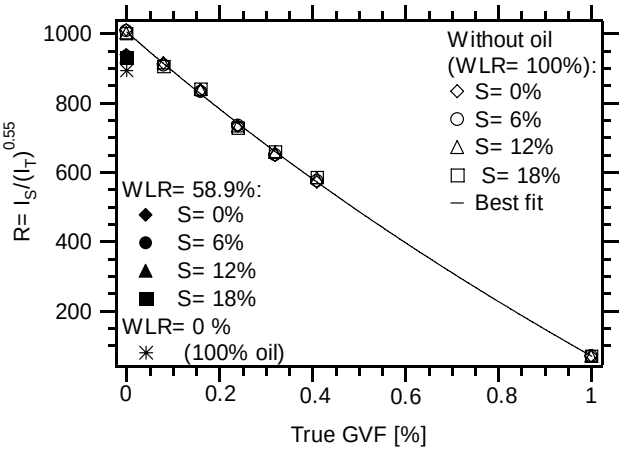

Figure 3. Calibration curve yielding GVF from measurements of I_T and I_S for homogeneously mixed fluid conditions 4. The water salinity (w/w NaCl) percentage is listed with the legends, so is the WLR in the case of GVF=0.

An experiment using one fan-beam collimated gamma-source and 9 detectors to cover the full pipe cross section was carried out at the flow loop facility of Christian Michelsen Research 2. The apparatus, which is shown on the top in Figure 4, was mounted in a tilt section and several measurement series were performed with horizontal, 45° tilted and vertical flows. The results for a typical series are shown in Figure 4. The counting or integration time of the 9 detectors are 30 ms, meaning each of the 3 s long sequences presented are composed of 100 individual measurements. All tree cases are typical slug flow regimes where it is difficult to measure the GVF accurately using one beam densitometer and model compensation. But by dividing the flow into short segments as presented in Figure 4, it is possible to continuously identify the instant cross sectional flow pattern. For the horizontal case it can be seen that this typically varies between what would be stratified and bubble type of regime if it was continuous. Likewise the vertical case is composed of bubble and annular flow. For the tilted flow case a mixture of all patterns can be identified although it can be most closely associated with horizontal flow. This is probably because the measurement position is just about 2 m above the floor level where the flow enters the tilt section. It would look different if the tilted flow was allowed to develop further. In all cases the limited spatial measurement resolution makes bubble flow, which is typical for low gas fractions, appear as homogenously mixed flow for the detectors.

The conclusion of this work was that it is possible to use multiple gamma-ray beams to continuously identify the instantaneous flow pattern in multiphase pipe flow. This can in turn

be used to calculate the GVF more accurately and also to correct other measurements, such as the DMD GVF, according to their dependency.

A practical implementation of the MGB principle needs to be simpler and more compact than the system shown in Figure 4. A system with the source and detectors partially embedded in the pipe wall has been built and successfully tested 7. This uses only two transmission detectors to identify the regime. A similar set-up is presented in the next section.

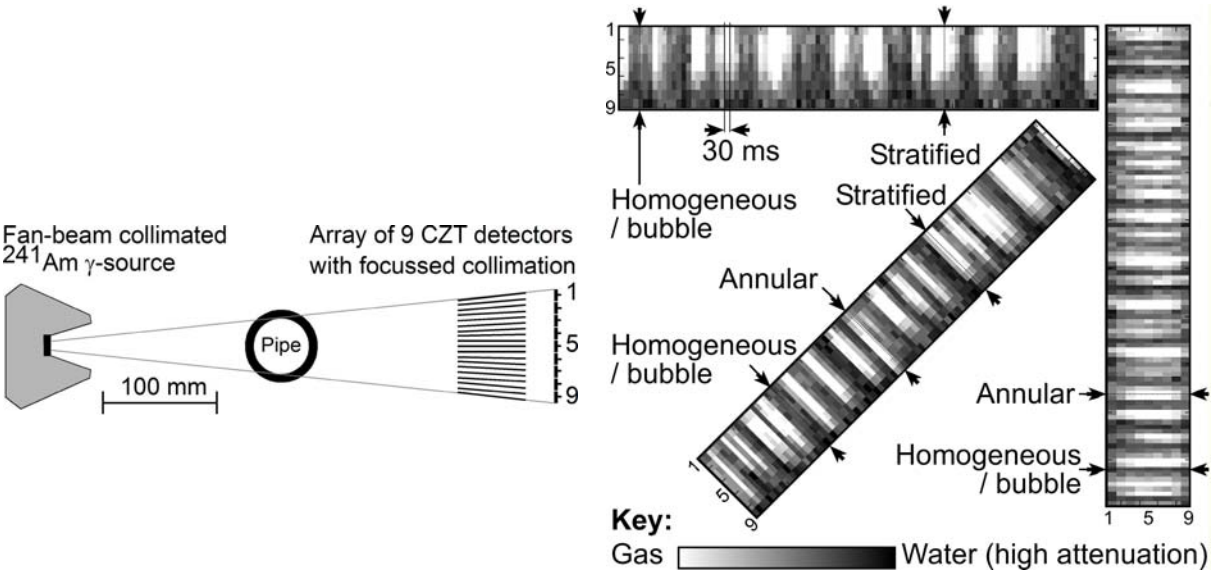

Figure 4. Experimental set-up (top) and measured three phase flow pattern sequences with Q_{oil}=5 m^3/h, Q_{water}=25 m^3/h and Q_{gas}=20 Am^3/h (83% WLR and 67% GVF) average reference data at horizontal, 45° tilted and vertical flow. Each of the 3 s long sequences is composed of 100 separate measurements with 3 ms counting (integration) time. The numbers refer to the array of 1 cm^2 detectors shown at the set-up on the top.

2.4 Experimental Set-up for Rig Tests

To further investigate the DMD and MGB principles an experiment was carried out using a basic circulation flow loop rig which uses Diesel oil, saline water and compressed air as gas. The WLR is set by filling the bottom tank, which also is the gas/ liquid separator, with the desired amount of oil and water before each run. Compressed air is injected continuously under the runs through a separate valve. The actual salinity and WLR for each run are determined by sampling the fluid at a point with fairly homogeneous mixing. An YSI Model 30M/10FT probe is used for salinity measurement, whereas the WLR is determined by fractional measurements of the liquid sample after separation. Compared to a large flow loop facility where the oil and water are continuously separated in a large volume tank, the limited volume of this system makes it fairly easy to change the water salinity (using NaCl) before each run. For all runs the flow is allowed to stabilize before the data acquisition is started.

The measurement geometry for the experiments is shown in Figure 5 and based on the conclusions of previous work as presented in sections 2.2 and 2.3. A PVC spool piece with 81 mm diameter was used in the measurement cross section. This has approximately the same

attenuation properties as PEEK or reinforced epoxy which typically are used in a real flow meter system. All four detectors are CsI(Na) scintillation counters with integrated read-out electronics and counter output. The size of the crystals is Ø= 13 mm x38 mm. Both DMD scatter detectors (S1 and S2) have fairly relaxed collimation to allow higher count-rate and make it comparable with that of the transmission detectors. The transmission detectors (T1 and T2) are collimated to reduce build-up for the DMD measurements, and to reduce their fields of view for the flow pattern identification. The experiments were to a large extent carried out by an MSc student 8.

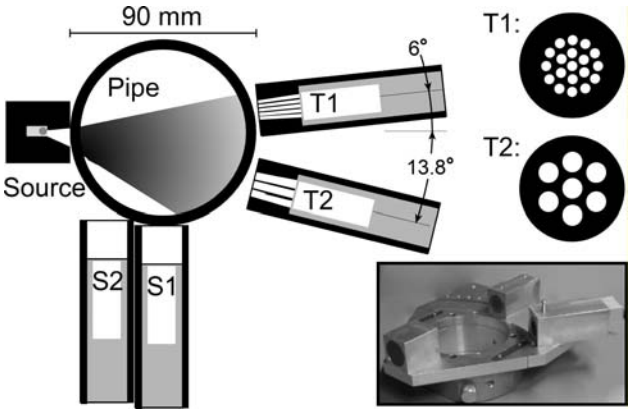

Figure 5. The MBG DMD measurement geometry used for the rig experiments. The shaded area in the pipe is the beam as defined by the source collimation. The shading indicates the exponential decay in the number of interactions across the pipe for homogeneously mixed flow. This is highest in the dark area close to the source. The insert show the source and detector support system (without scatter detectors) which is clamped onto the pipe. Also shown are cross sections of the focused collimators used for T1 and T2 with Ø= 2 mm and Ø= 4 mm holes, respectively.

3. RESULTS

In Figure 6 the ratio given in Equation 2 is plotted for all four combinations of scatter and transmission detector intensities. The *WLR* is close to 100%, i.e. there is virtually without oil, and three different salinities are used. As can be seen the salinity independent *GVF* principle is confirmed for all ratios, however, the R_{11} ratio clearly provides the highest sensitivity.

In Figure 7 R_{11} is plotted as a function of *GVF* for three different salinities and four different *WLRs* ranging from 20% to 99%. The results presented in Figure 3 are partially confirmed as the presence of oil in the flow reduces the slope of the calibration curve (*R -vs- GVF*) as expected. But it also shows that the WLR need to be known (which it is in multiphase flow meters) to maintain salinity independent GVF measurements at low WLRs. In the plot this is most clearly seen for *WLR*= 20% and *WLR*= 25% at *GVF*= 0; these should appear on the same spot, but they do not. The effect of a range of the *n*-values (the exponent in Equation 2) was investigated, but did not make a significant change. The same plot was made for R_{12}, R_{21}, and R_{22}, and for their mean R_{AVG}, but the results were the all same. The only difference was the slope of the calibration curve, i.e. the sensitivity, as can be seen for R_{AVG} in Figure 7.

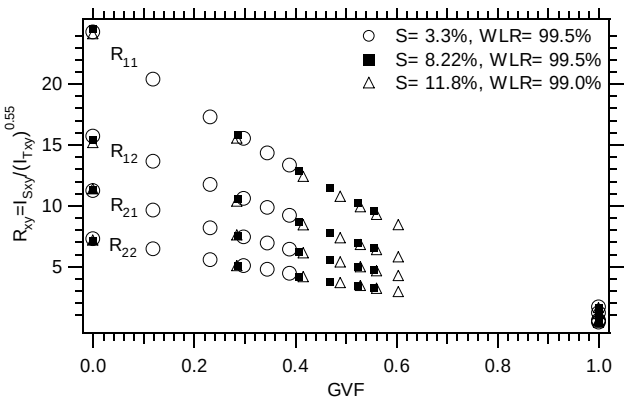

Figure 6. Plot of the R ratio (Equation 2) -vs- GVF of the four possible combinations of transmission and scatter detectors shown in Figure 5 ($R_{12}= I_{S1}/(I_{T2})^{0.55}$ etc.) with three different salinities (S) and WLR≈ 100%.

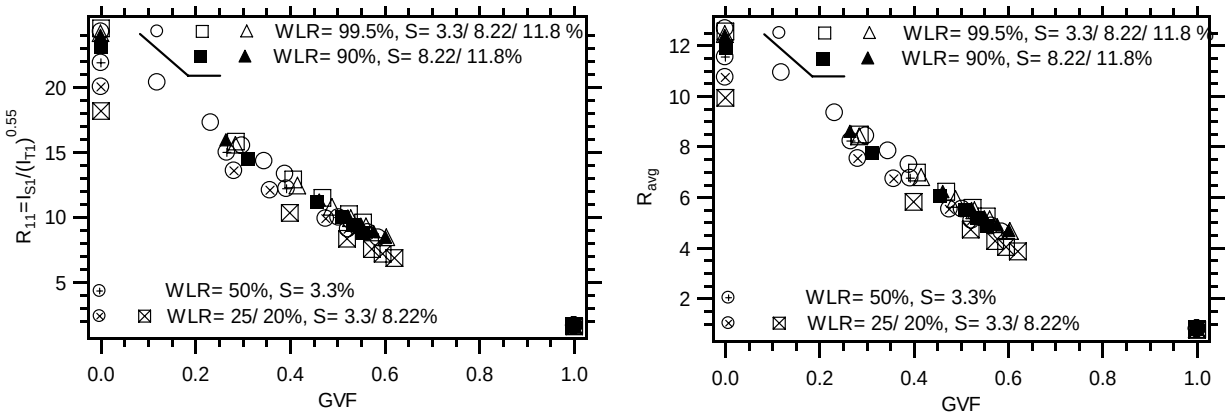

Figure 7. The ratio R_{11} (Equation 2) -vs- GVF at three different salinities and four different WLRs (left) and with the average ratio $R_{AVG}= (R_{11}+R_{12}+R_{21}+R_{22})/4$ (right).

Previous experiments 4 indicate that annular type of flow would have the same effect on the salinity independence as seen here although it does not explain the deviation of identical WLRs at *GVF*= 0. Whilst there is no possibility that annular flow has developed fully at the measurement point in the loop, it is likely that there will be slug flow with temporal annular type of pattern as can be seen in the vertical plot in Figure 3. To check for this the GVF was calculated from both T1 (*GVF1*) and T2 (*GFV2*) intensity measurements, I_T 5:

$$GVF \approx \ln\left[\frac{I_T}{I_W}\right] \Big/ \ln\left[\frac{I_G}{I_W}\right] \tag{3}$$

Here I_W and I_G are calibration measurements at *GVF*= 0 and 1, respectively. Since there is no reference data available for the GVF in the flow rig, *GVF2* is plotted as a function of *GVF1* in Figure 8. The result shows that *GVF1* in all cases are higher than *GVF2*. To see how this relationship would be with an exact GVF reference and a true annular flow pattern, a MCNP5 Monte Carlo model was developed for the system and benchmarked at *GVF*= 0 and 1, and at WLR= 0 and 100% for all detectors. A cylinder shaped gas bubble was introduced along the

center axis of the pipe and simulations were made with stepwise increases in the radius of this cylinder. The results are also plotted in Figure 8 where *GVF1* and *GVF2* and their errors are shown as functions of the true GVF determined by the ratio of the cylinder. Simulations of homogenously mixed flow end up on the straight line as one would expect.

4. DISCUSSION

The measured results presented in Figure 8 predict that there is a predominant distribution of gas along the center axis of the pipe for all measurements. This is confirmed by the simulations. The deviation between the measurements and the simulations at low *GVFs* is explained by the fact that it is unlikely to have a stable gas core at the pipe center at these conditions. The simulation results presented in Figure 8 confirm that there, except for high gas fractions, always is a difference between *GVF1* and *GVF2* with this geometry.

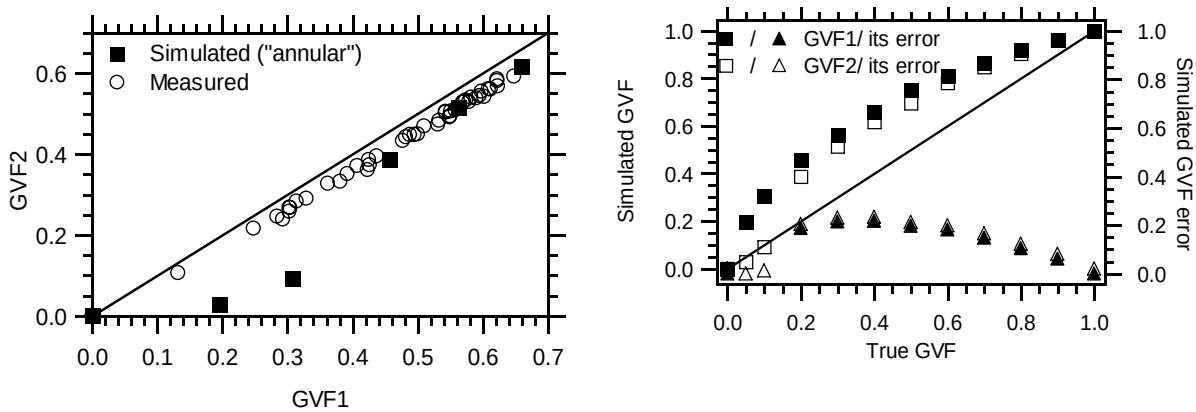

Figure 8. Calculated GVF2 plotted versus calculated GVF1 for all measured data sets and for simulations on annular type flow with 3.3% brine (left), and calculated GVF1 and GVF2 and their errors based on simulations plotted as functions of the true GVF with 3.3% brine as liquid phase (right).

This means that the actual *GVF* is less than that presented in Figs. 6, 7 and 8. This adds uncertainty to the quality of the data presented in these figures. Further Monte Carlo simulations would be helpful here since these provide accurate reference data.

Regarding positioning of the scatter detectors the results confirm that S1 is an ideal position because it has higher sensitivity than S2 to the full pipe cross section. The less favorable result with S2 may be explained by its higher contribution from the pipe wall and partly source collimator, and correspondingly less from the fluid. Better results would probably be achieved with S2 if it were tilted slightly towards the center of the pipe.

5. CONCLUSIONS

The lack of accurate reference data for the measurements makes it difficult to make solid conclusions. Nevertheless the support of Monte Carlo simulations confirms that the applied measurement geometry can be used to identify the average flow pattern and correct for GVF

errors. However, the sensitivity to annular type of flow pattern would be higher with detector T2 placed at a higher angle, such as 25° or slightly more.

The results also show that the DMD principle for salinity correction has highest sensitivity with the scatter detector positioned as S1 with a large field of view. On the other hand the results indicate that the DMD salinity compensation fail at low WLR, but this is uncertain because of lack of accurate reference data.

Further research should be carried out with Monte Carlo simulations since this provides accurate reference data which experimentally is very difficult to achieve in any flow loop. A major advantage in both the DMD and MBG principles is that they rely on pulse counting only; there is no need for detectors with high energy resolution and read-out electronics to perform energy analysis.

ACKNOWLEDGEMENTS

The support on Monte Carlo simulation by Prof. Robin P. Gardner and the CEAR members at North Carolina State University is very much appreciated.

REFERENCES

1. S. Corneliussen, J.-P. Couput, E. Dahl, E. Dykesteen, K.-E. Frøysa, E. Malde, H. Moestue, P.O. Moksnes, L. Scheers and H. Tunheim *Handbook of Multiphase Flow Metering*, Rev. 2, 2005 (www.nfogm.no) NFOGM/ Tekna.

2. S.-A.Tjugum, B. T. Hjertaker and G. A. Johansen "Multiphase flow regime identification by multibeam gamma-ray densitometry" *Meas. Sci. & Technol*. 2002, **13**, 1319-1326.

3. A. M. Scheers, "Multiple Energy Gamma Ray Absorption (MEGRA) Techniques Applied to Multiphase Flow Metering", 1998, *Proceedings of the 4th Int. Conf. on Multiphase Techniques*, London 26 & 27 March.

4. G. A. Johansen and P. Jackson "Salinity independent measurement of gas volume fraction in oil/gas/water pipe flows", 2000, *Appl. Rad. and Isotopes* **53** No. 4-5, 595-601.

5. G. A. Johansen and P. Jackson *Radioisotope gauges for industrial process measurements* John Wiley & Sons, Ltd. (2004) 336 pp.

6. S.-A. Tjugum, G. A. Johansen and J. Frieling "A multiple voxel model for scattered gamma radiation in pipe flow" *Meas. Sci. & Technol.* **14** No 10 (2003) 1777-1782.

7. S.-A. Tjugum, J. Frieling and G. A. Johansen "A compact low-energy multibeam gamma-ray densitometer for pipe-flow measurements" *Nucl. Instr. & Meth.* **B197** (2002) 301-309.

8. L. Ratnam *DMD experiments in a three phase flow loop* (in Norwegian) MSc thesis at the Department of Physics and Technology, University of Bergen (2006).

Wet Gas Metering Using Sonar-based Flow Meters and Piping Pressure Loss Gradients

Daniel L. Gysling – CiDRA Corporation
Douglas H. Loose – CiDRA Corporation
Nicolas Morlino – BP America, EPTG
Alex van der Spek - Zdoor, BV

---

1. ABSTRACT

Convenient and accurate measurement of gas and liquid rates of wet gas mixtures represents a long standing challenge within the oil and gas industry. Recently, sonar-based flow meters have been demonstrated to provide accurate measurement of the mixture flow rate of wet gas mixtures on a clamp-on basis. This paper describes an approach which combines sonar-based flow meters with the measured pressure drop across a section of pipe to provide gas and liquid flow rates. The approach leverages recognition that variations in the pressure gradient along a given section of pipe containing a wet gas mixture are primarily determined by the flow rate and liquid content of the mixture. In this approach, a sonar-based flow meter provides the mixture flow rate, and the measured pressure drop across a section of fixed geometry piping provides a basis to determine the liquid loading. The interpretation of the measured quantities in terms of gas and liquid flow rates is performed using either empirical data-based model or with the assistance of a multiphase flow model. The approach is of particular interest in applications in which pressure gradient measurements either exist, or can be installed without requiring a process shutdown. Two data sets are provided demonstrating the utility of this approach: 1) a laboratory test with data spanning range of flow rates and pressures with wetness levels predominately in range of 0 to 2.0 Liquid Gas Mass Ratio, and 2) a field test in which the measured produced gas and liquid rates from a wet gas well are compared to test separator measurement over a range of flow rates and wetnesses ranging from 0.08 to 0.15 Liquid to Gas Mass Ratio.

2. INTRODUCTION

Measuring wet gas flows is important for a wide range of upstream oil and gas measurement applications. While measuring dry gas flow rate is a well-served application for a wide range of gas flow metering technologies, accurate and cost-effective measurement of wet gas flow remains a long-standing multiphase flow measurement challenge for the upstream oil and gas industry. The paper is targeted at Type I and Type II wet gas mixtures [1] and, broadly speaking, applies primarily to gas continuous mixture with a relatively small amount of liquid by volume (~< 10%). It should be noted that there are many parameters defined in the wet gas literature to quantify the liquid loading or wetness of a wet gas mixture. In this paper, the liquid to gas mass ratio is the predominate parameter used to quantify wetness. For a more in depth discussion of wet gas terminology, the reader is referred to a recent discussion paper on the subject [2].

Sonar-based flow measurement leverages sonar array processing technology to determine the speed at which coherent flow patterns convect past an array of strain-based sensors attached to the pipe. These naturally-generated, coherent flow patterns exist in virtually all types of industrial fluid flows, allowing sonar-based flow measurement to be broadly applicable to a wide range of single and multiphase flows. The sonar-based flow measurement technique was developed in 1998 for use in the upstream oil and gas industry and was the flow measurement principle used in the world's first downhole, fiber-optic flow meter on the Mars platform in 2000 [3]. Since then, sonar-based flow measurement has evolved to include clamp-on versions and has been applied to a wide range of single and multiphase flow applications [4].

Sonar-based flow measurement is well-suited to measure volumetric flow rate of wet gas mixtures. For well-mixed wet gas mixtures, Sonar-based flow meters have been shown to accurately measure the mixture flow rate, relatively independent of the liquid loading.

The relative insensitivity of sonar-based flow meters to liquid loading can be contrasted to the response of flow meters based on correlating the differential pressure (DP) created by flow through a cross-sectional area restriction, such as venturis, orifice plates and cone devices. An approach, termed DP plus SONAR is described in [5] in which and approach is developed which measures wet gas flows by leveraging this dissimilar response of sonar-based and differential pressure-based to liquid loading.

The approach developed in this paper is similar to the one described by [5], however, the differential pressure measurement is measured across an existing section of fixed geometry piping rather than a discrete flow restriction. Conceptually, the pressure losses through either a discrete flow constriction or a distributed section of piping will scale with the liquid loading of the wet gas mixture. Due to the complex nature of multiphase flows in piping networks, interpreting changes in pressure drop across a distributed section of piping in terms of liquid loading has the potential to be significantly more complicated than correlating increases in pressure loss with liquid loading through a discrete device. Thus, this paper presents two methodologies to perform this interpretation. The first employs a relatively simplistic empirical correlation between pressure drop and liquid loading, and the second employs an iterative process employing a mechanistic multiphase flow model.

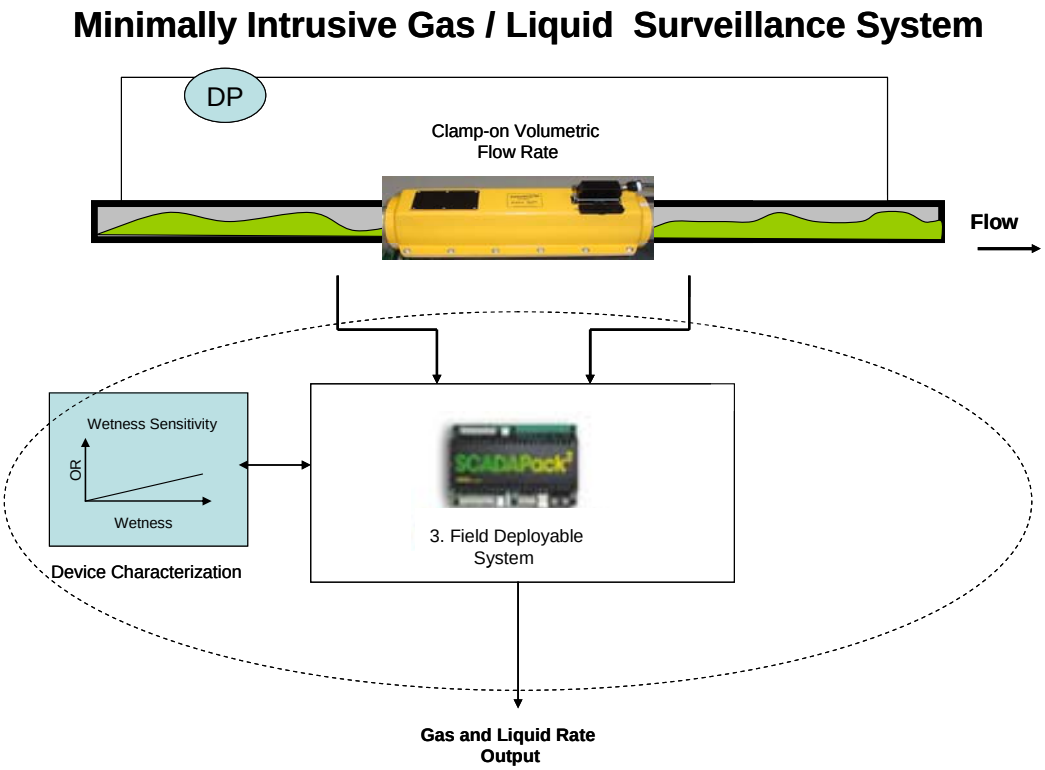

Figure 1: Schematic of DPDX plus SONAR approach for Wet Gas Measurement

2.1 Scope

The scope of this paper is limited to evaluating the practicality of measuring gas and liquid rates of wet gas flows by interpreting the measured flow rate from a sonar-based flow meter and a measure of the two-phase pressure gradient with a section of fixed geometry piping. It is

stipulated that the quantitative accuracy of this approach will, in general, be a function the specific application and the details of the empirical flow correlations and/or multiphase flow models used in defining the wetness sensitivity of both the pressure gradient measurement and the sonar-based flow measurement. It is beyond the scope of this paper to provide a critical evaluation of the various multiphase flow models that could be employed in this approach. Rather, the objective of this paper is to illustrate, using two approaches on two different data sets, the extent to which the output of such models can provide a means for measuring the gas and liquid rates of wet gas flow.

3.0 THEORETICAL DEVEOPLEMENT

The proposed approach, termed DPDX plus SONAR, determines the gas and liquid rate by measuring the mixture flow rate and the pressure drop across a given section of piping. The approach is shown schematically in Figure 1. The accuracy with which the measured quantities can be interpreted to determine gas and liquid flow rate will be a function of many multiphase flow parameters including the sophistication of the empirical correlations and / or multiphase models used in the interpretation.

3.1 Homogeneous Flow Model

Recognizing that a homogeneous multiphase flow model will likely be overly simplistic to provide the accuracy requirement for a majority of applications, it is present here since it does provide a useful first principles illustration of the DPDX plus SONAR concept for wet gas measurement.

One of the key aspects of the DPDX plus SONAR approach is that for well mixed flows sonar-based flow meters provide a flow rate that closely tracks the volumetrically averaged flow velocity of the wet gas mixture. Thus, the flow velocity reported by the sonar-based flow meter (VSONAR) can be related to the superficial gas velocity, the gas and liquid densities, and the liquid-to-gas mass ratio (LGMR) as follows.

$$V_{SONAR} = V_{mix} = V_{S_{liq}} + V_{S_{gas}} = V_{S_{gas}}(1+\frac{V_{S_{liq}}}{V_{S_{gas}}}) = V_{S_{gas}}(1+\frac{\rho_{gas}}{\rho_{liq}}\frac{\rho_{liq}V_{S_{liq}}}{\rho_{gas}V_{S_{gas}}}) = V_{S_{gas}}(1+\frac{\rho_{gas}}{\rho_{liq}}LGMR) \quad (1)$$

Where V_{mix} is the volumetrically averaged mixture flow velocity, Vs_{liq} and Vs_{gas} are the superficial velocities of liquid and gas phases and ρ_{gas} and ρ_{liq} are the gas and liquid densities. The superficial velocity of the phase of fluid (gas or liquid) is the volumetrically averaged flow that would exist if only that phase were present. The volumetric flow (Q) a given phase of fluid is given by the superficial velocity times the cross sectional area of the pipe.

Treating the well mixed flow as single phase flow, the pressure loss, ΔP, across a section of pipe of length(L) gradient can be related to the flow rate using the Darcy-Weisbach equation [6].

$$\Delta P = \left(\frac{dP}{dx}\right)L = f * \left(\frac{L}{D}\right) * \left(\frac{1}{2}\rho_{mix}V_{mix}^2\right) \quad (2)$$

Where f is the friction factor and D is the diameter.

For well mixed flows, we can define the following relationships:

$$\rho_{mix} = \rho_{gas} * GVF + \rho_{liq}(1-GVF) \quad (3)$$

$$V_{mix} = V_{S_{liq}} + V_{S_{gas}} \quad (4)$$

$$LGMR = \frac{\rho_{liq}V_{S_{liq}}}{\rho_{gas}V_{S_{gas}}} = \frac{\rho_{liq}}{\rho_{gas}}(\frac{1-GVF}{GVF}) = sqrt(\frac{\rho_{liq}}{\rho_{gas}})X \quad (5)$$

Where GVF is the gas volume fraction, Vs is the superficial velocity, and LGMR is the liquid to gas ratio, and X is the Lockhardt-Martinelli Number [2].

Using these relationships, the pressure drop across a section of pipe of length L can be expressed as follows

$$\Delta P_{1,2} = f\left(\frac{L}{D}\right)\left(\frac{1}{2}\rho_{gas}V_{gas}^2\right)\left(1+\left(1+\frac{\rho_{gas}}{\rho_{liq}}\right)LGMR+\frac{\rho_{gas}}{\rho_{liq}}LGMR^2\right) \qquad (6)$$

Generalizing for a fixed geometry piping without any elevation change and normalizing the pressure drop by the superficial dynamic head of the gas flow ($q_{gas}=\rho_{gas}V^2_{gas}/2$), the pressure drop can be expressed as follows:

$$\Delta\tilde{P} = \frac{\Delta P}{q_{gas}} = f\left(\frac{L}{D}\right)\left(1+\left(1+\frac{\rho_{gas}}{\rho_{liq}}\right)LGMR+\frac{\rho_{gas}}{\rho_{liq}}LGMR^2\right) \qquad (7)$$

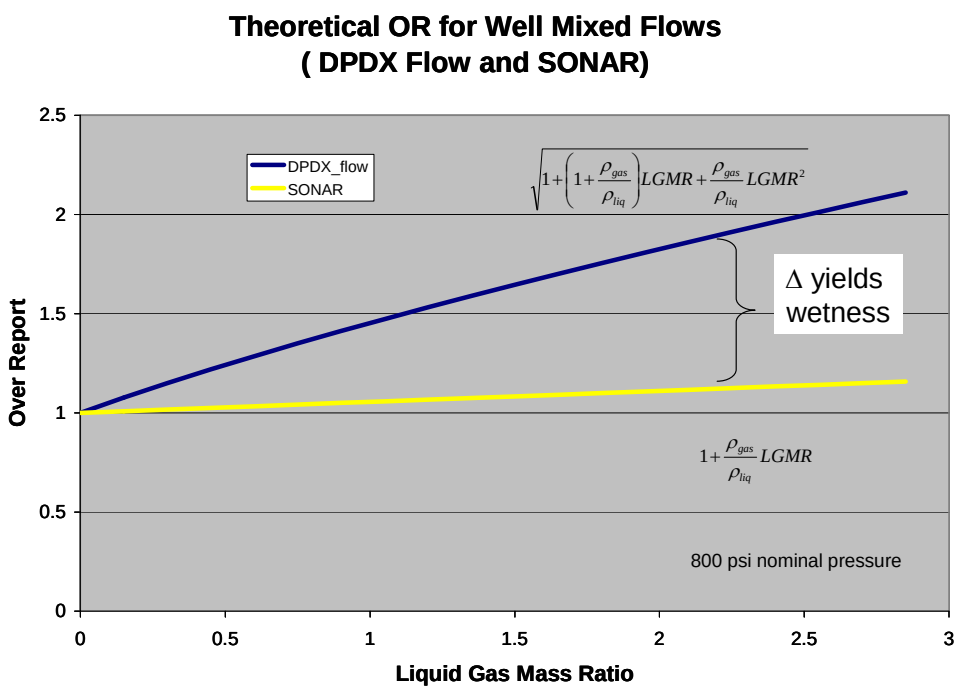

Figure 2: Theoretical Flow Rate Over Report as Function of Liquid to Gas Mass Ratio for Flow line differential pressure and sonar-based Flow meters in well mixed flows

The equation derived above for well mixed flow illustrates the impact that wetness, expressed as liquid to gas mass ratio, has on the normalized pressure drop between two locations. In this simplified model, a wet gas flow gas and liquid properties and fixed flow line geometry, the normalized pressure loss across a given section of piping provides a means to measure the liquid loading. Defining the over-report (OR)of a measuring device as the ratio of the flow rate reported in wet gas to the flow rate that would be reported with only the gas phase present, the wetness sensitivity of the two dissimilar measurements to the flow rate can be expressed as follows:

$$OR_{DPDX} = \sqrt{1 + \left(1 + \frac{\rho_{gas}}{\rho_{liq}}\right) LGMR + \frac{\rho_{gas}}{\rho_{liq}} LGMR^2} \qquad (8)$$

$$OR_{SONAR} = 1 + \frac{\rho_{gas}}{\rho_{liq}} LGMR \qquad (9)$$

The DPDX plus SONAR method for wet gas measurement is shown schematically in Figure 2 for a gas to liquid density ratio of 0.055. As depicted in Figure 2, DPDX plus SONAR is conceptually similar to DP plus SONAR described in [5].

4.0 FLOW LOOP TESTING

A flow loop test was conducted in February 2007 at the Colorado Engineering Experimental Station, Inc (Ceesi) designed to 1) evaluate the relationship between pressure loss and flow rate for wet gas mixtures in a straight, horizontal section of pipe and to 2) assess the practicality of using this approach for gas and liquid rate measurement. The differential pressure over an 86 foot and 8 inch (26.4 meters) section of 4 inch, schedule 80, pipe (273.5 L/D) was measured over a range of wet gas flow conditions as shown in Figure 3. The tests were conducted using natural gas (mostly methane) and Stoddard fluid (mostly decane) for the gas and liquid phases, respectively.

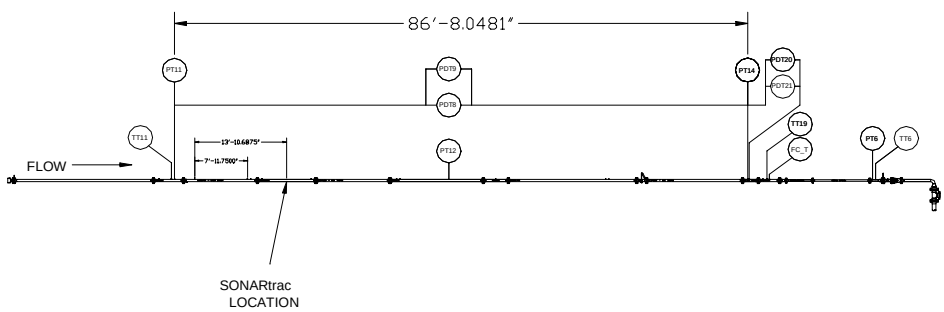

Figure 3: Piping Layout for Flow line Differential pressure and SONAR-based flow measurement test

4.1 RESULTS

The test results are summarized in Table 1. The tests were conducted predominately over a range of wetnesses from 0.0 to 2.0 LGMR, mixture velocities of 20 to 80 ft/sec and pressures of 300 psia and 800 psia.

Table 1: Results for DPDX plus SONAR Flow Loop testing

Test ID Number:	Pressure psia	Gas Superficial Velocity ft/sec	Liquid Superficial Velocity ft/sec	Gas density (kg/m^3)	Liquid Density (kg/m^3)	Froude Number (gas)	Lockhart-Martinelli Parameter	LGMR	SONAR trac Velocity (ft/sec)	SONAR OR	DP (psi)	DP/q	DP /q OR
18	299	51.73	0.00	14.7			0.00	0.00	51.91	1.00	1.032	3.902	1.000
11	308	50.52	1.66	15.1	756.3	2.26	0.23	1.64	53.48	1.04	3.505	13.532	3.468
12	306	51.18	1.26	14.9	755.7	2.27	0.18	1.24	53.34	1.03	3.104	11.784	3.020
13	303	51.56	0.80	14.8	755.6	2.28	0.11	0.79	53.15	1.02	2.516	9.492	2.432
14	300	50.88	0.39	14.7	755.3	2.24	0.06	0.40	42.55	0.83	1.941	7.581	1.943
15	299	51.60	0.25	14.6	755.3	2.27	0.03	0.25	53.37	1.03	1.809	6.896	1.767
16	298	50.94	0.16	14.6	755.3	2.24	0.02	0.17	49.20	0.96	1.692	6.631	1.699
17	297	50.97	0.08	14.5	756.1	2.24	0.01	0.08	52.22	1.02	1.629	6.391	1.638
17.5	296	51.12	0.04	14.5	756.6	2.24	0.01	0.04	52.22	1.02	1.544	6.043	1.549
18.5	300	23.43	0.00	14.9			0.00	0.00	23.50	1.00	0.212	3.867	1.000
19	304	23.64	1.67	15.2	760.7	1.06	0.50	3.59	30.33	1.28	1.531	26.774	6.924
20	300	23.36	1.22	15.0	760.1	1.04	0.37	2.68	26.55	1.13	0.913	16.524	4.273
21	299	23.48	0.80	14.9	759.9	1.04	0.24	1.76	10.04	0.43	0.664	11.983	3.099
22	297	22.94	0.42	14.8	760.1	1.01	0.13	0.96	22.84	0.99	0.444	8.465	2.189
23	296	22.98	0.25	14.7	760.6	1.01	0.08	0.56	22.40	0.97	0.377	7.202	1.863
24	295	23.11	0.16	14.6	761.2	1.01	0.05	0.37	22.20	0.96	0.344	6.525	1.687
25	294	23.17	0.08	14.6	761.7	1.01	0.03	0.19	22.40	0.97	0.310	5.886	1.522
26	293	23.32	0.04	14.5	762.6	1.02	0.01	0.10	22.60	0.97	0.288	5.410	1.399
27	291	23.28	0.00	14.4			0.00	0.00	23.00	0.99	0.204	3.875	1.002
40	808	77.90	0.00	41.6			0.00	0.00	78.95	1.00	6.647	3.907	1.000
48	823	78.29	1.69	42.1	739.7	6.03	0.09	0.38	80.17	1.01	8.481	4.874	1.248
47	821	78.18	1.24	42.0	738.0	6.02	0.07	0.28	80.31	1.02	8.308	4.801	1.229
46	820	78.78	0.82	41.9	737.8	6.06	0.04	0.18	80.40	1.01	8.166	4.658	1.192
45	818	78.39	0.61	41.8	737.9	6.02	0.03	0.14	79.88	1.01	8.034	4.635	1.186
44	816	78.76	0.40	41.8	738.5	6.04	0.02	0.09	80.24	1.01	8.045	4.607	1.179
43	816	78.92	0.32	41.7	738.6	6.05	0.02	0.07	80.38	1.01	8.048	4.593	1.176
42	815	78.30	0.25	41.7	738.8	6.00	0.01	0.06	79.65	1.01	7.901	4.585	1.174
41	813	78.39	0.17	41.6	739.2	6.00	0.01	0.04	79.63	1.00	7.844	4.548	1.164
48.5	808	77.97	0.00	41.5			0.00	0.00	79.04	1.00	6.812	4.005	1.025
49	811	40.79	0.00	42.2			0.00	0.00	40.94	1.00	1.873	3.957	1.000
57	817	40.16	1.73	42.7	738.4	3.11	0.18	0.75	40.31	1.00	3.725	8.031	2.029
56	817	40.52	1.42	42.6	737.4	3.14	0.15	0.61	40.65	1.00	3.499	7.430	1.878
55	816	40.72	1.24	42.6	737.2	3.16	0.13	0.53	41.18	1.01	3.405	7.157	1.809
54	814	41.11	0.82	42.5	737.1	3.18	0.08	0.35	42.47	1.03	3.092	6.394	1.616
53	811	40.21	0.43	42.4	737.6	3.11	0.04	0.19	41.09	1.02	2.626	5.686	1.437
52	809	40.39	0.25	42.3	738.3	3.12	0.03	0.11	41.01	1.01	2.500	5.374	1.358
51	808	40.41	0.17	42.3	738.8	3.12	0.02	0.07	41.15	1.01	2.471	5.314	1.343
50	808	40.56	0.08	42.2	739.5	3.13	0.01	0.04	41.11	1.01	2.381	5.087	1.286
49.5	805	40.51	0.00	42.1			0.00	0.00	40.60	1.00	1.844	3.961	1.001
58	796	20.33	0.00	41.4			0.00	0.00	20.03	0.98	0.457	3.961	1.000
59	797	19.89	1.68	42.0	738.6	1.53	0.35	1.49	13.52	0.68	1.452	12.973	3.275
60	791	20.43	0.82	41.7	738.5	1.57	0.17	0.71	22.30	1.09	1.027	8.742	2.207
61	788	20.64	0.39	41.6	739.2	1.58	0.08	0.34	21.76	1.05	0.796	6.657	1.681
62	787	20.26	0.21	41.4	739.9	1.55	0.04	0.18	20.68	1.02	0.652	5.686	1.436
63	786	20.37	0.12	41.3	739.9	1.55	0.03	0.11	20.48	1.00	0.607	5.255	1.327
64	786	20.38	0.08	41.3	740.0	1.55	0.02	0.07	20.25	0.99	0.583	5.047	1.274
65	784	20.45	0.04	41.3	742.6	1.55	0.01	0.04	20.03	0.98	0.554	4.766	1.203
66	782	20.17	0.00	41.1			0.00	0.00	19.97	0.99	0.442	3.925	0.991

4.1.1 Pressure Loss as Function of Wetness

Figure 5 shows the pressure loss data normalized by the dry gas pressure loss as a function of wetness (LGMR) for each data set. The pressure ratio over report as predicted by the homogeneous model developed above is also shown. For the range of pressures and velocities tested the dry gas pressure drop was shown to be largely independent of flow rate and pressure and measured 3.9 dynamic heads, translating into a Darcy friction factor of 0.014. As shown in Figure 4, the pressure drop increased with liquid to gas mass ratio, increasing sharply with the introduction of the initial liquids, and then building more gradually with wetness. For liquid loadings beyond the onset of wetness (LGMR < 0.05%), the pressure drop is shown to increase in a reasonably linear manner with wetness for each Froude number. The densimetric Froude number is defined as the square root of the ratio of the superficial gas dynamic head to the

gravitation head generated associated with a column of liquid with height equal to the diameter of the pipe corrected for the buoyancy of the gas.

$$Fr \equiv \sqrt{\frac{\rho_{gas} V_{S_{gas}}^2}{(\rho_{liq} - \rho_{gas}) g D}} \qquad (10)$$

Where g is the acceleration of gravity.

As shown, the data and the simplified model demonstrate similar behavior. Given the complexity of the two phase flows over the parameter space investigated, the data does exhibit an encouraging level of parametric simplicity. Since the Froude number is the first order parameter influencing the mixedness of gas/liquid flows, it is reasonable that the Froude number would influence the wetness sensitivity of the two phase pressure gradient. The data set with the lowest wetness sensitivity corresponds to the highest Froude number.

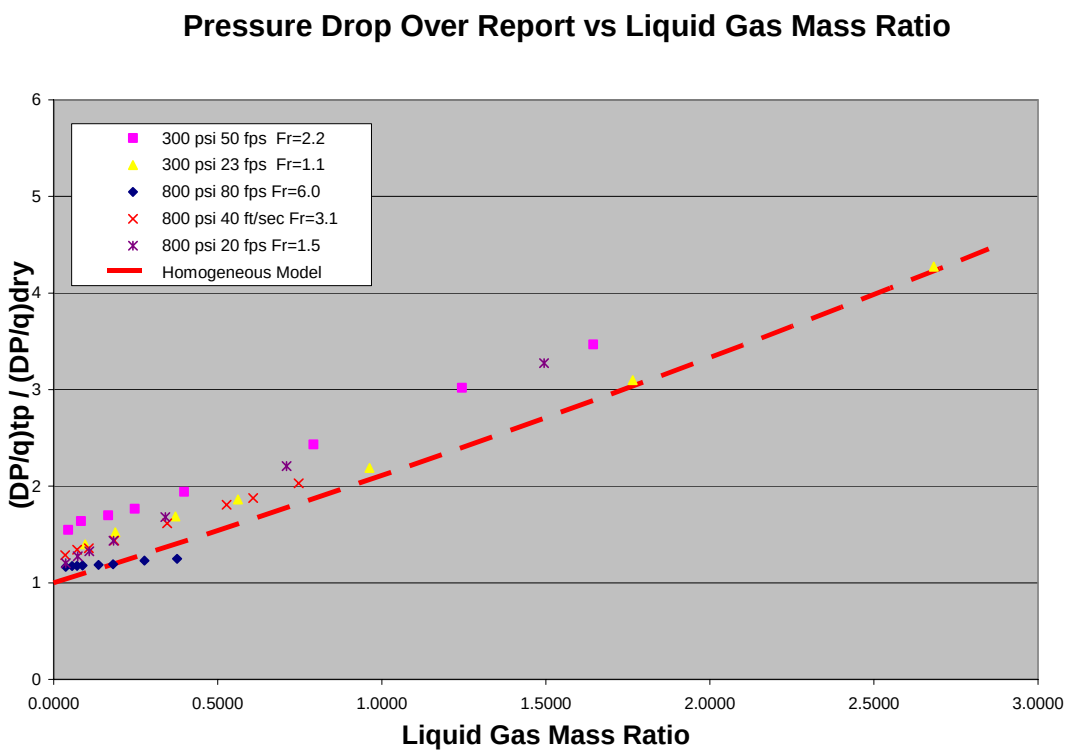

Figure 5: Over report of the Two Phase Pressure Loss over an 273.5 L/D section of pipe normalized by dry gas pressure loss as a function of wetness (LGMR) with Homogeneous Model

4.1.2 SONAR Flow Rate as Function of Wetness

For well mixed flows (i.e. wet gas flows with Fr >~2.0), the velocity reported by sonar-based flow meters have been shown to be relatively insensitive to wetness. Figure 5 shows the over-report, defined as the ratio between the reported flow velocity and the reference superficial gas velocity. The theoretical over report for well mixed flows, assuming that the SONAR meter reports the mixture velocity, is shown for reference for the two pressures. As shown, the data and theory are in relative good agreement for the higher Froude numbers. Specifically, the all the data points associated with Froude No. of 6.0 and 3.1 are within 5% of the well mixed model.

At lower Froude numbers, Fr<~2, gas / liquid flows tend to stratify and the interpretation of SONAR flow measurement is less well defined. Four data points for Froude numbers of 2.2 and lower exhibited anomalous behaviors associated with stratification and are shown as circled data points. These anomalies can often be "corrected" with advanced post-processing interpretation of SONAR meter diagnostic information, however, a detailed discussion of performance of the sonar- based flow meter for non-well-mixed flows is beyond the scope of this work.

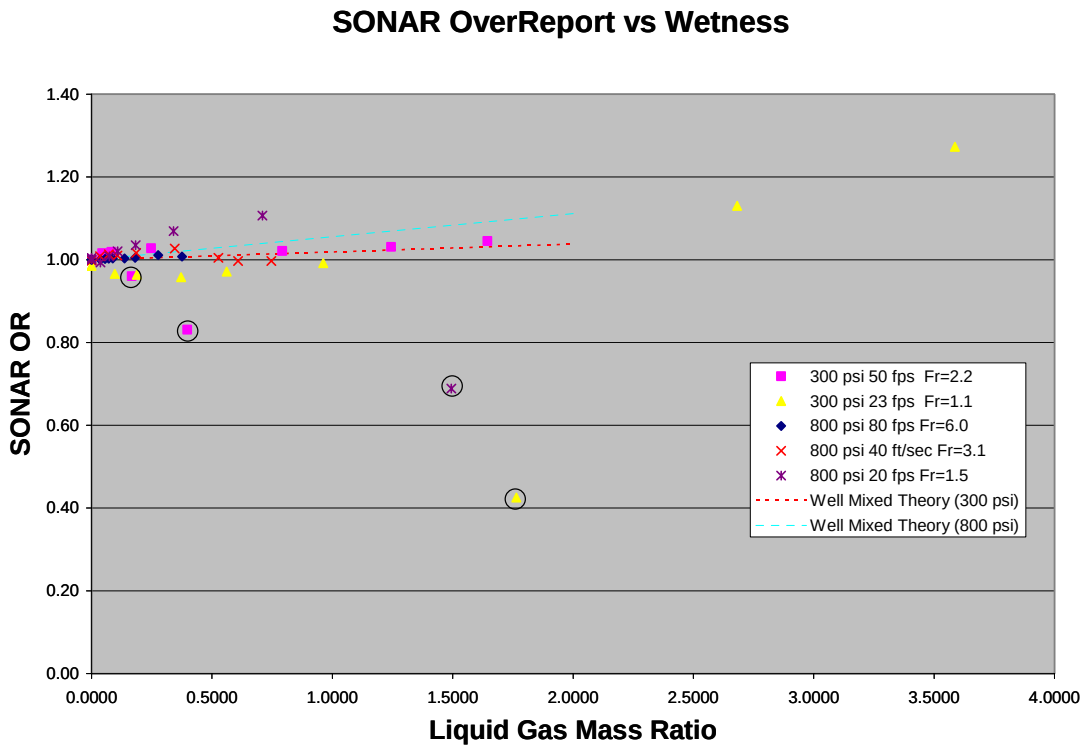

Figure 5: Over report of SONAR flow meter normalized by dry gas reading as a function of wetness (LGMR) with prediction from homogeneous flow model at two pressures

5.0 IMPLEMENTATION OF FLOW MEASURMENT METHODOLOGY

A goal of this work was to develop methods to measure the gas and liquid flow rates leveraging the dissimilar response of the SONAR meters and the axial pressure gradient to changes in liquid loading. In this paper we present two approaches to interpret the combined output of a sonar-based flow meter and the measured of the axial pressure gradient: 1) the first uses an empirical characterization of each device to measure wetness and, 2) the second uses an optimization algorithm in conjunction with a mechanistic multiphase flow model to provide a measure of the gas and liquid flow rates.

5.1 Empirical DPDX plus SONAR Methodology

As shown schematically in Figure 6, the wetness sensitivity of the differential pressure across the test section was fairly linear with increasing liquid to gas mass ratio, except for the initial onset of

wetness for LGMR < ~0.05. The wetness sensitivity of the pressure drop was parameterized assuming that the pressure loss increases linearly with liquid to gas mass ratio.

$$\frac{\Delta P}{\frac{1}{2}\rho_{gas} V_{S_{gas}}^2} = K^*_{DRY} + \beta * LGMR \qquad (11)$$

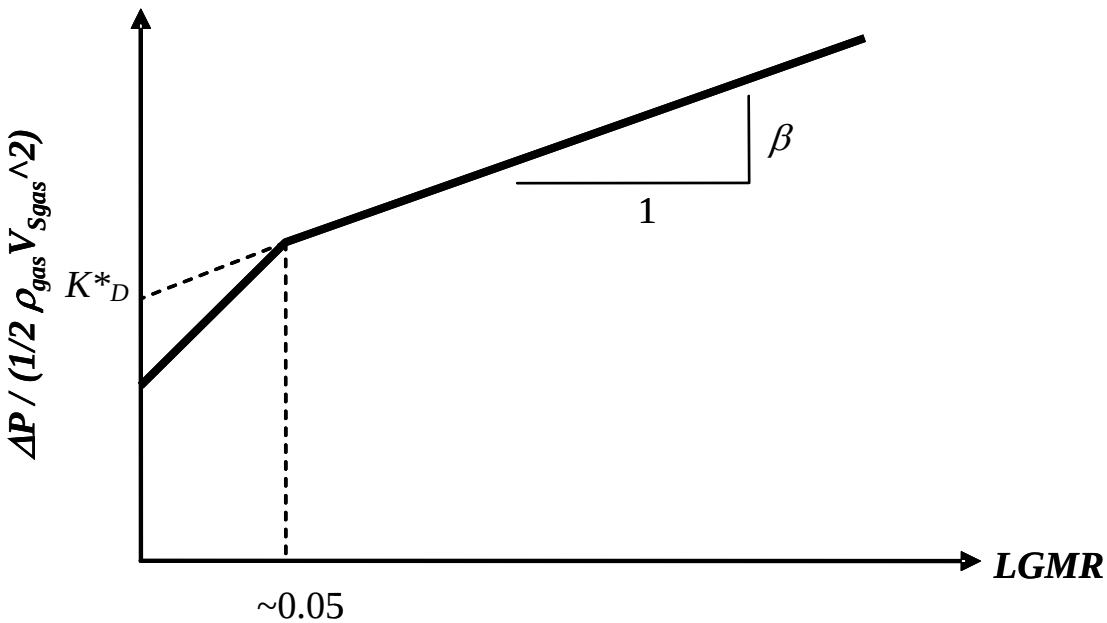

Figure 6: Schematic of the parametric model of the pressure loss as a function of wetness (LGMR) illustrating effective (psuedo) Dry Gas pressure drop

In this model, the wetness sensitivity is defined by a slope and offset, with the offset defining a pseudo dry gas pressure loss coefficient. These wetness sensitivity parameters were determined using a linear curve fit of the pressure loss data as a function of wetness for each data set of constant pressure and velocity (Froude number), excluding the dry gas pressure point. The wetness sensitivity parameters for the straight pipe test section determined in this manner are tabulated in Table 2.

Table 2 Wetness Sensitivity Parameters for 86 ft Section of 4 inch, Schedule 80 pipe

Pressure (psi)	Velocity (ft/sec)	Froude Number	Density Ratio	Kdry*	Beta
300	51	2.1	0.02	5.83	4.7
300	23	1.1	0.02	4.86	4.27
800	79	6	0.056	4.4	0.949
800	40	3.1	0.056	4.96	4.11
800	20	1.5	0.056	4.66	5.61

The wetness sensitivity of the sonar-based flow meter is parametrically assumed to increase with alpha times the liquid to gas mass ratio. For the well mixed model, alpha is equal to the ratio of gas and liquid densities as shown below.

$$\frac{V_{SONAR}}{V_{S_{gas}}} = 1 + \alpha LGMR = 1 + \frac{\rho_{gas}}{\rho_{liq}} LGMR \qquad (12)$$

The expressions for theoretical over-report for the SONAR meter and the empirical over-report of the pressure gradient can be solved to determine the LGMR consistent with a measured pressure loss and SONAR velocity and a given set of wetness sensitivity parameters (Kdry, and Beta, and Alpha). Identifying the LGMR enables the determination of the gas and liquid rates from the SONAR flow measurement.

$$V_{S_{gas}} = \frac{V_{SONAR}}{1 + \left(\frac{\rho_G}{\rho_L}\right) LGMR} \qquad (13)$$

$$Vs_{lig} = V_{S_{gas}} \left(\frac{\rho_G}{\rho_L}\right) LGMR \qquad (14)$$

The gas and liquid volumetric flow rates are then determined by multiplying the superficial flow velocities times the cross section area of the pipe. The interpreted gas and liquid flow rates are shown versus reference in Figures 7 and 8.

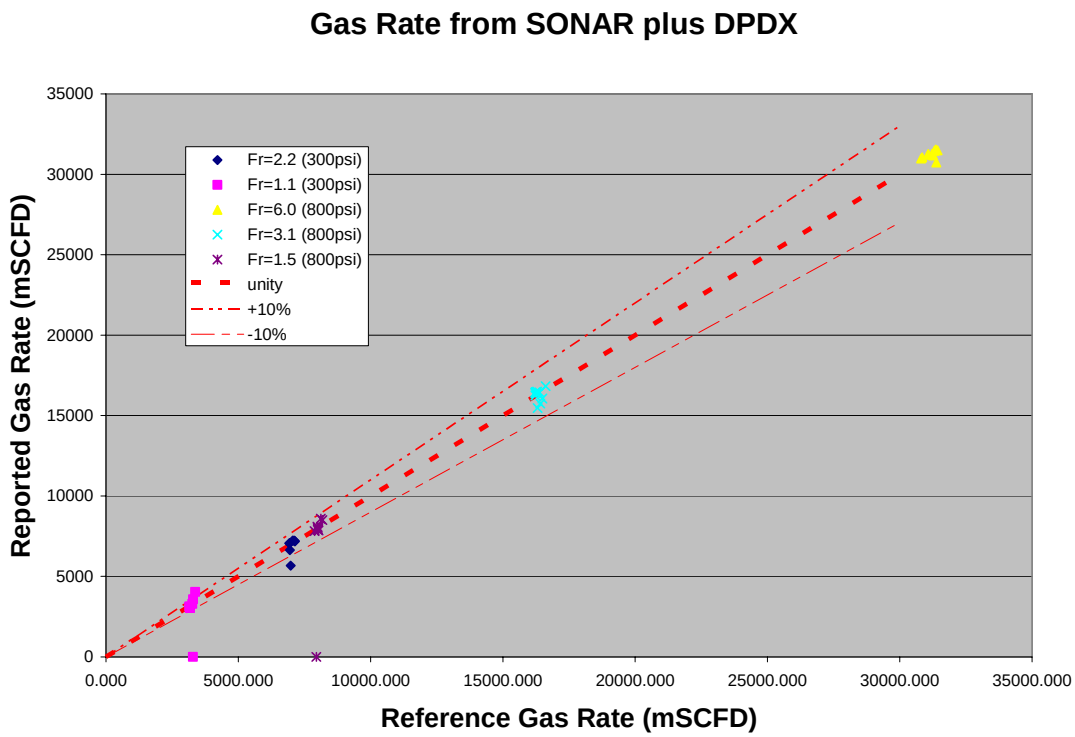

Figure 7: Gas Rate reported by DPDX plus SONAR System versus reference

As shown, the DPDX plus SONAR approach reported the majority of the gas flow rates within 5% of reference and the Majority of the Liquid Flow rates to within +/- 20% of reference.

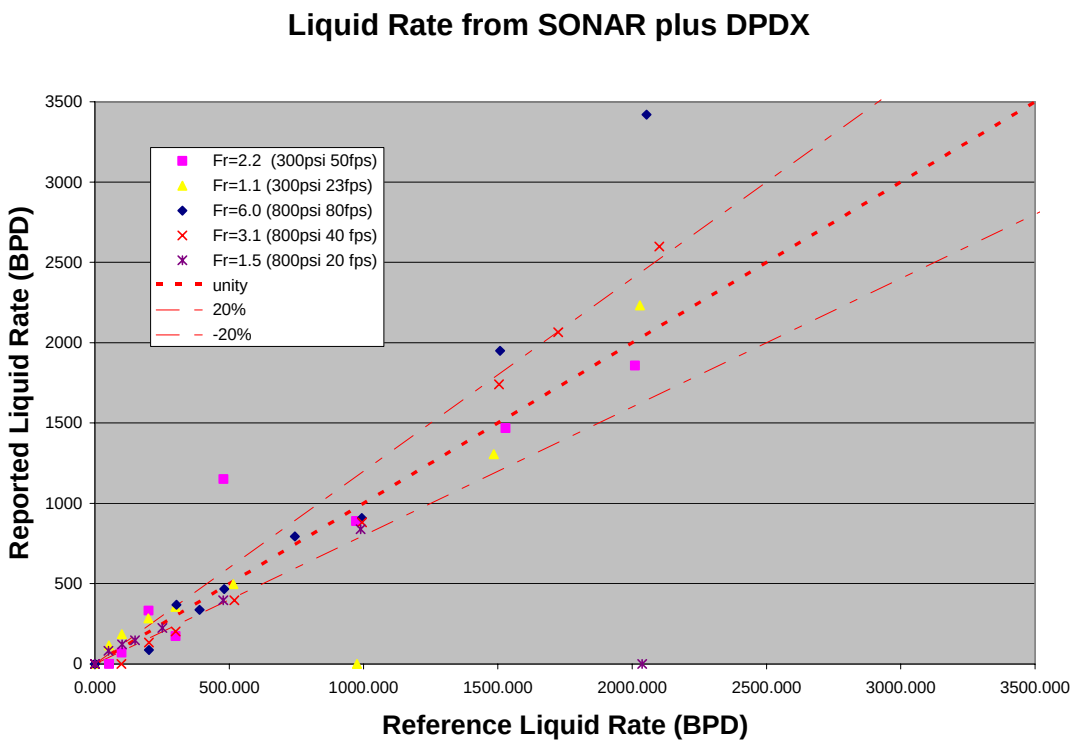

Figure 8: Liquid Rate reported by DPDX plus SONAR System versus Reference

5.2 Mechanistic DPDX plus SONAR

The empirical method described will in general require in-field calibration and will be applicable over a limited range of flow parameters. An alternative approach is to interpret the pressure loss across a section of pipe and the SONAR flow measurement using and optimization procedure and a mechanistic multiphase flow model. Most flow model operating in this forward fashion in which the input gas and liquid rates are specified and the model then computes the various flow parameters such as liquid hold-up, pressure drop and flow regime information. In this work, a mechanistic two fluid flow model described in [7] was used to compute two phase flow characteristics such as the liquid holdup and the pressure gradient associated with a specified input liquid and gas flow rates. For DPDX plus SONAR approach, the problem is inverted in that the flow rate and pressure gradient are measured and the input gas and liquid flow rates need to be determined. To accomplish this inversion, an optimization procedure was developed in which the input liquid and gas rates are determined by minimizing the error between measured and calculated flow parameters. A flow chart of the optimization procedure is shown in Figure 10.

In the mechanistic DPDX plus SONAR approach, the SONAR meter was assume to measure the actual gas velocity, whereas, in the empirical version, the SONAR meter was assumed to measure the mixture velocity of a well mixed flow. The importance of the distinction scales with the degree of stratification, a parameter that the empirical interpretation does not consider.

Flow Model Assisted Interpretation of DPX and SONAR

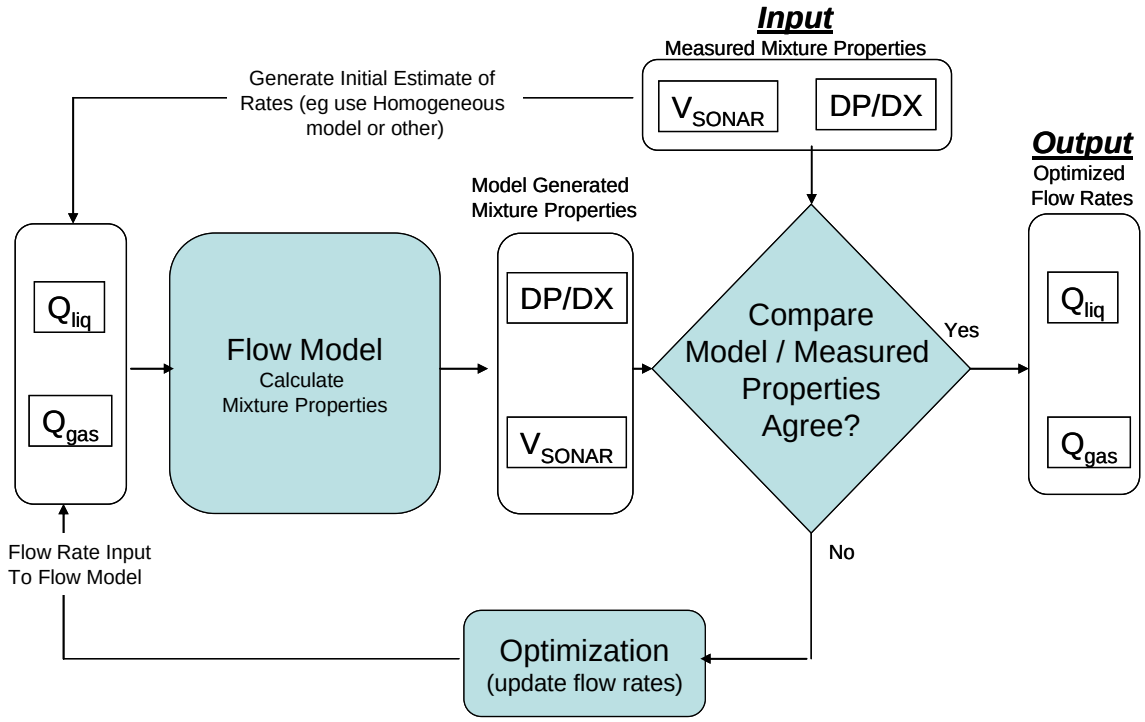

Figure 9: Flow Chart of the Multiphase Flow Model Assisted Interpretation Procedure

To assess the effectiveness of determining gas and liquid flow rates using the approach, the model was exercised to evaluate the characteristics of the optimization process used to determine the gas and liquid rates.

The optimization procedure is based on minimization of an error term that represents the difference between the calculated pressure gradient and gas velocity for a given gas and liquid flow rate and the measured values. This error function, termed chi-squared, is defined below. As defined, the chi-squared function is minimized at 0 when the measured flow rate and pressure gradient are equal to the calculated flow and pressure gradient, respectively.

$$\chi^2(Vs_{liq}, Vs_{gas}) = \left(\frac{V_{SONAR} - Vg_c}{V_{SONAR} + Vg_c}\right)^2 + \left(\frac{(dp/dx)_m - (dp/dx)_c}{(dp/dx)_m + (dp/dx)_c}\right)^2 \qquad (15)$$

Where m and c indicate measured and calculated values respectively.

Figure 10 shows contour plots of the chi-square error function for two representative cases, one with high liquid loading and another with low liquid loading. The right hand panel (TagID 03-2), is a 2-inch schedule 80 pipe at high Froude Number (Fr=8.3) and relatively high liquid loading. The actual gas rate is 260 m3/h (Vs_{gas} = 39.0 m/s) and liquid rate is 8 m3/h (Vs_{lig} = 1.20 m/s) corresponding to a liquid gas mass ratio of 1.5 and a Lockhardt-Martinelli No of 0.21. The left hand panel (TagID 02-2) is also in a 2-inch schedule 80 pipe with a slightly lower Froude Number (Fr=6.3) and a significantly lower liquid loading. The actual gas rate is 205 m3/h (Vs_{gas}= 30.9 m/s) and liquid rate is 0.5 m3/h (Vs_{liq}= 0.08 m/s) corresponding to a liquid gas mass ratio of 0.13 and a Lockhardt-Martinelli No of 0.02. As shown, the chi-squared function exhibits a well defined

minimum located at the bottom of a long extended valley that turns toward the Vs_{lig} axis as higher superficial liquid velocities. The overlaid reference, measurement and endpoint do not coincide with the minimum since the simulated pressure gradients do not exactly coincide with the measured gradients. The objective of this section is more to provide qualitative insight into the behavior of the chi-squared function of equation (15) rather than provide a quantitative comparison between the flow model and the flow loop data.

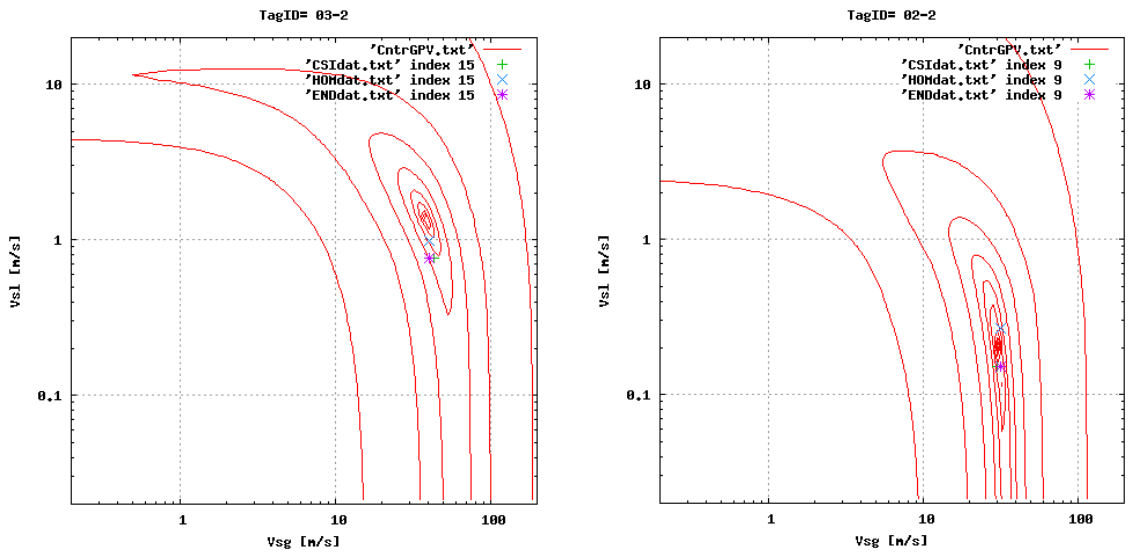

Figure 10: Contour plot for SONAR/DPDX type measurement.

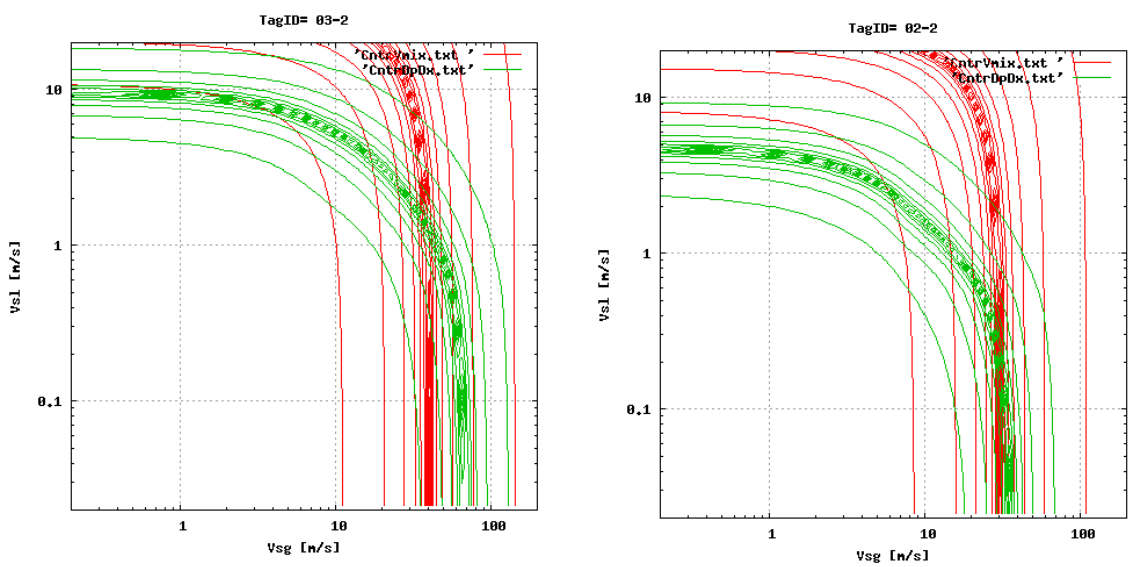

Figure 11: Component of chi square error function Separate contours for sonar (red) and dpdx (green)

The behavior of the chi-squared function of equation (15) can further be examined by considering the topology of its two error terms separately as shown in Figure 11. The right half applies to the relatively high liquid loading case and the left half applies to the lower liquid loading case. The red contours are associated to the velocity term; the green contours are associated with the pressure gradient term. As shown, the red and green contours are close to being parallel over a large part of the area of interest. This causes the long valley in the chi-squared function. The error term associated with measured velocity is relatively insensitivity to liquid loading for liquid volume fraction below roughly 10%. The error term associated with the pressure gradient is significantly

more influence by the liquid loading, with the intersection of the green and red minima combining to determine the gas and liquid rates.

Around a Vs_{lig} equal to 1 m/s the two sets of contours finally intersect which produces the sought for minimum It is to be expected that for conditions at lower values of Vs_{lig}, the point of intersection for the two contour sets will be less well defined. At lower values of Vs_{lig}, the red and green contours will be less "offset" from each other at the Vs_{gas} axis leading to a much more drawn out minimum. The right hand panels in Figure 11 demonstrate this for the case of test point with a Vs_{lig} = 0.08 m/s.

5.2.1 Interpretation of Flow Loop Data using Mechanistic DPDX plus SONAR

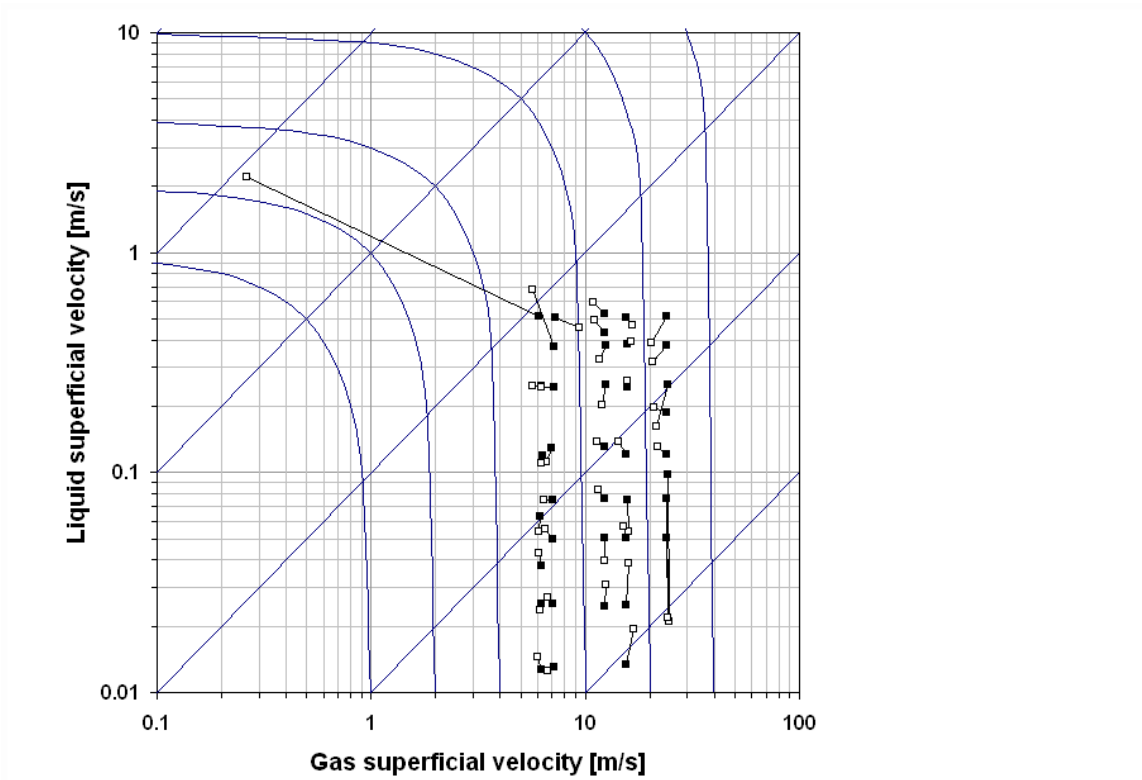

Figure 12: Two Phase flow map showing Reference data (closed symbols) and Measured Data (Open Symbols) Using the Mechanistic Flow Model Interpretation of the DPDX plus SONAR Flow Loop Data

The result of the flow model assisted interpretation of the SONAR plus DPDX data recorded in the flow loop test described above are shown in Figure 12. In calculating the results, the mechanistic flow model was run with the following assumptions.

- Entrainment factor [8] for the calculations was assumed to be zero. Calculations show that the entrainment is very low in virtually all conditions. This is consistent with the relatively low velocities in 4".
- Roughness, surface tension and gas/liquid viscosity set to give best match on pressure drop for the first 6 dry gas points.
- Flow patterns calculated. In total 3 of the two phase points are stratified. At such low superficial liquid/gas velocities, the stratified/annular transition is extremely sensitive to the pipe inclination. An exact value of 0° (horizontal) was used.

In the above flow map, the straight lines represent constant input phase fraction and the curved reference lines represent constant input mixture flow velocity. Each flow loop set point is plotted with a solid symbol, the open symbols of the interpreted results. The line connecting the reference point to the interpreted value is a measure of the error in the measurement, with each grid line representing a 10% relative error. As shown, the flow loop interpreted SONAR plus DPDX data is in reasonable agreement with the reference data. The largest errors in gas rate occur at the highest liquid loadings and the lowest superficial gas velocities. Relatively large errors in liquid rate are also exhibited at the high gas rate, low liquid loading. Errors in the region can likely be attributed in part to the zero entrainment assumption in the multiphase flow model.

6.0 Well Test Data

The empirical DPDX plus SONAR approach was evaluated through field testing on a wet gas well in November 2006. A 4-inch SONARtrac VF-100 meter manufactured by CiDRA Corporation was installed between the well-head and the test separator. The pressure drop used for the DPDX plus SONAR calculations was measured using a pressure gauge installed at the same location as the SONAR meter near the well head and a pressure gauge located near a well test separator, approximately 2000 ft away. The majority of the flow line between the two locations was 6-inch, horizontal flow lines, with short section of vertical pipe and the associated elbows.

In processing the data, it was assumed that the watercut was relatively constant so the liquid density was fixed. The gas density will vary with pressure, temperature and composition and therefore must be calculated for each point. To simplify the gas density calculation it was assumed that the gas composition was constant and that small changes in barometric pressure are insignificant so gas density changes only with line pressure and temperature.

Several well tests were conducted so that the DPDX plus SONAR results could be compared to the test separator reference. The operating condition of the well under test was changed by choking back the well. The change in flow rate caused a change in the produced gas to liquid ratio, with the liquid to gas mass ratio decreasing with decreasing flow rate.

Table 2: Well Test Data Using Empirical DPDX plus SONAR

Well Test Results	Test1	Test 2	Test 3	Test 4	Test 5
Well Test Ref Gas Rate (mmscfd)	31.2	19.9	27.5	39.3	36.3
Well Test Liquid Rate, calculated (bpd)	685	350	620	1015	873
Well Test LGMR	0.11	0.09	0.11	0.13	0.12
Densimetric Froude (4 in)	6.4	4.3	5.8	8.0	6.6
Average DP / Dynamic Pressure	33.8	32.4	34.0	35.1	34.0
Average Gas Density (kg/m3)	54.0	52.0	53.1	56.4	67.9
SONAR Gas Rate (mmscfd)	31.0	20.3	27.8	39.1	35.4
Deviation	-0.6%	2.4%	1.2%	-0.6%	-2.5%
SONAR Plus DP Liquid Rate (bpd)	684	360	631	1030	822
Deviation	-0.1%	3.1%	1.9%	1.5%	-5.8%

The constants K_D* and beta are defined as the offset and slope of the pressure drop versus LGMR relationship for LGMR greater then 0.05 (see Figure 6). Both of these constants were calculated from the data to provide a best-fit between the DPDX plus SONAR and the test separator results, resulting in 26.99 and 62.34, respectively. Note that effective Dry gas pressure loss through the pipe network in the field data of ~27 gas dynamic heads is approximately 7 times the dry gas dynamic pressure loss measured in the flow loop data, consistent with the longer and more complicated flow path associated with the well test pressure loss. It should also be noted that due to constraints in the amount of field data available, the pressure gradient as a function of LGMR was assumed to behave linearly with liquid to gas mass ratio even though the Froude number for each test point varied.

The results of the well testing are summarized in Table 2 below. Note that the gas rates are better than ±3% and the liquid rates better than ±6%.

The well E-06 testing demonstrated that the DPDX plus SONAR approach could accurately measure both the gas and liquid flow rates (and therefore gas-liquid ratio, GLR) for liquid-to-gas mass ratios greater than approximately 0.05.

The Froude Number indicated in Table 3 is the densimetric Froude Number in the 4 inch Schedule 80 line and is the relevant number for assessing the wetness sensitivity of the SONAR-based flow meter. However, since the majority of the flow line length was 6 inch, schedule 80, the relevant Froude number for characterizing the pressure gradient should based on the Froude Number in the 6-inch flow lines, which is approximately one half of the Froude number in the 4 inch lines.

The flow conditions in the well were varied by changing the choke position, resulting in the produced liquid to gas mass ratio varying with flow rate. As such the data represents Froude numbers in the 6 inch sections ranging from ~2 at the lowest LGMR to ~4 at the highest LGMR, reasonable consistent with the flow data discussed above.

Figure 13 shows the well test data flow over report (square root of the pseudo-dry gas normalized two phase pressure drop) plotted versus liquid to gas mass ratio. The theoretical over-report predicted by the simplified homogenous flow model for both pressure loss and the SONAR meters are also included. Data from the flow loop test at a pressure= 800 psi and Fr=3.1, normalized by the pseudo-dry gas pressure loss is also shown. As shown, the well test data and the flow loop data at similar conditions each follow the trend predicted by the simplistic model, providing a good first-principles confirmation DPDX plus SONAR measurement approach.

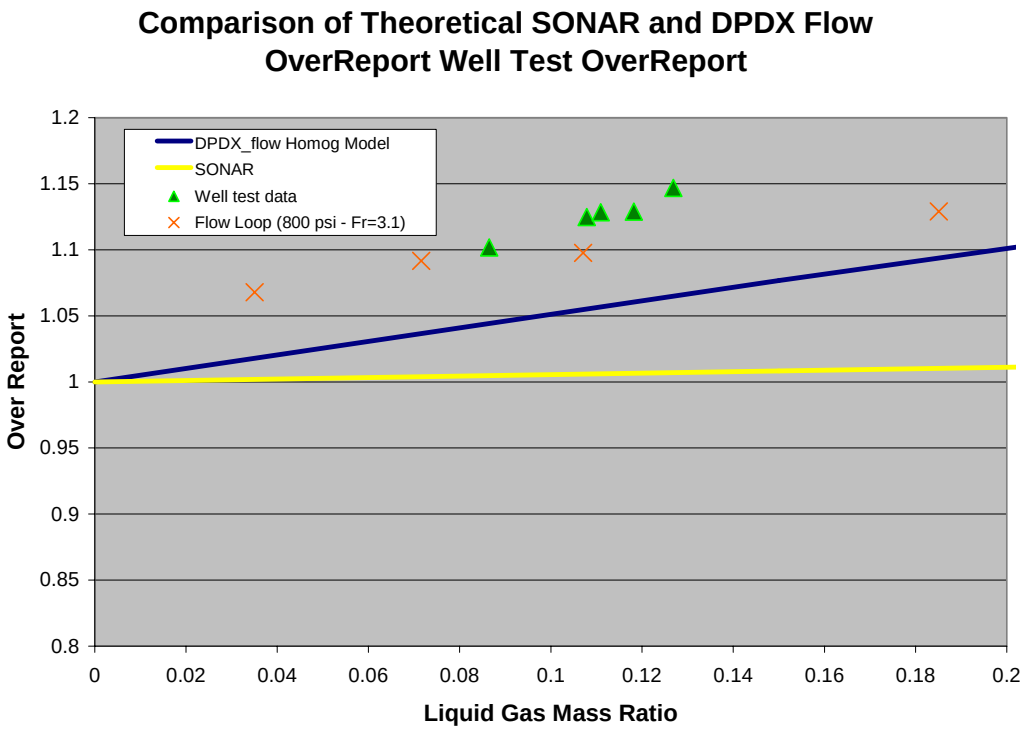

Figure 13: Flow rate Over Report as a Function of Wetness comparing the Flow Over report for the Homogenous flow model, SONAR flow meter, Flow Loop and Well test data

6.0 CONCLUSIONS

This paper demonstrates a minimally intrusive approach to measuring the gas and liquid rates of wet gas mixture using the combination of a clamp-on, sonar-based flow meter and a measurement of the pressure gradient over a given section of piping network. A key advantage of this approach is the ability to provide a gas and liquid measurement on a minimally intrusive basis.

Two approaches were demonstrated; one based on an empirical characterization of the wetness sensitivity a piping network with fixed geometry and another approach which used an optimization procedure in conjunction with a mechanistic two-phase flow model to interpret the measured pressure gradient and SONAR flow measurement in terms of gas and liquid rates of wet gases. Wet gas flow loop data was presented for the pressure loss over a straight section of pipe and the output of the SONAR meter over a range of flow conditions. The gas and liquid rates determine using both the empirical method and the Multiphase Flow model assisted interpretation were presented versus reference rate. The DPDX plus SONAR method was also applied to well test data using and empirical correlation of pressure loss versus wetness defined from test separator data. For the well test data, the piping network over which the pressure drop data was recorded was significantly longer and more complicated than the straight test section from the flow loop, yet demonstrated similar non-dimensional sensitivity to wetness.
The accuracy of either of these methods will be dependent on many application specific parameters, include the flow and fluid properties and the sophistication of the model used for interpretation. The densimetric Froude number of the wet gas flow through the sonar-based meter is an important parameter influencing measurement accuracy, with Froude Numbers greater than ~2 providing the best results.

7.0 ACKNOWLEDGEMENTS

The authors would like to acknowledge BP America and CiDRA Corporations for their support and permission to present this work, as well as the many colleagues who have contributed to this effort.

8.0 REFERENCES

[1] MEHDIZADEH, P., et al, "Wet Gas Metering: Trends in Application and Technical Developments", SPE Paper 77351, Presented at SPE Annual Technical Conference, San Antonio, September, 2002.

[2] A. HALL, D. GRIFFIN, R. STEVEN, " A Discussion on Wet Gas Flow Parameter Definitions", Presented at the 26th International North Sea Flow Meter Workshop, organized by the National Engineering Laboratory, East Kilbride, Scotland, UK, Oct 2007.

[3] KRAGAS, T. K., et al., "Downhole Fiber-Optic Multiphase Flowmeter: Design, Operating Principle, and Testing," Presented at Society of Petroleum Engineers Annual Conference, SPE Paper #77655, September 2002.

[4] GYSLING D.L., LOOSE, D.H., VAN DER SPEK, "Clamp-on, SONAR-based, Volumetric Flow and Gas Volume Fraction Meter Industrial Applications", presented at the 13th International Flow Measurement Conference, organized by the National Engineering Laboratory, East Kilbride, Scotland, UK, June 2005.

[5] GYSLING, D. L., LOOSE, D. H., AND VOLZ, R., " Wet Gas Metering Using a Combination of Differential Pressure and SONAR Flow Meters", presented at the 24th International North Sea Flow Measurement Workshop, organized by the National Engineering Laboratory, East Kilbride, Scotland, UK, Oct 2006.

[6] J. P. BRILL AND H. MUKHERJEE, "Multiphase Flow in Wells", SPE Monograph Volume 17, 1999.

[7] R.V.A. OLIEMANS, "Multiphase science and technology for oil/gas production and transport", Lecture notes for course P2.24 on Multiphase flow in wells and pipelines, Shell Internationale Research Maatschappij B.V., 1994.

[8] S.W. CHURCHILL, "Friction factor equation spans all fluid flow regimes", Chem. Eng, **7**, November 1977, p 91.

25th International North Sea Flow Measurement Workshop
16th – 19th October 2007

A PROTOTYPE WET-GAS AND MULTIPHASE FLOWMETER

E. S. Johansen (Weatherford Intl.), A. R. W. Hall (BP Exploration & Production)
Ö. H. Ünalmis, D. J. Rodríguez, A. Vera, V. Ramakrishnan (Weatherford Intl.)

ABSTRACT

A wet-gas flowmeter based on the field-proven downhole fiber-optic multiphase flowmeter has been developed. The flowmeter is based on an extended throat Venturi-nozzle and a Sonar flowmeter. This combination exploits the characteristics of these two devices in wet-gas flows. For the Venturi, there is a well-defined and large over-reading with increasing liquid-loading, whereas this has a significantly lower impact on the total flow rate measured by Sonar.

The Sonar-Venturi wet-gas flowmeter has been in development over the past several years and has been tested extensively in industry flow loops. Particular emphasis has been placed on developing a flowmeter with a broad operating envelope that includes a large span of fluid properties, a high turndown ratio, and well characterized response both within and outside its intended operating envelope. The wet-gas performance has been demonstrated at the recently commissioned CEESI 3 phase wet-gas flow loop, yielding total and gas flow rates better than ±5%,[*] liquid flow rate better than ±0.5 m^3/hr in Type I wet gas,[1] and better than ±20% in Type II wet gas. A Red Eye 2G near-infrared (NIR) water cut meter is used to differentiate the oil/condensate and water. The Red Eye 2G has field proven performance in low gas volume fraction (GVF) flows for full range of water cut. A prototype version has demonstrated ±5% water cut uncertainty in high GVF multiphase[2] flows and initial testing of the Red Eye in wet-gas flows is showing great promise.

The wet-gas flowmeter was also tested at the NEL multiphase flow facility to evaluate whether the measurement capability could be extended beyond the wet-gas envelope. Although the performance in low-pressure multiphase flows did not match the performance seen in high-pressure wet-gas flow, measurement capability was maintained and reasonable performance was demonstrated for the entire range of GVF.

INTRODUCTION

Test separators and portable well testing services are the most common technologies used to generate a measurement snapshot, typically every 30 days, but often less frequent. It is, however, widely accepted that real-time individual wellhead production monitoring is an effective tool to monitor the health and maximize the performance and ultimate recovery of producing oil and gas wells. Measurement technologies have been developed to monitor individual wells in real-time; however, the high cost has generally limited the install base to prolific wells or multiple wells multiplexed with multi-port selector valves. Furthermore, many are being used as mobile well-testing devices. Other factors complicating wide implementation include limited operating envelope, fragile mechanical and sensing characteristics, and sensitivity to changes in fluid chemistry or composition. To date, only a few meter types claim to operate both in wet-gas and

[*] All performance numbers quoted herein are relative measurements with 95% confidence interval, unless otherwise noted.

multiphase regimes. Most other wet-gas or multiphase meters may report highly erroneous results outside their intended operating range. Therefore, as wells mature with increasing gas fractions and water cut, the flow measurement conditions at the wellhead necessitate flowmeters with a wider operating envelope and a lower sensitivity to compositional changes than is available today.

The Sonar flowmeter technology platform offers the potential for a cost-effective and robust flowmeter with a broad operating envelope that may bridge the gap between traditional multiphase flowmeters and high gas-fraction metering. Sonar flow measurement is derived from the field-proven downhole fiber optic multiphase flowmeter.[3-5] It is non-intrusive, has no wetted sensors and offers excellent resilience to erosion and corrosion. Sonar flowmeters offer accurate and repeatable flow measurement with a small and well-behaved Reynolds number dependence and a large turndown ratio. Sonar can measure liquid and gas flows with no changes in hardware or software.

The conventional types of differential pressure meters (e.g. Venturi, cone or orifice plate meters) still remain the flowmeters of choice in the vast majority of gas wells. The over-reading of such devices when there is liquid in the flow stream is well understood and documented in literature.[6,7] However, the liquid content can be very difficult to estimate and hence correct for in the field. Consequently, the erroneous readings must be corrected by back allocation. Sonar tends to have a very well-behaved and low over-reading with liquid loading in wet-gas flows. The combination of a differential pressure meter with a Sonar flowmeter therefore offers an over-reading contrast that is exploited to yield the total and gas flow rates and the liquid content.

FLOWMETER DESCRIPTION

The Sonar-Venturi flowmeter is a combination of a Sonar sensor array located in the extended throat section of a Venturi-Nozzle, shown in Fig 1. The higher mixture velocity in the throat is favorable to the passive Sonar array as it improves signal to noise ratio and enhances mixing. The Sonar flowmeter consists of an array of electronic strain gauges (non-fiber optic) combined with fully integrated data acquisition and processing electronics housed in a spool-mounted enclosure. The prototype flowmeter also employs a multivariable pressure, temperature, and differential pressure transmitter for the Venturi. The flowmeter also includes Modbus and diagnostic communications over RS 485 and Ethernet. The entire assembly is powered by 12-36 VDC, consumes less than 10 W, and is Class I, Division 1 compliant.

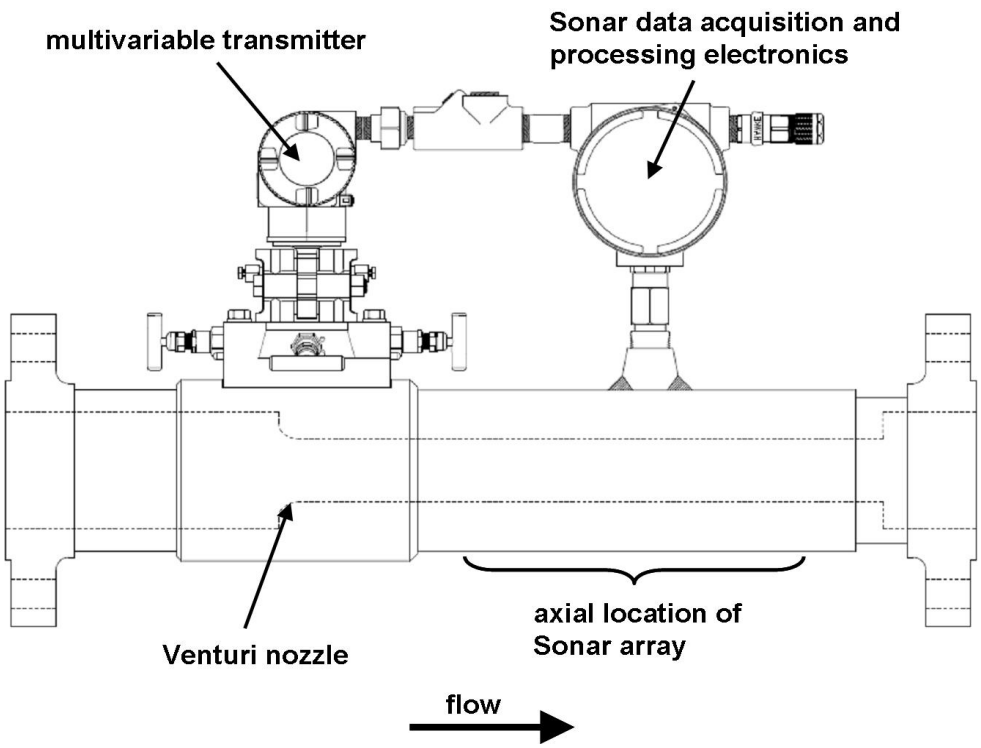

Figure 1 - Sonar-Venturi flowmeter schematic.

Sonar Flowmeter

Turbulent pipe flow contains self-generating vortical structures that convect with the fluid. These vortices remain coherent for several pipe diameters, and they decay as they convect through the pipe. Meanwhile new vortices are continuously generated by frictional forces acting between the fluid and pipe wall and within the fluid itself. An array of circumferentially mounted and axially distributed pressure sensors measures dynamic pressure fluctuations associated with the convecting turbulent eddies. The convection velocity is calculated from the unsteady pressures by array processing algorithms. The volumetric flow rate is directly proportional to the convective velocity measured by Sonar and a single Reynolds number calibration yields a flow rate for liquid or gas. with an uncertainty typically better than ±1%.

The calibrated performance of the Sonar meter in single-phase (oil, water and gas) is presented in Fig. 2. A Reynolds number "turndown" of nearly three orders of magnitude is demonstrated for six different fluids at three different test facilities with no change in the three calibration constants. The calibration values are also consistent with what is typically seen in a fiber-optic flowmeter. In wet-gas conditions, the calibrated Sonar velocity yields a volumetric flow rate that is slightly higher than the actual mixture velocity. The over-reading of Sonar is well behaved with respect to liquid loading and is readily correlated with the Lockhart-Martinelli parameter.

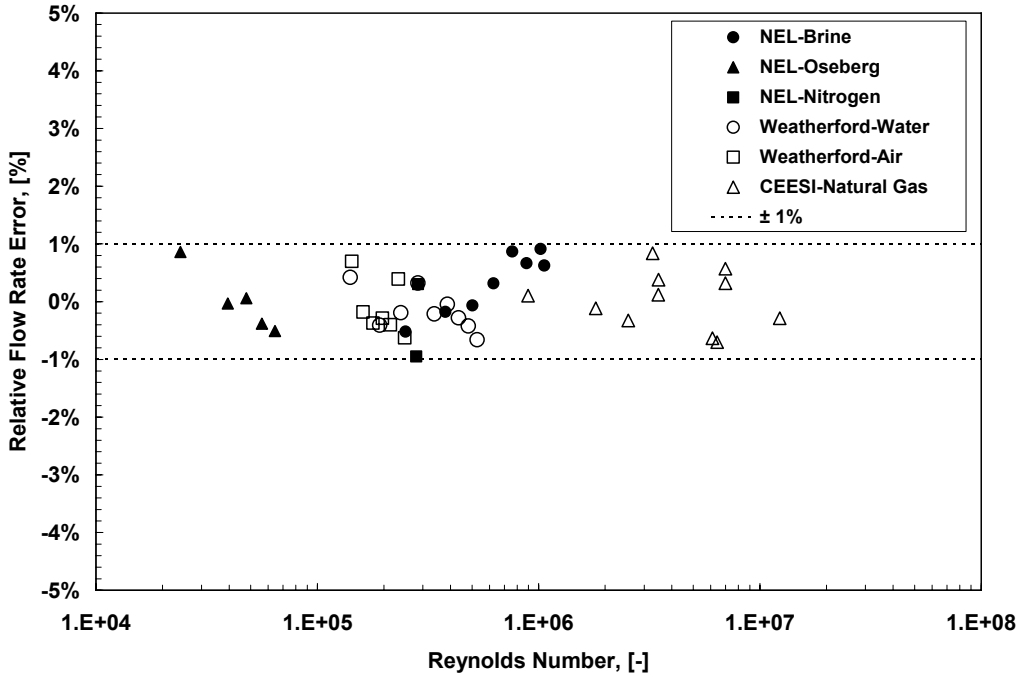

Figure 2 - Baseline Sonar performance over broad Reynolds number range.

Venturi

The extended throat Venturi-nozzle performance was verified with the same dataset and was found to measure single-phase flow rates within ±1.4%. The Venturi behavior is well described in literature. Tests conducted with the Sonar-Venturi combination throughout single-phase, multiphase, and wet-gas flow were consistent with published values of discharge coefficients.

The turndown ratio of the differential pressure sensor is 84:1 from the multivariable transmitter specification sheet. In practice, the wet gas differential pressure on a horizontal Venturi-nozzle was observed to depart from the deLeeuw correlation at pressure turndown ratio of 30:1. Since ΔP is proportional to V^2 the velocity turndown ratio for the Venturi-nozzle is at best 9:1 and, in practice, it can be as low as 5:1. Thus, in terms of flow velocity turndown, the performance of the Sonar meter far exceeds that of the Venturi-nozzle.

Water Cut Meter

The Red Eye 2G water cut meter is based on the principles of spectroscopy and relies on the large difference in the absorption of near infrared (NIR) radiation between oil and water. Differentiation is achieved by operating over a very narrow band of radiation with maximum intensity occurring at wavelengths where crude oil and water exhibit large differences in opacities. The Red Eye measures transmissions at multiple infrared wavelengths simultaneously and calculates the water fraction from the ratio of attenuation at different wavelengths. The technique operates consistently across the full range of 0% to 100% water cut, and is effectively insensitive to free gas.

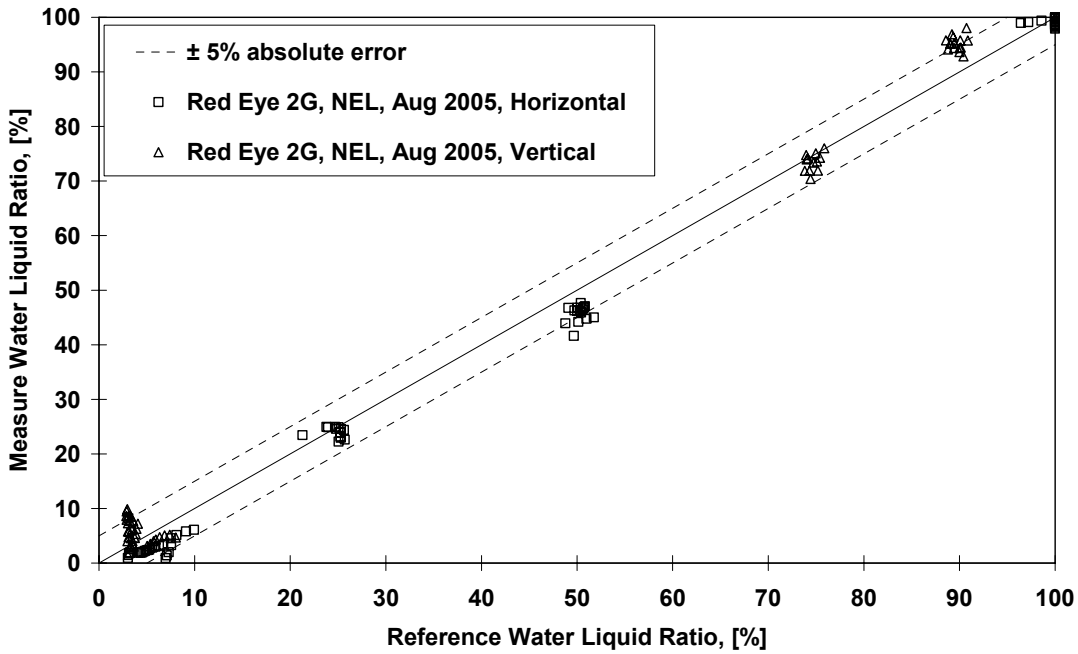

Figure 3 - Performance of water cut measurement.[2]

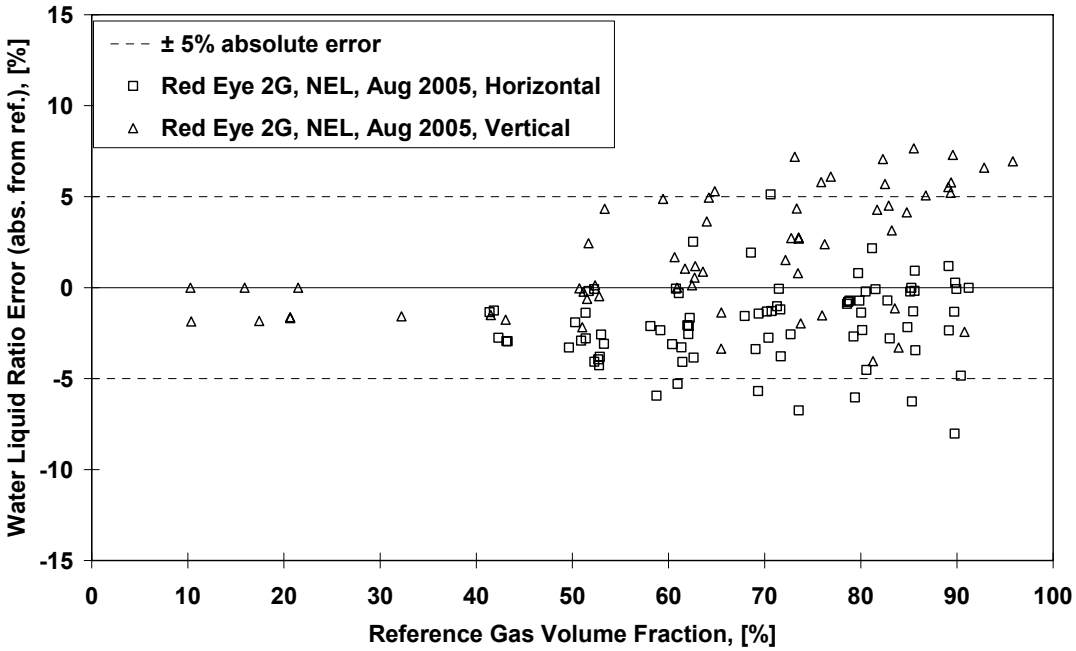

Figure 4 - Performance of water cut measurement for wide GVF range.[2]

Data shown in Figs. 3 and 4 range from 10 to 95% GVF at low pressures.[2] Even those points at the highest GVF do not constitute wet-gas flows with Lockhart-Martinelli parameter significantly higher than 0.3 (due to the low pressure and high liquid/gas density contrast)[1]. However, recent tests conducted at CEESI show very good sensitivity, correlation, and measurement capability in wet-gas flows at GVF up to 99.9%. The water cut measurement has been verified in separate studies and the remainder of the discussion in this paper will focus on the ability to measure liquid and gas flow rates by the Sonar-Venturi combination.

TEST ENVELOPE

The flowmeter was tested at NEL (multiphase) and CEESI (3-phase wet gas) in August and September of 2007 respectively. The CEESI tests were conducted in the recently commissioned 3-phase wet-gas flow loop.

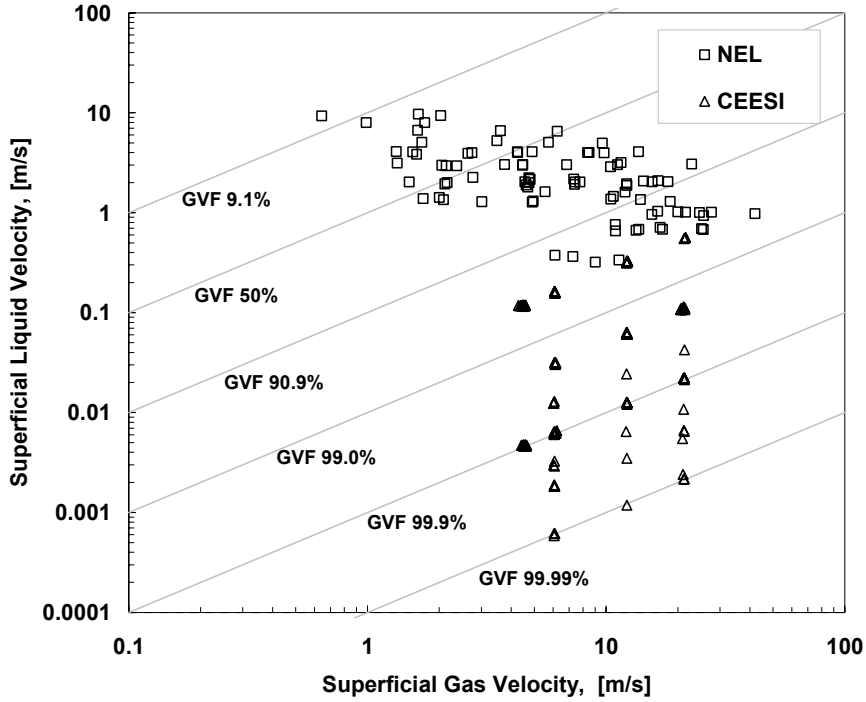

Figure 5 - Phase superficial velocity and GVF variations for NEL and CEESI test matrices.

Figure 5 shows the entire test matrix for both facilities in terms of superficial liquid and gas velocities with no-slip GVF as isolines. From this view, it appears as though the two tests overlap, however, the test pressure at NEL ranged from 2 to 7.5 bar, whereas the test pressures at CEESI ranged from 14 to 55 bar yielding very different liquid/gas density contrasts (see table below). Consequently the high GVF points in the NEL test matrix are not representative of wet-gas conditions because the relatively low gas density results in a relatively low gas Froude number, Fr_g and a relatively high Lockhart-Martinelli parameter, X_{LM}. The CEESI test envelope, on the other hand, covered Fr_g and X_{LM} within the regions defined by API as Type I and Type II wet-gas flow.[1]

	CEESI	***NEL***
Pressure	14, 28, 55 bara	2 – 7.5 bara
Temperature	28-35 °C	22-42 °C
WLR	0 – 100%	1, 40, 75, 100%
GVF (no slip)	97.5-100%	0 - 100%
Total Volume Flow Rate	85-655 m^3/hr	14 – 460 m^3/hr
Liquid/Gas Density Ratio	16 at 55 bara 40 at 28 bara 98 at 14 bara	106 at 7.5 bara 485 at 2 bara
Frg Sonar	1.5 - 20	0.07-2.6
Frg Nozzle	0.5 -5.5	0.02.-0.7
X_{LM}	0 - 0.26	0.3-167
LMQ	0 – 0.72	0-1

WET-GAS TESTS

CEESI Test Facility

The CEESI (Colorado Engineering Experiment Station, Inc.) wet-gas facility, originally built in 1998, was designed for two-phase flow studies consisting of natural gas and hydrocarbon liquids. The loop has been recently redesigned for three-phase operation. Figure 6 shows the block diagram of the three-phase wet-gas loop used for the current tests.

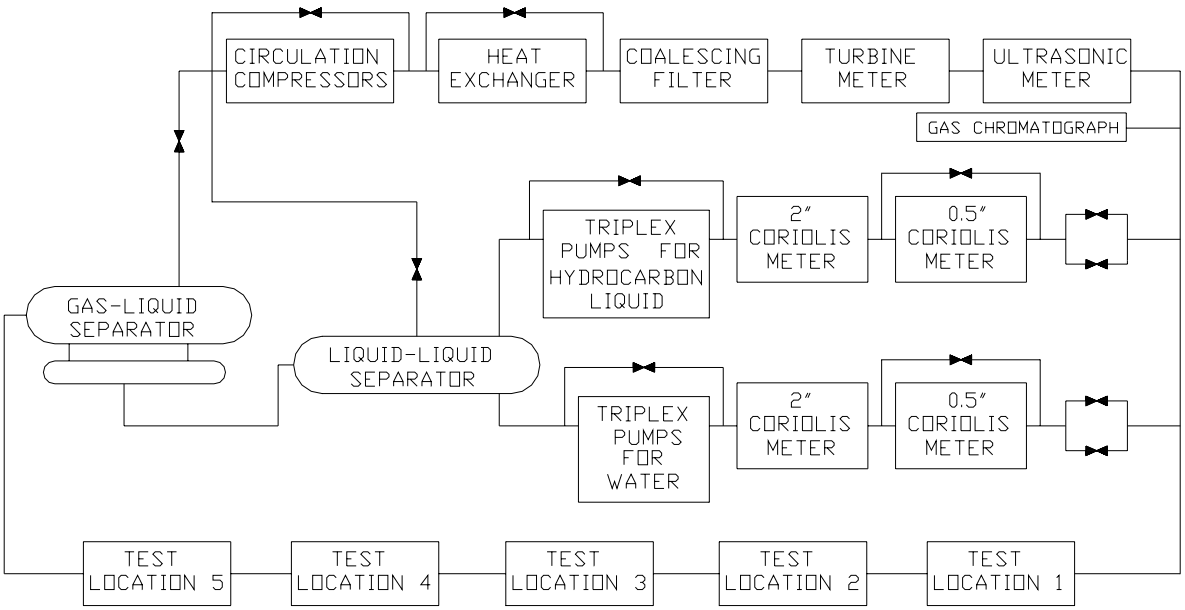

Figure 6 - Block diagram of wet-gas research loop, 4-inch test line

Both a turbine meter and an ultrasonic meter measure the flow rate of the natural gas. The difference in mass flow rate between these two meters is monitored; if the difference exceeds a specified amount, the data is scrutinized for detrimental effects such as pulsation. If the difference is within tolerance, then all other meters installed in the research loop can be compared to the natural gas mass flow rate as measured by the turbine meter. Pressure and temperature measurements at various locations on the loop (including the test locations) are used to calculate local gas density.

The hydrocarbon liquid and the water, which reside in the liquid-liquid separator, can be injected into the gas stream by positive displacement pumps (Triplex pumps). Coriolis meters measure the mass flow rate and the density of the liquids to be injected. The gas stream carries the liquid mixture through the meter test locations and on to the horizontal gas-liquid separator where it is then returned to the liquid-liquid separator. Stability of liquid density, gas composition, pressure, temperature and flow rate is monitored to determine steady state conditions.

During each test point, a gas chromatograph obtains a sample of the natural gas on a 6-minute time interval. Using the average natural gas composition during the test point and the measured pressure and temperature at any given location in the test loop, the gas density at that location is determined using AGA-8. The composition of the gas has some seasonal variation with the methane composition ranging from approximately 83% to 95% during the year. The hydrocarbon liquid (Exxsol™ D80) is very similar to kerosene with less than 2 ppm sulfur.

Figure 7 - Sonar-Venturi flowmeter installed vertically in flow loop.

Figure 7 shows the vertical installation of the Sonar-Venturi flowmeter in the 4-inch wet-gas flow loop. The flowmeter was mounted immediately downstream of a blind T.

Measurement Contrast

The flowmeter has two independent measurements – the Sonar velocity and the Venturi ΔP. It has been established (as evidenced in literature and through tests at multiple flow facilities by the authors) that both instruments measure dry-gas flow-rates very well. In wet-gas flow, it is desirable for each instrument to have an over-reading that is dependent primarily on liquid loading and minimally on other flow parameters such as gas Froude number and line pressure. A modified version of the de Leeuw correlation (developed for horizontal flows) was found to work very well and has been adopted for the Venturi. The basis for the Venturi over-reading (ORV) and subsequent correlation is

$$ORV = \frac{Q_{g,apparent}}{Q_{g,ref}}, \tag{1}$$

with

$$ORV = f_1(X, Fr_g), \tag{2}$$

where the Lockhart-Martinelli parameter is defined herein, as:

$$X = \frac{m_l}{m_g}\sqrt{\frac{\rho_g}{\rho_l}}. \tag{3}$$

The over-reading correlation for the Sonar meter (ORS) was established based on the measured flow velocity and the liquid mass quality (LMQ):

$$ORS = \frac{Q_{t,apparent}}{Q_{t,ref}}; \tag{4}$$

$$Q_{t,apparent} = V_m A; \tag{5}$$

$$ORS = f_1(LMQ, Fr_g); \tag{6}$$

$$LMQ = \frac{m_l}{m_t}; \tag{7}$$

where V_m is the Sonar mixture velocity after applying the Reynolds calibration. A necessary condition for solving for both unknowns (i.e., total flow rate and liquid loading), is to have two independent equations that characterize ORV and ORS.

A convenient way to quantify the independence of the over-reading characteristics is to depict the contrast (i.e., difference in slope) of both over-reading trends. The apparent nozzle gas flow rate and the apparent Sonar bulk flow rate were divided by the reference total flow rate and plotted against X_{LM} in Fig. 8. The contrast between the two trends is what allows for a successful iterative solution for the unknowns.

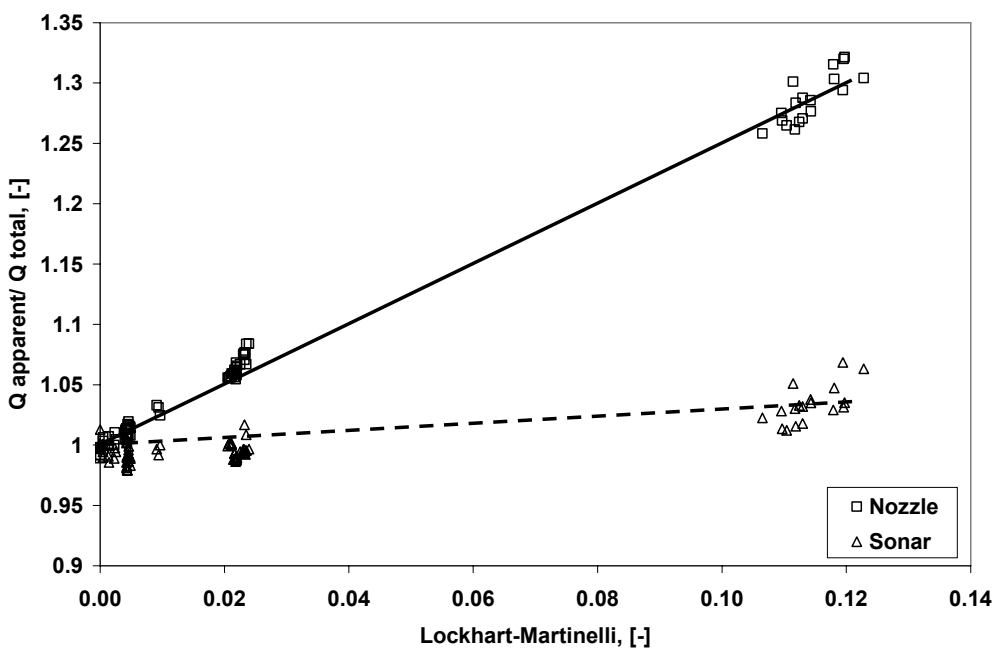

Figure 8 - Difference in slope between the over-reading trends of Sonar and Venturi reveals the contrast between the two devices in wet-gas flow.

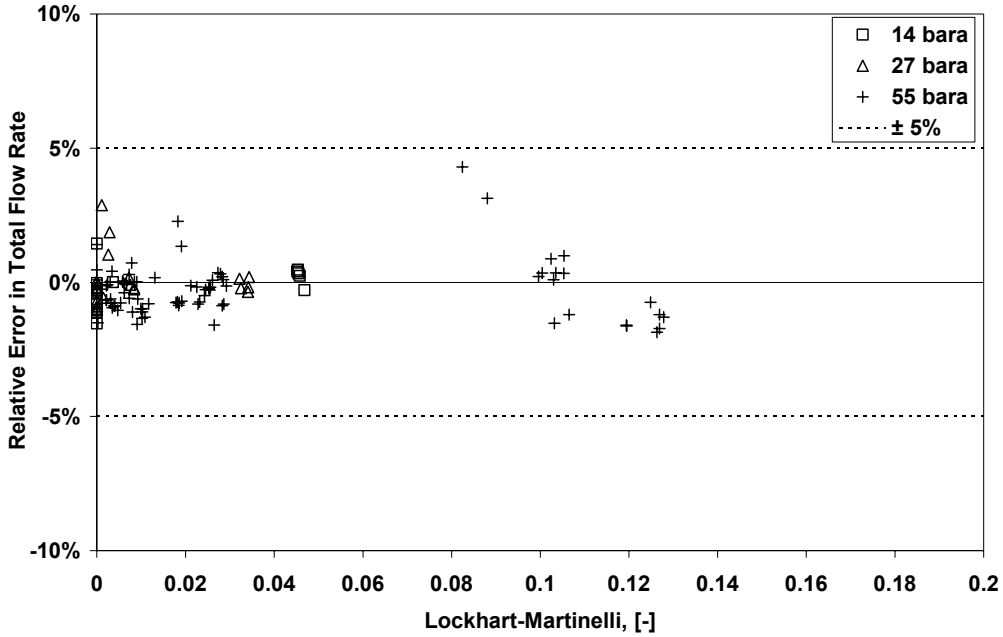

Figure 9 - Total flow rate relative error for wet gas.

Figure 9 shows the total flow rate relative error predicted over all test pressures for the Sonar-Venturi flowmeter. Total flow rate is predicted well within ±5% for the test points across the full range of Lockhart-Martinelli parameter tested. The gas flow rate relative error is shown in Fig. 10. As expected, the gas rate performance follows the total flow rate since the liquid content by volume is negligible for a majority of the test matrix.

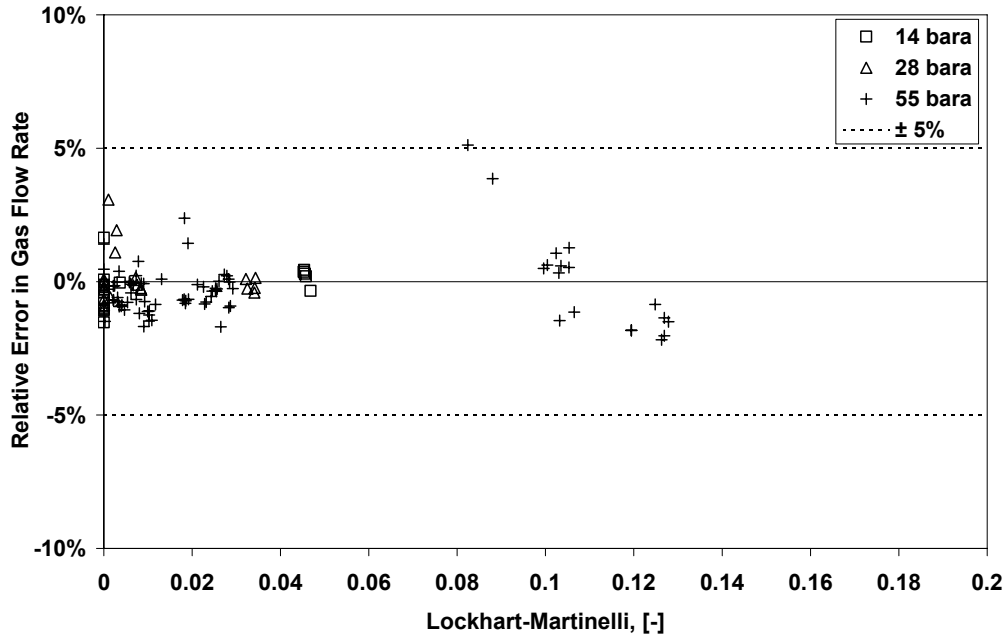

Figure 10 - Gas flow rate relative error for wet gas.

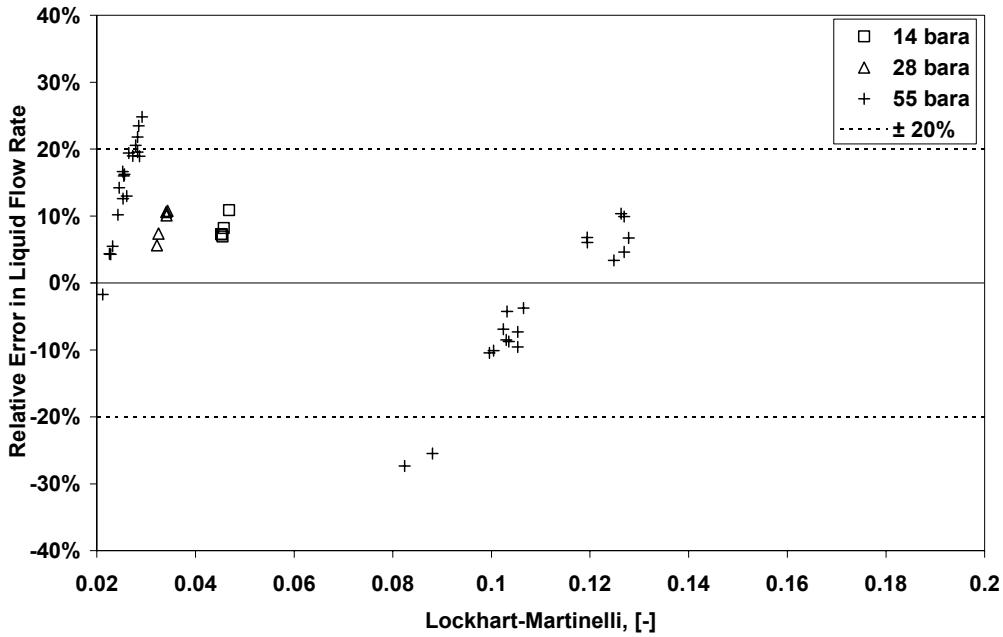

Figure 11 - Liquid flow rate relative error for API Type II wet gas.

Figure 11 shows the relative error in liquid flow rate for API Type II wet gas, defined by having $X_{LM} > 0.02$. The dashed lines show that most of the points are contained within a ±20% relative error band. Figure 12 shows the error in liquid flow rate for API Type I wet-gas flows, where $X_{LM} < 0.02$. In this case the data has been presented in absolute terms and is shown to be within ±0.5 m^3/hr.

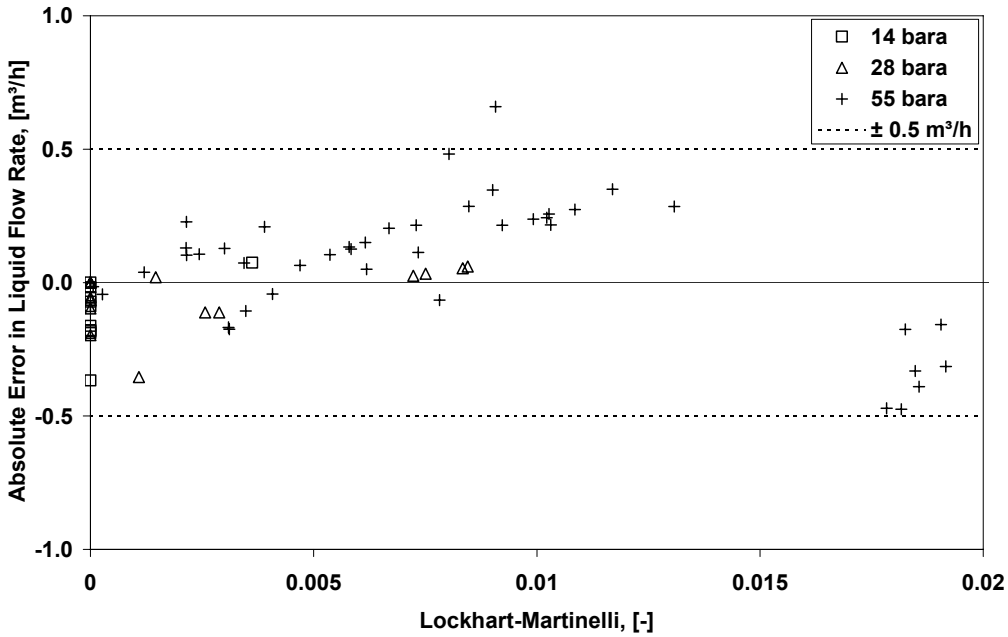

Figure 12 - Liquid flow rate absolute delta for Type I wet gas.

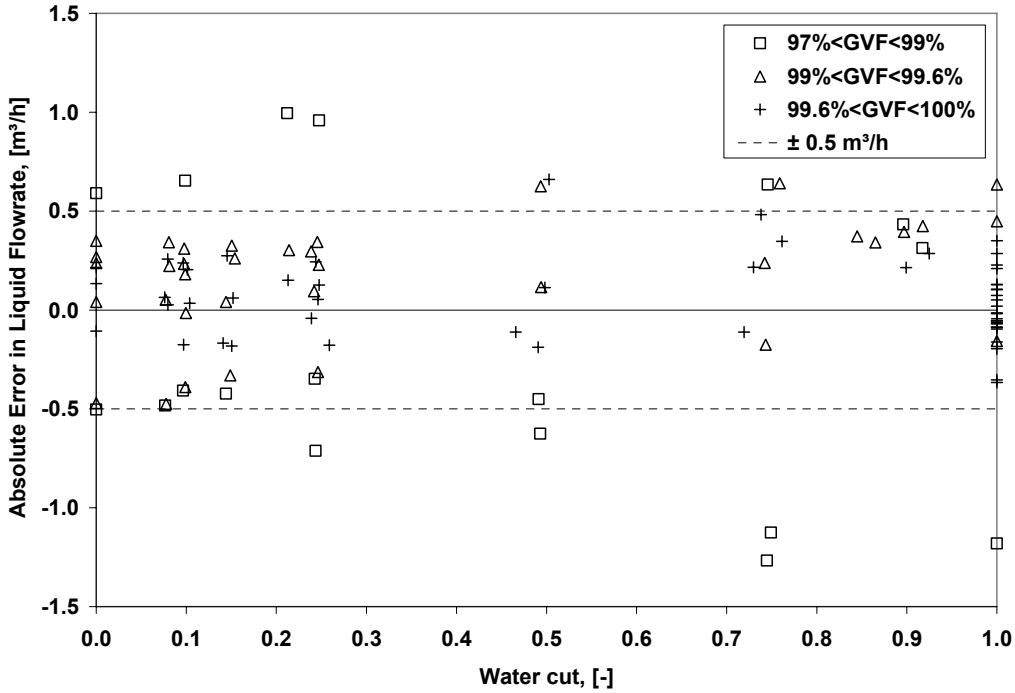

Figure 13 - Error in liquid flow rate prediction vs. water cut.

Figure 13 shows the effect of water cut on the measured liquid flow rate demonstrating that there is no discernable effect of liquid viscosity and to a certain degree density.

MULTIPHASE TESTS

The Sonar-Venturi is primarily designed for wet-gas flow; however, it was also tested at NEL to evaluate the performance in off-design conditions. An extension of the wet-gas iterative solution described above was devised for resolving the liquid and gas flow rates under multiphase flow conditions. While analogous *ORS* and *ORV* concepts are used in characterizing the multiphase response of the single phase devices, the definitions of these quantities as well as their correlating parameters are different from the ones used for wet gas. The ORV in multiphase flows follows published methods and is analogous to variations in discharge coefficient in multiphase flow conditions.[8,9] The Sonar over-reading was characterized in a form similar to the wet-gas methodology. No refinement was attempted for this first evaluation of multiphase performance and no effort was made to asymptotically match the multiphase and wet-gas models.

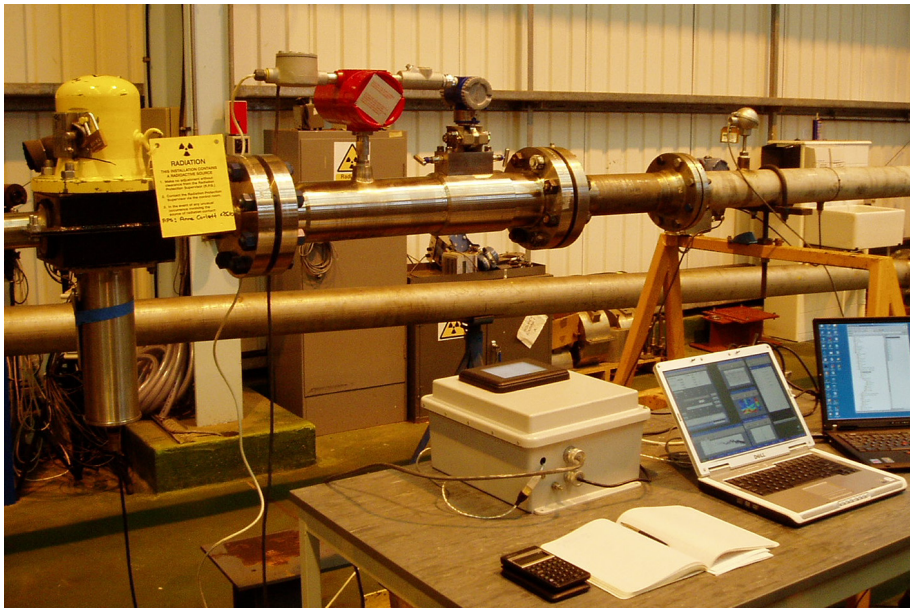

Figure 13 - Sonar-Venturi flowmeter at NEL multiphase test facility. The gamma densitometer in picture is for R&D only and has not been used in the Sonar-Venturi flowmeter calculations.

The results were categorized using three gas volume fraction (GVF) ranges namely *0<GVF<60%*, *60<GVF<80%*, and *80<GVF<97.5%*. It is worth emphasizing that even the highest GVF in this facility does not constitute wet-gas flows and that intermittent flow conditions occurs at all GVF above 30%.

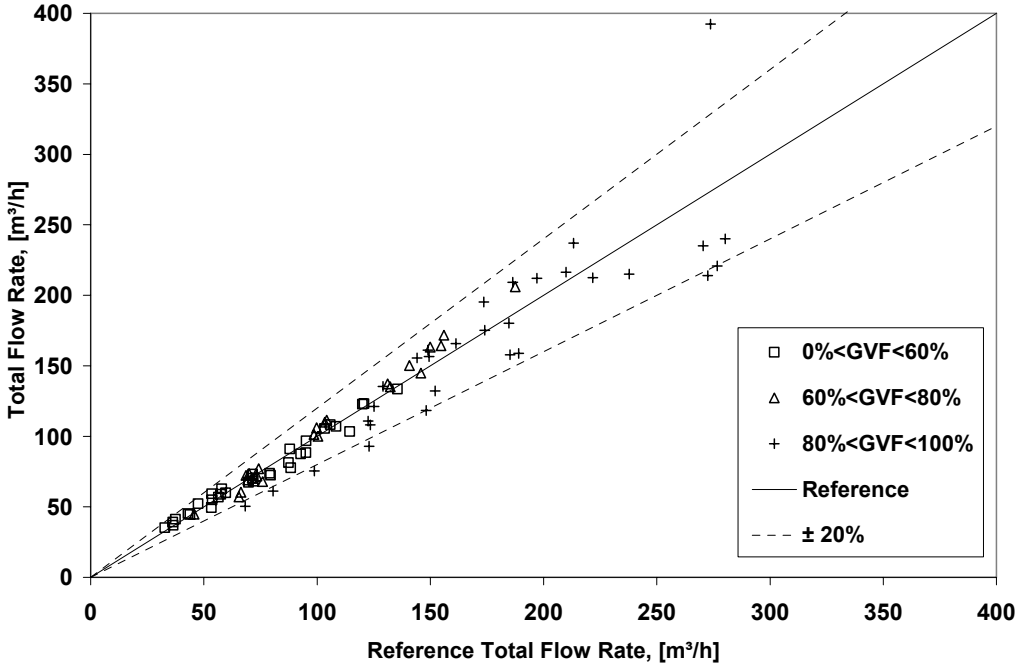

Figure 14 - Total flow rate in multiphase

Figure 14 shows the total flow rate for all GVFs ranging from 0 to 100% and all water cuts ranging from 5 to 75%. It can be seen that the total flow rate is predicted to within ±20% for *GVF<80%*, however, at higher GVF the measurement is erratic. The velocity reported by Sonar at these

conditions is not deemed representative as a time-averaged total flow rate. Further refinement of Sonar processing is required to resolve these flow conditions accurately.

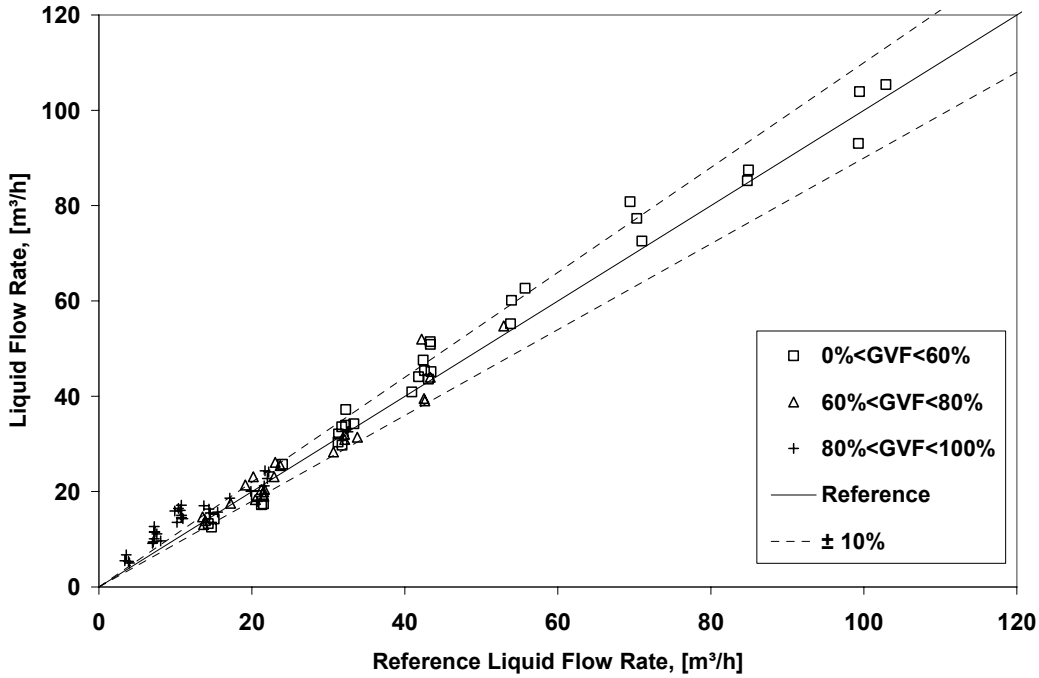

Figure 15 - Liquid flow rate in multiphase.

Similar to the total flow rate, Fig. 15 shows that liquid flow rate is measured to within 20% for GVF<80%. The effect of the inaccurate Sonar velocity between 80 and 97.5% GVF exacerbates the liquid error.

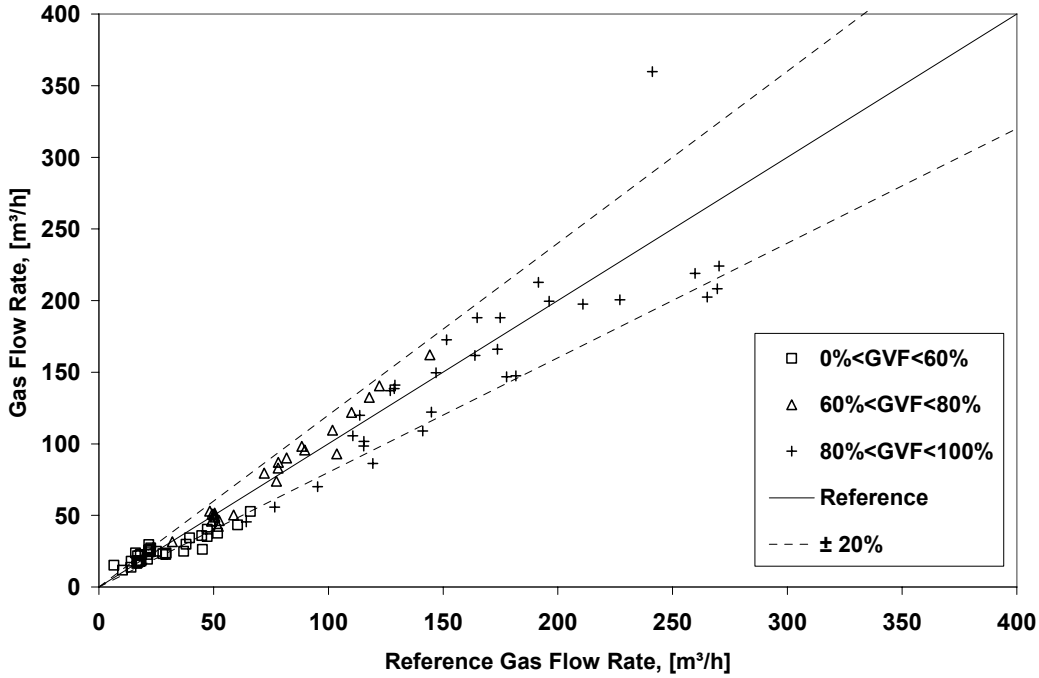

Figure 16 - Gas flow rate in multiphase.

Figure 16 shows the gas flow rate. The gas rate is predicted to within 20% between 60 and 80% GVF, but larger errors are prevalent at lower GVF. Again, the measurement performance between 80 and 97.5% GVF is reduced due to low accuracy of the Sonar in this regime to the widely time-varying properties of the flow. Currently Sonar algorithms do not attempt to capture transient properties, but is rather reporting volumetric and time-averaged flow properties. It is worth noting that the Sonar processing algorithms can readily identify the slugs and offer potential to calculate both slug and bubble velocity and volume.

CONCLUSIONS

The Sonar-Venturi-(Red Eye) flowmeter constitutes a high-accuracy top-side evolution of the downhole fiber-optic flowmeter technology. The flowmeter combines Sonar sensors with an extended throat Venturi that enables measurement of liquid and gas rates in wet-gas and multiphase flows. Addition of a Red Eye 2G water cut meter enables distinction of oil/condensate and water. This flowmeter has been tested in a range of wet-gas and multiphase flow conditions at CEESI and NEL where it was found that for wet-gas flows the total and gas flow rates are measured to within ±5% and liquid rate is determined to be within ±20% in API Type II wet gas and ±0.5 m^3/hr in API Type I wet gas.

In multiphase flows, liquid and total rates are predicted to better than ±20% at GVF below 80%. In low pressure highly unsteady slugging flows, there is a reduction in Sonar measurement capability and hence the measurement performance is reduced. This was evident between 80 and 97.5% GVF in the multiphase facility. Additional work is required to improve the multiphase and especially Sonar performance in unsteady flow conditions. The Red Eye water cut meter has been demonstrated in other work to be within ±5% (absolute) over the full range of GVF and WLR and is not significantly affected by slugging flow conditions.

ACKNOWLEDGEMENTS

The authors gratefully acknowledge BP Exploration Operating Company Limited and Weatherford Intl. for permission to present this work. We would also like to thank our co-workers who have directly or indirectly contributed to this work.

NOMENCLATURE

Acronyms and Symbols

A	=	Area, [m^2]
API	=	American Petroleum Institute
CEESI	=	Colorado Engineering Experiment Station, Inc
f	=	Function
Fr	=	Densimetric Froude Number, [-]
GVF	=	Gas Volume Fraction, [-]
LMQ	=	Liquid Mass Quality
m	=	Mass flow rate, [kg/s]
NEL	=	National Engineering Laboratory
NIR	=	Near-Infrared
ORS	=	Over-Reading Sonar, [-]
ORV	=	Over-Reading Venturi, [-]
Q	=	Volumetric Flow Rate, [m^3/s], [m^3/hr]
V	=	Velocity, [m/s]
WLR	=	Water Liquid Ratio, [-]

X_{LM} = Lockhart-Martinelli parameter, [-]
ΔP = Differential Pressure, [bar]

Subscripts

g = Gas
l = Liquid
m = Mixture
s = Superficial
t = Total

REFERENCES

[1] "State of the Art Multiphase Flow Metering" API Publication 2566, First Edition, May 2004.

[2] Hall, A., Lievois, J., and Adejuyigbe, B., "Testing of the Red Eye Near-Infrared Water Cut Monitor for Application as a Water Cut Sensor in Multiphase Flow Conditions," Multiphase Pumping and Technologies, International Conference & Exhibition, Abu Dhabi, 10-14 February 2007.

[3] Kragas, T.K., Johansen, E.S., Hassanali, H., and Da Costa, S. L.: "Installation and Data Analysis of a Downhole, Fiber Optic Flowmeter at BP's Mahogany Field, Offshore Trinidad," SPE 81018, SPE Latin American and Caribbean Petroleum Engineering Conference, Port-of-Spain, 27–30 April 2003.

[4] Johansen, E. S., Kragas, T. K. and Beaumont, P., "Downhole Fiber Optic 3-Phase Flowmeter Field Test at BP Mungo," 21st North Sea Flow Measurement Workshop, Tønsberg, 28-30 October 2003.

[5] Sandøy B., *et al*. "Improved Reservoir Management with Intelligent Multi-Zone WAG Injectors and Downhole Optical Flow Monitoring," SPE 95843, SPE Annual Technical Conference and Exhibition Dallas, 9-12 October 2005.

[6] De Leeuw R., "Liquid Correction of Venturi Meter Readings in Wet-gas Flow", North Sea Workshop 1997.

[7] Stewart, D., *et al*. "Wet-gas Venturi Metering" North Sea Flow Measurement Workshop, Tønsberg, Norway, 2003.

[8] Hall, A.R.W., Reader-Harris, M.J. and Millington, B.C., "A Study of the Performance of Venturi Meters in Multiphase Flow," 2nd International Conference on Multiphase Technology, Banff, 22 June 2000.

[9] Vilagines, R. and Hall, A.R.W., "Comparative Behaviour of Multiphase Flowmeter Test Facilities," Oil and Gas Science Technology, Vol. 58, No. 6, pp. 647-657, 2003.

A Discussion on Wet Gas Flow Parameter Definitions

Andrew Hall, BP Exploration Operating Co. Ltd., Pipeline Systems Team, Aberdeen, UK. E-mail: andrew.hall@bp.com
Douglas Griffin, Head, Petroleum Measurement & Allocation, BERR (formerly DTI) Energy Group, Aberdeen, UK. E-mail: douglas.griffin@berr.gsi.gov.uk
Richard Steven, Colorado Engineering Experiment Station, Inc., 54043 WCR 37-Nunn, Colorado 80648, USA. E-mail: rsteven@ceesi.com

1. Introduction

For more than a decade, the technical papers presented at flow meter conferences have included papers that have discussed the issues of wet gas flow metering. This is directly related to the continued increase in the development and use of wet gas flow in the natural gas production industry. Wet gas meter technologies had previously been developed primarily for steam measurement within the power generation industry. However, the steam industry's research into this topic had wound down by the early 1980s. When the natural gas production industry restarted this research on the strength of earlier publications, some terminology was taken from these records and other terminology was created by the new research. However, there has never been any attempt to unify the terminology. Therefore, the result is that researchers, meter manufacturers and meter users are free to produce their own definitions for commonly used terms, which often do not match those of others, and as a result of this there has been confusion and misunderstanding.

There are now a few documents that can be referenced but there is no guarantee that the definition given by any one document will match that of any other document. Furthermore, the authors of wet gas flow metering papers presented at previous North Sea Flow Measurement Workshops sometimes have different definitions for the same term and this has gone unquestioned or un-remarked upon by the audiences.

It is not beneficial to any research topic for no common language to be agreed upon. In some instances at NSFMW question periods, arguments have initiated because the two parties did not realise they were not using the same definitions. In this paper there is an attempt to explain the different terminologies being used and the authors offer suggested definitions that they believe to be the most appropriate for stated technical reasons as a starting point for a debate.

2. Definitions of Two phase Flows, Multiphase Flows and Wet Gas Flows

There can be confusion between the terms *two phase flow*, *multiphase flow* and *wet gas flow*. With no agreed standard to define these terms it is not surprising that different organizations and individuals have created their own definitions and that these do not always agree.

In his presentation at the NSFMW in 2006, Jamieson [1] suggested that industry should adopt the term *unseparated flow* to encompass all hydrocarbon production fluid flows upstream of any process equipment. Unseparated flow is a term that can describe any flow whether it is a single phase homogenous flow or not. This is seen by the authors as a reasonable suggestion. However, even if this term is adopted there is still considerable scope for confusion when trying to define sub-sets of unseparated flow, i.e. two phase flow, multiphase flow and wet gas flow.

In classical physics there are three phases: solids, liquids and gases. It could therefore be reasonably assumed then that the term *multiphase flow* would be used to describe a flow of more than any two possible phases, i.e. solids, liquids and gases. Likewise, it could be reasonably assumed then that the term *two phase flow* would be used to describe a flow that consisted of any two of the three possible phases, i.e. a gas / liquid flow, a gas / solid flow, or a liquid / solid flow. However, in the terminology that has developed in the hydrocarbon production industry these assumptions can in fact be wrong. Flow meters labelled as multiphase flow meters do not typically measure combined flows of solids, liquids and gases but rather the flows of gas and liquid where the liquid phase has more than one component, with different liquid components labelled as different phases. In reality this generally means natural gas, hydrocarbon liquids and water. The multiphase meters on the market do not typically have the ability to indicate or measure the flow of any solids entrained in the gas and liquid flow but they do differentiate the liquid component flowrates, although it is recognised that devices are available for the detection of solid components within multiphase flow streams.

The hydrocarbon production industry commonly defines *two phase flow* as exclusively gas / liquid flows. Furthermore, it is common, but by no means universal, to assume that two phase flow is the flow of a gas with one liquid component. However, with the strict use of the scientific word "phase" a two phase flow of gas and liquid could consist of several different components of each phase (i.e. the gas and the liquid). Almost universally gas is denoted as one phase regardless of the number of components in the gas, whereas it is common to describe a liquid flow of hydrocarbon liquid and water as a flow of two "phases".

In the flow metering industry terminology an unseparated flow could be used as an all-encompassing term to describe any flow of any combination of gases, liquids and solids (as proposed by Jamieson). It is proposed here that *two phase flow*, which is currently ill-defined by the hydrocarbon production industry, should be any gas and liquid flow. That is, two phase flow is the combined flow of gases and liquids where the phases can consist of one or more components. This then is a subset of unseparated flow. Two phase flow is all unseparated flow that is not a single phase flow and has no solids flowing. As industry is certain to keep the almost universally accepted terminology of *multiphase flow*, it could be said that multiphase flow is a flow of gas and liquid with more than one liquid component. That is, it is a subset of two phase flow as it is a gas and liquid flow where there is more than one liquid component. Figure 1 shows this graphically.

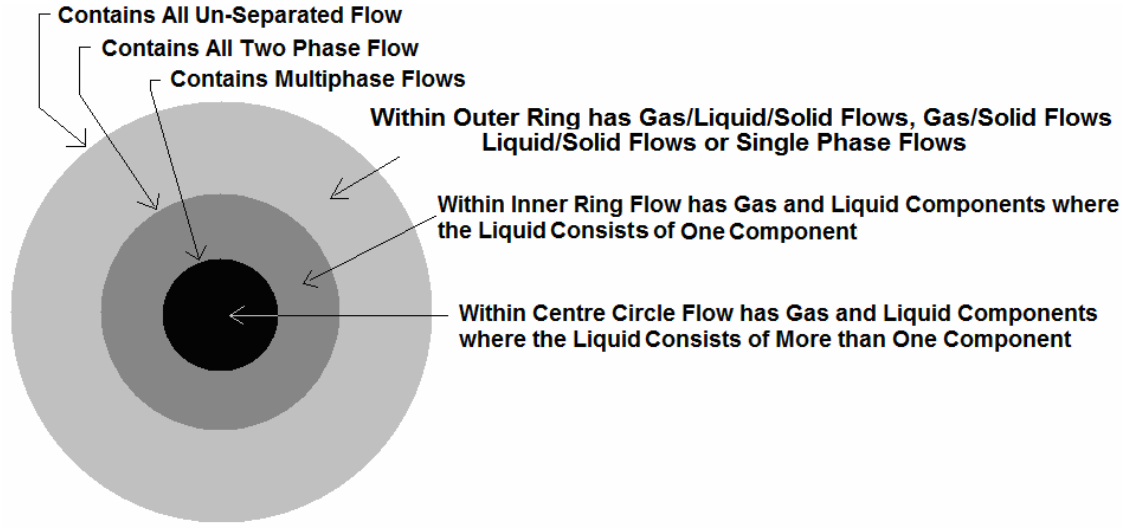

Figure 1. Pictorial view of suggested definitions

In many production flows that are called multiphase flow there could be solid particulates entrained in the liquid and gas flow (e.g. sand, hydrate crystals, etc.). In such cases, the flow would be unseparated flow outside the subsets of two phase or multiphase flow described above. Industry still tends to call this situation multiphase flow which is one of the inconsistencies the adoption of the term unseparated flow could help resolve.

No mention has yet been made of the relative quantities of the phases and the phase components. *Wet gas* is a term that has possibly caused more confusion than the two phase and multiphase flow terms. The details of different definitions given to this term over the years will be dealt with in turn but for the current discussion we will say the term loosely means a relatively small amount of liquid (of any composition) by volume in a flow that is predominantly of gas by volume. All definitions discussed later are on how to quantify relative magnitudes of gas and liquid flowrates and not on what liquid components are flowing. A wet gas flow is always a two phase flow and depending on the liquid phase composition it may be a multiphase flow.

There is sometimes confusion on just what is meant by the flow metering industry with regards to the liquid phase. Gas flows that include components that are evaporated liquids (such as humid air containing water vapour) but have no condensed liquids flowing with them are not usually considered to be two phase, multiphase or wet gas flows from the measurement point of view. One way to explain this is to consider an aircraft flying in humid air (i.e. a relative humidity greater than 0% and less than 100%). The aircraft would not be considered to be flying through a wet gas. If it was flying in the rain that would be a different story.

The Norwegian Society for Oil and Gas Measurement [2] explain this issue in the following way:

"Hydrocarbon gases that contain heavy components that will condense during further processing (but at a particular pressure and temperature behaves as a pure gas) are not considered to be a wet gas from the measurement point of view."

3. Defining Wet Gas Flow

It is now appropriate to discuss a quantitative definition of wet gas flow. Different researchers and organizations have used various parameters for describing the relative quantity of liquid in a flow predominately of gas; even those that used the same parameters did not necessarily use the same definition for what was the maximum quantity of liquid that would be the cut-off between wet gas and general two phase flow. One of the most commonly used parameters to describe the relative quantity of liquid in a two phase flow is called the *Lockhart-Martinelli parameter* (denoted here as X_{LM}). However, it is crucial that this term is precisely defined as it has been given different definitions over the years, and without a precise definition of the Lockhart-Martinelli parameter, any definition of wet gas flow using this term will be ambiguous. Five different Lockhart-Martinelli parameter definitions have been used, and this has caused considerable confusion. The history of these different definitions and the confusion this has caused is now explained.

3.1. The history of the Lockhart-Martinelli parameter

The term *Lockhart-Martinelli parameter* so often used by the oil and gas industry has a protracted origin. There are now four different equations for this term (and arguably five definitions as one of these equations can de derived in two different ways). To understand these definitions, where they come from, how they relate to each other, why there has been so much confusion and why industry is slowly beginning to favour one of these terms, the discussion starts 58 years ago.

Lockhart and Martinelli [3] discussed the pressure losses occurring in two phase flow in unit lengths of straight, constant area, smooth pipes. This work produced a parameter which Lockhart and Martinelli denoted as X. It was defined, for a unit length of smooth pipe, as the square root of the ratio of the head losses (i.e. friction induced pressure losses) if the liquid and gas phases of a two phase flow flowed alone in the conduit, equation (1),

$$X = \sqrt{\frac{\Delta P_{l,hl}}{\Delta P_{g,hl}}} \ . \qquad (1)$$

Where $\Delta P_{g,hl}$ and $\Delta P_{l,hl}$ are the head losses of the gas and liquid phases of a two phase flow if they were to flow alone in the unit length of pipe. It can be seen that the original term *Lockhart-Martinelli parameter* was not developed as a wet gas flow metering tool but rather as a pressure loss predictor for unit lengths of smooth pipe with two phase flow. Lockhart and Martinelli derived these pressure losses using a generalised Blasius friction factor equation which is applicable only to smooth pipes. For cases where both the liquid and gas phases flowing alone in the pipe had Reynolds numbers greater than

2000 Lockhart and Martinelli stated that the parameter X was found from equation (2). No upper Reynolds number limit was given although it is known that the Blasius friction factor equation is not generally applicable at high Reynolds numbers. However, the maximum Reynolds number in the Lockhart and Martinelli data set was 124,000, so the use of a generalized Blasius friction factor was a reasonable method for Lockhart and Martinelli to derive the pressure loss in their data.

$$X^2 = \frac{\Delta P_{l,hl}}{\Delta P_{g,hl}} = \left(\frac{m_l}{m_g}\right)^{1.8} \frac{\rho_g}{\rho_l} \left(\frac{\mu_l}{\mu_g}\right)^{0.2}, \tag{2}$$

where m_g and m_l are the gas and liquid mass flowrates, ρ_g and ρ_l are the gas and liquid densities, and μ_g and μ_l are the gas and liquid dynamic viscosities.

However, unlike the flow conditions Lockhart and Martinelli were discussing, in most hydrocarbon production flows the pipes can not be presumed to be smooth and usually conditions are such that if the gas and liquid flowed alone in the pipe, for the gas flow at least, the Reynolds numbers would be too high for the application of a Blasius friction factor equation to be appropriate. Therefore, if the original Lockhart-Martinelli parameter definition is to be used in these cases, a more appropriate method is needed for predicting the head losses for the phases flowing alone.

For higher Reynolds numbers, the head loss for a single phase flow per unit length of pipe is predicted in general hydraulic theory by the product of the fluid density and a factor called the "major losses" (usually denoted by the symbol h_l). For horizontal flow this major loss is defined by equation (3),

$$\frac{P_1 - P_2}{\rho} = \frac{\Delta P_{hl}}{\rho} = h_l, \tag{3}$$

where P_1 and P_2 are the upstream and downstream pressures across a unit length of pipe, ΔP_{hl} is the head loss for a single phase flow along a unit length of pipe. For turbulent single phase pipe flows h_l is calculated by equation (4),

$$h_l = f \frac{L}{D} \frac{\bar{U}^2}{2}, \tag{4}$$

where L and D are the unit length of pipe and pipe diameter, $\bar{U}$ is the average flow velocity of the single phase flow and f is the friction factor which is traditionally predicted by the Moody[1] diagram which shows curves of friction factor against Reynolds number for smooth pipes and for pipes of increasing relative roughness, denoted by the term e/D.

[1] Moody published the Moody Diagram (building on the work of Rouse) in 1944, so this work was known and available to Lockhart and Martinelli. This, and the fact that the highest Reynolds number used in the Lockhart and Martinelli data set was 124,000, shows that Lockhart and Martinelli were not aiming their research at the Reynolds numbers range typical to modern day natural gas production flows. Lockhart and Martinelli would therefore have been unlikely to have agreed that their parameter was suitable for such industrial applications.

For two phase, multiphase and wet gas flows when one phase is imagined to flow in the pipe alone the associated average velocity is called the superficial velocity. The liquid superficial velocity ($\bar{U}_{sl}$) and the gas superficial velocity ($\bar{U}_{sg}$) are calculated by equations (5a) and (5b),

$$\bar{U}_l = \frac{m_l}{\rho_l A}; \tag{5a}$$

$$\bar{U}_g = \frac{m_g}{\rho_g A}, \tag{5b}$$

where A is the cross sectional area of the pipe.

For wet gas flows, the average liquid velocity if the liquid flowed alone is significantly smaller than the gas velocity if the gas flowed alone. It is also true that usually the liquid viscosity μ_l is order(s) of magnitude greater than the gas viscosity μ_g. Therefore, from the Reynolds number definition, equation (6),

$$\mathrm{Re} = \frac{Inertia\ \ Forces}{Viscous\ \ Forces} = \frac{\rho \bar{U}\, D}{\mu} = \frac{4m}{\pi \mu D}, \tag{6}$$

it can be seen for a wet gas flow that the liquid Reynolds number if the liquid flowed alone is much lower than the gas Reynolds number if the gas flowed alone.

The friction factor is, for a given pipe roughness, solely a function of the Reynolds number. In this case it is always the same pipe in question with two different flows (i.e. that of the liquid and the gas phases of the wet gas flow as if they were flowing alone in that particular pipe) and therefore the relative pipe roughness (e/D) is constant. Therefore, from the Moody diagram for any given pipe roughness, it can be seen that the difference in Reynolds numbers between the gas and liquid flows means different friction factor values, say f_l and f_g, for the liquid and gas friction factors and because $\mathrm{Re}_l << \mathrm{Re}_g$ the condition $f_l > f_g$ exists. From equations (3) and (4) the single phase major pressure loss in a pipe is given by

$$\Delta P = \rho h_l = \rho f \frac{L}{D} \frac{\bar{U}^2}{2}. \tag{7}$$

Substituting equation (7) into equation (1) for liquid and gas gives the original Lockhart and Martinelli parameter definition (i.e. the square root of the single phase pressure drop ratio) calculated using an appropriate friction factor calculation for rough pipe and the Reynolds numbers in use with typical wet natural gas production flows, X_M,

$$X_M = \sqrt{\frac{\Delta P_{l,hl}}{\Delta P_{g,hl}}} = \frac{\sqrt{\rho_l f_l \frac{L}{D}\frac{\overline{U}_l^2}{2}}}{\sqrt{\rho_g f_g \frac{L}{D}\frac{\overline{U}_g^2}{2}}} = \sqrt{\frac{f_l}{f_g}}\frac{\overline{U}_l}{\overline{U}_g}\sqrt{\frac{\rho_l}{\rho_g}} . \tag{8}$$

Substituting equations (5a) and (5b) into equation 8 gives

$$X_M = \sqrt{\frac{\Delta P_{l,hl}}{\Delta P_{g,hl}}} = \sqrt{\frac{f_l}{f_g}}\frac{m_l}{m_g}\sqrt{\frac{\rho_g}{\rho_l}} . \tag{9}$$

Equation (9) is the mathematical expression for the original meaning of the Lockhart-Martinelli parameter as published by the engineers R.W. Lockhart and R.C. Martinelli in 1949 using the appropriate calculation method for typical flow range encountered in natural gas production. Equation (9) and equation (2) are essentially the same, with the only difference being the method of calculating the friction factors.

Murdock [4] used a parameter which has subsequently been denoted by X by some engineers applying Murdock's work (although Murdock himself never used this symbol). This parameter was used by Murdock during the discussion of the behaviour of orifice plate meters in general two phase flow. For clarity, in this paper $X_{Murdock}$ will denote this Murdock parameter. Murdock described the relative amount of liquid and gas in a given pipe two phase / wet gas flow by using the square root of the ratio of the differential pressures ΔP_l and ΔP_g that would be read by a given orifice plate meter if the liquid and gas phases flowed alone, equation (10),

$$X_{Murdock} = \sqrt{\frac{\Delta P_{l,m}}{\Delta P_{g,m}}} , \tag{10}$$

where subscript m means meter-induced pressure drop.

The standard differential pressure (DP) meter equation is

for gas: $$m_g = EA_t \varepsilon C_{d,g}\sqrt{2\rho_g \Delta P_{g,m}} ; \tag{11a}$$

and for liquid: $$m_l = EA_t C_{d,l}\sqrt{2\rho_l \Delta P_{l,m}} , \tag{11b}$$

where E is the velocity of approach, A_t is the orifice area, ε is the expansibility factor (denoted as Y by Murdock), $C_{d,g}$ and $C_{d,l}$ are the discharge charge coefficients of gas and liquid, and $\Delta P_{g,m}$ and $\Delta P_{l,m}$ are the differential pressures which would be observed if the gas and liquid phases flowed alone through the meter. Equation (10) can also be written in the form

$$X_{Murdock} = \sqrt{\frac{\Delta P_{l,m}}{\Delta P_{g,m}}} = \frac{C_{d,g}\varepsilon}{C_{d,l}}\frac{m_l}{m_g}\sqrt{\frac{\rho_g}{\rho_l}} . \tag{12}$$

Murdock never called this parameter the Lockhart-Martinelli parameter although some in industry now confuse the terms.

Chisholm [5, 6] published a general two phase flow correlation for orifice plate meters and used a similar, but not identical, parameter denoted by upper case X. For clarity, in this paper $X_{Chisholm}$ will denote this Chisholm parameter. This is shown as equation (13) where x is the flow quality as described by equation (14). The equation for Chisholm's correlating parameter (13) can be rewritten as equation (15),

$$X_{Chisholm} = \frac{1-x}{x}\sqrt{\frac{\rho_g}{\rho_l}}\,; \tag{13}$$

$$x = \frac{m_g}{m_g + m_l}\,; \tag{14}$$

$$X_{Chisholm} = \frac{m_l}{m_g}\sqrt{\frac{\rho_g}{\rho_l}}\,. \tag{15}$$

Chisholm derived equation (15) similarly to the way that Murdock derived equation (12). However, unlike Murdock, Chisholm called the parameter he derived *"…the Lockhart-Martinelli correlating group"*. The reference he cites as his reference 13 is the Lockhart-Martinelli paper, reference [3] in this paper.

Chisholm therefore appears to have erroneously called the parameter defined in equation (15) the Lockhart-Martinelli parameter. Returning to equation (15) it can be seen that it is the same as equation (12) only if there is the added assumption that

$$C_{d,g}\varepsilon = C_{d,l}\,. \tag{16}$$

This is an approximation that could be treated as valid under some, but not all, two phase flow conditions. However, although equation (15) can be found from equation (12) by making this assumption, Chisholm did not state as much, but it can also be formed by an alternative derivation. For any given pipe cross sectional area and any given two phase flow imagine that the phases were to flow alone. Then, if the square root of the ratio of the inertia of these gas and liquid phase flows across that given cross section of the pipe is taken, this would give a parameter which can be denoted as X_{LM},

$$X_{LM} = \sqrt{\frac{Liquid\ \ Flowing\ \ Alone\ \ Inertia}{Gas\ \ Flowing\ \ Alone\ \ Inertia}} = \sqrt{\frac{\rho_l U_{sl}^2 D^2}{\rho_g U_{sg}^2 D^2}}\,, \tag{17}$$

with $Liquid\ \ Flowing\ \ Alone\ \ Inertia = \rho_l U_{sl}^2 D^2$ and $Gas\ \ Flowing\ \ Alone\ \ Inertia = \rho_g U_{sg}^2 D^2$. Therefore , substituting in equations (5a), (5b) and equation (17) and comparing the result to equation (15) gives,

$$X_{LM} = \sqrt{\frac{\rho_l U_{sl}^2 D^2}{\rho_g U_{sg}^2 D^2}} = \frac{U_{sl}}{U_{sg}}\sqrt{\frac{\rho_l}{\rho_g}} = \frac{m_l}{m_g}\sqrt{\frac{\rho_g}{\rho_l}} = X_{Chisholm}\,. \tag{18}$$

The importance of this simple result in terms of wet gas flow metering is considerable.

The original Lockhart-Martinelli parameter, X, is only applicable to smooth pipes and low Reynolds numbers. The associated equation developed here that is valid for typical wet gas natural gas production flow conditions, equation (9), is dependent on the friction factors and therefore the condition of the particular pipe in question. Two identical wet gas flow conditions flowing in pipes that only differ by having different relative roughness values, will have different Lockhart-Martinelli parameters. Hence, as a tool to define a wet gas flow so that a simple and direct comparison between flows can be made this is clearly an impractical parameter to use.

The Murdock parameter, $X_{Murdock}$, that some have mistakenly called the Lockhart-Martinelli parameter, is not only dependent on the relationship of meter discharge coefficient with Reynolds number and the gas expansibility factor, but is solely useable for the case of wet gas flow metering with DP meters. It is also dependent on the geometry of the DP meter in question. It is not directly applicable to non-DP meter wet gas flow metering systems. Hence, this is not a practical tool to help characterise a wet gas flow so that a simple and direct comparison between flows can be made.

However, the Chisholm parameter $X_{Chisholm}$, when derived by this different method, unlike the original Lockhart-Martinelli parameter, X, is shown to be independent of the relative pipe roughness. Further, the Chisholm parameter $X_{Chisholm}$, unlike Murdock's parameter, $X_{Murdock}$, is independent of any DP meter technology. It is simply the square root of the ratio of the liquid inertia to the gas inertia at any given cross section of the pipe if the phases of a two phase flow flowed alone. It can therefore be used to describe the liquid to gas content of any wet gas flow, in any roughness of pipe, whether any type of meter is present or not. This parameter is therefore a very useful non-dimensional way of describing the relative amount of liquid in a gas flow.

By the 1990's some in industry were calling Chisholm's version of the parameter $X_{Chisholm}$ the Lockhart-Martinelli parameter, as Chisholm had erroneously done. However, the developed version of the original Lockhart-Martinelli parameter, the Murdock parameter and the Chisholm parameter are only the same if equation (19a) holds. This in fact is never the case. All real two phase flows follow equation (19b),

$$\sqrt{\frac{f_l}{f_g}} = \frac{C_{d,g}\varepsilon}{C_{d,l}} = 1; \tag{19a}$$

$$\sqrt{\frac{f_l}{f_g}} \neq \frac{C_{d,g}\varepsilon}{C_{d,l}} \neq 1. \tag{19b}$$

For a wet gas flow condition, the square root of the ratio of the friction factors of the liquid and gas flows if these phases were to flow alone in a straight unit length of pipe is not equal to unity; the ratio of the product of gas discharge coefficient and expansibility of the gas flow flowing alone to the liquid discharge coefficient of the liquid flowing alone is not equal to unity. Therefore, the Lockhart-Martinelli, Murdock and Chisholm parameters that have all been commonly denoted by X are all different. The term Lockhart-Martinelli parameter is now extensively used by the metering fraternity to describe either the Murdock or Chisholm parameters with little in the literature to state

that these are two different definitions and neither of these are the actual Lockhart-Martinelli parameter as defined by Lockhart and Martinelli.

These authors of this paper promote the use of the Chisholm parameter due to its independence from pipe friction factors and DP meter characteristics. However, it is understood that the term Lockhart-Martinelli parameter is entrenched in industry and therefore it is suggested that the term should remain and the preferred definition be denoted by X_{LM}, that is,

$$X_{LM} = \sqrt{\frac{Superficia\ l\ Liquid\ Inertia\ Force}{Superficia\ l\ Gas\ Inertia\ Force}} = \frac{m_l}{m_g}\sqrt{\frac{\rho_g}{\rho_l}} = \frac{Q_l}{Q_g}\sqrt{\frac{\rho_l}{\rho_g}}\ . \qquad (20)$$

This definition is also written in terms of the gas and liquid volume flowrates Q_g and Q_l as this is also a commonly used equation.

3.2. Is there really an incompatibility in definitions within the industry?

Unfortunately, it is not simply the case that most engineers use one definition and only those not familiar with the industry mistakenly revert to another, as shown by some examples. In these examples it must be remembered that with no formal standard agreed upon engineers are free to use what ever definition they wish and therefore nobody is incorrect. They are simply using the same term to define different phenomena. Examples:

1. If an engineer did not know the definition of the Lockhart-Martinelli parameter it would be reasonable practice to look up the original paper and assume that the given term is the universally used definition as this is common practice in the scientific community. The original Lockhart-Martinelli parameter definition was briefly discussed by Falcone [7] at the NSFMW in 2006. The paper indicated that there are other definitions but did not explain further.
2. Murdock's original plot of the gas flowrate error of a meter vs. $X_{Murdock}$ [4], is now widely referred to as a Murdock plot and is the almost universal method of plotting DP meter wet gas data. However, nearly all recent graphs use gas flowrate error of a meter vs. $X_{Chisholm}$ instead, with no mention of this inconsistency being made. The Murdock parameter definition is indirectly suggested by Geach and Jamieson [8] who made the comment, "the correlations used to correct for liquid entrainment in wet gas require both the gas and liquid discharge coefficients which are not the same." However, this would only be true if the correlation were designed for use with the Murdock parameter $X_{Murdock}$.
3. In many papers and publications, the Chisholm parameter is used in plots and correlations and called the Lockhart-Martinelli parameter without any comment being made regarding the difference, e.g. de Leeuw [9], Hall and Steven [10].

3.3 Impact of the different definitions in practical applications

This is not academic trivia. There is a direct relevance to the current practices involving wet gas flow metering as there can be significant differences between the four equations. A worked example will indicate this point.

Consider a wet natural gas flow in a 4 inch schedule 80 pipe (inside bore diameter of 0.09718 m) with a relative roughness level of 0.001. The pressure is 50 bara at 300K and the natural gas molecular weight is 17.4. The gas density is therefore approximately 38 kg/m^3 and the gas viscosity is approximately 0.01124 cP. The gas flowrate is 400 m^3/hr (approximately 17.5 MMSCFD or 4.23 kg/s). In this example, the liquid flowrate is 1.937 kg/s (1317 US barrels per day or 8.72 m^3/hr), the density is 800 kg/m^3 and the liquid viscosity is 1.92 cP. The flow is through an ISO 5167 Part 2 standard orifice plate meter of beta 0.7 with D and D/2 tappings fitted.

What are the values of the original Lockhart-Martinelli parameter, X, the roughness-modified Lockhart-Martinelli parameter, X_M, the Murdock parameter $X_{Murdock}$, and the Chisholm parameter $X_{Chisholm}$, and how do they compare to each other?

Applying the original Lockhart-Martinelli parameter, equation (2), unaware that it is not applicable to these rough pipes with high Reynolds numbers would give

$$X = \sqrt{\frac{\Delta P_{l,hl}}{\Delta P_{g,hl}}} = \sqrt{\left(\frac{m_l}{m_g}\right)^{1.8} \frac{\rho_g}{\rho_l}\left(\frac{\mu_l}{\mu_g}\right)^{0.2}} = 0.180\,. \tag{21}$$

The Reynolds number of the gas phase if it flowed alone in the pipe is approximately 4.93×10^6. The Reynolds number of the liquid phase if it flowed alone in the pipe is approximately 1.32×10^4. From the Moody diagram for a relative roughness of 0.001, the gas friction factor f_g is 0.0196 and the liquid friction factor f_l is 0.032. Therefore the original Lockhart-Martinelli parameter when modified for the case of rough pipes and high Reynolds numbers is

$$X_M = \sqrt{\frac{\Delta P_{l,f}}{\Delta P_{g,f}}} = \sqrt{\frac{f_l}{f_g}}\,\frac{m_l}{m_g}\sqrt{\frac{\rho_g}{\rho_l}} = 0.128\,. \tag{22}$$

From Table A.2 of ISO 5167 Part 2 the orifice plate meter discharge coefficient at a Reynolds number of 4.93×10^6 is 0.608 and at a Reynolds number of 1.32×10^4 is 0.639. Using ISO 5167 part 2 the expansibility factor in this example is 0.9887. Therefore Murdock's parameter from equation (12) is

$$X_{Murdock} = \sqrt{\frac{\Delta P_{l,m}}{\Delta P_{g,m}}} = \frac{C_{d,g}\,\varepsilon}{C_{d,l}}\,\frac{m_l}{m_g}\sqrt{\frac{\rho_g}{\rho_l}} = 0.094\,. \tag{23}$$

Chisholm's parameter is calculated from equation (15) and (17),

$$X_{Chisholm} = X_{LM} = \frac{m_l}{m_g}\sqrt{\frac{\rho_g}{\rho_l}} = 0.100\,. \tag{24}$$

Therefore, for the same wet gas flow conditions,

Calculation	Symbol	Value
Original Lockhart-Martinelli	X	0.180
Roughness modified Lockhart-Martinelli	X_M	0.128
Murdock	$X_{Murdock}$	0.094
Chisholm	$X_{Chisholm}$	0.100

Taking X_{LM} as the most appropriate definition it can be seen that the original Lockhart-Martinelli parameter is 80% higher, the modified original parameter for this particular pipe roughness is 28% higher and the Murdock parameter for this particular DP meter is 6% lower. Hence, the difference between these parameters is not trivial.

3.4. Correlation sensitivity to Lockhart-Martinelli parameter errors

The error in the gas flowrate prediction when using a gas DP meter wet gas correlation when there is an error in the Lockhart-Martinelli parameter definition is, while still significant, not as serious as the errors in the Lockhart-Martinelli parameter itself due to the sensitivity of the correlations to the Lockhart-Martinelli parameter. To show this point the above worked example is continued by applying Chisholm's[6] orifice plate wet gas correlation,

$$Over-reading = \frac{m_{g,apparent}}{m_g} = \sqrt{1+\left\{\left(\left(\frac{\rho_g}{\rho_l}\right)^{1/4} + \left(\frac{\rho_l}{\rho_g}\right)^{1/4}\right)X_{LM}\right\} + \left(X_{LM}\right)^2}\,, \tag{25}$$

where $m_{g,apparent}$ is the uncorrected gas flowrate prediction. With a gas to liquid density ratio of 0.0475 the associated over-readings (or positive error in the gas flowrate prediction) are:

Calculation	Symbol	Value	Gas flowrate over-reading
Original Lockhart-Martinelli	X	0.180	22.6%
Roughness modified Lockhart-Martinelli	X_M	0.128	16.1%
Murdock	$X_{Murdock}$	0.094	12.0%
Chisholm	$X_{Chisholm}$	0.100	12.7%

Chisholm used $X_{LM} = X_{Chisholm} = 0.100$, so the Chisholm correlation is saying the over-reading is 12.7%. However, an incorrect choice of definition can cause an error in the final gas mass flowrate prediction. In this case a 0.63% over-estimation for

$X_{Murdock} = 0.094$, a 3% under-estimation for $X_M = 0.128$ and an 8.8% under-estimation for $X = 0.180$. This is a bias, not an uncertainty.

The prediction of a DP meter wet gas correlation is therefore affected by which parameter is being used. Different DP meters and correlations will have different sensitivities to varying Lockhart-Martinelli parameter values. For example, a Venturi meter is more sensitive to the Lockhart-Martinelli parameter than an orifice meter. For the case of a Venturi the above results would most likely have shown greater biases, although the calculation in equation (23) requires the discharge coefficient which for a Venturi requires a flow calibration. The risk of a relatively large bias if the Murdock parameter is applied where a Lockhart-Martinelli parameter should be applied is somewhat mitigated by the Venturi meter's tendency to have a relatively small shift in discharge coefficient across a large Reynolds number range compared to the orifice plate.

These are errors and not uncertainties. Typical DP meter wet gas correlations correct the over-reading to an uncertainty of 2% so small differences may not be noticeable but the added error in this case is avoidable. As this example is randomly chosen it is possible that in many production wet gas flow metering cases the error could be larger.

3.5. Another definition for the Lockhart-Martinelli parameter

The Lockhart-Martinelli parameter can be defined as the square root of the ratio of the gas densimetric Froude number and the liquid densimetric Froude number. This is in fact the same parameter as equation (18). The definition of the gas densimetric Froude number is the square root of the gas flow inertia if the gas flowed alone to the liquid phase gravitational force. The definition of the liquid densimetric Froude number is the square root of the liquid flow inertia if the liquid flowed alone to the liquid phase gravitational force. This is shown by equations (26) and (27),

$$Fr_g = \sqrt{\frac{Superficia\ l\ Gas\ Inertia}{Liquid\ Gravity\ Force}} = \frac{U_{sg}}{\sqrt{gD}}\sqrt{\frac{\rho_g}{\rho_l - \rho_g}} = \frac{m_g}{A\sqrt{gD}}\sqrt{\frac{1}{\rho_g(\rho_l - \rho_g)}}\,; \quad (26)$$

and

$$Fr_l = \sqrt{\frac{Superficia\ l\ Liquid\ Inertia}{Liquid\ Gravity\ Force}} = \frac{U_{sl}}{\sqrt{gD}}\sqrt{\frac{\rho_l}{\rho_l - \rho_g}} = \frac{m_l}{A\sqrt{gD}}\sqrt{\frac{1}{\rho_l(\rho_l - \rho_g)}}\,, \quad (27)$$

where g is the gravitational constant. Taking the ratio of the liquid densimetric Froude number and gas densimetric Froude number gives the Chisholm parameter,

$$X_{LM} = \frac{Fr_l}{Fr_g} = \frac{\sqrt{\frac{Gas\ Superficid\ Inertia}{Liquid\ Gravity\ Force}}}{\sqrt{\frac{Liquid\ Superficid\ Inertia}{Liquid\ Gravity\ Force}}} = \sqrt{\frac{Gas\ Superficia\ l\ Inertia}{Liquid\ Superficia\ l\ Inertia}} = \frac{m_l}{m_g}\sqrt{\frac{\rho_g}{\rho_l}}\,. \quad (28)$$

3.6. Definitions of wet gas flow conditions

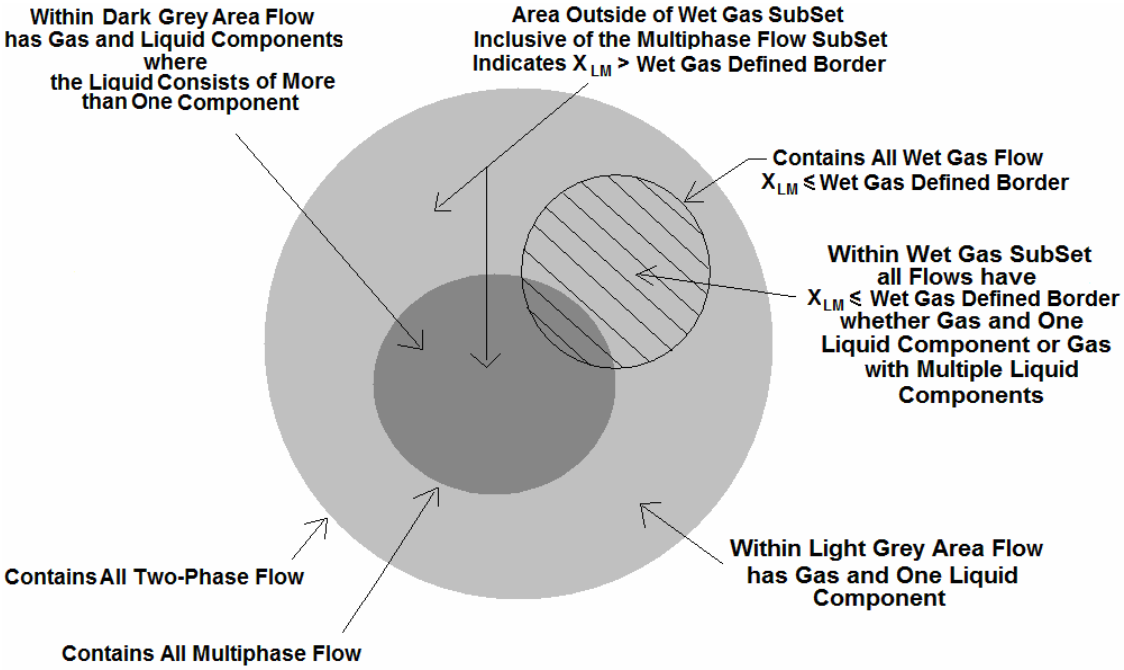

Figure 2. Wet gas as a subset of two phase and multiphase flow

There are several different wet gas flow definitions. For example, many engineers in the steam industries typically call any saturated steam with a quality, *x,* defined in equation (14), less than unity, wet steam (i.e. a wet gas), but others say wet steam is any steam quality greater than 0.5. Some in the oil and gas industry call wet gas any flow with a gas volume fraction (GVF) greater than 90%. Others have said wet gas flow should be defined as having a Lockhart-Martinelli parameter of 0.35 or 0.3, although they don't all confirm what they definition of Lockhart-Martinelli parameter has been used. (The $X_{LM} \leq 0.35$ definition is an early definition for wet gas used by Shell that came about due to experimental evidence suggesting that slugging in the pipe can become significant at $X_{LM} > 0.35$.) There are other definitions over the years, but recently, with the exception of those that continue to talk of GVF > 90%, the trend is to define wet gas flow as any two phase flow (i.e. any number of liquid components) by using a limiting value of the Lockhart-Martinelli parameter. Figure 2 shows a pictorial view of wet gas.

Just at what value of Lockhart-Martinelli parameter the border between wet gas and general two phase flow should be set is a matter of some debate. Three organisations promote a border in the region of a Lockhart-Martinelli parameter of 0.3. Those are the Norwegian Society for Oil and Gas Measurement [2], the American Petroleum Institute (API) [11[2]] and the American Society of Mechanical Engineering (ASME[3]) [12].

[2] It is understood by the authors that at the time of writing API has not yet ratified this document.
[3] At the time of writing this ASME document is under ballot and is due for general release in early 2008.

It is difficult to find a technical review that promotes the use of another wet gas defining parameter with technical reasoning. All three publications listed above give a description of the Lockhart-Martinelli parameter that is fundamentally the same, i.e. equation (18).

The ASME document states that the wet gas definition is $X_{LM} \leq 0.30$. The Norwegian Society for Oil and Gas Measurement defines wet gas as a two phase flow with a maximum Lockhart-Martinelli parameter value of approximately 0.30. That is, they state $X_{LM} \leq 0.30$ as an approximate border between a wet gas flow and a general two phase flow but they stop short of declaring this an absolute border and allow room for individual interpretation.

The API document [11] has a more detailed approach. The definition of wet gas flow is separated into three "types":

API Type I Wet Gas:
"Wet gas Type I is defined as the region with Lockhart-Martinelli number X equals or less than 0.02…" That is $X_{LM} \leq 0.02$.

API Type II Wet Gas:
"Type II wet gas is defined as the region above Type I … [*and*] … constrained to the liquid content limit by the following Lockhart-Martinelli relationship equal to or less than 0.3." That is $0.02 < X_{LM} \leq 03$.

API Type III Wet Gas:
"All the regions above the boundaries defined by the Lockhart-Martinelli relationship of 0.3 can be designated as a 'Multiphase Measurement System' … ". That is $X_{LM} > 0.3$.

The API Type I definition appears to be based solely on single phase differential pressure (DP) meter design wet gas performance and is not general to all wet gas flows. It is accepted by some in industry that at $X_{LM} \leq 0.02$ most DP meters give small gas flowrate errors and a DP meter can therefore be used instead of a more sophisticated wet gas or multiphase meter. At $X_{LM} > 0.02$ the use of a wet gas meter becomes thought of by many as a more valid option. However, the Lockhart-Martinelli parameter value of 0.02 is not universally important to all gas flow meter types and hence it could be argued it is inappropriate to use this value to give a general non-meter specific definition of wet gas flow. Furthermore, it is debatable whether this $X_{LM} \leq 0.02$ limit for DP meters is a particularly precise value for when a wet gas meter shows advantage over a standard gas meter. Figure 3 shows a typical wet gas test result on a 4 inch, 0.4 beta Venturi meter, reproduced from Steven [13]. The solid points are the uncorrected wet gas flow gas flowrate predictions from the meter and the hollow points the de Leeuw [9] Venturi correlation corrected gas flowrate predictions for a known liquid flowrate. It can be seen that at a Lockhart-Martinelli parameter of 0.02 the over-reading can be in the order of 5%. It is arguable that a 5% gas flowrate error could be improved upon by some wet gas flow meter devices.

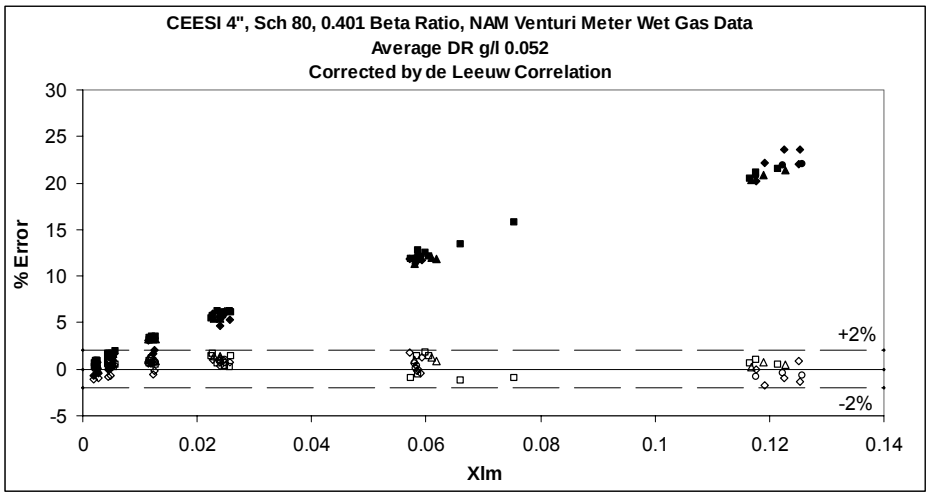

Figure 3. CEESI wet gas test data on a 4 inch 0.4 beta Venturi meter

The API Type II definition is bound at the lower end by the Type I definition which has the above issues.

The API Type III is ambiguous as there is no upper liquid content limit. According to this definition, an infinitely small quantity of gas in an infinitely large quantity of liquid is still technically a Type III wet gas flow. A diagram in the API report [11] tends to suggest the upper limit of Type III is perhaps a GVF of 80% but this is not precisely stated.

Therefore, the API gave no upper liquid content limit to wet gas flow. The Norwegian Society for Oil and Gas Measurement left the upper liquid quantity limit of wet gas flow deliberately vague by calling the border a Lockhart-Martinelli parameter of approximately 0.3. The border of the Lockhart-Martinelli parameter of 0.3 is rather arbitrary. In terms of fluid flow it has no special significance, with no fundamental physical condition change between a flow just above and just below this 0.3 value. Some wet gas and some multiphase flow metering technologies may have operating envelopes that straddle this arbitrary border. For example, one particular wet gas meter design could be claimed to operate in the range $0 \leq X_{LM} \leq 0.35$. Some multiphase meter technologies claim to operate at $GVF \leq 0.95$, which, depending on the flow conditions, could mean a minimum Lockhart-Martinelli parameter of less than 0.3.

To the authors of this paper, it seems far more important that operators using wet gas meters agree on the definition of terms to be used when describing flow ranges and mathematical equations than it is to give a precise scientific definition of the border between wet gas flow and general two phase / multiphase flow.

3.7. Equivalent wet gas parameters and conversions

A common requirement from the increasingly accepted wet gas definition of approximately $X_{LM} \leq 0.30$ is an ability to express this boundary in the units normally encountered in production situations.

The Lockhart-Martinelli parameter is typically asked to be expressed in terms of one of five common alternative parameters. These are:

- Gas volume fraction (GVF). the gas volume flowrate to the total volume flowrate as shown by equation (29a);
- Liquid volume fraction (LVF), the liquid volume flowrate to the total volume flowrate as shown by equation (29b);
- flow quality (sometimes termed the dryness fraction), and defined by equation (14);
- liquid to gas mass flowrate ratio, the ratio of the gas mass flowrate to liquid mass flowrate;
- liquid to gas volume ratio, the ratio of the gas volume flowrate to liquid volume flowrate.

GVF and LVF are defined by

$$GVF = \frac{Q_g}{Q_g + Q_l} \; ; \tag{29a}$$

and

$$LVF = \frac{Q_l}{Q_g + Q_l} \; . \tag{29b}$$

Unfortunately, conversion isn't as straightforward as a direct equivalent numerical answer as these parameters are all related via the gas to liquid density ratio. The various parameters are related as shown in the following equation series:

$$X_{LM} = \frac{m_l}{m_g}\sqrt{\frac{\rho_g}{\rho_l}} = \frac{Q_l}{Q_g}\sqrt{\frac{\rho_l}{\rho_g}} = \frac{1-(GVF)}{(GVF)}\sqrt{\frac{\rho_l}{\rho_g}} = \frac{1-x}{x}\sqrt{\frac{\rho_g}{\rho_l}} = \frac{(LVF)}{1-(LVF)}\sqrt{\frac{\rho_l}{\rho_g}} \; ; \tag{30a}$$

$$GVF = \frac{1}{1+\left(\frac{m_l}{m_g} * \frac{\rho_g}{\rho_l}\right)} = \frac{1}{\left(\frac{Q_l}{Q_g}\right)+1} = 1-(LVF) = \frac{\sqrt{\frac{\rho_l}{\rho_g}}}{X_{LM} + \sqrt{\frac{\rho_l}{\rho_g}}} = \frac{\left(\frac{\rho_l}{\rho_g}\right)}{\left(\frac{\rho_l}{\rho_g}\right)+\left(\frac{1-x}{x}\right)} \; ; \tag{30b}$$

$$x = \frac{1}{1+\left(\frac{m_l}{m_g}\right)} = \frac{1}{1+\left(\frac{\rho_l}{\rho_g}\frac{Q}{Q_g}\right)} = \frac{1}{1+X_{LM}\sqrt{\frac{\rho_l}{\rho_g}}} = \frac{1}{1+\left(\left(\frac{1-(GVF)}{(GVF)}\right) * \frac{\rho_l}{\rho_g}\right)} = \frac{1}{1+\left(\left(\frac{(LVF)}{1-(LVF)}\right) * \frac{\rho_l}{\rho_g}\right)} \; ; \tag{30c}$$

$$\frac{m_l}{m_g} = X_{LM}\sqrt{\frac{\rho_l}{\rho_g}} = \frac{\rho_l}{\rho_g}\frac{Q_l}{Q_g} = \frac{1-(GVF)}{GVF}\frac{\rho_l}{\rho_g} = \frac{LVF}{1-LVF}\frac{\rho_l}{\rho_g} = \frac{1-x}{x}; \quad (30d)$$

$$\frac{Q_l}{Q_g} = X_{LM}\sqrt{\frac{\rho_g}{\rho_l}} = \frac{\rho_g}{\rho_l}\frac{m_l}{m_g} = \frac{1-(GVF)}{GVF} = \frac{LVF}{1-(LVF)} = \left(\frac{1-x}{x}\right)\frac{\rho_g}{\rho_l}; \quad (30e)$$

$$LVF = 1-(GVF) = \frac{X_{LM}\sqrt{\frac{\rho_g}{\rho_l}}}{1+X_{LM}\sqrt{\frac{\rho_g}{\rho_l}}} = \frac{\left(\frac{1-x}{x}\right)}{\left(\frac{1-x}{x}\right)+\frac{\rho_l}{\rho_g}} = \frac{\frac{\rho_g}{\rho_l}}{\frac{\rho_g}{\rho_l}+\frac{\dot{m}_g}{\dot{m}_l}} = \frac{\frac{\dot{Q}_l}{\dot{Q}_g}}{1+\frac{\dot{Q}_l}{\dot{Q}_g}}. \quad (30f)$$

It can be seen from equation (30a) that setting the upper limit of wet gas flow at a Lockhart-Martinelli parameter of 0.3 does not set a value for any of the alternative five parameters since they are related through the gas to liquid density ratio. It is a fair and understandable request from meter users and operating engineers to have the seemingly abstract concept of the Lockhart-Martinelli parameter expressed in units they can more readily understand, but an example shows how this is not necessarily possible. Taking the GVF as an example, a conventional wet gas definition is to say that wet gas flow has a GVF limit of 90%. Engineers get asked whether this GVF > 90% flow is approximately the same as a $X_{LM} \leq 0.30$ flow. From equation (30a), if $X_{LM} = 0.30$ and $GVF = 0.90$ then this would define the density ratio, ρ_g/ρ_l as 0.137174. This is clearly a meaningless statement. In fact, setting any two of the six parameters also then sets the gas to liquid density ratio value. (More details were supplied by one of the authors to ASME [12].) There is therefore no equivalent expression to $X_{LM} \leq 0.30$ without including a function of the gas to liquid density ratio.

Figure 4 shows a graphical form of equations (30). The abscissa is the gas to liquid density ratio and the ordinate is the Lockhart-Martinelli parameter. There are four coloured series of lines. These are black for the quality, blue for the GVF, orange for the liquid to gas mass flowrate and green for the liquid to gas volume flowrate. (Since GVF = 1 – LVF, the LVF lines overlap the GVF lines and so are not shown.)

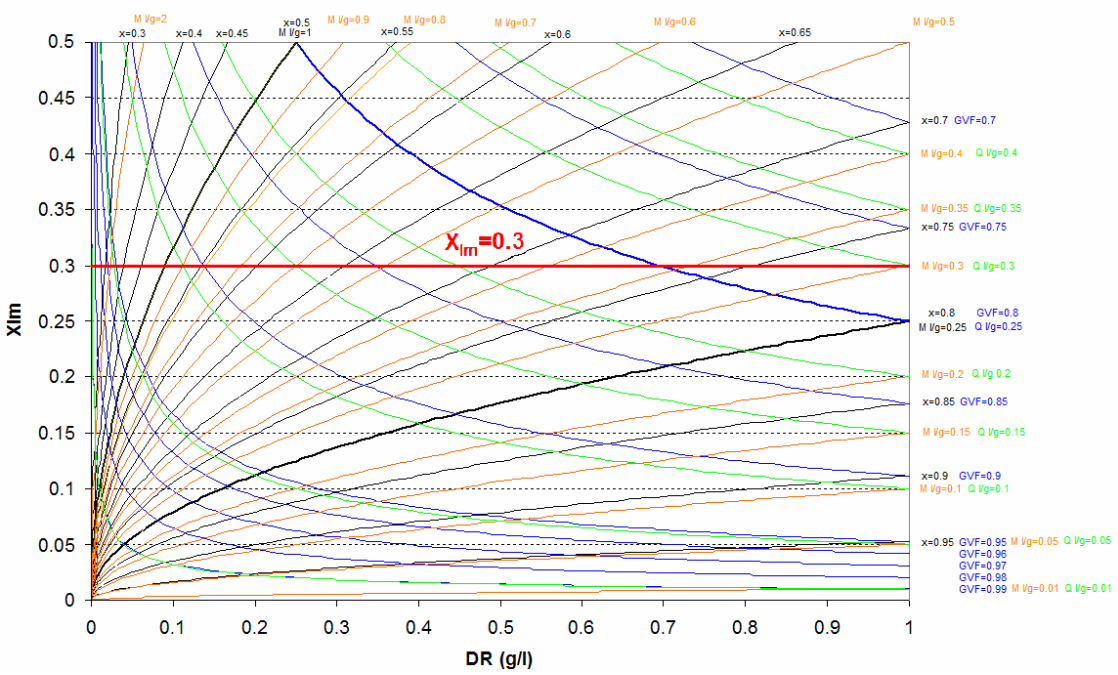

Figure 4. Sample wet gas / two phase flow parameter comparison graph

As an example take a gas to liquid density ratio of 0.2 and a quality of 0.8. Finding this point in Figure 4 immediately allows the other parameters to be read off for quick comparisons, that is:

$$X_{LM} = 0.11;\ GVF = 0.955 = 1 - LVF;\ LVF = 0.045;$$

$$m_l/m_g = 0.25 \text{ and } Q_l/Q_g = 0.05.$$

Such graphs are useful only when the flow conditions fit the graph. In general two phase flows the Lockhart-Martinelli parameter can be much greater than 0.5 and a larger scale is needed. Also in most real world flows the gas to liquid density ratio is less than 0.2 and a span of up to 0.2 gives more resolution. Therefore ASME [12] gives a series of such graphs and this figure is given as an example only.

4. The Difference Between the Gas Volume Fraction and the Gas Void Fraction

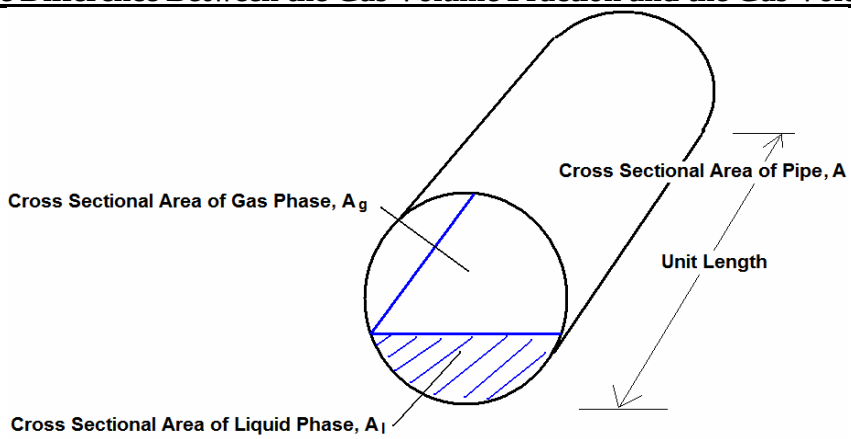

Figure 5. A sketch of stratified flow in a pipe

The *gas volume fraction* is defined as the ratio of the gas volume flowrate to the total volume flowrate, given by equation (31). The *liquid volume fraction* is defined as the ratio of the liquid volume flowrate to the total volume flowrate, given by equation (32). The name gas volume fraction has led to some confusion in the industry as this is sometimes mistakenly thought to be the actual ratio of the volume of the gas to the pipe volume along a unit section of pipe in two phase flow at any given instant in time. The *gas void fraction* (α_g) is defined as the ratio of the cross-sectional area occupied by the gas to the total cross-sectional area, at any given instant in time, and this is shown in equation (33),

$$GVF = \frac{Q_g}{Q_g + Q_l} \; ; \tag{31}$$

$$LVF = \frac{Q_l}{Q_g + Q_l} \; ; \tag{32}$$

$$\alpha_g = \frac{V_g}{V_g + V_l} = \frac{A_g L}{A_g L + A_l L} = \frac{A_g}{A_g + A_l} \; . \tag{33}$$

V_g is the gas volume in a unit volume of constant area pipe, V_l is the liquid volume in a unit volume of constant area pipe, A_g is the gas cross-sectional area, A_l is the liquid cross-sectional area and L is a unit length of constant area pipe, as shown in Figure 5.

The gas volume fraction is not the same parameter as the gas void fraction unless the average gas velocity and average liquid velocity are the same. The slip ratio denoted here by K, which is defined as the ratio of the average gas and liquid velocities, equation (34), must be unity, for the GVF and the gas void fraction parameters to be equivalent,

$$K = \bar{U}_g \big/ \bar{U}_l \; . \tag{34}$$

This statement may be further explained by deriving an expression to relate the GVF to the cross-sectional area occupied by the gas and the liquid. Starting with equation (35),

$$Q = A\bar{U}\,, \tag{35}$$

where Q is the volume flowrate, A the area that the flow in question flows through and $\bar{U}$ is the average velocity of the flow. Equation (36) can now be derived,

$$GVF = \frac{Q_g}{Q_g + Q_l} = \frac{A_g \bar{U}_g}{A_g \bar{U}_g + A_l \bar{U}_l} = \frac{A_g}{A_g + \left(\dfrac{\bar{U}_l}{\bar{U}_g}\right) A_l} = \frac{A_g}{A_g + \left(\dfrac{1}{K}\right) A_l}\,; \tag{36}$$

Whereas the void fraction is defined by equation (33) which is only equivalent to equation (36) with $K = 1$.

The expression *hold-up* can be defined as the ratio of the liquid to total cross sectional area and this is shown as equation (37). Hold up is therefore the same as the liquid to pipe volume ratio for a steady flow in a constant area pipe,

$$Liquid\ \ holdup = \alpha_l = \frac{A_l}{A_g + A_l}\,. \tag{37}$$

Clearly from equations (33) and (37),

$$\alpha_g + \alpha_l = 1\,. \tag{38}$$

In most two phase flows, the slip, while difficult to measure in practice, is known to often be considerable, so an approximation of unity is not valid in the vast majority of cases.

A numerical example helps show this point, continuing with the worked example started in section 3.3. Chisholm created a slip model [6] which stated that for stratified flow the slip of a wet gas was

$$K = \frac{\bar{U}_g}{\bar{U}_l} = \left(\frac{\rho_l}{\rho_g}\right)^{1/4}\,. \tag{39}$$

There are many slip models in the literature and they should only be applied according to the limits of the models assumptions and the suitability of the model to the application in question. These authors make no claim on the validity of any particular slip model, and Chisholm's slip model used here only as an example. In the example, the gas density is 38 kg/m^3 and the liquid density is 800 kg/m^3, so the slip according to Chisholm's expression is

$$K = \frac{\bar{U}_g}{\bar{U}_l} = \left(\frac{800}{38}\right)^{1/4} = 2.14\,. \tag{40}$$

The meaning of this value is that the average gas velocity is 2.14 times that of the average liquid velocity. From equations (33), (36) and 39),

$$\alpha_g = \frac{1}{1+\left\{K\left(\frac{1}{GVF}-1\right)\right\}}. \tag{41}$$

Using the example values of 400 m^3/hr for the gas flowrate and 8.72 m^3/hr for the liquid flowrate, the GVF and LVF are

$$GVF = \frac{Q_g}{Q_g + Q_l} = 0.979\,; \tag{42a}$$

$$LVF = 1 - GVF = \frac{Q_l}{Q_g + Q_l} = 0.021\,; \tag{42b}$$

and the void fraction is

$$\alpha_g = \frac{1}{1+\left\{K\left(\frac{1}{GVF}-1\right)\right\}} = \frac{1}{1+\left\{2.14*\left(\frac{1}{0.979}-1\right)\right\}} = 0.956\,. \tag{43}$$

Hence the hold up is

$$\alpha_l = 1 - 0.956 = 0.044\,. \tag{44}$$

The Armand coefficient, C_A is a very rarely used parameter that indicates the difference between GVF and gas void fraction. It was quoted by Chisholm in his derivation of equation (25). This is shown in equation (45) along with the value in this example,

$$C_A = \frac{\alpha_g}{GVF} = \frac{0.956}{0.979} = 0.977\,. \tag{45}$$

The Armand coefficient would take a value of 1 where there is no slip, i.e. K=1.

So it should be understood that the GVF and the gas void fraction are not the same parameter. In this particular example a small difference in GVF and gas void fraction is noticeable but it is important to note that other flow conditions and other slip models can have greater differences between the parameter values. Furthermore, sometimes engineers are more interested in the liquid flowrate of a wet gas flow. In these cases the LVF is often found by equation (42b). If the GVF in this example has been erroneously described as the gas void fraction the difference between a GVF of 0.979 and gas void fraction of 0.956 is a small difference of -2.4%. However, if the GVF was taken as 0.955 when calculating the LVF , this would give a value of 0.044 instead of the actual 0.021, i.e. a difference of 110%!

The relevance of this discussion regarding the difference between GVF and gas void fraction is that it is generally the gas void fraction, or the liquid holdup that is the parameter measured. This is because the measuring device will see the fluids as they

flow in the pipe, unless somehow the gas and liquid have been homogenised to remove all slip. The GVF on the other hand is typically derived from other measured parameters. Either the slip, in addition to the holdup, must also be directly measured, or it must be modelled.. If the GVF could be independently measured in some way the value would be available for input into equation (30a) and hence for known gas and liquid densities the Lockhart-Martinelli parameter would be known. This in turn would allow the use of any single phase meter wet gas correlation based on the Lockhart-Martinelli parameter to predict the gas and liquid flowrates.

5. Summary and recommendations

Wet gas can be considered a subset of two phase flow, and is a condition described as a relatively small amount of liquid (of any composition) in a flow that is predominantly gas by volume. The upper boundary of this condition can be numerically described in dimensionless terms as having a *Lockhart-Martinelli parameter* of approximately 0.30.

The Lockhart-Martinelli parameter has been defined differently by several frequently-cited authors in the field over the last 6 decades, and by subsequent interpretation of those authors' works. The present authors recommend the definition for the Lockhart-Martinelli parameter of the correlating parameter defined by Chisholm, which is independent of pipe roughness and friction factor, and independent of any type of differential pressure meter. This quantity should be denoted by X_{LM} and is defined by

$$X_{LM} = \frac{m_l}{m_g}\sqrt{\frac{\rho_g}{\rho_l}} \,. \tag{20}$$

Finally, attention has been drawn to the difference between the quantities *gas void fraction*, which represents the actual cross-sectional distribution of the gas and liquid phases within the pipe, and *gas volume fraction* which is a volumetric ratio of the gas and liquid rates.

Nomenclature

α	Holdup (-)
ΔP	Pressure drop (Pa)
ε	Expansibility factor (-)
μ	Dynamic viscosity (Pa.s)
ρ	Density (kg/m^3)
A	Cross-sectional area (m^2)
A_t	Differential pressure meter restriction area (m^2)
C_A	Armand coefficient (-)
C_d	Discharge coefficient (-)

D	Pipe diameter (m)
e	Pipe roughness (m)
E	Velocity of approach (-)
f	Friction factor (-)
Fr	Froude number (-)
GVF	Gas volume fraction (-), commonly expressed as a percentage
K	Slip ratio (-)
L	Unit length of pipeline (m)
LVF	Liquid volume fraction (-), commonly expressed as a percentage
m	Mass flowrate (kg/s)
P_1	Upstream pressure (Pa)
P_2	Downstream pressure (Pa)
Q	Volumetric flowrate (m^3/s)
Re	Reynolds number (-)
U	Velocity (m/s)
x	Quality (-)
X	Dimensionless parameter defined by Lockhart & Martinelli (-)
$X_{Chisholm}$	Dimensionless parameter defined by Chisholm (-)
X_{LM}	Alternative definition of Chisholm dimensionless parameter (-)
X_M	Roughness-modified version of dimensionless parameter defined by Lockhart & Martinelli (-)
$X_{Murdock}$	Dimensionless parameter defined by Murdock (-)

References

1. Jamieson, A. *et al,*, "Neftemer – A versatile and cost effective multiphase meter," North Sea Flow Measurement Workshop, St Andrew's, UK, Oct 2006.
2. "Handbook of multiphase flow metering," Revision 2, Norwegian Society for Oil and Gas Measurement, March 2005.
3. Lockhart, R.W. & Martinelli, R.C., "Proposed correlation of data for isothermal two phase, two component flow in pipes," Chem. Eng. Prog., Jan 1949, Vol 45, no 1., pp 39-48.
4. Murdock, J.W., "Two phase Flow measurements with orifices," Journal of Basic Engineering, Vol. 84, pp 419-433, December 1962.
5. Chisholm, D., "Flow of incompressible two phase mixtures through sharp-edged orifices," Journal of Mechanical Engineering Science, Vol. 9, No.1, 1967.
6. Chisholm, D., "Research note: Two phase flow through sharp-edged orifices," Journal of Mechanical Engineering Science, Vol. 19, No. 3, 1977
7. Falcone, G., "Critical review of wet gas definitions," North Sea Flow Measurement Workshop, Tønsberg, Norway, Oct 2005.
8. Geach, D. and Jamieson, A., "Wet gas measurement in the Southern North Sea," North Sea Flow Measurement Workshop, St Andrew's, UK, Oct 2006.
9. de Leeuw., R, "Liquid correction of Venturi meter readings in wet gas flow," North Sea Flow Measurement Workshop, Norway, Oct 1997.

10. Hall, A.R.W., Steven, R., "New data for the correlation of orifice plate measurements with wet gas flow conditions," 6th South East Asia Hydrocarbon Flow Measurement Workshop, Kuala Lumpur, March 2007.
11. "State of the art multiphase flow metering," American Petroleum Institute Publication 2565, 1st Ed., August 2004.
12. Wet Gas Flow Metering Technical Report, American Society of Mechanical Engineering MFC, under ballot at time of writing.
13. Steven., R., "Horizontally installed differential pressure meter wet gas flow performance review," North Sea Flow Measurement Workshop, St Andrew's, UK, Oct 2006.

25th North Sea Flow Measurement Workshop
16-19 October 2007 – Gardermoen, Norway

WET GAS PERFORMANCE OF DIFFERENTIAL PRESSURE FLOWMETERS

Russell Evans
Stephen Ifft
Emerson Process Management, Rosemount Division

David Hodges
TUV NEL Ltd

ABSTRACT

Wet gas flow measurement is becoming vital to the production of natural gas. New wells with marginal outputs cannot justify gas-liquid separation equipment and must transfer gas which contains some liquid volume. The flow measurement device on each well dictates the allocation earnings and must therefore provide gas flow measurement as accurately as possible.

Several types of differential pressure based flowmeters are currently being used in wet gas flow measurement. Differential pressure based flowmeters share many performance characteristics in wet gas applications. However, studies have also found that there can be significant differences in the correlations between meter over-reading and liquid content depending on the type of differential pressure meter being tested.

Emerson Process Management conducted a series of wet gas tests on a standard orifice plate, a V-Cone, a Venturi and two Rosemount conditioning orifice plates at TUV NEL Ltd in Scotland. Previously, tests of conditioning orifice plates in wet gas were conducted at the Colorado Engineering Experiment Station, Inc. (CEESI). The work described in this paper is aimed at investigating the similarities and differences in the performance of these meter types in wet gas flows. Comparisons of these data to those from previous studies on the meter types tested are presented. Also, as a result of these studies, a general method for correcting the over-reading of DP-based, wet gas flowmeters using process measurements and the flow computing capabilities of modern multivariable DP transmitters was developed and is presented.

NOMENCLATURE

A_p = pressure coefficient (-)

A_{Vg} = gas velocity coefficient (-)

A_β = beta ratio coefficient (-)

$\dot{m}_g$ = gas mass flow rate (kg/s)

$\dot{m}_l$ = liquid mass flow rate (kg/s)

OR = over-reading (-)

P = line pressure (bar)

U = gas velocity (m/s)

X_{LM} = Lockhart Martinelli parameter (-)

β = beta ratio (-)

ΔP_{tp} = differential pressure of wet gas (bar)

ΔP_g = differential pressure of dry gas (bar)

ρ_g = gas density (kg/m^3)

ρ_l = liquid density (kg/m^3)

WET GAS FLOW

For the purposes of this paper, wet gas flow shall be defined as the flow of a two phase mixture of gas and liquid where the Lockhart-Martinelli parameter is less than or equal to 0.3. This follows the de facto standard used in the natural gas industry. The parameter, $X_{LM,}$ is calculated by equation (1):

$$X_{LM} = \frac{\dot{m}_l}{\dot{m}_g}\sqrt{\frac{\rho_g}{\rho_l}} \qquad (1)$$

All the testing reviewed in this paper was conducted using a single homogeneous liquid. Real world applications can include a mixture of liquids that make up the liquid phase of wet gas, such as a combination of water, compressor oil, and hydrocarbon liquids. This paper and the conclusions drawn will relate to wet gas flow with a single liquid component.

DIFFERENTIAL PRESSURE FLOWMETERS

Single phase differential pressure (DP) flowmeters are the most common type of meters for the measurement of wet gas. These meters are either stand-alone measurement points or as the primary element of a wet gas/multi-phase flow measurement system. The most common types of DP meters used are the standard orifice plate and Venturi, the McCrometer V-Cone and the Rosemount conditioning orifice plate.

This paper will focus on the use of DP meters as stand alone wet gas flow measurement points. DP meters tested in wet gas flow have shown a characteristic over-reading which is proportional to the Lockhart-Martinelli parameter (or other estimations of liquid loading). As the Lockhart-Martinelli parameter increases, the differential pressure created by the primary element will over-read by as much as 50%.

Each DP meter has a slightly different response to the introduction of liquid during wet gas testing, though all will over read, with the exception of orifice plates at very small values of the Lockhart-Martinelli parameter.

TESTING CRITERIA

CEESI Criteria

Initial wet gas testing on four conditioning orifice plates was completed at the Colorado Engineering Experiment Station, Inc. (CEESI) in Nunn, Colorado during 2004. The purpose of these tests was to confirm the performance of the four hole conditioning orifice plates in wet gas applications. In homogeneous fluid applications, whether liquid or dry gas, the conditioning plates performed in a similar way to traditional orifice plates with the same beta ratio, with respect to their values of discharge coefficient, gas expansion factor, permanent pressure loss and accuracy.

CEESI tested two models of conditioning orifice plates, each with two different beta ratios, and tested at two different line pressures. The wet gas was a combination of natural gas and decane, a hydrocarbon liquid. Liquid loading ranged from zero (dry gas) to a Lockhart-Martinelli value of 0.3. The line size for all CEESI tests was 3”. A turbine meter and a subsonic Venturi jointly measured the flowrate of dry gas. Coriolis meters measured the liquid mass flowrate and the density of the injected liquid. Fig. 1 is a photo of the test setup at CEESI’s wet gas testing facility.

Test meter locations

Fig. 1 Test setup at CEESI wet gas testing facility

The Rosemount conditioning orifice plate is a proprietary design of Emerson Process Management. The two models tested were the Rosemount 1595 and 405C. The 1595 is a paddle-type orifice plate (see Fig. 2). The paddle-style plate requires flanges taps in the mating flanges. The flange taps are located 1 inch (25.4 mm) from both the upstream and downstream faces of the plate.

The 405C is a compact orifice design, see Fig. 3. Compact orifice meters include corner taps in the body of the meter as well as a mounting head with isolation and equalization valves. Orifice corner taps are located at the upstream and downstream faces of the plate. The compact meters can be installed between standard ASME and DIN flanges.

Fig. 2
Rosemount model 1595

Fig. 3
Rosemount model 405C

The beta ratios tested were 0.40 and 0.65. Conditioning orifice plates have equivalent beta ratios to standard orifice plates in terms of open area. Low and high line pressures were 200 and 700 psi (14 and 48 bar) respectively. The use of two line pressures illustrated any performance changes due to changing gas density.

TUV NEL Criteria

Testing with wet gas was continued and extended at TUV NEL Ltd in Glasgow, Scotland. This test series was expanded to include other DP technologies. The following meters were tested at TUV NEL in 2005:

1. 4 inch ISO 5167 orifice plate with 0.65 β, see Fig. 4.
2. 4 inch Rosemount model 405C with 0.65 β, see Fig. 3.
3. 4 inch classical Venturi with 0.75 β, see Fig. 5.
4. 4 inch McCrometer V-Cone with 0.75 β, see Fig. 6.

The Venturi tested was provided by TUV NEL from their laboratory supply of differential pressure primary elements and was of standard design with a 21º convergent section.

The V-Cone is a proprietary device of McCrometer, Inc. The V-Cone creates differential pressure with a cone located in the center of the pipe. The high pressure measurement is taken upstream of the cone at the pipe wall, while the low pressure measurement is taken through the center of the cone, with the port facing downstream.

Fig. 4
ISO 5167 Orifice Plate

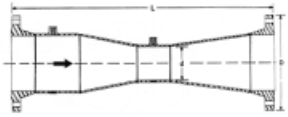

Fig. 5
Classical Venturi

Fig. 6
McCrometer V-Cone

DP elements are commonly used in wet gas applications, with the above elements the most widely used. This study was intended not only to expand the data available on the wet gas performance of the conditioning orifice plate, but also as a wider study of DP flow elements in wet gas. The goal was to find a common thread among DP devices which would more accurately correlate flow measurement in wet gas conditions.

TUV NEL tested all the above DP elements under similar conditions for direct comparison of results. The test gas was nitrogen. The test liquid was a kerosene substitute, trade name EXXSOL D80. The Lockhart-Martinelli parameter value ranged from 0 to 0.3. Two pressures were tested at 215 and 870 psi (15 and 60 bar). Fig. 7 is a photo of the test setup at TUV NEL's wet gas test facility.

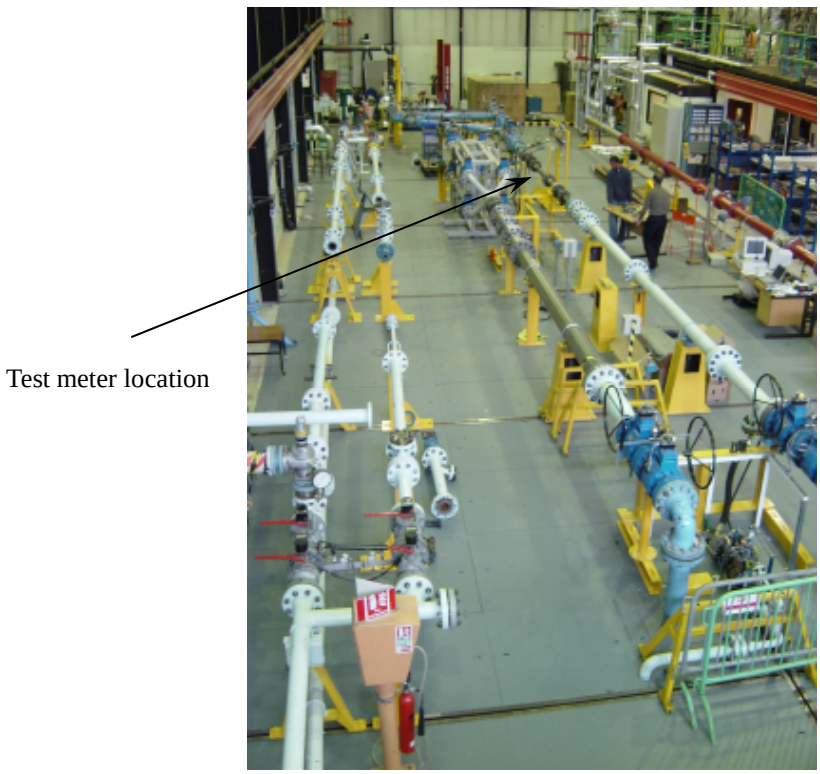

Fig. 7 Test setup at TUV NEL wet gas testing facility

TEST RESULTS

The response of a differential pressure flow element tested in wet gas is typically graphed as the over-reading vs. the Lockhart-Martinelli parameter value. The over-reading increases as the X_{LM} value increases. The over-reading is calculated by equation (2).

$$OR \cong \sqrt{\frac{\Delta P_{tp}}{\Delta P_g}} \qquad (2)$$

To correct for this type of offset, the user of a wet gas DP flow element would determine the Lockhart-Martinelli parameter value, look at the response of the element at that liquid load (i.e. the over-reading), and decrease his flow reading accordingly. Thus the user will obtain an estimate of the actual gas flowrate by correcting for the known quantity of liquid flowing in the pipe.

CEESI Results

The CEESI wet gas study of 2004 showed that the conditioning orifice plates responded as would be expected of a standard single hole orifice plate. See Fig. 8 for results from the Model 1595 conditioning orifice plates, both beta ratios. See Fig. 9 for results from the model 405C plates, both beta ratios.

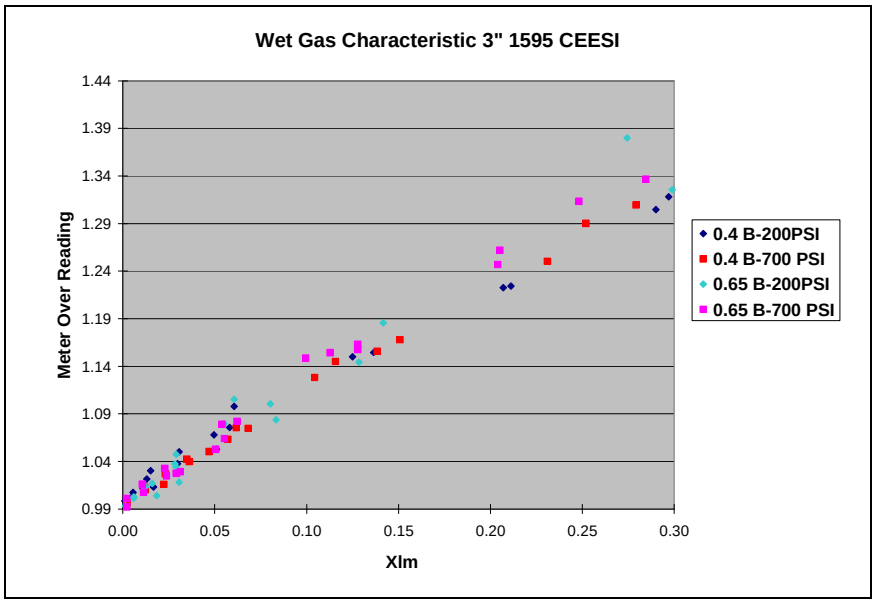

Fig. 8
Meter over reading vs. Lockhart-Martinelli parameter for conditioning orifice plate, CEESI data

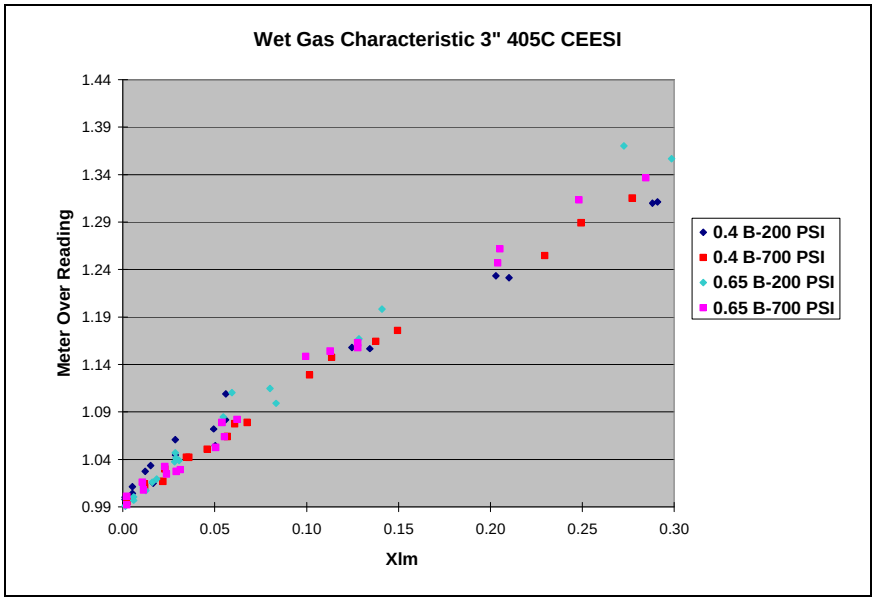

Fig. 9
Meter over reading vs. Lockhart-Martinelli parameter for conditioning orifice plate, CEESI data

The response of both the 1595 and 405C plates could be corrected for wet gas loading using a linear model correlation. As liquid loading increased, the plates created more DP than under dry gas conditions. The relation of over-reading to X_{LM} was linear and repeatable. Equations (3), (4), (5), and (6) are derived corrections from the CEESI wet gas tests.

Equation for Model 1595 0.40 β

$$OR = 1.0998 \cdot X_{LM} + 1 \qquad (3)$$

Equation for Model 1595 0.65 β

$$OR = 1.2306 \cdot X_{LM} + 1 \qquad (4)$$

Equation for Model 405C 0.40 β

$$OR = 1.1062 \cdot X_{LM} + 1 \qquad (5)$$

Equation for Model 405C 0.65 β

$$OR = 1.2684 \cdot X_{LM} + 1 \qquad (6)$$

The accuracy of correction equations is perhaps of most interest to wet gas flow element users. The accuracy of the linear relationships in equations 3 to 6 was checked by applying those equations to the test results and comparing to the direct measurement of dry gas in the CEESI test loop. Fig. 10 and Fig. 11 show the error in corrected wet gas measurement when compared to the dry gas measurement. Most points lie within a ±2.0% range, with a few points in the range 2.0% to 3.5%. This compares favorably against previous results using other DP flow elements[1], [2]. These results are published and are available from Emerson Process Management[3].

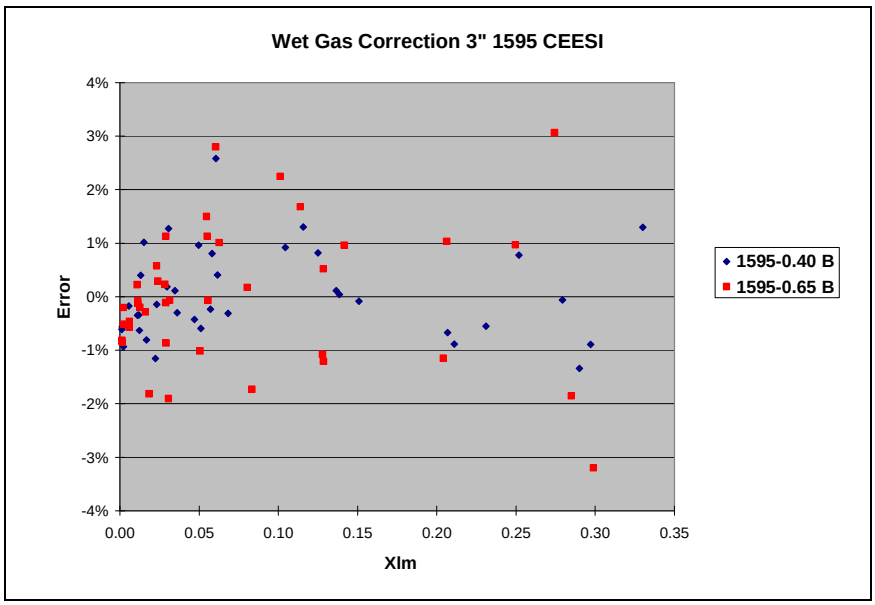

Fig. 10
Error vs. Lockhart-Martinelli parameter for conditioning orifice plate

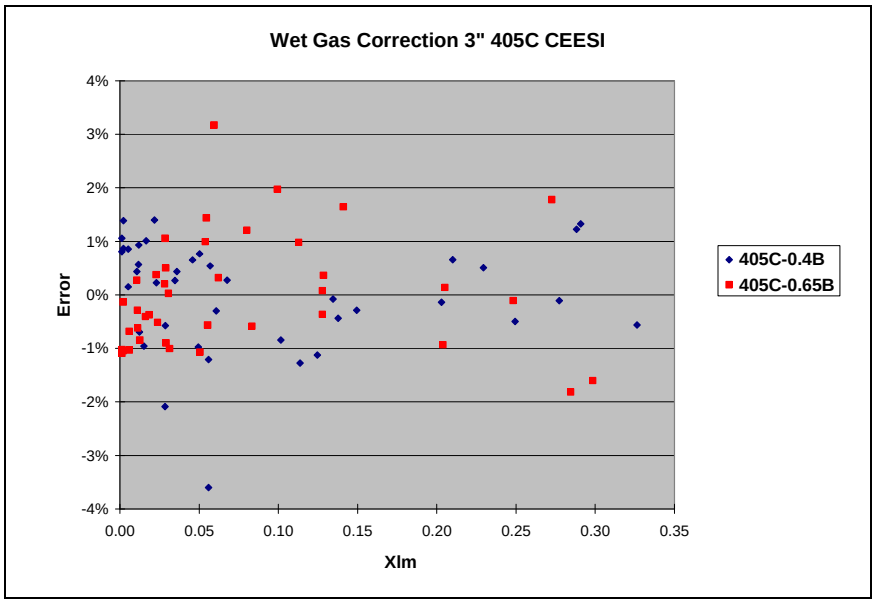

Fig. 11
Error vs. Lockhart-Martinelli parameter for conditioning orifice plate

TUV NEL Results

Results from the TUV NEL tests appear consistent with earlier findings for each of the flow element types. The ISO 5167 standard orifice plate results matched those of Murdock[4]. The 405C data concurred with the CEESI test results. The Venturi results matched those from de Leeuw[5], while the V-Cone performance was consistent with data presented by McCrometer[1]. For the TUV NEL results from these elements, see Fig. 12 through Fig. 15.

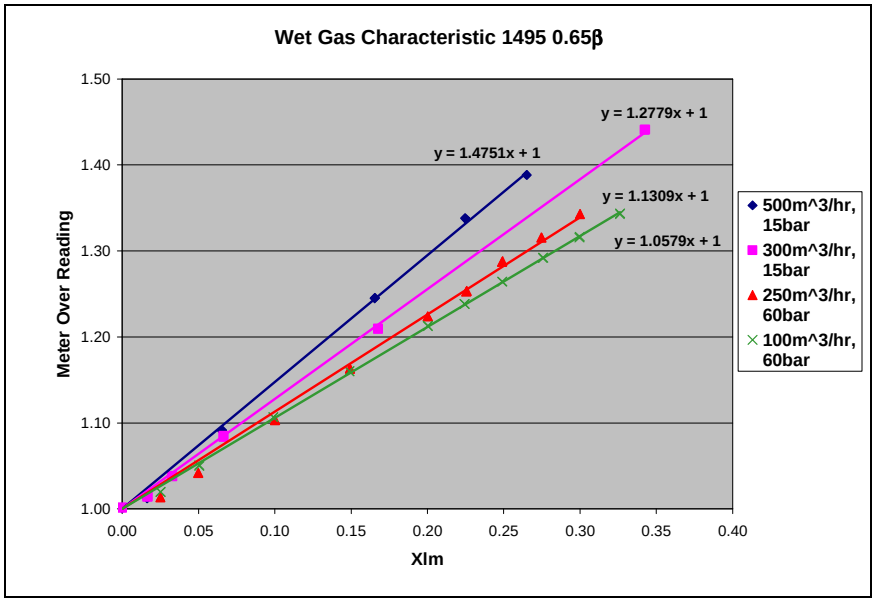

Fig. 12
Meter over reading vs. Lockhart-Martinelli parameter for standard orifice plate, beta 0.65

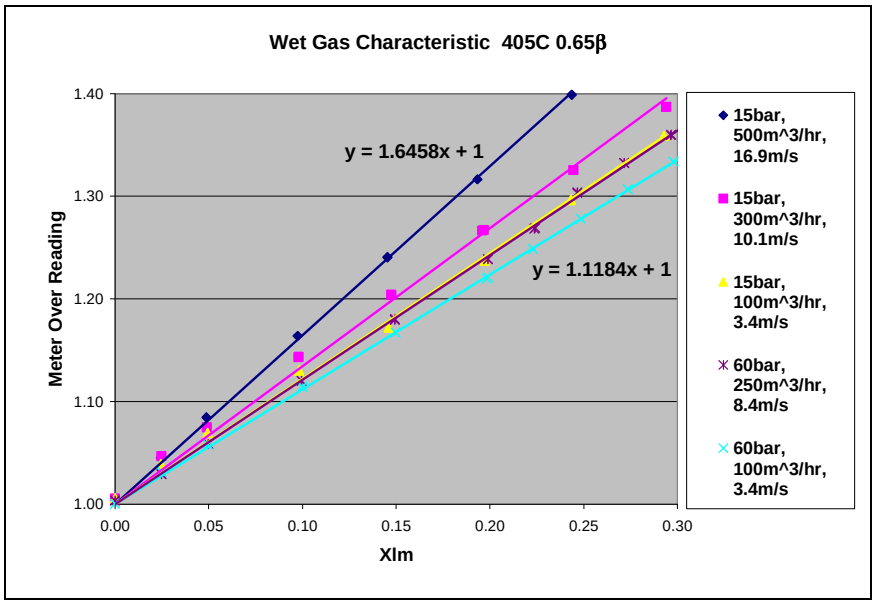

Fig. 13
Meter over reading vs. Lockhart-Martinelli parameter for conditioning orifice plate, beta 0.65

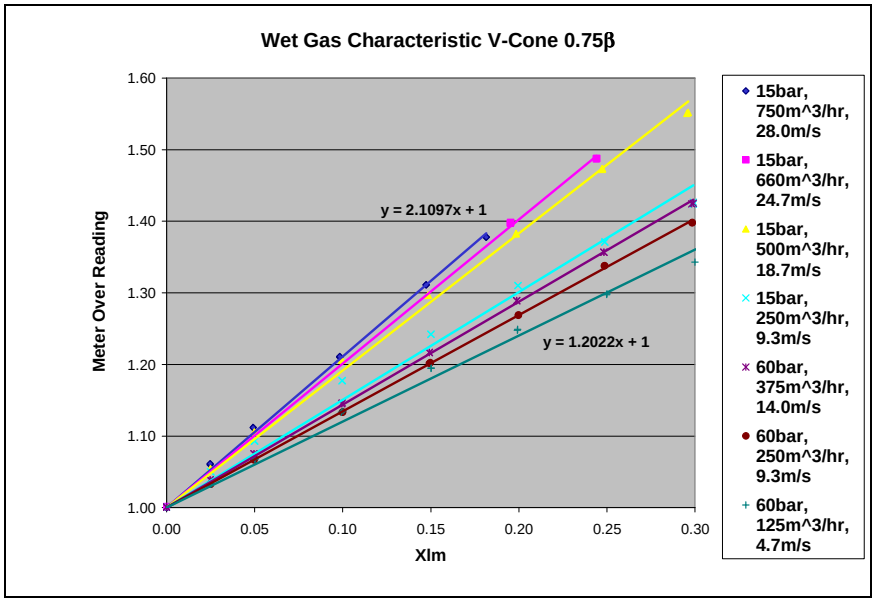

Fig. 14
Meter over reading vs. Lockhart-Martinelli parameter for V-Cone, beta 0.75

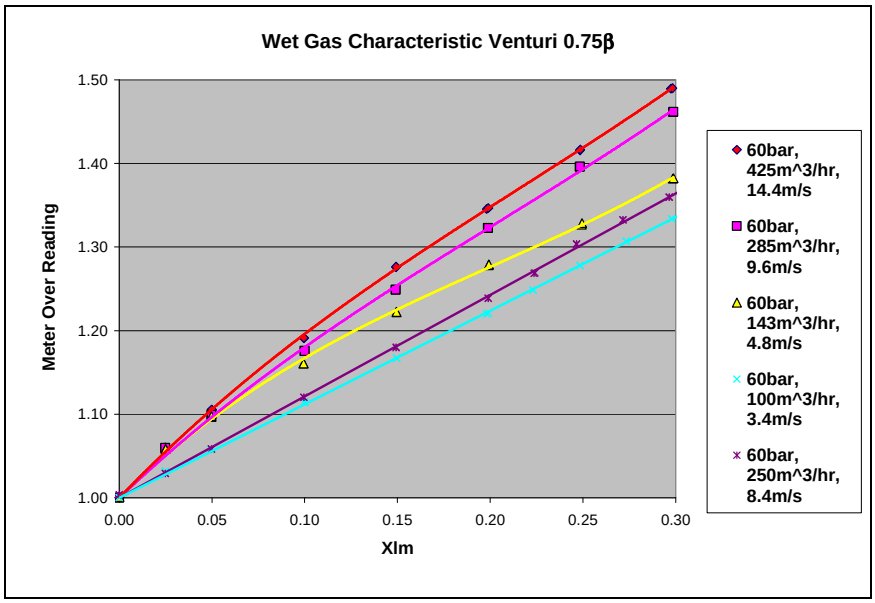

Fig. 15
Meter over reading vs. Lockhart-Martinelli parameter for venturi, beta 0.75

A closer examination of the data, however, showed characteristics not explored in the earlier study. With flow elements that have a linear over-reading response to X_{LM}, there was a correlation with certain test parameters. For instance, if gas velocity is isolated in the data, there is a relationship between the slope of the OR vs. X_{LM} curve and the gas velocity. In other words, the characteristic wet gas correction curve for DP meters is affected by gas velocity. This relationship is shown in Fig. 16 for tests on the 405C flow element.

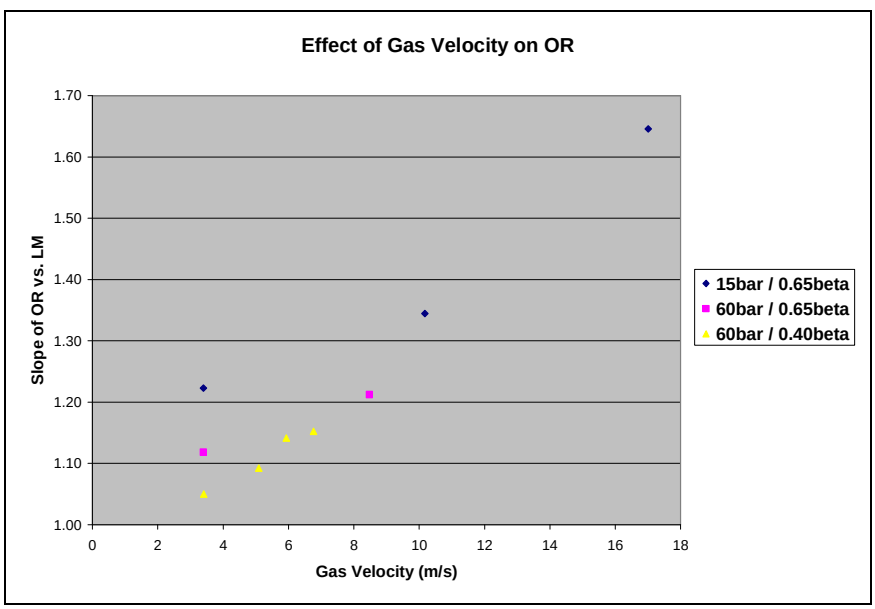

Fig. 16
Effect of gas velocity on meter over reading for 405C

A similar effect was also found to exist in relation to pressure (i.e. gas density or gas-liquid density ratio). As shown in Fig. 17, there is an inverse relationship between pressure and the slope of the OR vs. X_{LM} curve.

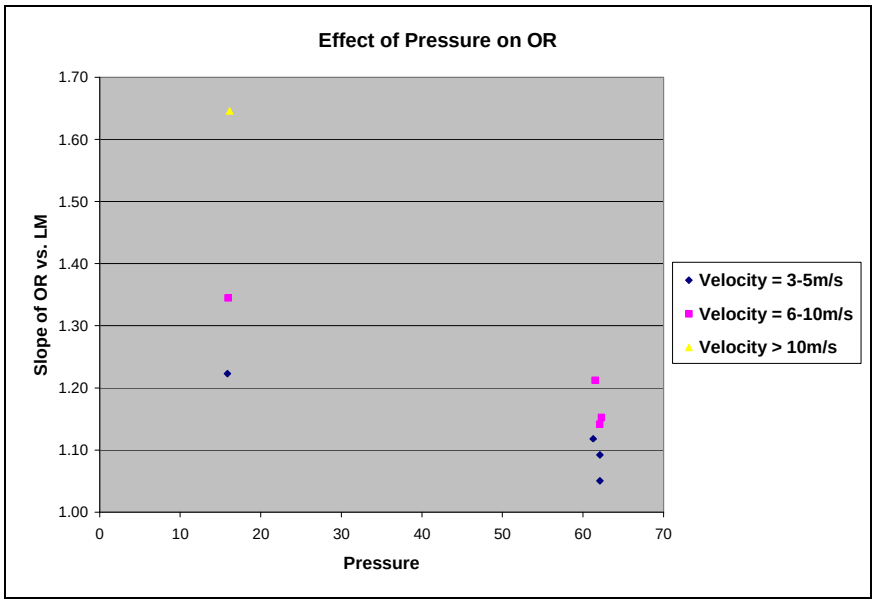

Fig. 17
Effect of gas pressure on meter over reading for 405C

LINEAR CORRELATION

By revisiting the data shown in Fig. 12 through Fig. 14, a linear fit can be applied to each test condition and the corresponding slope calculated for each combination of pressure, gas velocity and beta ratio. The Venturi was not included in this analysis because of its non-linear response to wet gas loading.

With slope as a function of pressure, gas velocity and beta ratio, a regression of the data produced a linear model that can be applied across the scope of the TUV NEL data.

This derivation was also applied to the previous CEESI data on the 405C model. While the CEESI testing did not cover the scope of the TUV NEL testing, it did show similar dependencies. The form of linear equation used is shown in Equation (7).

$$\text{Slope of OR vs. } X_{LM} = \text{Intercept} + A_P \cdot P + A_U \cdot U + A_\beta \cdot \beta \qquad (7)$$

Table 1 shows the regression coefficients generated for both the CEESI and the TUV NEL data sets.

Table 1
Regression Coefficients

	Intercept	A_p Pressure Coeff.	A_U Gas Vel. Coeff.	A_β Beta Coeff.
405C / CEESI	1.6956	-3.52E-03	0.0361	-1.2675
405C / TUV NEL	1.0460	-2.47E-03	0.0298	0.1445
V-Cone / TUV NEL	1.3554	-5.27E-03	0.0300	N/A
ISO O-Plate / TUV NEL	1.2033	-3.48E-03	0.0172	N/A

Table 2 shows the correlation coefficients generated for the CEESI and the TUV NEL data sets.

Table 2
Correlation Coefficients

	Pressure	Gas Velocity	β
405C / CEESI	-0.3510	0.6750	-0.0233
405C / TUV NEL	-0.7590	0.9293	0.5801
V-Cone / TUV NEL	-0.7990	0.9575	N/A
ISO O-Plate / TUV NEL	-0.8023	0.8429	N/A

APPLICATION OF THE LINEAR MODEL

As in the case of the previous CEESI tests, the multi-variable linear model was applied to the TUV NEL results and the outputs compared to the actual gas flow measurement. Figures 18-21 show the results of that analysis for the ISO 5167 orifice plate, V-Cone and the two 405C conditioning orifice plates, respectively. Also shown in those figures are the results of the application of other commonly used wet gas correlations applied to the same data set. As can be seen from these results, the multi-variable linear model yields residual errors that are comparable and in some cases less than those obtained from more commonly used correlations.

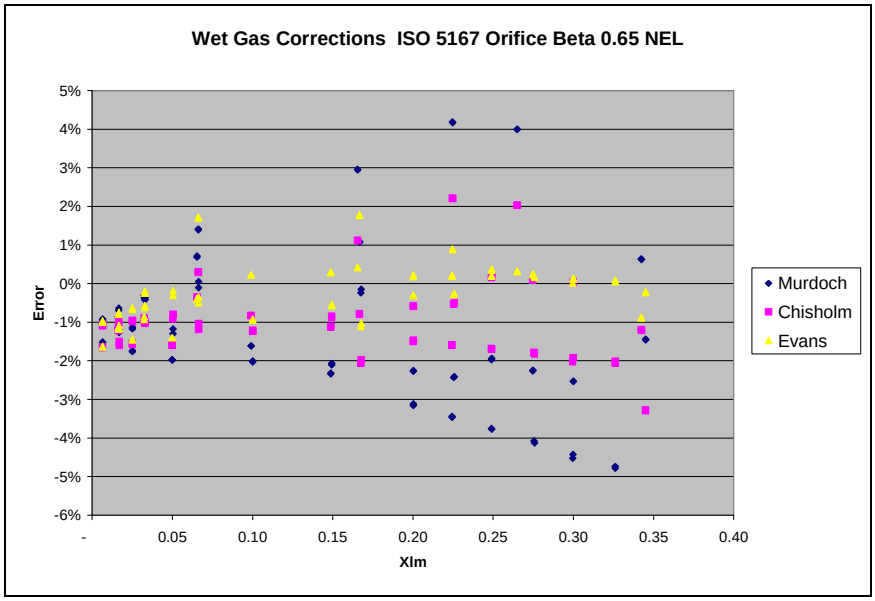

Fig. 18
Error vs. Lockhart-Martinelli parameter for standard orifice plate, beta 0.65

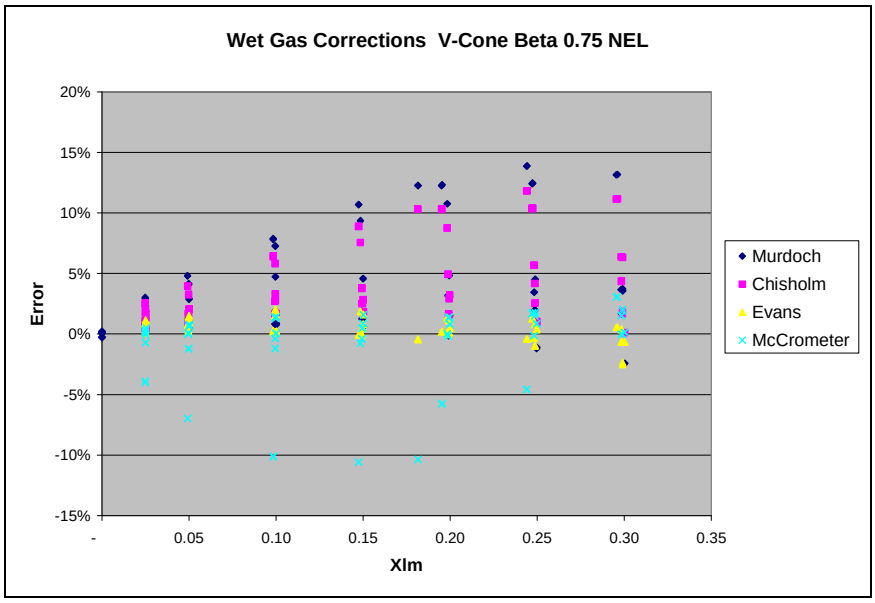

Fig.19
Error vs. Lockhart-Martinelli parameter for V-Cone, beta 0.75

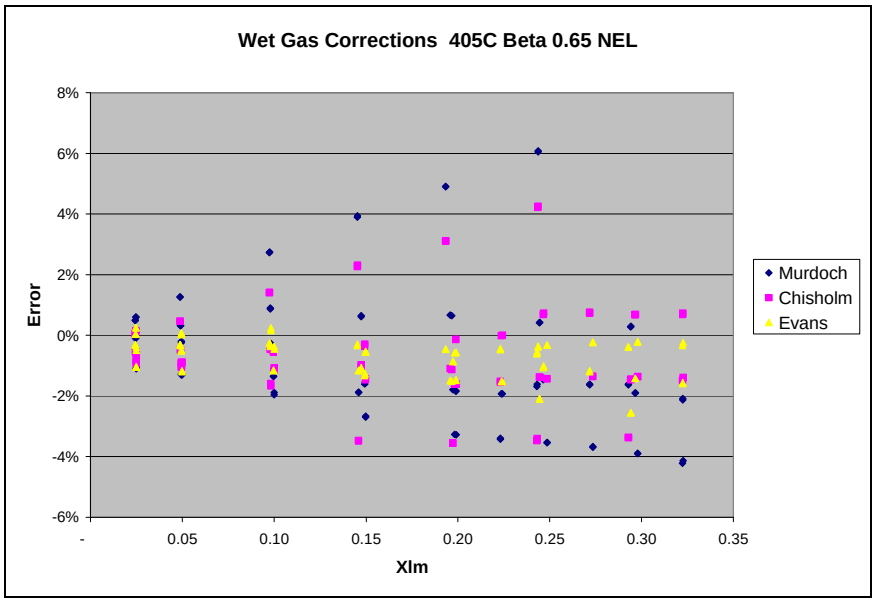

Fig. 20
Error vs. Lockhart-Martinelli parameter for conditioning orifice plate, beta 0.65

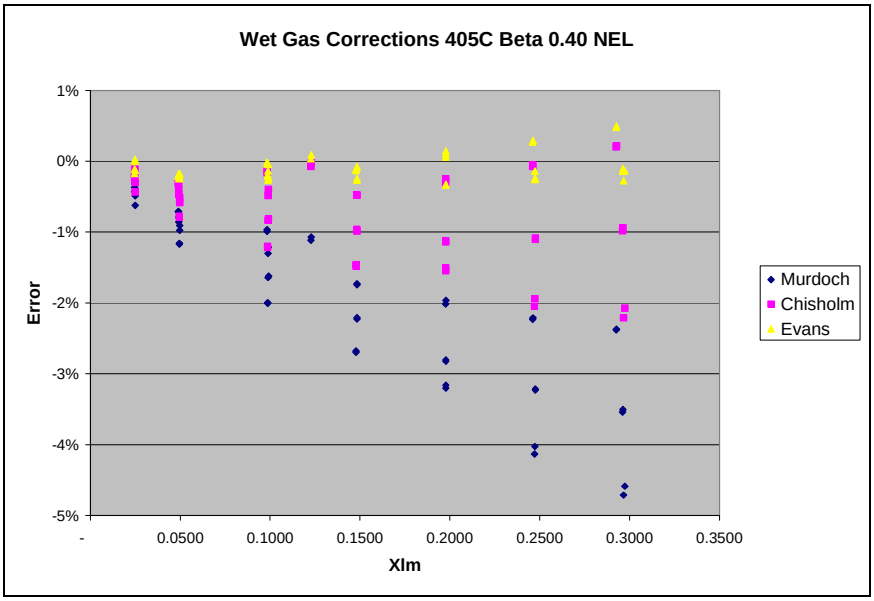

Fig. 21
Error vs. Lockhart-Martinelli parameter for conditioning orifice plate, beta 0.40

It would be expected that applying a linear model to the data set which was used to generate the model should yield positive results. A better test of the validity of the model is to apply it to other independent data. The multi-variable linear model (based on the TUV NEL results only) has been applied to the previous CEESI data for the same meter types. The results of that analysis are shown in Figs. 21 and 22 for the 0.40β and 0.65β 405C conditioning orifice plates, the only common meter types between the two data sets.

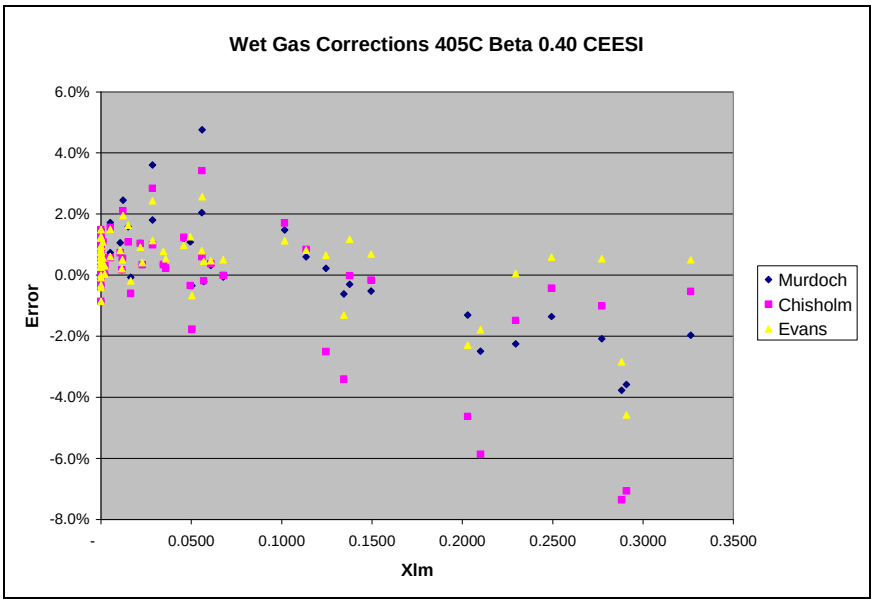

Fig. 22
Error vs. Lockhart-Martinelli parameter for conditioning orifice plate, beta 0.40
This data shows the TUV NEL correction to the previous CEESI data set.

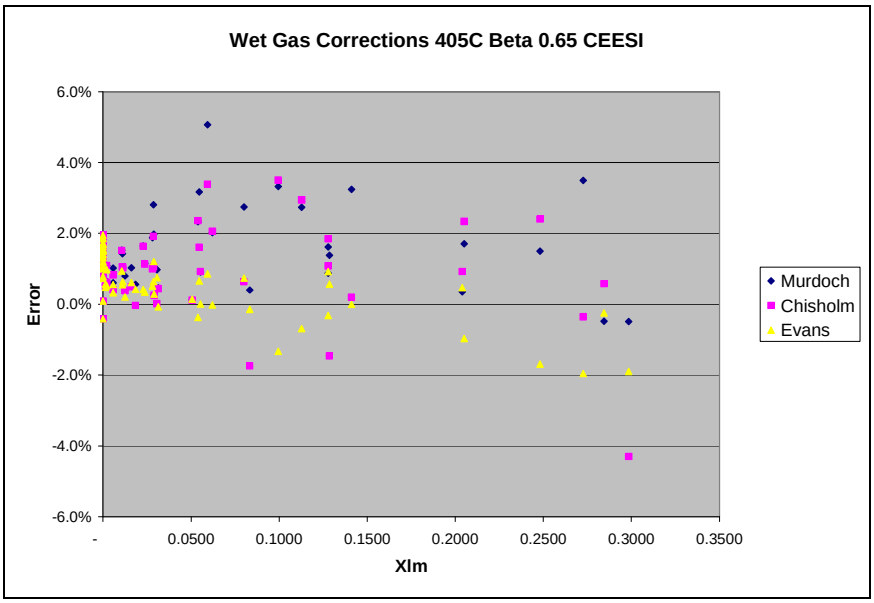

Fig. 23
Error vs. Lockhart-Martinelli parameter for conditioning orifice plate, beta 0.65
This data shows the TUV NEL correction to the previous CEESI data set.

When applied to the independent CEESI data, the multi-variable linear model can be seen to yield corrections that are again comparable to that obtained by more traditional correlations.

RESULTS DISCUSSION and CONCLUSIONS

These results have significant implications when it is considered that the independent variables in the model are values that are already available in modern multi-variable flow transmitters. The process pressure is typically a measured value and the gas velocity is calculated from the standard flow computation in the multi-variable

transmitter. Using these values and a compact, simple iterative process, the proper wet gas correction curve can be determined and applied. This presents the possibility that once the correct linear model coefficients for a particular primary element type are determined, the wet gas correction can be made entirely within the field mounted instrument.

Results obtained from the CEESI and the TUV NEL test fluids are comparable when using the multi-variable linear correlation approach. This is a small sample data set but confirms the validity of the correlation method between flow labs and across different test fluids. While the coefficients listed in Table 2 are not intended as definitive for any of the technologies tested, the success of the method on this limited data set is encouraging and suggests that it may be a viable correlation strategy for wet gas measurement. Further work in this area is planned through additional tests and by analysis of the results of other available data sets with this method.

REFERENCES

[1] Steven, R., and Peters, R., 2004, "Wet Gas Metering with V-Cone Meters", 3rd International SE Asia Hydrocarbon Flow Measurement Workshop.

[2] Steven, R., 2006, "Wet Gas Flow Metering with Gas Meter Technologies", Ciateq 2006.

[3] White Paper, "Rosemount Conditioning Orifice Plate in Wet Gas", www.rosemount.com.

[4] Murdock, J.W., "Two-Phase Flow Measurement with Orifices", Journal of Basic Engineering, 1962, Vol. 84, pp. 419-433.

[5] de Leeuw, R., "Liquid Correction of Venturi Meter Readings in Wet Gas Flow", North Sea Flow Measurement Workshop, 1997.

V-Cone Wet Gas Metering

Richard Steven
Colorado Engineering Experiment Station Inc.
54043 WCR 37-Nunn, Colorado 80648, USA
Tel: US 970-897-2711, Fax: US 970-897-2710, E-mail: rsteven@ceesi.com

1. INTRODUCTION

Single phase differential pressure (DP) meters can be used to meter wet gas flows if the liquid flow rate can be obtained from an independent source and a suitable wet gas correction factor is available. As it is not a trivial task to measure the liquid flow rate of a wet gas flow, sophisticated wet gas flow meters have been developed that meter the gas and liquid phases simultaneously. The complexity of most wet gas meters means that they tend to be expensive (relative to standard gas meters). Therefore, due to economic necessity, many wet gas flow applications still have single phase gas meters being fitted to meter wet gas flows. This situation is not ideal, as it means poorer metering performance than what is really desired.

An industry goal is to reduce the cost of wet gas metering by producing simpler wet gas metering systems so as all wet gas flow metering applications can have a wet gas meter installed. One simple design concept is the use of a downstream pressure tapping on a Venturi meter to give a second primary reading. This is used in conjunction with the classical DP to derive the gas and liquid phase flow rates simultaneously. This paper describes a decade long DP meter research project that started with Venturi meters and led to the creation of a simple wet gas DP meter design that utilises the V-Cone DP meter and a downstream pressure tapping with a novel, yet simple, methodology for deriving the gas and liquid phase flow rates. The details of the fluid mechanics principles applied, the errors made at various stages of the development and the subsequent lessons learned that led to the successful system are described along with descriptions of the wet gas meters performance. Data from a NEL Venturi meter test and different V-Cone meters at NEL, CEESI and K-Lab's wet gas test facilities are shown.

2. DEFINITION OF WET GAS FLOW PARAMETERS

In this paper wet gas flow is defined as any two phase flow (i.e. gas and liquid flow) that has a Lockhart Martinelli parameter [1] value (X_{LM}) less or equal to 0.3. The Lockhart Martinelli parameter is:

$$X_{LM} = \sqrt{\frac{Superficial\ Liquid\ Inertia}{Superficial\ Gas\ Inertia}} = \frac{\dot{m}_l}{\dot{m}_g}\sqrt{\frac{\rho_g}{\rho_l}} \quad \text{---- (1)}$$

where $\dot{m}_g$ & $\dot{m}_l$ are the gas and liquid mass flow rates and ρ_g & ρ_l are the gas and liquid densities respectively. Many gas meters have wet gas flow responses that are dependent on pressure. It is possible to non-dimensionalise this effect when analyzing meter wet gas responses by using the gas to liquid density ratio. Often, the gas to liquid density ratio is indicated by the letters "DR". That is $DR \equiv \rho_g / \rho_l$.

The gas and liquid densiometric Froude numbers are expressed as Equations 2 and 3:

$$Fr_g = \sqrt{\frac{Superficia\ l\ Gas\ Inertia}{Liquid\ Gravity\ Force}} = \frac{U_{sg}}{\sqrt{gD}}\sqrt{\frac{\rho_g}{\rho_l - \rho_g}} = \frac{\dot{m}_g}{A\sqrt{gD}}\sqrt{\frac{1}{\rho_g(\rho_l - \rho_g)}} \quad \text{---- (2)}$$

$$Fr_l = \sqrt{\frac{Superficia\ l\ Liquid\ Inertia}{Liquid\ Gravity\ Force}} = \frac{U_{sl}}{\sqrt{gD}}\sqrt{\frac{\rho_l}{\rho_l - \rho_g}} = \frac{\dot{m}_l}{A\sqrt{gD}}\sqrt{\frac{1}{\rho_l(\rho_l - \rho_g)}} \quad \text{---- (3)}$$

Note, "g" is the gravitational constant, A is the pipe cross sectional area, D is the pipe inside bore diameter and U_{sg} and U_{sl} are the superficial gas and liquid velocities respectfully. Note that:

$$U_{s_g} = \frac{\dot{m}_g}{\rho_g A} \text{ ---- (4)} \quad \text{and} \quad U_{s_l} = \frac{\dot{m}_l}{\rho_l A} \text{ ---- (5)}$$

Finally, it is a recurring theme for DP meters that the liquid present in a gas flow tends to induce a positive bias or "over-reading" in the gas flow rate prediction. When a gas DP meter is used with wet gas flow the uncorrected gas mass flow rate prediction is often called the "apparent" gas mass flow ($\dot{m}_{g,Apparent}$). The over-reading is the ratio of the apparent gas flow rate to actual gas flow rate. Often the over-reading (denoted by "*OR*") is expressed as approximately the square root of the ratio of the actual wet gas (or "two-phase") differential pressure (ΔP_{tp}) read and the differential pressure (ΔP_g) that would be read if the gas flow flowed alone (Equation 6) or as a percentage (Equation 6a).

$$OR = \frac{\left(\dot{m}_{g,Apparent}\right)_{TM}}{\dot{m}_g} \cong \sqrt{\frac{\Delta P_{tp}}{\Delta P_g}} \text{ -- (6)}, \quad OR\,(\%) = \left(\frac{\left(\dot{m}_{g_{Apparent}}\right)_{TM}}{\dot{m}_g} - 1\right) * 100\% \cong \left(\sqrt{\frac{\Delta P_{tp}}{\Delta P_g}} - 1\right) * 100\% \text{ -- (6a)}$$

Note subscript "TM" indicates "traditional meter" as it will later be necessary to identify the traditional meter from an unorthodox meter design to be discussed in this paper.

3. PRE - 1997 TWO-PHASE / WET GAS FLOW METER DESIGNS

Prior to the modern oil and gas industries wet gas metering research drive there were several different two-phase designs discussed in the literature. In 1972 Medvejev [2] discussed positioning a positive displacement (PD) meter upstream of an orifice plate meter. Figure 1 reproduces Lin's [3] representation of the Medvejev system. From suitable manipulation of the data from the two independent meters Medvejev showed the gas and liquid phase flow rates could be predicted. In 1982 Chen et al. [4] did similar work and it was claimed that "within the experimental range the root mean square of this method for volumetric flow rate of each phase is less than 7%".

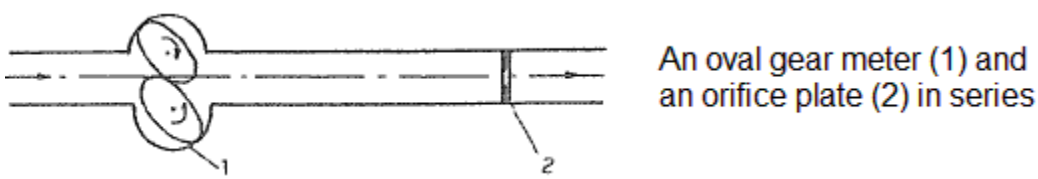

Figure 1. Medvejev Two-Phase Flow Metering System

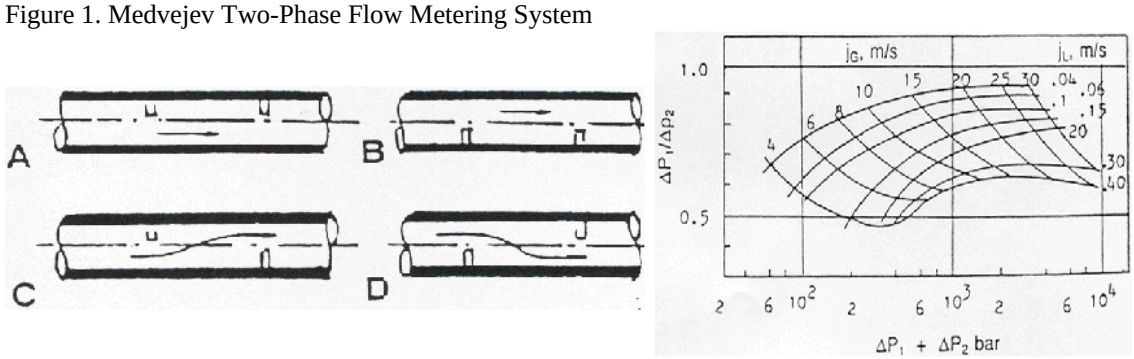

Figure 2. The Sekoguchi Segmental Orifice Plates in Series with a Sample Sekoguchi Data Plot.

In 1978 Sekoguchi [5] placed variously orientated segmental orifice plate meters in series as shown by Lin [3] in Figure 2. The analysis of the data was however, unsophisticated. Sekoguchi plotted constant superficial gas and liquid velocity lines on graphs with the abscissa as the sum of the two differential

pressures and the ordinate as the ratio of the two differential pressures. Note Sekoguchi used j_G and j_L to denote superficial gas and liquid velocities. The methods reported accuracy was poor with flow rate errors of $\pm 30\%$. However, this appears to be the first attempt to meter two-phase flow with DP meters in series.

In the 1980's Nguyen [6], patented measuring two-phase flow by placing an orifice plate meter in series with a Venturi meter (see Nguyen's Figure 3 - it is not known if Nguyen took a classical DP or the DP across the Venturi meter as shown in his patent sketch.) Nguyen [7] then patented two orifice meters in series. By the early 1990's British Gas was investigating pairs of DP meters as a wet gas flow metering system. This led to the SolartronISA Dualstream II [8] product. Other derivatives of this generic idea exist. A common theme of these two-phase flow meters is that they rely on two gas meters in series having different wet gas flow responses so as a measurement by difference technique can be utilised.

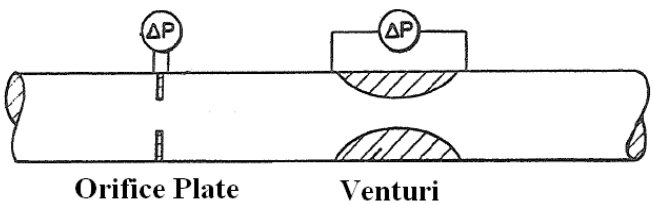

Figure 3. Nguyen's Patented Orifice Plate and Venturi Meter Two-Phase Flow Metering System.

4. DE LEEUW 1997: A SINGLE VENTURI WET GAS FLOW METER CONCEPT

The modern era of wet gas flow meter research started in erhnest with a paper by de Leeuw [9] in 1997. This paper described the response of a Venturi meter to wet gas flow. It was found that a Venturi gas meter has a gas flow over-reading due to liquid present with the gas that is dependent on the Lockhart Martinelli parameter, the gas to liquid density ratio and the gas densiometric Froude number, i.e:

$$OR = \frac{\left(\dot{m}_{g,Apparent}\right)_{TM}}{\dot{m}_g} = f\left(X_{LM}, \frac{\rho_g}{\rho_l}, Fr_g\right) = f\left(\frac{\dot{m}_l}{\dot{m}_g}\sqrt{\frac{\rho_g}{\rho_l}}, \frac{\rho_g}{\rho_l}, \frac{\dot{m}_g}{A\sqrt{gD}}\sqrt{\frac{1}{\rho_g\left(\rho_l - \rho_g\right)}}\right) \quad \text{---- (7)}$$

De Leeuw gave the form for the function "f" and this equation is now the most common correction factor for Venturi meters with wet gas flow. The Achilles heel of this metering method is the same as that which exists for all DP meters[1] with wet gas correction factors. That is, the system requires that the liquid flow rate is found from an independent source. The common liquid prediction methods are not continuous and have relatively large uncertainties. This then has a knock affect on the gas prediction method uncertainty.

De Leeuw [9] discussed research that aimed to alieviate this limitation. It was suggested that the permanent pressure loss across the Venturi meter was affected by the liquid presence in the gas flow. Therefore, reading the upstream to throat DP and also the upstream to downstream DP could potentially give enough information to predict both phase flowrates without any requirement for an independent liquid flowrate estimation. Figure 4 shows such a Venturi meter installation [9]. Note a tracer dilution method is also shown but this is outwith the scope of this discussion. The crux of the de Leeuw argument is that it was found that the "pressure loss ratio", which de Leeuw defined as the ratio of the permanent pressure loss (ΔP_{PPL}) to the classic DP read by the Venturi meter (ΔP), is different between dry and wet gas flows. Furthermore, de Leeuw suggested that the change in the pressure loss ratio is directly related to the Lockhart Martinelli parameter, gas to liquid density and gas densiometric Froude number. Figure 5 shows a de Leeuw graph [9] indicating for a set pressure / gas to liquid density ratio, how the Lockhart Martinelli parameter and the gas densiometric Froude number affect the pressure loss ratio. Hence, it was suggested that a function of the form shown as equation 8 (found by data fitting) could be substituted into equation 7 to give some function "h" (as shown in equation 7a), and where, for known fluid properties, a known meter

[1] In this paper the term "DP meter" excludes the cases of pitot static devices and laminar element devices.

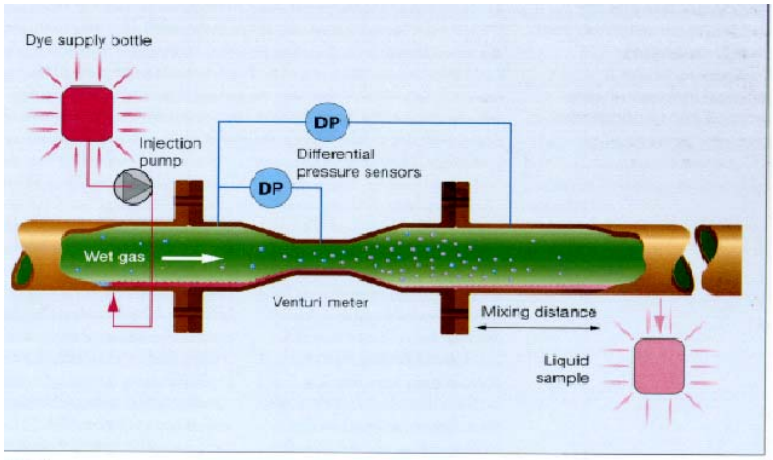

Figure 4. De Leeuw's Double DP Venturi Meter Set Up (with a Tracer Dilution System Indicated).

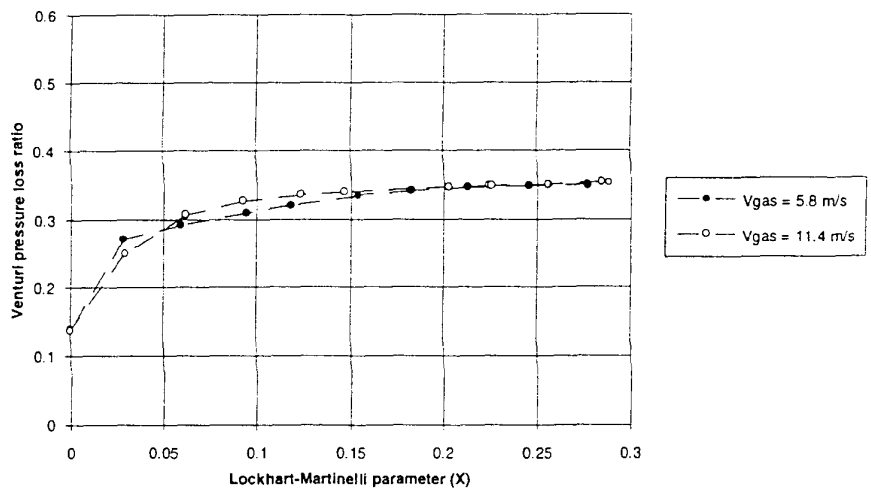

Figure 5. 4", 0.4 Beta Ratio Venturi Meter Pressure Loss Ratio vs. X_{LM} at 45 Bar.

geometry and read DP's, the only unknown in equation 7a is the gas mass flow rate. Once this value is found equation 1 could be utilised to calculate the liquid mass flowrate hence making the stand alone Venturi meter a wet gas meter. A limitation of this method was found independently by de Leeuw [9], Steven [10] and NEL [11] to be that while the relationship is extremely sensitive at low Lockhart-Martinelli parameters it becomes less sensitive at higher Lockhart-Martinelli parameters (e.g. see Figure 5). This idea is therefore seen as useful as a wet gas metering tool, especially at low liquid loadings, but also limited, due to the reduced sensitivity of the permanent pressure loss ratio to the Lockhart-Martinelli parameter at higher wet gas liquid loadings. (Note that in equations 8 and 7a subscript "tp" indicates "two-phase" or "wet gas" conditions.)

$$X_{LM} = g\left(\frac{\Delta P_{PPL_{tp}}}{\Delta P_{tp}}, \frac{\rho_g}{\rho_l}, Fr_g\right) \text{--(8) \&} \quad \frac{\left(\dot{m}_{g,Apparent}\right)_{TM}}{\dot{m}_g} = h\left(\frac{\Delta P_{PPL_{tp}}}{\Delta P_{tp}}, \frac{\rho_g}{\rho_l}, \frac{\dot{m}_g}{A\sqrt{gD}}\sqrt{\frac{1}{\rho_g(\rho_l - \rho_g)}}\right) \text{--(7a)}$$

5. A WET GAS FLOW VENTURI METER PhD PROJECT (1997-2001)

In October 1997, when de Leeuw [9] presented Shell's wet gas Venturi meter paper at the North Sea Flow Measurement Workshop (NSFMW), this author started a wet gas Venturi meter PhD project at NEL / Strathclyde University. This de Leeuw paper was to greatly influence this PhD as de Leeuw had remarked:

"The potential for the pressure loss measurement is to use it as a means to determine the liquid content of the flow, from which the over-reading factor can be determined accordingly. In essence this would form a simple two-phase flow meter. To date, however, no acceptable correlation formula has yet been found that would relate the pressure loss ratio to the actual liquid content and the over-reading. Additional requirements might be required."

The challenge was to sucessfully create a wet gas metering system that was simple and practical for industry. The challenge, on the face of it, this author was to dismally fail. By April 2001 the PhD viva discussion was focused on why the techniques developed had not worked. However, as will be explained in the following chapter the fix was somewhat closer than was then realised, although it was to take nearly four more years for this to become clear. To begin with though, to understand the later V-Cone meter work the PhD generic DP meter theories and test results must first be explained.

The initial PhD work was to review the fundamental single phase flow theories of the DP meter. It immediately became apparent that the same physical principles that apply to the traditional metering section of a DP meter (i.e. the geometric constriction section) could be applied to the downstream geometric expansion section. That is, for single phase gas flow, a flow rate prediction could be made by the classic reading of the difference in pressure between the upstream to throat (i.e. the minimum cross sectional area) or by reading the difference in pressures between a downstream section and the throat. Figure 6 shows a sketch of a generic Venturi meter. Figure 7 shows a sketch of the pressure fluctuation typical through generic DP meters such as Venturi and V-Cone meters. Note that the differential pressure between the upstream to throat (ΔP_t), the downstream to throat (ΔP_r) and the upstream to downstream (ΔP_{PPL}) is related by equation 9:

$$\Delta P_t = \Delta P_r + \Delta P_{PPL} \quad \text{--- (9)}$$

Equation 9 is true for all DP meters whether the flow is a gas, liquid or any mix of gas and liquid flow.

The single phase flow equation for the classical DP meter (i.e. using ΔP_t) is given by equation 10 and the unconventional single phase flow equation for the "expansion" DP meter (i.e. using ΔP_r) is given by equation 11. A full derivation of these equations from first principles is given in the Appendix.

$$\dot{m}_g = EA_t \varepsilon C_d \sqrt{2\rho \Delta P_t} = EA_t K_g \sqrt{2\rho \Delta P_t} \quad \text{--- (10)} \quad \text{and} \quad \dot{m}_g = EA_t K_g^* \sqrt{2\rho \Delta P_r} \quad \text{--- (11)}$$

Note "E" is the velocity of approach, A_t is the minimum cross sectional area (or "throat"), K_g and K_g^* are experimentally found coefficients and ρ is the gas density. It can be shown that all DP meters should have the conditions C_d<1, $\varepsilon < 1$ and therefore K_g <1, and, K_g^* >1.

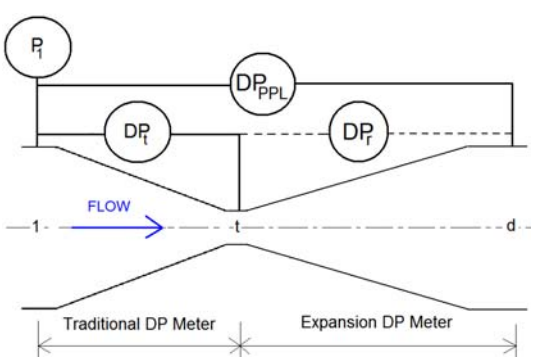

Figure 6. Venturi with DP's Marked Out

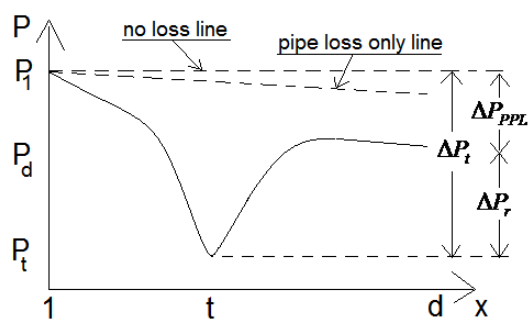

Figure 7. Pressure Fluctuations Through DP Meter.

Figure 8 shows a sketch of the ISA Controls (now known as Solartron ISA) supplied 6", sch 80, 0.55 beta ratio, ISO 5167 Part 4 compliant Venturi meter Steven [10] tested at NEL during commissioning of the

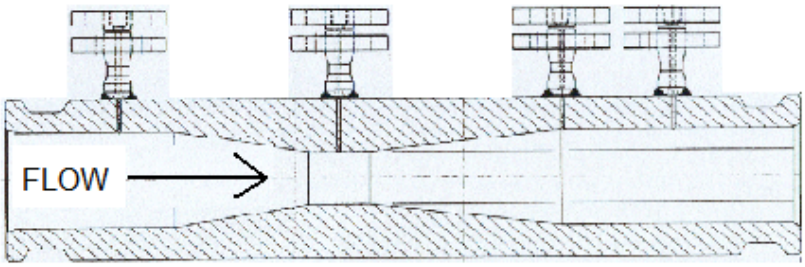

Figure 8. ISA Controls, 6”, 0.55 Beta Venturi Meter Wet Gas Tested at NEL.

NEL wet gas flow facility in September 1999. Note the two downstream tappings. One is at the junction of the diffuser exit and the other is one diameter further downstream. At the time of production early in the PhD project this author requested downstream tappings on the Venturi meter to test de Leeuw’s theories. On request from ISA Controls on where they should be placed this author did not then know. In this very early period of the research (1997) where this author was still learning basic DP meter theory it was guessed that as a Venturi meters diffuser section exists to recover the pressure, the exit of the diffuser must be the position of pressure recovery completion. As an after thought it was countered that this may not be true in reality so as a safe guard a second pressure tapping was included at a further one pipe diameter downstream. Of course, it was realised later in the project that this was a mistake. ISO 5167 part 4 suggests that full pressure recovery is not guaranteed to up to six diameters downstream of the diffuser exit. (However, the meter was built and the tests went ahead with the available equipment. Two differential pressures were read along with the upstream pressure. These were the traditional differential pressure (i.e. the upstream to throat, ΔP_t) and the permanent pressure loss, ΔP_{PPL} (or in this particular case the upstream to furthest downstream pressure tapping available).

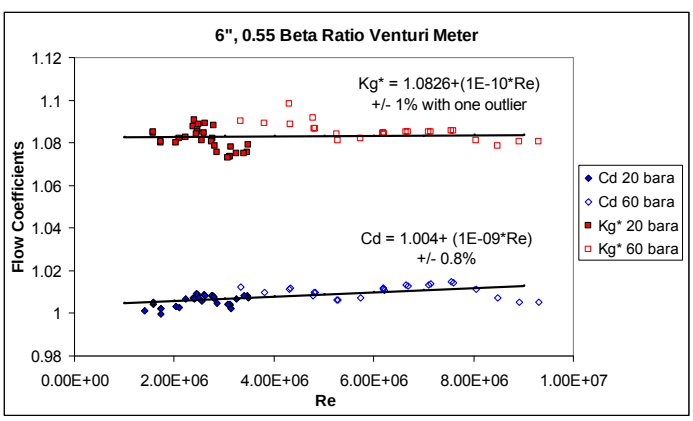

Figure 9. PhD Venturi Meter Traditional and Expansion Meter NEL Calibration Results.

Figure 9 shows the PhD Venturi meter dry gas flow calibration for equations 10[2] and 11[3]. The classic discharge coefficient was found to be slightly greater than unity which is a violation of the basic DP meter theory but a common result for Venturi meters due to the actual value being so close to unity and with real meters having non-ideal effects. The result is therefore a discharge coefficient linear fit slightly greater than unity and a traditional gas meter design with a ±0.8% performance across a ten to one turndown. The unconventional expansion flow coefficient was found to be greater than unity (as expected) and except for

[2] After 8 years the author could not find the zeroing data in the archived PhD raw data sets for the DP transmitters and hence when reproducing the discharge coefficient and expansion flow coefficient values the results are approximate and for explanation purposes only.

[3] In the PhD thesis [10] the Velocity of Departure term was combined with the expansion flow coefficient to simplify the flow equation. In hindsight this has not been done here as it is not convention in industry to combine the Velocity of Approach with the discharge coefficient and it is deemed best for explanatory reasons to keep the new equation as analogous to the conventional DP meter methods as possible.

one outlier (with a repeat point within the range) this downstream meter design had a ±1% performance across a ten to one turndown. (Note that Figure 8 shows pressure has no influence on the coefficient values.) Hence, the data shows that there are two metering opportunities in any one DP meter design and that the second downstream meter is of practical industrial use.

The NEL 6" 0.55 beta Venturi meter nitrogen & kerosene wet gas tests were for 21 Bara, 41 Bara and 61 bara between 400 and 1000 m^3/hr and $X_{LM} \leq 0.3$. The results showed the same Venturi meter wet gas flow trends as reported by de Leeuw [9]. Figures 10 and 11 show this for the three set pressures / gas to liquid density values tested (Figure 10) and for a sample of one pressure with varying gas densiometric Froude numbers (Figure 11). As the Lockhart Martinelli parameter increases for all other parameters constant a DP meters gas over-reading increases. As the gas to liquid density ratio increases for all other parameters held constant the over-reading reduces. As the gas densiometric Froude number increases for all other parameters constant the gas over-reading increases. Figure 11 shows that the apparent scatter for each set pressure (see Figure 10) is in fact not scatter but rather a gas densiometric Froude number effect.

The wet gas Venturi data was fitted using TableCurve 2D and 3D software to produce the correlation shown here as equation 12.

$$\dot{m}_g = \frac{\left(\dot{m}_{g,Apparent}\right)_{TM}}{\left(\dfrac{1 + AX + BFr_g}{1 + CX + DFr_g}\right)} \quad \text{--- (12)}$$

where A, B, C and D where functions of pressure. It was suggested by the PhD examiners in April 2001 that the function would have been more fitting with $B = D$ and the resulting A, B, C parameters functions of the gas to liquid density ratio to non-dimensionalise the terms.

The expansion meter wet gas data showed some scatter and a complicated relationship between the liquid induced gas flow rate error and the Lockhart Martinelli parameter, gas to liquid density ratio and the gas densiometric Froude number. Figure 12 shows the 61 bara wet gas data as an example. The plot shows the expansion meter "over-reading" (OR*) vs. X_{LM} for the set gas to liquid density of 0.088 and various gas densiometric Froude numbers. In fact, in this case the gas flow rate error is not always positive so the term "over-reading" is used here loosely only to prompt the reader to see the expansion meter liquid induced gas flow rate error as analogous with the traditional DP meter gas error over-reading. Note:

$$OR^* = \frac{\left(\dot{m}_{g,Apparent}\right)_{EM}}{\dot{m}_g} \cong \sqrt{\frac{\Delta P_{r,tp}}{\Delta P_{r,g}}} \quad \text{--- (13)}$$

where subscript "EM" denotes "expansion meter" and $\Delta P_{r,tp}$ and $\Delta P_{r,g}$ are the recovery (i.e. downstream to throat) differential pressures with two-phase (or "wet gas") and dry gas flows respectively. Even the simplest useable data fit (say function "j" – as shown in equation 14) was a complex equation.

$$\dot{m}_g = \frac{\left(\dot{m}_{g,Apparent}\right)_{EM}}{j\left(X_{LM}, \dfrac{\rho_g}{\rho_l}, Fr_g\right)} \quad \text{--- (14)}$$

It was considered unlikely that this complicated equation would fit subsequent data sets precisely as over fitting of data was a significant concern. Furthermore, this complex equation 14 could not have the Lockhart Martinelli parameter separated out to allow substitution into equation 12 (i.e. it was not possible to set up a solution procedure directly analogous to that described for de Leeuw's method). The only

practical method of finding a solution to the two wet gas correlations (i.e. equations 12 and 14) was to separate out the Lockhart Martinelli parameter from equation 12 and substitute that into equation 14.

The results were mixed. There were three types of result across the 243 point data set. The first type of result was the correct prediction of the gas and liquid mass flow rates with relatively small uncertainties. The second was an entirely incorrect prediction. The third was no prediction of any kind. With approximately a third of the results giving good gas and liquid flow rate predictions it was clearly not a coincidence and there was some useful data in the downstream to throat differential pressure reading[4]. It was therefore necessary to investigate why some data sets gave such poor results and others no results. This was done by selecting three individual data points, one for each type of result, and plotting a graph of gas mass flow rate vs. Lockhart Martinelli parameter. These graphs immediately showed the problems. Figures 13 to 15 replicate the graphs shown by Steven [10]. In the legend of these Figures note that "Meter 1" is the traditional Venturi meter and "Meter 2" is the downstream "expansion" meter.

Figure 13 shows one PhD result where the method worked well. Equations 12 and 13 intersected at a gas mass flow rate prediction of 10.45 kg/s and a Lockhart Martinelli parameter of 0.0186. The actual gas flow rate (i.e. reference gas meter reading) was 10.47 kg/s, i.e. a difference of -0.2%. The actual Lockhart Martinelli parameter (derived from the NEL gas and liquid reference meters and density calculations) was

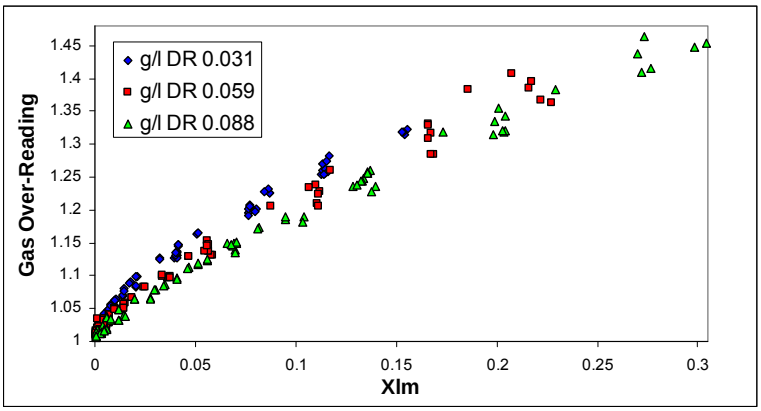

Figure 10. NEL PhD 6" 0.55 Beta Ratio Venturi Meter Wet Gas Data.

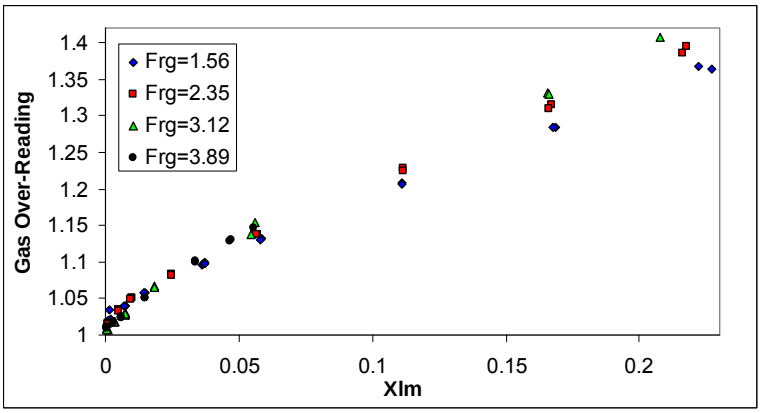

Figure 11. NEL PhD 6" 0.55 Beta Ratio Venturi Meter Wet Gas Data for 41 Bara / DR 0.059.

[4] The Venturi meter tested [10] had the traditional upstream to throat DP and the upstream to downstream DP recorded and the "recovery" DP, i.e. downstream to throat DP was derived from equation 9. There is therefore additional uncertainty in this data compared to if the recovery DP was measured directly. It should also be remembered that the "downstream" pressure tapping was at one diameter downstream of the diffuser exit and hence full recovery had not occurred at the measurement point. A pressure tap position further downstream could possibly reduce the level of scatter. Furthermore, the DP transmitter used was the only available instrument and had a higher Upper Range Limit than was ideal.

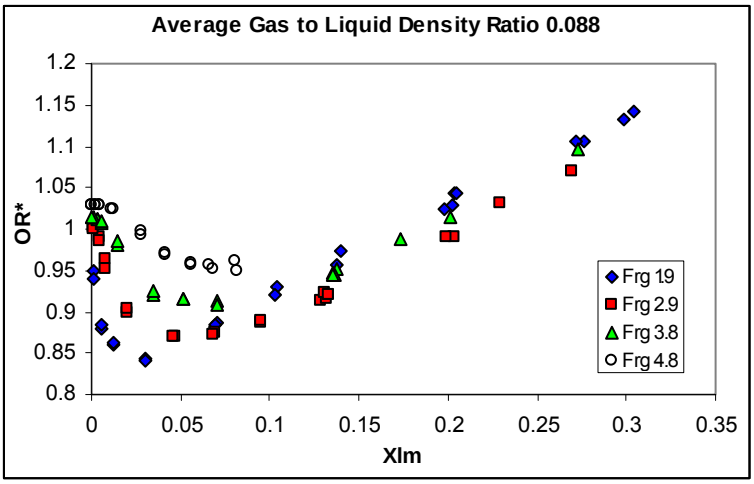

Figure 12. Venturi Downstream / Expansion Meter Equation 11 Wet Gas Response at 60 Barg.

0.0194. This is therefore an error of –3.955% and this error is then passed on to the liquid flow rate prediction. The predicted value of the liquid flow rate of was 0.78 kg/s compared with the NEL liquid reference meter value of 0.80 kg/s, a percentage difference of -3.4%.

Figure 13 shows a problem. It can be seen that for Figures 13 to 15, equation 12 is rather constant in that it always the same general shape when plotted on a gas mass flow rate vs. Lockhart Martinelli parameter graph. However, the complex equation 14 curve has more variation in shape and varies in position relative to equation 12's curve. In Figure 14 this has caused two intersections of the equations. That is, there is a correct result and a false (or "phantom") result. Whether the correct or phantom result is obtained is wholly dependent on what starting gas mass flow rate value is used in the iteration. As this is nothing more than an educated guess this is a problem. In Figure 14 the actual values were gas mass flow rate of 4.1 kg/s, Lockhart Martinelli parameter of 0.162 and a liquid mass flow rate of 3.63 kg/s. The "correct" convergence gives gas mass flow rate of 4.18 kg/s (+2%), the Lockhart Martinelli parameter of 0.144 (-11%) and the liquid mass flow rate as 3.30 kg/s (-9%). The "incorrect" convergence gives gas mass flow rate of 4.82 kg/s (+18%), the Lockhart Martinelli parameter of 0.039 (-76%) and the liquid mass flow rate as 1.03 kg/s (-72%). However, it is noteworthy that the differences in results are relatively large and an operator may be able to tell which result is the real result. However, this is far from ideal.

Figure 15 shows another adverse affect of the equations 14 complex nature. Naturally both equations 12 and 14 have uncertainty limits. That is, the actual data point values they predict do not necessarily lie on the equations but in the uncertainty band associated with each equation. In Figure 15 we see that there is no solution because the two equations do not intersect. As is required by mathematics both equations have the actual point within their respective uncertainty bands (shown in Figure 15 by broken lines). These intersect but the actual equations do not. The result is no solution by attempting to solve by simulatneous equations but when plotting the equations on a graph (Figure 15) it is obvious what the approximate result is. In Figure 15 this "visual estimate" and actual reference data point are marked. A visual estimate is a gas mass flow rate of 5.5 kg/s (compared to the actual 5.44 kg/s, i.e +1%) and a Lockhart Martinelli parameter of 0.1 (compared to the actual 0.122, i.e. -18%). The corresponding liquid mass flow rate estimation is 3.1 kg/s (compared to the actual 3.65 kg/s, i.e. -15%).

This then was the results of the PhD [10] research project. It was concluded it was technically possible to make a simple wet gas meter out of a stand alone standard DP meter using this method but much work was required to produce a workable system for industry. The PhD thesis fell short of offering this. One unanswered question was just what affect the downstream tapping position had had on the results. It was unknown if placing the downstream tapping at or beyond the full recovery point would reduce the complexity of the expansion meters wet gas response. It was also unknown what results other DP meter designs would give under similar test conditions. There was the possibility that another DP meter design would have a better performance than a Venturi meter.

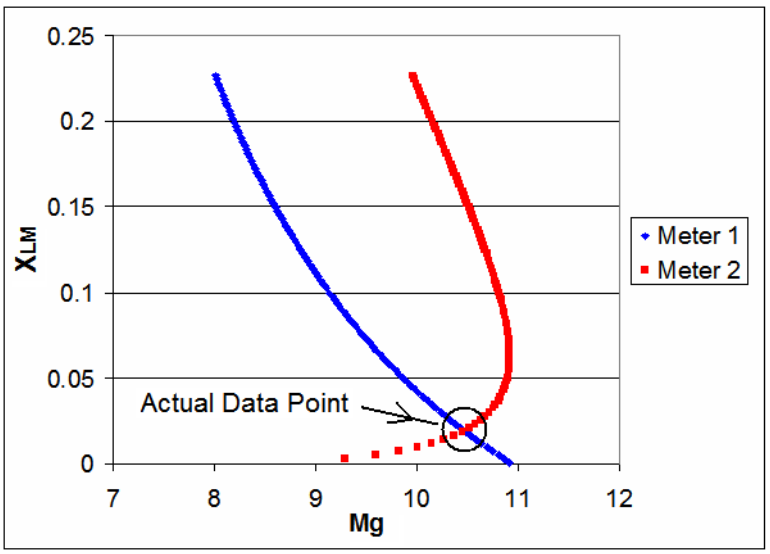

Figure 13. A Succesful Result of Combining Equation 12 and Equation 13.

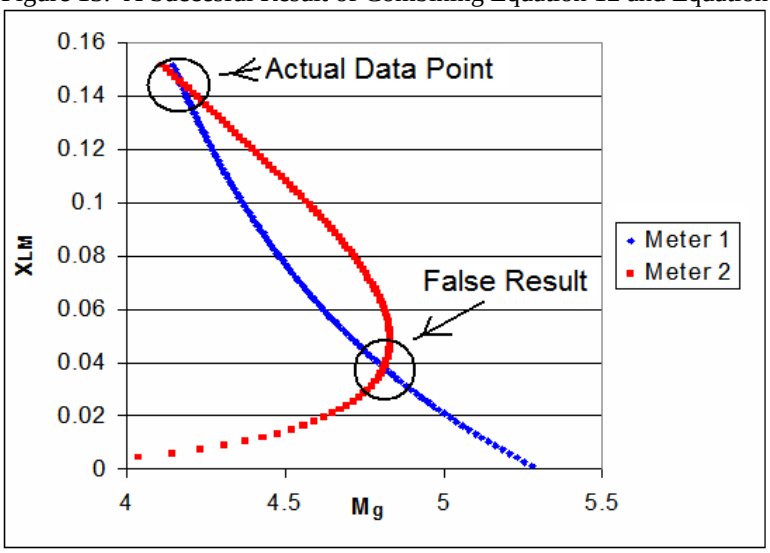

Figure 14. Correct and False Results of Combining Equation 12 and Equation 13.

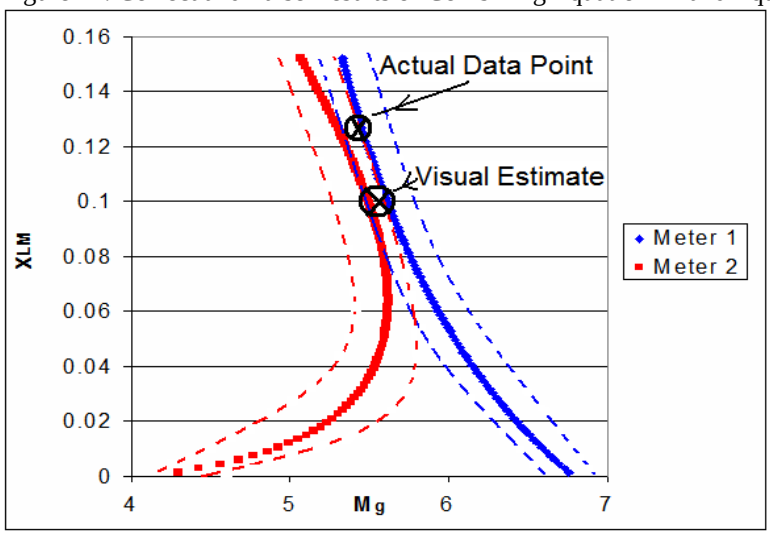

Figure 15. Non-Convergence Result of Combining Equation 12 and Equation 13.

5. McCROMETER 2001-2004, V-CONE METERS AND THE PhD THEORIES

During the final stages of the PhD research this author was interviewed by McCrometer who expressed a desire to develop a V-Cone based wet gas meter. The PhD generic DP meter wet gas flow theories were explained to McCrometer. In the UK, the NEL (where the author was still resident as a Post Graduate Training Partnership research associate) was preparing to carry out Flow Programme funded research into the reaction single phase gas meters had to wet gas flows. The NEL wet gas flow loop, commissioned with the PhD Venturi meter tests in late 1999, was the facility to be used. Two 6”, schedule 80, V-Cone meters (i.e. beta ratios of 0.55 and 0.75) were scheduled for Flow Programme testing in September 2001. On agreement of future employment McCrometer and this authour therefore requested that NEL also recorded the permanent pressure loss during these wet gas tests. The immediate hope was that the PhD generic DP meter theories and lessons could be directly transferred to V-Cone meters.

It was initially decided to place a downstream tapping in each meter body one diameter downstream of the back face of the cone as there was no room in the meter body to place it further downstream. Figure 16 shows a drawing of the 0.75 beta ratio V-Cone meter. However, it was one of the main lessons from the PhD research that it may be better to place the downstream tapping on a DP meter at or downstream of the full pressure recovery location. A problem was there had been no previous V-Cone meter research aimed at finding precisely where even the single phase pressure recovery position was. It was judged probable that the available pressure tapping downstream of the cone was not far enough downstream. A downstream spool was therefore built to give pressure tappings at the estimated / guessed recovery location four pipe diameters downstream of the back face of the cone.

It subsequently became clear that a 0.75 beta ratio V-Cone meter had the most stable wet gas flow response and therefore the rest of this paper concentrates on the 0.75 beta test results only.

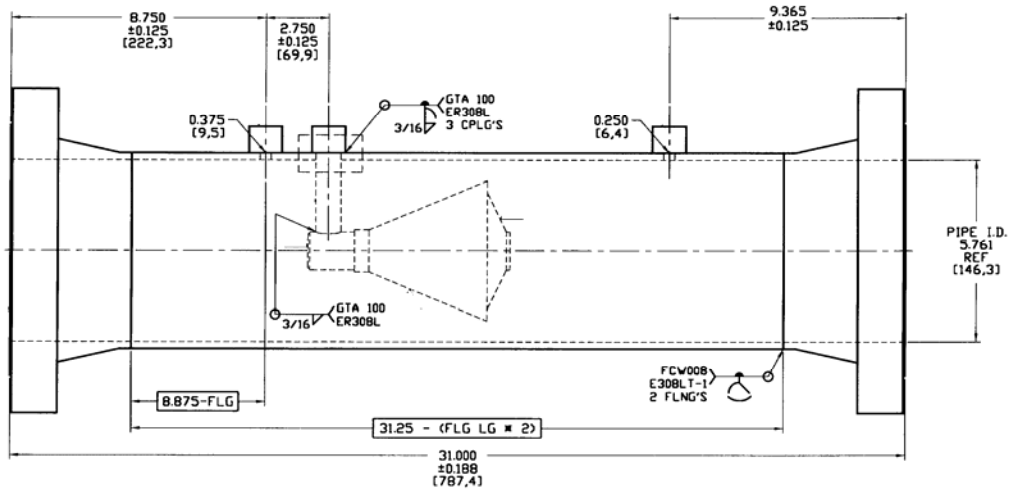

Figure 16. The 6”, 0.75 Beta Ratio V-Cone Meter Wet Gas Tested by the UK DTI’s Flow Programme.

The 6”, 0.75 beta ratio V-Cone meter was set up by NEL as sketched in Figure 17. That is, with traditional inlet pressure and DP transmitters and on request, although it was outwith the scope of the Flow Programme requirements, a second DP transmitter between the upstream pressure port and pressure port four diameters downstream of the back face of the cone. The recovery DP was found by equation 9. This added DP transmitter was the only available device and it had a higher upper range limit (1 bar / 400 ”WC) than would have been ideal. The result was that to reduce scatter on the recovery DP data only differential pressures read by this device greater than 1”WC were used. (This is why some points are missing from the expansion meter low Reynolds number calibration plots in Figure 18.)

Figure 18 shows the gas calibration results of the 6”, 0.75 beta ratio V-Cone meter across a 10:1 turndown. The traditional and expansion DP meter equations 10 and 11 were both calibrated by linear fits to less than

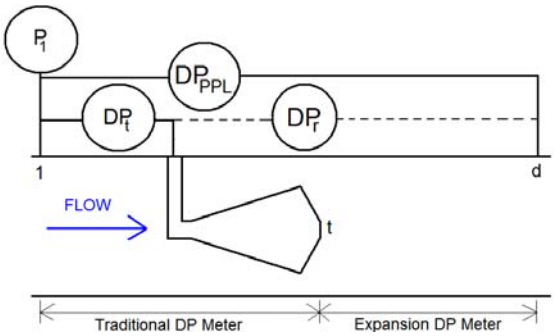

Figure 17. NEL V-Cone Meter Test Configuration.

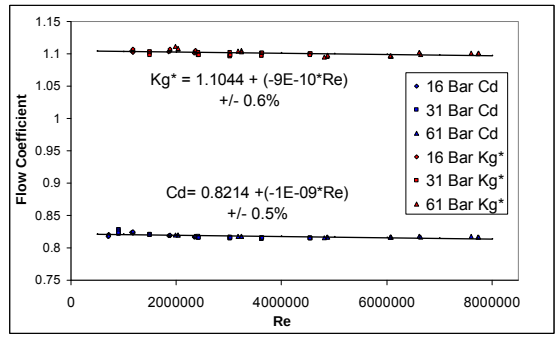

Figure 18. 6", 0.75 Beta V-Cone Gas Calibration.

±1%. Note that as expected, C_d<1 and K_g*>1. Also note that the pressure has no effect on either calibration. This result re-enforces the idea that the expansion meter equation of any DP meter is a practical gas metering method and not just an academic curiosity.

The wet gas over-reading results of the traditional V-Cone meter have been well documented. The test matrix (Table 1) and results of the Flow Programme tests at NEL were presented at the NSFMW in 2002 by Stewart et al [12]. The same wet gas flow trends were reported for a V-Cone meter as were reported by de Leeuw [9] for a Venturi meter. That is, a V-Cone meter with wet gas flow responds to changes in the Lockhart Martinelli parameter, gas to liquid density ratio and densiometric Froude number in the same general way as a Venturi meter.

Nominal Pressure (Barg)	Average Density Ratio	Fr_g range	X_{LM} range
15	0.0239	0.57 – 1.91	$0 \leq X_{LM} \leq 0.3$
30	0.0456	0.54 – 2.75	$0 \leq X_{LM} \leq 0.3$
60	0.0889	0.92 – 3.53	$0 \leq X_{LM} \leq 0.3$

Table 1 - Envelope for NEL 2001 Wet Gas Flow 6", 0.75 Beta Ratio V-Cone Meter Test

Further 0.75 beta ratio V-Cone meter repeat data from NEL and CEESI was shown by Steven et al in 2003 and 2004 [13,14] before a final summarising paper was given by Steven [15] in June 2005. This paper superimposed all the available NEL and CEESI data on to one graph. Figure 19 shows a further update with the inclusion of a data set from a CEESI Joint Industry Project. Steven et al [15] gave the latest 4" and 6" 0.75 beta ratio V-Cone meter wet gas correction factor (which is a slight modification to that originally shown by Stewart et al [12]) and this is reproduced here as equation set 12a and equations 15a to 15c. It is the performance of this V-Cone meter wet gas correlation that is used in Figure 19 for the case of a known liquid mass flow rate. It should be noted that equation 12a is in fact simply the PhD Venturi equation 12 form with the PhD examiners suggestions that B=D applied, and, that the resulting parameters A, B and C are functions of the gas to liquid density ratio. For a known liquid mass flow rate this correlation predicts the gas mass flow rate to ±2% (with a few outliers).

Although most V-Cone meter wet gas flow tests between 2001 and 2005 at NEL, CEESI and K-Lab have included the recording of downstream pressure tapping data, up until now no downstream wet gas flow data has been released by McCrometer. Figure 20 shows all the wet gas over-reading data taken from the Flow Programme tested 6", 0.75 beta ratio V-Cone expansion meter as produced internally by McCrometer in 2001. Figure 21 shows one gas to liquid density ratio set with the gas densiometric Froude numbers separated out. The finding was that, when using a V-Cone meter with a downstream tapping that is positioned to allow good pressure recovery, a wet gas flow trend was clearly visible and could be described by a relatively simple function. (This was a considerable improvement on the PhD Venturi meter with little distance for pressure recovery.) Figures 20 and 21 show a clear over-reading with an almost linear relationship with the Lockhart Martinelli parameter. A gas to liquid density ratio effect is also evident. In Figure 21 a gas densiometric Froude number effect is evident. The mid range gas to liquid density ratio data set was chosen as a sample graph. It should be remembered that this data was taken as an add on to the main test program and the permanent pressure loss transmitter was not ideal (i.e. over sized) so there is knock on affect of a high uncertainty in some of the lower value recovery DP measurements / low gas

densiometric Froude numbers. It is postulated that this is the reason that the lowest two gas densiometric Froude numbers do not show the same trend as the higher values.

$$\dot{m}_g = \frac{\left(\dot{m}_{g,Apparent}\right)_{TM}}{\left(\frac{1+AX_{LM}+BFr_g}{1+CX_{LM}+BFr_g}\right)}$$ --- (12a) where for $\rho_g/\rho_l < 0.027$, then A=2.431 , B=-0.151 , C=+1

and for $\rho_g/\rho_l \geq 0.027$, then[5]:

$$A = -0.0013 + \frac{0.3997}{\sqrt{\rho_g/\rho_l}} \text{ ---(15a)}, \quad B = 0.0420 - \frac{0.0317}{\sqrt{\rho_g/\rho_l}} \text{ ---(15b)}, \quad C = -0.7157 + \frac{0.2819}{\sqrt{\rho_g/\rho_l}} \text{ ---(15c)}$$

A 6”, 0.75 beta ratio V-Cone expansion meter wet gas correlation was formed (which is not designed for extrapolation). Unlike for the Venturi meter a relatively simple correlation form could be successfully applied. In fact, the PhD DP meter wet gas correlation form (equation 12a) was applicable. This is shown as equation 12b with equation 16a to 16c:

$$\dot{m}_g = \frac{\left(\dot{m}_{g,Apparent}\right)_{EM}}{\left(\frac{1+A'X_{LM}+B'Fr_g}{1+C'X_{LM}+B'Fr_g}\right)}$$ --- (12b)

where:

$$A' = -0.116 + \left(\frac{0.0094}{\left(\rho_g/\rho_l\right)^{1.5}}\right) \text{--(16a)}, \quad B' = -0.166 + \left(\frac{0.0009}{\left(\rho_g/\rho_l\right)^{1.5}}\right) \text{--(16b)}, \quad C' = -0.616 + \left(\frac{0.007}{\left(\rho_g/\rho_l\right)^{1.5}}\right) \text{--(16c)}$$

Figure 22 shows the uncorrected data for the 6”, 0.75 beta ratio V-Cone expansion meter and the performance of the correction (equation 12b with equations 16a to 16c) for the case of known liquid mass flow rates. The expansion meter wet gas correlation therefore predicts the gas flow rate to ±5% with a few outliers. This is therefore a poorer performance to the traditional meters wet gas correlation at ±2% (see Figure 19). Nevertheless it is a second working wet gas correlation for the same V-Cone meter body. The V-Cone meter is therefore, in affect, two DP meters in series with two wet gas correlations.

Figure 23 shows the mid pressure (DR 0.046) wet gas response of both the traditional and expansion meter equations. It appeared that there was a significant difference in the two metering methods and hence a measurement by difference technique was possible. Furthermore, unlike equation 14, equation 12b can have the Lockhart Martinelli parameter separated out (see equation 12c).

$$X_{LM} = \frac{\left(1+B'Fr_g\right)\left(1-OR^*\right)}{\left(OR^*C' - A'\right)}$$ --- (12c)

Therefore, a wet gas meter design attempt was made for a known gas and liquid density by substituting into equation 12a, equation 12c, equation 2, equations 6 and 13, equation set 15a to c and equation set 16a to c and solving for the only unknown, i.e. gas mass flow rate. The iteration was started with the expansion meter uncorrected gas mass flow rate (which we see from Figure 23 has a lower over-reading than the traditional V-Cone meter flow rate calculation method and therefore is the closest value to the gas mass flow rate).

[5] Note that Steven et al [15] gave the value of the parameter C at a gas to liquid density ratio less or equal to 0.027 as C = -0.669. This is an error. The correct value is in fact C = +1. 000.

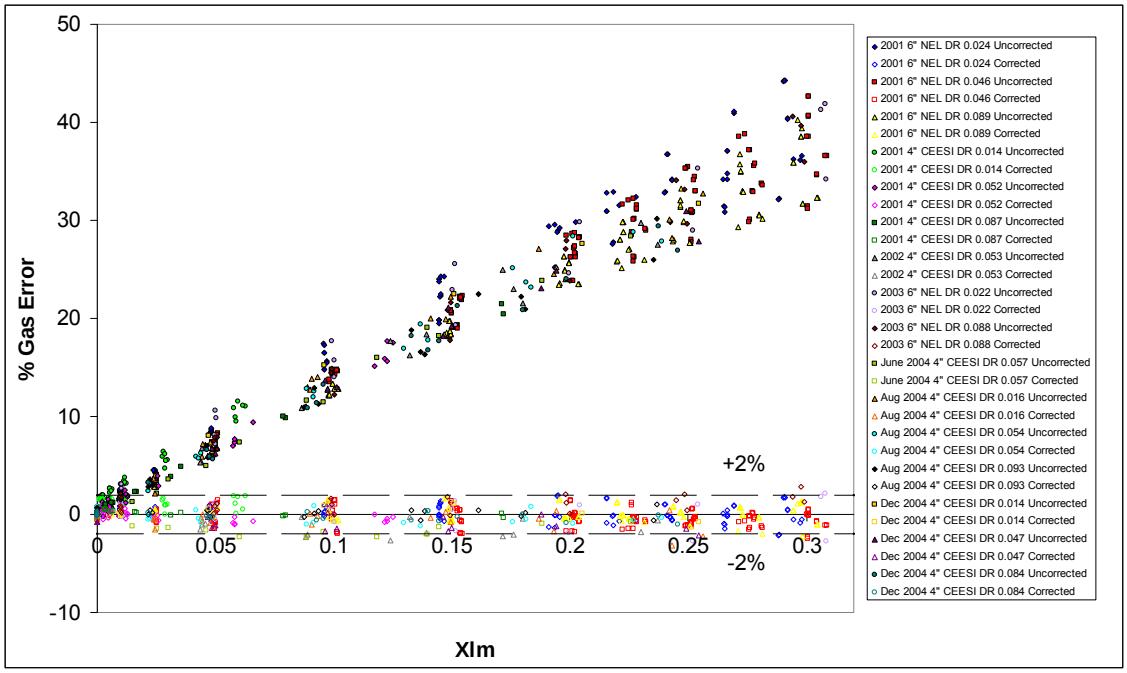

Figure 19. Flomeko 2005 [15] Graph with Additional CEESI JIP Data Showing Uncorrected and Corrected 4" and 6", 0.75 Beta V-Cone Meter Wet Gas Flow Response.

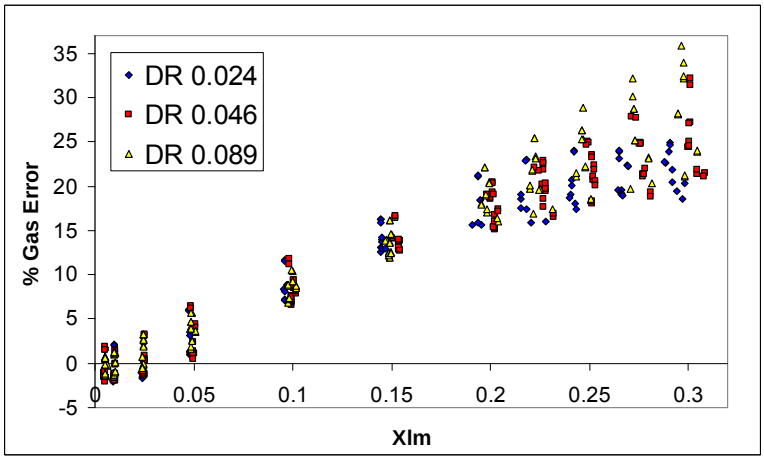

Figure 20. All NEL 6", 0.75 Beta V-Cone Meter Expansion Meter Wet Gas Response Data.

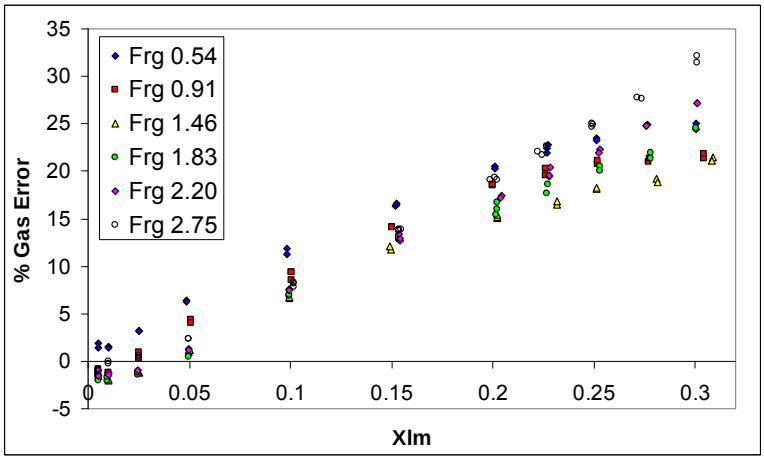

Figure 21. NEL 6", 0.75 Beta V-Cone Meter Expansion Meter Mid-DR 0.046 Wet Gas Response Data.

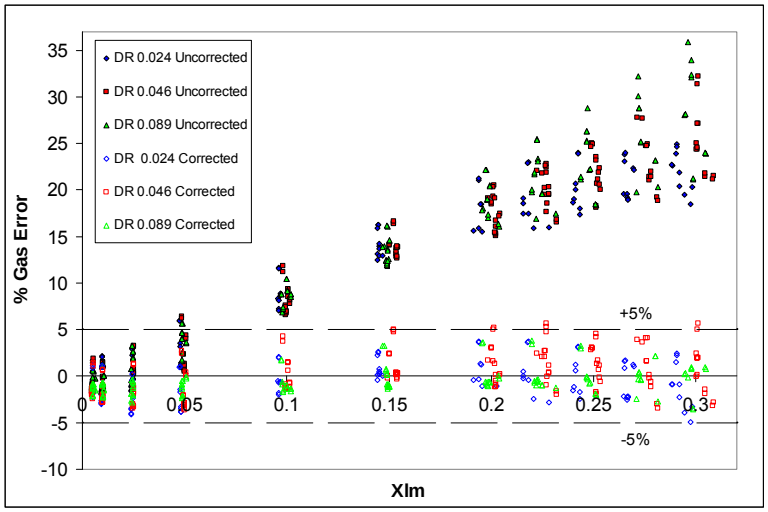

Figure 22. NEL 6", 0.75 Beta V-Cone Meter Expansion Meter Uncorrected and Corrected Results.

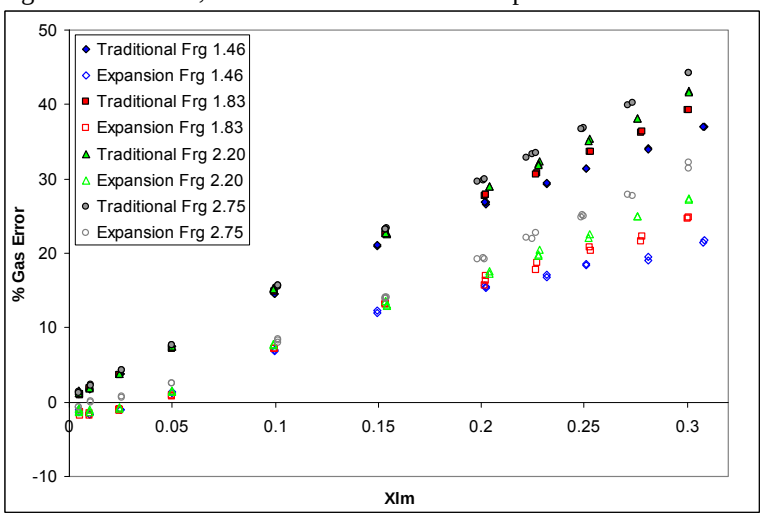

Figure 23. NEL 6", 0.75 Beta Ratio Traditional and Expansion Meter Wet Gas Responses.

The results were poor. Even though the traditional V-Cone meter had as good a wet gas correction factor as the PhD Venturi meter, and the V-Cone expansion meter wet gas response was relatively well predicted by a vastly simpler equation than found for the PhD Venturi meter, the method showed the same problems as the PhD research. Some data points had the phase flow rates predicted well, some poorly and again some data points had iterations that failed to converge. Again, plots of X_{LM} vs. gas mass flow rate were produced and they showed the same story.

Figures 24 shows a sketch representing a typical result. The traditional V-Cone meter over-reading equation gave a predictable shape on the X_{LM} vs. gas mass flow rate curves in all cases, similar to the PhD Venturi meter. However, the V-Cone expansion meter had a more predictable (less variable) wet gas curve than that found for the Venturi meter. This however was still not enough to alleviate the problem explained with the PhD data. The uncertainty bands of the V-Cone expansion meter wet gas correlation were still too large compared to the relative gradients of the two correlations. The actual data points always fell within the uncertainty bands of both equations. However, whereas for some data the equations intersection gave good predictions, for much of the data, due to the similarity in the traditional and expansion meter X_{LM} vs. gas mass flow rate gradients, there were very significant errors (see Figure 24). That is, the V-Cone expansion meter wet gas correlation was a considerable improvement on the PhD Venturi expansion meter wet gas correlation, but the uncertainty bands of the traditional and expansion V-Cone meters were still too large to allow the creation of a V-Cone meter wet gas system by solving these simultaneous equations.

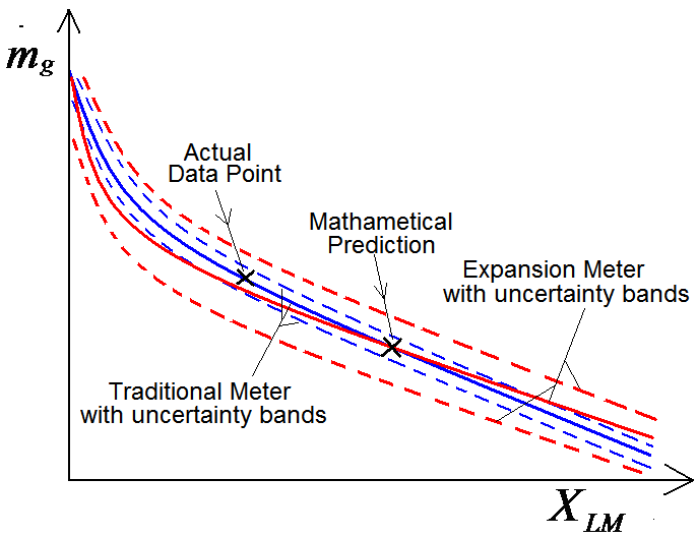

Figure 24. An Unsuccessful V-Cone Traditional and Expansion Meter Wet Gas Correlation Pairing.

6. McCROMETER 2004-5, V-CONE METERS, THEORIES & ALTERNATIVE DATA ANALYSIS

By early 2002 this author had reported to McCrometer that the research program had failed to produce a V-Cone wet gas meter. The decision was made to continue with other avenues of research. From October 2002 until August 2004 McCrometer carried out multiple theoretical wet gas meter design reviews and wet gas testing runs at NEL and CEESI. Theoretical design concepts investigated included (but were not restricted to) placing Venturi and V-Cone meters in series and orifice plate and V-Cone meters in series. Actual wet gas test projects at NEL and CEESI included (but were not restricted to) placing wedge and V-Cone meter in series, placing a vortex and V-Cone meter in series, changing the cone design for wet gas flow applications, placing a capacitance sensor and V-Cone meter in series and partnering with Petroleum Software Ltd. to investigate if the ESMER concept could be utilised with the V-Cone meter design (as described by Toral [16]). Much of this work is still held in confidence by McCrometer.

By the early summer of 2004 despite considerable effort and expense the research had not led to McCrometer getting any closer to a wet gas metering system. Radical steps were required. This author therefore decided that as there were wet gas flow meter systems on the market that were essentially two DP meters in series, operating by utilising measurement by difference techniques, it must be technically possible to produce this. What was evidently required in order to use the V-Cone meter in conjunction with a second meter design, was a second meter design with a wet gas over-reading value far in excess of that produced by the V-Cone meter. That is, when measuring by difference, the bigger the difference the better the measurement and the reduction of uncertainty levels.

In August 2004 CEESI wet gas tested an extreme design of DP meter (the details of which are held in confidence by McCrometer) in series with a V-Cone meter. The over-reading of this new design was significantly higher than that publicly released before for any DP meter design. The measurement by difference technique as applied above for the Venturi and V-Cone traditional and expansion meter pairs was attempted using the two DP meter traditional wet gas correlations. Again, the results were as before. At this stage, however, it was becoming very unlikely that any of the marketed wet gas meter products based on measurement by difference of gas meter over-readings could have a greater difference in over-reading values than this extreme test. Therefore, rather belatedly, this author began to wonder why these rival products worked and the McCrometer prototypes did not.

The answer was found in the literature. In 2003 Wood [17] had presented at the NSFMW a paper describing the operation of the Dualstream II wet gas meter. Graphs were presented to show the relationship between the two DP meter wet gas over-readings. These are reproduced as Figure 25. The term "DOR" appears to mean the "Difference in Over-Reading" between the two DP meters in series. In the autumn of 2004 this author re-read the paper, concentrating on all direct and indirect comments regarding

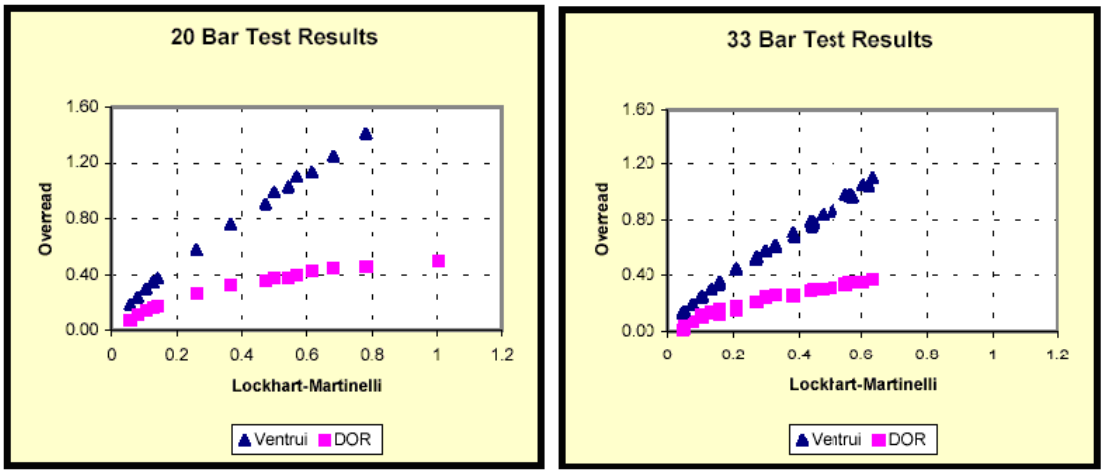

Figure 25. The 2003 Solartron ISA / Shell Wet Gas Flow Data Plots of A DualstreamII Wet Gas Meter.

the mathematical manipulation of the data. It became clear that SolartronISA were not using the same technique as described above. The Lockhart Martinelli parameter was directly shown as a function of the difference of the over-readings of the two DP meters. An immediate comparison was made between Woods DOR values and those found for the V-Cone traditional and expansion meter wet gas over-readings. They were of the same magnitude. It was also noticed that Wood [17] showed an equation pairing the two DP meter over-readings ratio to the Lockhart Martinelli parameter. All post 2002 research was immediately put on hold and this author returned to the original Flow Programme 6", 0.75 beta ratio V-Cone meter data sets to re-evaluate the data analysis techniques.

The ratio of the 6", 0.75 Beta Ratio V-Cone traditional and expansion meter wet gas over-readings (denoted here as "theta", ϕ) vs. Lockhart Martinelli parameter were plotted for set averaged values of gas to liquid density ratio and gas densiometric Froude number. Figure 26 shows this result. Note that theta, ϕ, is a measurable parameter as:

$$Theta, \phi = \frac{OR}{OR^*} = \frac{\left(\dot{m}_{g,Apparent} / \dot{m}_g\right)_{TM}}{\left(\dot{m}_{g,Apparent} / \dot{m}_g\right)_{EM}} = \frac{\left(\dot{m}_{g,Apparent}\right)_{TM}}{\left(\dot{m}_{g,Apparent}\right)_{EM}} \quad \text{--- (17)}$$

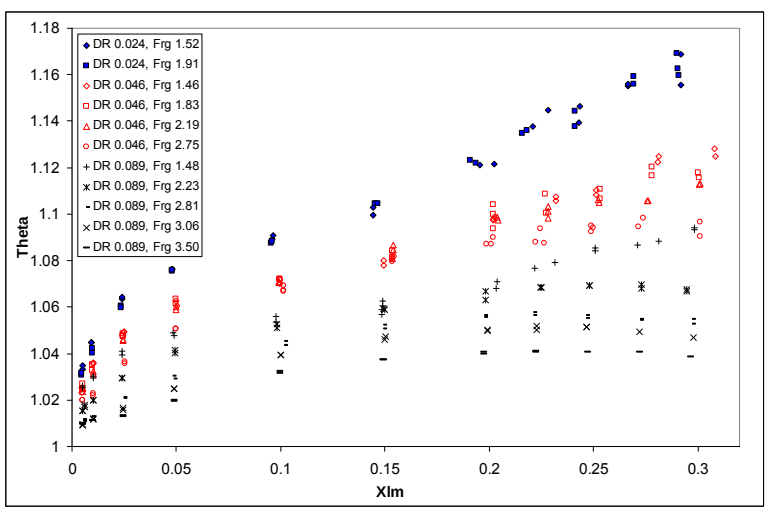

Figure 26. Plot of Theta (Equation 17) to X_{LM} for 2001 NEL 6", 0.75 Beta Ratio V-Cone Wet Gas Data.

The resulting curves were all fittable to a parabolic equation. That is:

$$(\phi-1)^2 = 4aX_{LM} \text{ --(18)}, \quad \text{i.e. } X_{LM} = \frac{(\phi-1)^2}{4a} = \left\{(\phi-1)^2\right\} \Big/ \left\{4\left[f_1\left(\frac{\rho_g}{\rho_l}, Fr_g\right)\right]\right\} \text{--(18a)}$$

$$\text{as } a = f_1\left(\frac{\rho_g}{\rho_l}, Fr_g\right) \text{--(19)}$$

The term "a" is the focus of the parabola which has been found to be solely a function of the gas to liquid density ratio and gas densiometric Froude number. From TableCurve3D a blind fit showed that in the case of the NEL / Flow Programme 6", 0.75 beta ratio V-Cone meter tests:

$$a = 0.0024 + \frac{0.00051}{\left(\rho_g/\rho_l\right)} - 0.00056Fr_g^2 \text{ --- (19a)}$$

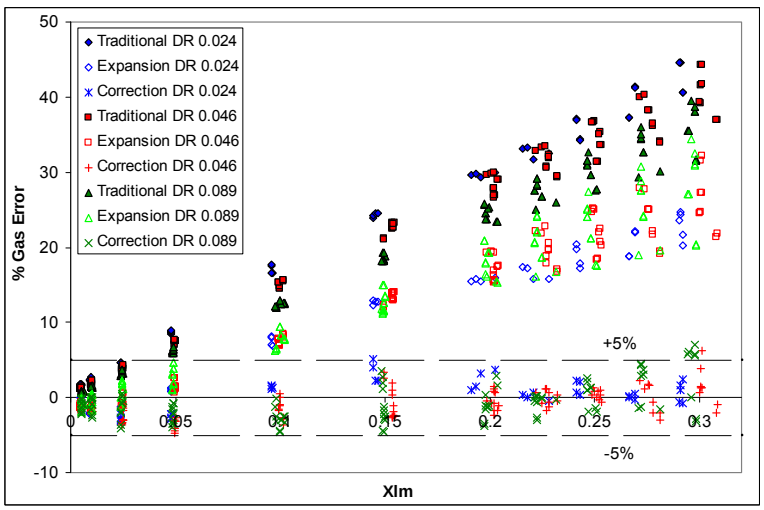

Figure 27. Results of Applying Iteration Sequence to 2001 NEL 6", 0.75 Beta Ratio V-Cone Wet Gas Data.

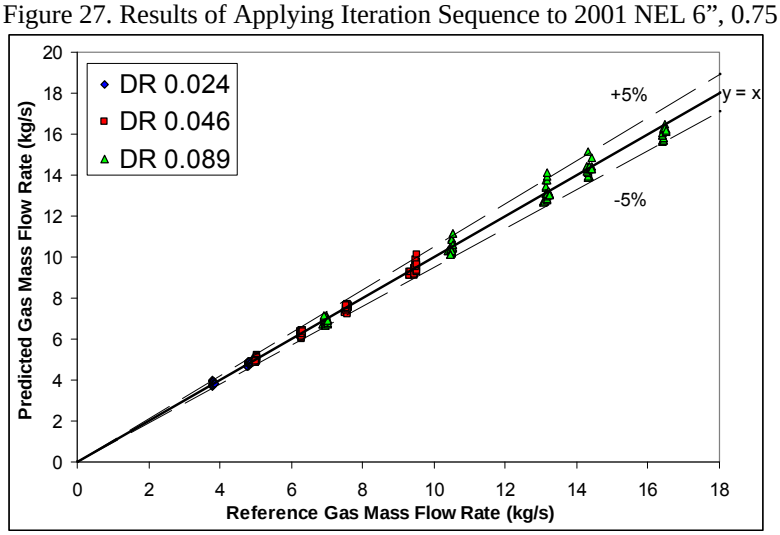

Figure 28. Alternative Plot of Results of Applying Iteration Sequence to NEL V-Cone Wet Gas Data.

Therefore, if we substitute equation 17 and equation 19a into equation 18a we have an expression for the Lockhart Martinelli parameter that is independent of the as yet unknown liquid flow rate. In fact it is solely a function of the known theta value, the known gas to liquid density ratio and the as yet unknown gas densiometric Froude number. Substituting this resulting Lockhart Martinelli parameter expression with

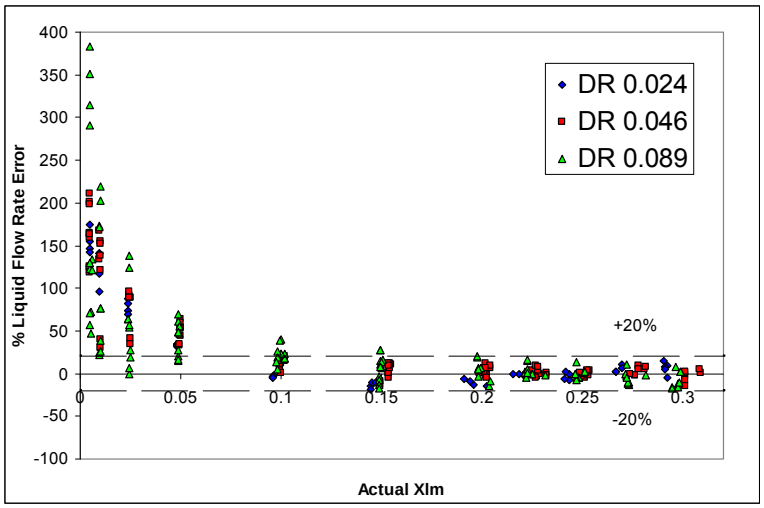

Figure 29. Results of Applying Liquid Flow Rate Calculation to 2001 NEL V-Cone Wet Gas Data.

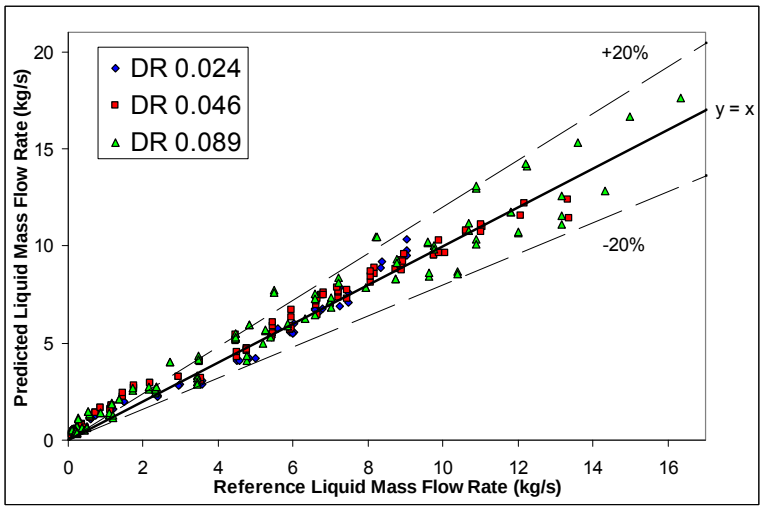

Figure 30. Alternative Plot of Results of Applying Liquid Flow Rate Calculation to NEL V-Cone Data.

equations 2 and equation set 15a to 15c into equation 12a results in an equation with only one unknown, i.e. the gas mass flow rate. Iterating, by starting say, with the uncorrected gas mass flow rate prediction of the V-Cone expansion meter equation, equation 12a will predict the gas mass flow rate.

The result of applying this technique to the NEL data is shown in Figures 27 and 28. The gas mass flow rate has been predicted to within ±5% with a few outliers at the very highest liquid loading. Of the 255 useable points (i.e. the permanent pressure loss was > 1"WC) there were 7 gas flow rate predictions > ±5%. The prediction method therefore has a 95% confidence level. The predicted Lockhart Martinelli parameter values can be substituted into equation 1 with the gas mass flow rate prediction and for a known gas to liquid density ratio a liquid mass flow rate prediction is obtained. Figures 29 and 30 show the results. The target of predicting gas mass flow rate to ±5% was achieved. The secondary target of predicting liquid mass flow rate to ±20% (until the liquid mass flow rate reduces to small quantities, i.e. X_{LM}<0.05) for a set meter geometry and known fixed fluid properties was approached but not fully achieved.

7. McCROMETER 2005 - A CONFIRMATION TEST AT CEESI

In March 2005 McCrometer tested a 4", 0.75 beta ratio V-Cone meter at the CEESI wet gas flow facility. The recovery differential pressure (ΔP_r) was now read directly. The test set up is sketched in Figure 31. Note that the downstream pressure tapping is shorter than sketched in the NEL set up (i.e. Figure 17). This

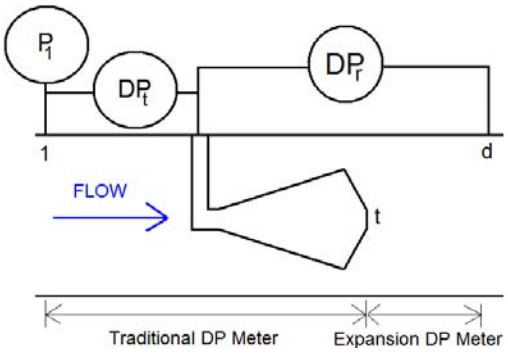

Figure 31. CEESI V-Cone Meter Configuration.

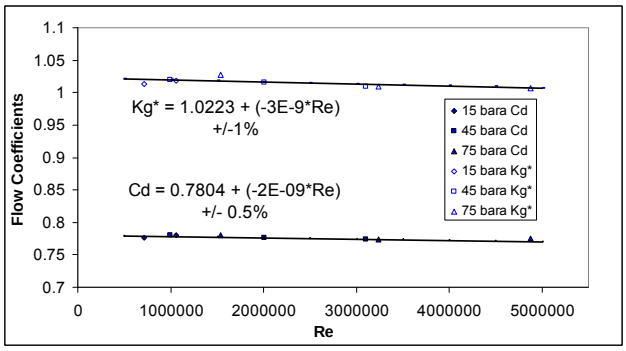

Figure 32. 4", 0.75 Beta V-Cone Gas Calibration.

indicates an effort to shorten the prototype meter design, i.e produce a more compact and lighter design. The downstream tapping was now approximately pipe 2.5 diameters downstream of the cones back face.

The V-Cone traditional and expansion meter calibration result is shown in Figure 32. The traditional meter operated to ±0.5% and the expansion meter to ±1% across a 10:1 turndown. Again we see that C_d <1, and K_g^* >1. However, whereas the discharge coefficient is a very familiar range for standard V-Cone meters the expansion flow coefficient is just above unity where as it was approximately 1.1 at the NEL test. This is evidence that the downstream pressure tapping position can significantly affect an expansion meters calibration. It is not certain if pressure recovery is complete by the downstream tap location in this meter installation. Nevertheless, the unconventional expansion meter still calibrates to ±1% across a 10:1 turndown which is acceptable for many conventional DP meter designs on the market.

Nominal Pressure (Bara)	Average Density Ratio	Fr_g range	X_{LM} range
15	0.015	0.90-1.50	$0 \le X_{LM} \le 0.27$
45	0.046	0.85-2.55	$0 \le X_{LM} \le 0.27$
75	0.083	1.15-3.50	$0 \le X_{LM} \le 0.27$

Table 2 - Envelope for CEESI 2005 Wet Gas Flow 4", 0.75 Beta Ratio V-Cone Meter Test.

Table 2 shows the CEESI natural gas / Stoddard solvent (mainly of C9-C12) test matrix. The standard reaction of the traditional V-Cone meter was as expected. That is, Figure 33 shows the over-reading to Lockhart Martinelli parameter graph with the results for a standard correction (equation 12a with equations 15a to 15c) for a known liquid flow rate being ±2%. Figure 34 shows this data sets plot of theta, ϕ vs.Lockhat Martinelli parameter. Again, as with the NEL data set, for set gas to liquid density and gas densiometric Froude numbers the data can be described well by a parabolic equation. Fitting the focus to the gas to liquid density and gas densiometric Froude number variables found the equation 19b.

$$a = \exp\left\{-2.74 + (-22.3\frac{\rho_g}{\rho_l}) + (-\frac{1.27}{Fr_g})\right\} \text{ --- (19b)}$$

Figure 35 shows the traditional ("TM") and expansion ("EM") V-Cone meter over-readings and the result of applying the correction method with equation 19b. Figure 36 shows the gas flow rate prediction result in an alternative format. Figure 37 and 38 show representations of the liquid flow rate predictions. The results are similar to the NEL results, that is, the gas flow rate is predicted to ±5% with a few outliers. The liquid flow rate is generally predictable to ±20% at X_{LM} > 0.1, but at lower values (X_{LM} < 0.1) this system – like most wet gas systems – has a considerable increase in liquid flow rate uncertainty.

Note that both NEL's Figure 26 and CEESI's Figure 34 show that for set gas to liquid density ratio and gas densiometric Froude numbers, theta vs. Lockhart Martinelli parameter can be fitted well using a parabolic equation. For both data sets, as the gas to liquid density increases the trend is for theta to tend to unity. However, the gas densiometric Froude number trends are different. The NEL data shows increasing gas

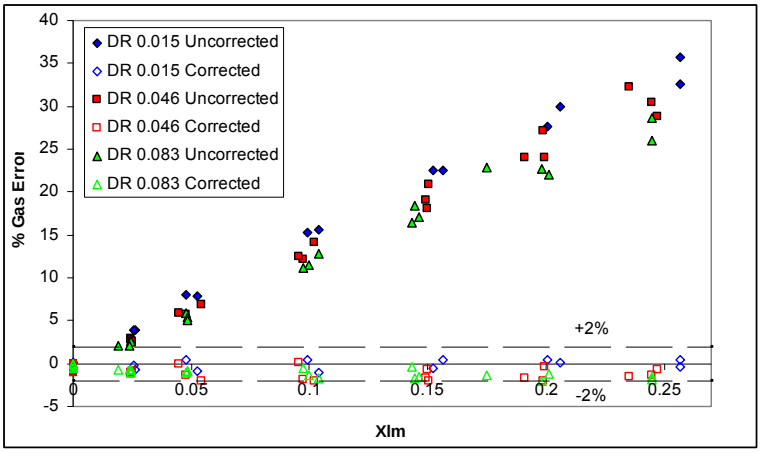

Figure 33. CEESI 2005 4", 0.75 Beta Ratio V-Cone Meter Uncorrected and Corrected Data.

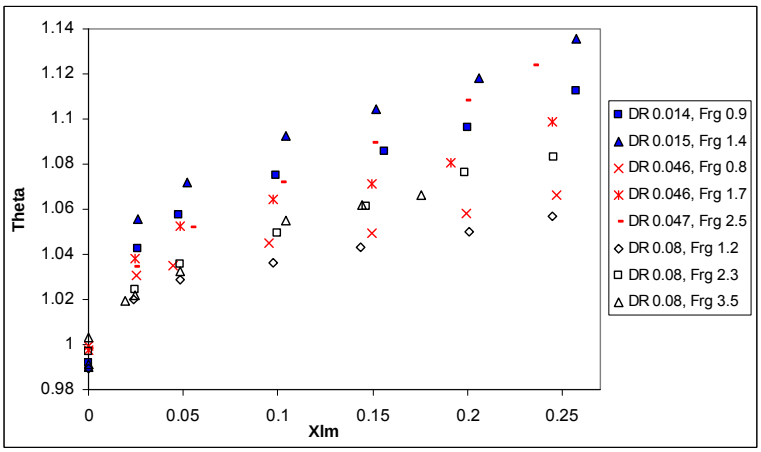

Figure 34. CEESI 2005 4", 0.75 Beta Ratio V-Cone Meter Theta vs. Lockhart Martinelli Parameter Data.

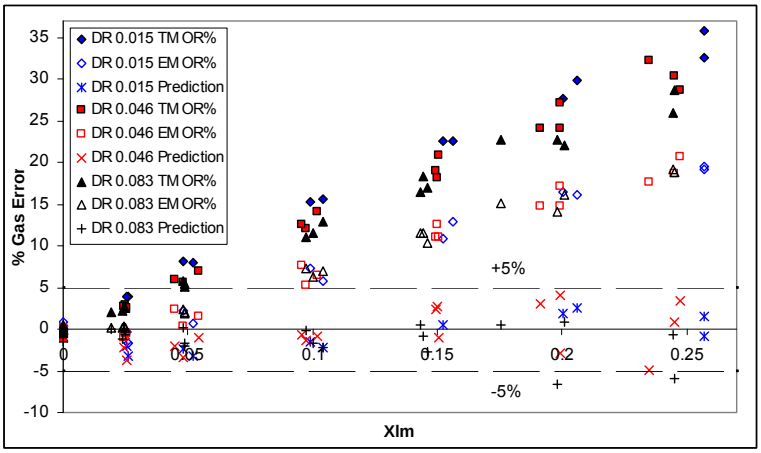

Figure 35. CEESI 2005 4", 0.75 Beta Ratio V-Cone Meter Traditional, Expansion and Corrected Results.

densiometric Froude numbers reducing theta's value but CEESI's data shows the opposite. Theoretically, as the gas dynamic pressure increases the wet gas flow should tend towards homogenous (i.e. pseudo single phase) flow and theta should therefore tend towards unity. It is possible that the CEESI result may be due to the short downstream tapping distance meaning recovery has not yet been completed. Whatever the reason the data fit on the relationship between the parabolas focus and the gas to liquid density ratio and gas densiometric Froude number is different for the two data tests. Both work well for the data set that created them but they are not similar. This suggests that until further research is conducted at least, such a

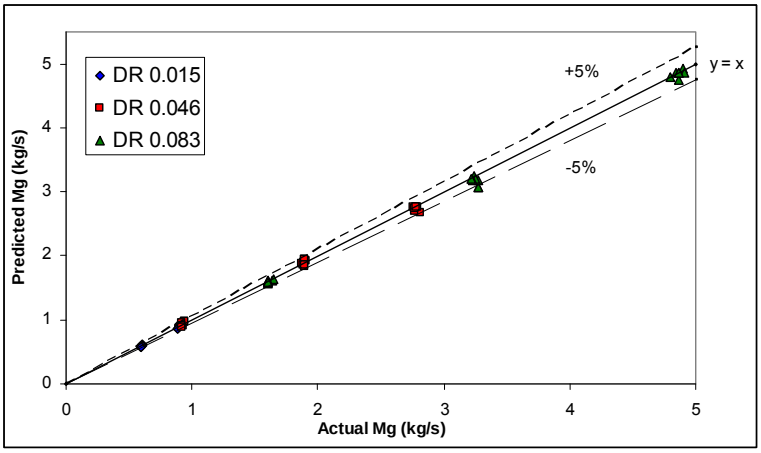

Figure 36. CEESI 2005 4”, 0.75 Beta Ratio V-Cone Meter Gas Flow Rate Prediction Results.

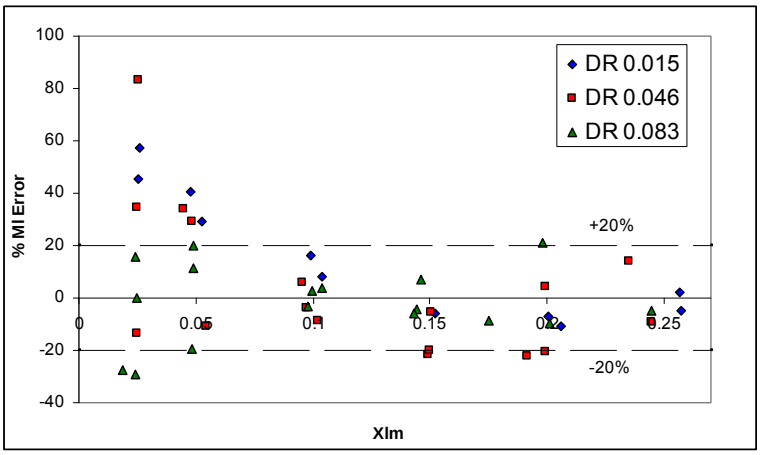

Figure 37. CEESI 2005 4”, 0.75 Beta Ratio V-Cone Meter Liquid Flow Rate Prediction Results.

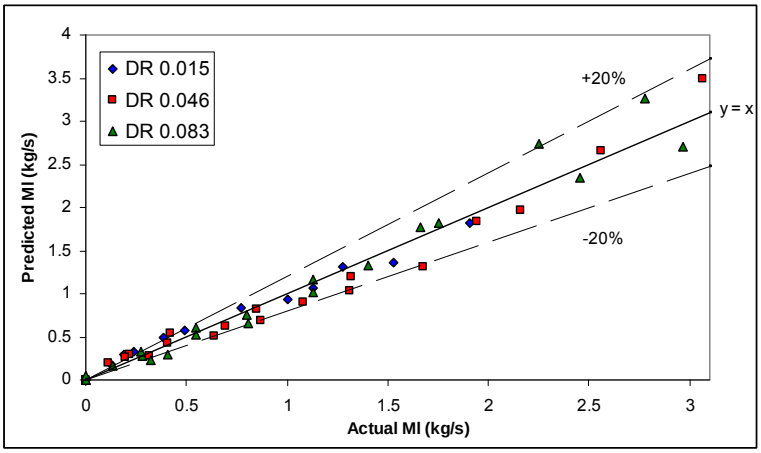

Figure 38. CEESI 2005 4”, 0.75 Beta Ratio V-Cone Meter Liquid Flow rate Prediction Results.

wet gas V-Cone meter would have to be calibrated in the range of conditions it was to be used.

8. A SPECIAL BG GROUP V-CONE METER WET GAS TEST AT K-LAB

In Feburary 2005 McCrometer tested a BG Group 6”, sch 160, 0.75 beta ratio V-Cone meter with wet gas flow at K-Lab. The test matrix was unusual as along with moderate (i.e. typical) flow conditions the meter was to be tested under extreme gas flow rate conditions. Table 3 shows the test matrix.

Nominal Pressure (Bara)	Average Density Ratio	Fr_g range	X_{LM} range
34	0.045	4.3 – 8.8	$0 \leq X_{LM} \leq 0.28$
49	0.060	6.7	$0 \leq X_{LM} \leq 0.26$

Table 3 - Envelope for K-Lab 2005 Wet Gas Flow 6", 0.75 Beta Ratio V-Cone Meter Test.

McCrometer requested K-Lab record the permanent pressure loss as well as the traditional DP. As no such tap existed on the meter body the tap was on the downstream spool and was approximately six pipe diameters downstream of the back face of the cone. Figure 17 indicates both the K-Lab and NEL V-Cone meter set ups (although this 6" meter had the pressure tapping two pipe diameters further downstream than the 4" NEL set up – 6 diameters downstream).

Figure 39 shows the K-Lab dry gas calibration result. The traditional discharge coefficient is in the typical region for a V-Cone meter at approximately 0.8. The linear fit gives a ±0.5% performance. The expansion flow coefficient is in the region of 1.14. The linear fit gives a ±0.6% performance. Here again, the expansion meter concept stated in this authors PhD as applicable to all DP meters is shown to work well for a V-Cone meter. It is notable that the CEESI test with a downstream tapping distance of 2.5D gave an expansion flow coefficient of approximately 1.02, the NEL test with a downstream tapping distance of 4D gave an expansion flow coefficient of approximately 1.1 and the K-Lab test with a downstream tapping distance of 6D gave an expansion flow coefficient of approximately 1.15. The downstream pressure tap location appears to affect the expansion flow coefficient. However, as long as the meter is calibrated to specific pressure tap locations this single phase flow metering system works well.

Figure 40 shows the three V-Cone meter wet gas test matrices on the Shell Flow Pattern Map. This map was based on 4" observations and so the 6" NEL and K-Lab flow pattern predictions have more uncertainty than the 4" CEESI predictions. However, these are all reasonable approximations. The meters tested at NEL and CEESI therefore saw very similar wet gas flow patterns whereas the meter tested at K-Lab had a significantly different flow pattern. Whereas CEESI and NEL had wet gas flow ranges where the flow conditions created stratified flow, a transitioning flow pattern between stratified and annular-mist flow or annular mist flow, at K-Lab the extremely high gas velocities and even lighter condensate hydrocarbon liquid[6] than used by other test facilities meant the flow was likely to be further into the annular-mist flow region. In fact, at these conditions it is expected the liquid could be close to fully atomised meaning the flow tends to homogenous flow. That is, the higher velocity K-Lab wet gas flows could act like pseudo-single phase flow. These flow conditions are at the extreme end of real industrial flow applications.

Figure 41 shows the K-Lab 6", sch 160, 0.75 beta ratio V-Cone traditional meter wet gas data with the released V-Cone meter wet gas correction factor (i.e. equation 12a with equations 15a to 15c) applied for the case of a known liquid mass flow rate. It is of interest to note that the gas to liquid density ratio range is well within the range tested by NEL and CEESI. The lowest gas densiometric Froude number (a relatively high value of 4.37) is just above the values tested at NEL and CEESI. That data set, with minimal extrapolation, is corrected well by the existing correlation. However, the higher gas densiometric Froude number values are poorly predicted by the current V-Cone meter wet gas correction factor. The correction factor considerably "over corrects" the gas flow rate prediction. This is an example of the dangers of extrapolating any correlation. It should be noted that this is not a problem specific to V-Cone meters. All DP meter designs have this problem. Similar trends were shown by Steven et al [20] for the orifice meter

[6] In 2006 [18] this author stated that wet gas flows with kerosene would, for otherwise set flow conditions, have a flow pattern further into the annular mist region than wet gas flows with water, as water is more viscous and has a higher surface tension than kerosene. There is an error in this statement. Kerosene is more viscous than water (but does have a lower surface tension than water). There is limited information on the combined effects of liquid viscosity and surface tension parameters on flow patterns. It is still assumed from limited indirect evidence (e.g. the Baker map or an argument can be based on the findings of Reader Harris et al [19]) that light oil wet gas flows become annular mist flows at lower gas dynamic pressures than water wet gas flows. This suggests that surface tension is more important in determining flow patterns than viscosity. It is assumed that K-Labs condensate has a lower surface tension than NEL or CEESI liquids and therefore K-Lab wet gas flows becomes annular mist at lower gas dynamic pressures.

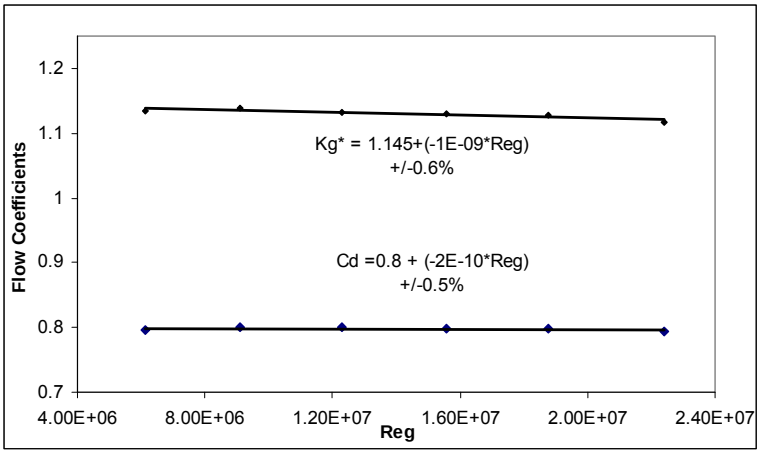

Figure 39. K-Lab 6", 0.75 Beta V-Cone Gas Calibration.

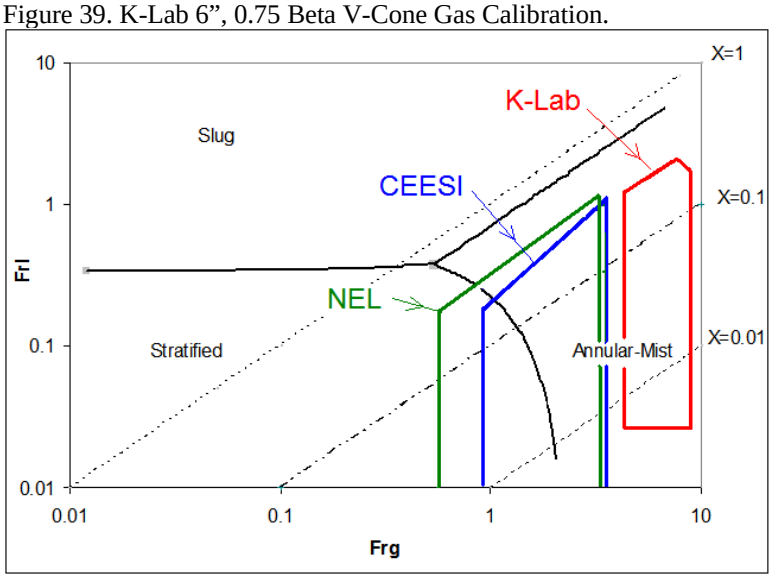

Figure 40. Shell 4" Natural Gas / Light Hydrocarbon Liquid Based Flow Pattern Map.

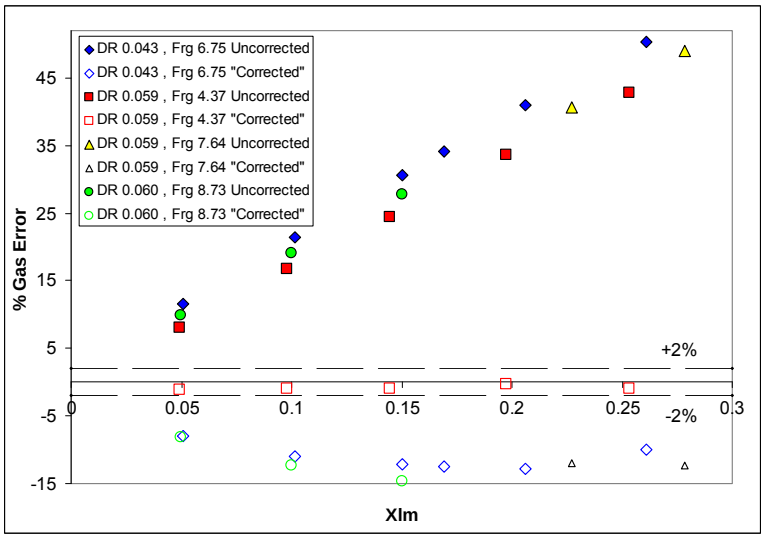

Figure 41. K-Lab 6", 0.75 Beta Ratio V-Cone Meter Uncorrected and Corrected Data.

and the Chisholm equation but the test conditions were not as extreme. Furthermore, this is not a limit of DP meter designs, but rather a limit on the available data sets in which to create the wet gas correlations. In

this case McCrometer set a new (unpublished) correlation for the BG Group that correctly (±3.5%) predicted the gas flow rate across the NEL/ CEESI / K-Lab ranges for known liquid flow rates.

In 2006 this author [18] suggested that when fitting wet gas data from any gas meter to create a wet gas correction factor it is advisable to set an upper boundary condition for extraploation of both gas to liquid density ratio and gas densiometric Foude number to the homogenous model. This data is a good example of why this is appropriate. A DP meters homogenous wet gas correction factor has been shown to be:

$$\dot{m}_g = \frac{\dot{m}_{g_{Apparent}}}{\sqrt{1 + CX_{LM} + X_{LM}^2}} \text{ ---- (20)} \quad \text{where:} \quad C = \left(\frac{\rho_g}{\rho_l}\right)^{\frac{1}{2}} + \left(\frac{\rho_l}{\rho_g}\right)^{\frac{1}{2}} \text{ ---- (21)}$$

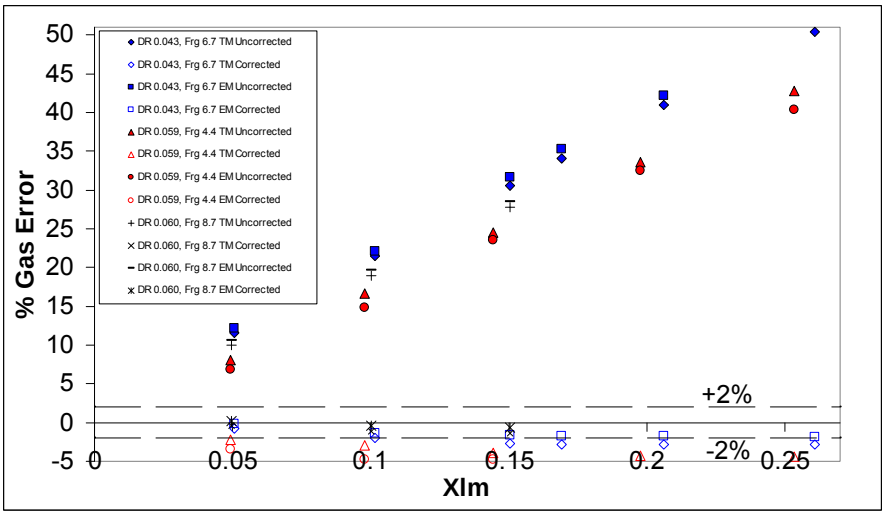

Figure 42. K-Lab 6”, 0.75 Beta Ratio V-Cone TM & EM Meters Data Corrected by Homogenous Model.

Figure 42 shows the K-Lab 6”, 0.75 beta ratio V-Cone traditional ("TM") and expansion ("EM") meter data superimposed on one graph with the homogenous model correction applied to both DP meter types for the case of a known liquid flow rate. One important observation is that there is no significant difference between the two metering methods. This is evidence that the wet gas flow is tending towards the homogenous flow pattern. Here the meters act like single phase flow meters as they are effectively metering a flow of a homogenous mixture. When a wet gas flow is perfectly homogenised any DP meters gas flow rate error would solely be caused by the gas density being applied to the flow rate calculation when the DP read is actually being caused by the flow with the homogenous mixes density. Hence, by theory, all DP meters in this special extreme condition give the same wet gas over-reading. Note that for the 0.059 / 0.06 gas to liquid density cases as the gas densiometric Froude number (i.e. gas flow rate) increases the performance of the homogenous correction model improves as would be expected.

Wet gas flows tending to homogenous flow is a theoretical limit to all DP meter in series wet gas meter techniques. With no difference between different DP meter wet gas over-readings no measurement by difference technique can be utilised. Fortunately, DP meters appear to influence the local flow pattern in such a way that, for any given gas to liquid density ratio, it takes the exceeding of different gas densiometric Froude number values for different DP meter designs to reach the homogenous flow model over-reading prediction. This fact extends the usefulness of the general technique considerably. In extreme pressure and flow rate condition wet gas flow cases where two DP meters in series give the same gas flow rate prediction the flow could be single phase gas or homogenised wet gas flow. With measurement by differrence not possible in this case it is postulated here that in such cases, phase fraction devices may predict the approximate density of the flow and therefore predicting the gas and liquid phase flow rates with a combination of a DP meter and phase fraction device would be at least theoretically possible. However, as yet no such reseach of this kind is known to have been published.

9. CONCLUSIONS

The PhD thesis's claim that the expansion section of any DP meter is a DP meter in its own right, first shown with one Venturi meter data set has now been backed by three V-Cone meter tests. The performance of these expansion meter designs is only slightly inferior to the traditional DP metering method.

When combining the V-Cone traditional and expansion meter wet gas flow data information it is possible, by use of appropriate mathematical analysis, to predict the gas and liquid flow rates. This creates a simple inexpensive wet gas metering system that could operate well across a significant range of industry wet gas flow applications. Currently, like most simple wet gas metering systems, it is necessary to data fit test results across the range of its use as extrapolation of the correlations (e.g. use with different liquid properties, meter diameters, higher gas flow rates, pressures etc.) is not adviseable.

The limitation of this method is the same as for all other DP meters in series wet gas flow meter designs. As the wet gas flow tends to a homogenous mix flow the measurement by difference technique is increasingly difficult as the difference diminishes. There are currently conceptual ideas as yet to be proven on how this limitation can be overcome.

10. ACKNOWLEDGMENTS

The author would like to acknowledge Strathclyde University, NEL and SolartronISA for their support of the PhD research and the ESPRC for their funding of the PhD research. This author would like to acknowledge the support of NEL and the Flow Programme for the wet gas testing of the V-Cone meter. Finally, CEESI would like to thank BG Group for the supply of valuable data.

9. REFERENCES

1. Steven. R., "A Discussion on Wet Gas Flow Parameter Definitions", Energy Institute & CEESI Wet Gas Flow Metering Seminar, Aberdeen, UK, 30th Nov 2006.
2. Medvejev V.F., "Gas and Liquid Flow Rate Measurement in Gas-Liquid Mixture", Journal of Instrumentation and Control System, No. 10, pp 18-20, 1972.
3. Lin. Z.H., "Two-Phase Flow measurement with Orifices", Encyclopedia of Fluid Mechanics, Ch. 29, 1986.
4. Chen Z.H., Chen Z.A.Y, and Xu Y.L. et al., "Two-Parametric Flow Measurement in Gas-Liquid Two-Phase Flow" Proceedings of the 7th Int. Heat Transfer Conference, Sept. 1982.
5. Sekoguchi et al. "Two-Phase Flow Measurement with Orifice-Couples in a Pipeline", Bul. JSME, Vol. 21, No. 162, Dec 1978, pp 1757 – 1761.
6. Nguyen T.V., "Methods for Metering Two-Phase Flow", US Patent No. 4,576,043, Date of Patent, March 18th, 1986.
7. Nguyen T.V., "Methods for Metering Two-Phase Flow", US Patent No. 4,662,219, Date of Patent, May 5th, 1987.
8. Daniel P., Lund J., "Meter for the Measurement of Multiphase Fluids and Wet Gas", US Patent Application Publication US 2004/0011139 A1, Published Jan. 22, 2004.
9. de Leeuw. R, "Liquid Correction of Venturi Meter Readings in Wet Gas Flow", North Sea Flow Measurement Workshop, Norway, Oct 1997.
10. Steven R., "Wet Gas Metering" PhD Thesis, Strathclyde University, Glasgow, UK, 2001.
11. NEL Wet Gas Measurement Training Course Notes – St Andrews, UK, 23rd October 2006.
12. Stewart. D and Steven R. et al., "Wet Gas Metering with V-Cone Meters", North Sea Flow Measurement Workshop 2002, St Andrews, Scotland, UK. Paper No.4.2.
13. Steven, R., "Research Developments in Wet Gas Metering with V-Cone Meters", North Sea Flow Measurement Workshop 2003.
14. Steven R. et al., "Wet Gas Metering with V-Cones", 3rd International South East Asia Hydrocarbon Flow Measurement Workshop, Singapore, 9th-11th March 2004.
15. Steven R. Et al.,"An Update on V-Cone Meter Wet Gas Flow Metering Research", Flomeko, Peebles, UK, June 2005.

16. Toral et al. “Estimating the Liquid Hold-Up in Wet Gas Flow by Analysis of Pressure Fluctuations across a V-Cone”, North Sea Flow Measurement Workshop 2005, Tonsberg, Norway.
17. Wood, I. et al. “Penguin Wet Gas Measurement”, North Sea Flow Measurement Workshop 2003, Tonsberg, Norway
18. Steven, R., “Horizontally Installed Differential Pressure Meter Wet Gas Flow Performance Review”, North Sea Flow Measurement Workshop 2006, St Andrews, Scotland, UK.
19. Reader Harris M., Hodges D., Gibson J., ”Venturi-Tube Performance in Wet Gas: Computation and Experimement”, SE Asia Hydrocarbon Flow Measurement Workshop, Kuala Lumpur, March 2007.
20. Steven R., Ting F., Stobie G.,”A Re-Evaluation of Axioms Regarding Orifice Meter Wet Gas Flow Performance” , SE Asia Hydrocarbon Flow Measurement Workshop, Kuala Lumpur, March 2007.

APPENDIX

It is convention for DP flow meters to use a geometric constriction to create the required momentum change. By applying the mass and energy conservation equations an expression for the flow rate is obtained that is a function of the geometry, fluid density and differential pressure across two points on the constriction. However, a geometric expansion can also be used. This was discussed by Steven [10].

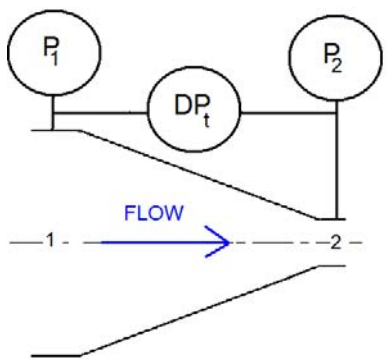

Figure A.1a. Generalised Constriction DP Meter

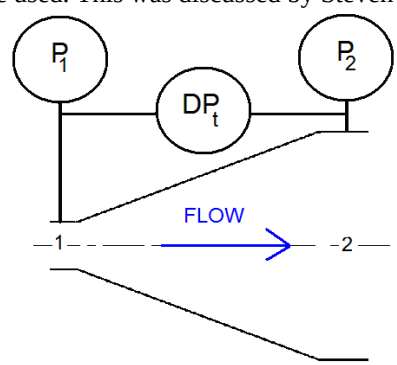

Figure A.1b. Generalised Expansion DP Meter

<u>Derivation of Single Phase Generalized Constriction DP Meter Generic Flow Equation</u>

Consider incompressible, horizontal, reversible flow through a meter of the geometry shown in Figure A.1a. Mass continuity (equation A.1) and energy conservation (equation A.2) gives:

$$\dot{m} = \rho \dot{Q} = \rho A_1 U_1 = \rho A_2 U_2 \quad \text{--- (A.1)} \qquad \text{and} \qquad \frac{P_1}{\rho} + \frac{U_1^2}{2} = \frac{P_2}{\rho} + \frac{U_2^2}{2} \quad \text{--- (A.2)}$$

where $\dot{m}$ is the mass flow rate, $\dot{Q}$ is the volume flow rate A_1 and A_2 are the inlet and outlet areas respectively, P_1 and P_2 are the inlet and outlet pressures respectively, U_1 and U_2 are the inlet and outlet velocities respectively and ρ is the density. Let β be defined by equation A.3 and re-arrange:

$$\beta = \sqrt{\frac{A_2}{A_1}} \text{ -(A.3)}, \quad \frac{P_1 - P_2}{\rho} = \frac{U_2^2 - U_1^2}{2} = \frac{U_2^2}{2}\left(1 - \left(\frac{U_1^2}{U_2^2}\right)\right) = \frac{U_2^2}{2}\left(1 - \left(\frac{A_2}{A_1}\right)^2\right) = \frac{U_2^2}{2}\left(1 - \beta^4\right) \text{-(A.2a)}$$

Let E (the velocity of approach) be defined by equation A.4 and substitute equation A.4 into equation A.2a and re-arrange:

$$E = \frac{1}{\sqrt{1-\beta^4}} \quad \text{--- (A.4)} \qquad , \qquad U_2 = \sqrt{\frac{2(P_1 - P_2)}{\rho(1-\beta^4)}} = E\sqrt{\frac{2(P_1 - P_2)}{\rho}} \quad \text{---- (A.2b)}$$

Substituting equation A.2.b into equation A.1 gives:

$$\dot{m} = \rho A_2 U_2 = E A_2 \sqrt{2\rho(P_1 - P_2)} \quad \text{---- (A.5)}$$

Derivation of Single Phase Generalized Expansion DP Meter Generic Flow Equation

Consider incompressible, horizontal, reversible flow through a meter of the geometry shown in Figure A.1b. Mass continuity (equation A.1) and energy conservation (equation A.2) still hold true. Let $\beta^{'}$ be defined by equation A.3a and re-arrange such that we get:

$$\beta^{'} = \sqrt{\frac{A_1}{A_2}} \text{ -(A.3a) , } \frac{P_2 - P_1}{\rho} = \frac{U_1^2 - U_2^2}{2} = \frac{U_1^2}{2}\left(1 - \left(\frac{U_2^2}{U_1^2}\right)\right) = \frac{U_1^2}{2}\left(1 - \left(\frac{A_1}{A_2}\right)^2\right) = \frac{U_1^2}{2}\left(1 - \beta^{'4}\right) \text{-(A.2c)}$$

Let $E^{'}$ (the velocity of departure) be defined by equation A.4a and substitute this into equation A.2c and re-arrange:

$$E^{'} = \frac{1}{\sqrt{1 - \beta^{'4}}} \text{ ----(A.4a) , } U_1 = \sqrt{\frac{2(P_2 - P_1)}{\rho\left(1 - \beta^{'4}\right)}} = E^{'}\sqrt{\frac{2(P_2 - P_1)}{\rho}} \text{ --- (A.2d)}$$

Substituting equation A.2.d into equation A.1 gives:

$$\dot{m} = \rho A_1 U_1 = E^{'} A_1 \sqrt{2\rho(P_2 - P_1)} \text{ ---- (A.6)}$$

Comparison of the Classic and Expansion Type DP Meter Results

Note equations A.5 and A.6 are mirror images of each other. As this analysis assumed incompressible and reversible flow through Figure A.1a, then the incompressible and reversible flow analysis for the flow through Figure A.1b is precisely the flow through Figure A.1a in reverse. In reality gas flows are compressible and irreversible. As a result the traditional DP meter style has corrections factors. The discharge coefficient is defined by equation A.7. This correction factor takes account of all real world factors that are not accounted for by the theory. With traditional gas DP meters the gas density drops with the pressure and hence the assumption of incompressible flow is not valid. The correction factor is called the expansion factor (denoted by ε in Europe). This is some function f_1 as shown by equation A.8:

$$C_d = \frac{\dot{m}_g}{\dot{m}_{g,theoretical}} = \frac{\dot{m}_g}{EA_2\sqrt{2\rho(P_1 - P_2)}} \text{ --- (A.7) and } \varepsilon = f_1(P_1, \Delta P, \kappa, \beta) \text{ --- (A.8)}$$

where $\dot{m}_g$ is the actual gas mass flow rate, $\dot{m}_{g,theoretical}$ is the value predicted by equation A.5 and κ is the gases isentropic exponent and note $\Delta P = P_1 - P_2$. From theory, for a traditional DP meter C_d <1 and $\varepsilon < 1$. Sometimes these two factors are accounted for by one "flow coefficient" ("K_g"), i.e. the flow coefficient is the product of the discharge coefficient and the expansion factor (and therefore $K_g < 1$). We now have:

$$\dot{m}_g = EA_2\varepsilon C_d\sqrt{2\rho(P_1 - P_2)} = EA_2 K_g\sqrt{2\rho(P_1 - P_2)} \text{ --- (A.5a)}$$

An expansion meter would have the equivalent discharge coefficient to that of the constriction meter (see equation A.9.). The flow expansion slows the flow causing an increase in gas density as the pressure increases. A compression factor ($\varepsilon^{'}$) would account for this phenomenon (see equation A.10).

$$C_d^{'} = \frac{\dot{m}_g}{\dot{m}_{g,theoretical}} = \frac{\dot{m}_g}{E^{'}A_1\sqrt{2\rho(P_2 - P_1)}} \text{ --- (A.9) and } \varepsilon^{'} = f_1\left(P_2, \Delta P^*, \kappa, \beta^{'}\right) \text{ --- (A.10)}$$

Note that here $\dot{m}_{g,theoretical}$ is the value predicted by equation A.6, and $\Delta P^* = P_2 - P_1$. For an expansion DP meter $C_d^{'} > 1$ and $\varepsilon^{'} > 1$. These two factors can be accounted for by one "expansion flow coefficient" (K_g^*).This is the product of the expansion discharge coefficient and the compression factor. Therefore, as

$K_g^* = C_d^{'}\varepsilon^{'}$ and as $C_d^{'} > 1$ and $\varepsilon^{'} > 1$ we get $K_g^* > 1$. When we include the expansion flow coefficient in the derived expansion DP meter gas equation we get:

$$\dot{m}_g = E^{'} A_1 C_d^{'} \varepsilon^{'} \sqrt{2\rho(P_2 - P_1)} = E^{'} A_1 K_g^* \sqrt{2\rho(P_2 - P_1)} \text{ ---- (A.11)}$$

Traditional DP Meters and the Downstream Expanding Flow

It was pointed out by Steven [10] that traditional DP meters expand the flow back to the pipe area. That is once the minimum area has passed (i.e. the vicinity where the low pressure is read) the flow expands back to the cross sectional area of the pipe as it flows downstream. Hence, from the minimum area point to the recovered pressure point there is in effect, a second DP meter imbedded within the body of the any traditional DP meter. That is, any DP meter is a constriction and expansion DP meter in series. For example Figure 6 shows a sketch of a Venturi meter. For traditional and expansion DP meters in series made from one meter body such as a Venturi meter we have $\beta = \beta^{'}$ and $E = E^{'}$ and the two flow equations are:

$$\dot{m} = EA_t K_g \sqrt{2\rho\Delta P_t} = EA_t K_g^* \sqrt{2\rho\Delta P_r} \text{ --- (A.12)}$$

where is $\Delta P_t = P_1 - P_t \equiv \Delta P = P_1 - P_2$ and $\Delta P_r = P_d - P_t \equiv \Delta P^* = P_2 - P_1$

Also note that the density of the downstream meter will be slightly different than the upstream meter due to pressure differences. However, with the exception of extremely high velocity gas flow this is a small difference.

In 2001, Steven [10] (in Chapter 7, section 2 of the PhD Thesis) stated that "…the same principles apply for metering with a DP Meter whether the pressure differential is produced by a constriction or expansion in the flow area." In other words, this statement is saying the above derivation is applicable to all DP meters. It therefore, is applicable to V-Cone meters.

PRESSURE AND TEMPERATURE EFFECTS FOR ORMEN LANGE ULTRASONIC GAS FLOW METERS

Per Lunde[1,2], Kjell-Eivind Frøysa[1] and Trond Folkestad[3]

[1)] Christian Michelsen Research AS (CMR), P.O.Box 6031 Postterminalen, N-5892 Bergen, Norway.
[2)] University of Bergen, Department of Physics and Technology, Allégaten 55, N-5007 Bergen, Norway.
[3)] StatoilHydro ASA, Sandsliveien 90, P.O.Box 7190, N-5020 Bergen, Norway.

ABSTRACT

Ultrasonic gas flow meters (USMs) may be influenced by pressure and temperature in several ways. Change of the meter body's cross-sectional area (the "pipe bore") influences directly on the amount of gas flowing through the meter. Change of the ultrasonic path geometry (i.e. change of the inclination angles and lateral chord positions, caused by e.g. meter body diameter change and change of the orientation of the ultrasonic transducer ports) influences on the transit times and the numerical integration method of the meter. Change of the Reynolds number influences on the integration method. Change of the length of the ultrasonic transducer ports influences on the acoustic path lengths, and thus on the transit times. Likewise, change of the length of the ultrasonic transducers influences on the acoustic path lengths, and thus on the transit times. In addition, changes of the transducer properties such as the directivity, influences on the diffraction correction, and thus on the transit times.

Some of these issues are addressed to some extent in current draft standards for such meters, such as the AGA-9 (1998) report, and the ISO/CD 17089-1 (August 2007). Other of these effects have not been described or treated in the literature.

In the present paper, pressure and temperature effects have been investigated for 18" Elster-Instromet Q-Sonic 5 ultrasonic flow meters (USMs) to be operated in the Ormen Lange fiscal metering system at Nyhamna in Møre and Romsdal, Norway, from October 2007. Pressure and temperature changes from flow calibration (Westerbork, at 63 barg and 7 ^{o}C) to field operation (Ormen Lange, nominally at 230 barg and 40 ^{o}C) conditions are evaluated. The effects addressed are changes related to (a) the meter's cross-sectional area, (b) the ultrasonic path geometry (inclination angles and lateral chord positions), (c) length expansion of the ultrasonic transducer ports, (d) length expansion/compression of the ultrasonic transducers, and (e) Reynolds number correction.

The various effects (a)-(e) contributing to the measurement error are discussed and quantified. Investigations are made using a combination of analytical modeling and finite element numerical modeling of the meter body and the ultrasonic transducers, combined with a model for USM numerical integration relevant for the Q-Sonic 5 multipath ultrasonic flow meter in question.

It is shown that for the Ormen Lange application, investigation and evaluation of all of the factors (a)-(e) mentioned above have been necessary to evaluate the effect of pressure and temperature on the meter. Expressions for pressure and temperature effects on ultrasonic flow meters proposed in ISO/CD 17089-1 do not appear to be preferred for the Ormen Lange fiscal metering system.

The study shows that pressure and temperature affects the Q-Sonic 5 by about 0.26 % in the Ormen Lange application. If this systematic measurement error is not corrected for, the Q-Sonic 5 will underestimate the volumetric flow rate by the same amount. Significant economic values are involved.

Two correction factors are thus proposed for the Q-Sonic 5 in this application: (1) one "nominal P&T correction factor" (accounting for by far the largest part of the correction, about 0.26 %), and (2) an "instantaneous P&T correction factor" (accounting for small deviations in pressure and temperature from nominal to actual Ormen Lange conditions), which is typically an order of magnitude smaller than the nominal P&T correction factor. The correction factors and the individual contributors to these are discussed and quantified.

1. INTRODUCTION

From October 2007 five 18" Elster-Instromet Q-Sonic ultrasonic gas flow meters will be operated at a land based fiscal gas metering station at Nyhamna, Møre and Romsdal, Norway, for export of

gas through the 1200 km Langeled pipeline, to an import metering station in Easington, UK, built by Statoil, cf. Fig.1. The Ormen Lange export station at Nyhamna was constructed and built by Norsk Hydro, and will be operated by Shell. The production life of Ormen Lange is estimated to 50 years.

The nominal flow rate of the Ormen Lange export metering station is 70 million Sm^3/day, or 25 billion Sm^3/year. At an assumed sales price of 2 NOK/Sm^3 this corresponds tentatively to 140 million NOK/day, or 50 billion NOK/year. An assumed systematic measurement error of only 0.3 % (as an example), would correspond to about 420 000 NOK/day, or about 153 million NOK/year, for such a tentative sales price.

Flow calibration of the flow meters have been made at the Westerbork laboratory in the Netherlands, at temperature and pressure conditions of 7 ^{o}C og 63 barg, respectively, with two meters in series installed in a "long pipe", and with flow conditioner upstream of the meters.

The high pressures in question at the Ormen Lange metering station, 230 barg nominal, have raised the question whether correction for pressure and temperature effects on the ultrasonic meters will be needed, relative to the 63 barg pressure used under flow calibration at Westerbork.

Pressure and temperature effects on the ultrasonic meters relates to factors such as e.g[1].

- Change of the meter's cross-sectional area,
- Change of the ultrasonic path geometry (inclination angles and lateral chord positions),
- Change of the length of the ultrasonic transducer ports,
- Change of the length of the ultrasonic transducers,
- Change of the Reynolds number.

The influence of these factors are addressed here, on basis of the results given in [1].

2. SPECIFICATIONS

The Ormen Lange metering station consists of 3 parallel meter runs, with in total 5 ultrasonic flow meters, cf. Fig. 1:

- 2 parallel runs, each with two 18" ultrasonic flow meters in series,
- 1 parallel run with one 18" ultrasonic flow meter, for backup measurement,
- Flow conditioner will be used (DN450 Laws type 316SS or Duplex Material),
- Elster-Instromet Q-Sonic 5 ultrasonic gas flow meters [2].

Table 1 gives various parameters of the USM, and Table 2 other specifications for the study.

---

[1] In general, the properties of an ultrasonic flow meter will also depend on the pressure and temperature properties of the ultrasonic transducers used in the meter that is, the electrical and acoustical properties of the transducers, which for a large part determine the signal form, etc.). These are factors which relate to the time detection of the meter (the signal processing). There is no evaluation of *such* factors in the present study, since these types of effects – if the transducers function as they should – are not considered to be very significant (several decades smaller than the other effects) in a 18" meter with reflecting paths. (However, if pressure and temperature cause effects such as period error, transducer error or defect, etc., that would of course be serious and significant.) Pressure test certificates for the K10 transducers used in Q-Sonic 5 given in [19] show that the transducers have survived pressure testing to 620 bar, in water at room temperature.

Table 1. Specifications of the ultrasonic flow meters used in the Ormen Lange metering station.

Parameter	Property	Conditions
Material type	Steel (Duplex)	
Length	1800 mm	(at assumed 20 ^{o}C, 1 atm.)
Outer diameter, *OD*	457.2 mm	(at assumed 20 ^{o}C, 1 atm.)
Inner diameter, *ID*	(366.5 ± 0.25) mm	(at assumed 20 ^{o}C, 1 atm.)
Inner radius, R_0	183.25 mm	(at assumed 20 ^{o}C, 1 atm.)
Wall thickness, *w*	45.35 mm	(at assumed 20 ^{o}C, 1 atm.)
w/R_0	0.25	(at assumed 20 ^{o}C, 1 atm.)
Young's modulus, *Y*	$2.0 \cdot 10^5$ MPa	
Poisson's ratio, σ	0.3	
Coeff. of linear thermal expansion, α	$12.6 \cdot 10^{-6}$ K^{-1} (ASME)	

Table 2. Specifications for the study.

Parameter	Westerbork flow calibration conditions	Ormen Lange metering station (line conditions, nominal)
Gas	Dry natural gas	Dried natural gas[a)]
Pressurel *P*	63 barg	230 barg (design)
Temperature	7 ^{o}C	40 ^{o}C (design)
Viscosity	$1.30 \cdot 10^{-5}$ Pa-s	$2.28 \cdot 10^{-5}$ Pa-s
Density	57.36 kg/m^3	186.6 kg/m^3
Metering configuration	2 USMs in series, with upstream flow conditioner	2 USMs in series, with upstream flow conditioner
Flow velocity	1.5 – 19 m/s	Volumetric flow rate 70 MSm^3/d (=> flow velocity = 15-16 m/s per run)
Reynolds number, *Re*	$2.4 \cdot 10^6$ – $3.0 \cdot 10^7$	$4.5 \cdot 10^7$

[a)] The gas composition is known, but has not been necessary to specify for the present study.

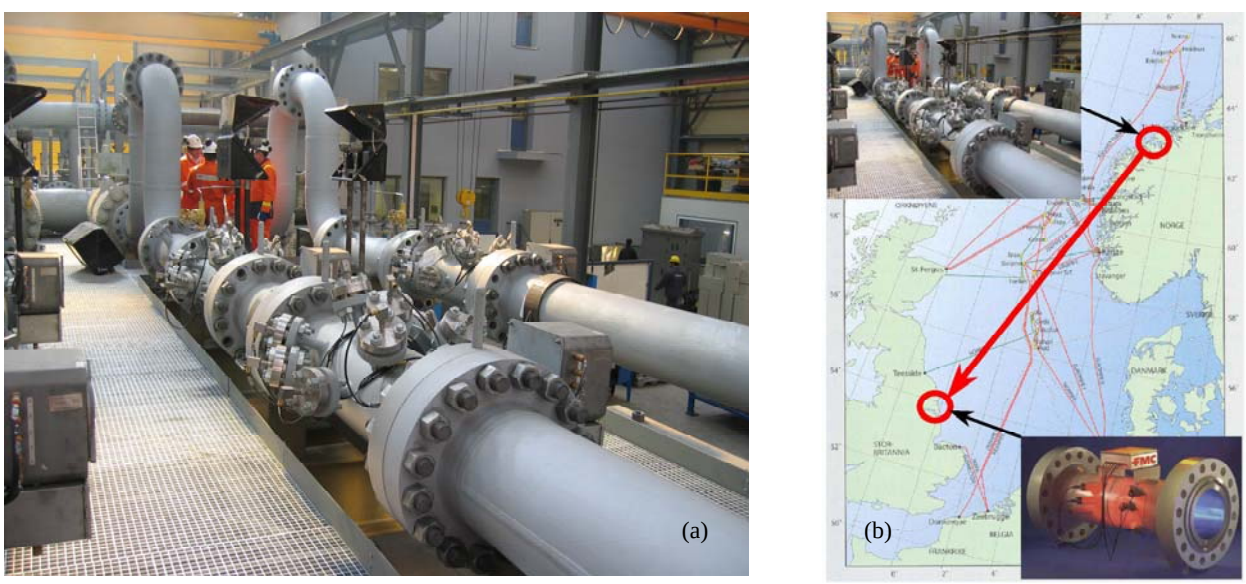

Fig. 1. *(a) Photograph of the Ormen Lange fiscal gas metering station, under factory acceptance test (FAT) in Athens, Greece, 2005.*
(b) Sketch of the Ormen Lange transport system, with fiscal metering stations at Nyhamna (Norway) and Easington (UK).

3. MULTIPATH ULTRASONIC GAS FLOW METERS

3.1 USM functional relationship

In ultrasonic transit time flow meters with reflecting and/or non-reflecting paths, the volumetric flow rate (at line conditions) is given as [3-5]

$$q_{USM} = \pi R^2 \bar{v}_A , \qquad \bar{v}_A = \sum_{i=1}^{N} w_i \bar{v}_i , \qquad \bar{v}_i = (N_{refl,i} + 1) \frac{2\sqrt{R^2 - y_i^2}\,(t_{1i} - t_{2i})}{t_{1i} t_{2i} \left| \sin 2\phi_i \right|} , \qquad (1)$$

where (cf. Fig. 2), R is the inner radius of the USM meter body; $\bar{v}_A$ is the axial volume flow velocity (at line conditions); N *is* the number of acoustic paths; i is the path number; w_i is the integration weight factor for path no. i; $\bar{v}_i$ is the average axial flow velocity along path no. i (i.e. the line integral along the path); y_i is the lateral distance from the pipe center (lateral chord position) for path no. i; L_i is the interrogation length for path no. i; ϕ_i is the inclination angle (relative to the pipe axis) of path no. i; t_{1i} and t_{2i} are the measured transit times for upstream and downstream sound propagation of path no. i; and $N_{refl,i}$ is the number of wall reflections for path no. i ($N_{refl,i}$ = 0, 1 or 2 in current USMs), i = 1, …, N.

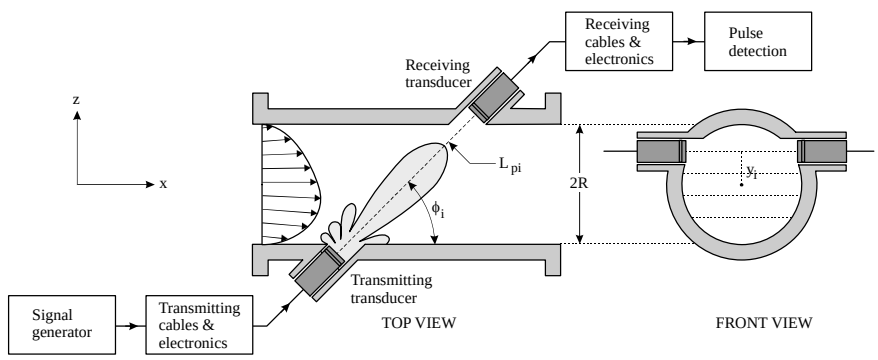

Fig. 2. Schematic illustration of a single path in a multipath ultrasonic transit time flow meter with non-reflecting paths (for downstream sound propagation). (Left: centre path example (y_i = 0); Right: path at lateral chord position y_i.)

3.2 Pressure and temperature influences on USMs

Ultrasonic gas flow meters may be influenced by pressure and temperature in several ways, cf. Table 3. Change of the meter body's cross-sectional area (the "pipe bore") influences directly on the amount of gas flowing through the meter. Change of the ultrasonic path geometry (i.e. change of the inclination angles and lateral chord positions, caused by e.g. meter body diameter change and change of the orientation of the ultrasonic transducer ports) influences on the transit times and the numerical integration method of the meter. Change of the Reynolds number influences on the integration method. Change of the length of the ultrasonic transducer ports influences on the acoustic path lengths, and thus on the transit times. Likewise, change of the length of the ultrasonic transducers influences on the acoustic path lengths, and thus on the transit times.

Table 3. Direct and indirect pressure and temperature influences on USMs.

	Direct P&T effect	Indirect P&T effect
A	Change of the meter body cross-sectional area	Affects amount of gas flowing through the flow meter
B	Change of the ultrasonic path geometry (changed inclination angles and lateral chord positions, caused by diameter change & changed transducer port orientation)	Affects acoustic path lengths and thus transit times. Influences on the numerical integration method.
C	Change of the length of the ultrasonic transducer ports	Affects acoustic path lengths and thus transit times.
D	Change of the length of the ultrasonic transducers	Affects acoustic path lengths and thus transit times.
E	Change of the Reynolds number	Influences on the numerical integration method.

3.3 Elster-Instromet Q-Sonic 5

The Q-Sonic 5 ultrasonic meter employs 5 acoustic paths. Three of these paths are single reflection paths. These paths are denoted path 1, 3 and 5, cf. Fig. 3. These paths are centre paths. This means that in the side view of Fig. 3, these 3 paths are represented by the three straight lines going through the centre of the pipe (y_i = 0). The inclination angle of these paths is typically 70° for the meters in question at Ormen Lange.

The two remaining paths are double reflecting paths. These paths are denoted path 2 and 4, cf. Fig. 3. These paths propagate at a lateral distance, y_i, of 0.5·R. In the side view of Fig. 3b, each of these paths is represented as a triangle. The inclination angle of these paths is typically 60° for the meters in question at Ormen Lange.

(a)

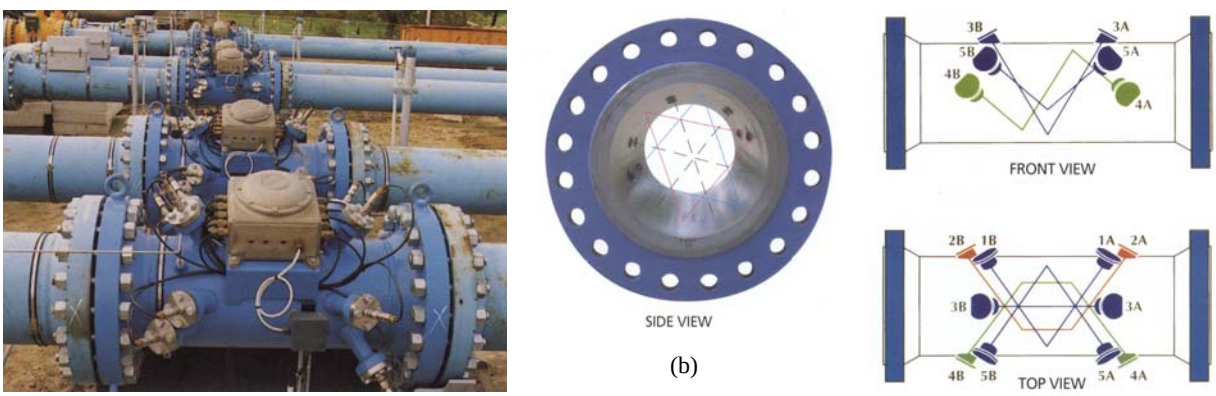

(b) (c)

Fig. 3. Meter body and path geometry of the Elster-Instromet Q-Sonic 5 ultrasonic gas flow meter (after [2].)

In the present work, pressure and temperature effects for each of the five acoustic paths are first analyzed individually. Thereafter, values for the pressure and temperature effect on the volumetric flow rate are found through integration over the five acoustic paths, using the integration weight factors, w_i, i = 1, …, 5, cf. Eq. (1) and e.g. [22]. The integration weights of the Q-Sonic 5 have not been available for the present study. A tentative set of integration weight factors, w_i, i = 1, …, 5, has thus been worked out for the Q-Sonic 5. This gives one integration weight factor for each of the three single-bouncing paths (centre paths), and a second one for each of the two double-bouncing paths (swirl paths). This set is the best estimate that has been possible to obtain for the present work, and has been used in the analysis presented here [1].

4. PRESSURE AND TEMPERATURE INFLUENCES ON THE METER CROSS-SECTIONAL AREA AND ULTRASONIC PATH GEOMETRY

The present section addresses changes in the USM's cross-sectional area (diameter) and ultrasonic path geometry (inclination angles and lateral chord positions) caused by changes in pressure and temperature, and the consequences of such changes for the measurement accuracy. In particular, this relates to

(a) changes in the Q-Sonic 5 ultrasonic meter's cross-sectional area and its path geometry, from factory ("dry calibration") to Westerbork (flow calibration) conditions,
(b) changes in the Q-Sonic 5 cross-sectional area and its path geometry, from Westerbork (flow calibration) to Ormen Lange (operating) conditions,
(c) the effect of these changes on the Q-Sonic 5 measurement uncertainty at Ormen Lange (operating) conditions.

In Section 4.1, simplified analytical models for pressure and temperature expansion / contraction are discussed and used for describing (a) - (c). In Section 4.2, finite element numerical modelling (FEM) is used, as a more accurate approach. Calculation results are given in Section 4.3.

4.1 Simplified analysis

Analytical models generally represent simplified descriptions of pressure and temperature effects on USM cross-sectional area and ultrasonic path geometry, both with respect to meter geometry and validity ranges, but may be useful for certain purposes, depending on their accuracy. Various models used in the literature and international standards to correct for pressure and temperature expansion of USMs are discussed.

4.1.1 Analytical Model A

At a temperature T and pressure P, the meter body radius (R), the lateral chord positions (y_i), and the inclination angles (ϕ_i), can be shown to be approximately given by [5,1]

$$R \approx K_T K_P R_0 , \quad y_i \approx K_T K_P y_{i0} , \quad \phi_i \approx \tan^{-1}\left(\frac{\tan(\phi_{i0})}{1-(1-\beta^*/\beta)(K_P-1)} \right), \quad i = 1, \ldots, N \tag{2}$$

where subscript "*0*" is used to denote the respective geometrical quantity at "dry calibration" conditions, i.e. R_0, y_{i0} and ϕ_{i0}. The correction factors for the inner radius of the meter body due to dimensional changes caused by temperature and pressure changes relative to "dry calibration" conditions, are given as (cf. e.g. [6,7,8,10])

$$K_T \equiv 1 + \alpha \Delta T_{dry} , \qquad \Delta T_{dry} \equiv T - T_{dry} , \tag{3}$$

$$K_P \equiv 1 + \beta \Delta P_{dry} , \qquad \Delta P_{dry} \equiv P - P_{dry} , \tag{4}$$

respectively, where P_{dry} and T_{dry} are the pressure and temperature at "dry calibration" conditions, e.g. P_{dry} = 1 atm. and T_{dry} = 20 ^{o}C. α is the coefficient of linear thermal expansion of the meter body material. β and β^* are the *radial* and *axial* linear pressure expansion coefficients for the

meter body, respectively (cf. Section 4.1.3). K_P and K_T are here referred to as the *radial* pressure and temperature correction factors for the USM meter body, respectively[2]. Eqs. (2)-(4) are referred to as the "analytical model A", and applies to all inclination angles.

4.1.2 Analytical Model B

For USMs where all inclination angles are equal to ±45°, i.e, $\phi_{i0} = \pm 45^o$, $i = 1, \ldots, N$, q_{USM} can - from Eqs. (1)-(4) - be written as [5,1]

$$q_{USM} \approx q_{USM,0} \cdot C_{tsm} \cdot C_{psm} \quad , \tag{5}$$

where

$$C_{tsm} = K_T^3 = (1+\alpha\Delta T_{dry})^3 \approx 1+3\alpha\Delta T_{dry}\,, \quad C_{psm} = K_P^3 = (1+\beta\Delta P_{dry})^3 \approx 1+3\beta\Delta P_{dry}\,, \tag{6}$$

are the *volumetric* thermal and pressure correction factors of the USM meter body[3], and $q_{USM,0}$ is given by Eqs. (1)-(2), with the "dry calibration" quantities R_0, y_{i0}, L_{i0}, x_{i0} and ϕ_{i0} inserted instead of the quantities R, y_i, L_i, x_i and ϕ_i, $i = 1, \ldots, N$. Eqs. (5)-(6) are referred to as the "analytical model B".

For USMs with inclination angles equal to ±45°, thus, the analytical model B is equivalent to the analytical model A. For other inclination angles it represents an approximation to the more accurate analytical model A [5]. This is the case for Q-Sonic 5, which employ inclination angles of 60° and 70°. Eq. (D.28) in [5] gives the relative error by using this approximation. It turns out that for moderate pressure deviations ΔP_{dry} (a few tens of bars), the errors made by using analytical model B may be neglected, and that this model may be used for inclination angles in the range of relevance for current USMs, 40° to 60°. However, for larger pressure deviations, and especially for inclination angles approaching 60°, the error introduced by using Eqs. (5)-(6) increases.

The main advantage of analytical model B over A lays in the fact that in model B, the P and T corrections of the geometrical quantities of the meter body can be separated from the basic USM functional relationship and put outside of the summing over paths, as illustrated by Eq. (6). Consequently, since the analytical model A is not easily applicable for use in the "instantaneous correction factor" to be implemented at the flow computer level, Eqs. (5)-(6) is the model proposed for the "instantaneous correction factor" described in Section 7.2, used for relatively small pressure changes only (a few bar).

4.1.3 Coefficients of linear pressure expansion

The radial and axial linear pressure expansion coefficients β and β^* involved in the analytical models A and B depend on the type of support provided for the meter body installation (i.e. the

---

[2] The *radial* pressure and temperature correction factors for the USM meter body, K_P and K_T, should not be confused with the corresponding *volumetric* pressure and temperature correction factors of the meter body, C_{psm} and C_{tsm}, cf. e.g. Eqs. (6).

[3] For the correction factor of the *meter body*, a notation is used according to "common" flow metering terminology, where subsripts *t*, *p*, *s* and *m* refer to "temperature", "pressure", "steel" and "meter", respectively, cf. e.g. [6-8].

model used for the meter body pressure expansion / contraction). For thin-walled cylindrical and isotropic elastic meter bodys, β and β^* are related by [1]

$$\frac{\beta^*}{\beta} \approx \begin{cases} -\sigma = -0.3 & \text{for the cylindrical pipe section model (ends free),} \\ 0 & \text{for the infinite-length cylindrical pipe model (ends clamped),} \\ \dfrac{1-2\sigma}{2-\sigma} = 0.235 & \text{for the cylindrical tank model (ends capped),} \end{cases} \tag{7}$$

where the values given for β^* / β apply to steel ($\sigma = 0.3$).

With respect to K_T and K_P, there seems to be general agreement in the literature that temperature and pressure expansion/contraction can be described by expressions such as Eqs. (3)-(4). However, there is widely varied practice with respect to which model is used for the coefficient of linear radial pressure expansion, β. Table 4 gives different models in use for β, and a discussion of these is given in [1]. Note that all models in use represent simplifications.

Table 4. Models used by USM manufacturers, standards, etc. for linear pressure expansion of the inner radius of the USM meter body (isotropic material assumed), under uniform internal pressure.

Reference / USM manufacturer	**Models for the coefficient of linear radial pressure expansion, β**	**USM meter body assumptions**
AGA-9 (1998) [10], Roark (2001), p. 592 [11]	$\beta = \frac{R_0}{wY}$	• Cylindrical pipe section model (ends free) • Thin wall, $w < R_0/10$
Daniel Industries (2001) [20,5]	$\beta = \frac{1}{Y}\frac{1.3(R_0+w)^2 + 0.4R_0^{\,2}}{(R_0+w)^2 - R_0^{\,2}}$ ($\beta \approx 0.85\frac{R_0}{wY}$ for $w << R_0$)	• Cylindrical tank model (pipe with ends capped) • Thick wall • Steel material ($\sigma = 0.3$)
FMC Technologies (2001) [21], [5], Roark (2001), p. 593 [11]	$\beta = \frac{R_0}{wY}\left(1 - \frac{\sigma}{2}\right)$ ($\beta = 0.85\frac{R_0}{wY}$ for $\sigma = 0.3$ (steel))	• Cylindrical tank model (pipe with ends capped) • Thin wall, $w < R_0/10$
Instromet (2001) [12], [5]	No P or T correction used. Pressure expansion analysis based on: $\beta = 0.5\frac{R_0}{wY}$	• Infinitely long pipe model (ends clamped, no axial displacement) • Radial expansion taken to be = 0.5 · radial expansion for ends-free model • Thin wall, $w < R_0/10$
ISO/CD 17089-1 (2007) [3]	$\beta = \frac{1}{3}\frac{3D_0}{4wY} = 0.5\frac{R_0}{wY}$	• Flanged-in meter body • Thin wall, $w < R_0/10$ (?)
ISO/CD 17089-1 (2007) [3]	$\beta = \frac{1}{3}\frac{7D_0}{4wY} = \frac{7}{6}\frac{R_0}{wY} = 1.17\frac{R_0}{wY}$	• Welded-in meter body • Thin wall, $w < R_0/10$ (?)

The "cylindrical pipe section model (ends free)" [11] (1st row of Table 4) applies to a finite-length pipe section with free ends and does not account for flanges, bends, etc. It is considered to be relevant for thin-walled meter bodies mounted in pipe sections where ends can move relatively freely (note that according to the FEM analysis of Section 4.2, axial displacements are in the sub-mm range), e.g. with U-bend as part of the pipe section. Calculations using this model are confirmed relatively well by the FEM calculations described in Section 4.2 (which do account for flanged meter bodies), cf. Section 4.3. For the Ormen Lange metering station, this model for β is

considered to be the most relevant of the analytical models given in Table 4, and consequently used here (cf. Section 7.2).

The two expressions proposed in ISO/CD 17089-1 [3], given in the latter two rows of Table 4, and claimed to cover "flanged-in meter body" (5th row) and "welded-in meter body" (6th row), respectively, give 50 % smaller and 17 % higher radial displacement than the ends-free model (1st row). These models are not found to be very relevant for use in correction factors for the Ormen Lange fiscal metering station, basically for two reasons: (a) no documentation or references for the β expressions has been given in ISO/CD 17089-1 (i.e. no traceability), and (b) the expressions given in ISO/CD 17089-1 are not confirmed by the FEM calculations, cf. Section 4.3.

4.2 Finite element modelling (FEM) analysis

The analytical models A and B described in Section 4.1 represent simplified descriptions, accounting for "average" effects only, and are in general not able to account very precisely for the effects of P&T on the meter body. To analyze such effects in more detail and more accurately (including effects of flange thickness, wall thickness, the resulting form of the meter body (e.g. pipe bulging), influence of the transducer ports and their location, displacement of the transducer ports, precise calculation of the ultrasonic path lengths, etc.), a numerical finite element model (FEM) is needed.

Thus, as a second and considerably more accurate step to analyze pressure and temperature effects on the Q-Sonic 5 ultrasonic meter, a FEM approach was used. The finite element mesh used for FEM calculations of the Q-Sonic 5 meter body is shown in Fig. 4a. Dimensional changes caused by temperature and pressure changes, at any position of the meter body, are calculated using FEM. Details are given in [1].

With respect to boundary conditions, the model of the meter body is fixed as follows, cf. Fig. 4:

- In vertical direction (x-direction) in two points corresponding to bolts in 3 o'clock and 9 o'clock positions.
- In axial direction (y-direction) in the bolt's circle diameter.
- In transveral direction (z-direction) in one point corresponding to a bolt in 6 o'clock position.

This means that the centre of the pipe in principle does not move in vertical and transversal direction, and that no constraint loads will appear.

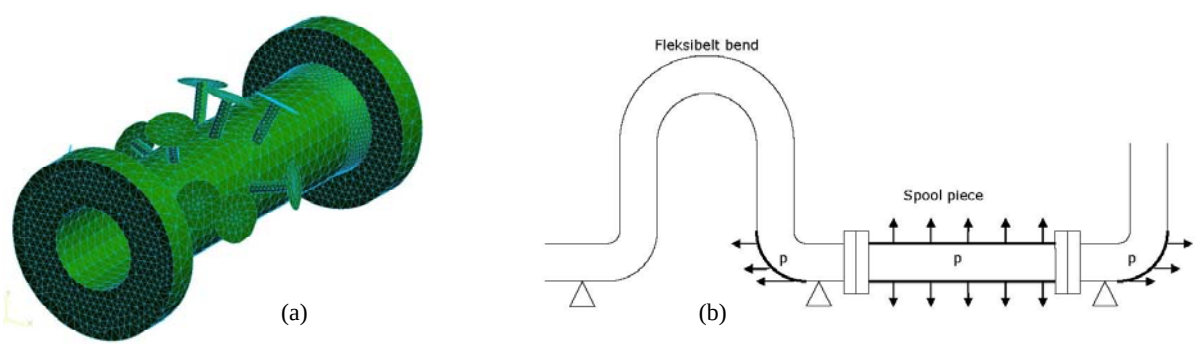

Fig. 4. (a) Finite element grid used for FEM analysis of P & T effects on the meter body (spoolpiece) of the Q-Sonic 5 ultrasonic gas flow meter. (b) Sketch of pipe section accounted for in the FEM analysis.

Due to the U-bend and the header at the opposite side of the USM in the Ormen Lange metering station (cf. Fig.1), it is assumed that the meter body can expand freely in the axial direction (as for the ends-free analytical model for β chosen in Section 4.1.3) (note that axial displacements are in the sub-mm range). Flanges and the 10 transducer mounting ports of the Q-Sonic 5 meter body are all accounted for, as well as axial forces on the meter body flanges caused by the associated 18" pipe section in which the Q-Sonic 5 is mounted, cf. Fig. 4 [1]. The material data used for the calculations are given in Section 2.

The FEM calculations give the change of position for every point of the meter body. Thus, the change of diameter in the horizontal and vertical directions and changes with respect to the transducer ports (i.e. inclination angles and directional orientation of the port (rotation, etc.)), are calculated. This includes the rotation around the vertical, axial and transversal axes, of the back plane of the transducer ports.

The results of the FEM calculations are used as input data to calculation of the pressure and temperature effects on the individual acoustic paths, and the pressure and temperature effects on the USM volumetric flow rate measurement, through integration over the 5 acoustic paths of the USM, using the tentative Q-Sonic 5 weight factors discussed in Section 3.3 [1].

4.3 Calculation results

First, consider the accuracy of the different models for radial linear pressure expansion coefficient β given in Table 4. Table 5 provides a comparison of 4 of the different β models given in Table 4, compared to the results of the FEM analysis[4]. It appears from the pressure effect results given in the table that the cylindrical pipe section model (ends free) (1st row of Table 4) gives the best approximation to the FEM results. A relatively good agreement is found between the FEM calculations and this β model, for both cases. The flanged-in and welded-in models proposed in ISO/CD 17089-1 [3] represent another type of correction than found to be recommended here, and is not used for the Ormen Lange fiscal metering station,

Table 5. Calculated change in USM meter body radius, ΔR [mm], due to pressure and temperature expansion/contraction, for 4 different models for β given in Table 4, compared to the results of the FEM analysis. Two cases are considered: (a) "dry calibration" to flow calibration (Westerbork) conditions, and (b) flow calibration (Westerbork) to operating (Ormen Lange) conditions.

	Flow calibration (Westerbork) 7 °C, 63 barg			**Operation (Ormen Lange) 40 °C, 230 barg**		
	Temperature effect ΔT = -13 °C ΔP = 0 bar	Pressure effect ΔT = 0 °C ΔP = 63 bar	**P & T effect ΔT = -13 °C ΔP = 63 bar**	Temperature effect ΔT = 33 °C ΔP = 0 bar	Pressure effect ΔT = 0 °C ΔP = 167 bar	**P & T effect ΔT = 33 °C ΔP = 167 bar**
Cylindrical pipe section β model (ends free) [AGA-9, 1998] [Roark, 2001, p.592]	-0.03002	**0.02332**	-0.00670	0.07619	**0.06183**	0.13804
Cylindrical tank β model (ends capped) [Roark, 2001, p.593]	-0.03002	**0.01983**	-0.01019	0.07619	**0.05255**	0.12877
Flanged-in meter body β model [ISO 17089]	-0.03002	**0.01166**	-0.01836	0.07619	**0.03091**	0.10711
Welded-in meter body β model [ISO 17089]	-0.03002	**0.02729**	-0.00273	0.07619	**0.07234**	0.14856
FEM	-0.03002	**0.02388**	-0.00614	0.07665	**0.06329**	0.13994

4 In the FEM analysis of pressure effects, the calculated diameter change is different in the vertical and horizontal directions, due to the asymmetric distribution of the transducer ports (all located at the upper half of the meter body, cf. Fig. 4a). In the FEM results of Table 5, the vertical and horizontal diameter changes have been averaged.

Next, consider the error in the volumetric flow rate as measured by the USM caused by pressure and temperature effects on the meter diameter and the ultrasonic path geometry.

For the change from flow calibration (Westerbork) to field operation (Ormen Lange) conditions, there is a significant systematic shift in the volumetric flow rate due to pressure and temperature effects, ranging approximately from about 0.24 (double reflecting paths) to about 0.27 % (single reflection paths) for the various acoustic paths [1]. Integrated over the 5 acoustic paths the effect is calculated to 0.2457 %, cf. Fig. 5. It is also seen from Fig. 5 that the effect of the pressure effect isolated is calculated to 0.1208 % and the temperature effect isolated is calculated to 0.1247 %, which act in the same direction since both the temperature and the pressure increases from Westerbork to Ormen Lange conditions. If not corrected for, the Q-Sonic 5 will thus underestimate the volumetric flow rate.

For the analytical model approaches, the corresponding results become 0.250 % for the analytical model A (0.125 % both for temperature and pressure effects isolated), and 0.226 % for the more simplified analytical model B, valid at inclination angles of 45° (0.10 % for the pressure effect isolated and 0.126 % for the temperature effect isolated) [1]. The difference between the results from the analytical model A and the FEM results are therefore only 0.0043 %, and the difference between the FEM results and the results from the simplified analytical model B is 0.0207 %.

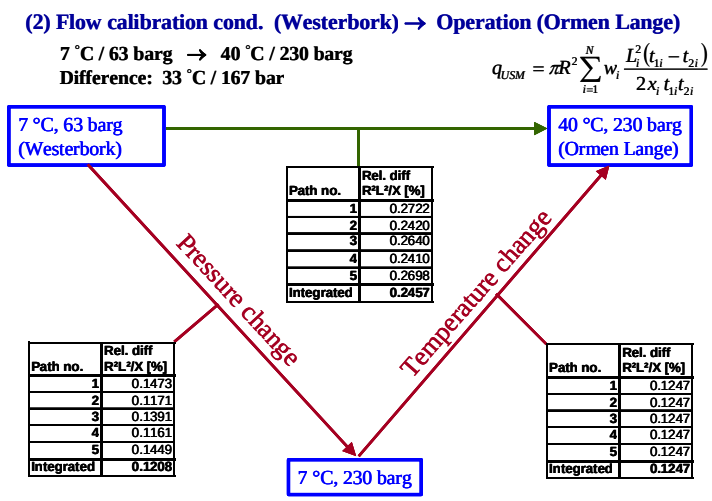

Path no.	Rel. diff R^2L^2/X [%]
1	0.2722
2	0.2420
3	0.2640
4	0.2410
5	0.2698
Integrated	0.2457

Path no.	Rel. diff R^2L^2/X [%]
1	0.1473
2	0.1171
3	0.1391
4	0.1161
5	0.1449
Integrated	0.1208

Path no.	Rel. diff R^2L^2/X [%]
1	0.1247
2	0.1247
3	0.1247
4	0.1247
5	0.1247
Integrated	0.1247

Fig. 5. Effect of pressure and temperature on the measured volumetric flow rate for the Elster-Instromet Q-Sonic 5 ultrasonic gas flow meter, calculated from the FEM analysis results, for Westerbork (flow calibration) to Ormen Lange (operational). conditions (After [1].)

This result is of high interest in the sense that the FEM results may be used for the correction from Westerbork conditions to nominal Ormen Lange conditions (the "nominal PT correction factor"), and the analytical model B may be used for the remaining correction from nominal to the actual Ormen Lange line conditions (the "instantaneous PT correction factor"), cf. Section 7.2.

5. PRESSURE AND TEMPERATURE INFLUENCES ON TRANSDUCER PORTS, TRANSDUCER LENGTH AND ACOUSTIC PATH LENGTH

Changes in pressure and temperature influence on the length of the transducer ports in which the ultrasonic transducers are mounted, the length of the ultrasonic transducers themselves, and consequently on the length of the acoustic paths, and thus the measured transit times. The present section addresses these length changes, and the consequences for the measurement error. In particular, this relates to

(a) length changes from Westerbork (flow calibration) to Ormen Lange (operating) conditions,
(b) the effect of these changes on the Q-Sonic 5 measurement uncertainty at Ormen Lange (operating) conditions.

5.1 Expansion / compression of the transducer ports

Changes in pressure and temperature will induce expansion/compression of the transducer ports and thus changes in the length of the ports, which influences on the acoustic path lengths, and thus on the transit time measurements. A detail study of the pressure and temperature induced expansion / compression of the transducer ports of the Q-Sonic 5 ultrasonic meter is given in the following, for the Ormen Lange application. The analysis is based on the finite element modelling (FEM) numerical calculations described in Section 4.2.

Fig. 4a gives the finite element mesh used for modeling of the Q-Sonic 5 meter body with transducer ports, and Fig. 6 a detail drawing of a transducer port of this meter. In the FEM calculations, each transducer port is assumed to be covered with a pressure tight and rigid plate (instead of the transducer flange), so that pressure-induced length changes of the port can be described, from Westerbork (flow calibration) to Ormen Lange (operating) conditions. Actual and realistic length changes are calculated for each of the 10 ports in the 5 acoustic paths.

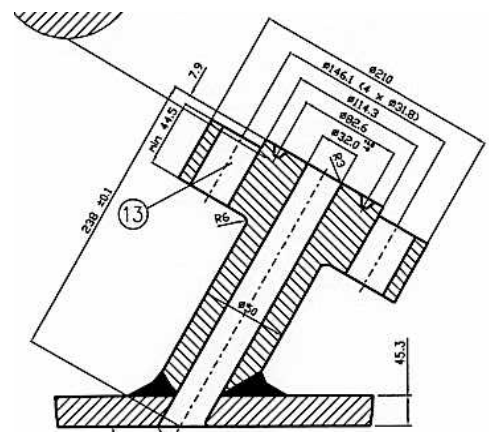

Fig. 6. Detail drawing of a transducer port of the Q-Sonic 5 meter body, as accounted for in the FEM analysis of the meter body.

The calculated length changes of the transducer ports range from 0.1038 mm to 0.1658 mm, depending on the path no., cf. Table 6 [1]. To illustrate the basic analysis and indicate the level of significance, consider an average length change of about, say, 0.12 mm, as a simplified and preliminary approach. If the length change is not corrected for, the (isolated) measurement error due to port length changes becomes, approximately [1],

$$\frac{\Delta \bar{v}_i}{\bar{v}_i} \approx -2\frac{\Delta L_i}{L_i} = -2\frac{2 \cdot 0.12\,mm}{780\,mm} \approx -0.0006 = -0.06\,\%\,, \tag{8}$$

where L_i is the interrogation length of path no. i, $i = 1, \ldots, N$, and ΔL_i is the change of L_i due to pressure and temperature effects.

However, note that when the two effects of the changed transducer ports and the changed transducer length are combined, the influence on the Q-Sonic 5 volumetric flow rate measurement in the Ormen Lange application becomes different from Eq. (8), cf. Section 5.3.

5.2 Expansion / compression of the ultrasonic transducers

Fig. 7 shows photographs of an Q-Sonic 5 ultrasonic transducer of the K2 type used in the Ormen Lange application. Changes in pressure and temperature will induce expansion/compression of

the transducers, which influences on the acoustic path lengths, and thus on the transit time measurements.

An extract of a detail study of the expansion / compression of the Q-Sonic 5 ultrasonic transducer in the Ormen Lange application is given in the following. The analysis is based on finite element (FEM) numerical calculations of pressure and temperature induced length changes of the transducer [1]. In particular, this relates to

(a) changes of the transducer length, from Westerbork (flow calibration) to Ormen Lange (operating) conditions, and
(b) the effect of these changes on the Q-Sonic 5 measurement uncertainty at Ormen Lange (operating) conditions.

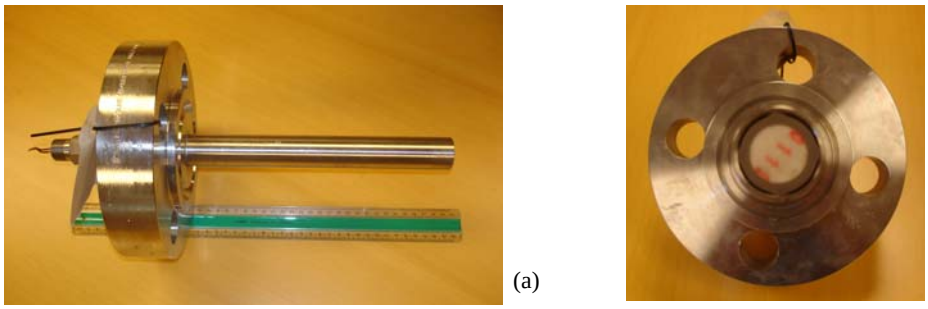

Fig. 7. Photographs of an Elster-Instromet Q-Sonic 5 ultrasonic transducer of the K2 type used in the Ormen Lange application. Left: side view; Right: front view. (After [1].)

The FEM analysis is based on information provided by Elster-Instromet [12], in addition to "qualified guess" on some of the construction details of the transducer. It is known that the active acoustic part of the transducer (the piezoelectric element, etc., in the front of the transducer) is pressure equalized, that the pressure barrier is located behind this region, and that important parts of the transducer interior are made up of epoxy [12]. However, the information provided on the construction details of the transducer was in general insufficient to do a precise FEM analysis of the pressure and temperature expansion/compression of the transducer. Thus, some assumptions had to be made in relation to constructional details, materials used, and material properties. The calculations given below are based on the best possible "qualified guess" of the constructional details of the transducer one could establish. A finite element model mesh of the transducer was thus developed, and finite element calculations made, in two steps:

(i) changes of the transducer length, from factory ("dry calibration") to Westerbork (flow calibration) conditions, and
(ii) changes of the transducer length, from factory ("dry calibration") to Ormen Lange (operating) conditions.

These are then combined to evaluate the changes of the transducer length, from Westerbork (flow calibration) to Ormen Lange (operating) conditions.

In short, the FEM calculations indicate that a pressure increase from 63 to 230 barg leads to a change in the transducer length of –0.0889 mm (compression) [1]. A temperature increase from 7 to 40 ^{o}C leads to a calculated change in the transducer length of +0.1945 mm (expansion) [1]. Some further details are given in [1]. The combined effect of the calculated pressure induced

compression of –0.0889 mm and the calculated temperature induced expansion of +0.1945 mm becomes [+0.1945 – 0.0889] mm = +0.1056 mm (expansion). Thus, the FEM results indicate that the temperature effect dominates and that the transducer increases in length by 0.1056 mm from Westerbork to Ormen Lange conditions.

It should be emphasized that, from the above discussion on the FEM analysis of the transducer, it is evident that due to the uncertainties in relation to some of the constructional details and the materials used, the calculated change in transducer length (0.1056 mm) is associated with some uncertainty (which is difficult to estimate, however).

If this length change is not corrected for, the measurement error due to transducer expansion becomes, approximately [1] (by noting that a transducer expansion corresponds to negative ΔL_i),

$$\frac{\Delta \bar{v}_i}{\bar{v}_i} \approx -2\frac{\Delta L_i}{L_i} = -2\frac{2\cdot(-0.1056)\,mm}{780\,mm} \approx +0.00054 = +0.054\,\% \,. \tag{9}$$

However, note that when the two effects of the changed transducer ports and the changed transducer length are combined, the influence on the Q-Sonic 5 volumetric flow rate measurement in the Ormen Lange application becomes different than predicted by Eq. (9), cf. Section 5.3.

5.3 Combined effect, in relation to change of acoustic path length

The results of Sections 5.1 indicate that pressure and temperature effects on the transducer ports will lead to increased acoustic path length, in the range from 2 · 0.1038 mm to 2 · 0.1658 mm, depending on the path no. On the other hand, the results of Sections 5.2 indicate that pressure and temperature effects on the transducers themselves will lead to a decreased acoustic path length, by about 2 · 0.1056 mm.

Consequently, in the Ormen Lange application the effect of changed transducer port length and changed transducer length partly cancel each other, and by combining them, one finds an increased acoustic path length, in the range from 0.0017 mm to 0.1089 mm, depending on the path no., cf. Table 6 [1].

First, consider a simplified analysis of the effect of the increased acoustic path length, to illustrate the basic analysis. The average calculated length change for the five acoustic paths is about, say, 0.04 mm, as a very rough figure. If this average length change is not corrected for, the measurement error (misreading) due to transducer port and transducer length changes becomes, approximately [1],

$$\frac{\Delta \bar{v}_i}{\bar{v}_i} \approx -2\frac{\Delta L_i}{L_i} = -2\frac{2\cdot 0.04\,mm}{780\,mm} \approx -0.000205 \approx -0.021\,\% \,. \tag{10}$$

If this error is not corrected for, the ultrasonic flow meter thus underestimates the volumetric flow rate. Consequently, the effect of this average acoustic path length change on the USM is positive, +0.021 %.

The above simplified analysis effectively illustrates the basic idea of the analysis, but does not account for changes in the acoustic path lengths of the individual paths. A more thorough analysis has thus been made, where calculated changes in the individual acoustic path lengths are accounted for. This analysis - given in the following - reveals that the tentative figure given by Eq. (10) may represent a rough but still reasonable estimate. Table 6 gives the calculated change in acoustic path length based on the calculated change in transducer port length and the calculated change in transducer length, calculated using FEM in Sections 5.1 and 5.2, respectively.

Table 6. Combined effect of (a) calculated transducer port length change and (b) calculated transducer length change, due to pressure and temperature effects, from flow calibration (Westerbork) to field operation (Ormen Lange) conditions, for each of the 5 paths of the Q-Sonic 5. Results both for individual paths and for the integrated effect are given. (After [1].)

Path no.	Port no.	Change in port length [mm]	Change in transducer length [mm]	Change in acoustic path length [mm]	Interrogation length [mm]	Effect on acoustic path [%]
1	1A	0.1080	0.1056	+0.0044	780	+0.0011
	1B	0.1076	0.1056			
2	2A	0.1543	0.1056	+0.1089	1100	+0.0198
	2B	0.1658	0.1056			
3	3A	0.1172	0.1056	+0.0252	780	+0.0065
	3B	0.1192	0.1056			
4	4A	0.1511	0.1056	+0.1013	1100	+0.0184
	4B	0.1614	0.1056			
5	5A	0.1038	0.1056	-0.0017	780	-0.0004
	5B	0.1057	0.1056			
Integrated effect, using the assumed USM integration weight factors:						**+0.0165**

Based on these numbers, the effect on the velocity measured on each acoustic path can be calculated similar to Eqs. (8)-(10), for each of the 5 paths of the Q-Sonic 5. The integrated value is then found based on the tentative Q-Sonic 5 integration weights discussed in Section 3.3. The integrated value (typical value for the effect on the flow meter in total) is found to be about +0.0165 % ≈ +0.017 %. The positive sign is an effect of increased transit times, meaning that the USM is underestimating the volumetric flow rate if this acoustic path length effect is not corrected for.

6. PRESSURE AND TEMPERATURE INFLUENCES ON THE REYNOLDS NUMBER CORRECTION

The Reynolds number used at the Westerbork flow calibration is lower than at Ormen Lange operating conditions, cf. Table 2. At Westerbork, the Reynolds number was in the range $2.4 \cdot 10^6$ - $3.0 \cdot 10^7$, and at Ormen Lange, it is about $4.5 \cdot 10^7$. For constant flow velocity, the Reynolds number is about a factor 2 larger at Ormen Lange than at Westerbork conditions.

This means that the flow profile is different at Westerbork conditions than at Ormen Lange conditions, for the same flow velocity. In the Q-Sonic 5 software, a Reynolds number correction is made by Elster-Instromet, with intention to account for this difference [12]. The Reynolds number correction for the Ormen Lange metering station is discussed in the following.

The effect of the change in Reynolds number from Westerbork to Ormen Lange conditions is here studied by a set of measured axially symmetric flow profiles, reported by a series of

laboratories [13-17]. In one laboratory, both smooth and rough pipe walls were used. In the other laboratories smooth pipes were used. The Reynolds number range covered by these experiments is about $7{\cdot}10^3$ - $35{\cdot}10^6$. For each Reynolds number (flow velocity profile), the deviation from reference is calculated using the tentative Q-Sonic 5 integration weights discussed in Section 3.3. The results are shown in Fig. 8a over a wide Reynolds number region.

(a)

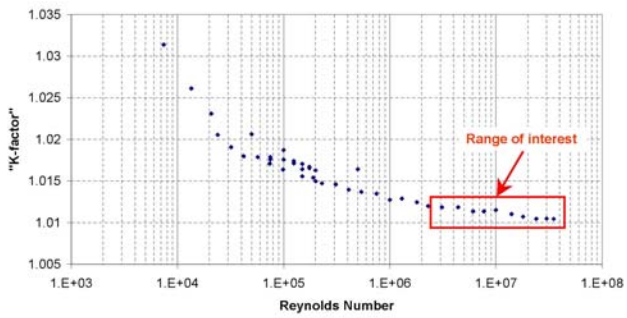

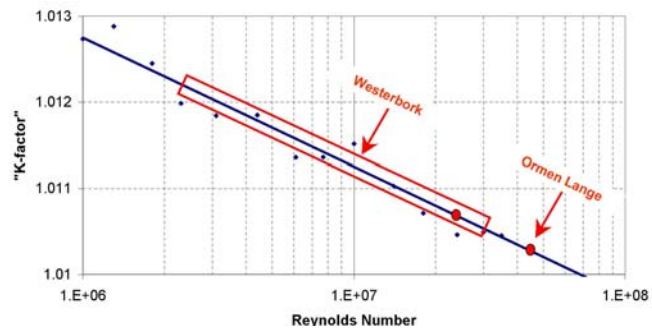

(b)

Fig. 8. Tentative Q-Sonic 5 USM integration method used on a set of measured symmetric flow profiles taken from the literature, over (a) a wide Reynolds number range, and (b) the Reynolds number range of interest here. The Q-Sonic 5 results are shown with blue dot markers. In (b), the Reynolds number correction curve proposed by Eq. (11) is shown using the blue line. The Westerbork and Ormen Lange Reynolds number ranges are indicated with a red rectangular box and a red marker, respectively. Corresponding Reynolds numbers at Westerbork and Ormen Lange for constant flow velocity of 15 m/s are shown with red markers.

In Fig. 8b, the same results are shown over the Reynolds number region of interest here. In addition, a fitted straight line is added, given as

$$RC = 1.01275 - \frac{\ln(10^{-6}\,\mathrm{Re})}{\ln 10} 0.0015\,, \tag{11}$$

where *RC* is the Reynolds number correction, and *Re* is the Reynolds number. Fig. 8b may be interpreted as follows:

At Westerbork, the flow calibration is intended to ensure that at 15 m/s, the USM gives 15 m/s as output value, at the Reynolds number $2.43{\cdot}10^7$. At Ormen Lange conditions, however, use of the USM at 15 m/s gives (erroneously) a lower output flow velocity value than 15 m/s, since the Reynolds number corresponding to 15 m/s is $4.5{\cdot}10^7$, and the curve in Fig. 8b decreases by increasing Reynolds number. At Ormen Lange conditions, thus, the USM underestimates the flow velocity. This is a property of the integration method of the USM (i.e. the integration weigth factors).

The underestimation made by the USM can be corrected using a Reynolds number correction factor for the Q-Sonic 5 flow meter, from Westerbork to Ormen Lange conditions,

$$q = q_{USM}\, C_{W-OL}^{RE-Number}\,, \tag{12}$$

where

$$C_{W-OL}^{RE-Number} = \left.\frac{RC_{Westerbork}}{RC_{OrmenLange}}\right|_{v=15\ m/s} \approx \frac{1.01067}{1.01027} \approx 1.00040 \tag{13}$$

is the Reynolds number correction factor from Westerbork to Ormen Lange conditions, evaluated at 15 m/s flow velocity at both locations (Re = $2.4 \cdot 10^7$ and $4.5 \cdot 10^7$, respectively). The Reynolds number correction from Westerbork to Ormen Lange conditions is thus about +0.040 %. It can be shown that this Reynolds number correction of about +0.04 % applies to all flow velocities of relevance here, 1 – 19 m/s.

The actual Reynolds number correction carried out in the Q-Sonic 5 has not been available for the present work. However, Elster-Instromet claims that the Reynolds number correction they use is 90 % correct [12]. Now, assume that the magnitude of the correction is about 0.04 %, as argued above, and assume that the Reynolds number correction made in the Q-Sonic 5 is at least 50 % correct. Then the error of the Q-Sonic 5 Reynolds number correction will be less than 0.02 %. Consequently, the Reynolds number correction already carried out in the Q-Sonic 5 is assumed to be sufficient, and no further correction is introduced here. (It would also be difficult to device any additional Reynolds correction.)

7. CORRECTION MODEL FOR PRESSURE - TEMPERATURE EFFECTS

Correction models for pressure and temperature effects are proposed on basis of the calculation results given in Sections 3-6. Correction factors have been designed to be implemented at the flow computer level, and not at the USM level (i.e. not in the Q-Sonic 5 software).

7.1 Combined measurement error

Table 7 gives an overview of the calculated contributions, and their combined effect on the USM [1].

Table 7. Various contributions to the measurement error, and their combined effect, caused by pressure and temperature changes, from flow calibration (Westerbork) to field operation (Ormen Lange) conditions, for the Q-Sonic 5 ultrasonic flow meter. (Cf. also Table 8, which is an extract of Table 7.) (After [1].)

Contributing factor to measurement error, due to pressure and temperature changes	**Path no.**	**Contribution to error**	**Integrated contribution to error (all 5 paths)**	**Combined contribution to error**	**Source (further details)**
Cross-sectional area and acoustic path geometry (inclination angles & lateral chord positions), effect on paths 1-5:	1	+ 0.272 %	+ 0.246 %	+ 0.246 %	Fig. 5
	2	+ 0.242 %			
	3	+ 0.264 %			
	4	+ 0.241 %			
	5	+ 0.270 %			
Expansion transducer ports, effect on paths 1-5:	1	+ 0.055 %	+ 0.057 %		Table 6
	2	+ 0.058 %			
	3	+ 0.061 %			
	4	+ 0.057 %			
	5	+ 0.054 %			
Expansion transducers, effect on paths 1-5:	1	- 0.054 %	- 0.041 %		Table 6
	2	- 0.038 %			
	3	- 0.047 %			
	4	- 0.033 %			
	5	- 0.047 %			
Combined integrated effect, expansion transducer ports & expansion transducers, all 5 paths:				+ 0.017 %	Table 6
Reynolds number correction (assumed deviation from Elster-Instromet Reynolds number correction):				0 %	Sect. 6
Combined effect, total (%)				**+ 0.262 %**	

The contribution to the measurement error from the cross-sectional area and the acoustic path geometry (the inclination angles and the lateral chord positions), integrated over all 5 paths, is calculated to be +0.246 %, cf. Fig. 5. The contribution from expansion of the transducer ports, integrated over all 5 paths, is calculated to be +0.057 %. The contribution from expansion of the transducers themselves, integrated over all 5 paths, is calculated to be +0.041 %. The contribution from Reynolds number correction (assumed deviation from the Elster-Instromet Reynolds number correction), is taken to be 0 %, cf. Section 6.

Thus, according to the models used, the combined effect accumulates to +0.262 %. If effects caused by pressure and temperature changes are not corrected for, the Q-Sonic 5 will underestimate the volumetric flow rate by the same amount. A graphical visualization of the same data is given in Fig. 9.

The estimates of the various contributions are obtained by calculations, and are of course associated with uncertainties. The estimates used here are considered to be the best possible on basis of the information at hand.

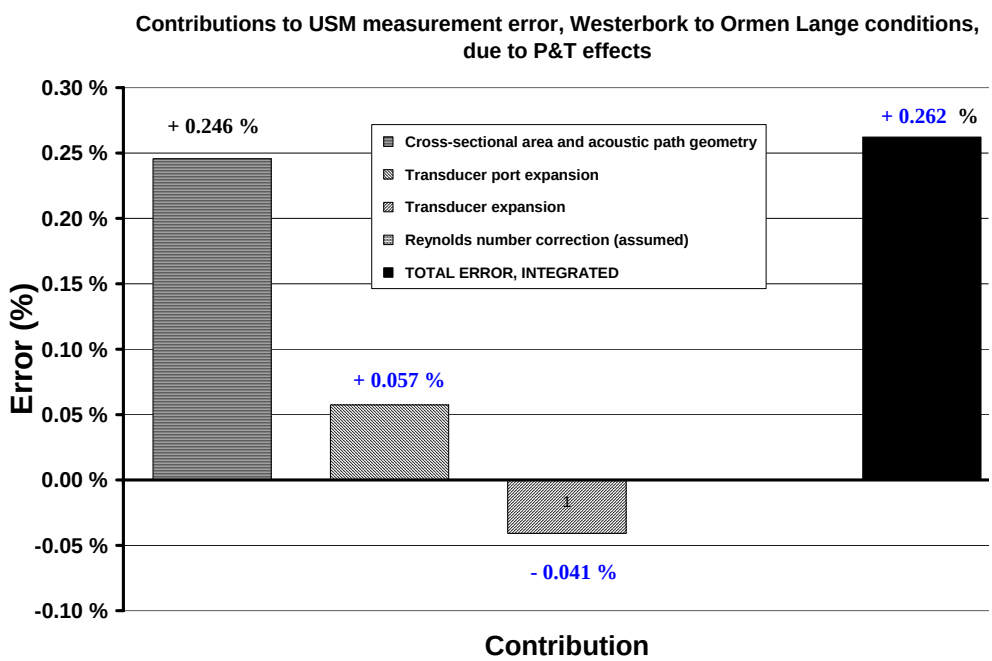

Fig. 9. Various contributions to the measurement error, and their combined total effect, caused by pressure and temperature changes, from flow calibration (Westerbork) to field operation (Ormen Lange) conditions, for the Elster-Instromet Q-Sonic 5 ultrasonic flow meter. (After [1].)

7.2 Correction factors

Correction of the volumetric flow rate for the effects of pressure and temperature changes from flow calibration (Westerbork) to field operation (Ormen Lange) conditions, as discussed in Chapters 4-6 and summarized in Section 7.1, is proposed to be done by multiplication of the measured volumetric flow rate with two correction factors, as outlined in the following:

(1) A "nominal P&T correction factor", C_{W-OL}^{PT-nom}, representing the main correction:

- Westerbork (63 barg, 7 ^{o}C) → Ormen Lange (nominal P&T, 230 barg, 40 ^{o}C),

- Fixed correction factor, based on the FEM calculations.
- Accounts for the effects A - E in Table 3.
- Implemented in the flow computer (not in the USM software).

(2) An "instantaneous P&T correction factor", $C_{OL}^{PT-inst}$, representing an adjustment for smaller P&T changes:
- Ormen Lange (nominal P&T, 230 barg, 40 ^{o}C) → Ormen Lange (actual P&T),
- Westerbork (63 barg, 7 ^{o}C) → Possible new flow calibration (new P&T conditions).
- Online "living" correction factor, based on the (simplified) analytical model B.
- Accounts for the effects A and B in Table 3.2.
- Implemented in the flow computer (not in the USM software).

The following correction model is thus proposed for the Ormen Lange application,

$$q = q_{USM} \cdot K_{Westerbork}^{Flow} \cdot C_{W-OL}^{PT-nom} \cdot C_{OL}^{PT-inst}, \tag{14}$$

where

q: Corrected volumetric flow rate at Ormen Lange line conditions [m^3/s].

q_{USM}: Output volumetric flow rate of the Q-Sonic 5 at Ormen Lange line conditions [m^3/s].

$K_{Westerbork}^{Flow}$: Flow calibration correction factor [dimensionless], established under flow calibration at Westerbork. Flow dependent. Not addressed here.

C_{W-OL}^{PT-nom}: "Nominal P&T correction factor" [dimensionless], for pressure and temperature changes from flow calibration (Westerbork) to field operation (Ormen Lange) conditions (nominal), accounting for:
- Changes of cross-sectional area (diameter) (based on FEM)
- Changes of acoustic path geometry (inclination angles and lateral chord positions) (based on FEM)
- Expansion / contraction of transducer ports (based on FEM)
- Expansion / contraction of transducers (based on FEM)
- Changes of the Reynolds number.

$C_{OL}^{PT-inst}$: "Instantaneous P&T correction factor" [dimensionless], for
(a) instantaneous (small) changes of Ormen Lange pressure and temperature conditions, i.e. deviation between actual and nominal Ormen Lange P&T conditions, and
(b) in case of a future recalibration at Westerbork or another flow calibration lab, pressure and temperature changes from "old" to "new" flow calibration, both accounting for
- Changes of cross-sectional area (diameter)
- Changes of acoustic path geometry (inclination angles and lateral chord positions), both based on the analytical model B.

The two proposed correction factors are given as (from Table 7 and Eqs. (6))

$$C_{W-OL}^{PT-nom} = 1 + 0.262\ \% = 1.00262, \qquad C_{OL}^{PT-inst} = (1+3\alpha\Delta T)(1+3\beta\Delta P), \qquad (15)$$

respectively, where

- ΔT = the temperature deviation between the nominal (40 ^{o}C) and the actual line temperature at Ormen Lange [^{o}C],
- ΔP = the pressure deviation between the nominal (230 barg = $230\cdot10^5$ Pa-g)[5] and the actual line pressure at Ormen Lange [Pa],
- β = the radial linear pressure expansion coefficient of the meter body [Pa^{-1}],

given as (cf. Section 4.1)

$$\Delta T = (T_{OL}^{inst} - T_{OL}^{nom}) - (T_{cal}^{new} - T_{cal}^{old}), \qquad \Delta P = (P_{OL}^{inst} - P_{OL}^{nom}) - (P_{cal}^{new} - P_{cal}^{old}), \qquad \beta = \frac{R_0}{wY}, \qquad (16)$$

where

- T_{OL}^{inst} = the instantaneous (actual measured) line temperature at the Ormen Lange metering station [^{o}C],
- T_{OL}^{nom} = the nominal line temperature at the Ormen Lange metering station [^{o}C] = 40 ^{o}C,
- T_{cal}^{new} = the line temperature in the USM at a possible (future) new flow calibration [^{o}C]. As long as a new flow calibration has not been made, T_{cal}^{new} is set equal to T_{cal}^{old},
- T_{cal}^{old} = the line temperature in the USM at the initial Westerbork flow calibration of the USM [^{o}C] = 7 ^{o}C,
- P_{OL}^{inst} = the instantaneous (actual measured) line pressure at the Ormen Lange metering station [Pa-g],
- P_{OL}^{nom} = the nominal line pressure at the Ormen Lange metering station [Pa-g] = 230 barg = $230\cdot10^5$ Pa-g,
- P_{cal}^{new} = the line pressure in the USM at a possible (future) new flow calibration [Pa-g]. As long as a new flow calibration has not been made, P_{cal}^{new} is set equal to P_{cal}^{old}.
- P_{cal}^{old} = the line pressure in the USM at the initial Westerbork flow calibration of the USM [Pa-g] = 63 barg = $63\cdot10^5$ Pa-g,

7.3 Correction factor calculation example

Fig. 10 shows an example of calculation of the corrected volumetric flow rate, q, including calculation of the instantaneous P&T correction factor, $C_{OL}^{PT-inst}$, and the total P&T correction factor, $C_{OL}^{PT-inst} \cdot C_{W-OL}^{PT-nom}$.

---

[5] Here, for brevity, the unit notation "Pa-g" is used for the gauge pressure (the excess pressure in Pascal relative to 1 atm.), i.e. in the meaning "Pa gauge" normally used in the SI unit system, analogous to the notation "barg" used for the excess pressure in bar relative to 1 atm.

In the example the following quantities are used: T_{OL}^{inst} = 45 ^{o}C and P_{OL}^{inst} = 240 barg, i.e. ΔT = (45-40) ^{o}C = 5 ^{o}C and ΔP = (240-230) bar = 10 bar = $10 \cdot 10^5$ Pa. The nominal P&T correction factor is $C_{W-OL}^{PT-nom} \approx$ 1.00262 (fixed), the instantaneous P&T correction factor becomes $C_{OL}^{PT-inst} \approx$ 1.00025 (calculated), and the total P&T correction factor thus becomes $C_{OL}^{PT-inst} \cdot C_{W-OL}^{PT-nom} \approx$ 1.00287 (calculated).

Due to the simplifications and approximations on which the calculations are based, at maximum four significant digits are considered to be valid for the present analysis. The total P&T correction factor for this example is thus rounded to $C_{OL}^{PT-inst} \cdot C_{W-OL}^{PT-nom} \approx$ 1.0029, corresponding to correcting for an error of +0.29 % (underreading).

Fig 10. Example of calculation of the corrected volumetric flow rate, including calculation of the instantaneous P&T correction factor and the total P&T correction factor.

(A)	**Nominal P&T correction factor:**					
	Nominal correction factor:	$C_{W-OL}^{PT_nom}$	=	**1.00262**		
(B)	**Instantaneous P&T correction factor:**					
	Fixed quantities:	R_0	=	0.183250	m	
		w	=	0.045350	m	
		Y	=	2.0E+11	Pa	
		α	=	1.260E-05	1/K	
		T_{OL}^{nom}	=	40.0	^{o}C	
		T_{cal}^{new}	=	7.0	^{o}C	
		T_{cal}^{old}	=	7.0	^{o}C	
		P_{OL}^{nom}	=	23000000.0	Pa-g	(= 230 barg)
		P_{cal}^{new}	=	6300000.0	Pa-g	(= 63 barg)
		P_{cal}^{old}	=	6300000.0	Pa-g	(= 63 barg)
	Input from instruments:	T_{OL}^{inst}	=	45.0	^{o}C	
		P_{OL}^{inst}	=	24000000.0	Pa-g	(= 240 barg)
	Calculations:	ΔT	=	5.0	K	
		ΔP	=	1000000.0	Pa	
		β	=	2.02040E-11	1/Pa	
		$1+3*\alpha*\Delta T$	=	1.00018900		
		$1+3*\beta*\Delta P$	=	1.00006061		
	Instantaneous correction factor:	$C_{OL}^{PT_inst}$	=	**1.00025**		
(C)	**Total P&T correction factor:**	$C_{W-OL}^{PT_nom} * C_{OL}^{PT_inst}$	=	**1.00287**		
⇨	**Corrected volumetric flow rate:**	$q = q_{USM} * K_{Westerbork}^{Flow} * 1.00262 * 1.00025 = q_{USM} * K_{Westerbork}^{Flow} * 1.00287$				

8. CONCLUSIONS

Ultrasonic gas flow meters may be affected by pressure and temperature changes in several ways, such as (cf. Table 3)

- (A) Change of the meter's cross-sectional area,
- (B) Change of the ultrasonic path geometry (inclination angles and lateral chord positions),

- (C) Change of the length of the ultrasonic transducer ports,
- (D) Change of the length of the ultrasonic transducers,
- (E) Change of the Reynolds number.

In the present work, pressure and temperature effects have been evaluated for the Elster-Instromet Q-Sonic 5 ultrasonic flow meter for operation in the Ormen Lange metering station at Nyhamna in Norway. The study addresses pressure and temperature changes from flow calibration (Westerbork, at 63 barg and 7 ^{o}C) to field operation (Ormen Lange, nominally at 230 barg and 40 ^{o}C) conditions.

The study shows that for the Ormen Lange application, investigation and evaluation of all of the factors (A)-(E) mentioned above have been necessary to evaluate the effect of pressure and temperature on the meter.

A theoretical approach has been chosen to establish such pressure and temperature corrections, since a screening of available flow laboratories in Europe and elsewhere has shown that currently no flow calibration laboratory can offer calibration or flow testing under process conditions which are relevant for Ormen Lange. This is particularly so with respect to the high pressure in question, 230 barg. Most flow calibration laboratories can not operate above about 60 barg with such large piping.

Investigation and evaluation of the pressure and temperature effects have been made by theoretical calculations, using various types of numerical and analytical models. Effects (A)-(D) have been evaluated very accurately using finite element modeling (FEM), in combination with a CMR model for USM numerical integration. In addition, effects (A)-(B) have been evaluated using two analytical models, as a simplified approach, for comparison. Effect (E) has been evaluated using a CMR model for USM numerical integration.

Accurate FEM calculations show that the combined effect of (a) change of the meter's cross-sectional area (diameter change) and (b) change of the ultrasonic path geometry (inclination angles and lateral chord positions) is by far the largest and most dominant effect, amounting to about 0.246 %. For this effect, a fair agreement has been obtained between FEM and the analytical models A and B, for the P&T conditions considered here. This indicates that the analytical model B may be used for the instantaneous correction factor in the Ormen Lange application, see below. How general this fair agreement is, however, and whether it can be extrapolated to other conditions, has not been investigated here.

With respect to the combined effects of (a) transducer port length changes and (b) transducer length change, accurate FEM calculations show that the two individual contributions are both significant for the Ormen Lange application, but effectively cancel each other to a large extent when combined, so that an error of about 0.017 % remains, cf. Table 8. This is an effect of the P&T conditions in question at Westerbork and Ormen Lange. In general (at other P&T conditions), such cancellation might not be the case, and a "reinforcement" effect may be experienced instead of cancellation. It is thus in general recommended to calculate or by other means investigate both the change of the transducer port length and the change of the transducer length.

The effect of Reynolds number change from Westerbork to Ormen Lange is relatively small (about 0.04 %), but still significant if Reynolds number correction were not used in the USM. For the Q-Sonic 5 flow meter a Reynolds number correction from Westerbork to Ormen Lange conditions is used by the manufacturer [12], but the actual magnitude of the manufacturer's correction has not been available for the present study. In a dialogue with Autek, Elster-Instromet and the Ormen Lange project, it has been assumed here that the manufacturer's Reynolds number correction is sufficiently close to the Reynolds number correction calculated here (0.04 %), so that an additional Reynolds number correction is not devised.

When combining the above mentioned contributions, the pressure and temperature effect on the Q-Sonic 5 in the Ormen Lange application is estimated to +0.262 %, cf. Table 8. Several factors contribute to this number: (a) cross-sectional area and acoustic path geometry (inclination angles and lateral chord positions) +0.246 %, (b) expansion of transducer ports +0.057 %, (c) expansion of the transducer -0.041 %, (d) Reynolds number correction 0 % (cf. Table 7 and Fig. 9).

Table 8. Extract of Table 7: Various contributions to the measurement error, and their combined effect, caused by pressure and temperature changes, from flow calibration (Westerbork) to field operation (Ormen Lange) conditions, for the Elster-Instromet Q-Sonic 5 ultrasonic flow meter. (After [1].)

Contributing factor to measurement error, due to pressure and temperature changes	**Integrated contribution to error (all 5 paths)**	**Combined contribution to error**
Cross-sectional area and acoustic path geometry	+ 0.246 %	+ 0.246 %
Expansion transducer ports, effect on paths 1-5:	+ 0.057 %	
Expansion transducers, effect on paths 1-5:	- 0.041 %	
Combined effect, expansion transducer ports & expansion transducers, all 5 paths:		+ 0.017 %
Reynolds number correction (assumed deviation from Elster-Instromet Re no. correction):		0 %
Combined effect, total (%)		**+ 0.262 %**

If the effects caused by pressure and temperature changes are not corrected for, the Q-Sonic 5 will underestimate the volumetric flow rate by the same amount.

Consequently, 2 correction factors are proposed for implementation in the flow computer, to account for pressure and temperature effects from flow calibration (Westerbork, 63 barg, 7 ^{o}C) to field operation (Ormen Lange, nominal P&T = 230 barg, 40 ^{o}C) conditions:

(1) A "nominal P&T correction factor", C_{W-OL}^{PT-nom}, representing the main correction, as a fixed number, equal to 0.262 %.

(2) An "instantaneous P&T correction factor", $C_{OL}^{PT-inst}$, representing an adjustment for smaller P&T changes at Ormen Lange (nominal P&T = 230 barg & 40 ^{o}C to actual P&T). This is an online "living" correction factor, based on the (simplified) analytical model B described in Section 4.1.

In case of a future flow calibration at possibly another pressure and temperature condition than the Westerbork condtions (63 barg, 7 ^{o}C), the P&T effects of that possible change of calibration conditions may also be accounted for in the "instantaneous P&T correction factor", cf. Eqs. (14)-(16).

A closer discussion of the two correction factors C_{W-OL}^{PT-nom} and $C_{OL}^{PT-inst}$ is given in Section 7. Note that $C_{OL}^{PT-inst}$ is calculated using the approximate analytical model B, strictly valid for inclination angles equal to $\pm 45^{o}$ only. Although an alternative and more accurate model is available (analytical model A), this model B has been chosen since the correction factor needs to be implemented at flow computer level, and not in the USM software.

The results and proposed correction factors are based on calculations, using theoretical models (analytical and numerical models). The question was therefore raised at an early stage in the project whether the calculations could by some means be verified experimentally, such as e.g. by doing static measurements with an 18" Q-Sonic 5. The purpose would be to supply or verify parts of the theoretical calculations. However, an analysis has indicated [1] that with the dimensional changes in question here, the effects on the transit times will be so small that control with time delay correction (transducer, electronics and diffraction correction delay, etc.) will be required beyond what is considered to be realistic today. Until such challenges are solved, it seems like one has to rely on theoretical models and calculations when pressure and temperature corrections of ultrasonic flow meters are required.

ACKNOWLEDGEMENTS

The authors wish to thank the Ormen Lange partners for the possibility to publish the present paper. Reidar Bø, CMR, is acknowledged for assistance in the ultrasonic transducer expansion / contraction analysis. FEM simulations of the P&T expansion / contraction of the Q-Sonic 5 meter body and ultrasonic transducers were performed by Øyvind Torvanger and Katrine Osgjerd, CMR Prototech. The authors wish to thank Autek and Elster Instromet Ultrasonics for having provided valuable information to the study, in particular on transducer construction issues, and for their review of [1]. Comments given in project meeting discussions with the Ormen Lange project, the Norwegian Petroleum Directorate (NPD), Shell and Gassco have been of great value to the study.

REFERENCES

[1] **Lunde, P. and Frøysa, K.-E.:** "Ormen Lange ultrasonic gas flow meters. A study for establishment of corrections for pressure and temperature effects", CMR report no. CMR-06-A10048-RA-01, Christian Michelsen Research AS, Bergen, Norway (March 2007).

[2] Elster-Instromet Q-Sonic 5 ultrasonic flow meter web site, Elster-Instromet NV, Rijkmakerlaan 9, B-2910 Essen, Belgium (2006); http://www.elster-instromet.com/en/ultrasonic_flow_metering.html

[3] "Measurement of flow in closed conduits – ultrasonic meters for gas – Part 1: meters for custody transfer and allocation measurement", ISO/CD 17089-1, August 31, 2007, International Organization for Standardization, Genéve, Switzerland. (Committee Draft.) (Reference number ISO/TC 30/SC 05 N210.)

[4] **Lunde, P., Frøysa, K.-E. and Vestrheim, M. (eds.):** "GERG project on ultrasonic gas flow meters, Phase II", GERG TM11 2000, Groupe Européen de Recherches Gazières (VDI Verlag, Düsseldorf, 2000).

[5] **Lunde, P. and Frøysa, K.-E.:** "Handbook of uncertainty calculations. Ultrasonic fiscal gas metering stations". Handbook prepared on behalf of the Norwegian Society of Oil and Gas Measurement (NFOGM) and the Norwegian Petroleum Directorate (NPD) (December 2001), 279 p. (ISBN 82-566-1009-3). (Free download available from www.nfogm.no.)

[6] "Manual of petroleum measurement standards. Chapter 12 - Calculation of petroleum quantities. Section 2 - Calculation of liquid petroleum quantites measured by turbine or displacement meters", First edition. American Petroleum Institute, U.S.A. (September 1981). (Paragraphs 12.2.5.1 and 12.2.5.2.)

[7] "Manual of petroleum measurement standards. Chapter 12 - Calculation of petroleum quantities. Section 2 - Calculation of liquid petroleum quantites using dynamic measurement methods and volumetric correction factors. Part 1 - Introduction", Second edition. American Petroleum Institute, Washington D.C., U.S.A. (May 1995). (Paragraphs 1.11.2.1 and 1.11.2.2.)

[8] "Institute of Petroleum. Petroleum Measurement Manual. Part X - Meter Proving. Section 3 - Code of practice for the design, installation and calibration of pipe provers", Published on behalf of The Institute of Petroleum, London (J. Wiley & Sons, Chichester, 1989), Section 10.7, p. 31 (ISBN 0 471 92231 5).

[10] "Measurement of gas by ultrasonic meters", A.G.A. Report no. 9, American Gas Association, Transmission Measurement Committee (June 1998). (Presently under revision.)

[11] **Young, W. C. and Budynas, W. C.,** *Roark's formulas for stress and strain*, 7th edition (McGraw-Hill, New York, 2001).

[12] Personal communication between Per Lunde, CMR, and Per Salvesen, Autek, Norway (Elster-Instromet's Norwegian sales representative) (2001, 2006 and 2007), including communication with Timo Smits, Elster-Instromet NV, Holland (2006 and 2007).

[13] **Zagarola, M. V. and Smits, A. J.**, "Experiments in high Reynolds number turbulent pipe flow". *Phys. Rev. Lett.* 78, (1997).

[14] **Perry, A. E., Henbest, S. M. and Chong, M. S.**, "A theoretical and experimental study of wall turbulence ". *J. Fluid Mech.* 165, 163-199 (1986).

[15] **den Toonder, J. M. J.,** "Drag reduction by polymer additives in a turbulent pipe flow". Ph. D. thesis, Delft University of Technology (1995).

[16] **Durst, F., Jovanovic, J. and Sender, J.,** "LDA measurements in the near-wall region of a turbulent pipe flow". *J. Fluid Mech.* 295, 305-335 (1995).

[17] **Laufer, J.,** "The structure of turbulence in fully developed pipe flow." Report 1174, National Bureau of Standards, 1952.

[18] "Regulations relating to measurement of petroleum for fiscal purposes and for calculation of CO_2 tax", Norwegian Petroleum Directorate, Stavanger, Norway (November 1, 2001).

[19] Test reports for K10 ultrasonic transducers, 44005-R114 to -R119, dated December 2004, and 54012-5005, -5008 and -5009, dated January 2005. Elster-Instromet NV, Rijkmakerlaan 9, B-2910 Essen, Belgium (2004).

[20] Personal communication between Per Lunde, CMR, and Klaus Zanker, Daniel Industries, Houston, USA (2001).

[21] Personal communication between Per Lunde, CMR, and Skule Smørgrav, FMC Kongsberg Metering, Kongsberg, Norway (2001).

[22] **Hallanger, A., Frøysa, K.-E. and Lunde, P.:** "CFD simulation and installation effects for ultrasonic flow meters in pipes with bends", International Journal of Applied Mechanics and Engineering, **7(**1), 33-64 (2002).

IMPACT OF REGULATOR NOISE ON ULTRSONIC FLOW METERS IN NATURAL GAS

MR. IDRIZ KRAJCIN, E.ON Ruhrgas AG
MR. MARTIN UHRIG, E.ON Ruhrgas AG
MR. ANDREW WRATH, SICK (UK) Ltd.
MR. TORALF DIETZ, SICK | MAIHAK GmbH
DR: VOLKER HERRMANN, SICK | MAIHAK GmbH

ABSTRACT

The impact of pressure regulator noise on the performance of ultrasonic meters has been discussed for several years now. This is one of the problems still to be solved in ultrasonic flow metering technology. Engineers have so far attempted to solve the problem by installing complex spatial pipe arrangements at high costs to reduce interfering noise levels.

The issue has been examined systematically both in field tests in the measuring station of a transportation pipeline and on the E.ON Ruhrgas high-pressure test facility in Lintorf to determine the limits of use and potential applications of an ultrasonic gas meter with chordal path layout in combination with a regulator. The tests made on a 16-inch meter in the measuring station confirmed that proper functioning of the meter with respect to pressure differential and flow rate can be guaranteed even under the most extreme conditions.

For further systematic testing on the Lintorf high-pressure test facility, an 8-inch ultrasonic meter was equipped with two four-path systems working independently of each other. This approach made it possible to directly compare a system with 210 kHz ultrasonic sensors with the latest technology of 350 kHz sensors. It was found that the 350 kHz sensors are clearly less sensitive to interfering noise signals and therefore improve measurement reliability under worst case conditions. Based on auto-diagnosis parameters such as signal-to-noise ratio and performance, the meter was confirmed to be capable of clearly detecting and rejecting disturbed signals.

The paper describes the test results and the information derived with respect to an expanded use of ultrasonic technology.

1. INTRODUCTION

Pressure regulators are a major source of noise in gas pipelines. In recent years, continuous optimization of the regulator design has led to a noticeable noise reduction, in particular in the audible range. However, the amount of noise generated at frequencies above the audible range may be problematic for ultrasonic gas flow meters. The reliability and accuracy of the signal transit time detected and thus the quality of the measured value provided by an ultrasonic gas meter are defined by the minimum signal level differential required between the sensor sound pulse to be analyzed and the signal interfering with the sound pulse (the signal-to-noise ratio). The spectral distribution of noise and its dependence on the pressure difference and flow rate at the regulator are of particular interest in this paper. Fig. 1 is a general presentation of the situation.

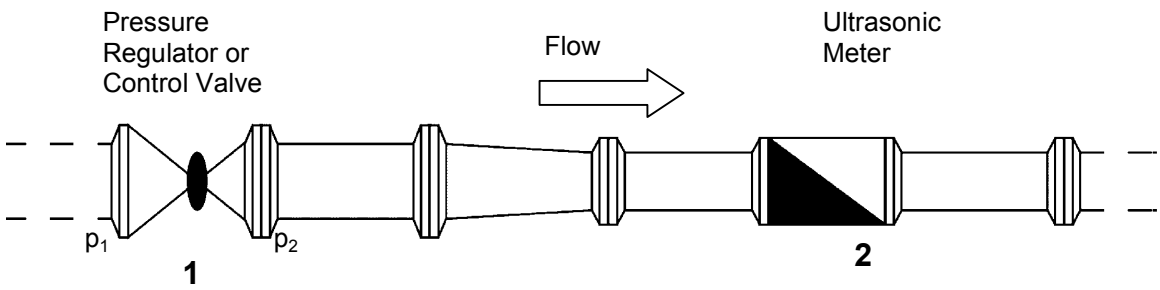

Fig. 1: Pressure regulator or control valve applied together with ultrasonic meter

1.1 INTERFERING NOISE FROM GAS PRESSURE REGULATORS

Energy loss and the consequential noise generated during pressure reduction are proportional to the flow rate and pressure difference. These relationships of noise sound pressure were already referred to in other literature [1]:

$$p_{noise} = f(\sqrt{Q}, \frac{p_1 - p_2}{p_2}) \tag{1}$$

$p_{1,2}$ pressure upstream (1) and downstream (2)

Q flowrate

The following approximation of the noise level produced by a sonic nozzle can be found e.g. in [2]:

$$L_{noise}[dB] \sim 93dB + 10 \cdot \log(Q \cdot c^2) - 10 \cdot \log\left[1 + 6\left(\frac{p_2}{p_1 - p_2}\right)^{2.5}\right] \tag{2}$$

L_{noise} sound pressure level

c speed of sound

For verification of this equation, the noise level emitted by a compressed air gun was recorded and the frequency spectra of a real signal and the theoretical model were compared. Fig. 2 shows the result of this test. A sufficient degree of congruence in the frequency range in question could be found.

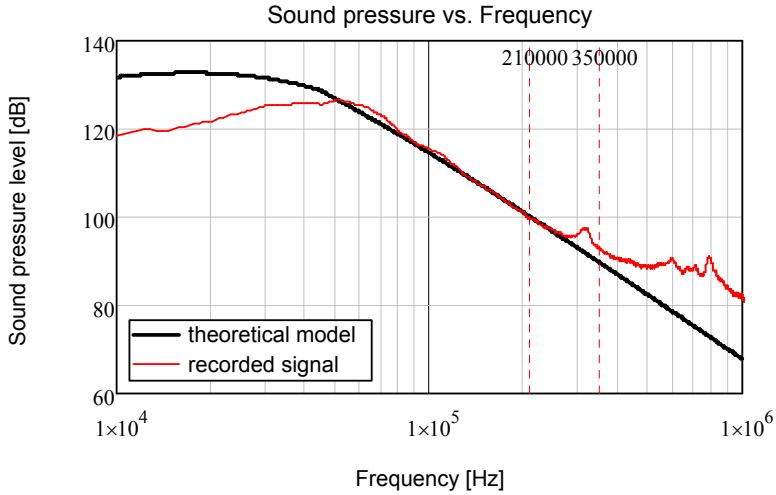

Fig. 2: Noise spectrum of a pressure regulator, simulated by means of a compressed air gun

A pressure regulator generates sound waves over a wide frequency range that may well be in the typical working frequency ranges of ultrasonic gas sensors (80...200 kHz). These sound waves travel through the gas from where they originate and superimpose the ultrasonic sound pulses emitted by an ultrasonic gas meter at the location where it is installed. It should be noted in this context that the gas industry uses various types of regulators that differ with respect to noise emission behavior. The rough approximations contained in this paper are only intended to assess the nature of noise generation.

1.2 SIGNAL-TO-NOISE RATIO (SNR)

To further investigate the matter, the ratio of

- useful signal (sound burst emitted) to
- interfering signal (broadband sound signal of pressure regulator)

will be examined.

The theory of noise emission and propagation is described comprehensively in [2]. Basically, sound waves in a gaseous medium always propagate in a directional fashion from their source. The sound pressure at a certain point is proportional to the amplitude of the sound-emitting source and decreases exponentially with the distance l to the source of sound. During its propagation, the sound wave is weakened as a result of interactions with the medium (attenuation α). Sound energy is transformed into thermal energy due to the viscosity of, and heat conduction in the medium. The attenuation is very dependent on the medium and on the signal frequency f_{sig} used. Since, in the case under investigation, a similar medium is used all the time, this relation can be simplified as follows:

$$\alpha = f(f_{sig}^{\ 2}) \tag{3}$$

If a sound wave hits an interface, its energy will be distributed into a different direction. The ratio of wavelength and dimensions of the disturbing object play a major role here. On the one hand, there will be diffraction effects, which is why “one can hear around a corner”. On

the other hand, the sound wave can be reflected. The ratio of reflector to transmitter surface area defines the resulting reflection signal loss [2]. The ratio of useful signal to interfering signal can thus be expressed as follows, taking into account attenuation, geometric distances and reflection signal losses:

$$\frac{L_{S,2}}{L_{N,2}} = \frac{L_{S,0} \cdot k_{bounce} \cdot e^{-\alpha(2\pi \cdot f) \cdot l_{path}}}{L_{N,0}(2\pi \cdot f) \cdot k_{damp} \cdot e^{-\alpha(2\pi \cdot f) \cdot l_{1,2}}} \tag{4}$$

$L_{N,0}$	noise sound level emitted by the pressure regulator
$L_{S,0}$	signal sound level emitted by the ultrasonic transducer
$L_{N,2}; L_{S,2}$	noise and signal at the receiving ultrasonic transducer
k_{bounce}	reflection signal loss; $k \leq 1$
k_{damp}	noise damping measures; $k \leq 1$
$\alpha(2\pi \cdot f)$	acoustic attenuation
$l_{path}; l_{1,2}$	distance between the ultrasonic transducer; pressure regulator and ultrasonic flow meter respectively

Equation (5) defines the ratio in equation (4) as a logarithmic measure in the unit *dB*. If a logarithmic measure is also used for attenuation α, the signal-to-noise ratio can also be expressed as follows using equations (4) and (5):

$$SNR = 20 \cdot \log\left(\frac{L_{S,2}}{L_{N,2}}\right)[dB] \tag{5}$$

$$\begin{aligned} SNR = {} & 20\log(L_{S,0}) + 20\log(k_{bounce}) - \alpha(2\pi f) \cdot l_{path} \\ & - 20\log\big(L_{N,0}(2\pi f)\big) - 20\log(k_{bounce}) + \alpha(2\pi f) \cdot l_{1,2} \end{aligned} \tag{6}$$

2 POSSIBLE SOLUTIONS

From equation (6) the measures can be derived that are necessary to optimize the SNR and thus the measured value quality of an ultrasonic gas meter. Measures can be taken to reduce the sound level of the interfering signal or to increase the sound level of the useful signal. Both solutions increase the SNR.

2.1 REDUCTION OF THE SOUND LEVEL OF THE INTERFERING SIGNAL

The interfering noise sound level depends on the type of pressure regulator used. The noise produced can be attenuated by appropriate acoustic measures. To date, engineers have attempted to solve the problem by installing complex and costly spatial pipe arrangements [3] to reduce interfering noise levels. In installations that require a flow conditioner and where the noise source is upstream the flow conditioner already provides a considerable attenuation of the noise level. For the PTB type flow conditioner, which is shown in Fig. 3a), an attenuation of 6 dB was recorded across the entire frequency range. A further improvement of the noise attenuation can be achieved if the flow conditioner is combined with metal foam

panels [4], see Fig. 3b). Because of the different thickness and structural density of the metal foam panels, an acoustically selective attenuation system can be created which is adapted to the working frequency of the ultrasonic transducers. This leads to further attenuation amounting to 3–6 dB. Because these structures are always symmetrical, this type of muffler can be used in conjunction with ultrasonic gas flow meters in bidirectional operation.

a) PTB design

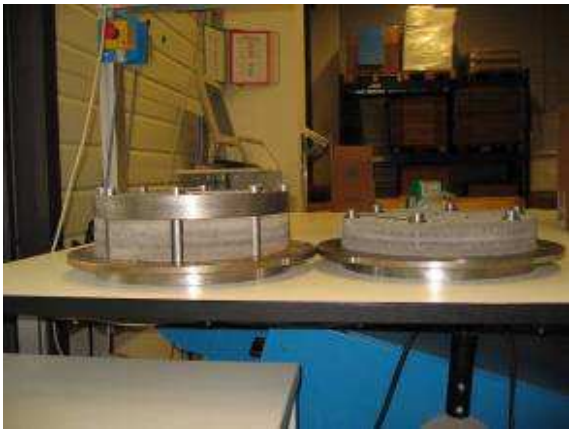

b) Metal foam structure for noise attenuation [4]

Fig. 3: Flow conditioner

2.2 INCREASE THE SOUND LEVEL OF THE SIGNAL

Path Layout

The sound burst emitted from the transmitting ultrasonic sensor is attenuated in the same way as the interfering signal. The geometric distances between the ultrasonic sensors of a measurement path should therefore be as short as possible to ensure maximum useful signal levels at the receiving ultrasonic sensor. It is also obvious that each point of reflection in the measuring path normally further weakens the useful signal level.

The signal level chart in Fig. 4 may serve as an exemplary illustration. It shows the signal level passing from the transmitter to the receiver of the ultrasonic measuring path for a single-reflection arrangement in contrast to a direct arrangement. This is a theoretic consideration according to equation (3). The sensor frequency and the angle between measuring path and flow axis shall be the same in both cases. The signal emitted at the position of the transmitter (level A) is attenuated on its way to the receiver. While the direct signal still has about e.g. 70 % (level B) of its original level in this example when it arrives at the receiver, the bounced signal is further attenuated because it travels twice the distance, and because there is an additional loss at the point of reflection.

The noise level in the received signal consists of both electric noise caused by the signal amplifiers and additive noise signals collected by the receiving sensor. Modern, closed-loop amplifier electronics modules (automatic gain control AGC) allow dynamic amplification ranges of 86 dB (1 : 20,000) to be processed without any limitation through electronic noise.

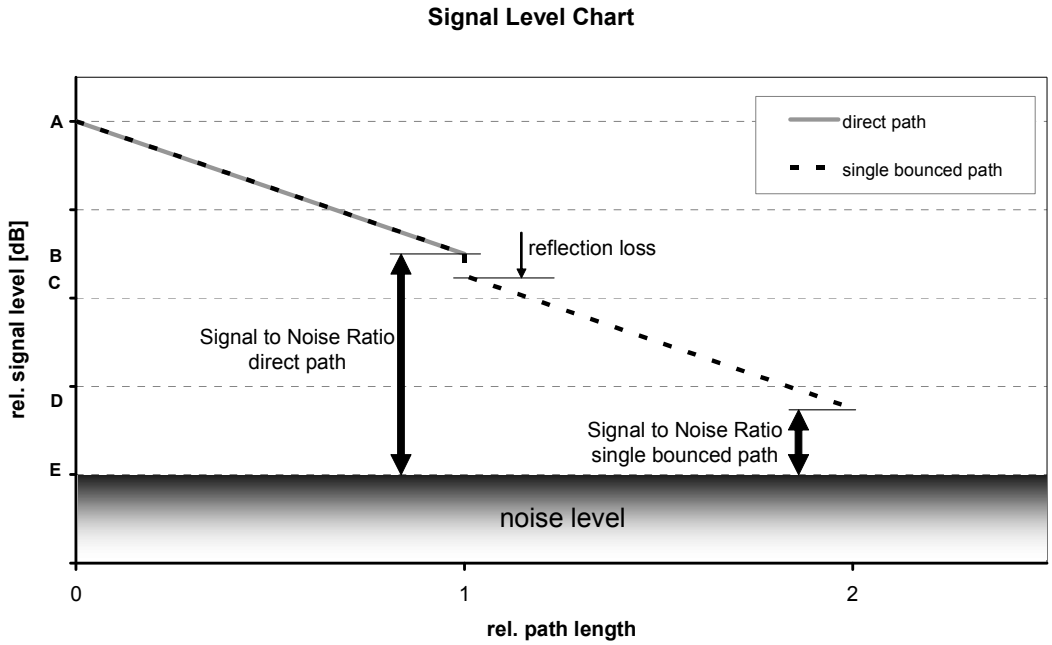

Fig. 4: Signal level chart, basic principle

Ultrasonic Sensors

Transducers for ultrasonic gas metering are usually of a piezo-ceramic type. The piezoelectric transducer itself is basically a thin disc. Two different vibration modes can be distinguished:

- the radial vibration mode and
- the thickness vibration mode.

If an alternating voltage is applied to the electrodes of the piezo-ceramic elements, their geometry will change. This generates a mechanical oscillation with the frequency of the alternating voltage. The maximum usable electric energy is limited because of the intrinsically safe design of the sensor circuits, which is required in this specific application. Further, because of the acoustic impedance jump between the oscillating surface and the gaseous medium, only a small portion of the energy is transmitted into the medium. In order to achieve the necessary efficiency of the energy transformation and to increase the sound pressure transmitted into the gas, the mechanical oscillation amplitude is amplified by a coupled mechanical oscillator.

Due to their simple design, bimorph transducers (see Fig. 5a) are widely used. These transducers have an acoustic matching layer which adheres to the ceramic element and performs this energy transformation. This layer is made of epoxy resins using hollow glass spheres and its thickness is dependent on the working frequency of the ultrasonic sensor. The alternating electrical field excites the piezoelectric disc so that it starts oscillating radially. The radial movement is transformed into an axial movement by the adhering matching layer. Great shear forces must be transmitted by the adhesive layer. In order to protect the epoxy resin of the matching layer from the material-changing effects of gaseous components such as hydrogen sulfide, the layer may be covered by a thin metal foil. However, this leads to a reduction in the amplitude of the transmitted acoustic signal and in the reception sensitivity [5].

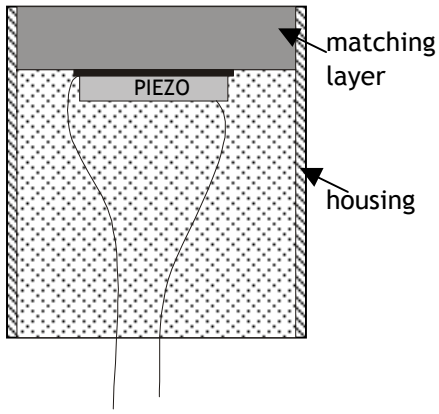

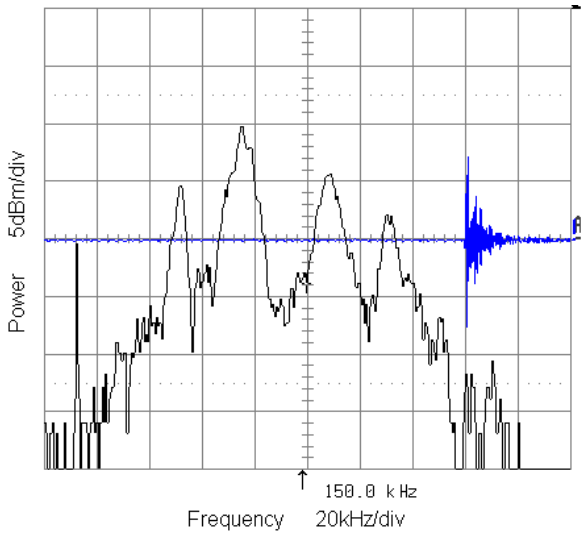

a) Schematic diagram

b) Acoustic spectrum of the emitted sound signal

Fig. 5: Bimorph transducer

This sensor type is characterized by a sound that means different pure tones which are close to each other. This is of course also reflected in the spectrum of absolute amounts of the acoustic signal (Fig. 5b). These sensors are therefore also often referred to as broadband sensors. In order to be able to generate maximum sound energy, the sensor is run in the resonance region with the greatest amplitudes (transmitter side). On the reception side, the additional, neighboring resonance regions are problematic, where possible noise signals superimpose the received measuring signal.

The acoustic matching layer could be left out if it were possible to achieve sufficient vibration amplitudes at the sound emitting surface. This idea leads to a stacked piezoelectric transducer in the form of a resonance converter. A metallic spring-mass-system is used to increase the amplitude at resonance (see Fig. 6a). Utilizing numerical optimization of mechanical and electrical parameters it is possible to produce sensors which exhibit

- sufficient bandwidth for short signals at great amplitude, and
- a maximum acoustic efficiency.

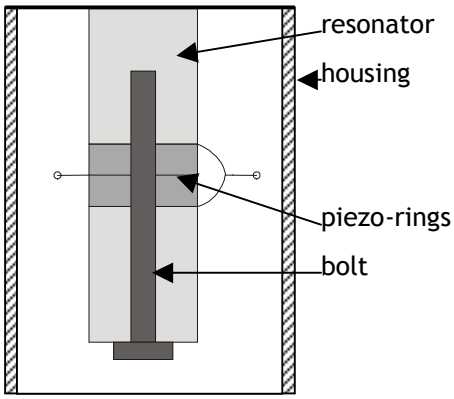

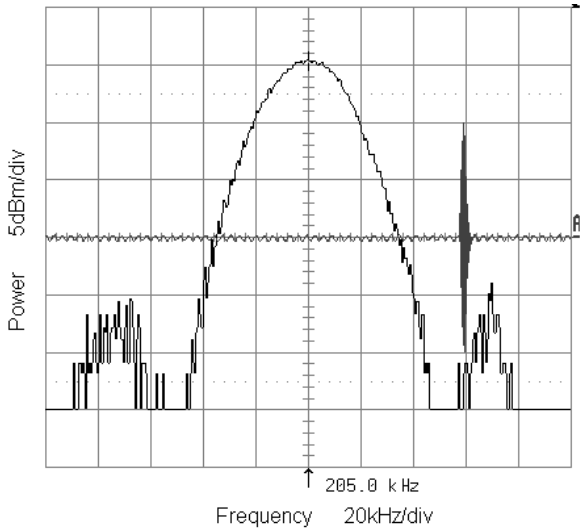

a) Schematic diagram

b) Acoustic spectrum of the emitted sound signal

Fig. 6: Stacked ultrasonic transducer

This sensor concept is characterized by pure tone resonance mode and a well-defined working range (see Fig. 6b). There are several advantages:

- the energy is efficiently transformed into acoustic energy,
- the transducer is hermetically sealed and has a full metal housing and
- the bandwidth allows relatively short pulse signals.

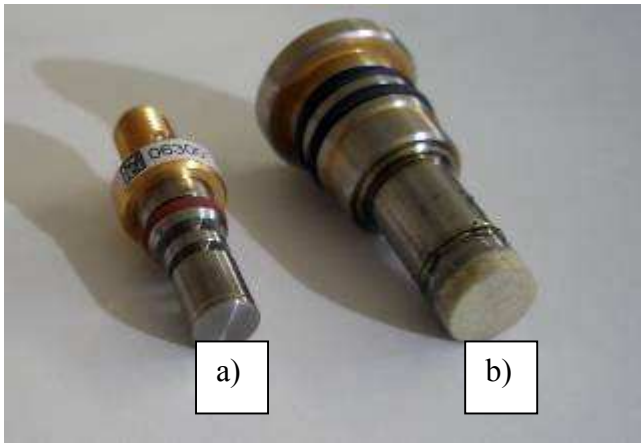

Fig. 7: Examples of the two different transducer designs
a) without and b) with the matching layer

<u>Signal Processing</u>

Generally, the SNR may be improved with the help of signal averaging methods or signal coding. However, specifically in gas flow metering applications the problem is that the signal path is modulated due to turbulence in the flowing gas. This limits the efficiency of the averaging and encoding methods. According to the signal theory, correlation methods provide optimum results in signal transit time measurements, but they cause great computational load during the digital signal processing.

If the SNR falls below a minimum threshold defined by the signal processing algorithm, faulty measurements of the signal transit time may occur. This must be prevented through adequate monitoring and analysis of the received signal quality, otherwise significant measuring errors of the gas velocity would occur.

3 NOISE-INSENSITIVE DESIGN OF ULTRASONIC GAS FLOW METERS

Based on the previous general explanations, optimization criteria applicable to ultrasonic gas flow meters near pressure regulators can easily be derived:

1. Selection of ultrasonic sensors with a working frequency which is as high as possible because
    - the noise signals emitted by the pressure regulator are significantly weakened at frequencies greater than 100 kHz;
    - the frequency-dependent attenuation of the noise signals at a given distance to the pressure regulator causes lower noise levels compared with lower frequencies.
2. Selection of ultrasonic sensors which work within a very defined frequency range which minimizes the collection of undesired noise signal components.
3. Selection of a suitable path layout in order to ensure a maximum ultrasonic burst signal level.
4. Selection of a signal processing method which
    - makes only minimum demands on the required SNR;
    - securely avoids faulty triggering and thus prevents biased measuring results.

The aforementioned requirements have been considered in the development of a noise-insensitive ultrasonic gas flow meter (FLOWSIC600) tested in this paper. The ultrasonic transducers mounted in the meter are stacked type transducers, which work according to the thickness vibration principle, and are available with working frequencies of 210 kHz and 350 kHz (Fig. 9). The path layout is the chordal direct path design with four independent paths which are configured in parallel in one plane (see Fig. 8) so as to cover the entire cross-section of the pipe. This layout also boasts the advantage that it is very insensitive to turbulent flow profiles.

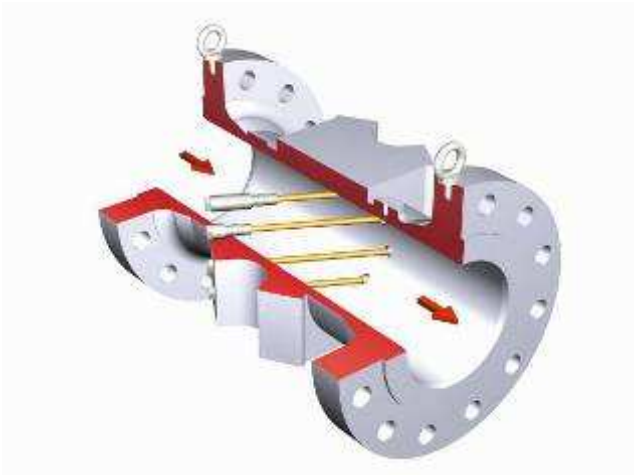

Fig. 8: Chordal 4-path layout of the FLOWSIC600

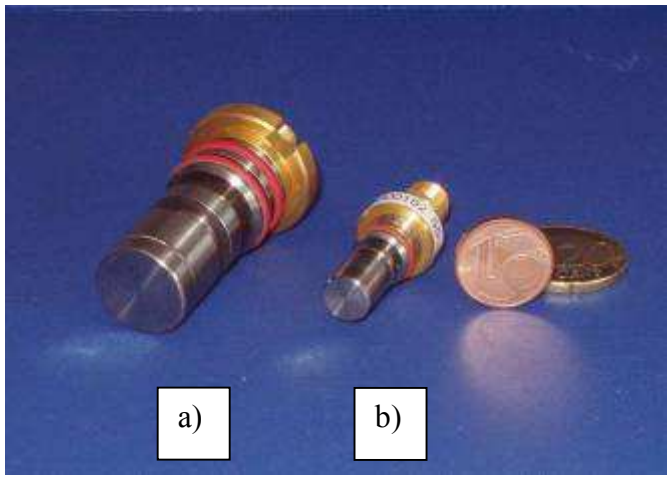

Fig. 9: High performance ultrasonic transducer, a)210 kHz and b) 350 kHz

Further robustness is achieved by the signal processing technology in the investigated ultrasonic gas flow meter. A model-based correlation method is used in combination with several plausibility criteria, so that even at a minimum SNR of just 6 dB the position of the ultrasonic signal burst is clearly detected in the received signal, see Fig. 10.

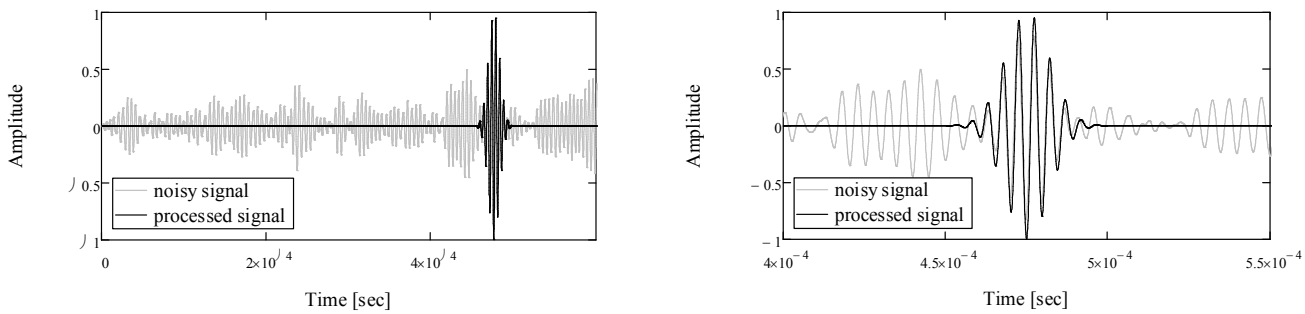

a) noisy signal at SNR = 6 dB

b) zoomed detail showing the ultrasonic burst

Fig. 10: Signal processing in the FLOWSIC 600 with the example of a noisy signal reception (SNR = 6 dB)

In the received signal, the signal processing algorithm determines the signal portion which comes closest to the signal model. Thanks to an extensive plausibility check, it can be ensured that the measured value is correct even at a performance of as low as 5 % (i.e. 95 out of 100 received signals had to be rejected). The signal is evaluated with respect to:

- the position in a time frame (not too early or too late)
- the amplitude (not too small or overloaded)
- the SNR (above the minimum required level) and
- the degree of congruence with the model signal

Only if all of these criteria are met, will a threefold transit time calculation be conducted according to different criteria in the signal. At least two of the three calculated transit times must be identical for the result to be validated.

4 RESULTS

This chapter presents results obtained from tests on the high-pressure test rig of E.ON Ruhrgas in Lintorf and at an M&R station. On the high-pressure test rig, the already proven 210 kHz sensors were directly compared with the newly developed 350 kHz sensors under near-field conditions. At an M&R station, a FLOWSIC600 fitted with 210 kHz sensors was tested under most extreme conditions for a regulator installed downstream of a flow meter.

4.1 210 KHZ SENSORS VS. 350 KHZ SENSORS TESTED AT THE LINTORF FACILITY

E.ON Ruhrgas operates a high-pressure test facility used for testing and optimizing bulk gas metering instruments. While the pigsar™ test rig [6] of E.ON Ruhrgas is used for high-precision calibration and verification of meters with natural gas under high pressure, the Lintorf facility [7] serves to

- test new measurement instruments under near-field conditions,
- investigate special factors influencing measurement behavior,
- optimize measurement instruments and other components,
- solve operational problems,
- examine new measurement technologies.

The test facility is shown in Fig. 11.

Fig. 11: Lintorf test facility

The configuration of the test facility is shown in Fig. 12. The pressure is controlled at the inlet to the test facility while the desired volume flow can be adjusted at the outlet using a flow control valve. The working standards (test rig standards) used are five parallel meter runs, four of which are orifice plate meter runs (DN 200) built according to ISO 5167 and calibrated with high accuracy. The other is a DN 150 meter run fitted with a turbine meter and an ultrasonic meter. The working standards provide reference values for the meters and

pressure regulators to be tested. A turbine flow meter (DN 300), which is permanently installed upstream of the working standards, and an ultrasonic flow meter (DN 300) permanently installed downstream of the test run are used for investigating long-term stability and for quality control purposes. The technical data are summarized in Table 1.

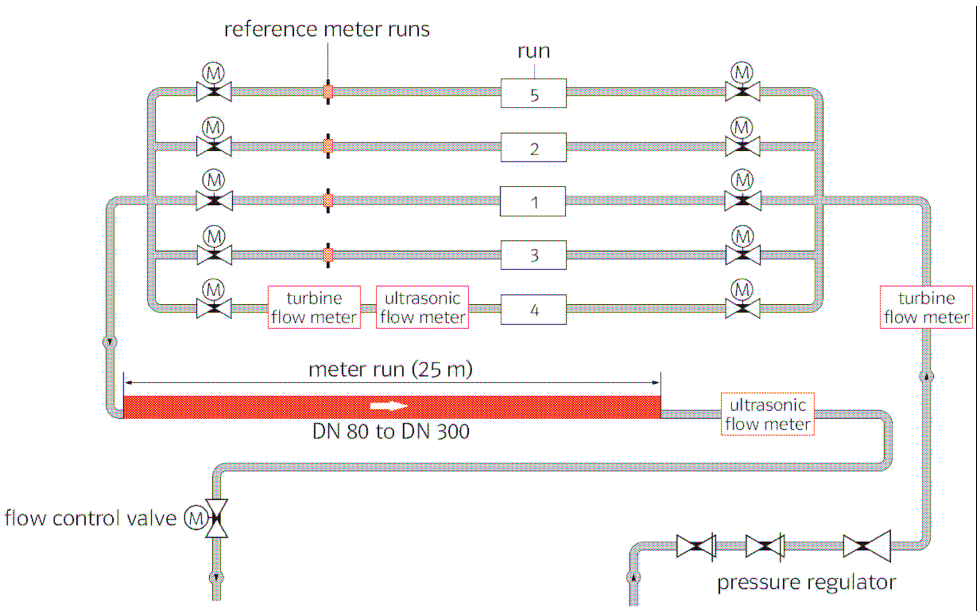

Fig. 12: Configuration of Lintorf test facility

Table 1: Technical data of Lintorf test facility

Flow range	100 m^3(N)/hr to 100,000 m^3(N)/hr
Pressure range	10 bar to 40 bar
Test gas	low-calorific natural gas (from the Netherlands)
Sizes	DN 80 to DN 300
Length of meter run	25 m
Working standards	orifice plates (calibrated individually), turbine and ultrasonic flow meters
Total uncertainty of measurement	0.3 %
Repeatability and reproducibility	0.1 %

4.2 TEST RESULTS FROM LINTORF TEST FACILITY

On the test rig, a regulator of RMG was installed upstream of the 8-inch ultrasonic meter tested. The distance between the regulator and ultrasonic meter was 15D. The regulator used was fitted with a sound damper to reduce audible sound. This regulator is normally always fitted with a sound damper. Fig. 13a) shows the regulator without sound damper and

Fig. 13b) with sound damper. For test purposes, the systems were examined both with and without sound damper.

In the case of the ultrasonic meter tested (see Fig. 13c)) two independent systems were installed in one housing. The measurements were made with a four-path 210 kHz sensor system as well as with a four-path 350 kHz sensor system. The tests with the 350 kHz system were completely independent of the 210 kHz system tests to allow direct comparison of the two systems. Basically, two systems are installed in one housing to ensure identical test conditions. The path configurations of the two systems are presented in Fig. 13d).

a) Regulator without sound damper

b) Regulator with sound damper

c) Ultrasonic meter tested

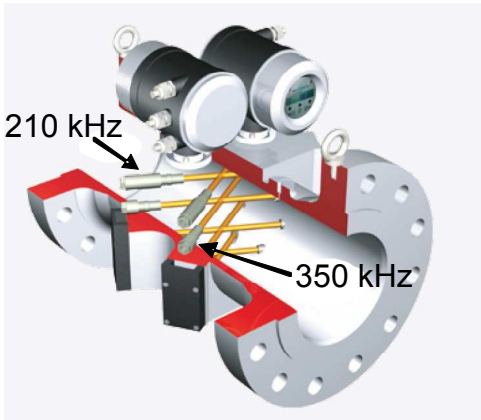

d) 210 kHz and 350 kHz systems

Fig. 13: Test set-up at Lintorf facility

Fig. 14 describes the basic findings for the 210 kHz and 350 kHz systems (both systems were not calibrated before testing) with a non-disturbed upstream straight length of 66D. The regulator was not installed in the test run in this case. The measurement deviation is very low for system 1. The deviation for system 2 is approx. -0.5% and remains virtually constant over the entire flow range.

It is known from previous tests that a regulator installed upstream of an ultrasonic meter affects the meter more strongly than a downstream regulator. The tests described in this paper only focused on the less favorable case where the regulator is installed at a distance of 15D upstream of the meter. The effects on the ultrasonic meter were examined for different pressure differentials across the regulator, absolute pressures and flow rates.

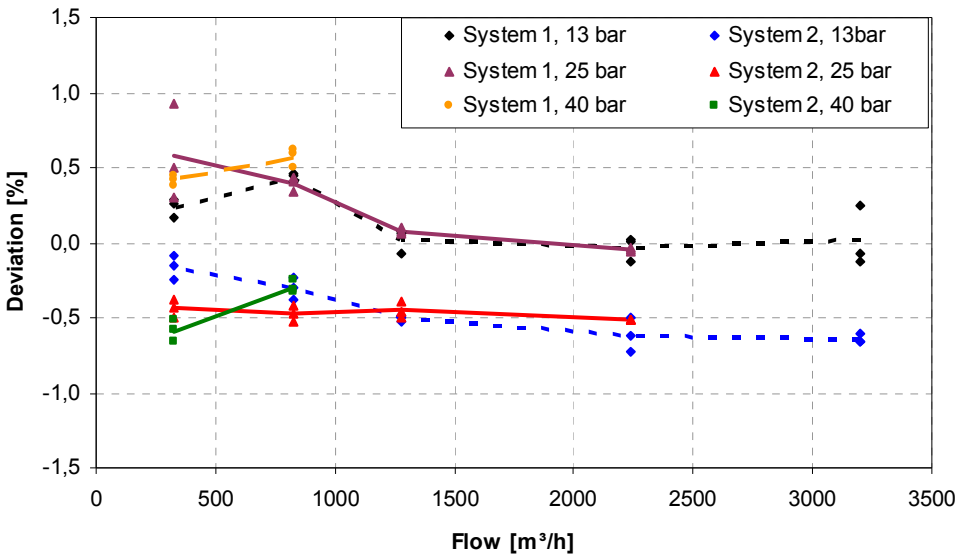

Fig. 14: Basic findings with 60D undisturbed upstream straight length (system 1: 210 kHz sensors, system 2: 350 kHz sensors)

In a first step, the regulator was installed together with the associated sound damper. The interfering effects can be very well evaluated based on the SNR. Fig. 15 directly compares the SNRs of the two systems for a pressure reduction from 40 bar to 10 bar across the regulator. It is obvious that the 350 kHz sensors are significantly less sensitive to the interfering sound emitted by the regulator than the 210 kHz sensors. With this high decrease in pressure and the extreme flow velocities (> 25 m/s), the conventional sensor system (210 kHz) is already at its stability limits. The meter did not fail but operation of the configuration tested in a situation where the pressure loss is so extreme should be limited to maximum flow velocities of 20 .. 25 m/s.

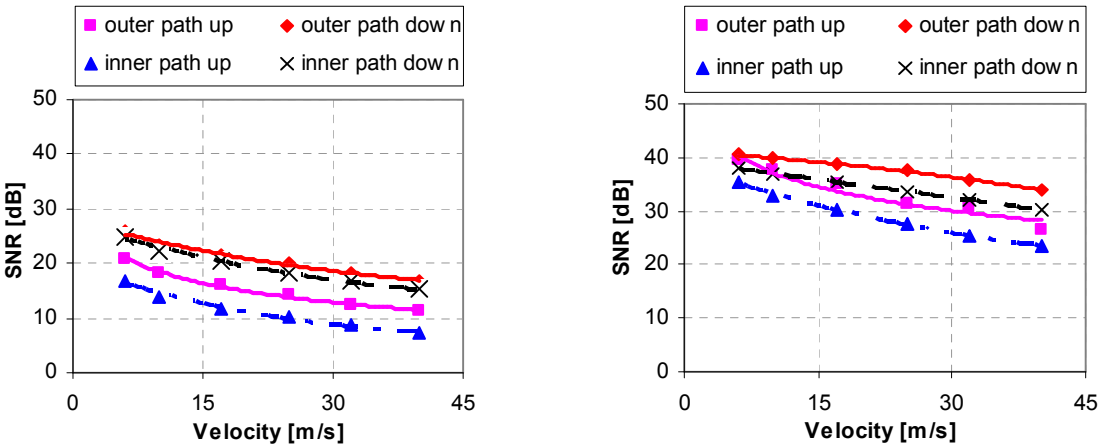

a) 210 kHz system b) 350 kHz system

Fig. 15: SNR as a function of velocity for a pressure reduction from 40 bar to 10 bar across a regulator with sound damper

While they are influenced by the noise emitted by the regulator, the 350 kHz sensor signals are still sufficiently strong with respect to the SNR. It would be possible to use the meter for this extreme pressure reduction and the high flow rates in the configuration tested without

further measures such as sound attenuation being required. The measurement error was within ± 0.5 % for both systems. As the 350 kHz sensors were prototypes, the tests focused on sensitivity to interfering noise rather than on measurement accuracy at this stage of development.

The results plotted in Fig. 15 were obtained for the greatest pressure differential across the regulator that was feasible on the test rig (10 bar to 40 bar test pressure). No further tests were made for this configuration as the results obtained were good and the 350 kHz sensor system proved robust to interfering noise and was sufficiently strong under most extreme conditions.

The following figure presents results for the regulator with the sound damper removed. It should be noted in this context that the regulator is normally always used with a sound damper. The tests were made to determine the limits of the 350 kHz sensors. The system with the 210 kHz sensors already failed in these tests at low flow rates and pressure differentials across the regulator from Δp 10 bar. With the 350 kHz system, the meter did not fail until higher flow rates were set. Some results are shown in the following as examples.

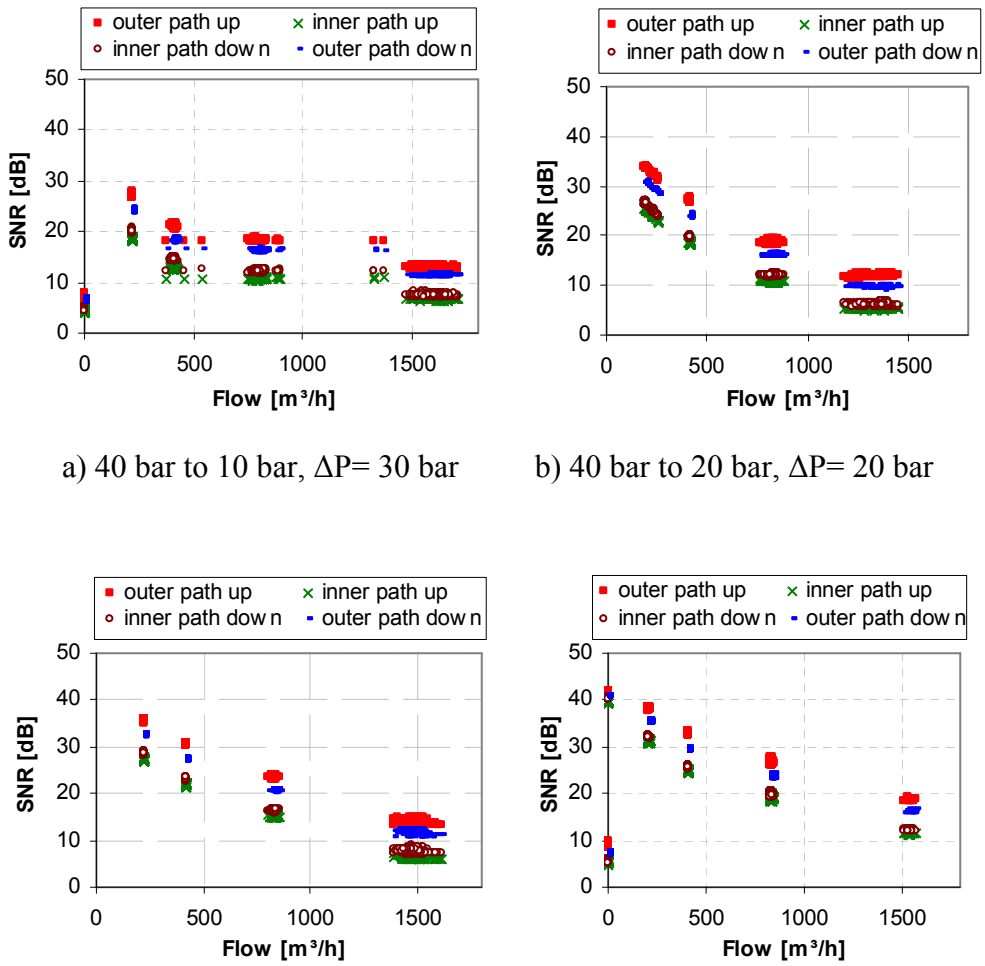

a) 40 bar to 10 bar, ΔP= 30 bar

b) 40 bar to 20 bar, ΔP= 20 bar

c) 40 bar to 25 bar, ΔP= 15 bar

d) 25 bar to 10 bar, ΔP= 15 bar

Fig. 16: SNR over flow for 350 kHz system at different pressure differentials across the regulator

It would not be possible to use the meter in this configuration without sound damper for the operating parameters tested here. It is also obvious that the 350 kHz sensors are a significant improvement compared to the 210 kHz sensors. Fig. 16 shows how the ultrasonic meter is influenced by flow rate, pressure differential and absolute pressure. The SNR falls, though with a decreasing gradient, as flow rate increases. It is also clear from Fig. 16a), Fig. 16b) and Fig. 16c) that the influencing effect is only slightly stronger for higher pressure differentials. Fig. 16c) and Fig. 16d) plot the results for a constant pressure differential of 15 bar and different absolute pressures. The influencing effect is stronger in this case for higher pressures (40 bar to 25 bar) than for lower pressures (25 bar to 10 bar) at the same pressure differential of ΔP=15 bar. Testing at low absolute pressures and extrapolation of the results to higher pressures is considered critical.

4.3 USE OF A FLOWSIC600 IN AN M&R STATION

In an M&R station, a FLOWSIC600 ultrasonic gas meter with standard sensors (210 kHz) was installed near a regulator. The risk was that the pressure regulator would produce noise interfering with the ultrasonic meter because of the very high flow velocities and pressure differentials across the regulator. To investigate the matter, some tests were made in a station. The meter run configuration is shown in Fig. 17.

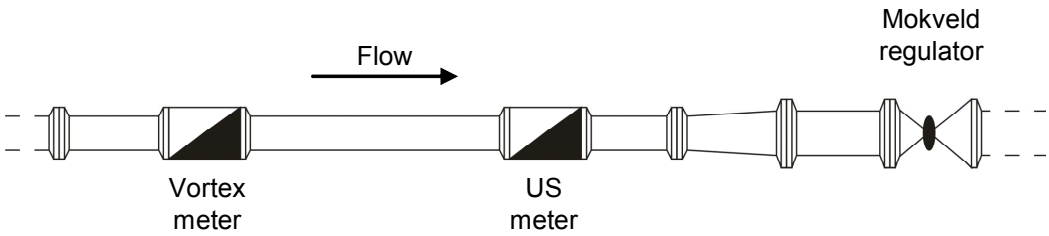

Fig. 17: Meter run configuration

The ultrasonic meter used had a nominal width of 16-inch and the downstream regulator a nominal width of 20-inch. A flow rate of up to 500,000 m³(n)/h may be set for the meter run at a pressure of 50 bar to 85 bar and a pressure reduction across the regulator of 0 bar to 30 bar.

Several flow rates and pressure differentials across the regulator were set for the tests. The deviation between the vortex meter and the ultrasonic meter was measured. The diagnosis parameters of the ultrasonic meter were also recorded to be able to better analyse the influencing effect of the regulator on the ultrasonic meter. In this context, the parameters

- relative number of faulty signals (performance) and
- calculated signal-to-noise ratio (SNR)

proved very useful for determining and assessing regulator influence.

An acoustic broadband pressure sensor was installed between the regulator and the ultrasonic meter to measure the noise in the gas line. Fig. 18 plots the frequency spectrum of the noise measured. The graph shows the results for higher pressure differentials from 23 bar to 30 bar and for various flow velocities. It can be seen from the graph that flow velocity has a significant effect on the noise level produced by the regulator. In the frequency range of the 210 kHz ultrasonic meter sensors the interfering noise measured is between 128 dB and

136 dB. Fig. 19 presents the SNRs obtained from the tests made. The log files were analyzed for each measurement point.

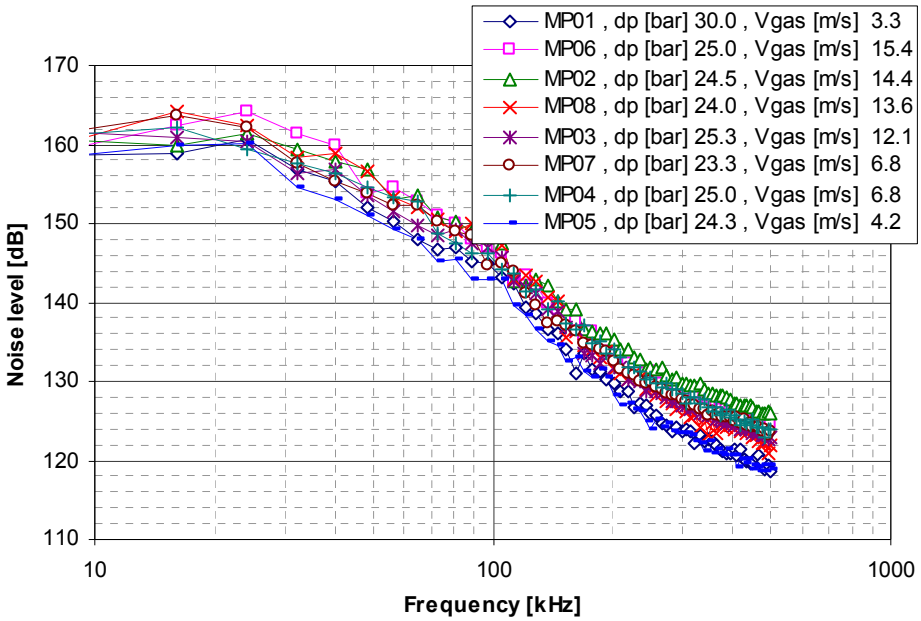

Fig. 18: Noise Level

From the diagnosis data, the lowest SNR of the four paths was selected and presented. Average meter performance was 98% .. 100% for all flow rates and pressure differentials tested.

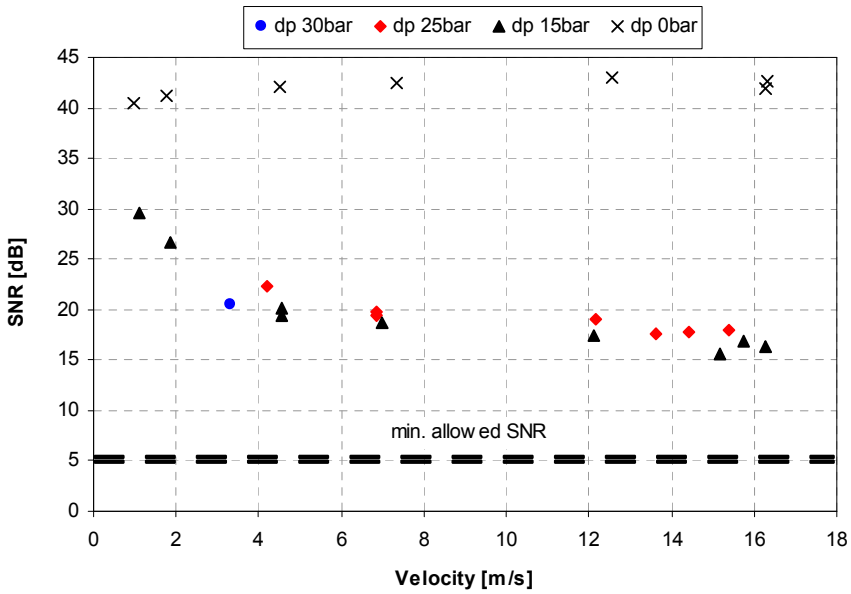

Fig. 19: SNR of ultrasonic meter

As can be seen from Fig. 19, the SNR is above 40 dB for a 0 bar pressure differential across the regulator. While the meter is influenced by pressure differentials across the regulator, the

distance to the critical 5 dB level is still sufficient to ensure reliable measurements even for the extreme conditions tested here. It is also obvious that the effect of flow velocity at constant pressure differentials on the SNR and thus on meter performance increases, though with a decreasing curve gradient, as velocity increases.

Fig. 20 shows the deviation between the vortex meter and ultrasonic meter. The ultrasonic meter was not high pressure-tested before the tests. The results are therefore very satisfactory. With the positive results obtained, the ultrasonic meter was calibrated on the pigsar™ and used in the M&R station.

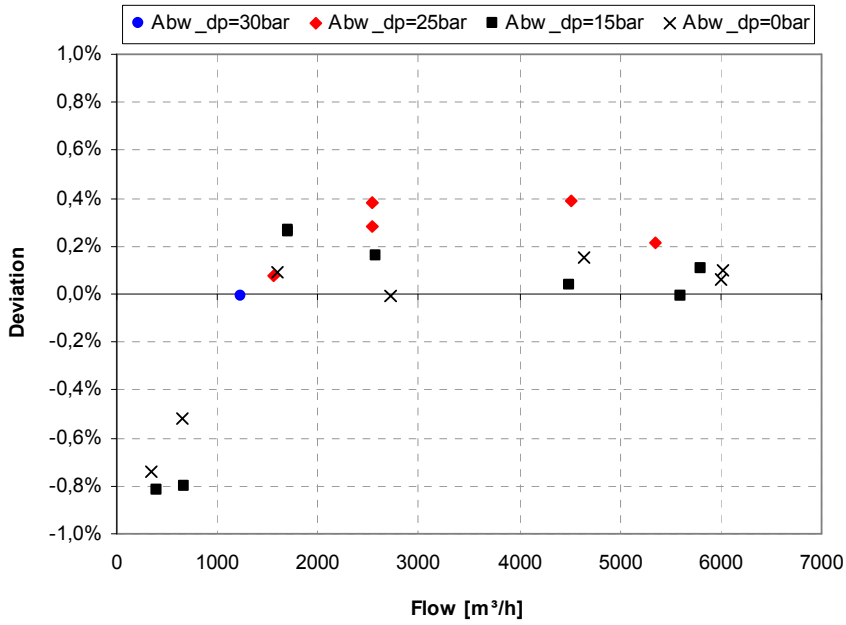

Fig. 20: Deviation between ultrasonic and vortex meters

5 CONCLUSION AND OUTLOOK

This paper presents the relationship between interfering noise emitted by a regulator and an ultrasonic meter. Theoretic considerations describe how an ultrasonic meter is influenced by interfering noise. Aside from theoretic considerations, the paper includes results from both tests in the field and on a test rig. The results define the limits of the application and show that good results were obtained from the field test even under most extreme conditions.

Different regulators have different characteristics with respect to interfering noise emission, in particular in the ultrasonic range (100 kHz .. 400 kHz of interest here) so prior to system design the following should be considered

- The interfering effects of a regulator and potential noise should be determined.
- Different regulators / control valves or the same valves with different trims will generate different noise spectrums. The results contained in this paper only apply to the regulator examined here and the FLOWSIC600.
- The tests did not examine in how far nominal pipe width is important but from theory it can be expected.

The tests focused on the more critical application where the regulator is installed upstream of the meter. Under these conditions, the meter reached its limits. But, compared to the proven 210 kHz sensors, the newly developed 350 kHz sensors again considerably improved the meter's robustness to interfering noise in the pipelines and good results were obtained under the extreme conditions tested. The 350 kHz system did not reach its limits until it was installed and tested with the modified regulator. For this the built-in sound damper was removed. But this situation is not to be expected for practical operations as the regulator is normally always used in standard configuration. The tests show that the FLOWIC600 may be used in installation configurations that have not been possible using traditional ultrasonic technology.

The 350 kHz sensors will be optimized further and again tested on the Lintorf test rig. The solution with the 350 kHz sensors is an attractive alternative to the use of noise-reducing devices such as sound dampers, flow straighteners or complex piping. Development work will therefore be continued.

6 REFERENCES

[1] Warner K., Zanker K., "Noise Reduction in Ultrasonic Gas Flow Measurement", 4th International Symposium on Fluid Flow Measurement, Denver, Colorado USA, 1999

[2] Müller G., Möser M., "Taschenbuch der Technischen Akustik", published by Springer, 2003

[3] ISO/CD 17089, "Measurement of flow in closed conduits – ultrasonic meters for gas; meters for custody transfer and allocation measurement"

[4] www.koetter-consulting.com

[5] Smørgrav et al., "Developments Of Transducer Technology And Reciprocity In Ultrasonic Flow Meters", 5th International South East Asia Hydrocarbon Flow Measurement Workshop, 2006

[6] pigsar™, high-pressure test facility and national standard for natural gas in Germany, www.pigsar.de

[7] High-pressure test facility of E.ON Ruhrgas in Lintorf, www.eon-ruhrgas.com

EuroLoop: Metrological concepts for efficient calibrations and primary realization of accurate reference values in flow

Mijndert P. van der Beek
Netherlands Measurement institute, dept. VSL-Flow/www.nmi.nl
Mvanderbeek@nmi.nl

Abstract

In a previous introductory paper [1], the ranges, possibilities and operation practice of the new calibration facilities for Natural Gas and several Oil products in Europe, are depicted.
The stringent claim on CMC or 'Calibration and Measurement Capability' is the driving force for criteria set for process stability, day-to-day reproducibility, long-term behavior of working standards and finally accuracy of the international linked reference value at the position of the device under test. The superb CMC claims imply highest demands in innovative designing.
This paper focuses on a 'metrological engineering' concept in which via an iterative process a balance is found between: optimal piping configuration, smallest uncertainties, sustainable traceability maintenance at one side and effective operation, lowest operational and capital expenses on the other.
The International traceability of the Hydro Carbon calibration facility (HyCal) will be realized by unique piston provers covering a range up to 5000 m^3/h. Theoretic and empirical correction methods will be avoided and most 'sensitive' parameters will be determined on the spot to increase credibility of estimated uncertainty sources. For instance, e.g. seal leakage, line-pack effects, diameter change will be measured and processed.
International acceptability of these rather small uncertainties will increase when uncertainty estimations are supported by 'on scale demonstration of auxiliary instrument performance' therefore a significant set of tests is scheduled in the near future.
The design of the intelligent piston will be shown as well as simulations of the piston behavior related to pump performance, inertia's, control characteristics of valves etc.
The primary realization will be intrinsic in the piston prover itself and changes of the reference volumes due to pressure, temperature and oil movement will be measured on line.
Traceability of the HP Gas Calibration laboratory will be based upon a Gas Oil Piston Prover and the Dutch-German-French Harmonized Reference Value. The prover was built in 2001 together with a multiplier and carrier of reference values, embodying the new traceability chain. The paper also focuses on the methods and steps to validate and certify such large Natural Gas calibration loop. In due coarse, the public will be informed regularly through series publications.

INTRODUCTION

In the past decade it became clear that the need for test facilities that offer primary standards for large flows in the oil and gas working field is still expanding. New metering principles like Ultrasonic-, Coriolis, Clamp-on US and pipe wall vibration sensing principles seem to always need at least one or repeated validation measurements somewhere in the life-cycle of the instrument, even when manufacturers claim the 'dry-calibration is sufficient' philosophy. The economics of valuable goods on the 'downstream oil and gas side' demands smaller uncertainties and comparable reference values between buyers and sellers (third party access..). For the 'upstream side' the demand focuses upon

behavior of instruments, higher MTBF, smaller pressure drops, reliability and scaling of meter behavior at difficult process conditions. NMi has been working over 40 years in the field of large flow HP Gas and intermediate flow hydrocarbons and water for the up- and downstream fields. Round the millennium, manufacturers and end-users communicated concerns about the security of supply of the popular large gas test facilities of 'Bergum' (due to the discontinuous 'gas-sink': the electricity plant) and 'Westerbork' of Gasunie (due to seasonal restrictions) and the lack of test facilities for large hydrocarbon flows with several viscosities in Europe. NMi's answer to that challenge is found in 'EuroLoop': one multiple large flow calibration and test facility offered to the up- and downstream oil and gas field, operational in 2008 (HyCal) and 2009 (GasCal).

What is 'EuroLoop'?
EuroLoop is a 'Center for flow technology' and a 'European facility for testing under industrial conditions'. It is located in the harbors of Rotterdam, close to refineries and a broad infrastructure.
The separate facilities are distinguished in three sections:

1) 'HyCal', Hydrocarbon Calibration facility;
2) 'GasCal', Gas Calibration facility;
3) 'GasSep', Gas Separation test facility (which details will be presented in another publication).

The facilities are partially owned/partially rented by NMi. NMi will be responsible for the operational management, plant facilities, marketing and order intake and planning, service, metrological status and -maintenance. This modus of operandi was chosen to certain the three 'Cornerstones' of a National Metrology Institute: absolute independency, -impartiality and -integrity.
Obviously, putting the three facilities together at one site, optimal synergy in client- and operation facilitation is obtained.

Overview of the ranges:

HyCal: Calibration facilities for Oil and Oil products

Overview of specs:

Type	Closed circuit, master meter method and provering method
Flow	10 – 5000 m^3/h
Line sizes	4" – 24"
Traceability	Piston prover, on-line geometric
Medium	several oil products
Viscosity	1, 10, 100 cSt (1200 cSt)
Piston Provers	2 (40 meters long, $U_{k=2} \leq 0.02\%$)
Master Meters	18 ($U_{k=2} < 0.05\%$)
Temperature stability	better than 0.5 ^oC
Line pressure	Up to 10 bara
Line temperature	19 – 35 ^oC (freely adjustable)
Number of test runs	6 (2 per test liquid, simultaneous operation of six metering runs possible)
Capacity	600 calibrations per year

GasCal: Calibration facilities for Low to High pressure Natural Gas

Overview of specs:

Type	Closed circuit, master meter method
Flow	5 – 30 000 m^3/h at working pressure
	5 – 1 800 000 m_0^3/h equivalent atmospheric conditions
Line sizes	2" - 30"
Medium	Air, Natural Gas, CO_2, variable mixtures (like H_2/CH_4 in the future)
Traceability ladder	Gas Oil Piston Prover and step up flow
Line pressure	1 – 78 bara (freely adjustable)
Line temperature	5 – 35 ^oC (freely adjustable)
Uncertainty	better than 0.20%, 0.15% typical, 0.10% possible (k=2)
Temperature stability	better than 0.05 ^oC
Pressure stability	better than 5 mbar
Number of test runs	5
Capacity	800 – 1500 calibrations per year

Metrological designing

The design process that is used in EuroLoop is shown in a simplified flowchart in Figure 1.
The main feedback loops are:

- Metrologic (re) designing, an iterative process of innovative thinking, feasibility study of uncertainty claim, conservative estimation of uncertainty budgets;
- Front-end engineering, Process and instrumentation diagrams, calculation of operating points, defining rotation equipment, heat exchangers, and other critical equipment (long lead items);
- Capital Expenses calculation, decision point whether to simplify the design, to accept a higher CMC or to find extra funding;
- Detail engineering with process simulations to prevent from process instabilities leading to lower reproducibility of the measurements;
- Realization, commissioning and fine tuning;
- Commissioning, 1st calibration, certification and acceptance;

The grand loop at the right side (Metrological acceptance procedure) is also dependent on international acceptance which can only be achieved after participation in one or more 'Key Comparison programms' organized by the BIPM, the ultimate 'examination board' for National Measurement Institutes.

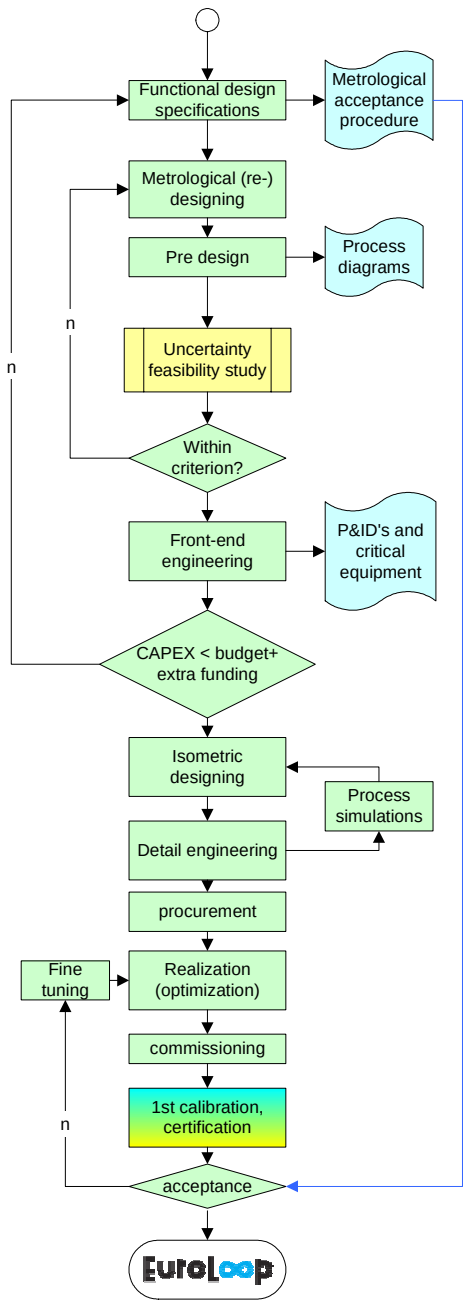

Figure 1: Euroloop Flowchart

Feasibility study claimed Calibration and Measurement Capability

As depicted in the previous section, the feasibility study of uncertainty budgets is crucial to prevent from disappointments or to put lost efforts in parameters that does hardly play a role and vice versa.
In this example, the uncertainty analyses of the HyCal facility is given as an example because related to GasCal in HyCal, more innovations had to be examined. In the modeling phase, the departure point is the mass balance that in all cases will remain stable during the measurement process (‘quasi stationary flow’).
The main dependencies are:

A) Provers’ displaced reference liquid volume is related to:

- Length between switches (base travel length of the piston);
- Average Diameter of the prover (base area);
- Prover wall temperature (expansion of the prover due to temperature);
- Mixed cup temperature of the liquid between the switch sensors (density of the liquid);
- Gauge pressure in the prover (expansion of the prover cylinder due to pressure);
- Absolute pressure inside the prover (compression of the liquid and thus density);
- Prover wall gauge (expansion of the cylinder area);
- Young’s modulus (elasticity of the wall material);
- Cubic expansion factor of prover material (temperature) ;
- Cubic expansion factor of liquid;
- Compressibility factor of the liquid.

B) The base volume determined at the reference point of the meter under test is related to:

- Temperature change in the dead volumes between piston prover and DuT during test run;
- Mixed cup temperature at the reference point of the DuT;
- Leakage between DuT and prover (e.g. through piston sealing);
- Geometry of the pipe length, -diameter, -wall gauge (elasticity and thermal expansion during test);

Some aspects like vapor bubbles inside the system will cause extra line pack effects due to instable process pressure ‘in- and expiration’ effects that are hardly calculable. It is of crucial importance to keep this amount of uncontrolled vapor as small as possible for it will lead to a decrease in repeatability.
The basics of uncertainty analyses read like:

$U = \sqrt{\sum_{par=1}^{par=n} \left(\frac{\delta V_{ref}}{\delta x} * \Delta x\right)^2}$, in other words: the effect of each individual parameter on the final uncertainty in reference volume (at the reference point of the DuT) is the square root sum of all individual contributions. The sensitivity factors are determined either analytical or numerical. For complicated models, often the numerical method is used and is presented in table 1

The sensitivity factors $\frac{\delta V_{ref}}{\delta x}$ are shown in the table as a percentage of Volume equivalence for easy comparison and to get a feeling which parameter is significant and which is not.

In this example, the small prover design is scrutinized on uncertainty budgets and crucial parameters can be appointed and further optimized if needed.

Parameter	value	unit	uncertainty (k=2) dX	unit	sensitivity factor	uncertainty in volume (k=2)	Impact on Vref %
					% / dX	%	
						0.017	100.0
Length between switches	20	m	0.002	m	5.000E+00	0.010	33.1
Diameter prover	0.564	m	0.0000123	m	3.546E+02	0.0044	6.3
Q operation	1200	m3/h					0.0
E mod	2.00E+11	kPa	2.00E+10	kPa	-1.283E-14	-0.00026	0.0
Wall gauge	0.05	m	0.2	mm	-1.128E-02	-0.002	1.7
Operation pressure	500000	Pa	1000	Pa	9.106E-08	0.0000911	0.0
Rho ref	800	kg/m3	2	kg/m3	-1.238E-04	-0.00025	0.0
Cub exp prover gamma	2.23E-05	C-1	2.23E-06	C^-1	1.360E+00	0.000003	0.0
T prover	15.00	C	0.10	C	-9.038E-02	-0.009	27.0
Pressure dead vol @ time 1	400000	Pa	1000	Pa	-1.119E-07	-0.00011	0.0
Press rise/min	500	Pa					0.0
Pressure dead vol @ time 2	400125	Pa	1000	Pa	1.119E-07	0.00011	0.0
T dead vol @ time 1	18	C	0.1	C	9.922E-02	0.002	1.6
dT dead volume netto			0.02	C			
Temp rise/ min	0.05	C/min					0.0
T dead vol @ time 2	18.01	C	0.02	C	-9.922E-02	-0.002	1.6
Dia connectionpipe	0.3048	m	0.005	m	-8.100E-03	-0.000041	0.0
Length connect pipe	**75**	m	1	m	-1.634E-05	-0.000016	0.0
Wall thickness dead v	0.01	m	0.001	m	-1.822E-04	-0.0000002	0.0
Pressure at DuT	1.00E+05	Pa	200	Pa	-8.539E-08	-0.000017	0.0
T at DuT	15.00	C	0.10	C	9.285E-02	0.009	28.5
Repr,due to mech. instability			0.00	%	1.000E+00	0.00	0.0
Leakage			0.00	%	1.000E+00	0.00	0.0

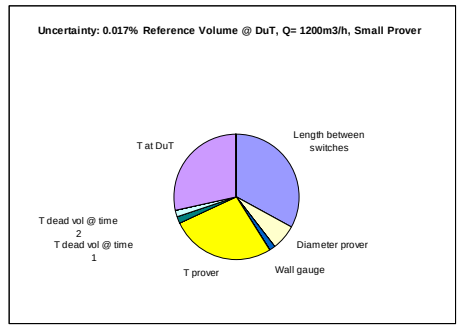

Figure 2: Impact of several uncertainty budgets

Table 1: 0.017% feasible uncertainty

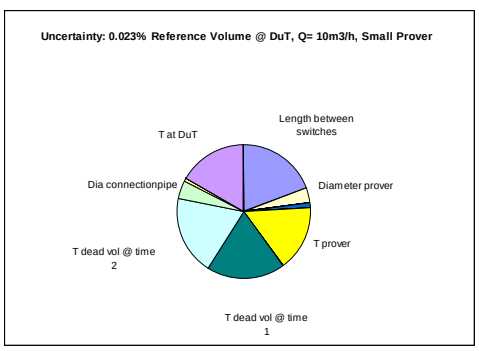

Figure 3: 'balancing' uncertainty

In the example, the feasible Best Measurement Capability of the Small prover at a flow rate of 1200 m^3/h is 0.017%
The significant parameters are apparently:
Length, diameter and the temperatures of the liquid in the prover and DuT. A remarkable fact is that the temperature measurement of the dead volumes does hardly play a role of importance. However when the flow rate is decreased to 10 m^3/h other parameters start to play a larger role like the dead volumes and every related parameter to that (temperature of dead volumes, diameter of connection pipes) and uncertainty tends to 0.023%.

What do we learn from these exercises?

1) For reaching highest accuracies, temperature effects need to be determined with small uncertainties. This is not a surprise; volume flow measurements are highly depending on temperatures as we see in gas as well as liquid metering. Temperature effects (unknown, uncorrected) often cause measurement noise.
2) It is not necessary at this stage to improve diameter accuracy ('on line diameter determination'), it won't help to improve the final uncertainty at this stage unless parameters length, and several temperature are improved first.

Note that the uncertainty budgets for reproducibility (a.o. due to axial vibration of the prover) and leakage are set to zero. See section 'Added value of an intelligent prover' for the motivation.

Such a high accuracy claim in metering 'mixed cup temperature' is this realistic for large pipes?

Temperature metrology in general is a rather strange working field. In fact measuring temperature of a substance is done by measuring the temperature of the tip of the sensor assuming that this tip is representing the representative (in liquid sometimes referred to 'mixed cup') temperature, which hardly ever will be the case. This is exactly the problem with temperature determination of large volumes, what does the profile look like?
The mixed cup temperature is defined as the temperature that would be read if the amount of passing liquid had been stirred. Mathematically it looks like:

$$T_{mixed} = \frac{2}{R^2} \int_{r=0}^{r=R} T_r \cdot r \cdot \delta r$$

Especially at the low flow rates/small turbulence (small Reynolds numbers) the temperature gradient in the liquid follows can be quite steep due to heat flow through the pipe wall via the stem of the thermo well. In the next graph, an example of a theoretical temperature profile is depicted. The study focuses on the large piston prover: Diameter prover cylinder 1.127 meter, pipe wall gauge 50 mm, ambient temperature 18°C, ambient air velocity 1 m/s, liquid temperature in center of the pipe 30 °C , flow rate 70 m^3/h and pipe insulation: 100 mm of mineral wool.

The left graph represents the cross section of the prover pipe in the temperature domain. The other graph focuses on the detail temperature profile inside the prover pipe and shows the deviation of the measured temperature related to the real liquid temperature. The temperature reference point position (sensor tips) is indicated by the red dots on the graph. The difference amounts about 0.25°C (see arrows) which would be a disaster considering the high accuracy claims.

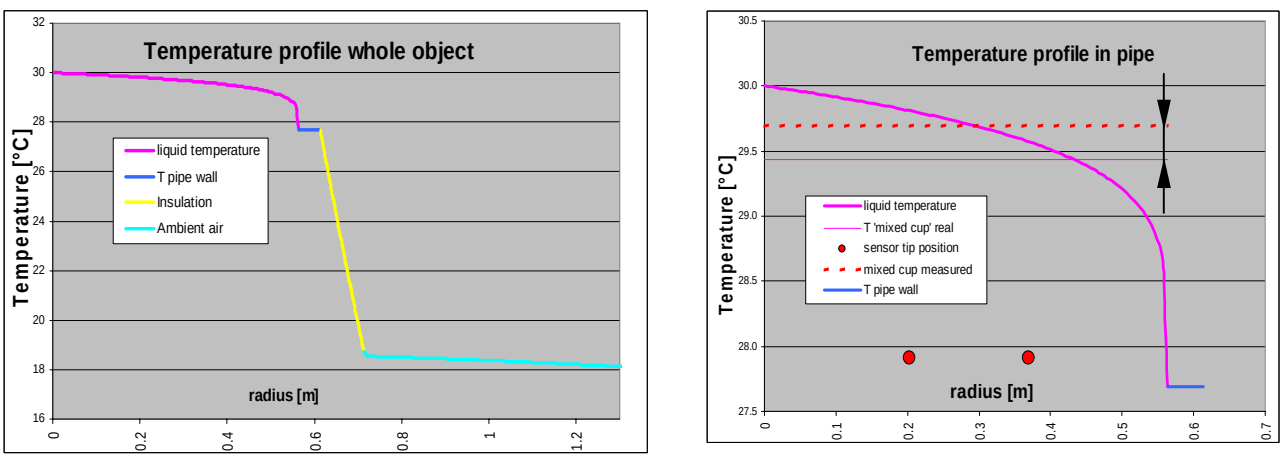

Figure 4: Temperature profiles

Fortunately the temperature profile will be less violent as in this theory, because of higher turbulence due to lots of bends in the closed circuits. However it is hard to estimate the uncertainty budget of this deviation and therefore NMi decided to put efforts in a system that could minimize these measurement deviations (See next section).

Mixed cup temperature measurement with ultrasound techniques.

In general, the speed of sound of a fluid is defined by: $c = \sqrt{\frac{B}{\rho}}$ m/s in which B is the 'Bulk modulus' or volumetric elasticity defined as: $B = \frac{\delta P}{\delta V / V}$ (reciprocal of compressibility of the fluid). In the following section, the speed of sound is presented as a function of reference density of the fluid and the mixed cup temperature.

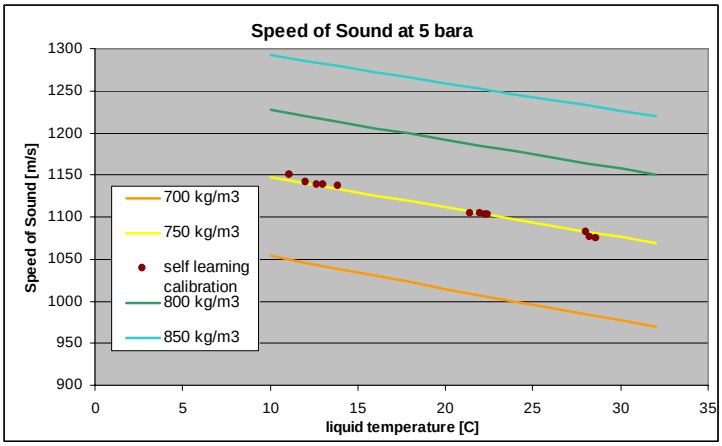

Figure 5: Speed Sound at 5 bara

The decay in speed of sound (slope) is roughly 3.5~4 m/s/°C.
For the indicated small temperature range, the relationship T=f(SoS) can be given by the linear relation: T=*a*+*b**SoS.

In HyCal, both factors *a* and *b* will be determined on site with an on line 'SoS calibrator'. The working principle is depicted in the next diagram.
It is of crucial importance to have a high resolution in the timing parameters of the ultrasound signal.

For the 1.127 diameter prover, the traveling time difference (resolution) of the ultrasound signal at a 0.01 °C temperature change of the fluid amounts 25 ns at minimum. For the small prover, the timing becomes more critical: 6 ns. Fortunately state of the art ultrasonic timing techniques offer these claims easily. In HyCal, the reference density will be stable for a certain period in time while circulated in the calibration loop. The loop will be provided with a 'self learning calibrator' to find the SoS for a given process condition (the a and b coefficients).

The SoS will be related to a high precision temperature reference standard in an on line passive thermostatic bath (see Figure 6). At the start up, factor b (slope) will be based upon literature and factor *a* ('zero shift') will be determined on the spot.

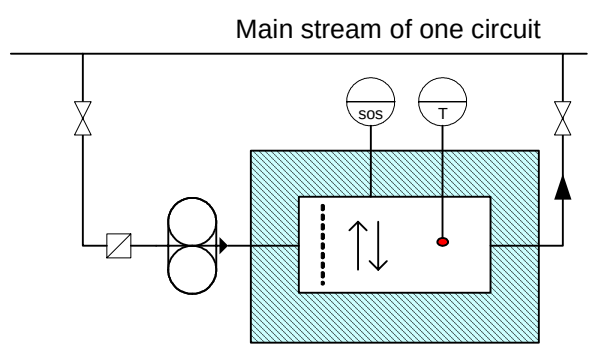

Figure 6: online T=f(SoS) calibrator

Design Details 'HyCal'

In this section, the design of the hydrocarbon liquid calibration facility 'HyCal' will be discussed.

Process flow diagram

The design consists of the following parts (see Figure 7):

- Three separate circuits (only circuit 1 has been drawn in Figure 7) for 3 types hydrocarbon liquids with viscosities in the order of 1, 10 and 100 cSt;
- A large and a small piston prover, that can be alternated to each circuit;
- Crossover headers for primary calibration enabling to put the small and large reference runs and metering runs in series;

  Per circuit:
- One small and one large reference loop (6", 10" and 16" multipath ultrasonic meters);
- Two meterruns (12"and 24");
- A set of pump trains, variable speed drives, heat exchanger, flow regulating valves each loop;
- One automatic liquid expansion/pressure control system that works also as an analyser for line pack effects.

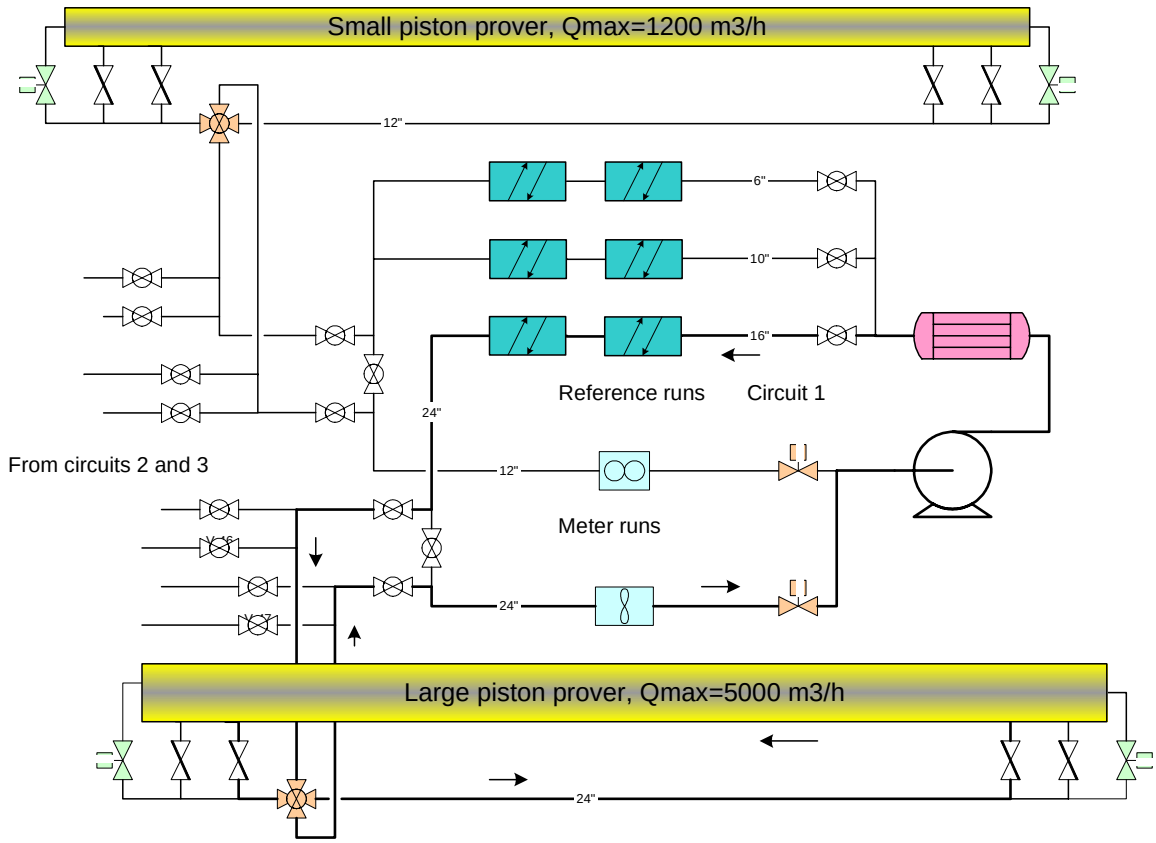

Figure 7: Simplified process flow diagram

A focus point in this design is to have all circuits connected and considering as small dead volumes as possible between DuT, reference meters and piston provers. Most globe valves are double block and bleed types for the obvious reason to prevent from the smallest internal leakage.

Piston provers
The two 40-meter long bi-directional piston provers respectively 1127 and 564 mm in diameter are provided with intelligent pistons (see below). The main challenge in the design lies in the way the pistons are to be launched and stopped at the desired position.
Extensive simulation studies have shown that three in- and outlets were needed for each of the provers to get full control over the dynamics. Furthermore, the in- and outlet grating patterns needed optimization in order to reduce pressure peaks when operating in piston launch- and decelerate modes, especially when taking water hammer into account on a prover containing almost 40 tons of liquid.

Simulation of the acceleration and the deceleration process of the pistons
The following issues were taken into account in the design process:

- The piston has to reach a steady velocity before the first 'start sensor' is reached;
- Water hammer needs to be avoided at all times;
- Cavitation needs to be avoided at all times;
- The acceleration and deceleration strokes need to be as short as possible to reduce investments on high precision pipe;
- The acceleration and deceleration strokes need to be as short as possible to reduce precious waiting time;
- The piston must have a slow speed when the end buffer is approached and a 3-point calibration of the proximity sensors can be achieved each piston stroke (see section 'intelligent piston').
- The deceleration shall be 'fail safe' e.g. when choking valves fail to close down during the run

Traceability chain, HyCal

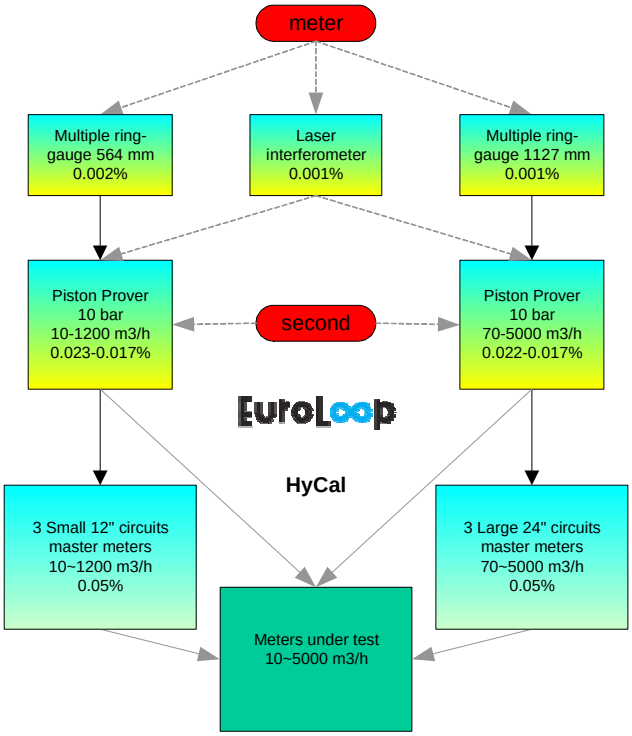

Figure 8: Traceability scheme HyCal

In the next traceability chart the dissemination of SI-units throughout the range of 'HyCal' is based upon geometric determination of reference volume by online diameter comparison of the cylinders with a multi-step ring gauge (diameter) and with a laser interferometer (length between the switches). The complete rangeability is based upon the intelligent piston provers without interference of step up TRMs or multiplier techniques. Advantage of that is:

- Transparent uncertainty analyses;
- Small uncertainties;
- Efficient full range recalibration of the master meters;
- No down times for the calibration of prover diameters.

Simulation backgrounds and results of the piston movement to assure safe and stable operation

A pre-study of the piston movement was necessary for two reasons.

- The piston must have a stable velocity before reaching the first inductive timer switch to enhance mechanical reproducibility;
- The piston must decelerate in a controlled and safe way.

The basics of the simulations were as follows:

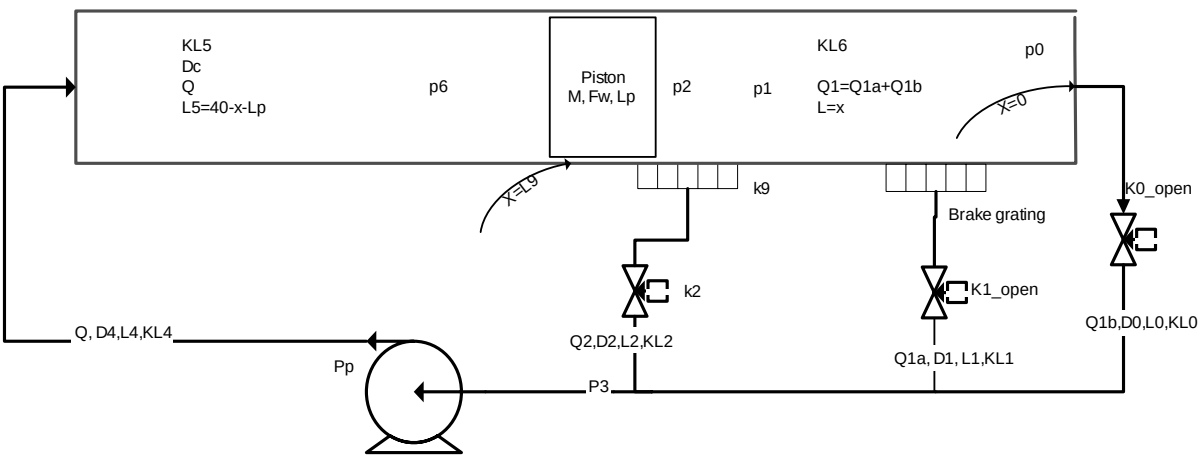

Figure 9: Simulation of the decelerating mode of the piston approaching the terminal

General:

A=Area in m^2

$$dP_{pipeline} = \xi \bullet \frac{L}{D} \bullet 1/2 \bullet \rho \bullet \frac{Q^2}{A^2} \quad \text{or simplified} \quad dP_{pipeline} = k_L \bullet Q^2$$

$$dP_{acceleration} = \frac{L}{A} \bullet \rho \bullet Q' \ (\text{with } Q' = \frac{\delta Q}{\delta \tau}) \quad \text{or simplified} \quad dP_{acceleration} = I \bullet Q'$$

Phase 1: assume Q1b=0 (valve K0 is closed) so that Q1a=Q1

$$Q = Q_1 + Q_2 = \text{Constant} \qquad (1)$$

so that

$$Q' = Q_1' + Q_2' = 0 \quad \text{therefore} \quad Q_1' = -Q_2' \qquad (2)$$

<u>Pressure relations focusing differential pressure p2-p3:</u>

counter clockwise

$$p_3 = p_2 - k_9 \bullet Q_2^2 - k_2 \bullet Q_2^2 - k_{L2} \bullet Q_2^2 - I_2 \bullet Q_2' \ \Rightarrow \ p_3 = p_2 - (k_9 + k_2 + k_{L2}) \bullet Q_2^2 - I_2 \bullet Q_2'$$

or simplified $p_3 = p_2 - X \bullet Q_2^2 - I_2 \bullet Q_2'$ (3)

clockwise $p_3 = p_2 - (k_6 + k_1 + k_{1_open} + k_{L1}) \bullet Q_1^2 - I_1 \bullet Q_1'$

or simplified $p_3 = p_2 - Y \bullet Q_1^2 - I_1 \bullet Q_1'$ (4)

from (3) and (4) $X \bullet Q_2^2 + I_2 \bullet Q'_2 = Y \bullet Q_1^2 + I_1 \bullet Q'_1$ (5)

from (5), (1) and (2): $X \bullet Q_2^2 + I_2 \bullet Q'_2 = Y \bullet (Q - Q_2)^2 - I_1 \bullet Q'_2$ (6)

leads to $(X - Y) \bullet Q_2^2 - Y \bullet Q^2 + 2 \bullet Y \bullet Q \bullet Q_2 = -(I_2 + I_1) \bullet Q'_2$ (7)

combining the constants: a=(X-Y), b= $-YQ^2$, c=2YQ and d= $-(I_2+I_1)$ (8)

=> $aQ_2^2 + b + cQ_2 = dQ'_2$ (9)

Goal is to solve Q_2 and Q'_2 for this step at time τ_n calculation.

$$Q'_2 = \frac{(Q_{2,n} - Q_{2,n-1})}{\Delta\tau} \quad (10)$$

in which $\Delta\tau$=time step per calculation and n = calculation step in progress

Because the previous calculation (n-1) is finished, $Q_{2,n-1}$ was solved and used as input.

Combining (9) and (10) leads to

$$\frac{a}{d}Q_2^2 + (\frac{c}{d} - \frac{1}{\Delta\tau})Q_2 + (\frac{b}{d} + \frac{Q_{2,n-1}}{\Delta\tau}) = 0 \quad (12)$$

From which Q_2 can be solved with the quadratic equation:

$$Q_{2,n\,(I,II)} = \frac{-(\frac{c}{d} - \frac{1}{\Delta\tau}) \pm \sqrt{(\frac{c}{d} - \frac{1}{\Delta\tau})^2 - 4\frac{a}{d}(\frac{b}{d} + \frac{Q_{2,n-1}}{\Delta\tau})}}{2\frac{a}{d}} \quad (13)$$

for the nth calculation step.

If two solutions for $Q_{2,n}$ are present, the one closest to $Q_{2,n-1}$ will be used.

Phase 2:

As soon as the piston approaches brake grating k1, k0 will be opened gradually (in the calculation.)

In normal conditions, k0 is open during the whole run to a certain degree to ascertain a maximum fixed braking flow rate and inherent piston velocity <0.1 m/s

Given: $Q_1=Q_{1A}+Q_{1B}$ (14) And $K_A \bullet \frac{Q_{1A}^2}{A_A^2} = K_B \bullet \frac{Q_{1B}^2}{A_B^2}$ (15)

from which the ratio between the two streams can be calculated:

(Assumption: $Q'_{1B}=0$) (14) and (15) leads to

$$Q_{1A} = \frac{Q_1}{1 + \frac{A_B}{A_A}\sqrt{\frac{K_A}{K_B}}} \quad \text{and} \quad Q_{1B} = \frac{Q_1}{1 + \frac{A_A}{A_B}\sqrt{\frac{K_B}{K_A}}} \quad (16)$$

<u>Position and progress of the piston:</u>

If the piston is at the left side of k9 grating: $x = x - \frac{Q}{A} \bullet \Delta\tau$

If piston on the right side of k9 grating and left side of k1 grating: $x = x - \frac{Q_1}{A} \bullet \Delta\tau$

If piston on the right side of k1 grating: $x = x - \frac{Q_{1B}}{A} \bullet \Delta\tau$

If the friction pressure of the piston (due to the seals) exceeds dP over line 1 or line 2 (dependant on position of the piston) then the piston will not move anymore (x will remain constant)

Equivalent k-factor of route 1, bypassed by bottom pipe line

The equivalent k-factor due to parallel configuration of line 1_A and 1_B that should be used in formula (4) is calculated according to:

$$K_{equivalent} = \left(\frac{A_c\sqrt{K_a}\sqrt{K_b}}{A_a\sqrt{Kb} + A_b\sqrt{K_a}}\right)^2 \qquad (17)$$

Ka = k_pipeline1 + k1(grating) + k1(valve)
Kb = k_pipeline0 + k0(grating)

Results simulated deceleration of the piston, water hammer and cavitation prevented?

The results of the simulations made clear that the wall gratings should have a smooth k-value as a function of passing ('plugging') piston. Besides possible damage of the delicate electronics inside the piston a large water hammer effect due to the intense deceleration crossing grating k9 would appear at the cylinder bottom and the piston. Secondly, the sudden flow reduction in pipeline L2 would definitely lead to cavitation (see graph below, smallest piston prover at 1200 m^3/h):

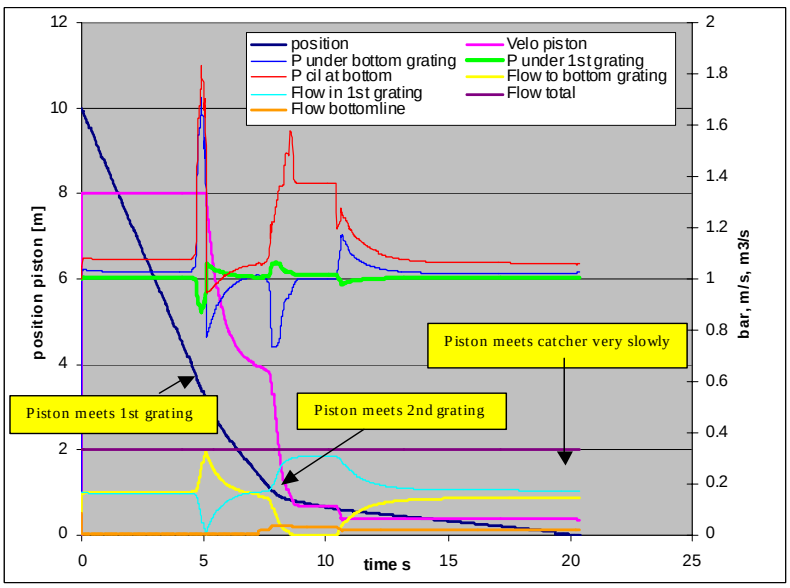

Figure 10: Simulation of the braking process of the piston inside the prover

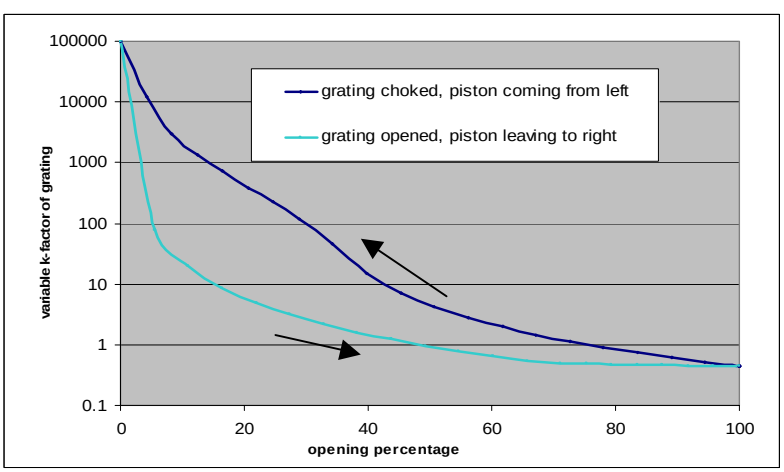

Figure 11: non symmetric grating characteristics

Transients of most important parameters at the phase where the piston approaches the two gratings (piston moves from left to right) are:

- Two small water hammer transients at 1st and 2nd block off
- Two under pressure peaks at both block offs.

These 'friendly' transients could only be achieved when the gratings were fine tuned to the process, see design in Figure 12.

Mind that the average process pressure is put at 1 bara, in operation, this pressure would be around 8 bara to avoid any cavitation, decrease volume of vapor bubbles etc.

The grating/piston (piston serves as a plug) combination is used as fail safe (hydraulic) controlled valve during the deceleration process. Interesting to see that the valve has a very asymmetric curve. The 'valve' smoothes the movement of the piston running into the right direction. As soon as the 'valve' opens again, the average flow rate will not exceed $Q_{max}/2$ and thanks to the

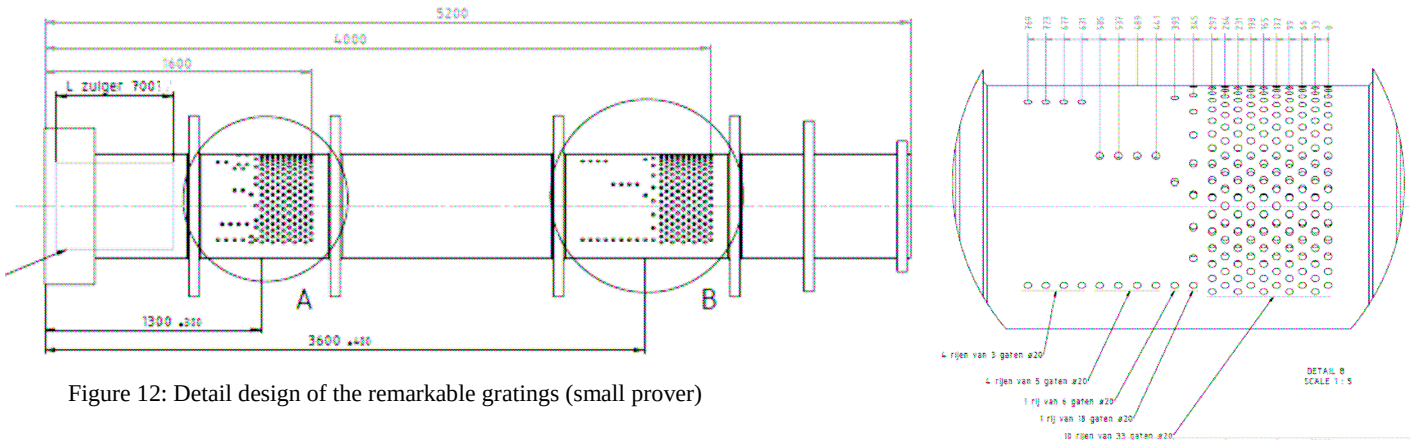

Figure 12: Detail design of the remarkable gratings (small prover)

liquid inertia in line 2, the flow builds up slowly despite the sudden ‘nasty’ opening of the grating.

Launching the piston and keeping the start-up transients under control enhancing calibration stability

The launching mode of the piston prover differs completely from the deceleration mode. In opposite to the later, launching the piston requires the following functionality:
- The stationary flow equilibrium and inherently response of the meter under test may not significantly be affected. (Deviation curve of meter under test is often very much related to actual flow rate)
- The piston should travel with a steady velocity when passing the first and successive inductive timing switches. (Enhancing the repeatability of the piston/run timing configuration)

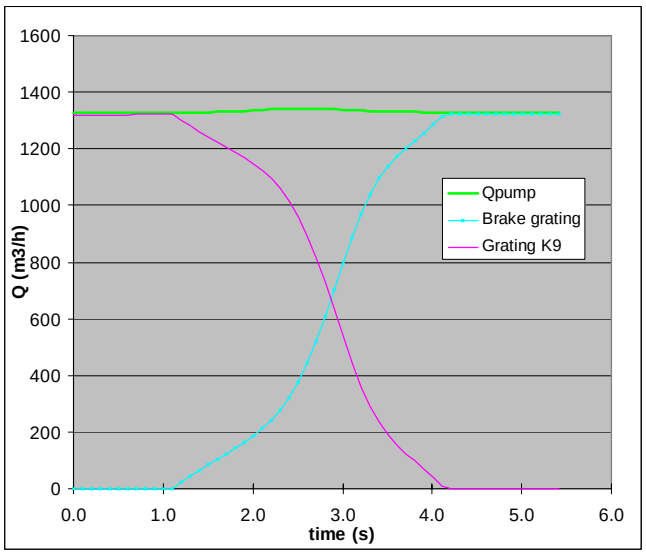

Figure 13: Simulation of the piston launch mode

During startup phase, the prover wall grating hydraulic friction is kept constant and the flows will only be controlled by motor operated fast control valves.
In Figure 13, the wall grating valves (butterfly types) are closed vice versa opened with a constant rotational speed of the valve stem within 3 seconds. Depending on the delay times between the two valves and the friction-factor as a function of opening ratio, the flow rate stability can be optimized so that the piston velocity is as stable as possible when passing the start timer switch.

What is the added value of an intelligent piston?
After some feasibility studies related to uncertainty budgets, NMi concluded that the only way to reach such demanding accuracies was to get a continuous online geometric calibration of the piston switch volumes available for each measuring run. (See section 'feasibility uncertainty')
Furthermore, a National Measurement Institute has to offer transparency in uncertainty analyses, which means that there is a constant strive to determine the amplitude of each uncertainty source rather then proposing estimates of uncertainty budgets and wait for endless discussions such as:

- How can the uncertainty budget of seal leakage be quantified?
- How can be proven that the piston is traveling at a steady velocity?
- What is the real expansion of the prover under the given process pressure?
- What is the real deformation of the prover due to irregular mechanical load?
- What is the real diameter expansion of the prover, due to temperature differences along the 40 m long provers?

Expected deformation of the precision prover pipes after on site assembling and positioning

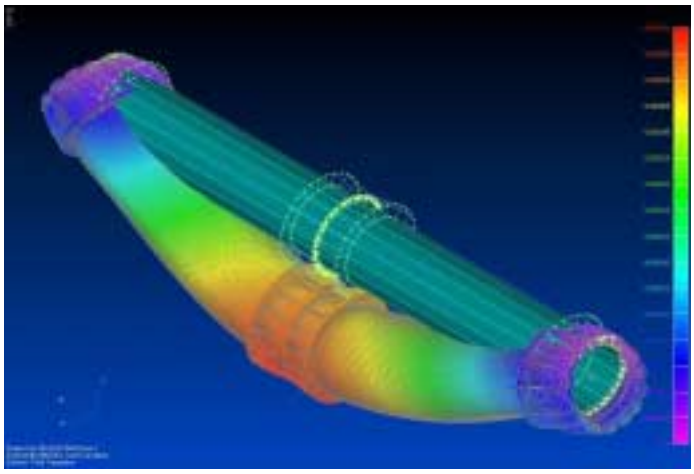

Figure 14: deformation of the precision prover pipes

The piston provers are very long and relatively thin. Various finite element calculations showed that special care should be taken at the design of the joint flanges to secure mechanical stiffness to reduce deformations at the joints. However, there is no guarantee for perfect regular mechanical support along the measurement partition. In the next figure, a case was analyzed assuming that some of the support piles were subsided only a few tenths of a millimeter in the soft soil of the site. The resulting forces bring about a considerable deviation of the cylinder circularity that should be taken into account.

With the online multipoint diameter gauge, this unknown non-circularity will be observed and compensated for.

The following schematic diagram depicts the several features of the intelligent pistons like:

- Diameter comparison with a primary ring gauge at the piston terminal, this is the most important feature. Twelve proximity sensors mounted on a rigid Invar base ring are used to detect the variation in prover diameter related to the ring gauge. (See section below for details);
- Pressure difference and leak flow detection, used for validation of the run related to seal wear or seal damage and inherent seal leakage;
- Several temperature sensors for correction purpose and safety checks (e.g. power consumption electronics)
- Acceleration sensor, to prove piston steady velocity within the calibration time window. The acceleration signal will be analyzed to calculate delta velocity (For details, see below);
- Radial angle sensor, to check for consistency of the piston position related to wearing of the sliding strips.
- Processor, inductive battery charger, HF transceiver

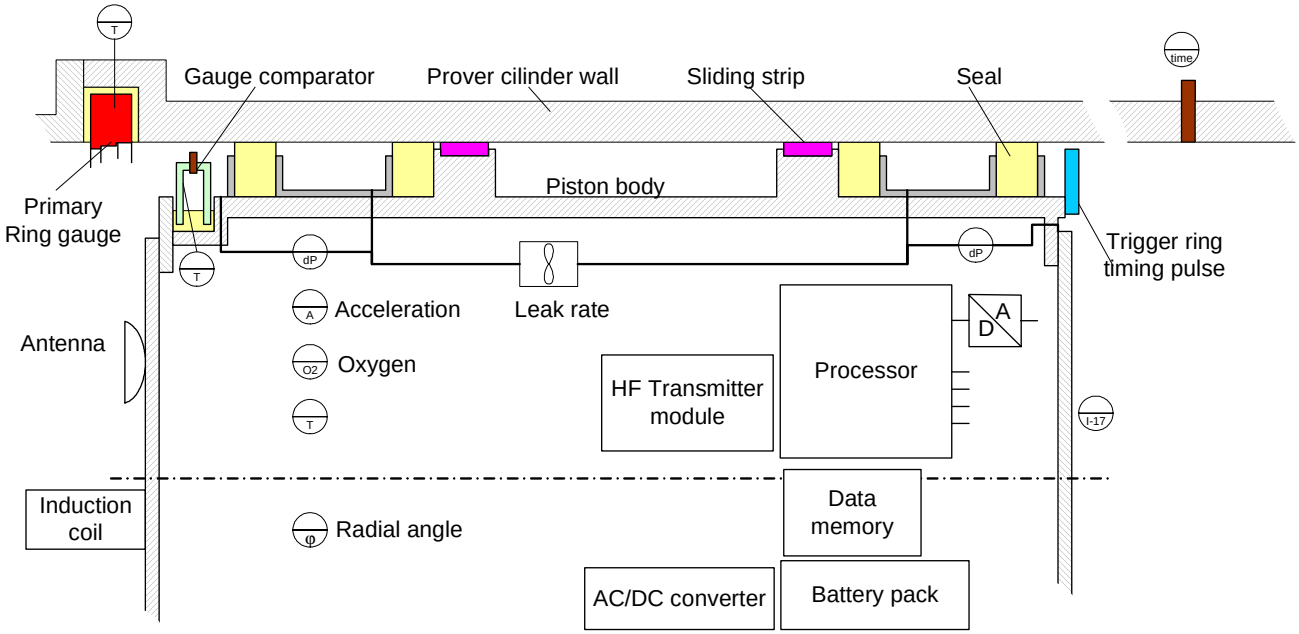

Figure 15: Overview of the piston's intelligent features

Gauge comparator: High resolution proximity sensors for 6 diametral on line measurement of geometry

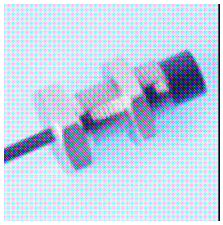

Fig. 16: proximity sensor (Ø 12mm)

The high-resolution inductive sensors are sensitive for the change in impedance of the coil distance related to the gap span to be determined. The impedance is also highly dependant on the material type of the 'conductor', which is the pipe wall. 12 of these sensors will be positioned at a rigged Invar support ring that travels along with the piston. The gap between the 'artifact' Invar support ring related to the prover wall is compared with a Primary Ring gauge (manufactured from the prover wall material) in order to disseminate the international unit of length along the prover wall. The temperature sensitivity of the inductive sensors is approximately 1 µm per °C.

Bearing in mind that the system is based upon analogue electronic techniques (long term drift), it was decided to design this piston-run cyclic calibration procedure to prevent from what metrologists call 'information loss'. The total range of the slit measurement is fixed at 3.5 mm for the large and 2 mm for the small prover. The resolution of the sensor/instrumentation amplifier is 0.12 respectively 0.08 µm at a refreshing rate of 1ms. At highest speed, the diameter could be determined nearly every 1 mm of piston travel at that speed. Each sensor will be calibrated when traveling along the three steps ladder ring gauge during the last couple of seconds when the piston arrives slowly at his terminal.

Figure 17: Example of a ring gauge

Calibration of inductive switch positions

Figure 18:Laser interferometer

The inductive switches are triggered by the ferrous metal ring attached to the piston (blue ring on Figure 15). The base reference volume sections of the pistons are dependant on the trigger moments of the inductive sensors attached in the prover wall.
The exact trigger positions of the inductive sensors will be calibrated with the aid of an artificial sliding piston with a laser reflector cube attached on the center line of that piston. A laser interferometer will be attached at the bottom of the prover and serves as a reference differential-length related pulse generator when the artificial piston is mechanically pulled through the open prover. When the inductive sensors are passed, the coinciding pulse is 'stamped' with the interferometers' position pulse counts. With this procedure, an accurate calibration of the length scale is realized. However, unfortunately the refractive index of air in the test site together with the reproducibility of the inductive sensors compels to estimate the accuracy at 0.5 mm per sensor. An extensive test program is schedules for the coming months to study the effects when an inductive sensor is replaced or when it is not completely mounted at the bottom of its thread hole. For this moment a rather high uncertainty budget of 2 mm is estimated as a total for 20 meters length (See uncertainty analyses)

Acceleration metering: advantageous for what?

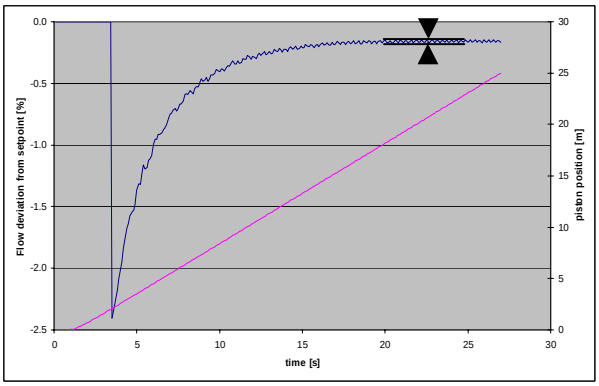

Figure 19: Piston approaching first trigger sensor

From the launching simulation, the observed maximum ripple of flow rate (and thus piston movement) is in the order of 0.025% (amplitude) at a frequency of 2.5 Hz and average flow rate of 5000 m^3/h.

At a diameter of 1127 mm (Large prover), the superposed velocity amplitude of the piston (dL/dt) and attached trigger ring for the timing pulses can be calculated at 0.35 mm/s. The smallest discrete switch length is 5 meter out of 4 times 5m total number of sections within 20meter net prover length. The effect of this ripple at the first and last timestamp will generate a standard deviation of dL/L*100=0.007% each 5 m sections. For the two timestamps combined (total travel time of the piston between the time sensor) it will generate $\sqrt{0.007^2 + 0.007^2} = 0.01\%$ 'noise' (or type A according to the GUM [2]) as additional uncertainty. It is obvious that the advantage of the accelerometer reading is that the reproducibility of the piston can be directly calculated in stead of waiting for another complete metering run. It can be concluded also that using the other metering sections as well, the standard deviation will be reduced by the square of the number of sections reducing to $0.01\% / \sqrt{4} = 0.005\%$. As a thumb rule one should keep the acceleration signal at the metering run below $\omega dL/dt = 2\pi f.dL/dt$ is 5.5 mm/s^2 or 5.10^{-4} times gravity. Inherently the accelerometer should be a low noise/high output type and should be able to handle transients at small frequencies down to DC such as e.g. Brüel and Kjaer offers.

Design details ‘GasCal’

In this section, the design of the High Pressure Gas calibration facility ‘GasCal’ will be discussed. The metrological principle of large conventional gas calibration facilities is mostly based upon a relatively long traceability chain, which inherently loses ‘information’ due to many intermediate step-up calibrations at different flow- and pressure ranges. This is not an option for the GasCal design. The facilities reference values will be based upon a very short and transparent traceability chain, leading to small uncertainties and straightforward uncertainty analyses. Small uncertainties are advantageous for society and short traceability chains are advantageous for the operational costs (‘maintaining traceability’) of GasCal.

Process flow diagram
GasCal can be distinguished into five parts:

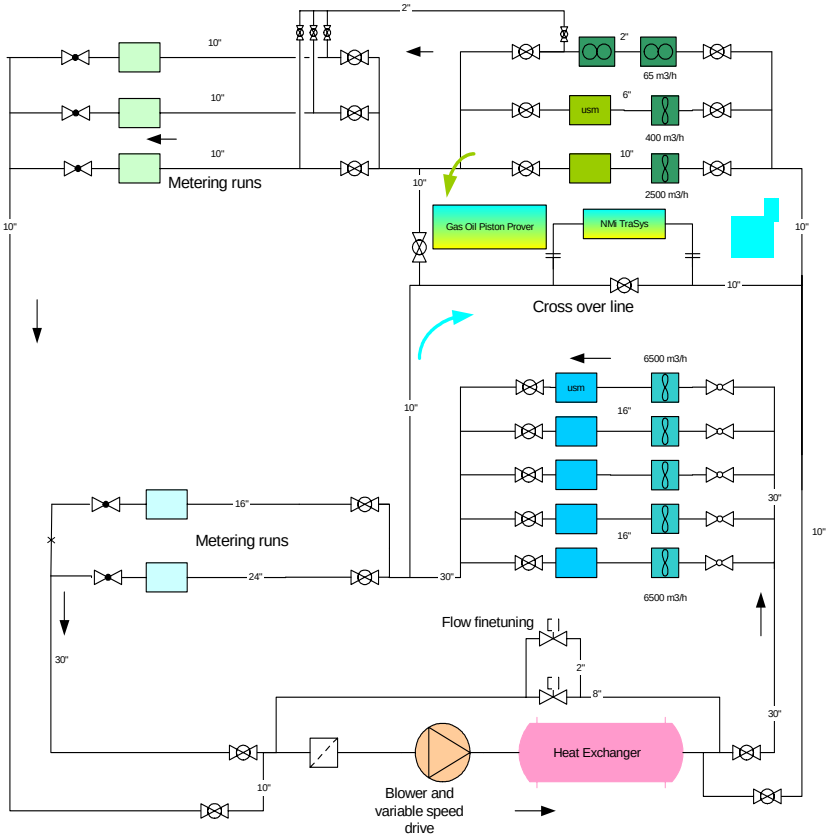

Figure 20: Process flow diagram

- 5 identical large reference runs, each consisting of one turbine reference meter and one ultrasonic monitoring meter, Q max 5 x 6500 m3/h. Total flow rate ads up theoretically to 32500 m^3/h and is depends on gas density.
- 3 small to very small reference runs, consisting of various reference meters and monitoring meters. Total flow rate up to nearly 3000 m^3/h
- Three identical metering runs for 12” and smaller meters
- Crossover for primary calibration (see section traceability chains) enabling to put the small and large reference runs in series for calibration maintenance, crosschecking etc. (see blue arrows).
- Variable speed drive, blower, flow fine tuning valves, filter and heat exchanger.

The design is such that dead volumes have been avoided as much as possible to reduce uncontrollable in- and expiratory effects (line pack) that might introduce poor repeatability.
The main transport line is a 30” diameter pipe, this extra large pipe is chosen to reduce pressure drop along the total circuit (energy consumption) and to minimize risk of low frequent oscillation effects and pulsations.
The monitoring meters (ultrasonic meters) are used to constantly monitor the behavior of the reference turbine meters but do not contribute in the determination of the reference value at the spot of the meter under test. Consistency has to be met during the calibration time frame. The question may arise why these meters are used while the reproducibility and repeatability cannot (yet?) compete with modern precision turbine metering. The answer to that is obvious, two turbine meters in series would be preferable from the metrologists’ perspective, but for the sake of ‘no’ extra pressure drop ultrasonic meters will be installed.

NMi concluded that this type of facility (closed loop with blower) is the best solution in the Netherlands to cope with the conflicting requirements of having a large gas flow at various pressure stages, reliability (risk of supply), no seasonal effects, stable flow and free of pulsations.
The drawback of this type facility is the energy consumption at large flow rates and the more complicated operation efforts, gas logistics etc. On the other hand, the enormous positive effect is found in the fact that the gas composition is absolutely constant and operation conditions are fully under control which lead to a considerable decrease in measurement uncertainty of reference mass flow.

Temperature stability: a prerequisite for high precision (gas) flow metering.

One of the challenges of the GasCal design is to keep the temperature variations within control.
The good news is that the facility’s process conditions are hardly depending on weather and/or ground conditions of the gas such as the case in conventional ‘tied-in’ test facilities. The laboratory hall has excellent temperature control. However, most important issues in gas metering related to temperature effects are a.o.:

- Unknown temperature variations in dead volumes between meter under test and reference meters (line pack effects); The past decades, NMi learn a lot from the facilities ‘Bergum’ and ‘Westerbork’ (owned by Gasunie). One of the best remedies are to use a large number of temperature transmitters in the dead volumes to determine the slow temperature transients during the calibration timeframe and to correct for the effects.
- Temperature stratification, especially at low flow rates in the long 24”and 16”metering runs; the phenomena was studied extensively by Gasunie and NMi[7]. GasCal will be provided with twin temperature measurements, both at the top of the pipe and at the bottom of the pipe.
- Unknown temperature profile of the fluid over the cross section, leading to wrong determination of ‘mixed cup temperature’ (See section before related to HyCal). Although this effect is not as large as in high viscous fluid circuits, the GasCal piping will be insulated anyhow to prevent from this risk. Mind that the process conditions can be quite different from the laboratory conditions.

Conventional and new traceability chain for the reference values for High Pressure Natural Gas Volume

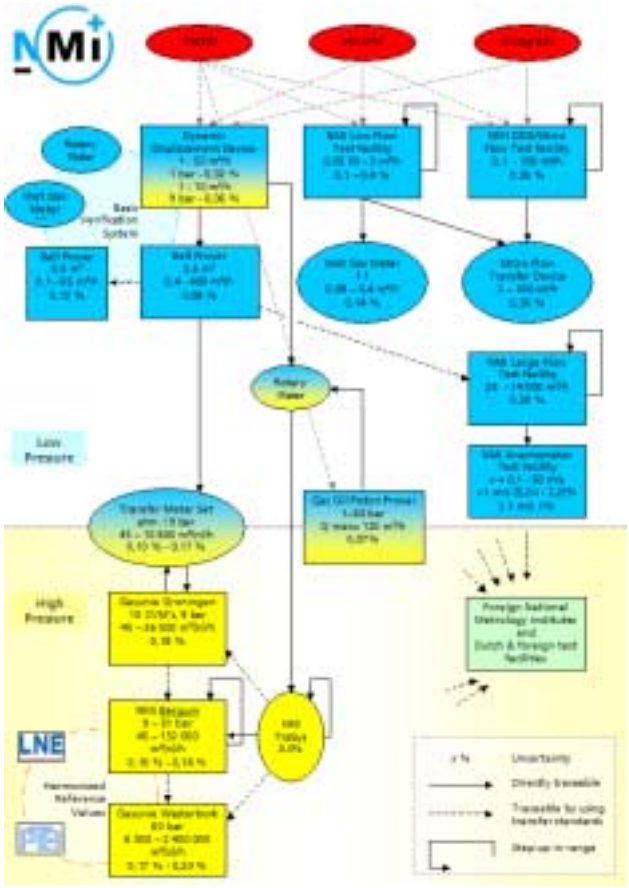

Figure 21: Situation until 2010

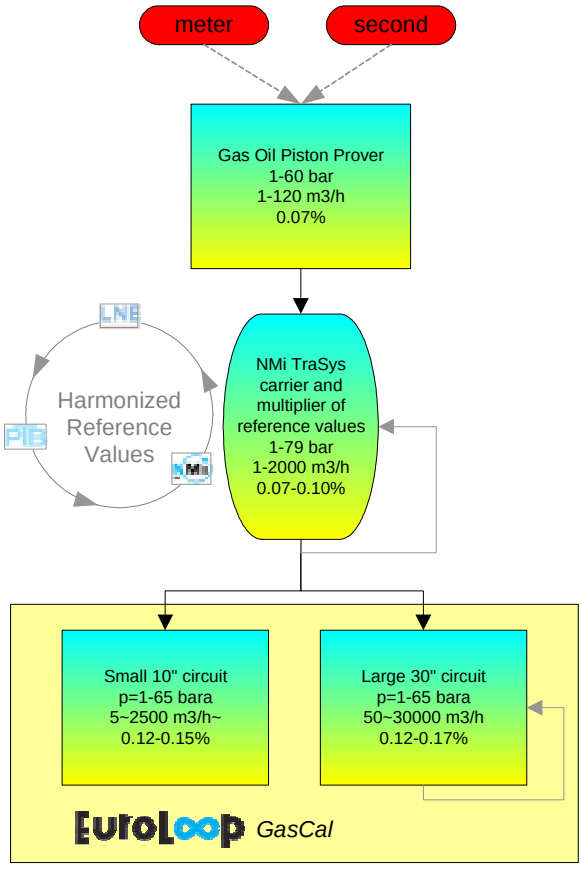

Figure 22: Situation commencing 2009

In the two presented traceability charts of ‘old’ and ‘new’ situation it is quite clearly that the dissemination of SI-units throughout the range of ‘GasCal’ is straight forward and will be realized in only a few steps. The main sources of these improvements are:

- The complete rangeability is placed under one roof, no dragging around with traveling reference meters (TRMs) to pressure and/or range restricted facilities.
- The primary realization will not be based upon the time consuming ‘pressure step up system’ but one Gas Oil Piston Prover together with traceability ‘booster’ called ‘NMi TraSys’ (‘*Traceability System*’).

These separate ‘mobile primary reference generators’ will be situated in the laboratory hall of GasCal. In the next figures, the operating principles are shown, for details see [3],[6]

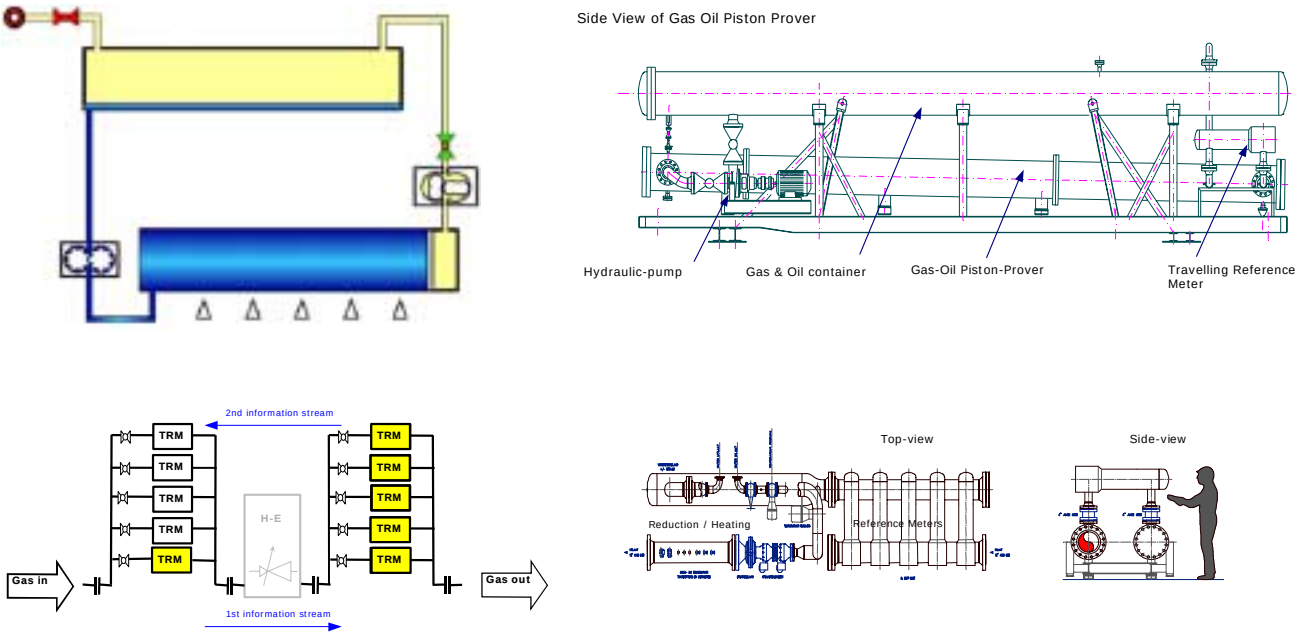

Figure 23: Primary and multiplied reference values, realized by the Gas Oil Piston Prover and TraSys

The left upper figure represents the Hydraulic driven Gas-Oil Piston Prover in a ‘closed circuit’ configuration for gas applications and will soon embody the national reference value for the volume of high-pressure gas. The advantage of the system is its process pressure independency. Another advantage is the stable operation of the piston as a result of the hydraulic smooth drive, resulting in small reproducibility figures.

Due to the restricted flow range of ‘GOPP’ another instrument is being used to boost up the flow range up to 2000 m^3/h which is carried out by NMi TraSys.

Obviously, the facilities ‘Bergum’ and ‘Westerbork’ will stay open until GasCal has been proven ‘stable’ and ‘consistent’ i.e. holding reference values that do not differ from earlier realized reference values.

The ultimate fine-tune procedure to diminish differences between (inter) national reference values is done by the ‘Harmonization Process’ which means that more independent national reference value attribute to realize the Global reference value for Natural Gas Volume [8]. This reference value that is currently realized by NMi, PTB and LNE will finally be embodied in EuroLoop GasCal for further dissemination of traceability with small uncertainties.

Sustainable operations: Low energy consumption and full recycling of Natural Gas

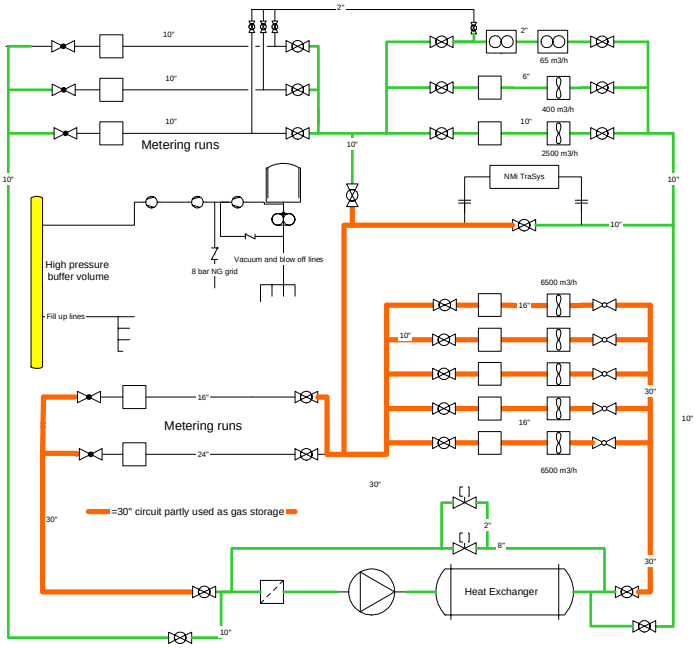

Figure 24: High pressure buffering and logistics

Recycling Natural Gas.

NMi values sustainable operations at her facilities and decided to avoid any (Natural) Gas spillage.
Mounting and dismounting the meters under test requires a complete meter run blow off containing up to 10 m^3 at 60 bar, equivalent to approximately 670 Nm^3. This amount of gas will be directed to either the 30" part or to the external high-pressure buffer volume. Complete removal will be done by vacumizing down to 20 mBar after which the spool pipe will be vented. For efficient operations, it is required to be able to blow off and to fill up again in a short time. An operation management study on gas logistics shows that four buffer volumes will work efficiently.

1. A small atmospheric gas holder as an intermediate storage for vacumized spool pipe gas;
2. The 30"loop partly used as temporary buffer (orange);
3. A separate High Pressure Volume (dead end pipeline, yellow);
4. The 10"circuit in operation mode (green, variable pressure)

The optimum operation sequence is to have batches of calibration of roughly the same pressure and to start operations at low-pressure ranges, climbing up during the week up to the highest pressures. The advantage of this cycle is to use the downtimes (e.g. weekends, overnights) to re-transport the gas into the high-pressure cavities.

Energy consumption by a large process blower.

In the design stage of the flow generating system, the energy consumption and related cooling power was one of the main considerations.

Two options are available:

- The blower/compressor has a fixed speed, electromotor and gearbox configuration with anti surge vanes at the inlet to control the smaller flow rates at high dP;
- The blower/compressor has a variable speed drive.

NMi opted for the variable speed drive to cover the complete range and maintaining high efficiency of the blower (durability). The maximum power at the blower shaft is 2400 kW at the full 30000 m^3/h actual flow rate, pressure difference of 2.5 bar across in- and outlet at 61 bara for Natural Gas. The system is suited for various other gases as well.
The installation will be fitted with a cooling system allowing the medium to be cooled to temperatures down to 5 and 10 ^oC. The main cooling power will be obtained from the river water that is available at about 50 meters outside the fence.

Conclusions

In the course of 2008 and 2009, two calibration facilities ‘under one roof’ will become available that are unique in their combination of line size, flow range, viscosity, pressure, temperature and measurement uncertainties.
As a National institute for Standards in Measurement, NMi VSL has a function to provide industry and society with applicable expertise and knowledge in Metrology, usually delivered as "Traceability Services". A prerequisite to this function for the Metrology of Flow is e.g., the capability to generate reliable reference values for measurement of large high-pressure gas flow and large mineral products flow.
EuroLoop is the creation of straightforward traceability-chains by innovative metrological concepts, realizing reference values covering wide ranges in pressure and flow-rates gas and liquid types.
Extending its capabilities NMi VSL keeps its dedication on track to reduce uncertainties in flow measurements and in this new facility specifically contributing to improvements in the Oil and Gas sector, at your service.

Acknowledgements

We have spend a couple of interesting hours together, dreaming, sparring and aiming for superb results, thank you folks, keep on bringing flow metrology onto a higher level:
Jan van Bekkum, ‘nestor’ for HyCal, top-level front end engineering!
Harry Dijstelbergen, Henk Bellinga ‘nestors’ for HP NG metering: learned a lot from you guys...
Peter van Brakel, Jan Pors, Yerke Boersma, Lukas IJmker (Krohne Altometer) for keeping shoe soles down to earth.
Henk Riezebos for making the vibration and dP analyses for GasCal and Aernout van den Heuvel, Jan de Boer (Gasunie) and Frans Doorman (NAM) for being our sparring-partners.
Bodo Mickan (PTB), Olivier Gorieu (GdF), Jean-Pierre Vallet (LNE), Gerard Blom (NMi-VSL) for ‘harmonizing HP NG reference values’ and friendship;
Jesper Busk and Kurt Rasmussen (Force, Denmark) ‘tak’ for sharing ideas related to storing HP Gas, big blowers and warning us for high dP’s to keep energy consumptions low.
Rens van den Brink one of my best colleagues in complicated simulation jobs. Ewout van der Beek for heat transfer calculations. Alex van de Spek for his ‘nasty’ remarks keeping us sharp.
Wim Volmer, Jan de Rouwe, Hans Elskamp, Gordon Foks (NMi CERTIN BV) for huge support.
André Beukers and Jan van Eerten (T-gradin) for having fun and keeping the budgets and timelines…
Many of our customers and relations that shared their suggestions for test facility improvements, their experiences and ‘wanna-haves’ with us.
Anneke, Ewout, Judith and Levi: thanks for supporting me again during this hectic but exciting period!

List of used symbols:

Symbol	Legend	unit	Symbol	Legend	unit
Q	Volume flow rate	m^3/h			
L	Length, pipe	m	τ	time	s
P	pressure	Bar, Pa	φ	Angle or meter deviation	Rad, %
dP	Delta pressure	bar	μ	micro	-
K	Loss coëfficiënt, in $dP=K\ ½\ \rho\ Q^2$	[1]	ω	Radial velocity	Rad/s
v	Velocity	m/s	ρ	Density	Kg/m^3
v’	Velocity derivative	m/s^2	T	temperature	K, °C
Q’	Flow derivative	m^3/s^2	R,r	Radius	Rad
I	Inertia		δ, Δ, d	Differential operator	-
A	Acceleration	m/s^2	D	Diameter	m
f	Pipeline friction factor according to Darcy-Weisbach	[1]	E	Young’s modulus	Pa
B	Bulk elasticity	Pa			

Abbreviations:

DuT	Device under test
MuT	Meter under test
SoS	Speed of Sound
TRM	Traveling Reference Meter
GOPP	Gas Oil Piston Prover
TraSys	Traceability System

References:

[1] Wim Volmer, 'EUROLOOP: Unique Oil and Gas Calibration Facilities', FLOMEKO 2007, Johannesburg, South Africa

[2] ISO, 'Guidelines for the expression of the Uncertainty of Measurement in calibrations (GUM)', ISO TAG4/WG3 1992, GENEVA, Switzerland

[3] M.P. van der Beek, R. van den Brink and I.J. Landheer, "Gas-Oil Piston Prover", a new concept to realize reference values for High-Pressure Gas-Volume in the Netherlands, FLOMEKO 2003, Groningen, the Netherlands

[4] H.J. Riezebos et al, 'Development of a tracer method to check flow meters in natural gas based on accurate speed-of-sound determination', FLOMEKO2007, Johannesburg, S A

[5] Mijndert P. van der Beek and Iman J. Landheer, 'Acceptance of variations in reference values of gas flow measurements', Flomeko 1998, Lund, Sweden.

[6] M.P. van der Beek, I.J. Landheer, 'NMi TraSys, The ultimate carrier&multiplier for the unit of volume for High Pressure Natural Gas', Flomeko 2003, Groningen, The Netherlands

[7] Aernout F. van den Heuvel et al, 'Fow measurement errors due to stratified flow conditions', FLOMEKO 2005, Peebles, UK

[8] T. Kurschat, G. Wendt, M.P. van der Beek and I.J. Landheer, 'NMi VSL and PTB establish common Reference Values for the unit of Volume for high-pressure Gas-Flow measurements', North Sea Flow Measurement Workshop 1999, OSLO, Norway

Uncertainty Modelling for Instruments, Systems & Plants – An essential Guide to Optimising Performance

Abstract:

Knowledge of the uncertainty of Custody Transfer and Allocation measurement is typically calculated following the published Guidelines & Standards using Manufactures Data. But what if there are environmental issues regarding the Installation or Type of Equipment.

This Paper identifies and illustrates ways of using established uncertainty theory as a tool for modelling the design of measurement equipment, the combination of that equipment into flow measurement systems and/or the modelling of complex Plants/Allocation Systems. By using these tools measurement exposure can be expressed in terms of uncertainty, units measured or financial risk, thereby giving an insight into the advantages of one method of measurement over another. In a similar way Design Houses can determine the optimum solution for a measurement system and Operators the most cost effective solution for Plant/Allocation metering.

The Paper is subdivided into three main Sections:

1. *Instrument Uncertainties – Examining the physics of the meter and determining its sensitivity to various aspects of its installation.*

2. *Meter System Uncertainties – Examining the algorithms used to determine flow rate from instruments and using a combination of sensitivity factor and calibration tolerances.*

3. *Plant & Allocation Systems – Examining the connectivity between the individual metering system associated with a Plant/Allocation System and assessing the cumulative uncertainty effect on reported figures.*

Authors:

Michael MacKay C.Eng
METCO Services Ltd., Emerson House, Kirkhill Drive, Kirkhill Ind. Est., Dyce, Aberdeen, AB21 0EU.
mike.mackay@metco-uk.com

Justin Walter
METCO Services Ltd., Emerson House, Kirkhill Drive, Kirkhill Ind. Est., Dyce, Aberdeen, AB21 0EU.
justin.walter@metco-uk.com

1.0 INTRODUCTION

1.1. GENERAL

In this day and age, engineers are under constant pressure to improve on what went before and nowhere is this more apparent in the Oil Industry than in the field of Fiscal & Allocation Hydrocarbon Measurement. Whether new installations or old, the emphasis is typically on minimising the "Uncertainty" of the measurement and therefore minimising the operators "Exposure" to unquantifiable losses (or gains).

Uncertainty is more formally defined as: "The interval within which the true value of the measured quantity can be expected to lie within a stated probability".

It is important to stress that Uncertainty is also dynamic; a measurement uncertainty will vary with changes to the active parameters. In flow metering that will mean that the measurement uncertainty varies with flow rate, pressure, temperature, density etc; similarly in measurement systems where fluid properties may change – a point often overlooked by Operators of Measurement Systems.

1.2. OBJECTIVES

The purpose of this paper is to analyse the techniques available to design engineers by Analysing system characteristics and Modelling individual component uncertainties rather than relying solely on the Monte Carlo Simulation approach for evaluation. Whether the engineer is designing Instruments, Measurement Systems or Processing Plants, the fundamental methodology is the same - generate a "Model" of the system identifying each element in the measurement chain, then attribute verifiable uncertainties and sensitivity factors to those elements prior to combining the uncertainties using the "Root-Sum-of-Squares" (RSS) method. Using this technique and following the recommendations laid down in various Measurement Standards & Guidelines the engineer is able to predict probable outcomes in terms of measurement uncertainty.

By analysing the individual component uncertainties and their corresponding sensitivity factors, the relative impact of each element in the chain and its significance with respect to the whole can be established. Modelling in this way allows the engineer to identify those elements of the system that have the greatest impact on the resultant measurement. This Analytical process can be extremely useful in providing guidance to Engineers on the choice of Instruments used in Measurement Systems and the choice of Measurement Systems used in Processing Plants/Allocation Systems. Ultimately, the Modelling could be applied to real time measurement, providing instantaneous diagnosis of instances where measurement systems are failing to meet their agreed Tolerances.

Each of the following Sections of this Paper addresses different levels of measurement Modelling; namely the Instrument, the Metering System Design and finally the Processing Plant/Allocation System.

The ultimately goal being to minimise measurement "Exposure" in terms of the cost that uncertainty represents when assessing the design and operation of measurement systems. Uncertainty Modelling in this way allows the engineer to avoid spending large amounts of money on elements in a system that contributes little to the desired outcome (i.e. concentrating on the elements of the system that give the best return in terms of reducing the financial "Exposure" to the Operator).

Authors Note: Whilst not specifically addressed in this document, often too much emphasis is placed on measurement uncertainty where the Tolerance is based on requiring the same measurement uncertainty over the whole operating range of the measurement system (e.g. ± 1.0% of Point for Gas, ± 0.25% of Point for Oil). But the "Exposure" at the low flow rates may be less than a quarter of that at the maximum flow rates when viewed purely in terms of units measured. I would suggest that Tolerances may be better expressed in terms of unitary or financial "Exposure" rather than ± 1.0%, or ± 0.25% of the flow over the full range – hence it could be argued that it is the "Exposure" that should the defining point, not the relative "Uncertainty".

2.0 INSTRUMENT UNCERTAINTIES

2.1. OBJECTIVES

This Section addresses the design issues associated with obtaining accurate measurement and the problems associated with assessing the uncertainty of that measurement as applied to a Particular Device (i.e. typically the Primary Instrument in a Metering System). Simple case studies looking at the "Physics" of the method of measurement and the impact of those effects on the measurement process will help to establish the anticipated "Uncertainty" of the device when in use. This methodology is especially useful when considering the implications of deviations from recommended practice such as improper installation or changes in Process Fluids that detrimentally effect the measurement (a factor often encountered when reviewing individual Metering Systems – see following Section for examples).

2.2. METHODOLOGY

2.2.1. The METCO Approach

We at Metco have implemented the principles set out in ISO TR 5168 and ISO GUM using the Root Sum or Squares method with sensitivities determined by partial differentiation. However we apply two additional stages of simple mathematical manipulation to significantly simplify the partial differentiation sensitivity coefficients. This manipulation is set-out below.

2.2.2. Fundamental Principals

It is appropriate to initiate a measurement uncertainty analysis with the equations that define the system under analysis. For example; let the "final result" be equal to the value "q", but 'q' may be calculated from other variables "x", "y" & "z" which may be measured quantities OR may in turn be calculated from further sets of variables that are ultimately derived from measured quantities.

In mathematical terms "q" is a Function of x, y & z i.e.

$q = F^n(x, y, z)$ Which means any equation incorporating the variables x, y & z.

But "x" may be a function of a, b, c & d.
And "y" may be a function of e, f & g etc.

To estimate the uncertainty of the value "q" it is necessary to determine the uncertainties of the contributing variables 'x', 'y, & 'z'. The fundamental equation of 'error' is:-

$$\delta q = \pm \frac{\partial(q)}{\partial(x)} \times \delta x \quad \pm \frac{\partial(q)}{\partial(y)} \times \delta y \quad \pm \frac{\partial(q)}{\partial(z)} \times \delta z$$

Where:

δq	Represents the error (in Engineering units) in the value "q"
δx	Represents the error (in Engineering units) in the value "x"
δy	Represents the error (in Engineering units) in the value "y"
δz	Represents the error (in Engineering units) in the value "z"
$\frac{\partial(q)}{\partial(x)}$	Represents the Partial Derivative of "q" by the variable 'x'
$\frac{\partial(q)}{\partial(y)}$	Represents the Partial Derivative of "q" by the variable 'y'
$\frac{\partial(q)}{\partial(z)}$	Represents the Partial Derivative of "q" by the variable 'z'

2.2.3. Relative Uncertainty

The Relative uncertainty is the 'error' (e.g. δq), in engineering units, divided by the measured, or calculated, value of the variable (q).

Relative Uncertainty $U_q = \frac{\delta q}{q}$

To develop the previous equation from an 'Error' equation to a 'Relative Uncertainty' equation both sides must be divided by "q" as follows:

$$\frac{\delta q}{q} = \pm \frac{\partial(q)}{\partial(x)} \times \frac{1}{q} \times \delta x \pm \frac{\partial(q)}{\partial(y)} \times \frac{1}{q} \times \delta y \pm \frac{\partial(q)}{\partial(z)} \times \frac{1}{q} \times \delta z$$

This may be manipulated to express each term on the RHS as a Relative uncertainty as follows:

$$\frac{\delta q}{q} = \pm \left(\frac{\partial(q)}{\partial(x)} \times \frac{x}{q} \times \frac{\delta x}{x} \right) \pm \left(\frac{\partial(q)}{\partial(y)} \times \frac{y}{q} \times \frac{\delta y}{y} \right) \pm \left(\frac{\partial(q)}{\partial(z)} \times \frac{z}{q} \times \frac{\delta z}{z} \right)$$

Where:

$\frac{\partial(q)}{\partial(x)} \times \frac{x}{q}$	Represents the "sensitivity" of Term "x" in the calculation of "q".
$\frac{\partial(q)}{\partial(y)} \times \frac{y}{q}$	Represents the "sensitivity" of Term "y" in the calculation of "q".
$\frac{\partial(q)}{\partial(z)} \times \frac{z}{q}$	Represents the "sensitivity" of Term "z" in the calculation of "q".

2.2.4. Root Sum Square

It is conventional to evaluate an uncertainty equation as a Root Sum Square. The above equation now becomes:

$$\frac{\delta q}{q} = \sqrt{\left(\frac{\partial(q)}{\partial(x)} \times \frac{x}{q} \times \frac{\delta x}{x}\right)^2 + \left(\frac{\partial(q)}{\partial(y)} \times \frac{y}{q} \times \frac{\delta y}{y}\right)^2 + \left(\frac{\partial(q)}{\partial(z)} \times \frac{z}{q} \times \frac{\delta z}{z}\right)^2}$$

Since Percentage Uncertainty is simply Relative Uncertainty expressed in terms of percentage and is normally assigned the symbol "E".

Percentage Uncertainty of "q" is: $E_q = \frac{\delta q}{q} \times 100 \quad \%$

Hence the above equation may be re-written as:

$$E_q = \sqrt{\left(\frac{\partial(q)}{\partial(x)} \times \frac{x}{q} \times E_x\right)^2 + \left(\frac{\partial(q)}{\partial(y)} \times \frac{y}{q} \times E_y\right)^2 + \left(\frac{\partial(q)}{\partial(z)} \times \frac{z}{q} \times E_z\right)^2}$$

2.2.5. Jokers

The above expressions are purely based upon the mathematical expressions used within the measurement. In the real world there are other factors that may degrade the uncertainty of measurement and it is advisable to incorporate these additional terms into the Root Sum Square equation where appropriate. In flow metering these terms may originate from effects such as:

Fluid Swirl
Fluid Profile Distortion
Flow Computer resolution
Etc

The final equation above thus becomes:

$$E_q = \sqrt{\left(\frac{\partial(q)}{\partial(x)} \times \frac{x}{q} \times E_x\right)^2 + \left(\frac{\partial(q)}{\partial(y)} \times \frac{y}{q} \times E_y\right)^2 + \left(\frac{\partial(q)}{\partial(z)} \times \frac{z}{q} \times E_z\right)^2 + E_{swirl}^2 + E_{profile}^2 + E_{fc}^2 + E_{etc}^2}$$

Authors Note: Addressing these "Real World" operating Uncertainties is a huge subject and will be the subject of a further Paper; however, a single example of the uncertainty derivation with respect to measurement instrumentation is illustrated in more detail in the Appendix of this document.

3.0 METER SYSTEM UNCERTAINTIES

3.1. OBJECTIVES

This Section addresses the design issues associated with obtaining an accurate Flow measurement as applied to a Metering System. It addresses the problems associated with assessing the uncertainty of measurement as applied to the collection of Primary & Secondary Instruments forming a Meter Tube or Metering Skid. The methodology follows on from the previous example, applying the same analytical techniques to by establish the sensitivity of each measurement element based on its place in the algorithm used to determine the flow measurement.

We would stress that it is by using these analytical techniques and deriving the sensitivity of each element of the calculation, that the engineer can get a better appreciation of those elements in the calculation that are most significant – and therefore warrant the most attention. This approach also means that those scenarios where the installation or process fluid does not meet the Manufacturers stated requirements (or comply with the relevant Statutory Guidelines) can be accommodated.

By adopting the following Methodology, it is hoped to demonstrate that uncertainty calculations can be generated that address all the elements affecting the measurement system (both instrument and process) and of the uncertainty assessed over the full operating range of the flow meter.

Using differential pressure flow meters as an example, it can be seen that the uncertainty of the flow meter degrades with reducing flow (typical of most types of meter). Hence, once the base condition of the metering system has been established, the turn-down with respect to flow rate can be demonstrated by reducing (adjustable) steps of differential pressure down to minimum applicable differential pressure. A change-over to a reducing step interval and a change-over between high range and low range differential pressure transmitters may be embedded and applied as required.

At METCO, Measurement System Models are be generated that reflect the uncertainty associated with each element of the system. This is done by breaking down the Uncertainty Calculation into a series of modules that encompass all the known uncertainty elements,. Each type of measurement system is then Modelled such that “Templates” are generated for future systems of a similar nature and uncertainty elements added as required by the application.

By assessing each element of the system and any anomalies associated with its installation one can slowly build up an appreciation of their impact and the final Measurement Uncertainty

Listed below are typical examples of anomalies found in flow measurement systems:

- Primary Instrument without adequate Upstream & Downstream Straight Lengths
- Secondary Instruments not located within the prescribed distance with respect to the Primary Element

- Operating too close to the Phase Envelope in Gaseous Systems, or the Vapour Pressure in Liquid Systems
- Inadequate mixing prior to Sample Loop or Manual Sample Point
- Relative Impact of increasing BS&W on corrected Flow Measurements

Some of the above examples are clearly design issues and can only be properly assessed once the condition is remedied by redesigning the Measurement System, Others can be evaluated either by analysis, or by reference to the Standards/Guidelines (as in the case of Orifice Plate deviations from the Standards) and their uncertainty contribution to the system determined.

Also, it is most important to take into account the verifiable uncertainty of measurement (normally deemed its "Calibration Tolerance") under operating conditions. This is particularly relevant to DP based measurement systems where the Manufacturers Specification may state admirable uncertainty tolerances that just cannot be demonstrated in the field. An example of this might be DP Transmitters operating at extremely high static pressures (normally accommodated by "Footprinting" the DP Transmitter at an approved Laboratory), or by a DP Transmitter being required to operated over an extremely low range of DP – say an averaging Pitot Tube operating over 0- 10 mbar (this low an operating range would be extremely difficult to verify in the field using standard test equipment because of resolution/repeatability issues).

Hopefully the above illustrations help to demonstrate the points to be considered when designing (or assessing) a flow measurement system and methods of assessing their significance.

Authors Note: It is only by having an appreciation of the significance of the issues (i.e. their Relative Uncertainty and – most importantly their Sensitivity Coefficient) that the design engineer and/or those assessing the measurement system can have real confidence in the measurements being made. By generating "Models" that analyse every detail associated with the metering system and its components, engineers will gain a better appreciation of the impact of each element of the system and its effect on the whole.

By using the above analytical techniques, it may be possible to avoid unnecessary mis-measurement corrections and if they occur - attribute an uncertainty to that mis-measurement.

3.2. METHODOLOGY

3.2.1. Root Equation

The example chosen to demonstrate the Methodology in this Section is the Orifice Plate Measurement System. The reason for choosing this method of measurement is that there already exist accepted algorithms for quantifying the Sensitivity of the Primary and Secondary Elements and hence allows a traceable demonstration of the Analytical Methods used to achieve those algorithms used in the Model.

Mass Flow: $$q_m = \frac{\pi d^2}{4} \times \frac{C \times \varepsilon}{\sqrt{1-(\beta)^4}} \times \sqrt{2 \times \Delta p \times \rho}$$

3.2.2. Accepted Sensitivity Algorithm

As can be seen, there are several elements within the calculation, each of which will have an associated uncertainty. A sensitivity analysis of the standard equation for Orifice Flow measurement uncertainty gives the following accepted equation:

$$E_{qm} = \sqrt{E_c^2 + E_\varepsilon^2 + \left(\frac{2 \times \beta^4}{1-\beta^4}\right) \times E_D^2 + \left(\frac{2}{1-\beta^4}\right)^2 \times E_d^2 + \frac{E_{\Delta p}^2}{4} + \frac{E_\rho^2}{4}}$$

But how was the above equation derived? The calculations shown below illustrate how each element in flow algorithm can be analysed in turn with respect to the whole and its sensitivity confirmed; the reasoning behind the above equation and (hopefully) demonstrate the value of the Analytical approach to Uncertainty.

3.2.3. Derivation of Algorithm

To derive this uncertainty algorithm the mass flow equation must be considered as being:

$$q_m = \frac{\pi d^2}{4} \times \frac{C \times \varepsilon}{\sqrt{1-\left(\frac{d}{D}\right)^4}} \times \sqrt{2 \times \Delta p \times \rho}$$

If the partial derivative with respect to “d” is taken of this expression it yields:

$$\frac{\partial(q)}{\partial d} = \frac{1}{2} \times \frac{\pi \times d \times C \times \varepsilon}{\sqrt{1-\left(\frac{d}{D}\right)^4}} \times \sqrt{2 \times \Delta p \times \rho} + \frac{1}{2} \times \frac{\pi \times d^5 \times C \times \varepsilon}{\left(1-\left(\frac{d}{D}\right)^4\right)^{\frac{2}{3}}} \times \frac{\sqrt{2 \times \Delta p \times \rho}}{D^4}$$

If this partial derivative is now divided by “q” i.e.:

$$\frac{\frac{\partial(q)}{\partial d}}{q} = \frac{\frac{1}{2} \times \frac{\pi \times d \times C \times \varepsilon}{\sqrt{1-\left(\frac{d}{D}\right)^4}} \times \sqrt{2 \times \Delta p \times \rho} + \frac{1}{2} \times \frac{\pi \times d^5 \times C \times \varepsilon}{\left(1-\left(\frac{d}{D}\right)^4\right)^{\frac{2}{3}}} \times \frac{\sqrt{2 \times \Delta p \times \rho}}{D^4}}{\frac{\pi d^2}{4} \times \frac{C \times \varepsilon}{\sqrt{1-\left(\frac{d}{D}\right)^4}} \times \sqrt{2 \times \Delta p \times \rho}}$$

Simplifying this becomes:- $= \frac{-2 \times D^4}{-D^4 + d^4} \times \frac{1}{d}$

Which may be written as:- $= \frac{2}{1 - \left(\frac{d}{D}\right)^4} \times \frac{1}{d}$

The Relative Uncertainty with Sensitivity becomes:- $\frac{2}{1-(\beta)^4} \times \frac{\delta d}{d}$

If the partial derivative with respect to "D" is taken of this expression it yields:

$$\frac{\partial(q)}{\partial D} = \frac{-1}{2} \times \frac{\pi \times d^6 \times C \times \varepsilon}{\left(1 - \left(\frac{d}{D}\right)^4\right)^{\frac{2}{3}}} \times \frac{\sqrt{2 \times \Delta p \times \rho}}{D^5}$$

If this partial derivative is now divided by "q" i.e.:

$$\frac{\frac{\partial(q)}{\partial d}}{q} = \frac{\frac{-1}{2} \times \frac{\pi \times d^6 \times C \times \varepsilon}{\left(1 - \left(\frac{d}{D}\right)^4\right)^{\frac{2}{3}}} \times \frac{\sqrt{2 \times \Delta p \times \rho}}{D^5}}{\frac{\pi d^2}{4} \times \frac{C \times \varepsilon}{\sqrt{1 - \left(\frac{d}{D}\right)^4}} \times \sqrt{2 \times \Delta p \times \rho}}$$

Simplifying this becomes:- $= \frac{-2 \times d^4}{-D^4 + d^4} \times \frac{1}{D}$

Which may be written as:- $= \frac{2 \times \left(\frac{d}{D}\right)^4}{1 - \left(\frac{d}{D}\right)^4} \times \frac{1}{d}$

The Relative Uncertainty with Sensitivity becomes:- $\frac{-2(\beta)^4}{1-(\beta)^4} \times \frac{\delta D}{D}$

Authors Note: The Relative uncertainties, $\frac{\delta d}{d}$ and $\frac{\delta D}{D}$ *may be expressed in terms of Percentage Uncertainty (*E_d and E_D respectively*). The negative sensitivity coefficient will be positive when squared; hence the negative sign may be "lost". In both cases a 'convenient' "d" and "D" forms on the denominator from the partial derivative to form the denominator of the Relative Uncertainty term.*

In the same way, it can be demonstrated that the partial derivative of the square root for the Δp *(differential pressure) and* ρ *(density) is ½ which when squared becomes ¼. The sensitivity coefficient for the uncertainties of C and* ε *can be seen to be unity.*

As can be seen, some elements are demonstrated to have a much more significant effect than others. It is by applying these techniques to any measurement application that one can assess the importance of each component of the measurement system and determine which element is most critical to the calculation.

Examination of the above example shows that (whilst important) the density uncertainty does not have as marked effect as it would in a linear equation (such as a Turbine, or Ultrasonic measurement system). In the same way, we can see that the uncertainty of the Diameters (in particular the orifice dimension) is mitigated in part by the Beta Ratio.

It is by analysing systems in this way that a true appreciation of the significance of each component is appreciated.

Thus, by breaking down the equation and considering how each element was determined, it is possible to accommodate most scenarios in measurement. As an illustration, the above equation can be further expanded to identify additional uncertainty factors such as orifice the use of drain holes in the plate, plate contamination and the additional uncertainty associated with the Discharge Coefficient as a result of contamination or flow profile distortion.

$$E_{qm} = \sqrt{\left(E_c + E_{add}\right)^2 + E_{drain}^2 + E_{\varepsilon}^2 + \left(\frac{2\times\beta^4}{1\text{-}\beta^4}\right)\times E_D^2 + \left(\frac{2}{1\text{-}\beta^4}\right)^2 \times E_d^2 + \frac{E_{\Delta p}^2}{4} + \frac{E_{\rho}^2}{4} + E_{fc}^2 + E_{jch}^2}$$

4.0 PLANT & ALLOCATION UNCERTAINTIES

4.1. OBJECTIVES

This Section addresses the design issues associated with combining measurement system uncertainties in order to assess their impact on a Processing Plant or Allocation System (i.e. when considering the uncertainty Processing Plant Balance, Allocation Systems, or the uncertainty in Allocation attributed to each participant in complex Pipeline Network). As previous, the methodology relies on building up an Uncertainty Model which is able to take into account all the elements of the network and establish "Group" uncertainties associated with Network Nodes and outputs.

It should also be noted that the uncertainty of measurement systems using the "by difference" approach (where there may be no direct measurement element) and in/out flows are based on the sum of other measurements in the system can be calculated using this modelling approach.

At this level of Modelling, the engineer can run "what if" scenarios looking at the implications of mis-measurement due to instrument failures and/or incorrect base data. Also engineers can establish the "Risk" associated with any element in the network - which is particularly useful when considering allowing new entrants to share pipelines or disputes relating to the measurement uncertainty of participants within an Allocation System.

Authors Note: As Allocation Systems become more complex, there may be pressures on participants to not only provide end of day reports on fluid movements, but also to attribute an uncertainty statement to accompany those figures. By monitoring instruments operating points and having a knowledge of their calibration tolerances, it would be a simple matter to assign uncertainties to measurement statements that can then be utilised to determine the Allocation Reporting "Exposure".

4.2. METHODOLOGY

The Partial Differentiation results illustrated in Section 1.0 can typically be simplified by algebraic manipulation to represent more complex measurement systems. This leads to a number of **"Standard Cases"** that represent common equation formats and common metering configurations. It is therefore not necessary to carry out partial differentiation action at every stage in an uncertainty analysis, where a 'standard' case equation occurs then the uncertainty expression follows logically.

A selection of common formats is given below.

4.2.1. Case 1: Multiples

The Function of "q" may be the multiple of x, y & z:

Multiplication Function:- $q = x \times y \times z$

The uncertainty equation becomes:

$$E_q = \sqrt{(1 \times E_x)^2 + (1 \times E_y)^2 + (1 \times E_z)^2}$$

Division Function:- $q = \dfrac{x}{y \times z}$

The uncertainty equation also becomes:

$$E_q = \sqrt{(1 \times E_x)^2 + (1 \times E_y)^2 + (1 \times E_z)^2}$$

In both cases all sensitivity terms reduce to unity.

4.2.2. Case 2: Powers

The Function of "q" may incorporate power terms of x, y or z:

Square Function:- $q = x \times y \times z^2$

The uncertainty equation becomes:

$$E_q = \sqrt{(1 \times E_x)^2 + (1 \times E_y)^2 + (2 \times E_z)^2}$$

Square root Function:- $q = x \times \sqrt{y \times z}$

The uncertainty equation becomes:-

$$E_q = \sqrt{(1 \times E_x)^2 + \left(\frac{1}{2} \times E_y\right)^2 + \left(\frac{1}{2} \times E_z\right)^2}$$

4.2.3. Case 3: Addition

The Function of "q" may be the summation of x, y & z:

Addition Function: $q = x + y + z$

In general terms: $q = \sum_{i=1}^{n} (x_i)$

Where "x_i" represents a number of variables from x_1 to x_n

The uncertainty of "q" may be calculated by:

$$E_q = \sqrt{\left(\frac{x}{q}\right)^2 \times (E_x)^2 + \left(\frac{y}{q}\right)^2 \times (E_y)^2 + \left(\frac{z}{q}\right)^2 \times (E_z)^2}$$

In general terms: $$E_q = \sqrt{\sum_{i=1}^{n}((\frac{x_i}{q})^2 \times E_{xi}^2)}$$

Though a general result; this is particularly applicable to parallel metered streams commingling into a common un-metered header and to gas composition calculations.

4.2.4. Case 4: By Difference

Case 3 may be considered to be a specific metering configuration where parallel streams are commingled into a metered common stream. All but one (i.e. "x" or in the general case "x_1") are metered. The un-metered stream is "metered by difference".

Metered by difference: $$x = q - (y + z)$$

In general terms: $$x_1 = q - \left(\sum_{i=2}^{n}(x_i)\right)$$

Uncertainty of Total Flow: $$E_x = \sqrt{\left[(E_q)^2 + (\frac{y}{q})^2 \times E_y^2 + (\frac{z}{q})^2 \times E_z^2\right] \times \left[\frac{q}{x}\right]^2}$$

Or in general terms is: $$E_{x1} = \sqrt{\left[E_q^2 + \sum_{i=2}^{n}((\frac{x_i}{q})^2 \times E_{xi}^2)\right] \times \left[\frac{q}{x_1}\right]^2}$$

It can be seen that where the 'metered by difference' stream flow rate is low compared with the flow through the remaining parallel streams then the uncertainty of the un-metered stream will become excessive. For example an uncertainty of 60 % is easily reported.

Authors Note: However, subject to the actual quantities involved, a 60 % uncertainty may translate to a relatively low quantity with respect to the quantities from the other systems. Due to the uncertainties of the other (i.e. metered) systems the stream metered by difference can be attributed with a negative quantity

4.2.5. Case 5: Attributed Quantity.

Case 5 may be considered to be a specific metering case. Multiple parallel metered streams are commingled into a common header and are then metered through a common stream.

This configuration normally relates to parallel Allocation meters commingling then being exported into a Pipeline through Fiscal quality meters. The actual quantity attributed to each input stream is Allocated by ratio against the 'more accurate' Fiscal meter quantity:

It must be assumed that, due to measurement uncertainties, the summation of the parallel Allocation streams does not equal the Fiscal meter reading.

Common Header "Total Produced Quantity" (tpq): $tpq = x + y + z$

Fiscal meter reading i.e. the Export Quantity is represented by: XQ

Due to metering uncertainties:- $tpq \neq XQ$

The Attributed quantities for the parallel streams are:

For meter stream "x": $AQ_x = \frac{x}{tpq} \times XQ$

For meter stream "y": $AQ_y = \frac{y}{tpq} \times XQ$

For meter stream "z": $AQ_z = \frac{z}{tpq} \times XQ$

If the "normal" uncertainty algorithm were to be applied the uncertainty equation would be:

Uncertainty in quantity allocated to stream "x": $E_{aqx} = \sqrt{E_x^2 + E_{tpq}^2 + E_{xq}^2}$

However: "Engineering Logic" indicates that this algorithm would return an excessive uncertainty for this configuration. This "Engineering Logic" leads to reconsidering the format of the attributed quantity equations as follows:-

For meter stream "x": $AQ_x = \zeta_x \times XQ$ Where:- $\zeta_x = \frac{x}{tpq}$

For meter stream "y": $AQ_y = \zeta_y \times XQ$ Where:- $\zeta_y = \frac{y}{tpq}$

For meter stream "z": $AQ_z = \zeta_z \times XQ$ Where:- $\zeta_z = \frac{z}{tpq}$

The uncertainty in the Allocation Fraction (ζ) can be demonstrated to be represented by:

Fraction for "x":- $$E_{\zeta x} = \sqrt{\left(\frac{y+z}{x+y+z}\right)^2 \times (E_x)^2 + \left(\frac{y}{x+y+z}\right)^2 \times (E_y)^2 + \left(\frac{z}{x+y+z}\right)^2 \times (E_z)^2}$$

Therefore the uncertainty in quantity attributed to stream "x" is:-

$$E_{aqx} = \sqrt{(E_{xq})^2 + \left(\frac{y+z}{x+y+z}\right)^2 \times (E_x)^2 + \left(\frac{y}{x+y+z}\right)^2 \times (E_y)^2 + \left(\frac{z}{x+y+z}\right)^2 \times (E_z)^2}$$

This can be expressed as a general case by the expression:

Uncertainty of mass fraction for any stream 'i':

$$E_{\varsigma.i} = \sqrt{\left(\frac{tpq - x_i}{tpq}\right)^2 \times E_{x.i}^2 + \left(E_{tpq}^2 - \left(\frac{x_i}{tpq}\right)^2 \times E_{x.i}^2\right)}$$

Where the uncertainty in the sum of the parallel streams (tpq) using Case 3 is:

$$E_{tpq} = \sqrt{(\frac{x_1}{tpq})^2 \times E_{x1}^2 + (\frac{x_2}{tpq})^2 \times E_{x2}^2 + \ldots + (\frac{x_n}{tpq})^2 \times E_{xn}^2}$$

Then the Attributed Uncertainty for input stream 'i' is: $E_{aq.i} = \sqrt{E_{\varsigma.i}^2 + E_{xq}^2}$

This expression correlates with an uncertainty evaluation using Monte Carlo Simulation (as do the other 'Case' equations given above).

4.2.6. Further Cases

This basic principle can be extended to cover other common metering configurations, for example phase change through separator vessels.

However: care must be exercised in implementing the mathematics to ensure that logical results are obtained. The above cases were checked by running the general root sum square equations against a Monte Carlo Simulation for the same input data. This was done using MathCAD Worksheets with the root sum square and Monte Carlo Simulation equations set-up in matrix format. Data was input with a variable number of meter streams, variable flow quantities and variable uncertainties against each stream. In all cases the uncertainty calculated using the root sum square algorithms correlated with the Monte Carlo Simulation (thus proving agreement between both the Statistical and Analytical Approach).

The applicable Standards require that the random (Type A) and systematic (Type B) elements of uncertainty are expressed individually. In practice, when assessing meter station uncertainty budgets it is extremely difficult differentiate between the random element and the systematic bias. In reality probably every term will have a random vector and a systematic vector and differentiating between these will be largely guesswork.

If the random & systematic uncertainties must, and can, be separated then the Case 3 expression:

$$E_q = \sqrt{\sum_{i=1}^{n}((\frac{x_i}{q})^2 \times E_{xi}^2)}$$

May be expanded to become:

$$E_{qT} = \sqrt{\sum_{i=1}^{n}((\frac{x_i}{q})^2 \times E_{x.random..i}^2) + \sum_{i=1}^{n}((\frac{x_i}{q})^2 \times E_{x.systematic..i}^2)}$$

Taking the particular case of a metering skid with a number of identical parallel meter streams, and where the systematic uncertainties are common to all streams then this expression may be simplified to:-

$$E_q = \sqrt{\sum_{x=1}^{n}((\frac{x_i}{q})^2 \times E_{x.random..i}^2) + E_{q.systematic}^2}$$

Also if the flow through each meter stream is balanced (i.e. equal flow through each stream) then the flow ratio simplifies to the number of meter streams on line:

$$E_q = \sqrt{\left(\frac{E_{random}}{\text{No of Streams}}\right)^2 + E_{systematic}^2}$$

The other “Case” equations would need to be similarly expanded.

4.3. SUB-ALLOCATION UNCERTAINTY

It is not expedient to provide a real case study of a Sub-Allocation or Pipeline Allocation uncertainty analysis as the Allocation methodology and data is confidential. However the principles involved can be illustrated in general terms.

Taking the example of a North Sea Installation producing from multiple reservoirs licensed to different consortiums; the financial exposure of each Partner in each consortium is dependant upon the relative flow rates of each source as well as the measurement point uncertainties.

A typical Sub-Allocation system for a multiple Reservoir production Installation could involve any of the following:-

Multiple Wells from each Reservoir
Multi-phase flow meter prior to commingling Reservoir fluids

Dedicated Separator for a Reservoir
Separation of Crude Oil, Natural Gas and Condensate phases
Commingling of Crude Oil after first stage Separator
Natural Gas commingled after first stage Separator
Natural Gas cross-flow from common second and third stage Separators
Condensate cross-flow from gas treatment plant
Crude Oil metered through common Fiscal Metering Station to Pipeline or shuttle tanker.
Separate Crude Oil Metering Stations
Common Gas Fiscal Metering Station to Pipeline
Common Condensate Fiscal Metering spiked to either Gas or Crude Oil Pipeline
Condensate spiked upstream of Crude Oil Fiscal Metering Station.
Fuel Gas metering
Flare Gas either metered or determined in some other way.
Lift gas metered and distributed to individual wells as required.

The starting point of the Sub-Allocation uncertainty analysis is to identify the primary mass flow paths through the Installation's Plant and to set-up the "Mass Ring-Fence". The Fluid mass flow Inputs into this Ring-Fence and the Fluid mass flow outputs from this Ring-Fence must be identified.

All inputs and all outputs should be measured, though a frequent alternative allows just one stream to be determined "by-difference".

The Mass Inputs into the Ring Fence will be the Natural Gas, Crude Oil and Produced Water from the individual Reservoirs; this measurement may be by multi-phase meter or as separate Gas, Oil and Water meters from a first stage Separator.

The Mass Outputs may include:

- Fiscally Metered Crude Oil
- Fiscally Metered Natural Gas
- Fiscally Metered Condensate
- Metered Fuel
- Metered Lift Gas
- Metered or estimated or "by-difference" Flare Gas.

The Sub-Allocation Procedure will incorporate the principles of the mass flow through the Installation and also equitable distribution of energy (both as produced energy in the exported products and consumed energy in extracting and treating those products).

This analysis is required to set-up a mathematical model of the Sub-Allocation System; once set-up this mathematical model of the mass (and energy) flow may be translated into an uncertainty analysis using the principles set-out in the combined flow "Cases" above.

These "Cases" will primarily involve:

- Parallel metered inputs to un-metered commingled stream (Case 3)
- Parallel metered inputs (excepting one by difference) to metered commingled. (Case 4)
- Allocation by Composition (Case 3)
- Gas / Liquid phase change through a Separator
- Parallel metered outputs (Case 3)
- Parallel metered outputs (excepting one by difference) to metered commingled. (Case 4)
- Attributed metered quantities against metered Commingled (Case 5)

Case 1 and Case 2 may be implemented as required. Gas / Liquid phase change through a Separator may be considered as “Case 6” (not illustrated above) where there is a mass fraction transfer between the vapour and liquid phases.

The final analysis results should be set-up to attribute the “risk” of the uncertainty associated with the Allocation to each Reservoir (and possibly extended to each Partner) in terms of Percentage uncertainty, actual quantity uncertainty and monetary uncertainty.

The attributed uncertainty is dependent upon the relative flow rates as well as the uncertainty of each measuring point; consequently the attributed uncertainty to any individual Reservoir may not directly reflect the quality of the measurements made by that Reservoir.

5.0 SUMMARY & CONCLUSIONS

5.1. GENERAL

The previous Sections were intended to illustrate the benefits of Analysing systems and deriving their associated measurement uncertainties using basic mathematical functions. By breaking down the uncertainty elements in this way, a true understanding of the essential elements of the measurement process may be better appreciated. For Example:

Instrument Design
By looking at the "Physics" of the measurement method and analysing the parameters that make the measurement process possible (as demonstrated in Section 2.0), then it is possible to get a better appreciation of which parts of the process effect the measurement the most. Thus the design engineers can concentrate on the "essential" elements of the measurement system as defined by their Sensitivity Coefficients and their Relative Uncertainty.

Metering Systems
Basic analytical methods can be used in the same way to address the formulae associated with deriving flow measurements in the preferred units (Mass, Standard Volume, Energy, Etc.). Each additional instrument may be assessed in terms of its Specification, its location and any process issues associated with that measurement. By building up "Templates" for different measurement systems and different instrument arrangements, a comprehensive selection of uncertainty measurement tools can be accumulated which can then be applied to Plant and Allocation Systems.

Plant & Allocation
The final (and often the most taxing) element in the uncertainty chain. Inevitably, these systems are unique to each client and must be built up based on the relative disposition of the measurement systems involved and the Process/Allocation issues associated with the particular application. Once built however, the uncertainty Model can be used to assess the respective benefits of using one measurement system as opposed to another and/or the effects of individual Instrument/Process uncertainties on the Plant/Allocation Model.

It should be noted that the Uncertainty Modelling Process can be run independently at each level, but the real strength of the philosophy is that each element of the uncertainty calculation can build on the previous level to provide a comprehensive analysis of "real" systems. It can be demonstrated that large measurement uncertainties can be missed by relying purely on Manufacturers data alone, or assuming that everything is operating within "design" parameters. It is only by Modelling the Equipment and Systems that a real insight into the measurement uncertainty of an Installation or Plant can be appreciated.

Authors Note: The assessment of "Measurement Uncertainty" really should be considered just the first step in assessing any measurement system. What is of more relevance is "what does this uncertainty mean in terms of Units Measured, or Product Value"; it would be very easy to convert the uncertainty measurement into terms that have a real meaning in the commercial world. Only when the measurement uncertainty is expressed in these terms can the real "Risk" associated with the measurement can be appreciated and decisions made as to its relevance.

Final Suggestion – most operators now have the data available and the computing capacity to assess the measurement uncertainty associated with their operating systems on a daily basis (i.e. the Daily Report). There could be great benefits, either internally or externally, in providing a "quality statement" associated with such Reports which may ultimately avoid the costly exercise of redressing "Mis-measurements" based on out of tolerance data.

APPENDICES

Case Study (Gas Ultrasonic Meter)

Uncertainty in Actual Volume

British Standard BS 7965: 2000 incorporates a method of assessing the uncertainty of an ultrasonic meter. The uncertainty terms in this Standard are mainly given as fixed values but this is not entirely appropriate as flow meters do not normally have a constant uncertainty over their operating envelope. However by using the principles of ISO 5168 and ISO GUM it is appropriate to analyse an ultrasonic meter uncertainty from the equations of measurement – the following illustrates the Methodology used.

The Ultrasonic Flow Meter measures fluid velocities at actual operating conditions consequently the initial flow quantity calculated is Gross Observed Volume (the conventional terminology for the Volume at Actual Operating conditions) as follows:

Gross Observed Volume = Mean Fluid Velocity x Pipe Cross Section Area

Or as an Equation: $$q_{gov} = v_{mean} \times \frac{\pi D^2}{4}$$

Where

v_{mean} Represents the mean fluid velocity in the pipe

D Represents the pipe internal diameter.

In a practical ultrasonic meter used for fiscal metering it is necessary to carry out a “Wet Calibration” hence the equation now becomes:

$$q_{gov} = v_{mean} \times \frac{\pi D^2}{4} \times MF$$

Where: “MF” is the Meter Factor determined by the Wet calibration.

The first level uncertainty equation for the Gross Observed Volume is therefore:

Uncertainty in Gross Observed (Actual) Volume: $E_{gov} = \sqrt{E_{vmean}^2 + (2)^2 \times E_D^2 + E_{mf}^2}$

As the Diameter term is squared it has a sensitivity factor of “2”. The remaining sensitivity factors are unity.

Mean Velocity Uncertainty

The mean fluid velocity is the combination of the individual measured path fluid velocities as a weighted summation:

In Daniel terminology:

$$v_{mean} = \sum_{path=1}^{\text{number of paths}} \left(\omega_{path} \times v_{\text{path}}\right)$$

Or expressing it slightly more mathematical where "np" = Number of Paths and "ip" = Individual Path.

$$v_{\text{m}} = \sum_{\text{ip}=1}^{\text{np}} \left(\omega_{\text{ip}} \times v_{\text{ip}}\right)$$

Other manufacturers use proprietary techniques but in terms of the uncertainty analysis this model should hold true.

By Partial Differentiation it can be shown that the 'mathematical' uncertainty of this equation may be expressed by the algorithm:

$$E_{v\text{m}} = \sqrt{\sum_{\text{ip}=1}^{\text{np}} \left[\left(\frac{\omega_{\text{ip}} \times v_{\text{ip}}}{v_{\text{m}}} \right)^2 \times \left(E_{\omega\text{ip}}^2 + E_{v\text{ip}}^2 \right) \right]}$$

Path Fluid Velocity

The individual path (subscript "ip") fluid velocity is calculated by:

Either:

$$v_{\text{ip}} = \frac{L_{\text{ip}}^2}{2\,X_{\text{ip}}} \times \frac{(\tau_{\text{du}} - \tau_{\text{ud}})}{\tau_{\text{du}} \times \tau_{\text{ud}}}$$

Or by:

$$v_{\text{ip}} = \frac{L_{\text{ip}}}{2 \times \cos(\theta)_{\text{ip}}} \times \frac{(\tau_{\text{du}} - \tau_{\text{ud}})}{\tau_{\text{du}} \times \tau_{\text{ud}}}$$

For a line of sight ultrasonic meter:-

Note that: $\frac{1}{X} \approx \frac{L}{\cos(\theta)}$ Hence $\frac{L_{\text{ip}}^2}{2\,X_{\text{ip}}} = \frac{L_{\text{ip}}}{2 \times \cos(\theta)_{\text{ip}}}$

And that: for any ultrasonic meter. $\frac{(\tau_{\text{du}} - \tau_{\text{ud}})}{\tau_{\text{du}} \times \tau_{\text{ud}}} = \frac{1}{\tau_{\text{ud}}} - \frac{1}{\tau_{\text{du}}}$

Where:

L_{ip} Represents the calibrated distance between a transducer pair.

X_{ip} Represents the 'Axial Beam Traverse'. That is the distance along the pipe that the ultrasonic beam sweeps as projected onto the pipe centreline.

θ Represents the Transducer inclination to the pipe wall.

τ_{du} Represents the Measured time period (second) of the ultrasonic pulse traverse from "down" to "up" (travelling UP stream against the fluid flow)

τ_{ud} Represents the Measured time period (second) of the ultrasonic pulse traverse from "up" to "down" (travelling DOWN stream with the fluid flow)

(The actual time measurement will be in micro second or nano second)

NOTE: The ultrasonic transducers are normally embedded into ports. Therefore the ultrasonic beam traverses a small DEAD SPACE prior to penetrating into the pipe cross section and hence the fluid flow.

For this reason the relationship: $\frac{1}{X} \approx \frac{L}{\cos(\theta)}$

Is not entirely true, it should be: $\frac{1}{X} = \frac{FPL}{\cos(\theta)}$

Where "FPL" represents the "Fluid Path Length", that is the actual ultrasonic beam length as it traverses the pipe cross section within the fluid flow.

$$FPL = L - 2 \times \text{Port Bay depth}$$

Basing the uncertainty analysis on the equation:

Measured Path Fluid Velocity: $v_{ip} = \frac{L_{ip}^2}{2\,X_{ip}} \times \frac{(\tau_{du} - \tau_{ud})}{\tau_{du} \times \tau_{ud}}$

Leads to an uncertainty algorithm:-

$$E_{vip} = \sqrt{(2)^2 \times E_{Lip}^2 + E_{Xip}^2 + \left(\frac{\tau_{ud}}{\tau_{du} - \tau_{ud}}\right)^2 \times E_{\tau du}^2 + \left(\frac{-\tau_{du}}{\tau_{du} - \tau_{ud}}\right)^2 \times E_{\tau ud}^2}$$

Where:

E_{Lip} Represents the uncertainty in the Ultrasonic Path

E_{Xip} Represents the uncertainty in the "Axial Beam Traverse"

$E_{\tau du}$ Represents the timing uncertainty in measuring the beam traversing UP stream

$E_{\tau ud}$ Represents the timing uncertainty in measuring the beam traversing DOWN stream

Further analysis, and evaluation, of these terms must consider the Geometry, the Physics and the Correction Factors applied to individual commercially available ultrasonic meters.

As the Transit Timing is carried out by the same electronic circuitry in both directions the ISO / GUM covariance term should be included with a correlation factor determined either by experiment or from manufacturer's data. The covariance term will be:-

$$\text{covariance} = \left(\frac{\tau_{ud}}{\tau_{du} - \tau_{ud}}\right) \times \left(\frac{-\tau_{du}}{\tau_{du} - \tau_{ud}}\right) \times v_m \times E_{\tau du} \times E_{\tau ud} \times \delta Cf$$

Where: δCf Is the Correlation Factor between the timing circuits.

Authors Note: The above example is intended to illustrate the analytical approach used to identify method used for calculating Flow Velocity. By identifying each element in the calculation, a greater understanding of the implications of incorrect equipment configuration and/or process effects can be seen, thereby allowing a more accurate determination of their effects on the measurement made (e.g. Path Length, Flow Profile, Etc.).

25TH INTERNATIONAL NORTH SEA FLOW MEASUREMENT WORKSHOP
October 16-19, 2007, Oslo, Norway

Erosion in a Venturi Meter with Laminar and Turbulent Flow and Low Reynolds Number Discharge Coefficient Measurements

Gordon Stobie, ConocoPhillips
Robert Hart and Steve Svedeman, Southwest Research Institute®
Klaus Zanker, Letton-Hall Group

1.0 ABSTRACT

Venturi meters are commonly used in single and multiphase flows. The ISO standard (ISO 5167-4) provides meter discharge coefficients for Venturi meters in turbulent flows with Reynolds numbers above 2 x 10^5. In viscous fluids, Venturi are sometimes operated in laminar flows at Reynolds numbers below the range covered by the standards. Venturi meters may also be subjected to erosion from sand entrained in the fluid. The effects of erosion on the Venturi meter performance is a concern for long-term field operations.

Test data were obtained on a classical Venturi meter operating in laminar flow to measure the discharge coefficient as a function of Reynolds number. Data were obtained over a range of flow rates and fluid viscosities. Modeling using computational fluid dynamics (CFD) was used to obtain additional insight into the Venturi meter performance in laminar flow conditions. The test setup and test results are presented, with the CFD modeling results.

Tests were also conducted to evaluate the effects of erosion on Venturi meters. Three Venturi meters were exposed to oil/sand and water/sand slurry erosion. The meters were flow tested before and after exposure to the slurry flows to measure changes in the meter discharge coefficients. Dimensional changes were also recorded.

2.0 INTRODUCTION

This paper describes the measurement of Venturi meter discharge coefficients at low Reynolds numbers (with viscous oil) and presents the results for tests conducted to determine the effect of solid particle erosion in Venturi meter measurements.

Discharge Coefficients. Viscous oil production is sometimes metered using multiphase meters that contain Venturi flow elements. The conditions encountered in metering viscous fluids can be beyond the range of applicability of the industry standards (ISO 5167-4). The ISO standard is limited to turbulent flows for Reynolds numbers (based on the upstream pipe diameter) above 2 x 10^5. Metering viscous oils may involve laminar, rather than turbulent flow at Reynolds numbers below the range covered by the ISO standard.

A test program was carried out at the Southwest Research Institute (SwRI®) Multiphase Flow Facility to determine the discharge coefficient of a nominal four-inch diameter Venturi flow meter at low Reynolds numbers (approximately 80 to 100,000), in single-phase viscous flows. In addition, simulations were conducted using CFD to model the Venturi meter performance.

Erosion. Field experience has shown that heavy oil production is often associated with sand production, and erosion of the flow meters is not uncommon in these cases. It is not known

how meter erosion affects the venturi flow meter performance. In order to investigate the effect of erosion on Venturi meter accuracy, tests were conducted to erode Venturi meters.

Two test facilities were assembled at SwRI. The first was a water flow rig that was used to measure the discharge coefficients of the test meters before and after erosion. The second was to run viscous oil containing sand through the Venturi meters. The Venturi meters were exposed to the oil slurry erosion three times and the meter discharge coefficients were measured after each slurry exposure. After the slurry exposure, the meter dimensions were re-measured to determine any dimensional changes.

3.0 VENTURI METER DISCHARGE COEFFICIENTS

Per ISO 5167-4, the mass flow rate in a Venturi meter (q_m) is given by:

$$q_m = \frac{C}{\sqrt{1-\beta^4}} \varepsilon \frac{\pi}{4} d^2 \sqrt{2(P_1 - P_2)\rho_1} \tag{1}$$

where:

C = Venturi discharge coefficient
β = Venturi beta ratio, d/D
d = Venturi throat diameter
D = Pipe diameter upstream of the Venturi convergent section
ε = Expansion factor
P_1 = Static pressure at the upstream pressure tap
P_2 = Static pressure at the Venturi throat tap
ρ_1 = Fluid density at the upstream tap location

When working with Venturi meters, Reynolds numbers based on inlet pipe diameter (D) and throat diameter (d) are frequently used. These are defined as follows:

$$\mathrm{Re}_D = \frac{\rho V D}{\mu} \tag{2A}$$

$$\mathrm{Re}_d = \frac{\rho V d}{\mu} \tag{2B}$$

where μ, δ and V are the dynamic viscosity, density, and average velocity, respectively, corresponding to either D or d.

Equation (1) is based on the assumptions that include steady, incompressible, and inviscid flow (no frictional pressure losses) and turbulent flow profiles (i.e., "flat" flow profiles) occur at the pressure tap locations. Two of the assumptions inherent in the Venturi equation do not apply when metering viscous fluids under laminar flow conditions. These are the assumptions that the flow is turbulent, so the velocity profile is uniform across the cross-section, and that the frictional pressure losses within the meter can be neglected.

Little data are available on Venturi discharge coefficients in laminar flow. Published results show that when the Reynolds number decreases below approximately 2 x 10^5, there is a small increase in the discharge coefficient before there is a steady decrease with decreasing Reynolds number. The strong dependence of the discharge coefficient on Reynolds number, for low Reynolds number flows makes it critical to know the operational conditions (so Reynolds number is known) for accurate metering.

A series of tests were conducted to obtain additional data on Venturi discharge coefficients under laminar flow conditions for Reynolds numbers below 2 x 10^5. The meter used was a four-inch ISO 5167-4 Venturi (Fluidic Techniques Model V-100) with a 21° convergent section and an 8° divergent section (included angles). Experiments were conducted over a range of flow rates and fluid viscosities. Dimensional details of the Venturi meter, were: D = 3.826 inches, d = 2.399 inches, and D = 0.627 inches.

In addition, CFD modeling was conducted to to simulate laminar flow in a Venturi meter. The objectives was to gain additional insight into low Reynolds number flows in Venturi meters to evaluate how well CFD modeling can predict the experimental results.

3.1 Experimental Setup

Testing was conducted in the flow loop at the SwRI Multiphase Flow Facility. Although the flow loop can be configured to accommodate multiphase flows, the testing did not require gas flow, so the loop was operated in single-phase flow. A heat exchanger controlled the loop temperature. Figure 1 shows a photograph of the test facility.

Figure 1. SwRI Multiphase Flow Facility Flow Loop

The Venturi meter was installed in the flow loop downstream of a pair of reference flow meters. These were a Coriolis meter (Endress-Hauser Promass® 83F) to measure the density of the oil, and a positive displacement flow meter (Metroval FA 600-SR) that was the volumetric flow rate reference.

The Venturi meter instrumentation consisted of a static pressure transmitter and a pair of "stacked" differential pressure (DP) transmitters. Low-range (0-50 inH_2O) and a high-range (0-250 inH_2O) DP transmitters were installed to reduce the uncertainty at low flow rates. The flowing temperature at the meter was determined from an RTD located in the pipe immediately downstream of the Venturi flow meter.

Since oil viscosity is a function of temperature, it was necessary to establish the viscosity versus temperature relationship of the oil so that the Reynolds number could be accurately determined at the various operating temperatures. For this a laminar flow viscometer was used. The viscometer consisted of 5/8-inch OD tubing with two pressure taps (for measuring pressure drop) located a known distance apart. To control the temperature of the oil in the viscosity test section, the tubing was strapped to the main test section piping and insulated. Before and after each series of test runs, flow would be diverted through the viscometer to measure the viscosity at the operating conditions. An average temperature associated with each measured viscosity was determined from RTDs located at the upstream and downstream ends of the viscometer. Using the measured DP and the mass flow rate and density from a Coriolis flow meter installed in the viscometer, the viscosity (μ) was calculated using the following equation:

$$\mu = \left(\frac{\pi}{128}\right)\frac{\rho \Delta P D_v}{ML} \tag{3}$$

where:

ρ = Fluid density
ΔP = Differential pressure between viscometer taps
D_v = Inside diameter of viscometer tube
M = Mass flow rate
L = Distance between viscometer taps

3.2 Test Conditions

For most of the testing, the flow loop was filled with Texaco Regal R&O 32 oil and pressurized with nitrogen. The static pressure in the loop was maintained between 150 and 200 psig over the course of the testing. (For each individual test run, the pressure was fixed.) Because of the difficulty in separating the gas from the viscous oil, care was taken to prevent the gas used to pressurize the loop from becoming mixed with the oil and carried to the test section. At the conclusion of the testing with oil, the loop was drained and filled with fresh water and a few test points were collected to check the performance of the Venturi meters in turbulent flow at higher Reynolds numbers. No effort was made to completely remove all oil from the loop, so the water was likely mixed with a small amount of oil.

132 test points were collected. Of these, 121 test points were completed with the oil and 11 were conducted with water. Table 1 summarizes the range of conditions covered.

Table 1. Range of Conditions for the Venturi Meter Testing.

METER SIZE	TEST FLUID	NUMBER OF TEST POINTS	Re_d	TEMPERATURE [°F]	REFERENCE FLOWRATE [kg/s]
4”	Oil	121	80 - 8514	53 - 123	1.9 - 19.9
	Water	11	22,110 - 100,914	87 - 89	3.5 - 17.2

3.3 General Test Procedure

Testing consisted of a number of datasets, with each dataset corresponding to a different nominal temperature (and oil viscosity). Each dataset was in turn, composed of a number of individual test points taken at different flow rates (and Reynolds numbers). For each test point, the discharge coefficient was computed by dividing the reference mass flow rate by the Venturi meter mass flow rate as calculated from Equation (1) with C = 1. As the temperature of the oil

tended to change over the course of a dataset, each dataset was bracketed by viscosity measurements made at the beginning and end of the dataset. All of the viscosity measurements were combined to create a viscosity-versus-temperature relationship that was used in post processing to calculate Reynolds numbers for the measured temperature of each test point.

3.4 Experimental Results

The objective was to measure the discharge coefficient of the Venturi meter over a range of Reynolds numbers, primarily in the laminar flow regime. The calculation of the discharge coefficient was straightforward as it depended only on measured and geometric parameters, such as flow rate, differential pressure, and meter dimensions. The calculation of Reynolds number was complicated by the fact that in addition to geometric and measured quantities, it also depends on the oil viscosity. Since oil viscosity is a function of temperature and the oil temperature tended to vary between test points, the Reynolds number needed to be determined during a particular test run.

Viscosity Measurements. The approach used for calculating Reynolds numbers for the tests with oil was to combine all of the viscosity measurements to determine a functional relationship between viscosity and temperature and then use this relationship to calculate a Reynolds number for each test point based on the average measured temperature during that run.

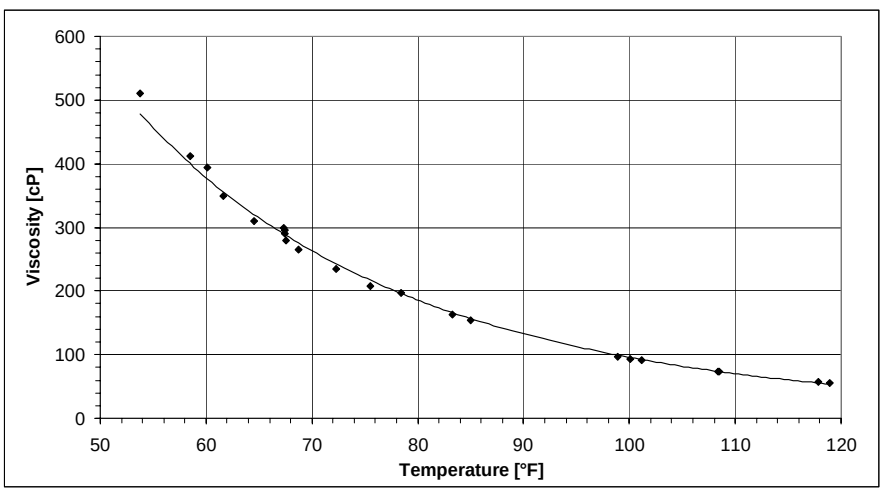

Figure 2. Oil Viscosity as a Function of Temperature.

Figure 2 presents the oil viscosity measurements with the curve fit that was used to characterize the data. The curve fit is of the form:

$$\mu = Ae^{B/T_{abs}} \tag{4}$$

which is the viscosity-versus-temperature model suggested by Fox and McDonald[2] for liquids. In Equation (4), A and B are constants and T_{abs} is the absolute temperature. A least-squares curve fit of all of the oil viscosity data points is shown as a solid line in Figure 2. Based on this fit, the values of the adjustable parameters in Equation (4) are as follows:

$A = 1.72618 \times 10^{-6}$
$B = 9980.58$

This curve fits the experimental data with an error that varies from -6.4% to +4.6%. The percentage error was calculated from the difference between each measured value of viscosity and the predicted value from the curve fit. Although this curve does not appear to fit the data

well at the highest viscosity (where there is a -6% error), the fit curve interpolates the remainder of the data points fairly well with errors that range from -4.8% to +4.6%.

Discharge Coefficients. The discharge coefficients for the Venturi meter are shown in Figure 3. The points below Reynolds number of 10,000 were obtained using oil as the test fluid, water was used for the points above 10,000. When plotted against the throat Reynolds number, the discharge coefficients, which were measured at a variety of temperatures, flow rates, and viscosities, all collapse onto a single curve. The overall behavior of the discharge coefficient curve is consistent with what is described in the literature and ISO 5167-4, including the "hump" that occurs as the Reynolds number decreases below 5,000. This hump is associated with the laminar-turbulent transition in the meter as explained by Benedict and Wyler[3]. At the highest Reynolds numbers, the experimental discharge coefficients agree with the values given in the ISO standard (0.970-0.977 for $5 \times 10^4 < Re_d < 1 \times 10^5$). The uncertainty in the Reynolds number is estimated to be ±1.3%, for all Reynolds numbers, and the uncertainty in the Venturi meter discharge coefficient ranges from approximately ±0.3% to ±0.8%.

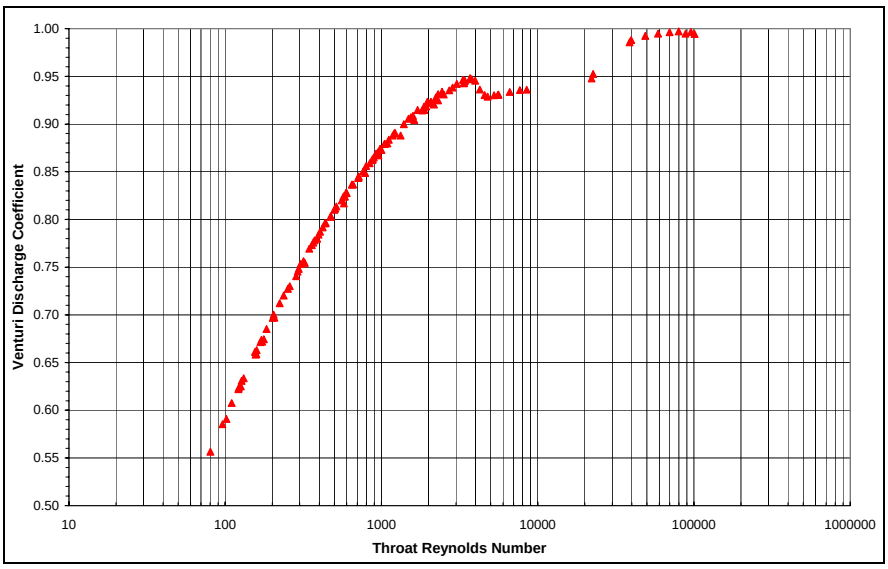

Figure 3. Experimentally-Determined Discharge Coefficients for the Four-Inch Venturi Meter.

In Figure 4, the discharge coefficients for the Venturi meter are compared to published data from several sources. Miller[4] presents data for 40 mm $\leq D \leq$ 100 mm and $0.3 \leq \beta \leq 0.7$, and the curve in Figure 4 is plotted assuming $\beta = 0.5$. Benedict and Wyler[3] proposed a generalized discharge coefficient for differential pressure-type flow meters. Figure 4 shows their proposed equation for laminar flow in a classical Venturi tube. The equations proposed by Pal[5] for the discharge coefficients for both stable and unstable water/oil emulsions are included, along with the data of Atkinson[6].

The discharge coefficients follow the same general trends as the published results, but do not agree exactly with any of the correlations. For Reynolds numbers below about 1,000, the data falls within the range of the various published results. Between Reynolds numbers of 1,500 to 5,000, the experimental points tend to be higher than the correlations would predict, but above a Reynolds number of 5,000 there is, good agreement. The transition "hump" found in the data of Miller is also seen in the experimental data, although it does not occur at the same Reynolds number. Since laminar to turbulent transition is facility dependent and does not occur at a

specific Reynolds number, it is not surprising that there would be some differences in the published and experimental discharge coefficients in the transitional range of Reynolds numbers.

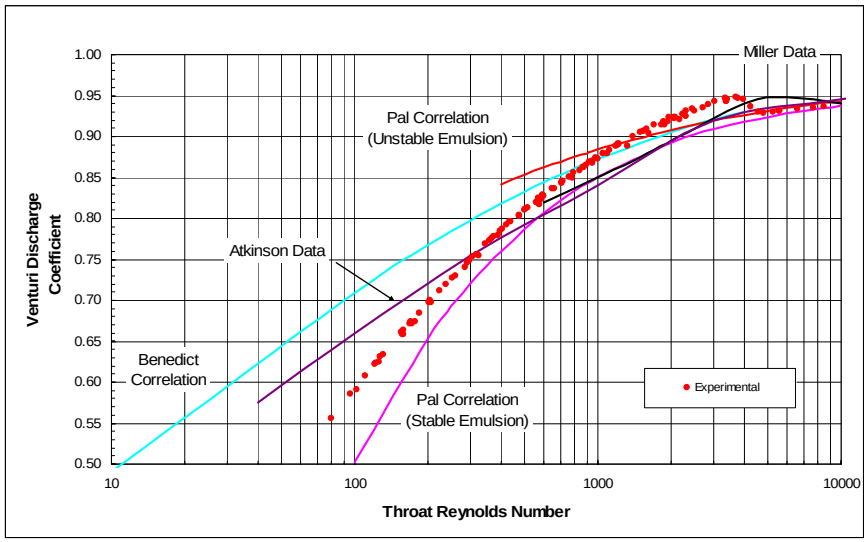

Figure 4. Comparison of Published Values of Venturi Meter Discharge Coefficients for Low Reynolds Numbers with the Experimental Results.

3.5 CFD Modeling

CFD modeling is a useful tool to gain an insight into the physics of the flow and to help understand the test results. The objective of the CFD work was to model the flow using two-dimensional CFD to obtain information about the flow that could not be obtained in the experimental test program. The CFD results were validated by running simulations for conditions within the range of the experimental test data and comparing the predicted discharge coefficients with the experimentally-determined values. Additional CFD simulations were conducted to predict Venturi meter operation at Reynolds numbers lower than could be simulated in the laboratory.

Model Description. The Fluent™ CFD model was used to simulate laminar flow through a Venturi meter. The Venturi geometry was modeled as a two-dimensional axisymmetric domain using a structured grid. The geometry was taken from the manufacturer's drawing of the Venturi meter. No pressure taps were included in the CFD geometry.

Figure 5 shows the CFD grid used for the contraction section of the meter. The modeled geometry included five diameters of straight pipe upstream of the contraction section and a diffuser section. A total of 41 grid points were used to detail the radial direction, and a total of about 450 grid points were placed along the inlet pipe, contraction section, and diffuser.

In simulating a fully-developed laminar flow profile at the Venturi meter inlet, a laminar velocity profile was prescribed at the pipe inlet, located five D upstream of the upstream pressure tap. This ensured a fully-developed laminar velocity profile at the Venturi upstream pressure tap location. The flow solutions were obtained for steady, incompressible flow.

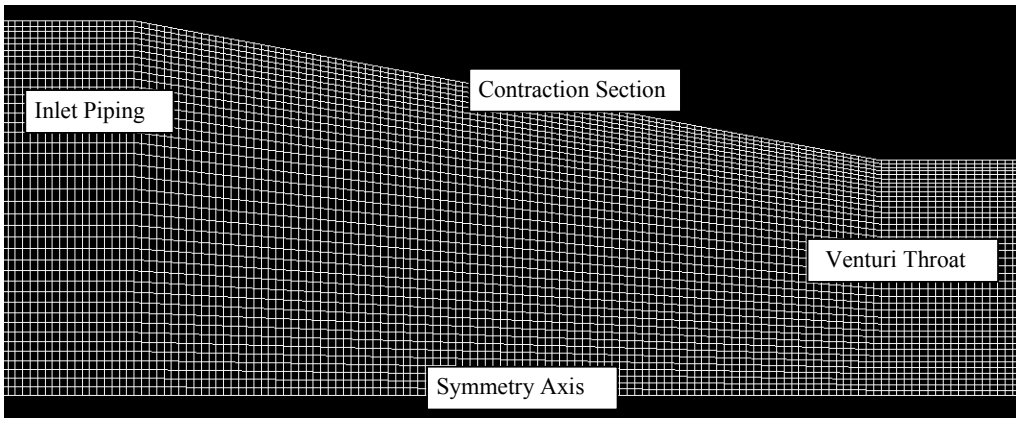

Figure 5. Computational Grid Used for the Contraction Section of the Venturi Meter Simulation.

Discharge Coefficients. CFD simulations were performed over a range of conditions. Venturi discharge coefficients were calculated from the predicted Venturi pressure drops and the flow rates. The simulations were done for oil viscosities of 250 cp, 500 cp, and 1,000 cp, a constant oil density of 889.9 kg/m^3 (27.5 API), and Reynolds numbers from 34 to 1,654.

Figure 6 shows the test data and the CFD results plotted together. The agreement between the experimental and CFD results is good; although it appears that the curves represented by the two sets of data have slightly different slopes. The results appear to cross between Reynolds numbers of 100 to 200, with the CFD slightly underpredicting the discharge coefficient for Reynolds numbers above 200. The CFD simulations were done before the experiments, and the CFD data was not "tweaked" to achieve the level of agreement shown.

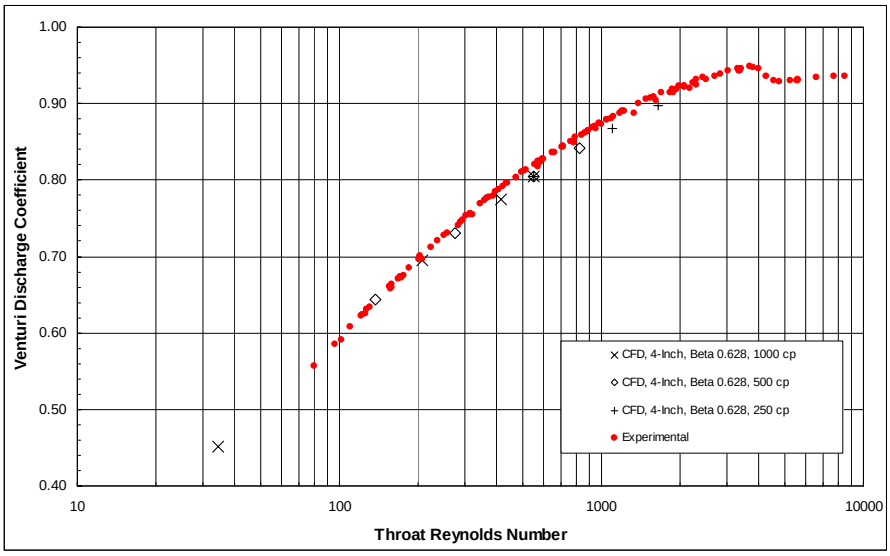

Figure 6. Comparison of Experimentally-Determined Venturi Meter Discharge Coefficients with the CFD Predictions.

Additional CFD simulations were carried out to predict Venturi discharge coefficients for Reynolds numbers below those that could be achieved experimentally. In these simulations, oil viscosities were increased to 30,000 cp to produce throat Reynolds numbers as low as two. The results show that the discharge coefficient tends toward zero as the Reynolds number is reduced. The discharge coefficient curve becomes very steep for Reynolds numbers below about 100.

These trends can be better seen when the data is plotted on a linear scale, as shown in Figure 7. One consequence of the nonlinear discharge coefficient curve is that a given uncertainty in the Reynolds number (viscosity or density uncertainty) will produce a larger uncertainty in the calculated discharge coefficient as the Reynolds number decreases.

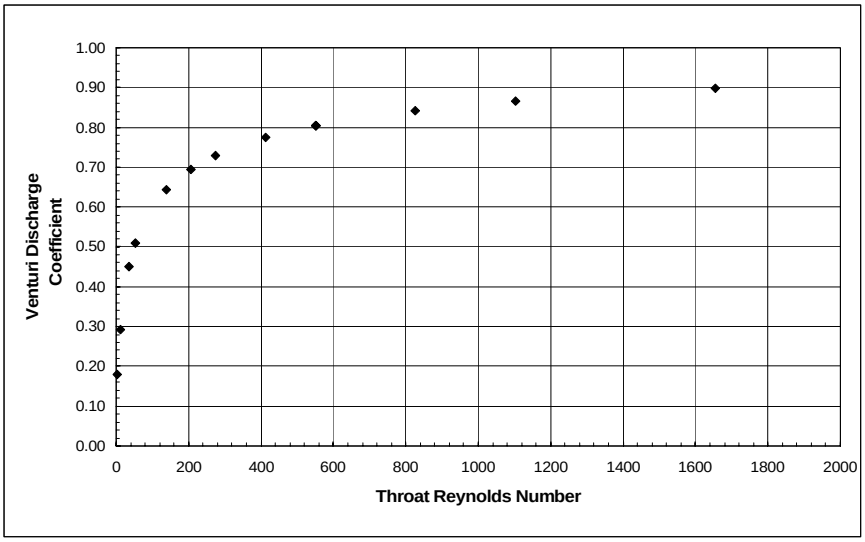

Figure 7. Venturi Meter Discharge Coefficient Versus Throat Reynolds Number Plotted Using a Linear Scale.

Frictional Pressure Loss. A large portion of the pressure drop measured across the Venturi pressure taps is due to frictional forces at the low Reynolds numbers used in the simulations. Figure 8 shows the frictional pressure loss as a percentage of the total pressure drop. At Reynolds numbers below about 50, about one-half of the measured pressure drop in the Venturi is due to frictional losses. These results show that one of the key assumptions (inviscid flow) inherent in Equation (1) is obviously not valid for viscous oil under laminar flow conditions.

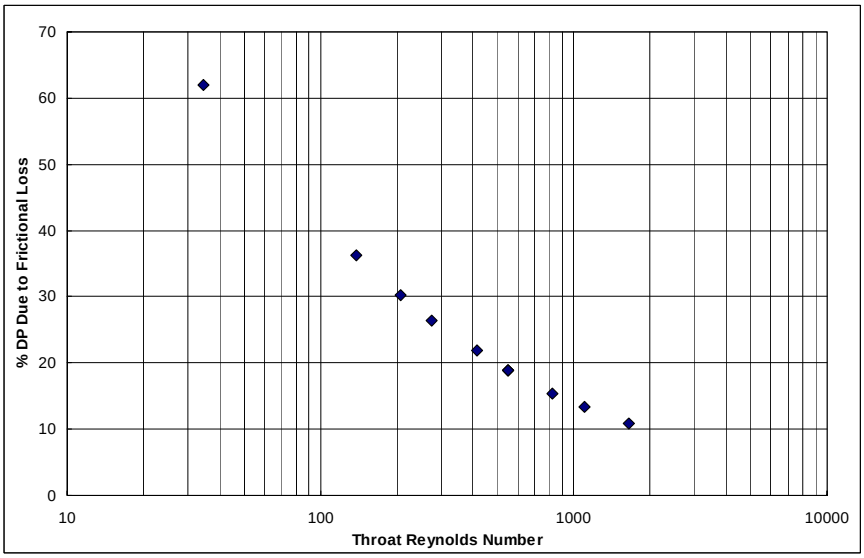

Figure 8. Percentage of the Measured Venturi Pressure Drop Due to Frictional Pressure Loss.

Throat Velocity Profile. CFD simulations were used to determine the kinetic energy correction factors at the Venturi throat pressure tap. Using the symbol v for the local velocity and V for the average velocity, the kinetic energy correction factor is defined as:

$$\alpha = \frac{1}{A}\int_A \left(\frac{\mathrm{v}}{\mathrm{V}}\right)^3 dA \tag{5}$$

The kinetic energy correction factor depends upon the velocity profile. For a fully-developed laminar flow profile, α is equal to exactly two. For a fully-developed turbulent flow profile, α will vary from about 1.02 for smooth pipe with a high Reynolds number to 1.2 for rough pipe at a lower Reynolds number. In most engineering computations for turbulent flow, the correction factor is usually neglected (set to equal 1.0), which is equivalent to assuming that the velocity profile is uniform.

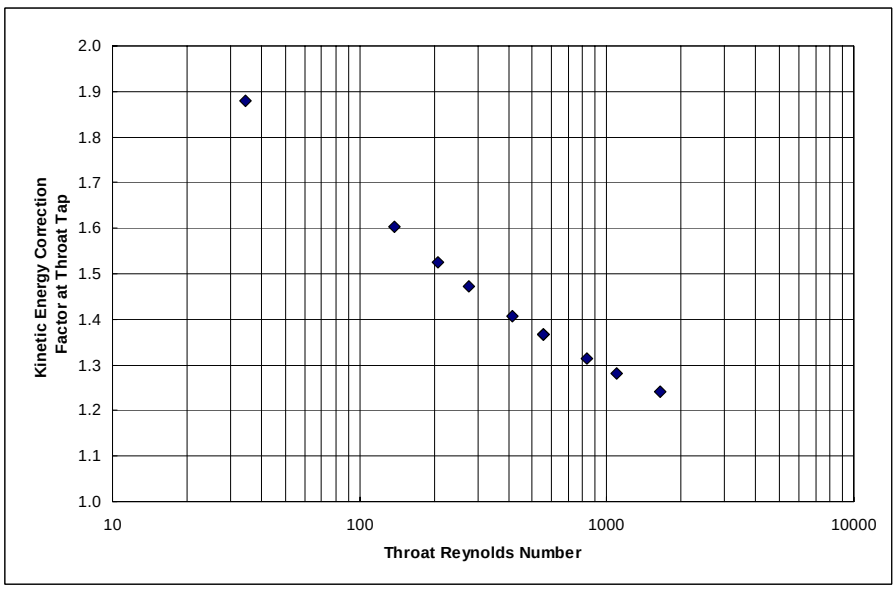

Figure 9. Kinetic Energy Correction Factor for the Venturi Meter Throat Pressure Tap.

Figure 9 shows the values of α as a function of the throat Reynolds number. The kinetic energy correction factor α varied from almost two at Re_d ~ 16 to 1.2 at Re_d ~ 2,000. As expected, as the Reynolds number increased, the throat velocity profile became flatter, approaching a turbulent velocity profile with an α value near 1. These results show that the second key assumption (flat or uniform velocity profile at the pressure taps) inherent in Equation (1) is not valid for viscous oil under laminar flow conditions.

4.0 VENTURI EROSION TESTS

Erosion tests were conducted to determine how erosion of the Venturi effects flow meter performance. The objective of the work was to subject Venturi meters to a viscous fluid stream containing sand to determine where Venturi meters eroded. The effect of erosion on the measurement accuracy of Venturi meters was determined by flow testing the meters before and after exposure to the erosive flow stream. Dimensional measurements of the Venturi meters were recorded before and after exposure to the erosive flow stream. After the oil slurry erosion tests were completed, additional erosion testing was conducted using a water/sand slurry.

Four identical Venturi meters were used in the test program. One meter, the "standard" meter, was not exposed to the erosive flow conditions. The "standard" meter was used to compare the discharge coefficients of the other three meters before and after each erosion test. The flow tests were to identify any shifts in the eroded meters' discharge coefficients. These flow tests were conducted using water flow and the Venturis were installed in accordance with ISO 5167-4 (straight pipe runs upstream and downstream of the Venturis).

Measurements were also made of the inside surfaces of the Venturi meters before and after the erosion tests to document changes to the surface finish and geometry.

4.1 Pressure Tap Hole Imperfection in Venturi V-2586-1A. In establishing the baseline discharge coefficients of the test meters, it was observed that one meter had a discharge coefficient of 0.973. This was significantly different from the other meters which were close to 0.995.

Visual inspection did not reveal any obvious defects. The problem was traced to a small burr on the upstream side of the "B" throat pressure tap. A casting of the pressure tap was made with a casting material so that the pressure tap contour could be seen (the throat tap was difficult to inspect since was located ~8" from the end flanges in a 1" diameter throat). Figure 10 shows a view of the casting at the intersection of the Venturi throat and the pressure tap. The burr stood up into the throat about 0.002".

The burr was sanded down and the flow test repeated. The meter discharge coefficient changed from 0.973 to 0.999, a change of about +2.6%. The surface roughness measurement upstream of the pressure tap changed from 43 micro-inches before sanding to 11 micro-inches after sanding. It is possible that the smoother surface finish may have affected the discharge coefficient after sanding (the discharge coefficients of the test meters were determined relative to an identical Venturi that was assumed to have a discharge coefficient of 0.995).

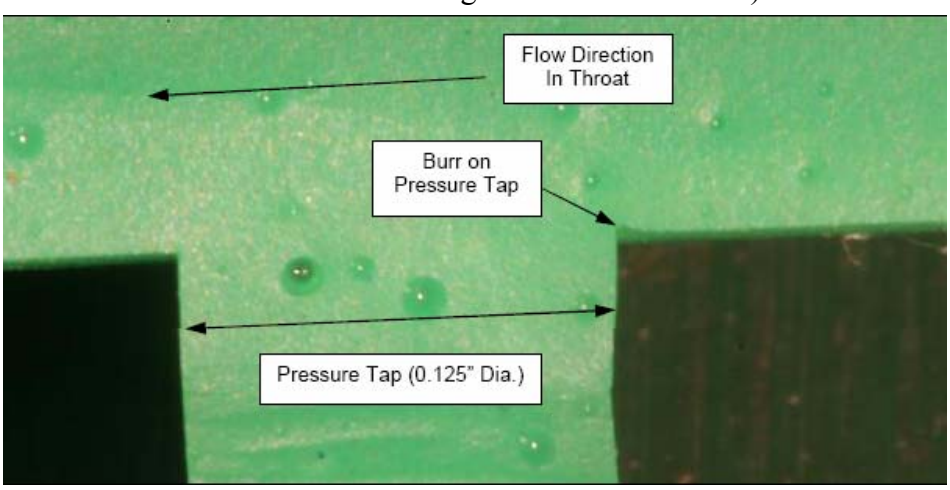

Figure 10: Burr on Venturi Meter V-2586-1A

4.2 Erosion Test Rig and Test Meters

An erosion test rig was set up to flow viscous oil-sand slurry through the Venturi meters to simulate the erosion exposure of the meters under field conditions. Three Venturi meters were installed in series, so each of the meters was exposed to the same fluid flow and sand loading. A schematic of the test rig is shown in Figure 11.

The Venturi meters were installed vertically with the flow passing through the Venturis in the upward direction. The Venturis were installed directly downstream of blind tees as they would typically be installed in multiphase flow meters. The geometry for the flow meter installation is shown in Figure 12.

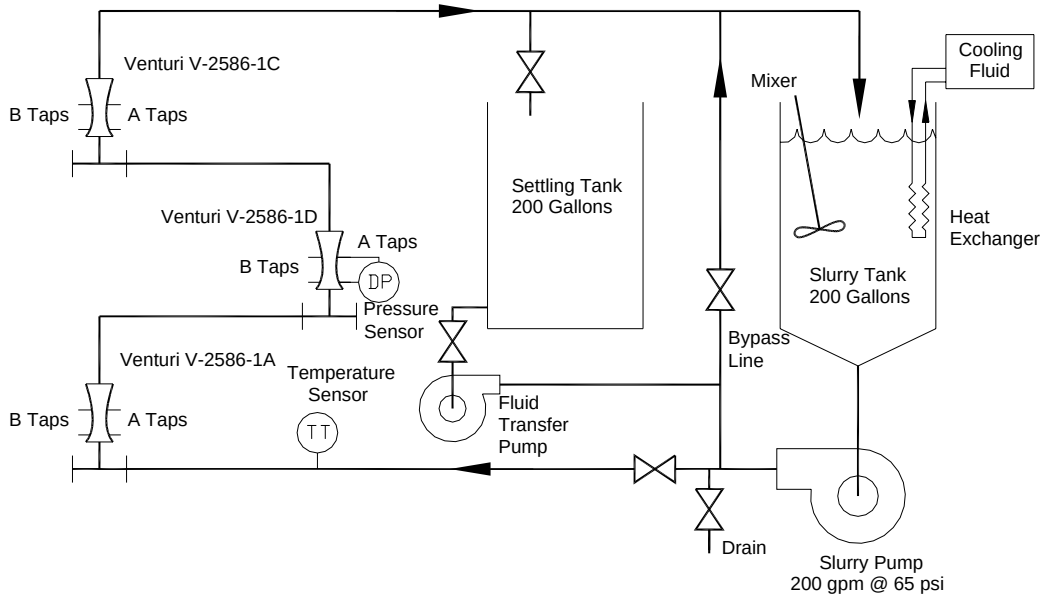

Figure 11. Schematic Diagram of the Erosion Test Rig.

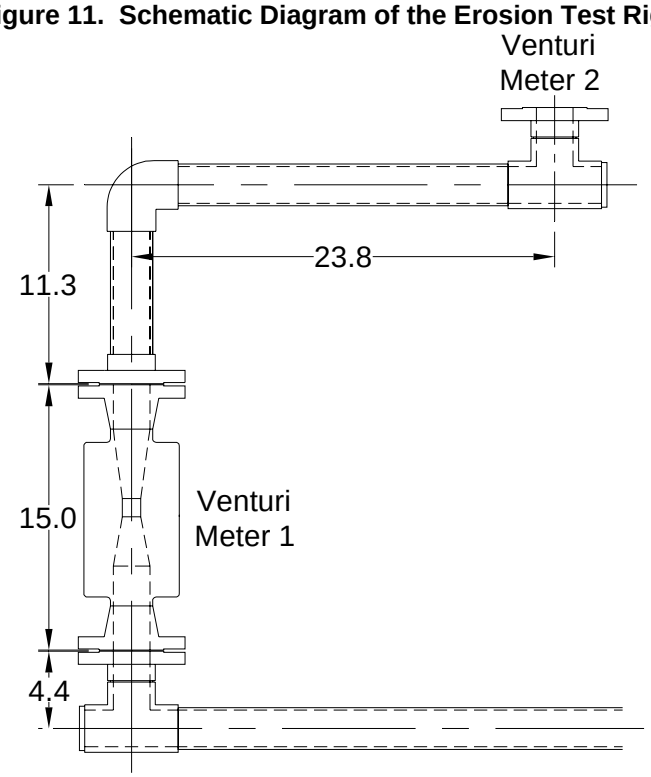

Figure 12. Flow Meter Installation Geometry.

Test Meters. Four matching Venturi meters were fabricated in 316 stainless steel, and is were designed to ISO 5167-4. The Venturis had a nominal two-inch inlet with 150# RF flanges and a Beta ratio of 0.5.

Solid Particles. The sand used for the erosion tests had a mean diameter of 276 microns. Figure 13 shows the result of a laser particle size analysis of the sand. The sand grains range in size from about 125 microns to about 600 microns. A photograph of the sand used in the tests is shown in Figure 14. The sand was made from crushed silica, so the particles were irregularly shaped and had sharp edges.

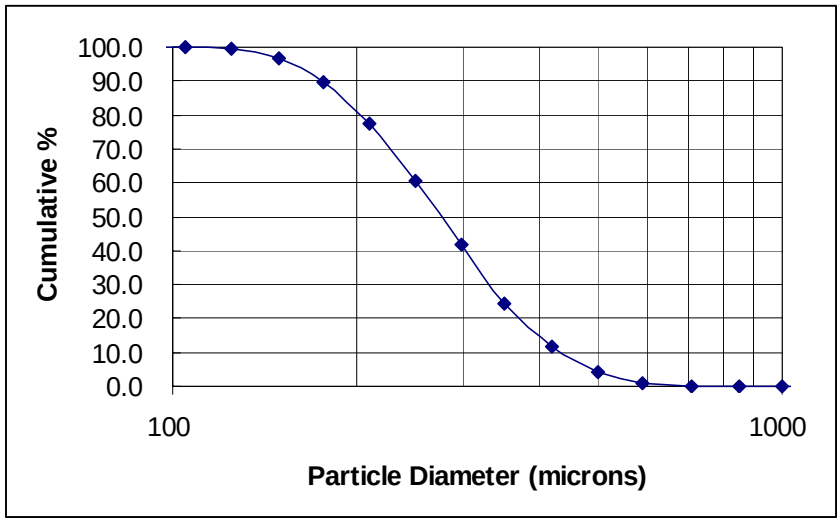

Figure 13. Plot of the Size Distribution of the Sand Used in the Erosion Tests.

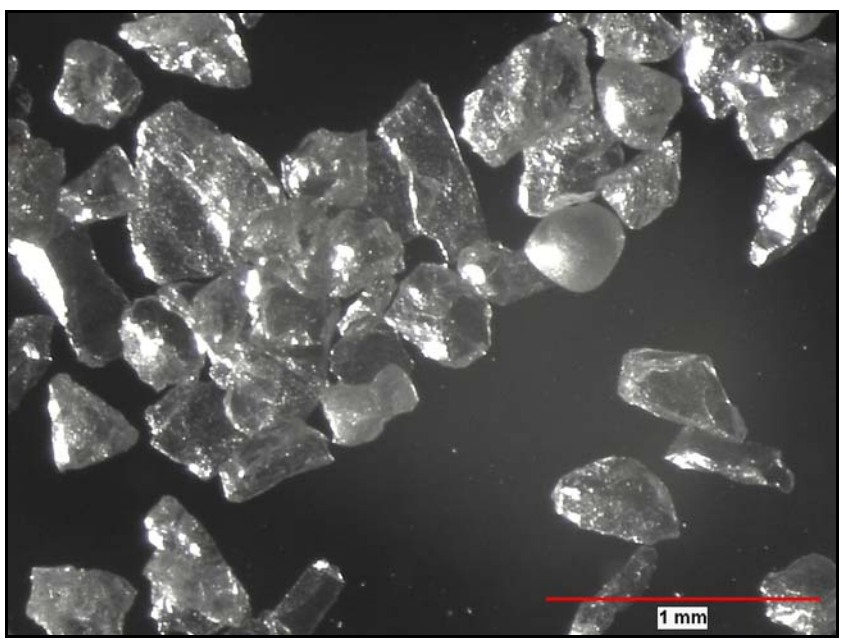

Figure 14. Photograph of the Sand Used in the Erosion Tests.

4.3 Viscous Oil Erosion Tests

The erosion test conditions were selected to accelerate the erosion rate. To maximize erosion, a high sand loading was used along with a minimal fluid viscosity, and as high a flow

rate as possible. The test conditions required a tradeoff between laminar flow, increasing the flow rate, and minimizing viscosity.

The erosion tests were run at 120 gpm (about 4100BPD), oil viscosity of 360 cP, oil density of 0.88 gm/cm^3 and a sand loading of 2% to 4% by mass. For these conditions, the pipe Reynolds number was 450 and the throat Reynolds number was 900. The meter pressure drop during the test was ~16 psi (1.1 bar). The pipe velocity was about 11 ft/sec and the throat velocity was 46 ft/sec.

The Venturi meters were exposed to oil slurry erosion over three separate periods. Between each period, the Venturi meters were removed and installed in the water flow loop to determine any changes in the discharge coefficients. A summary of the conditions during each of the three erosion runs is given in Table 2.

Table 2. Summary of the Erosion Test Conditions.

CONDITION	EROSION RUN 1	EROSION RUN 2	EROSION RUN 3
Run Time (hr)	28.13	145.80	140.41
Average Sand Concentration (% by wt)	1.63	4.73	4.52
Average Temperature (°F)	107.8	107.3	107.5
Fluid Viscosity (cP)	357	364	362
Throat Reynolds No.	918	882	892
Venturi Throat Velocity (ft/sec)	45.8	45.2	45.8
Venturi Inlet Velocity (ft/sec)	11.4	11.3	11.5
Mass of Sand Through Venturis (lbm)	24,400	368,000	344,000

The total mass of sand that passed through each Venturi during Run 1 was 24,400 lbm. After Run 1, the Venturi discharge coefficients did not indicate any erosion, so the duration of the erosion test and the sand concentration in the slurry were increased. At the end of test Run 3, the three Venturi meters had had a total of 732,000 lbm of sand pass through them.

The oil flow tests after each erosion run showed no measurable change in the discharge coefficient. The dimensional measurements made before and after the erosion tests also showed no measurable erosion.

Photographs taken of the pressure taps before and after the erosion tests confirmed that the viscous slurry had not produced any significant erosion of the Venturi bores. Figure 15 shows photographs of the throat tap for one of the Venturis before the erosion test and after completing Run 3. The flow direction in the photograph is from the bottom to the top. The photographs show that the tap hole geometry was unchanged and the surface of the Venturi around the tap hole still has visible machine grooves after the erosion tests. Figure 16 shows a photograph of a throat pressure tap hole after exposure to the erosion tests. A 0.124-inch diameter rod was inserted into the tap hole to provide a dimensional reference. The 0.125-inch diameter pressure tap hole had not changed due to erosion. The machine grooves on the bore are also still visible, indicating that there was no significant erosion of the Venturi throat.

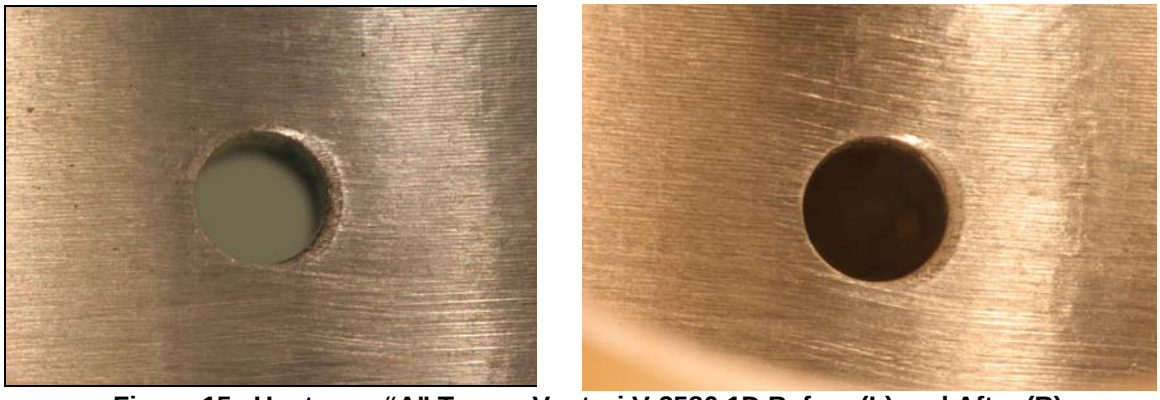

Figure 15. Upstream "A" Tap on Venturi V-2586-1D Before (L) and After (R) Exposure to the Sand Slurry.

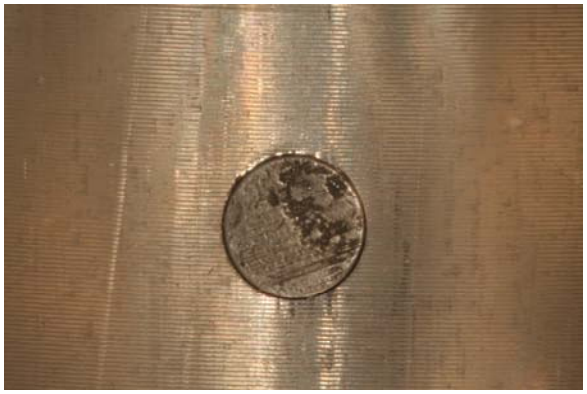

Figure 16. Throat Tap ("A" Tap) in Venturi V-2586-1A after the Erosion Tests.

4.4 Water Erosion Tests

After completing the oil slurry tests, further tests were conducted to expose the Venturi meters to a water/sand slurry. This was conducted using the same test rig, and sand size as the oil erosion tests. Total run time was 242 hours, and is summarized in Table 3.

Table 3. Flow Conditions for the Water/Sand Slurry Tests.

CONDITION	VALUE
Run Time (hr)	242
Average Sand Concentration (% by wt)	4.57
Average Temperature (°F)	77.5
Fluid Viscosity (cP)	0.884
Throat Reynolds No.	419,900
Venturi Throat Velocity (ft/sec)	44.7
Venturi Inlet Velocity (ft/sec)	11.2
Mass of Sand Through Venturis (lbm)	664,000

The total mass of sand that passed through each Venturi during the test was 664,000 lbm. The pipe water velocity during the test was 11.2 ft/sec and 44.7 ft/sec in the Venturi throat.

Discharge Coefficient Shift. The Venturi meter's discharge coefficients were measured before and after the water/sand slurry test to document changes in the meters due to erosion.

Discharge coefficients were measured in the water flow rig. The three Venturi meters that were exposed to erosion were tested against the "standard" meter that was not exposed to the erosive flow. The discharge coefficient for the "standard" meter was assumed to be 0.995 and the other meters' discharge coefficients were determined relative to the "standard" meter. Each Venturi had two sets of pressure taps located 180° apart. The two sets were labeled A and B Taps.

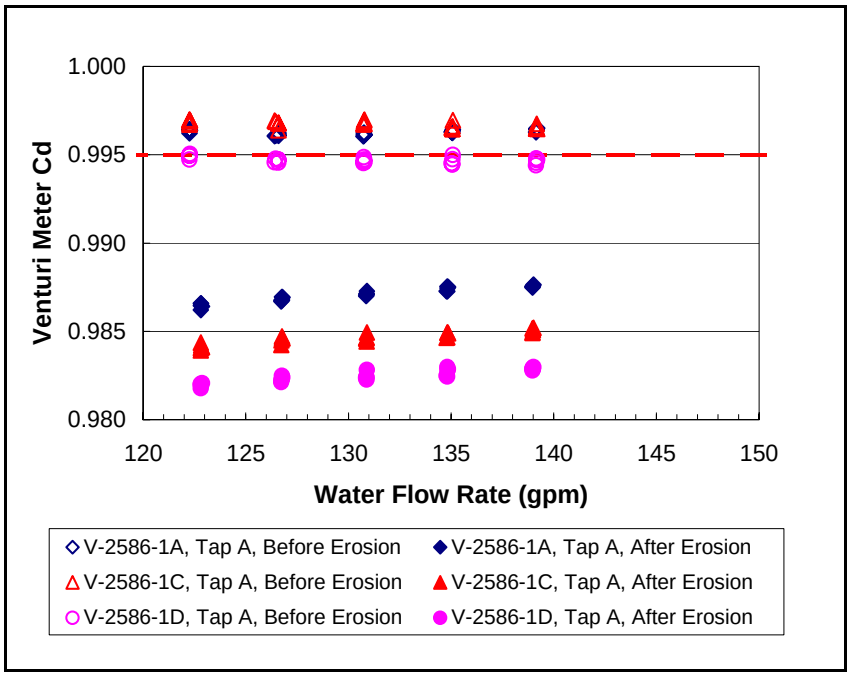

Figure 17. Venturi Meter Discharge Coefficients Measured Before and After the Water/Sand Slurry Exposure – "A" Taps.

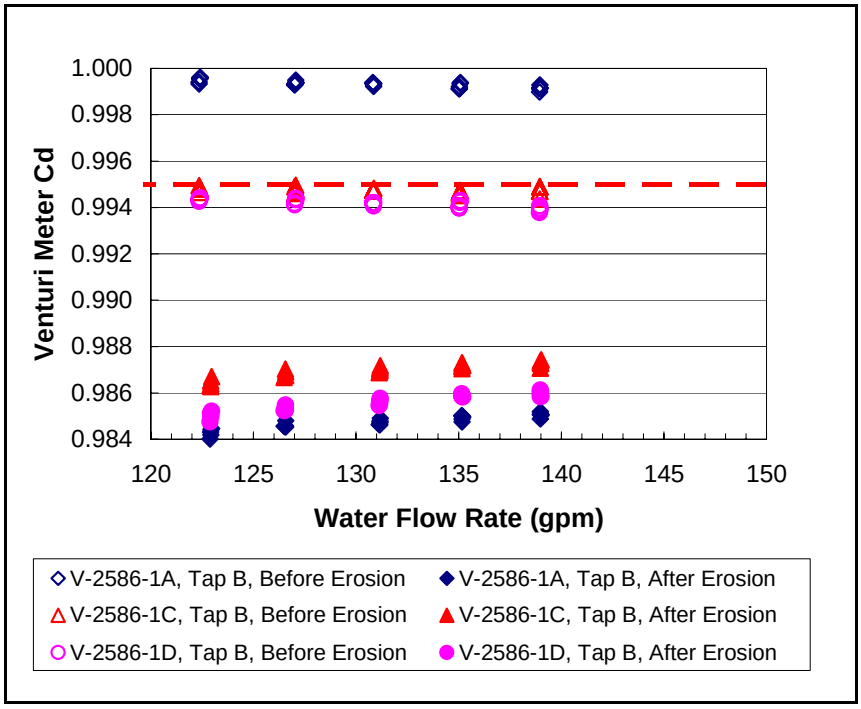

Figure 18. Venturi Meter Discharge Coefficients Measured Before and After the Water/Sand Slurry Exposure – "B" Taps.

The discharge coefficients measured before and after the water erosion test are shown in Figures 17 and 18. The discharge coefficients were measured in turbulent flow for a range of flow rates and at Reynolds numbers based on the pipe diameter between $4x10^5$ and $5x10^5$. Figure 17 shows the meter discharge coefficients when the differential pressure was recorded using the "A" Taps and Figure 18 shows the discharge coefficients recorded using the "B" Taps. The meter erosion caused an average change in the discharge coefficient of about -1%. The discharge coefficients recorded after the erosion test were computed using the meter geometry measurements taken before the erosion test.

Venturi Geometry Change. Measurements were made of the Venturi meter pipe and throat diameters, and the surface roughness prior to exposing the meters to the water slurry flow and were repeated after the erosion test. The upstream diameter was measured near the upstream taps (3.52 inches from the upstream flange face) with an internal micrometer. Measurements were made with the micrometer oriented at 0°, 90°, 180°, and 270° relative to the "A" Taps. Measurements of the throat diameter were also recorded. The diameter was measured just upstream of the throat pressure tap at a location 7.86 inches from the upstream flange face. The throat bore had a slight taper (diameter reducing in the direction of flow), so additional diameter measurements were made at a location 8.30 inches from the inlet flange face. Table 4 lists the average dimensions for the three test Venturis.

Table 4. Change in the Venturi Dimensions after the Water Erosion Test.

VENTURI #	VENTURI DIAMETER AND CHANGE IN DIAMETER	DIAMETER AT UPSTREAM TAPS-AT 3.52" (INCH)	DIAMETER AT THROAT TAPS-AT 7.86" (INCH)	DIAMETER IN THROAT-AT 8.3" (INCH)
V-2586-1A	Average Diameter	2.0642	1.0333	1.0327
	Change in Diameter	-0.0010	-0.0048	-0.0151
V-2586-1D	Average Diameter	2.0659	1.0332	1.0323
	Change in Diameter	-0.0009	-0.0048	-0.0153
V-2586-1C	Average Diameter	2.0640	1.0333	1.0327
	Change in Diameter	-0.0008	-0.0041	-0.0140

The average diameter change at the upstream tap was an increase of about 0.001 inches (negative values in Table 4 indicate the bore diameter increased in testing). The diameter of the Venturi throat increased about 0.005" just upstream of the throat pressure tap.

Before the water erosion test, the Venturi throat had a slight taper with the diameter decreasing in the direction of flow. After the erosion test, the throat diameter increased in the direction of the flow. Figure 19 show a plot of the throat diameter measured at different locations along the throat (the throat inlet is 7.55 inches for the inlet flange face and the end of the throat is 8.57 inches from the inlet flange face). Based on extrapolating the measurements made before the erosion test, the throat diameter at the inlet increased approximately 0.001 inches. The diameter at the outlet end of the throat increased by about 0.020 inches.

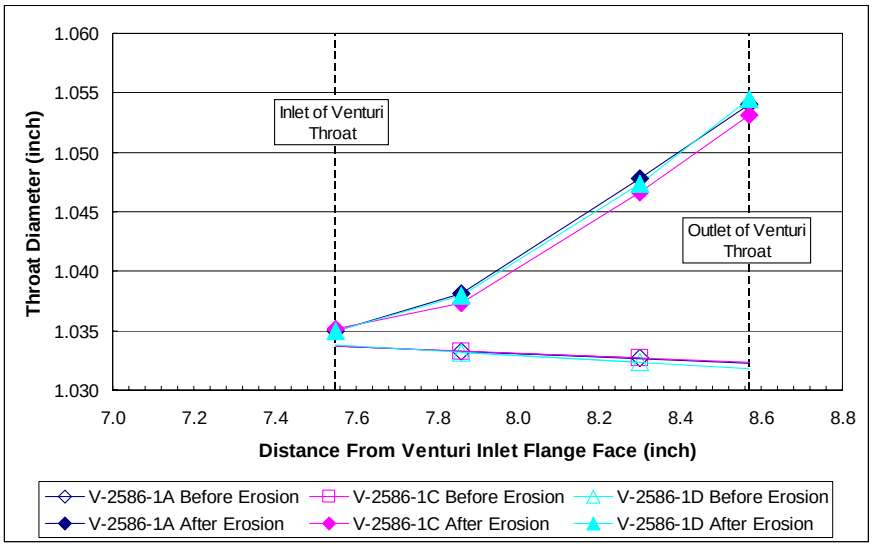

Figure 19. Plot of the Venturi Throat Diameter Measurements Before (Open Symbols) and After (Solid Symbols) the Water Erosion Test.

Photographs of Erosion.

Upstream (pipe) Taps. Photographs were taken of the pipe pressure taps after the water erosion test. There was considerable erosion on the downstream side of the tap holes. Figure 20 shows photographs of the upstream "A" and "B" pressure taps on Venturi V-2586-1C.

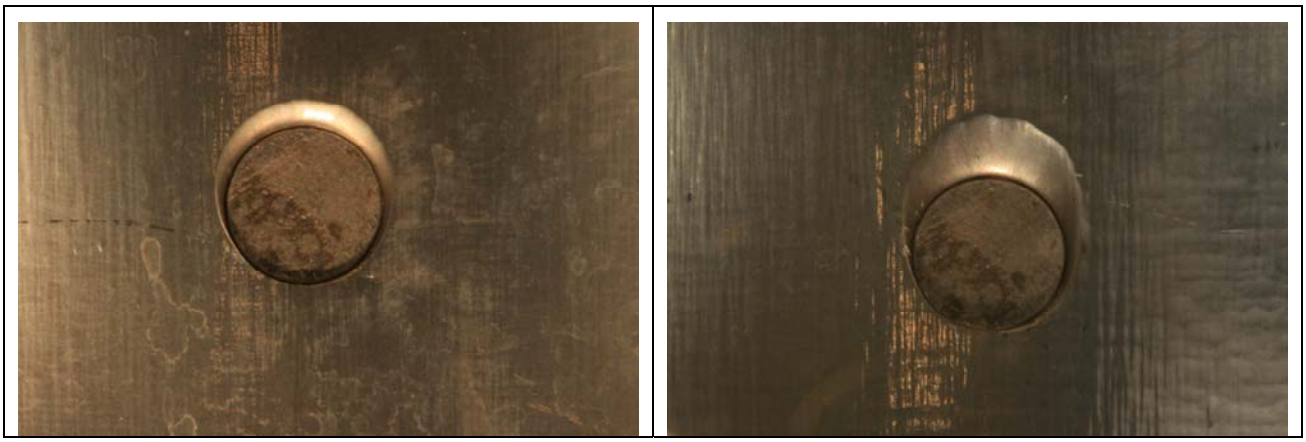

Figure 20. Upstream "A" (L) and "B" (R) Taps on Venturi V-2586-1C After the Water Erosion Test.

The direction of flow on the photographs is toward the top of the page. The "B" Tap had more erosion (right photograph, Figure 20) and was located on the outside of the flow bend created by the blind tee located just upstream of the Venturi. The upstream tap located on the outside of the flow bend had more erosion than the pressure tap located on the inside of the flow bend. This was true for all three Venturi meters.

The surface around the upstream pressure tap holes was eroded. The machine grooves that were visible before the erosion test (see Figure 15 for comparison) were eroded and erosion channels were cut into the surface, as seen in Figure 20. The eroded channels were aligned with the direction of the flow, which was towards the top of the photograph in Figure 20.

Throat Taps. The throat pressure taps were eroded by the water slurry. Figure 21 shows the downstream side (toward the top of the page) of the pressure tap, which was eroded into a shallow U-shaped cut. The surface around the throat taps was eroded smooth. The machine grooves visible before the erosion test were eroded away

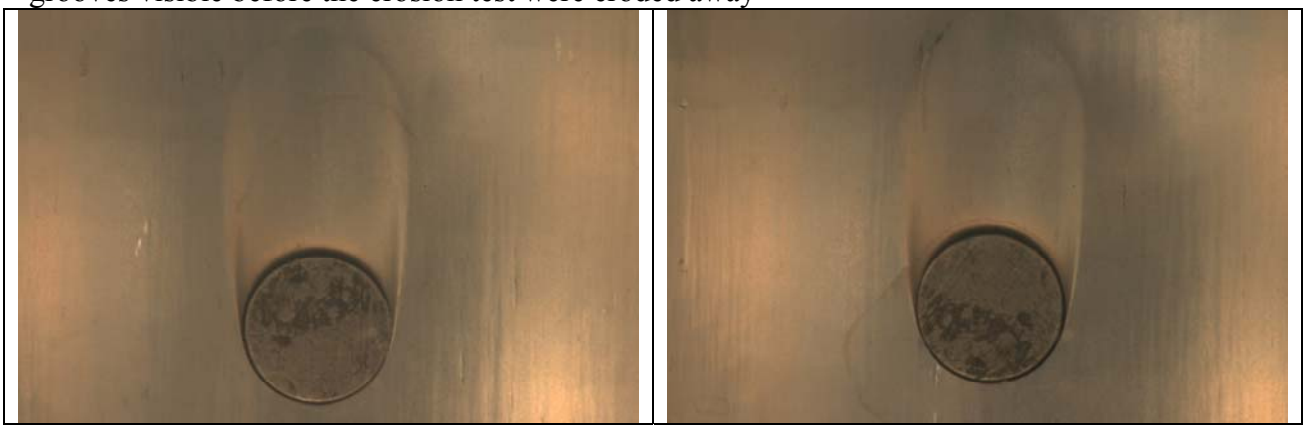

Figure 21. Throat "A" (L) and "B" (R) Taps on Venturi V-2586-1C After the Water Erosion Test.

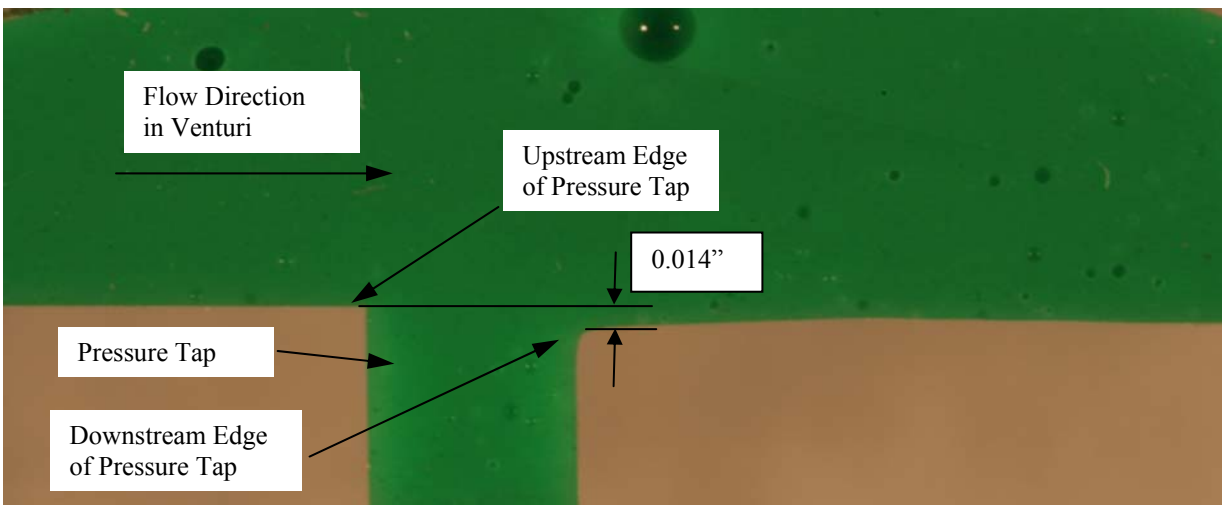

Figure 22. Cross-Section Cut from a Casting of the "A" Throat Tap of Venturi V-2586-1A.

A casting of the pressure tap and the throat surface around the pressure tap was made to determine the depth of erosion at the throat tap. Figure 22 shows a cross-section cut through the casting material. The cut plane passes through the centerline of the pressure tap and the plane was aligned with the direction of flow. The upstream edge of the pressure tap was sharp, but the downstream edge was eroded down by 0.014 inch below the upstream edge. The downstream edge had a radius of about 0.008 inch.

Changes in Discharge Coefficient Change. The discharge coefficients of the eroded meters changed by about -1% due to erosion. An increase in the throat diameter due to erosion would be expected to result in an increased discharge coefficient. The decrease in discharge coefficient was caused by the eroded pressure tap holes. The modified tap hole geometry increased the measured differential pressure to overcome the larger throat diameter and resulted in a decrease in the overall discharge coefficient.

If the erosion had only caused a change to the throat and upstream diameters, the shift in the discharge coefficient would have been expected to be about +1.8%. The shift in discharge coefficient that would result if only the pressure tap holes had eroded (no diameter change) was estimated to be about -2.5%.

Thus the diameter increase offset the changes caused by the pressure tap hole erosion.

5.0 CONCLUSIONS

Experiments were conducted on a four-inch Venturi flow meter over a range of flow rates and fluid viscosities with the objective of obtaining data on Venturi discharge coefficients under laminar flow conditions for a Reynolds number range below that given in ISO5167-4. Discharge coefficients were determined based on comparison of the calculated Venturi flow rate to the reference flow meter. In testing, both the flow rate and the temperature (and thus viscosity) were varied to obtain a range of Reynolds numbers that covered the laminar flow regime down to a Reynolds number of 80. The main conclusions reached from the investigation are:

- The discharge coefficients for the Venturi meter, fall on a single curve when correlated with the throat Reynolds number. This curve has a slight "hump" in the transitional range of Reynolds numbers before steadily decreasing as the Reynolds number is reduced. This is in contrast to the application of Venturi meters in turbulent flow, where the value of the discharge coefficient is taken as a constant.
- The discharge coefficients were compared to published correlations and it was found that the data followed the same general trends, but did not agree exactly with any of the correlations. The experimental discharge coefficients fell between the extremes defined by the various published results, except in the range of Reynolds numbers where transition from laminar to turbulent flow was occurring.

CFD modeling was performed to determine if CFD simulations could predict the performance of a Venturi flow meter under conditions typical of those encountered in metering viscous fluids. The CFD results were used to obtain detailed information on Venturi meter flow characteristics that could not be easily measured during experimental testing. Conclusions from the CFD modeling include:

- The agreement between the experimental and CFD results is good; although it appears that the two data sets have slightly different slopes. Comparisons with a range of experimental data were not made, the favorable agreement between the experimental and computational results suggests that CFD can be used to model the low Reynolds number flows when using Venturi meters.
- For laminar flow in a specific Venturi geometry (fixed D and β), discharge coefficient is a function of the throat Reynolds number over a range of viscosities and flow rates.

Three 2 inch Beta ratio 0.5 venturi meters were erosion tested. The venturi meters were flow tested with water to determine their discharge coefficients. One meter exhibited an unusual discharge coefficient which was the result of a small burr on the throat tap. Removal of the burr restored the discharge coefficient. Venturi pressure taps are critical components, and small discontinuities can and will create anomalous data.

The erosion test results showed that erosion of Venturi meters by a viscous fluid-sand slurry was not a major concern. The smooth flow of fluid through the Venturi meter combined with the viscosity of the fluid limited the sand impact, reducing erosion of the Venturi meters.

Significant Venturi meter erosion was experienced when exposed to a water/sand slurry. The erosion test conditions were similar to the viscous oil tests with a flow rate of about 120gpm (4100BPD). The flow for the water erosion test was turbulent with a Reynolds number >400,000. The test ran for ten days and 664,000 lbm of sand passed through each meter. In production operations, this would indicate that as water cuts increase (or bulk viscosity is reduced) significant erosion may be possible when sand is produced.

Erosion caused about a 1% decrease in the Venturi meter's overall discharge coefficient.

- The pressure tap holes experienced significant erosion with the downstream side of the tap holes being badly eroded. It is thought that this could have impacted the meter discharge coefficient by -2.5%.
- The surface finish inside the Venturi meters changed from the machine finish to a smooth, eroded surface, and the throat bore was eroded. It is thought that this could have impacted the meter discharge coefficient by +1.8%.
- The throat tap is a sensitive part of the venturi meter with respect to performance change due to defects and and erosion.

Dimensional measurements after the erosion test showed the Venturi throat had a significant taper, with the outlet end having a diameter that was about 0.020inches larger than the inlet end. The throat inlet end, just downstream from the contraction section did not experience much erosion. It appears that the nature of the flow entering the throat moved the sand away from the contraction cone and limited the erosion at the throat inlet.

6.0 REFERENCES

1. ISO 5167-4, "Measurement of Fluid Flow by Means of Pressure Differential Devices Inserted in Circular Cross-Section Conduits Running Full – Part 4: Venturi Tubes," 2003.
2. Fox, R. W., and McDonald, A. T., *Introduction to Fluid Mechanics*, Wiley and Sons, New York, 1992.
3. Benedict, R. P., and J. S. Wyler, "A Generalized Discharge Coefficient for Differential Pressure Type Fluid Meters," ASME Journal of Engineering for Power, pp. 440-448, October 1974.
4. Miller, R. W., *Flow Measurement Engineering Handbook*, McGraw-Hill, New York, 1996.
5. Pal, R., "Flow of Oil-in-Water Emulsions through Orifice and Venturi Meters," Industrial Engineering & Chemistry Research, Vol. 32, pp. 1212-1217, 1993.
6. Atkinson, D. I., et al., "Qualification of a Nonintrusive Multiphase Flow Meter in Viscous Flow," SPE 63118, 2000 SPE Annual Technical Conference and Exhibition, Dallas, TX, October 1-4, 2000.

25TH NORTH SEA FLOW MEASUREMENT WORKSHOP 2007

Experience with ultrasonic meters on high viscosity oil

Øyvind Nesse StatoilHydro

1 INTRODUCTION

Norsk Hydro has installed two ultrasonic metering stations for custody transfer of Grane heavy crude oil at the Sture terminal outside Bergen, Norway. The export metering station consists of five parallel meter runs with ultrasonic liquid flow meters and a 30" bi-directional ball prover with 20 m^3 volumes. The allocation metering station of Grane oil to Oseberg Transportation System has two meters in series and a bi-directional ball prover with 10 m^3 volumes. The ultrasonic liquid flow meters are respectively 12” and 6” Krohne 5-path Altosonic V.

The ultrasonic meters did not fulfil the linearity requirements of NPD. Hence it was not possible for a new K-factor to be automatically accepted by comparison with the average of the last 30 accepted K-factors with a predefined limit of acceptance of 0.3%.

Several measures were taken in order to improve linearity and gain control of development of the K-factor. The 6” allocation meters have been tested with and without the Reynolds number correction implemented in the KROHNE flow computer, and new weighing factors for high viscosities have been implemented. A test program was initiated to characterise the performance of the 12” export meters over a broad range of conditions, and a model for K-factor control limits has been established.

This paper will share the experience gained during testing and characterising of the ultrasonic heavy crude oil meters, and explains the final operating principles of the meters.

2 BACKGROUND

The Grane platform in the North Sea, in production since year 2003, sends heavy crude oil to shore through a 212 km pipeline to the Sture crude oil terminal in Norway, see Figure 1. The plateau production rate is about 40 000 Sm^3/day. The export of the heavy crude oil is through metering station named Grane Oil Handling Sture (GOHS) which consists of five parallel runs of 12” Krohne 5-path Altosonic V ultrasonic flow meters. The flow rate range of each run is 250-2500 m^3/h, however, maximum tanker loading rate is 8 000 Sm^3/h. In addition there is an allocation metering station exporting Grane oil into caverns of oil from the Oseberg Transportation System (OTS). This station, named New Oseberg Blend (NOB), consists of two 6” Krohne 5-path Altosonic V ultrasonic flow meters sin series with maximum flow rate of 600 Sm^3/h. Both metering stations have straight upstream length of 20 ID and Etoile flow conditioner. The provers are made quite large in order to ensure successful proving. The export metering station has a 30" bi-directional ball prover with 20 m^3 volumes, while the allocation station is provided with a bi-directional ball prover with 10 m^3 volumes. Schematic overview of the metering stations at Sture is shown in Figure 2.

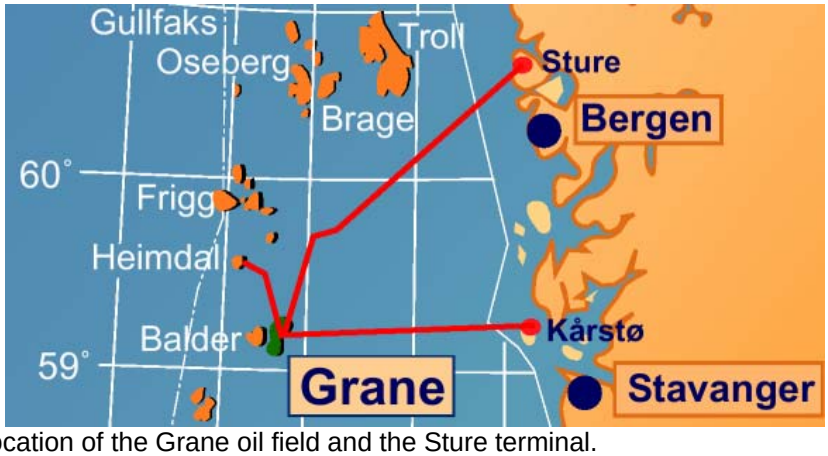

Figure 1. Location of the Grane oil field and the Sture terminal.

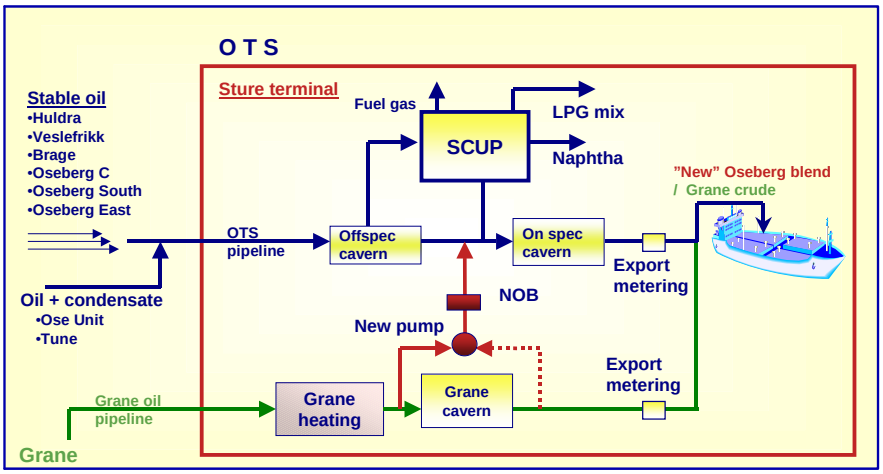

Figure 2. Schematic overview of the metering stations at Sture

3 GRANE OIL

The Grane crude oil has a viscosity during custody transfer varying between 215 and 540 mm^2/s (cSt) for temperatures between 30 ºC (normal loading temperature) and 15ºC. The density at 15 ºC is 943 kg/Sm^3 which yields an API of 18.53. A large heater system, placed upstream the two metering stations, increases the temperature of the Grane oil from nearly sea bed temperature up to 30 ºC, see Figure 2. The oil has characteristics of so called heavy crude oil, but from a metering point of view the main concern is the *conditions* during normal operation. Taking the oil properties and loading rates into account, we see that both metering stations operate at relative low Reynolds numbers, see Figure 3. Theoretically the meters will be used across three flow regimes, from laminar flow through the transition region to the preferred turbulent flow. For lower Reynolds numbers it is expected that the Krohne ultrasonic flow meters are not linear.

The two metering stations in question have a common low Reynolds-number-challenge. But due to dissimilar performance and measures taken in order control the meters long term stability, this paper describes the experience with the two ultrasonic meters separately, first the GOHS and thereafter the NOB metering station.

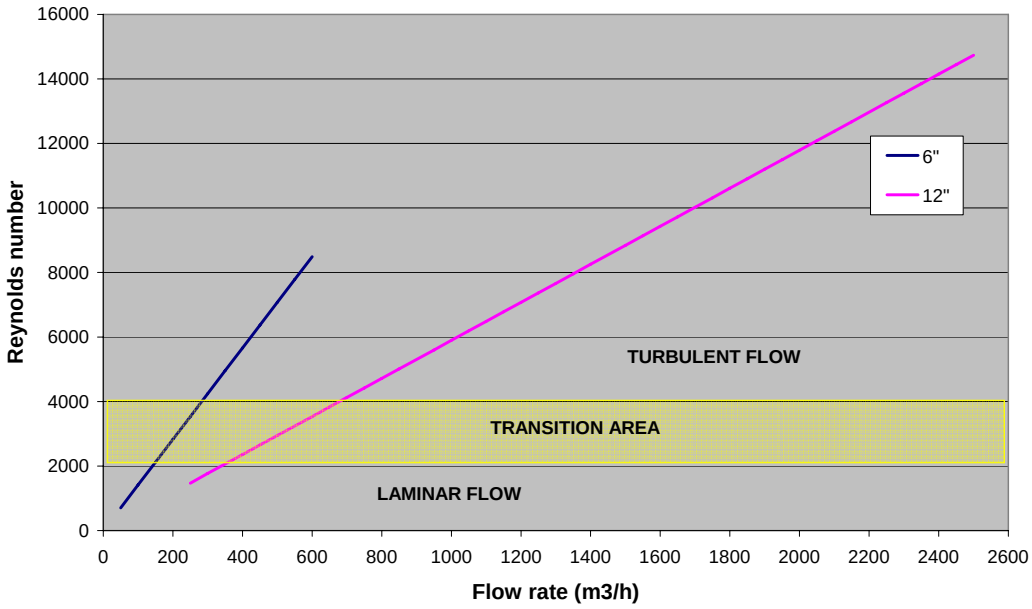

Figure 3. Reynolds number versus flow rate at normal operating conditions at GOSH and NOB

4 GOHS CHALLENGE

The Grane export ultrasonic meters went through a comprehensive testing in order to qualify the meters. The test results on heavy crude oil at SPSE in 2001 revealed a rather strong nonlinearity, as reported by Trond Folkestad at the NSFMW in 2001 [1]. Figure 4 shows an increasing K-factor with increasing Reynolds number. The Grane crude oil at Sture has lower Reynolds number at loading conditions which may enhance and invert the observed nonlinearity. The Norwegian Petroleum Directorate (NPD) required a careful k-factor follow up as part of the conditions to start using the ultrasonic metering station. Initial k-factor measurements at various loading rates certified the nonlinearity. However, opposite to the test results at SPSE the proving results on Grane crude oil show a strong decreasing k-factor with increasing flow rate, i.e. with increasing Reynolds number, see Figure 5. The Hydro repeatability requirement of 0.05% was easily fulfilled at all flow rates. Statistical method is applied.

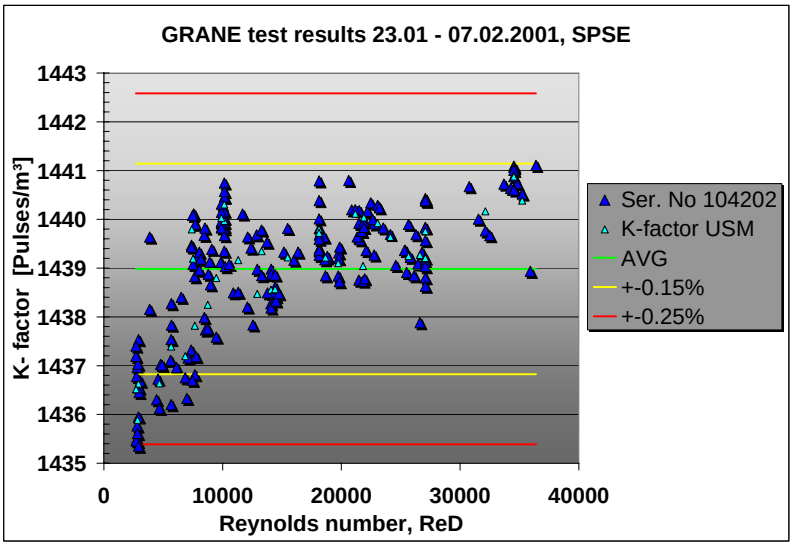

Figure 4. 12" Krohne 5-path Altosonic V ultrasonic flow meter tested on heavy crude oil

The NPD requirements for ultrasonic meters are 0.07% repeatability and 0.3% (band) linearity in 10:1 working range. On export metering stations Hydro requirements are 0.05% repeatability and the linearity requirement is defined as a long term k-factor stability of 0.15% (band). Figure 5 shows clearly that the GOHS ultrasonic meters do not fulfil the linearity requirements of neither NPD nor Hydro. Hence it is not possible for a new K-factor to be automatically accepted by comparison with the average of the last 30 accepted K-factors with a predefined limit of acceptance of 0.3%.

The GOHS challenge is to establish dynamic k-factor limits in order to have control with the ultrasonic meters long term stability. The solution is to make a k-factor model being a function of the loading conditions such as temperature, density, flow rate and so on.

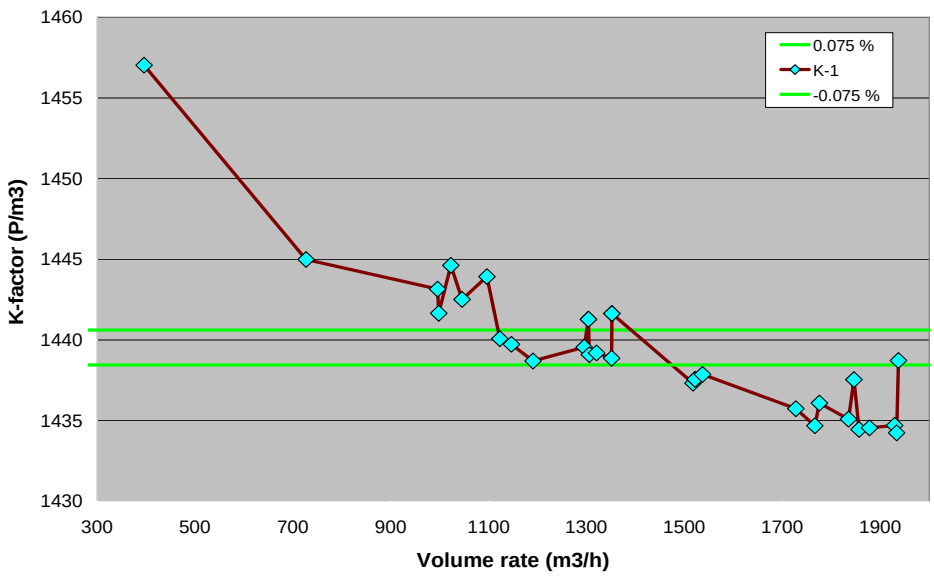

Figure 5. Initial k-factor results of the 12" Krohne 5-path Altosonic V ultrasonic flow meter, measured on Grane crude oil at Sture.

4.1 GOHS K-factor model

The first step made towards a k-factor model was to find relations between loading conditions and the k-factor it self. A test program was initiated to monitor the k-factor over a large range of flow rates, from below to above normal loading rates at 1900 m3/h. Correlations were carried out on the test results to find relations between the state variables temperature, pressure, density and flow rate, and the k-factor. Table 1 shows the correlation results for line 1. The negative correlation between temperature and density means that the density decreases with increasing temperature (of course). The results of the correlations clearly establish the most important k-factor variables, namely flow rate and temperature. Both variables have negative correlation with respect to the k-factor. In other words the k-factor decreases with increasing Reynolds number. This is also seen indirectly in Figure 5.

TABLE 1 Correlations between state variables at line 1

Correlation	*temp*	*pressure*	*Density*	*Rate*	*K-fact*
Temp	1				
Pressure	0.00668	1			
Density	**-0.862123**	0.191367	1		
Rate	0.2835064	0.564647	0.012204256	1	
K-fact	**-0.564329**	-0.41721	0.274322476	**-0.930956**	1

The next step made towards a k-factor model was to carry out a linear regression analysis based on the two main k-factor variables. Each regression analysis is based on 30 to 60 observations where each observation consist of accepted k-factor (repetition requirement fulfilled) and belonging mean value temperature and flow rate. The results of the regression analysis for all five ultrasonic meters are quite promising. Table 2 and 3 show the results for respectively line1 and 2. The R-square, which may be interpreted as the percentage explained, is for the five lines in the range 0.91 to 0.96. The linear k-factor model simply becomes the coefficients of the regression analysis times the respective measured stat variable, see Equation 1. Finally long term stability factor *limits*, ± 0.075%, are added to the calculated k-factor.

$$K\text{-}factor(T,Q)=Intercept + C_T \cdot T + C_Q \cdot Q \qquad (1)$$

where C_T is temperature regression coefficient and C_Q is volume flow rate regression coefficient, and T and Q are measured temperature and volume flow rate.

The k-factor model is applied in the following way: The measured k-factor with repeatability within the requirement of 0.05% (statistical method) is compared with the calculated k-factor, eq. 1, with belonging control limits of ± 0.075%. The new measured k-factor is accepted if it is within the calculated control limits.

TABLE 2 Linear regression coefficients and statistics for line 1

LINE 1			
	Coefficients	*Regression Statistics*	
Intercept	1473.03	Multiple R	0.97
Temp.(grC)	-0.78	R Square	**0.95**

Vol.rate (m3/h)	-0.01	Adjusted R Square	0.95

TABLE 3 Linear regression coefficients and statistics for line 2

LINE 2			
	Coefficients	*Regression Statistics*	
Intercept	1461.08	Multiple R	0.98
Temp.(grC)	-0.44	R Square	**0.96**
Vol.rate (m3/h)	-0.01	Adjusted R Square	0.96

4.2 Application of GOHS k-factor model

The GOHS k-factor model has been used by the operators at Sture since summer 2004. Measured k-factors being outside the control limits of ± 0.075% have been rejected. In the period January 2004 until august 2007 GOHS line 3 has carried out about 334 provings with successful repetition, and where 8 proving results were outside the long term stability control limits. Graphical presentation is given in Figure 6. This figure also includes simulations with fixed temperatures of 29, 31 and 33 ^{o}C and increasing flow rates. The temperature gradient yields a k-factor dependency of 0.04% per. ^{o}C for line 3. The storage of Grane export oil in large caverns improves the stability of the oil. Rarely the provings falls outside the repetition requirement of 0.05%. A histogram presentation of the proving results on line 3 is shown in Figure 7. The deviation in the histogram is the difference between calculated and measured k-factor. Similar results for line 5 are shown in Figures 8 and 9. Line 5 has a slightly broader distribution than line 3, but the gross proving results are within the long term acceptance limits.

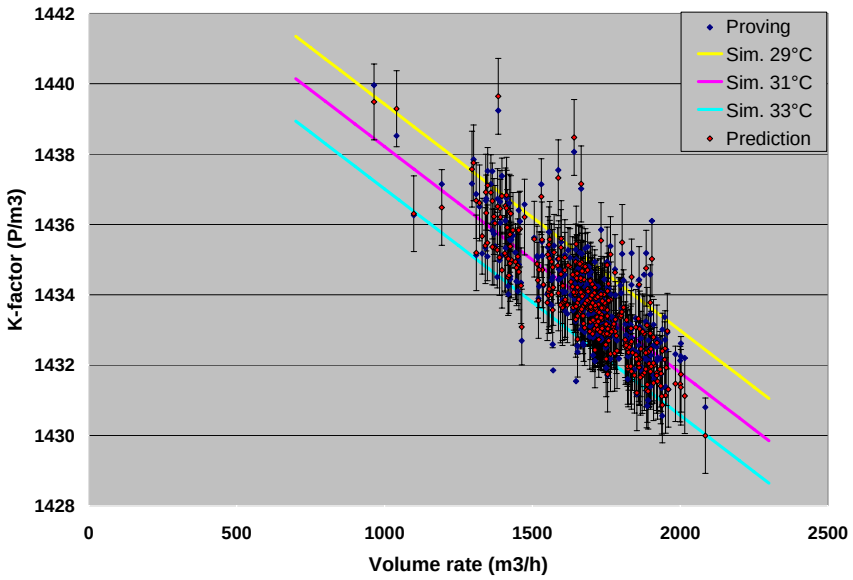

Figure 6. Measured and calculated k-factors for GOHS line 3. The error bars illustrate the control limits of ± 0.075%. The three simulations are carried out as a function of flow rates at fixed temperatures of 29, 31 and 33 ^{o}C.

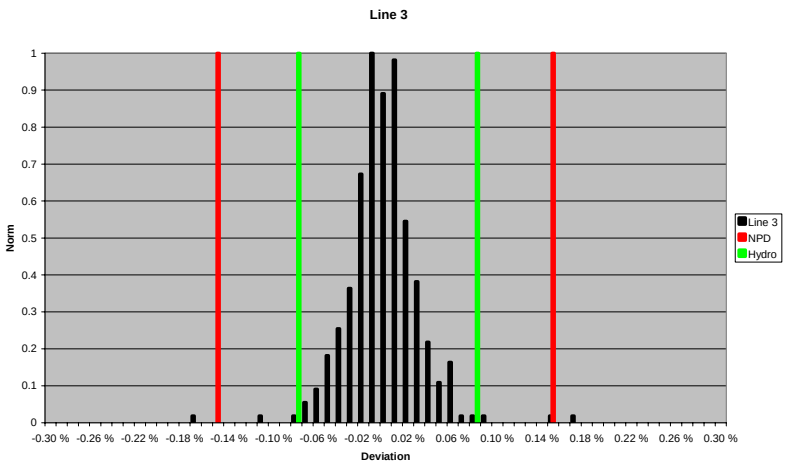

Figure 7. Histogram of the k-factor results shown in Figure 6. Deviation is the difference between calculated and measured k-factor. The Hydro and NPD long term control limits are shown respectively at ±0.075% and ± 0.15%.

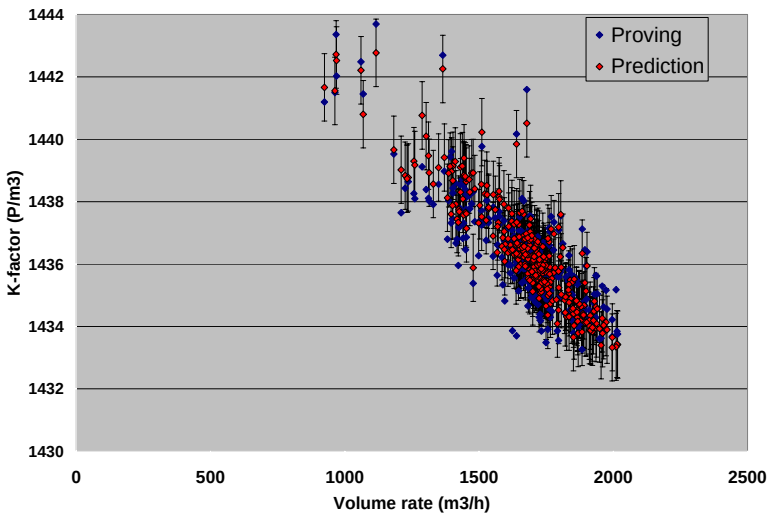

Figure 8. Measured and calculated k-factors for GOHS line 5

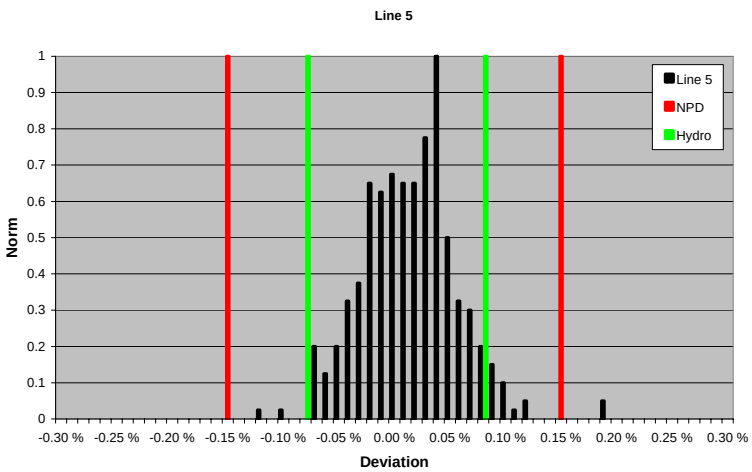

Figure 9. Histogram of the k-factor results shown in Figure 8. The Hydro and NPD long term control limits are shown respectively at ±0.075% and ± 0.15%.

4.3 Flow straightener collapse on GOHS

During the first 18 months most of the proving results on line 4 were accepted, see Figure 10. However, the slowly increasing deviation between measurement and proving model ended outside the control limits after august 2006. At the end of the year the deviation varied from -0.35% to 0.30%. Similar behaviour was also seen on line 1 at the end of year 2004, see Figure 12. By coincident an operator was present at the metering station during a proving and noticed a load metal-to-metal sound from line 4. It was assumed that the flow straightener was loose. The two lines in question were opened and the defect flow straightener assumption was verified. A picture of one of the defect flow straightener is shown in Figure 11. Once new flow straighteners were back in place most of the proving results finished within the long term stability control limits.

These results demonstrate that the k-factor model serves not only to keep control over the long term stability of the ultrasonic meters itself, but is also a mean to reveal defects on the metering stations. T the results achieved rely on a stable, hence predictable, Grane crude oil. The k-factor model has not been adjusted since initiation.

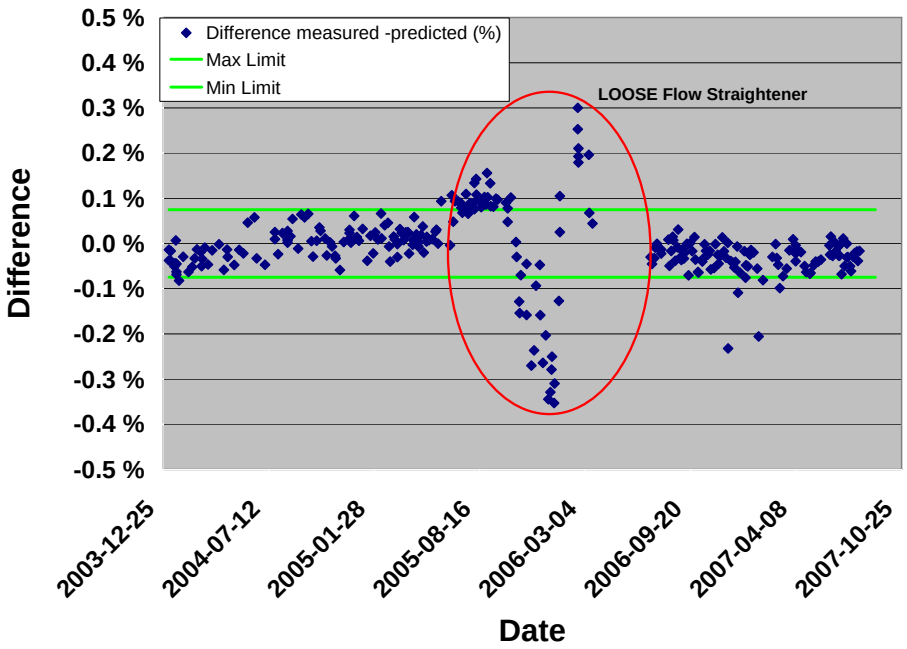

Figure 10. Deviation between measured and calculated k-factors on GOHS line 4

Figure 11. Defect flow straightener from GOHS line 4.

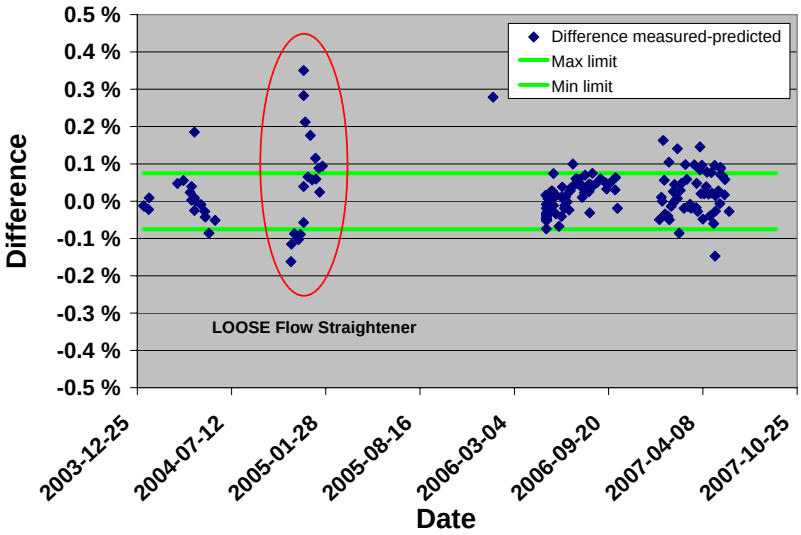

Figure 12. Deviation between measured and calculated k-factors on GOHS line 1

5 NEW OSEBERG BLEND CHALLENGE

The Krohne Altosonic V 6" ultrasonic meters went through standard FAT at Trapil metrology laboratory Paris in 2003. The calibration flow rate range was 63-630 m^3/h, see Figures 13 and 14, and the test product was Gasoil with viscosity of 3.5 to 8.0 mm^2/s at 20 ^oC. The viscosity of Grane oil is more than 25 times higher. The meters can be used with or without a Reynolds number correction which purpose is to improve the meter linearity. The correction must be applied to meet the vendor's specification. Thus the formal FAT was carried out with active Reynolds number correction. The correction, which may be interpreted as a profile correction, resembles most likely the k-factor model described for the GOHS ultrasonic liquid meters. But with active

Reynolds number correction the flow profile of the Krohne meter is *continuously* corrected. The user does not have access to neither the correction nor the correction parameters. Hydro policy for fiscal meters is to have access to all data, both fixed parameters and variable parameters. Therefore the meters were also calibrated with the Reynolds number correction turned off.

The red curve, see Figure 13 and 14, shows the formal calibration with Reynolds number correction on. The linearity of upstream and down stream meters are respectively 0,04 % and 0,02 %. The calibration without Reynolds number correction, blue curve, is close to the lower end of the NPD's linearity requirement (yellow lines). At lower flow rates the formal calibration curve of the upstream meter, see Figure 13, has an opposite trend relative to the uncorrected calibration. This may indicate that the Reynolds number correction overcompensates the true flow profile. The correction of the downstream meter yields an excellent linearity and with the same trend as the uncorrected meter, see Figure 14.

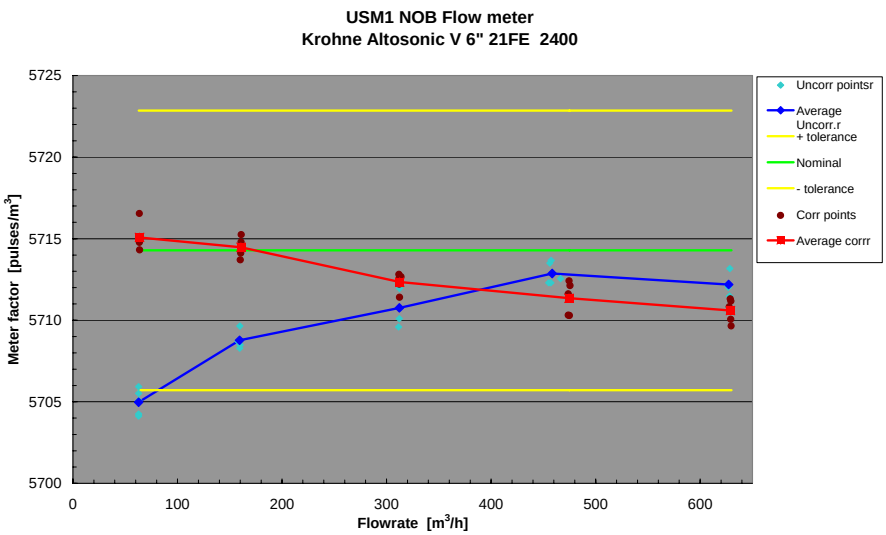

Figure 13. Pigsar calibration results of the NOB upstream ultrasonic meter. The meter was calibrated with and without Reynolds number correction.

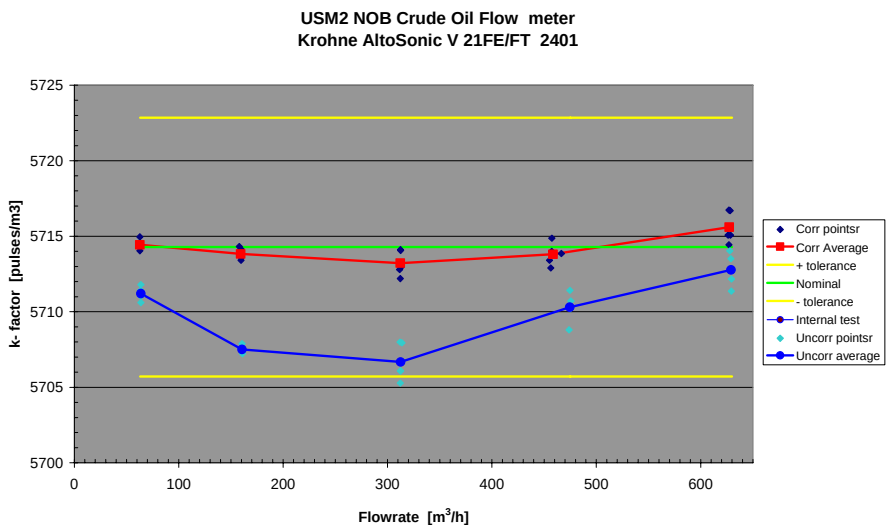

Figure 14. Pigsar calibration results of the NOB downstream ultrasonic meter. The meter was calibrated with and without Reynolds number correction.

The NOB challenge is to run the Krohne meters on Grane oil within the NPD requirements, and in accordance with the Hydro policy to have access to all applied and measured data.

5.1 NOB commissioning

Finally the commissioning phase could take place at Sture with real testing of the meters. In 2003 the Grane oil was heated up from about 7 to 30 ^{o}C with a conventional natural gas driven heat exchanger. The power consumption was about 16 MW and the Grane oil temperature varied more than 1 ^{o}C during a few minutes due to poor regulation. Initially the ultrasonic liquid meters were tested with Reynolds number correction turned off, and the meters' k-factor were characterised in the same way as the GOHS meters. Low Reynolds number in combination with unstable temperature proved to be worse than expected. It was not possible to achieve accepted k-factors because the repetition was outside the 0.07% limits. The k-factor could change as much as 0.3% from one proving trail to the next. Figure 15 shows strong correlation between temperature and k-factor. The k-factor decreases with increasing temperature. The GOHS meters possess the same relation.

The commissioning phase was scheduled to 1 month. In order to have a metering station up and running to start-up date the ultrasonic meters had to be characterised by Krohne to prepare for Reynolds number correction. Eventually with the Reynolds number correction turned on the k-factors fulfilled the repetition requirement. Statistical method was applied. Figure 16 shows a typical proving sequence. The k-factor dependency to temperature is now reversed, i.e. the k-factor decreases with decreasing temperature. Note that the new k-factor, found with statistical method, is above the traditional acceptance limits. The latter is based on the average of the 5 last proving trails.

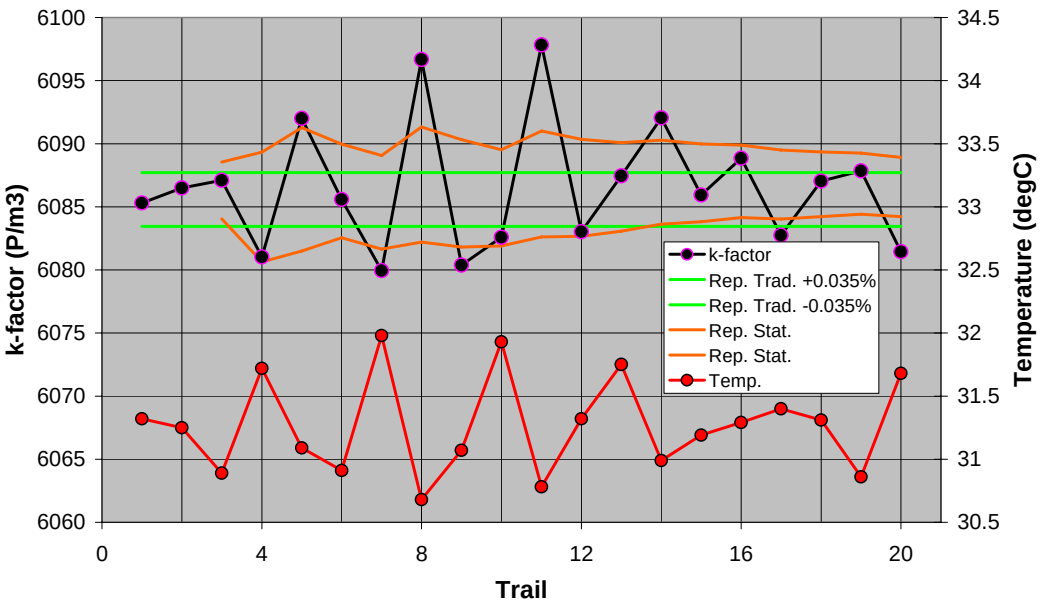

Figure 15. NOB USM1 proving sequence during commission phase. Statistical method is applied which allow maximum 20 proving trails. The flow rate is about 300 m^3/h.

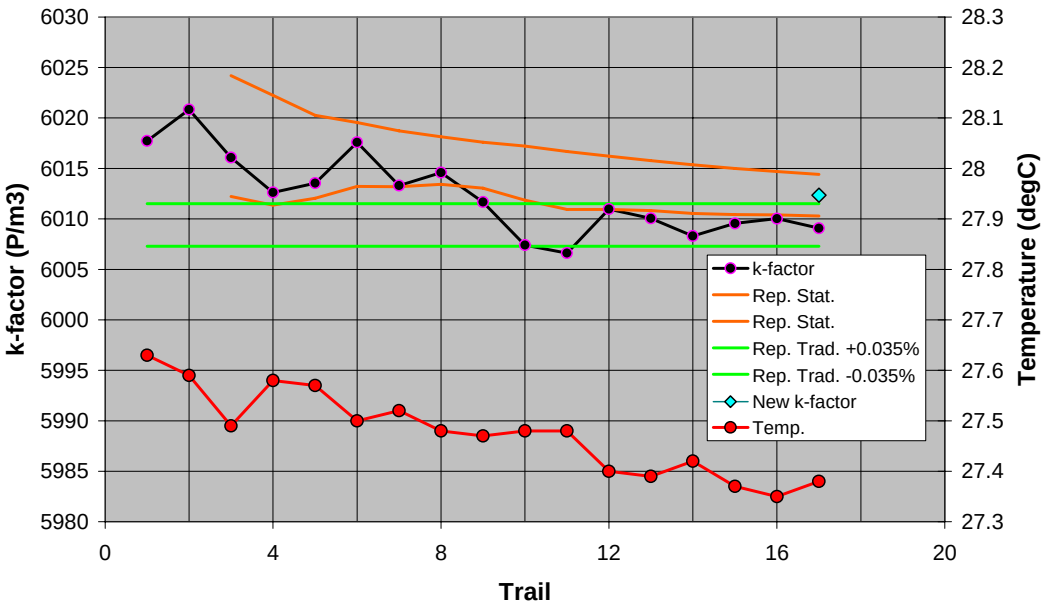

Figure 16. NOB USM1 proving sequence after start-up and Reynolds correction and statistical method are applied. The flow rate is 100 m^3/h and repetition is 0.068%.

5.2 NOB k-factor development

Krohne's Reynolds number correction was used from start-up of the New Oseberg Blend metering station. The majority of the provings fulfilled the k-factor repetition requirement of 0.07% band. However, the long term stability was not satisfied, see Figure 17. The control limits was set to 0.3%, being equal to the NPD linearity requirement. The k-factor variation was more than 3% band during the first 7 months. Thereafter in November 2004 the k-factor became more stable with a variation of about ± 0.5 %. The proving conditions did not change significantly in this period. The crude oil temperature during proving was still fluctuating, but the flow rate had decreased some. Figure 18 shows the development of temperature variation (temperature span) during proving and flow rate from start up to year 2007.

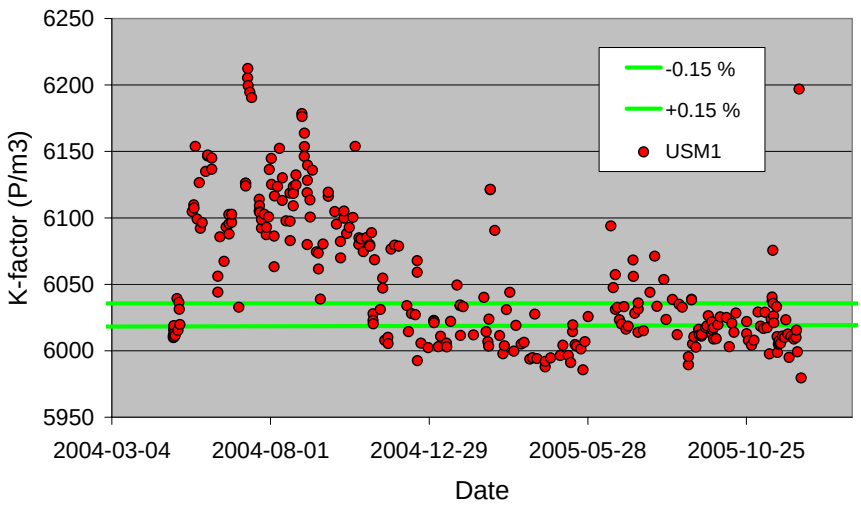

Figure 17. NOB USM1 proving results after start-up. Reynolds number correction is applied.

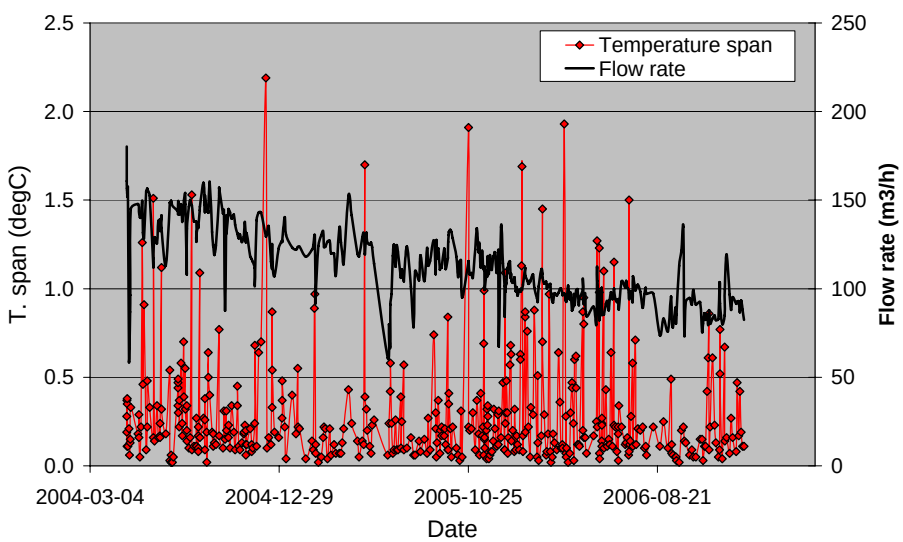

Figure 18. NOB USM1 temperature variation during proving and flow rate development from start-up to year 2007.

5.3 NOB ultrasonic path weights

The long term stability of the k-factor had to be improved. Moreover, the current Reynolds number correction partly masked the traceability of the fiscal measurements. The solution to these imperfections was to make the ultrasonic meters more *linear* at the existing conditions. The vendor Krohne carried out measurements at Sture at various flow rates and temperatures. The data were then used to estimate new weights for the ultrasonic paths. The normalised alternative weighing factors for high viscosity liquid are shown in Figure 19. The new configuration reduces weight of the centre path and increases the importance of path 1 and 5. Without using the Reynolds correction the meter should now be within the requirement of NPD. A proving sequence with new weighing factors and Reynolds correction turned *off* is shown in Figure 20.

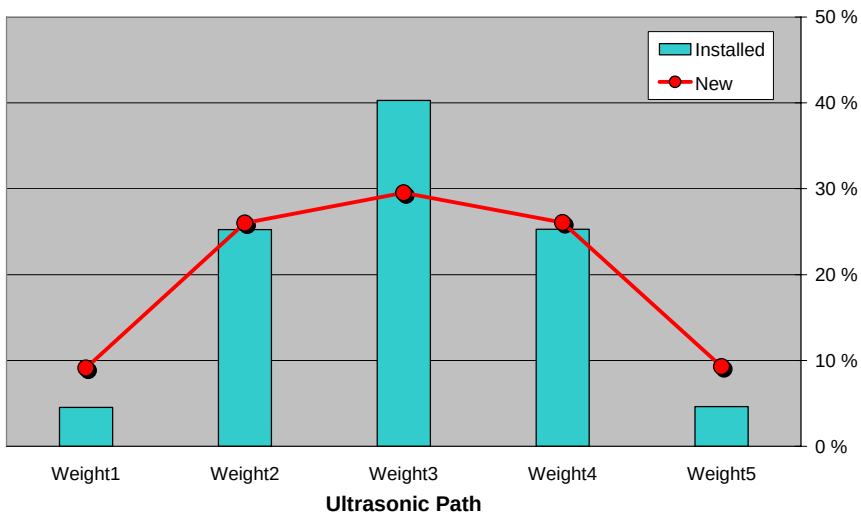

Figure 19. USM1 Old and new weighing factors

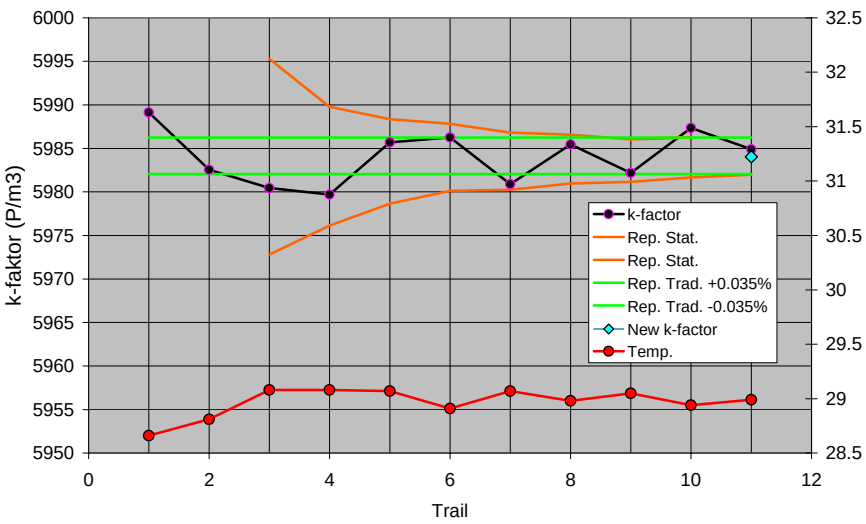

Figure 20. USM1 proving sequence with new weighing factors and without Reynolds correction. The flow rate is about 90 m^3/h.

The meters became significantly more linear with the new weighing factors. Figure 21 shows an overview of accepted k-factors since start-up until September 2007. These k-factors fulfil the repetition requirement. After implementation of new weighing factor most of the k-factors also are within the long term stability control limits of ± 0.15 %, a recent example is shown in Figure 22. The control limits are based on the average of the 30 last provings.

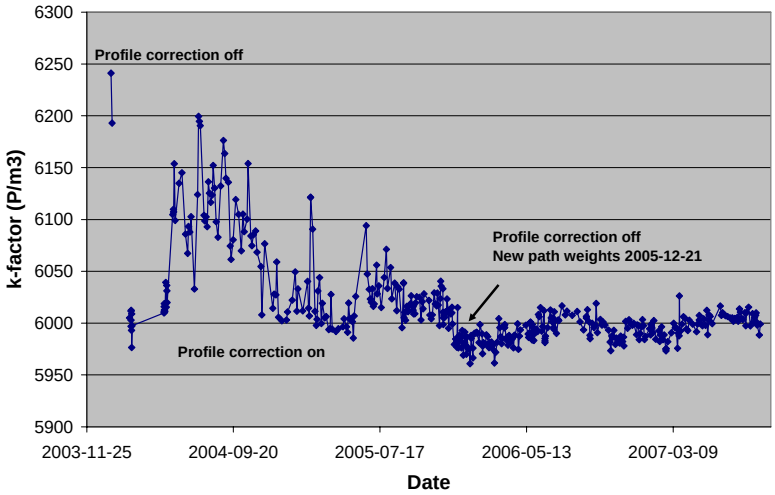

Figure 21. USM1 accepted k-factors (fulfil repetition requirement) from start-up to September 2007.

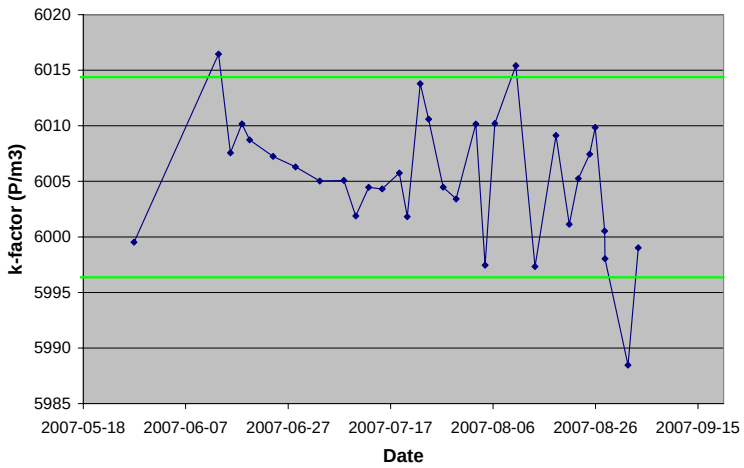

Figure 22. USM1 30 k-factors that fulfil the repetition requirement). The long term stability control limits of ± 0.15 % included.

6 CONCLUSION

Several measures were taken in order to improve linearity and gain control of the k-factor development of ultrasonic meters on high viscosity oil. The Reynolds number correction implemented in the Krohne flow computer has been turned off.

A test program was initiated to characterise the performance of the 12” export meters over a broad range of conditions. A model was made to predict the k-factor. The input to the model is temperature and flow rate, and output is long term k-factor control limits. The 12” export meters do fulfil the k-factor control limits of ± 0.075 %.

The 6” meters have got new weighing factors for high viscosities which made the meters more linear. The 6” allocation meters do now fulfil the long term stability control limits of ± 0.15 %.

REFERENCES

[1] Folkestad Trond, “Testing of a 12” Krohne 5-path Altosonic V ultrasonic liquid flow meter on Oseberg crude oil and on heavy crude oil”, NSFMW 2001.

25TH INTERNATIONAL NORTH SEA FLOW MEASUREMENT WORKSHOP
16th to 19th October 2007, Oslo, Norway

A New Approach to MPFM Performance Assessment in Heavy Oil

Martin Basil, SOLV Limited
Gordon Stobie, ConocoPhillips
Winsor Letton, Letton-Hall Group

1 Abstract

The performance of a MPFM (Multi Phase Flow Meter) is normally assessed with an observational data model obtained by comparison with a reference meter. Typically the vendor will provide the performance from their own databases using data from a wide range of sources including JIP's, client sponsored trials, field trials and the vendors own calibration facilities. This data is processed to model the MPFM and compiled into databases over a long period of time at considerable cost. Understandably the vendor regards this data as proprietary and seeks to control access by releasing only limited subsets specific to an application. In the early stages of a project, fluid properties and flow rates may not be well understood requiring repeated requests to the vendor for performance data which can be very time consuming. This reliance on vendor data that is not transparent does little to instil confidence in users who will often conduct costly independent trials to verify the suitability of the selected MPFM, or may revert to more conventional methods of measurement.

This paper presents an alternative analytical approach, developed for a heavy oil application, providing an independent assessment of a Dual Gamma Venturi MPFM performance from the physical properties of the fluids and sensors. Phase and line density performance of the Dual Gamma phase detector sensor are examined with the phase calculations taking into account the phase densities, attenuation factors and detector count rates. Mass flow rate performance of the Venturi meter is examined for a high viscosity emulsion with Reynolds Number of less than 2,000 that requires a correction to the Venturi Coefficient of Discharge. Dual Gamma and Venturi performance are combined to find overall performance of the MPFM meter for comparison with the vendor data.

The "Analytical MPFM Performance" from the physical properties of the sensors and fluids goes hand-in-hand with the "Observational MPFM Performance" from comparative trials giving the user an immediate and independent verification of the MPFM performance. This speeds MPFM selection building confidence in the suitability of the MPFM and eliminating the need for costly and time consuming trials at calibration laboratories.

2 Introduction

A Fiscal measurement of heavy oil entering a common pipeline was required for allocation of exports to each pipeline entrant between the existing and new development. The economics of the development did not allow for processing the heavy oil to a suitable standard for measurement with a LACT unit. An alternative approach was required that

would be acceptable to the pipeline entrants, the Royalty Owners and regulatory authorities. As there was no field ownership overlap between the developments all parties will be fully exposed to the heavy oil measurement uncertainty however there is a fifteen to one difference in relative rates of production between the existing and new development reducing the existing producer's relative exposure proportionally. The heavy oil producer is subject to the full exposure arising from measurement which is offset against the much greater cost of processing to Custody Transfer standards.

Heavy oil with gravity of 19 to 21 ºAPI will be produced at up to 20,000 bpd from wells with ESP's (Electrical Submersible Pumps). With the expected water production the produced fluids will be a tight emulsion. The viscosity of the emulsion is dependant on water-cut and line temperature with a range of 50 to 10,000 cP with a temperature range of 60 to 120 ºF and WLR (Water Liquid Ratio) of 0 to 60 %v/v. Line pressure is 150 to 300 psig.

Figure 1 shows the configuration of the Heavy Oil Measurement comprising a slugcatcher to reduce emulsion slugging and to constrain gas in the liquid leg to a GVF (Gas Volume Fraction) of 0 to 60 %v/v for measurement with a Dual Gamma Venturi MPFM. Gas will be entrained in the emulsion, without slip between the phases, as a froth of small bubbles similar to bubbles in treacle and is not expected to form voids at lower GVF levels. This flow regime and the WLR and GVF range are well within the capabilities of the MPFM Dual Gamma phase detector. The Venturi flow element does pose some difficulties due to the high viscosity and therefore low Reynolds Number (Rn) in the laminar flow region that requires a correction to the venturi Coefficient of Discharge (Cd) constant. A two-path ultrasonic meter in the gas leg measures the gas produced to account for gas and entrained liquids and is not part of the Fiscal measurement.

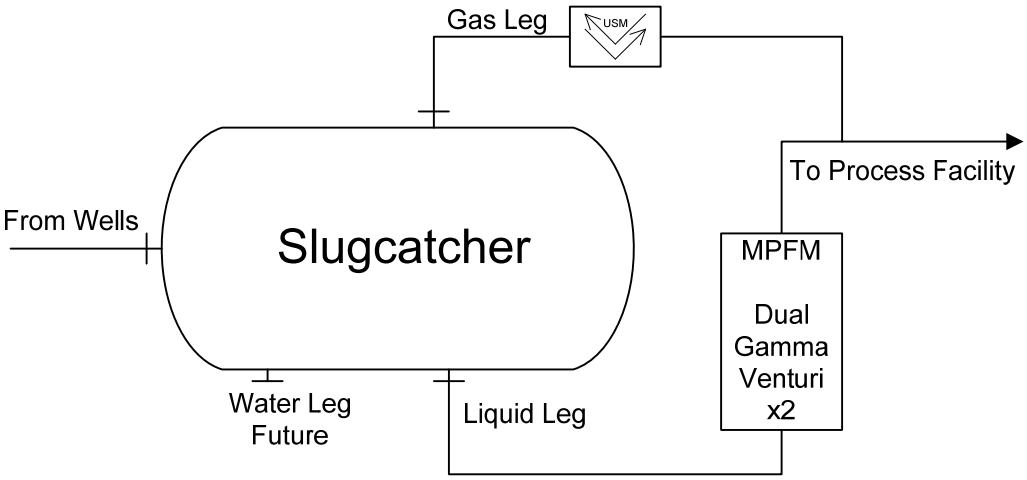

Figure 1 Heavy Oil Measurement

A model of the Dual Gamma Venturi MPFM phase detector and mass flow meter was developed to find the uncertainty and bias in the **oil standard volume Fiscal measurement**. The gas and produced water measurements in the Liquid Leg are not of interest for Fiscal measurement and are utilised as needed to implement the model.

The MPFM Model described in Section 3 includes a correction to the Venturi Cd constant for Rn based on published data, this being the main concern with the Heavy Oil measurement. The model is applied over the expected range of use to optimise the Venturi bore size selection for each of the two streams to minimise measurement uncertainty and cope with rapid changes in flow rate that arise due to slugging. This is achieved by switching the standby stream in or out of service as the flow rate changes to keep each MPFM within its optimum operating range, and maximise turndown.

The results for this application are discussed in Section 4, Conclusions including limitations of the current model and refinements to improve the model.

3 MPFM Model

The main components of the Dual Gamma Venturi MPFM shown in Figure 2 are:

1. Blind Tee — Mixer to improve the homogenous mixture of phases.
2. Venturi — Flow element with a calibrated bore and throat.
3. Temperature — Correction of oil volume to volume standard temperature.
4. Pressure — Correction of oil volume to volume at standard pressure.
5. Differential Pressure — Venturi ISO 5167 mass flow rate measurement.
6. Dual Gamma Detector — Measurement of WLR, GVF and mixture density.
7. Ambient Temperature — Dimensional correction.

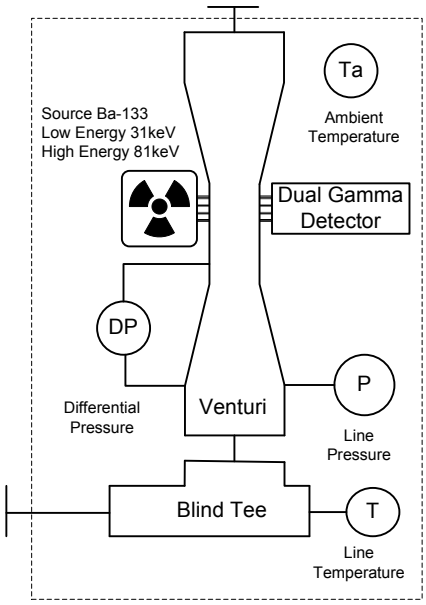

Figure 2 Dual Gamma Venturi MPFM

The MPFM model is constructed from a series of modules that calculate the measurement quantities, bias and uncertainty. Bias is found from duplicate calculations of the measurement quantities with the correct inputs and biased inputs respectively. Bias is found from the

difference between the results from the correct inputs and the biased inputs. By changing one input bias at a time the sensitivity of the measurement to each input can be found. Uncertainty is found with quadrature RSS (Root Sum Square) methods and MCS (Monte Carlo Simulation) methods in a hybrid RSS/MCS uncertainty model.

RSS is used for instrument measurements including line temperature, line pressure and venturi differential. RSS is also used to find the Venturi mass flow measurement using a modification to the orifice uncertainty method in ISO5167: 2003-2 [Ref. 5]. All other uncertainties are found by MCS including the API thermal and compressibility correction of oil volume from line to standard conditions and the AGA8 gas line density calculation, the Dual Gamma GVF, WLR and mixture density and the combination of all uncertainties. MCS takes account of all the dependencies and propagates uncertainty automatically eliminating the need to analyse the sensitivity of complex calculations. See "Uncertainty of Complex Systems by Monte Carlo Simulation" [Ref. 2] for explanation of MCS methods.

The MPFM modules are:

1.	Instrument Uncertainty	Differential Pressure, Static Pressure, and Temperature all by RSS.
2.	Line Conditions	Oil API thermal (Chpt. 11.1) and compressibility (Chpt. 11.2.1) correction for actual and standard density, Gas AGA8 actual density, Produced Water actual density from salinity all by MCS.
3.	Dual Gamma Phase	Uncertainty of GVF, WLR and Mixture Density from Oil, Gas and Produced Water actual density and mass attenuation with Low Energy and High Energy EPR (Empty Pipe Reference) count and Measurement count uncertainty all by MCS
4.	Venturi	Mass Flow calculation uncertainty from Mixture Density and Oil Standard Volume with a combination of RSS and MCS methods.
5.	Cd Correction	Reynolds Number found in the Venturi Module is used to find Cd from a correction curve for use in venturi mass flow calculation.
6.	Phase Envelope	Shows meter operating area and the mass attenuation factors limits.

The uncertainty and bias results are presented as three dimensional surfaces covering the GVF are WLR operating range in X-axis and Y-axis with the parameter of interest shown in the Z-axis. Figure 3 shows the Crude Oil Standard Volume Uncertainty surface for the conditions listed in Table 1. This includes the emulsion viscosity which increases with increasing water cut. The results at the four corners of the surface are summarised with other

results at the bottom of Table 1 which also shows bias due to oil and water input density bias discussed in the following sections.

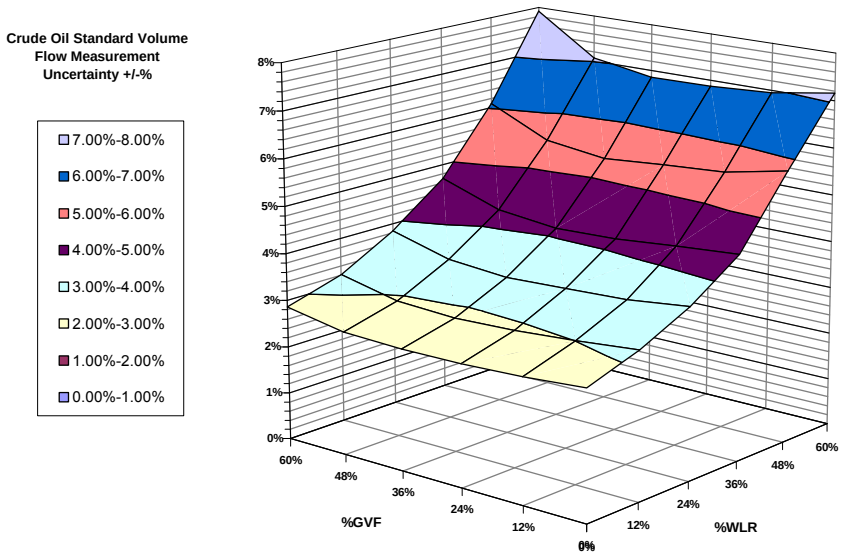

Figure 3 Crude Oil Standard Volume Uncertainty

Case	1			
Description	**Units**	**Measurement**	**Uncertainty**	**Bias**
Meter	Type	52mm		
Gamma Count Sample Rate	Seconds	40		
Liquid Line Flow Rate	bpd	20,000		
Gas Standard Density	SG	0.68	0.0023 lb/cf	0 lb/cf
Oil Standard Density	API°	20.6	0.58 lb/cf	1.87 lb/cf
Water Standard Density	lb/cf	64.30	0.32 lb/cf	1.87 lb/cf
Temperature	°F	78	0.45	
Pressure	psig	250.00	0.76	
Emulsion Viscosity	**%WLR**	**cP**		
	0%	121.00		
	12%	198.00		
	24%	361.00		
	36%	698.00		
	48%	1,806.00		
	60%	3,299.00		

Results	**Units**	**GVF=0%, WLR = 0%**	**GVF=60%, WLR=0%**	**GVF=0%, WLR=60%**	**GVF=60%, WLR=60%**
Oil Standard Volume Observed	stbpd	20,011	20,022	8,032	7,918
Oil Standard Volume Uncertainty	%	2.7%	2.8%	7.1%	7.6%
Oil Standard Volume Bias	%	-0.1%	-0.1%	-0.4%	-0.4%
GVF Observed	%GVF	-3.3%	58.7%	-3.1%	58.8%
GVF Uncertainty	%GVF	0.6%	0.5%	0.7%	0.5%
GVF Bias	%GVF	3.3%	1.3%	3.1%	1.2%
WLR Observed	%WLR	0.0%	0.0%	59.9%	59.9%
WLR Uncertianty	%WLR	1.0%	2.0%	1.5%	2.7%
WLR Bias	%WLR	0.0%	0.0%	0.1%	0.1%
Mixture Density Observed	kg/m^3	953.52	390.40	1,015.81	415.30
Mixture Density Uncertainty	%	1.1%	1.4%	0.9%	1.2%
Mixture Density Bias	%	-3.1%	-3.1%	-2.9%	-2.9%
Mixture Mass Flow Observed	kg/s	34.19	35.02	36.49	37.32
DP Observed	mbar	1515	3690	3108	5356
Viscosity Observed	cSt	131	53	3346	1339
Reynolds Number Observed		3459	21374	135	846
Discharge Coefficient Observed		0.932	0.955	0.672	0.819
Discharge Coefficient Uncertainty	%	2.164%	1.242%	5.960%	3.367%

Table 1 Crude Oil Standard Volume Conditions and Results with Bias

3.1 Dual Gamma GVF, WLR and Mixture Density

The proportions of oil, gas and water are found with a Dual Gamma detector which measures the attenuation of gamma counts from a Barium source at a Low Energy (31keV) and a High Energy (81keV) relative to an EPR (Empty Pipe Reference) count rate. The attenuation of the low energy source is predominantly dependant on the proportions of oil and water and the high energy source is predominately dependant on the proportion of liquid to gas although both count rates are affected to some degree by all phases.

The Phase Envelope in Figure 4 show linear mass attenuation for the full range of GVF from 0 to 100% and WLR from 0 to 100% in the outer triangle and the Heavy Oil MPFM range in the inner red triangle. The blue triangle illustrates the affect of undetected density bias discussed elsewhere. The corners of the triangle give the linear mass attenuation level single phase oil, gas and water.

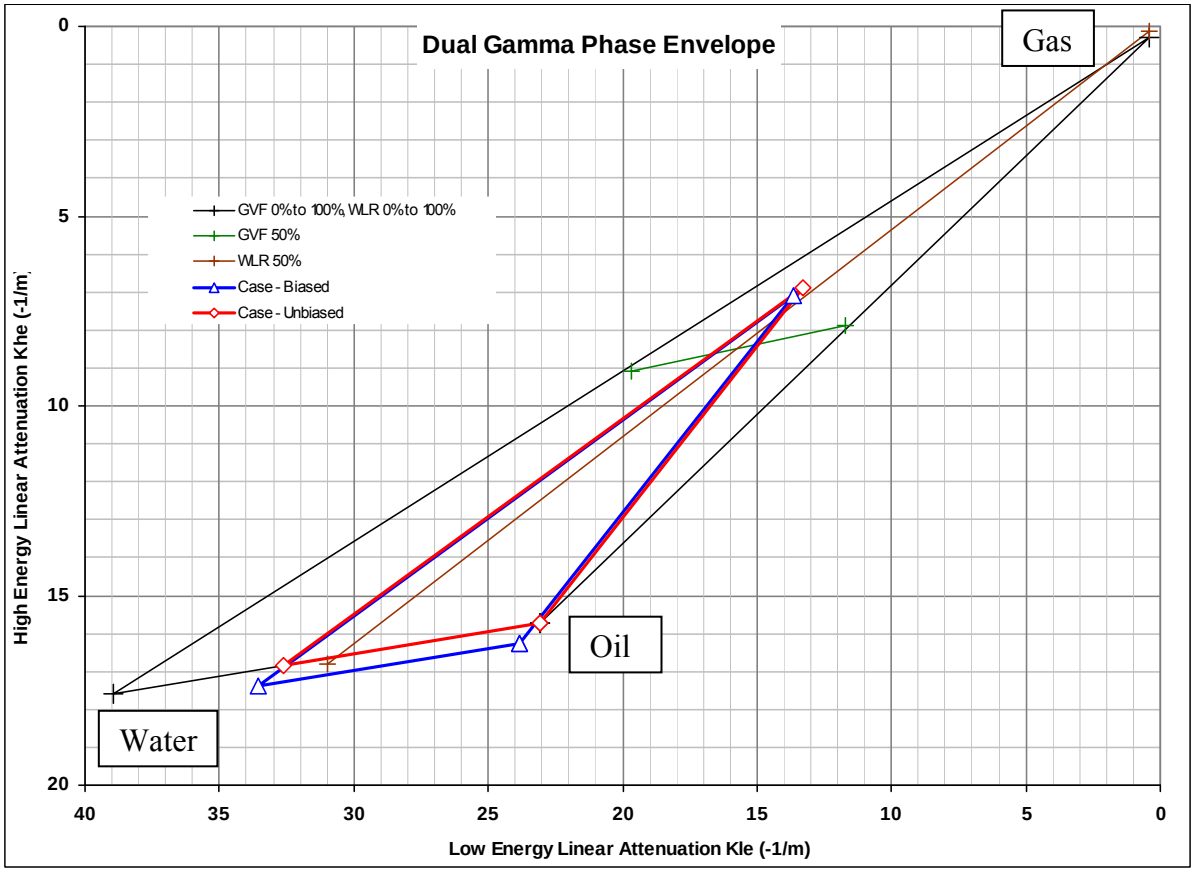

Figure 4 Phase Envelope

The attenuation can be found by calibration on actual fluid in single phase at each corner of the triangle or from the NIST X-Ray mass attenuation tables [Ref. 3] for the fluid composition.

The attenuation of gamma rays is dependant on the density of the mass attenuation coefficient of the penetrated material with the physical relationship:

$$N = N_o \cdot e^{-x\rho\mu}$$

where:

N	gamma detector count of the penetrated material
N_E	"empty pipe" gamma detector count
$x \cdot m$	gamma path length in metres
$\rho \cdot \frac{kg}{m^3}$	density of penetrated material in klogram per cubic metre
$\mu \cdot \frac{m^2}{kg}$	mass attenuation coefficient of penetrated material square meters per kilogram

Where the material is a mixture with oil, water and gas phases the equation is expressed as:

$$N = N_E \cdot e^{-x\left(\mu_o \cdot \rho_o \cdot \alpha_o + \mu_g \cdot \rho_g \cdot \alpha_g + \mu_w \cdot \rho_w \cdot \alpha_w\right)}$$

where:

α_{phase}	the fraction of oil, gas and water
$o \quad g \quad w$	subscripts identifying the oil, gas and water phases

The sum of the phase fractions is unity:

$$\alpha_o + \alpha_w + \alpha_g = 1$$

The detector has a low energy and high energy detection level which is expressed as:

$$N_{le} = N_{le0} \cdot e^{-x \cdot \left(\mu_{leo} \cdot \rho_o \cdot \alpha_o + \mu_{lew} \cdot \rho_w \cdot \alpha_w + \mu_{leg} \cdot \rho_g \cdot \alpha_g\right)}$$ Low energy

$$N_{he} = N_{he0} \cdot e^{-x \cdot \left(\mu_{heo} \cdot \rho_o \cdot \alpha_o + \mu_{hew} \cdot \rho_w \cdot \alpha_w + \mu_{heg} \cdot \rho_g \cdot \alpha_g\right)}$$ High energy

The equations can be represented in terms of linear attenuation constants for each energy:

$$K_{le} = \frac{\ln\left(\frac{N_{le}}{N_{le0}}\right)}{-x} = \mu_{leo}\cdot\rho_o\cdot\alpha_o + \mu_{lew}\cdot\rho_w\cdot\alpha_w + \mu_{leg}\cdot\rho_g\cdot\alpha_g$$

$$K_{he} = \frac{\ln\left(\frac{N_{he}}{N_{he0}}\right)}{-x} = \mu_{heo}\cdot\rho_o\cdot\alpha_o + \mu_{hew}\cdot\rho_w\cdot\alpha_w + \mu_{heg}\cdot\rho_g\cdot\alpha_g$$

The Dual Gamma Constant and Uncertainty Input in Table 2 lists all the inputs required to calculate Low Energy and High Energy counts over the required GVF and WLR range for input to the phase uncertainty module using the equations detailed above.

Dual Energy Gamma Densitometer – MCS Uncertainty					
Constants and Uncertainties					
Mixture	Name	Units	Minimum	Maximum	
Gas Volume Fraction	GVF	%gas/mix	0.0%	60.0%	
Water Liquid Ratio	WLR	%wtr/liq	0.0%	60.0%	
Density	Name	Units	Value	Uncertainty	Bias
Gas density	Rhog	kg/m^3	14.98	4.41%	0.00
Oil density	Rhoo	kg/m^3	923.7	1.00%	30.00
Water density	Rhow	kg/m^3	1027.3	1.00%	30.00
Gamma Detector	Name	Units	Value	Uncertainty	Bias
Path length	x	m	0.052	0.010%	0.00000
Low Energy	Name	Units	Value	Uncertainty	Bias
EPR Count Rate	Nle0	Hz	24,109.7	1.46	0.00
EPR Ave. Period	tle0	Sec	43,200		
EPR Samples	Sle0		1		
Measurement Count	mtle	Hz			0.00
Measured Ave. Period	tle	Sec	40		
Measured Samples	Sle		1		
Gas attenuation	Muleg	m^2/kg	0.025830400	0.50%	0.0000000
Oil attenuation	Muleo	m^2/kg	0.024967800	0.50%	0.0000000
Water attenuation	Mulew	m^2/kg	0.037914000	0.50%	0.0000000
High Energy	Name	Units	Value	Uncertainty	Bias
EPR Count Rate	Nhe0	Hz	12,541.4	1.06	0.00
EPR Ave. Period	the0	Sec	43,200		
EPR Samples	She0		1		
Measurement Count	mthe	Hz			0.00
Measured Ave. Period	the	Sec	40		
Measured Samples	Sle		1		
Gas attenuation	Muheg	m^2/kg	0.018003700	0.50%	0.0000000
Oil attenuation	Muheo	m^2/kg	0.017045900	0.50%	0.0000000
Water attenuation	Muhew	m^2/kg	0.017131700	0.50%	0.0000000

Table 2 Dual Gamma Constant and Uncertainty Input

The table includes the inputs for bias to enable investigation bias in the results arising from bias in the inputs. In the example the oil and water densities both have a +30kg/m3 bias. The effect of this can be seen in the Phase Envelope in Figure 4 which shows the linear attenuation bias in blue causing the small bias in Table 1, Crude Oil Standard Volume Conditions and Results with Bias illustrates relatively low sensitivity to large oil and water density biases. Other work has shown that oil density bias due to a change in the hydrocarbon composition has little effect on the oil mass attenuation factor. Small changes in the produced water density due to changes in salinity have a corresponding bias in the mass attenuation factor increasing the overall the WLR bias and dependant calculations.

Table 2 also shows the EPR and Measurement count rates including sampling intervals. The EPR is sampled for 12 hours to minimise the reference count uncertainty which is found from the square root of the number of counts divided by the count period in seconds to find the uncertainty in counts per second. It is also essential that the MPFM conditions are kept constant for this period of time. The Measurement count uncertainty is found in the same way however the count averaging period of forty seconds is chosen so the uncertainty is greater.

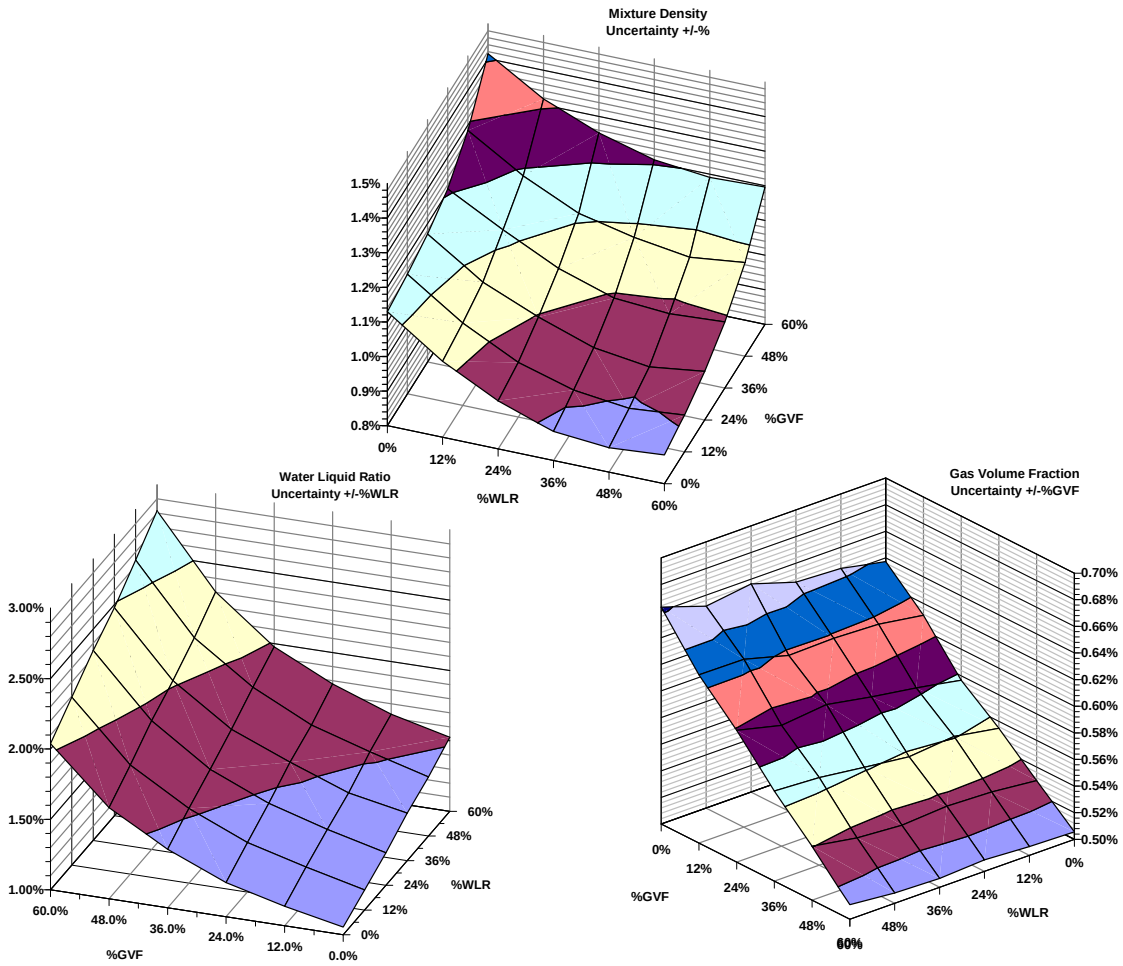

Figure 5 Dual Gamma WLR, GVF and Mixture density Uncertainty

Using the input data the uncertainty is calculated by MCS to find the Dual Gamma WLR, GVF and Mixture density Uncertainty surfaces shown in Figure 5 on the next page.

Oil, produced water and gas densities are calculated in the Line Condition module for use in the Dual Gamma module and Venturi module. Oil density is corrected to standard conditions using the API thermal and compressibility methods. Water density is calculated from the salt content and the gas densities are calculated from a gas composition using AGA8. Uncertainty is found with MCS for all densities. Pressure and temperature measurement uncertainties found by RSS are taken from the Instrument module. Table 3 shows the inputs, densities and uncertainty results for the Line Conditions module.

Fluid	Quantity	Name	Unit	Value	Uncertainty	
Conditions	Temperature	Tmix	°F	78.0		
			°C	25.56	0.45	
	Pressure	Pmix	psig	250.00		
			barg	17.042	0.76	
Oil	Gravity	APIoil	°API	20.6		
	Standard Density	ρsoil	kg/m^3	929.39		
	Vapour Pressure	Pvap	psig	10.00		
			barg	0.68		
	Thermal Correction	Ctloil	factor	0.992877		
	Pressure correction	Cploil	factor	1.001022		
	volume correct.	VCFoil	factor	0.993891		
	actual density	ρaoil	kg/m^3	923.71		
	standard volume correction factor			0.993891	0.10%	0.99399971
Water	standard density	ρswtr	kg/m^3	1,030.030		
	salinity		kg/kg	0.0429196		
	actual density	ρawtr	kg/m^3	1,027.319		
	standard volume correction factor			0.997368	0.10%	0.997866191
Gas	standard density	ρsgas	kg/m^3	0.83107		
	actual density	ρagas	kg/m^3	14.985		
	dyn. viscosity	μgas	cP @60°F	0.015		
	kin. viscosity	νgas	cSt	1.00102		
AGA8 Gas Density						
Line Conditions	Measurement	Uncertainty				Trial Values
Temperature deg C	25.56	0.450				25.43
Pressure bara	18.05	0.755				18.40
Gas Composition	Compostion mol%	Normalised mol%	Component Uncertainty %	Uncertainty mol%	Trials	Normalised Trials
Nitrogen mol%	0.720	0.720	1.00%	0.0072	0.7185	0.7174
Carbon Dioxide mol%	1.360	1.360	1.00%	0.0136	1.3676	1.3655
Methane mol%	85.330	85.330	2.00%	1.7066	85.4663	85.3403
Ethane mol%	6.150	6.150	1.00%	0.0615	6.1468	6.1377
Propane mol%	3.810	3.810	1.00%	0.0381	3.8206	3.8150
n-Butane mol%	2.020	2.020	1.00%	0.0202	2.0175	2.0145
i-Butane mol%	0.000	0.000	1.00%	0.0000	0.0000	0.0000
n-Pentane mol%	0.580	0.580	1.00%	0.0058	0.5807	0.5799
i-Pentane mol%	0.000	0.000	1.00%	0.0000	0.0000	0.0000
n-Hexane mol%	0.030	0.030	1.00%	0.0003	0.0297	0.0297
n-Heptane mol%	0.000	0.000	1.00%	0.0000	0.0000	0.0000
n-Octane mol%	0.000	0.000	0.00%	0.0000	0.0000	0.0000
n-Nonane mol%	0.000	0.000	0.00%	0.0000	0.0000	0.0000
n-Decane mol%	0.000	0.000	0.00%	0.0000	0.0000	0.0000
Total mol%	100.000	100.00			100.15	100.00
Normalised	True Result	Method Uncertainty	MCS Mean	MCS Uncertainty	Trials with Method	Trials
Line Density Kg/m3 (AGA8)	14.98	0.10%	14.98	4.41%	15.29	15.29
Standard Density Kg/m3 (AGA8)	0.8311	0.10%	0.83	0.34%	0.8310	0.8310
Line/Standard	18.03		18.02	4.40%	18.40	18.40

Table 3 Line Conditions Density Uncertainty

3.2 Venturi Mass Flow Rate

3.2.1 Venturi Method

The Venturi mass flow rate is calculated in accordance with ISO5167-4 [Ref. 6] and the uncertainty is calculated using a modified orifice uncertainty in ISO5167-2 [Ref. 5] which takes into account uncertainty in Cd, expansion factor, bore diameter, throat diameter, differential pressure uncertainty and the mixture density uncertainty from the Dual Gamma phase detector. In the model the mass flow rate is known enabling the calculation of the differential pressure for each GVF and WLR point with an inverse venturi calculation.

The model flow rates are for a constant Liquid Standard Volume which in this example is 20,000 stbpd therefore the line volume flow rates will vary with GVF and WLR with higher fluid velocity at high GVF resulting in high differential pressure with a 4:1 over the GVF, WLR range.

3.2.2 Cd (Coefficient of Discharge) Correction

Cd is dependant on Rn (Reynolds Number) which is found from the Velocity and the Kinematic Viscosity of the fluid, from Dynamic Viscosity and Density, and the Throat Diameter of the meter. Viscosity is dependant on the WLR of the emulsion. The viscosity may also be dependant on the GVF and has been combined in proportion to the GVF to find the viscosity of the mixture. Figure 6 shows the wide variation in viscosity over the operating range of the meter from 53cSt at WLR=0%, GVF=60% to 3,346cSt at WLR=60% and GVF=0%.

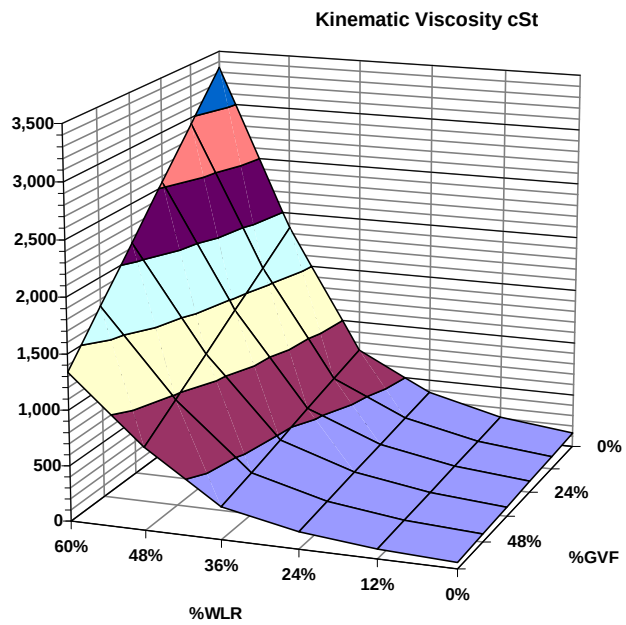

Figure 6 Viscosity Variation

The viscosity variation results in Reynolds Number range 135 to 21,374 in Figure 7.

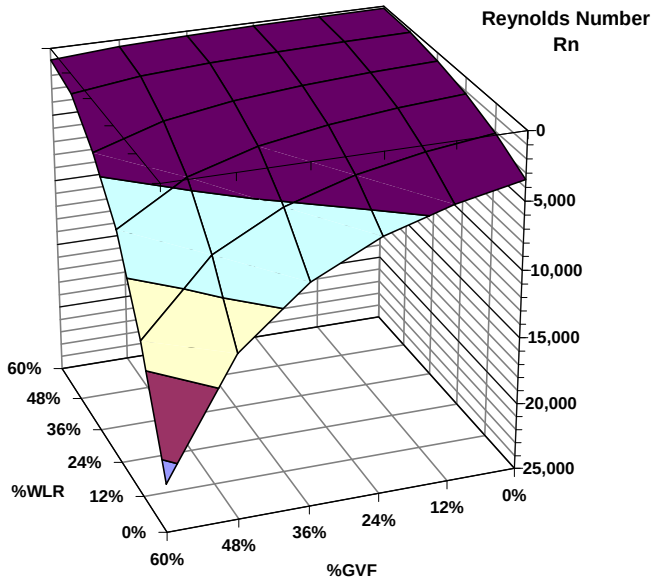

Figure 7 Rn Variation

At Rn below 10,000 the fluid is in transition from turbulent flow with a repeatable Cd= 0.95 to laminar flow with Rn progressively falling to 0.6 shown in Figure 8 below.

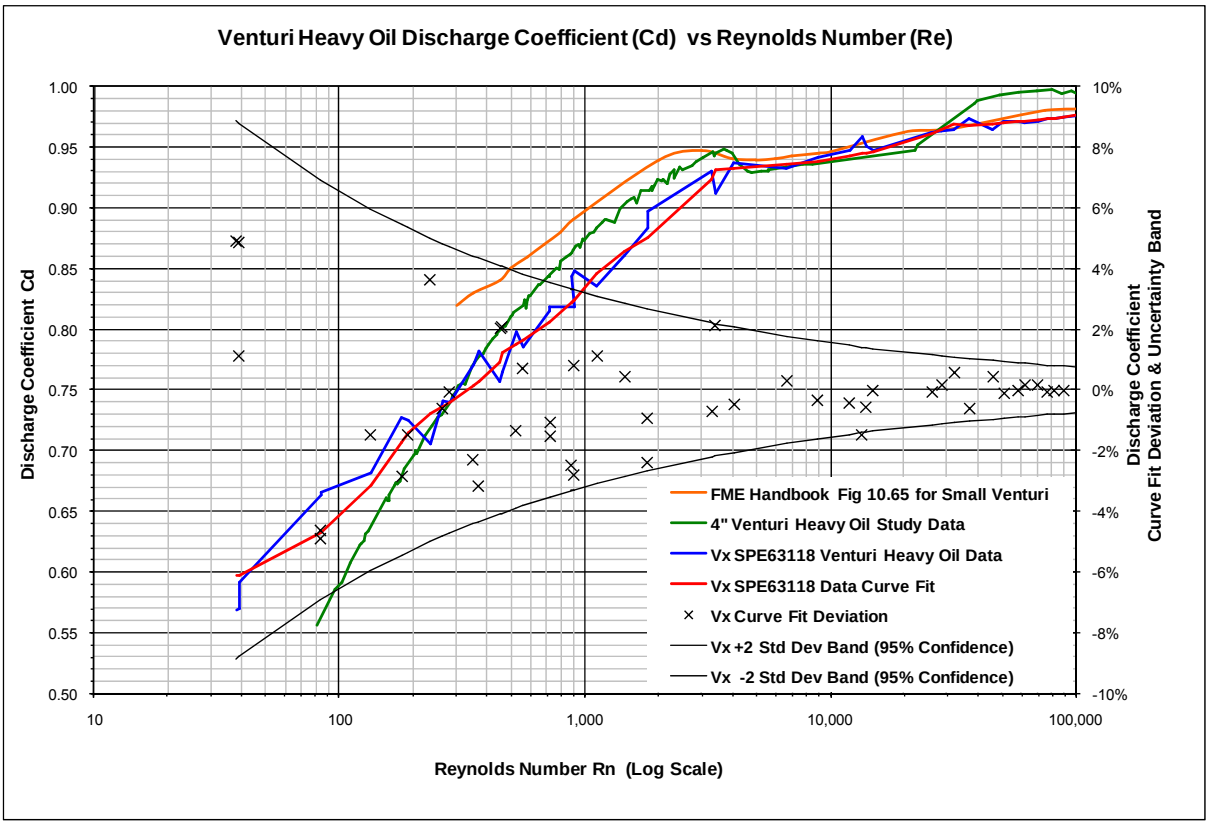

Figure 8 Change in Discharge Coefficient (Cd) with Reynolds Number (Rn)

Coefficient of Discharge (Cd) used in the Venturi equation is found from a Rn vs. Cd look-up table which is plotted as the red trace in Figure 8. This is a curve-fit of the data from the Heavy Oil MPFM paper SPE63118 [Ref.1] shown in the blue trace. This curve compares well with 4" Venturi Heavy Oil SWRI study data [Ref. 11] shown in the green trace and the orange trace from Figure 10.65 of the Flow Measurement Engineering Handbook [Ref. 10].

Data points "x" in Figure 8 are the deviation between the original SPE63118 data and the corresponding curve-fit point. The "trumpet" curve in Figure 8 is found from twice the standard deviation (95% confidence interval) of the "x" data points which represents uncertainty of the curve-fit. The uncertainty of Cd was taken from the curve-fit variability for the SPE63118 Heavy Oil data which did not have a stated uncertainty. The uncertainty is of a similar order to the FME data of ±2%OMV where the traces overlap. This increases to ±8%OMV at the lowest Rn. The Coefficient of Discharge (Cd) and Uncertainty (UCd) surfaces are shown in Figure 9 for the WLR and GVF in earlier examples.

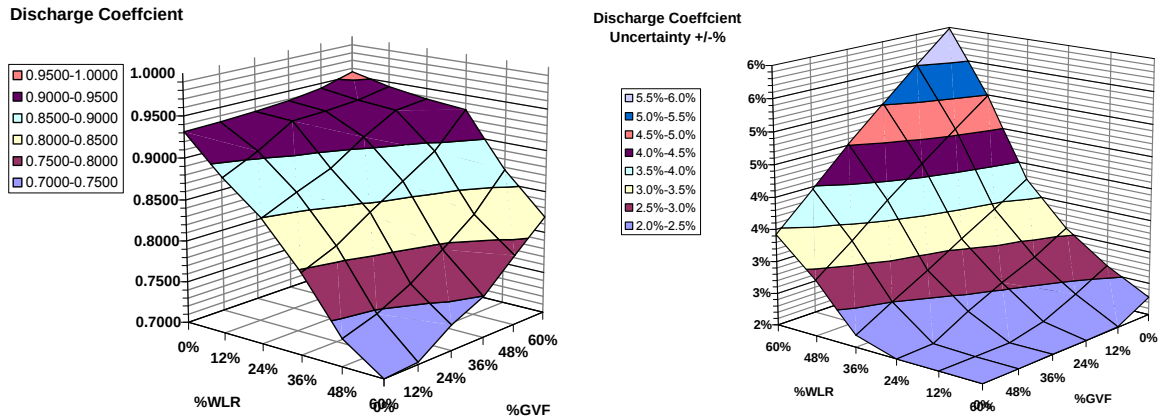

Figure 9 Coefficient of Discharge (Cd) and Uncertainty (UCd)

3.3 Combined Standard Volume

The Dual Gamma GVF, WLR, mixture density and Venturi mass flow rates are combined to calculate the Oil Standard Volume and Uncertainty as follows:

1. Mixture volume mixture mass flow divided by mixture density

   $Qv_{mix} = Qm_{mix} / \rho_{mix}$

2. Oil line volume is found from GVF and WLR

   $Qv_{oil} = Qv_{mix} \times GVF \times (1-WLR)$

3. Oil standard volume found from the API thermal and compressibility corrections

   $Qstdvol_{oil} = Qv_{oil} \times Ctl_{oil} \times Cpl_{oil}$

The uncertainty is found by propagating the uncertainty for each measurement through these calculations using MCS (Monte Carlo Simulation).

The Propagation of Uncertainties are summarised in Figure 10 below showing that high viscosity is the dominant influence on uncertainty with Heavy Oil due to low Reynolds Number.

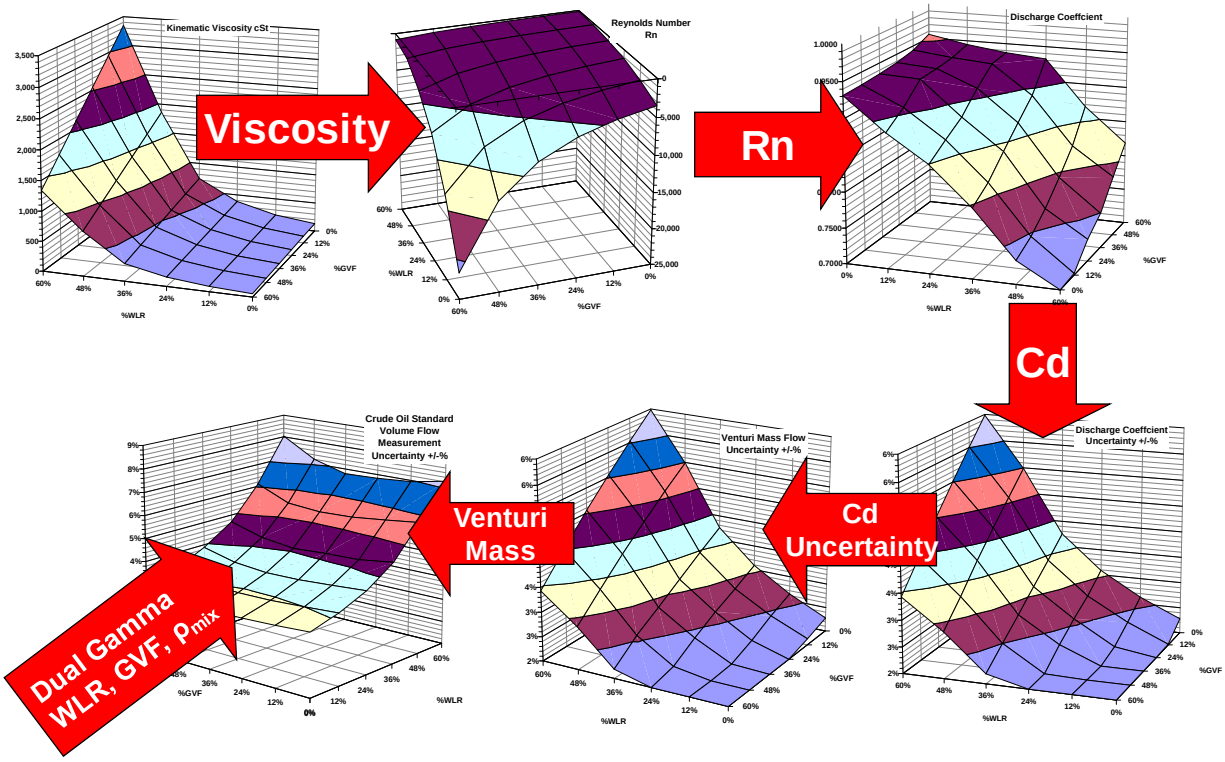

Figure 10 Propagation of Uncertainties

4 Conclusions

The Crude Oil Standard Volume Uncertainty for the base case in Figure 3 of ±3%OMV was within ±0.5%OMV of the vendor's uncertainty over the full GVF range from 0 to 60% for WLR from 0 to 12%. For WLR's above 12% the influence of the increase in the increasing viscosity of the emulsion with WLR and its influence on Reynolds Number and Coefficient Discharge do not appear to have been taken into account and the results diverged with a maximum difference of ±5%OMV at a WLR of 60%. Other documentation from the vendor and the SPE63118 paper [Ref. 1] has taken the increase in the oil measurement uncertainty due to viscosity into account and is of the order of ±5%OMV at a WLR of 60% whereas the model showed an uncertainty of ±8%OMV.

The model proved to be valuable in understanding bias due to produced water salinity variation which affects the density and mass attenuation factor additively whereas variation in oil composition impacts the oil density but has a negligible impact on the mass attenuation

factor so a relatively large oil density bias can be tolerated which has implication for sampling and analysis of oil and produced water.

The primary advantage of a model was the ability to evaluate the feasibility of various measurement options at each stage of production throughout the field life and when production conditions change. This enabled the selection of meter size, DP span and the number of meters for forecast production rates to be examined to find the optimum configuration.

The mass attenuation factors for oil, produced water and gas for this project were calculated in a separate mass attenuation model based on composition using NIST data [Ref. 3]. This was a great advantage for this project as the fluid properties were known from reservoir samples but samples were not available to measure the mass attenuation. The model could be improved incorporating the mass attenuation into the MPFM model to automate the mass attenuation calculation.

Whilst trials at a calibration facility do provide valuable information the production conditions can not be duplicated and the trials will only provide a rough indication of the meter performance. This also applies to observational data which is dependant on how well the observational data is matched to forecast and actual production conditions. A physical model also has limitations being dependant on knowledge of the production conditions and fluid properties which may be limited at the early stages of a project. As a project progresses knowledge of these conditions is gained and the model can be refined to provide an improved uncertainty prediction which can be used throughout the field life.

5 References

1. Atkinson, D. I., et al., "Qualification of a Nonintrusive Multiphase Flow meter in Viscous Flow", SPE63118, 200 SPE Annual Technical Conference and Exhibition, Dallas, TX, October 1-4, 2000.
2. Basil, M., Jamieson, A. W., "Uncertainty of Complex Systems by Monte Carlo Simulation", 16th North Sea Flow Measurement Workshop, Gleneagles, 26th to 29th October 1998.
3. Hubbell, J. H., Seltzer, S. M., Tables of X-Ray Mass Attenuation Coefficients and Mass Energy-Absorption Coefficients, National Institute of Standards and Technology, April 1996.
4. ISO 5167-1: 2003(E), Measurement of fluid flow by means of pressure differential devices inserted in circular cross-section conduits running full -Part 1: General principles and requirements
5. ISO 5167-2: 2003(E), Measurement of fluid flow by means of pressure differential devices inserted in circular cross-section conduits running full -Part 2: Orifice plates
6. ISO 5167-4: 2003(E), Measurement of fluid flow by means of pressure differential devices inserted in circular cross-section conduits running full -Part 4: Venturi tubes

7. ISO 5168: 2005(E),, Measurement of fluid flow – Procedures for the evaluation of uncertainties
8. ISO/IEC Guide 98: 1995, 2nd Edition; Guide to the expression of uncertainty in measurement (GUM).
9. ISO/IEC NP Guide 98: 1995/DSuppl 1.2, Propagation of distributions using a Monte Carlo method.
10. Miller, R. W., Flow Measurement Engineering Handbook, McGraw-Hill, New York, 1996, 3rd Edition: Page 10.63, Figure 16.5 Discharge coefficient for venturi.
11. Stobie, G. S., et al., "Erosion in a Venturi Meter with Laminar and Turbulent Flow and Low Reynolds Number Discharge Coefficient Measurement", 25th International North Sea Flow Measurement Workshop, October 16-19, 2007 Oslo, Norway.

6 Acknowledgement

Dr Andrew Hall's assistance with mass attenuation calculations was greatly appreciated.

LNG ALLOCATION METERING USING 8-PATH ULTRASONIC METERS

Gregor Brown, Cameron, UK
Herb Estrada, Cameron, USA
Don Augenstein, Cameron, USA
Terry Cousins, Cameron, USA

1 INTRODUCTION

This paper discusses the requirements and challenges of in-line allocation metering of LNG in facilities with common storage and shared offloading. Field trials conducted at an LNG test site are described and the results and conclusions of these tests are summarised. The design of the Caldon ultrasonic meter for LNG is discussed, with particular reference to the requirements for application at cryogenic temperatures and very high Reynolds numbers. The benefits of using an 8-path transducer arrangement to ensure transfer of calibration from the lab to the field are demonstrated, both analytically and with reference to the field test data.

2 BACKGROUND

2.1 LNG Supply and Demand

With the depletion of existing conventional oil and gas reserves, LNG is becoming an increasingly important source of fuel for many countries. This is illustrated in the UK gas forecast which shows a rapidly increasing supply gap (see Figure 1). Although much of the increasing demand will be met by gas imports by pipeline, LNG will play an important part in meeting future demands.

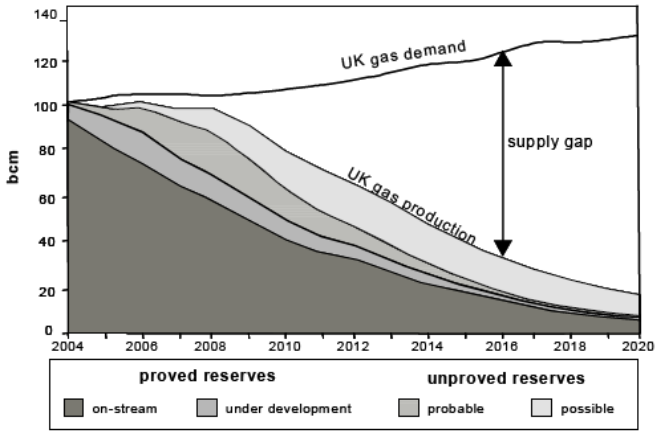

Figure 1 UK gas supply and demand forecast[1]

One of major players in the global supply of LNG is the State of Qatar. For example, the QGII project, which is just one part of the Qatargas facilities, will produce about

15.6 million tonnes of LNG annually. LNG from the first train of QGII is destined for the South Hook Terminal in Milford Haven UK, secured by a 25-year purchase agreement, and will fulfil approximately 20% of UK gas demand.

2.2 Common Facilities

Major savings in capital and operational expenditure can be achieved by using common facilities for storage and shared offloading thus reducing the number of storage tanks and berths required. This is the approach that has been adopted for the Qatar Common LNG Project, as illustrated in Figure 2 below, which comprises five separate joint ventures. Cost savings achieved by adoption of the common facilities approach are estimated to be in the region of 1 Billion US dollars ($1,000,000,000) [2].

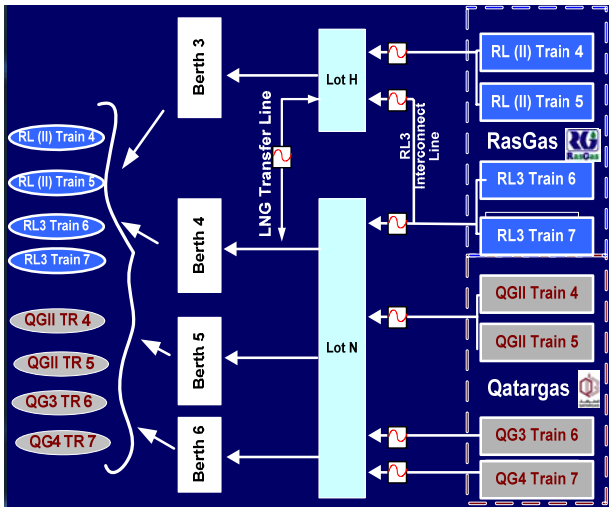

Figure 2 A Schematic of the Qatar Common LNG Project[2]

As a consequence of the fact that LNG from each plant is commingled in the common storage it is necessary to allocate production back to each venture by metering the LNG rundown from each plant. As such, accurate in-line LNG metering is a key enabling technology for this approach.

2.3 Metering Technology Selection Philosophy

As custody transfer measurement of LNG is normally performed by onboard tank measurements, limited research has been conducted regarding the performance of in-line LNG metering systems. In addition to the general shortage of information about in-line LNG metering, there is the added complication that conventional proving systems used for liquid metering can not be used on typical LNG applications. Therefore, a joint funded project was established to evaluate the performance of in-line metering technology for the Qatar Common LNG Project.

The philosophy that the partners agreed upon was to adopt the same technology for all of the metering stations in order that measurement uncertainties would also have a

common basis. Basic pre-qualification requirements used in the selection of technologies for evaluation were:

- No rotating parts
- No wetted sensors
- Advanced diagnostics
- Proven reliability in other applications
- Proven accuracy for liquid custody transfer
- Proven performance in (other) extreme temperature applications

On the basis of the above criteria, both ultrasonic and Coriolis technologies were selected by the project team for evaluation.

2.4 Qualification Requirements

In order to qualify for the use in the Common LNG Project, the flow meters would be required to have the following attributes:

- Ability to perform accurately in cryogenic conditions
- High reliability at cryogenic temperatures
- High reliability through large temperature cycles (-161 to +60°C)
- Ability to be used in a duty-and-check configuration
- Built-in diagnostic capabilities for dealing with unforeseen problems
- Low pressure drop to avoid vaporisation

Based on discussions with various manufacturers, two different makes of Coriolis meter and one ultrasonic meter were chosen for evaluation. The ultrasonic meter was a six-inch 8-path meter supplied by Caldon.

2.5 Field Qualification Tests

The qualification tests were performed at the ConocoPhillips LNG plant located in Kenai, Alaska. This location was selected as it was an operational facility with appropriate infrastructure for the meter evaluation. The test line is a bypass loop on the rundown line with double block and bleed valve, allowing installation and maintenance of the test meters without interfering with the production.

This infrastructure allowed the meters to be tested by using them to meter LNG into the plant's storage tanks. The storage tank measurements were in turn verified against previously certified tanker measurements. Figure 3 shows a schematic diagram and a photograph of the test set up.

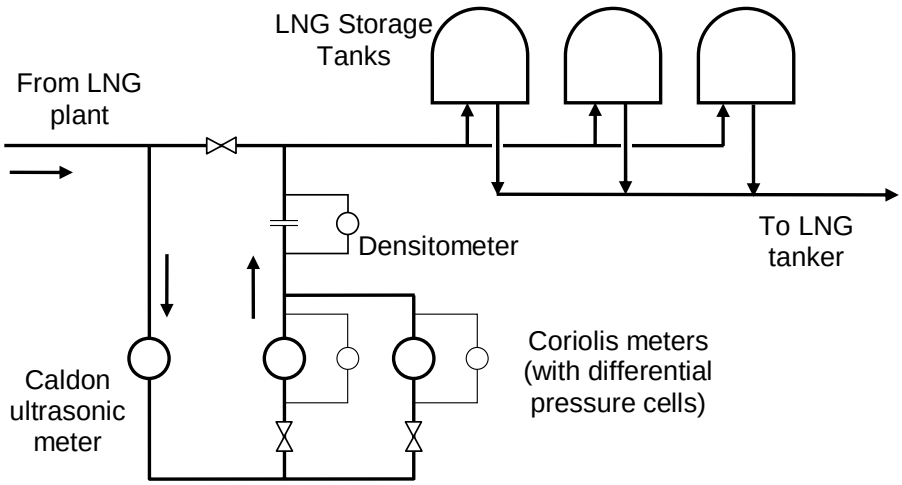

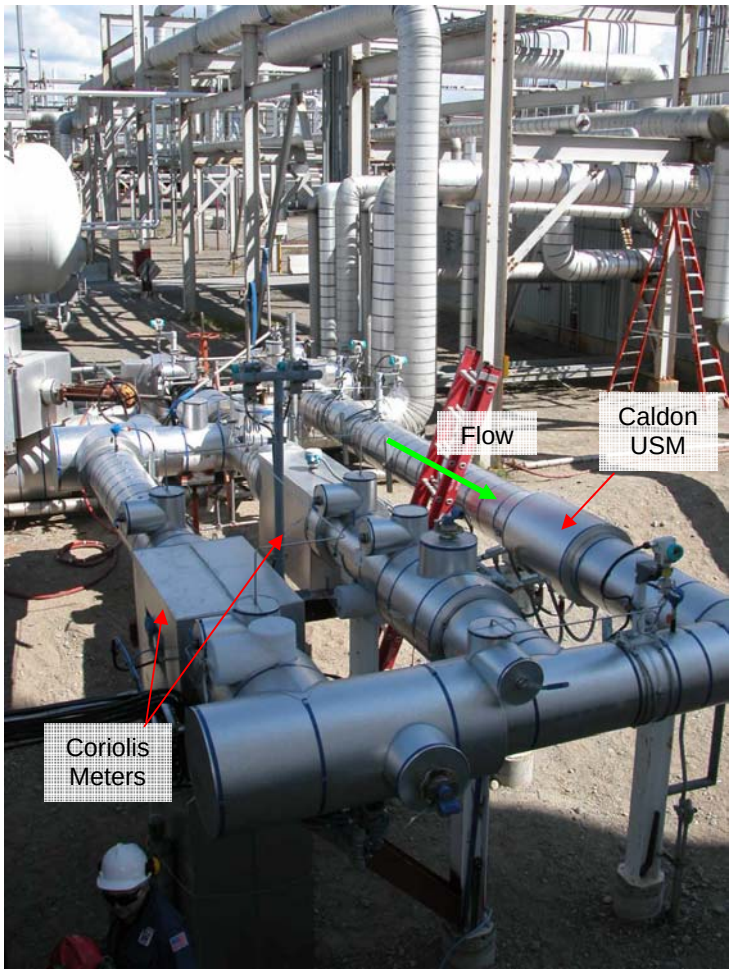

Figure 3 The Kenai test set-up

The qualification tests were performed over a three month period at the end of 2005.

3 CALDON LEFM TECHNOLOGY FOR METERING OF LNG

The Leading Edge Flow Meter (LEFM) ultrasonic technology upon which Caldon meters are based was originally developed by Westinghouse for high accuracy measurement of liquid flows in the late 60's. Following Caldon's acquisition of the LEFM technology in 1989 numerous improvements and additions were made to the product line, including development of transducers for challenging high temperature applications in nuclear power plants. From around 1980 onwards over 70 LEFM systems have been installed in nuclear power plants around the world. These meters are used to measure feedwater flows at temperatures of up to +235°C. In addition, many LEFM systems are now in service in oil custody transfer applications. These applications gave the engineers at Caldon the relevant measurement and design experience required to meet the challenges of high accuracy measurement at cryogenic temperatures.

3.1 Ultrasonic Transducers for Cryogenic Applications

Operation at cryogenic temperatures requires that the materials that are used in the meter body must perform reliably at low temperatures of around -161 °C and be able to withstand large changes in temperature. Furthermore, changes in temperature should not affect the accuracy of the flow rate measurement. The most critical parts of the ultrasonic meter in this respect are the ultrasonic transducers..

When designing an ultrasonic flowmeter for operation at low temperatures the designer must choose between placing the transducers close to the fluid or placing them at the end of some form of temperature buffer rod. Placing the transducers close to the fluid eliminates the buffer but demands that the transducers must produce good quality signals at low temperatures and be robust when subjected to changes in temperature. Using a buffer places lower demands on the transducers themselves but has the disadvantage of influencing the transit time measurements as a consequence of the long transit times in the buffer rods. Furthermore, the thermal gradients in the buffer rods can introduce uncertainties in the transit time measurements.

The approach adopted for Caldon ultrasonic meters is to place the transducers behind a stainless steel window in a welded stainless steel housing. The window, which is less than half an inch thick, serves as a pressure boundary and is in direct contact with the cryogenic liquid. The transducer housings are in turn welded into a manifold as shown in Figure 4. Importantly, this arrangement allows Caldon LNG meters to use the same physical design and path configurations as the standard range of liquid custody transfer meters.

The 8-path Caldon 280C configuration is recommended for LNG applications where high accuracy is important. The main reason for recommending the 8-path design is that it is very insensitive to swirl and distorted velocity profiles, without needing a flow conditioner, which is particularly important when considering pressure drop. A further benefit is that it provides greatest redundancy in case of transducer failure.

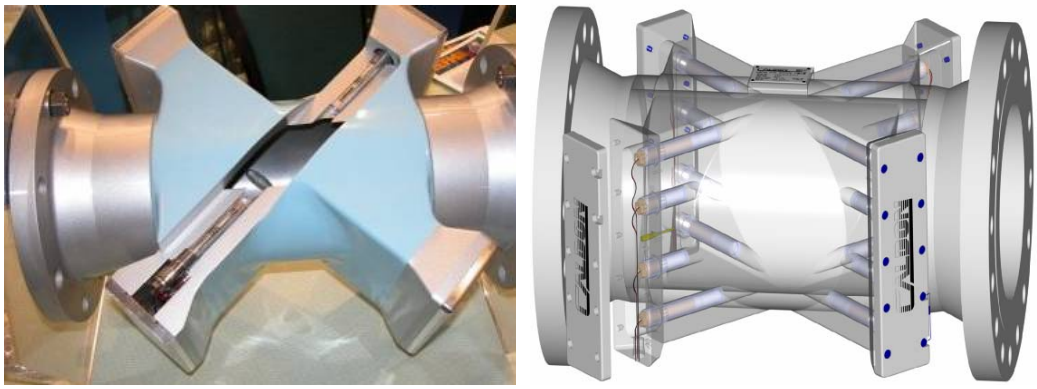

Figure 4 Transducer arrangement in an 8-path meter body

During the development of the transducers, various designs were evaluated by constructing and testing large batches of transducers. The testing included initial cryogenic measurements of signal strength on a large batch of transducers followed by cyclic temperature sample testing to cryogenic temperatures.

In terms of signal strength, it is vitally important that the signal-to-noise ratio (SNR) be sufficiently high in cryogenic conditions. Noise can be random or coherent. For transit time meters it is the signal-to-coherent-noise ratio (SNR_C) that is most important. As the transducers are such a critical part of the flowmeter, Caldon test each transducer as part of the factory acceptance test procedures and only those transducers that exhibit satisfactory signal strength ($SNR_C > 100$) are used.

Figure 5 below shows the distribution of measured SNR_C values (at cryogenic conditions of -191 °C) for a batch of 98 transducers tested by submersion in liquid nitrogen. In these tests 85% of the transducers had a SNR_C of greater than 100.

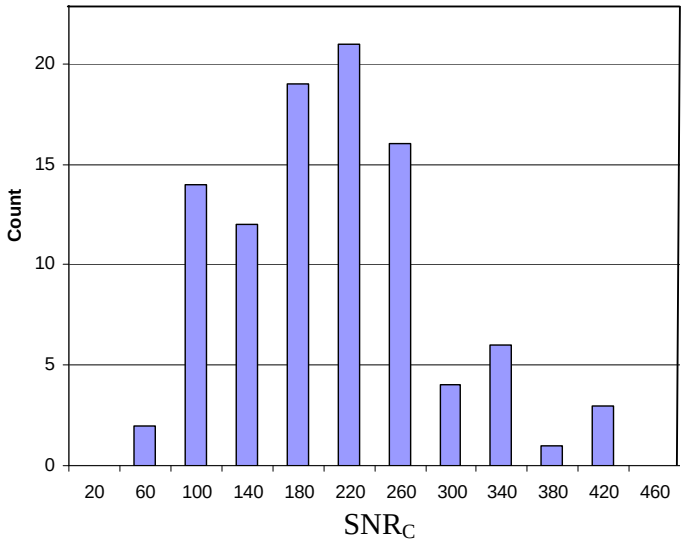

Figure 5 Measured SNR_C in liquid nitrogen

A photograph of the test set up is shown in Figure 6.

Figure 6 Transducer testing by submersion in liquid nitrogen

It can be observed that the average SNR_C in Figure 5 is approximately 200. However, when these transducers were tested in an actual meter (where there are fewer stray echo sources) their performance was much better and the average SNR_C was 740. An example of the cryogenic (liquid nitrogen) test setup with an assembled 10 inch meter is shown in Figure 7.

Figure 7 Cryogenic testing of an assembled meter

In addition to measuring the signal strength during factory acceptance tests, further tests have been carried out to ensure that the signal strength will not degrade if the meters are subjected to multiple thermal cycles. In these tests, the transducers were subjected to a rapid cycle from –191°C to +60°C by placing them in a test cell and submerging them in liquid nitrogen. Once submerged and cooled the signal strength was measured in terms of the gain applied to a transducer pair by the automatic gain

control in the flowmeter electronics. The nitrogen was then allowed to boil off and the samples were then transferred into an oven at 60 °C. Once the temperature had stabilised at 60 °C the process was repeated.

Figure 8 below shows the results from three transducer pairs subjected to 70 thermal cycles. It can be observed that there is no significant change in the gain levels over the duration of the test.

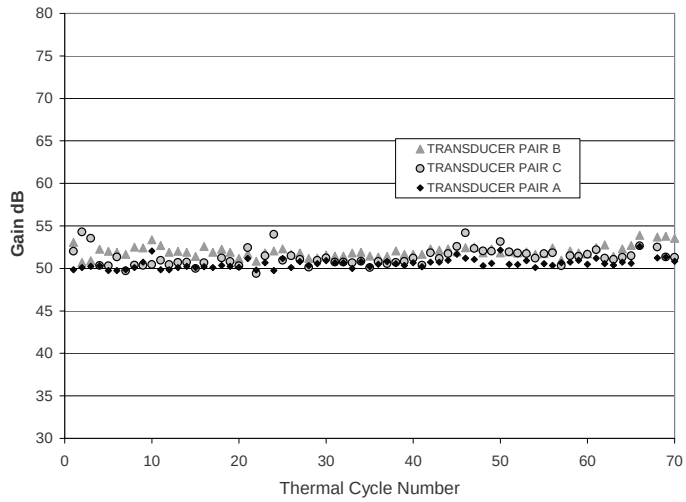

Figure 8 Transducer gain at cryogenic temperature during each thermal cycle

The thermal cycle test is extreme relative to the expected operating conditions for the meter in service for LNG. In general LNG lines will be kept cold to prevent boil-off, and even if the meter does experience temperature cycles the rate of change should be much less than in the Caldon lab tests.

3.2 Maintaining Traceability from the Lab to the Field

3.2.1 Laboratory Calibration and Accounting for Axial Profile Changes

For LNG applications it seems highly unlikely that typically sized ultrasonic meters will ever be calibrated in-situ. Therefore, the calibration must be performed in the factory or at a third-party laboratory. This presents a challenge as currently there are no test facilities using LNG or other cryogenic liquids as the calibration fluid that can achieve the flowrates typically required for ultrasonic meters. For example, the NIST cryogenic calibration facility has a maximum flow limitation of around 45 m^3/hr (or around 14% of the nominal maximum of a 4-inch ultrasonic meter).

To overcome this limitation Caldon have adopted a methodology that allows calibration of LEFM ultrasonic meters using another working fluid. The basis of this methodology is a rigorous analysis of the factors affecting the acoustic signals, and a process that accounts for variations in hydraulic conditions.

The influence of different fluid properties on the acoustic signals can be shown to be relatively small and can be included in the uncertainty budget for the final application [3]. Geometry changes are compensated as a function of temperature, which is measured in the meter body, and again the uncertainty in these corrections can be included in the overall uncertainty budget. This leaves one parameter, the meter factor (or velocity profile factor), to be accounted for.

The meter factor is analogous to the discharge coefficient of a differential pressure flow meter. Ultrasonic meters are velocity measuring devices that sample the velocity on a discrete number of paths. Therefore the 'discharge coefficient' of the ultrasonic meter is a function of the velocity profile of the fluid as it passes through the meter body.

Owing to the low viscosity of LNG, the Reynolds numbers (Re) experienced in LNG applications tend to be high (Re of 500,000 to 30,000,000 could be expected). At these high values of Re the boundary layer is relatively thin and velocity profile is flatter than experienced with a more 'normal' liquid. It is not possible to achieve such high Reynolds numbers in liquid calibration facilities (or at least it is not possible to achieve the maximum application Reynolds numbers), owing to the fact that typical calibration fluids, such as water, have a higher viscosity. Unfortunately achieving a higher Reynolds number by using a gas as the calibration fluid is not appropriate as the acoustic properties of liquids and gasses are too widely different.

However, the important fact is that the calibration of the ultrasonic meter is dependent on the time averaged velocity profile and not some other property of the high Reynolds number flow.

At this stage in the discussion it is important to emphasise some particular characteristics of Caldon 8-path (and 4-path) meters with respect to velocity profile. The first point is that is can be shown in theory (and backed up with laboratory data) that the Gaussian integration method applied in the design of Caldon meters results in a low sensitivity to changes in velocity profile at high Reynolds numbers. The data in Figure 9 below shows the velocity profile factor (or meter factor) for fully developed flow over Reynolds numbers of 32,000 to 35,000,000, calculated using velocity profile data from the Princeton University Superpipe experiments [4, 5]. It can be observed that for Gaussian integration using four chords the change in meter factor owing to profile changes is expected to be less than 0.07%, whereas for meters employing diametric paths the change in the meter factor is 3.9%.

Figure 10 shows results from the calibration of eleven Caldon 8-path LNG meters using water at Reynolds numbers of approximately 700,000 to 3,000,000. This data was obtained after applying a constant meter factor to the raw calibration results, i.e. no linearization was performed. The results demonstrate the excellent inherent linearity of the design, with all meters exhibiting linearity with +/- 0.08%.

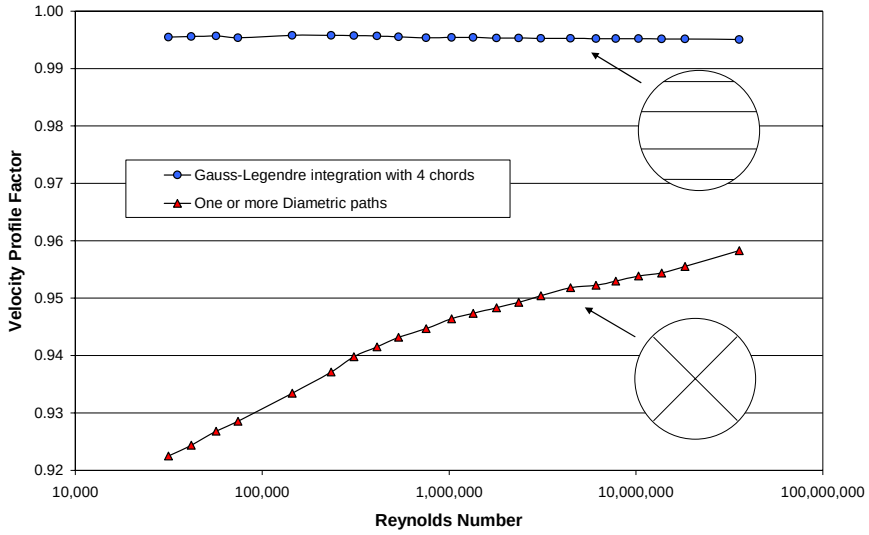

Figure 9 Velocity profile factor vs. Reynolds numbers for two different path configurations

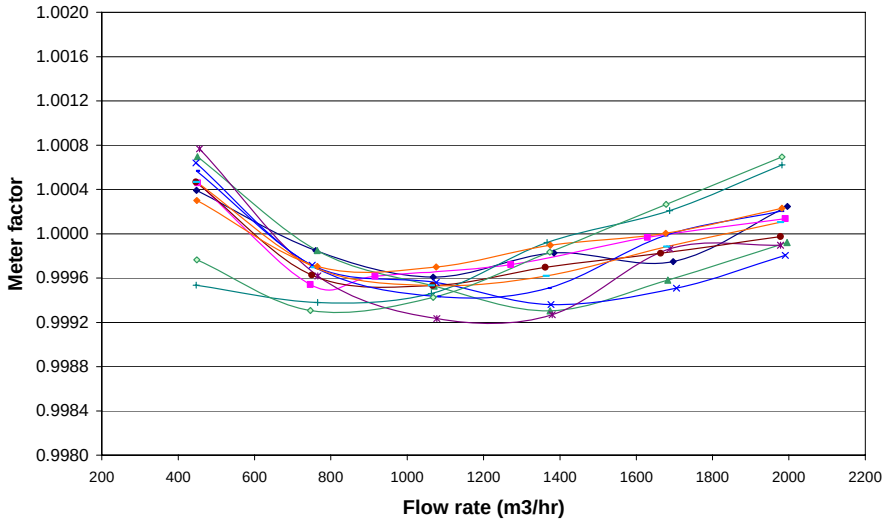

Figure 10 Meter factor versus flowrate for a batch of eleven 8-path LNG meters

The second important point about the Caldon chordal meter design is that the meter itself can characterise the shape of the velocity profile as a 'flatness ratio', which is the sum of the outside path velocities divided by the sum of the inside path velocities. This allows the meter factor to be determined as a function of flatness ratio, as illustrated in Figure 11 below, which shows the flatness ratio and profile factor derived from the Superpipe data for Reynolds numbers from 234,000 to 35,724,000. It should be noted that if two-path diametric or mid-radius designs are used it is not possible for the meter to calculate a flatness ratio, and the correction must rely on inference of Reynolds number.

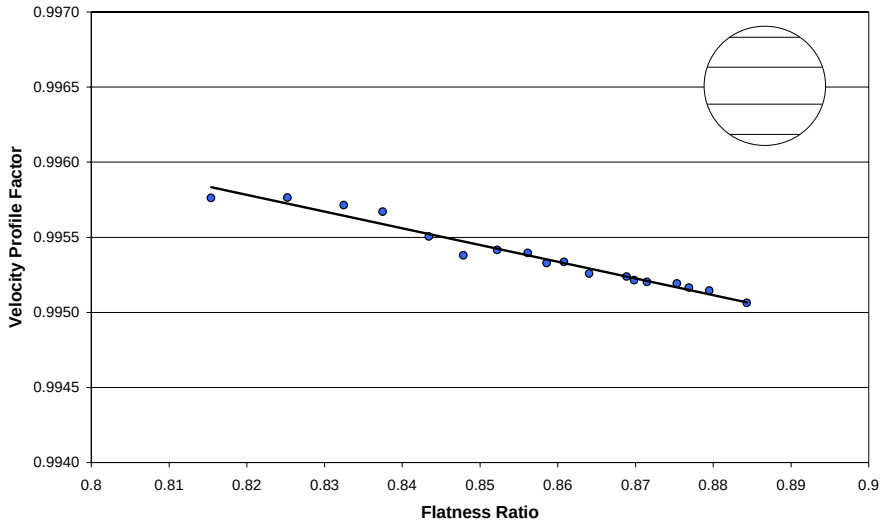

Figure 11 Velocity profile factor vs. flatness ratio for the Gaussian configuration

It is important to recognise that the shape of the velocity profile can be altered not only by changing Reynolds number but also by varying the upstream pipe conditions. For example, out-of-plane bends and reducers tend to thin the boundary layer and flatten the velocity profile. Although such profiles are not identical to fully developed profiles at higher Re, they do produce analogous variations in profile flatness and can be used to validate the calibration method over a range of velocity profile conditions that will encompass the high flatness ratio values seen in LNG applications. It should be noted that this process generates data that includes variation in upstream conditions and therefore also encompasses lab-to-site variations in axial velocity profile. This is in contrast to the limited capabilities of single-path or two-path systems, as illustrated below.

In Figure 12 the accuracy of Gaussian integration with flatness ratio correction has been compared with meter configurations using two paths for a selection of ten distorted axial velocity profiles. The index numbers in Figure 12 refer to the velocity profiles described in references [6] and [7], but with only half the magnitude of asymmetry (*m*). Contour plots of these profiles are shown in the Appendix. Details of the methodology and further examples of this type of analysis can be found in numerous papers, e.g. [6 -10]. In this case the profile factor was determined for each profile at 5 degree intervals of rotation. For the Gaussian configuration a linear relationship between flatness ratio and profile factor was applied before calculating the root-mean-square (RMS) error for each profile. For the 2-path configurations the RMS error for each profile was calculated relative to the velocity profile factor corresponding to fully developed flow in the form of a power law profile with $n = 7$.

The results presented in Figure 12 demonstrate the excellent performance of Gaussian integration with four chords and flatness correction, and highlight the relative weakness of the 2-path configurations. The Gaussian configuration is about 40 times more accurate than the diametric configuration and ten times more accurate than the mid-radius configuration. The two-path configurations fare so poorly in comparison

because they are more sensitive to velocity profile in the first place, and then have no ability to compute useful information about the shape of the velocity profile.

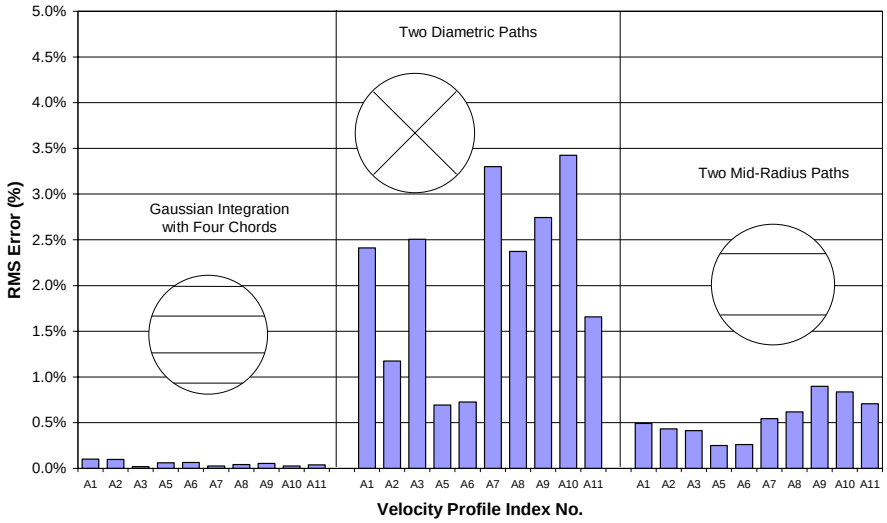

Figure 12 Errors owing to distortion and asymmetry for 10 different axial velocity profiles

For the lowest uncertainty and highest confidence, it is possible to calibrate the meter such that subsequent use relies on interpolation of the meter factor versus flatness ratio data. In that case multiple upstream configurations are required to produce an appropriate range of flatness ratio. However, owing to the low sensitivity of the meter design to velocity profile, extrapolation is possible with very little impact on the overall uncertainty.

The calibration methodology applied to Caldon meters is well supported by theory and an extensive database of laboratory test results obtained with different meter sizes and different pipe configurations. NMi, the Dutch weights and measures authority, have recently reviewed this information in the process of performing independent assessment of this calibration methodology for LNG. The assessment included reviewing uncertainty contributions for the effects of operation at cryogenic temperatures on the dimensional and acoustic aspects of the measurements. NMi's evaluation estimates the uncertainty in volumetric measurement of LNG using Caldon meters to be 0.2% for the case of interpolation using flatness ratio and 0.22% if extrapolation is used [3].

3.2.2 Eliminating the Influence of Non-Axial Flow (Swirl)

The preceding section deals with the issues of calibration and changes of axial velocity profile. It has been demonstrated that a Gaussian integration using four chords can be used to determine the mean velocity very accurately for a wide variety of axial velocity profile shapes, and that under the same conditions 2-path meters are susceptible to significant errors. However, inherent in the preceding analysis is the assumption that the axial velocity is being measured accurately on each of the ultrasonic paths, and that may not be so if there is swirl present.

When flow is forced to change direction, the fluid then travels with forward motion parallel to the pipe axis and motion at an angle to the pipe axis. 'Swirl' is the name generally used for these non-axial components of velocity that are produced downstream of bends and similar pipe fittings.

The means by which swirl interferes with the performance of ultrasonic meters is by introducing an unwanted non-axial component of velocity in the measurement paths. This unwanted component of velocity can be additive or subtractive. If the non-axial flow velocity is going in same the direction as the ultrasound when it travels from the upstream transducer to the downstream transducer then the effect will be to increase the measured velocity. If the non-axial velocity is opposite in direction to the downstream travel of the ultrasound then the effect will be to decrease the measured velocity.

Multipath meters have some in-built tolerance to swirl, but as we will see later, they are limited in terms of what forms of swirl they can tolerate without error.

Single-vortex swirl is a form of swirl that is normally associated with bends in different planes (i.e. configurations that cause a change of flow direction in more than one plane) and can perpetuate for many diameters downstream of the pipeline components that cause it. The rate of decay of swirl can be shown to be a function of the friction factor in the form $\exp(-4fz/D)$, where z is the downstream distance and D is the pipe diameter[11]. The friction factor is in turn a function of Reynolds number, with the result that swirl decays at a slower rate at high Reynolds numbers. This is important for LNG applications as the Reynolds number is typically very high.

Figure 13 below illustrates the rate of decay of swirl at Reynolds numbers of 30,000 (representing an oil flow) and 10,000,000 (representing LNG). An initial swirl angle of 25 degrees has been assumed. It can be observed that at Re = 30,000 the swirl angle is predicted to reduce to less than 2 degrees (the limit set by ISO5167 for orifice plates) in just over 25 pipe diameters. In comparison, at 10,000,000 Re it takes more than 50 pipe diameters for the same reduction in swirl.

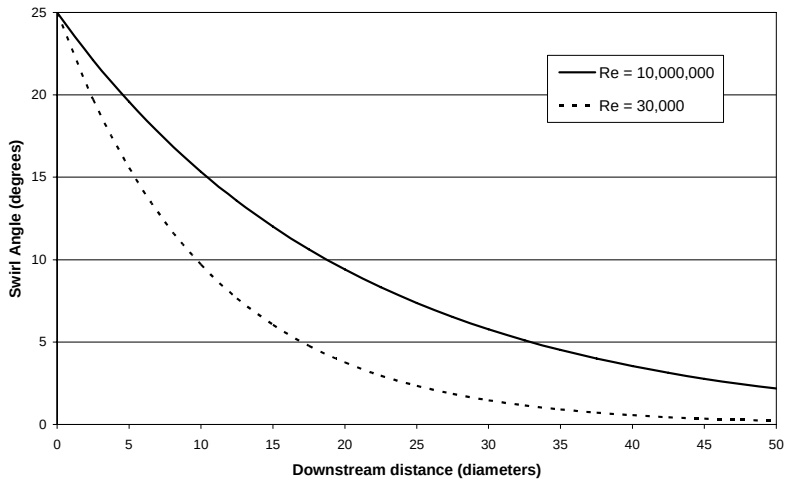

Figure 13 Decay of swirl downstream of a flow disturbance

Most ultrasonic meter designs are unaffected by swirl if the swirl takes the form of a single vortex centred perfectly in the middle of the pipe. However, if the swirl is slightly off-centre or has a more complex pattern containing multiple vortices, then potentially large errors can occur. Good illustrations of complex off-centred swirl downstream of bends can be found in studies where Computational Fluid Dynamics has been used to investigate meter performance [e.g. 12 - 14].

The potential effect of non-centred swirl on the performance of a meter can be evaluated using simulated swirl patterns such as that given by the following equation.

$$u_\theta = \frac{u_0 r_v \exp\left(-r_v^2\right)}{(1 - r + r_c)} \left(1 - r^2\right)^{1/n} \qquad (1)$$

where u_θ is the tangential velocity relative to the vortex centre, u_0 is the vortex strength and $r_v = r_c/r_0$, where r_c is the distance from the vortex centre and r_0 is the radius of the vortex. The value of n controls the manner in which the swirl velocity approaches zero at the walls, where r is the distance from the centre of the pipe normalised to the pipe radius.

Using the above model to create a vortex with parameters of $u_0 = 0.21$, $r_0 = 0.9$, $n = 15$, centred at $r_c = 0.1R$, $y = 0.1R$, and adding this to an axial velocity profile described by the power law in the form $(1 - r)^{1/15}$ generates a profile that has non-centred swirl with a maximum swirl angle of about 6 degrees. A plot of the swirl pattern produced by this model is shown in Figure 14 below.

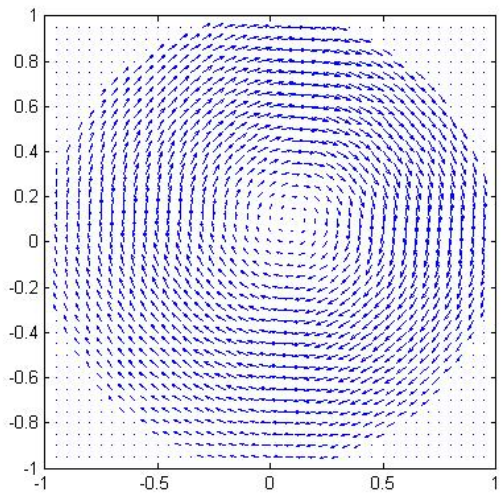

Figure 14 An example of non-centred swirl generated using Equation 1

In terms of the magnitude of effect on various meter configurations, the swirl pattern shown above would result in the errors given in Table 1 below.

Table 1 Swirl induced errors for the swirl pattern shown in Figure 13

Path configuration		Swirl Error Magnitude
Dual diametric paths	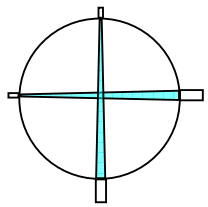	1.5%
4-Path Gauss-Legendre integration (single tilted plane)	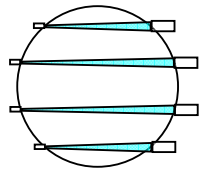	0.26%
5-Path Gauss-Jacobi integration (criss-crossed)	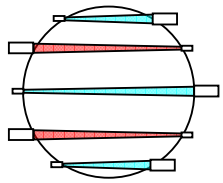	0.33%
8-Path Gauss-Legendre integration (two tilted planes)	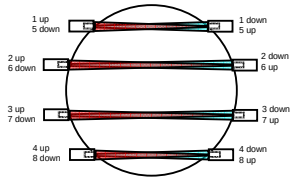	0%

The reason for the zero swirl error in the case of the 8-path meter is illustrated in Figure 15 below, which shows the path velocities for the 4-path (a), 5-path (b) and 8-path (c) meter designs. It can be observed that by averaging the paths in pairs the 8-path result is the same as the profile without swirl in (a) and (b), and hence the influence the swirl is eliminated.

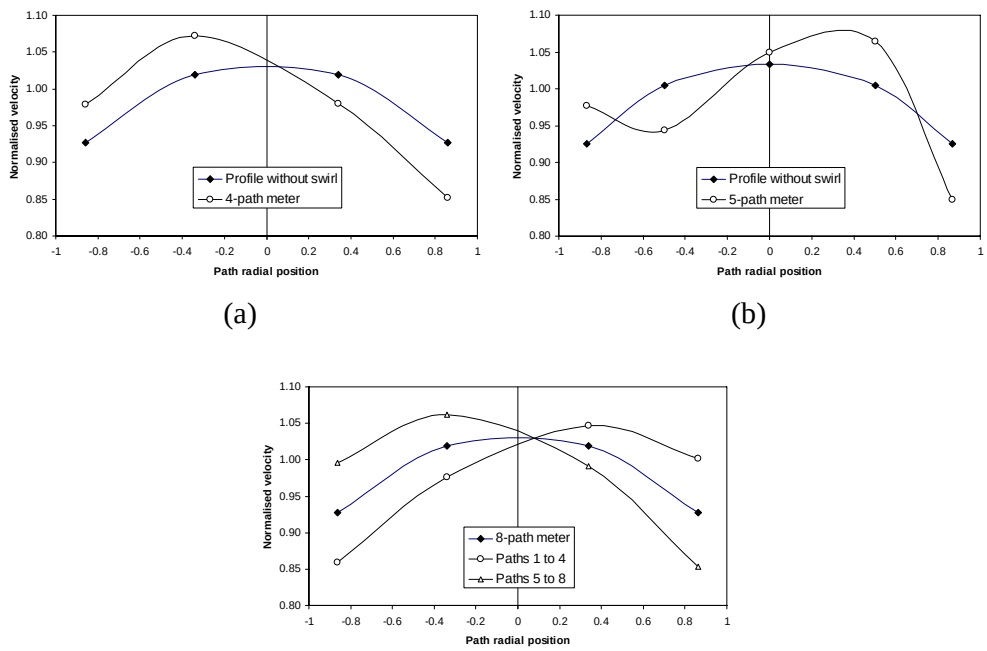

(a) (b)

(c)

Figure 15 Path velocities for (a) 4 paths, (b) 5 paths and (c) 8 paths with swirl

4 FIELD TEST RESULTS AND CONCLUSIONS

The Caldon meter and the two Coriolis meters were tested at Kenai over a three month period by using them to measure the LNG rundown to the storage tanks. The Kenai plant produces approximately 50,000 barrels/day of lean LNG. Photographs of the Caldon meter are shown in Figure 16. The right-hand photograph shows the two sets of electronics that are currently used for the 8-path meter. Each set of electronics produces an output corresponding to one set of four paths (the four paths are grouped in a single tilted plane, like a conventional Caldon 4-path meter, and are referred to as plane A or plane B). The two outputs were averaged externally in the Kenai data acquisition system.

Figure 16 Caldon LNG meter installed at Kenai in Alaska

4.1 Comparison Results

A limited number of runs were performed by comparing data taken directly against the shore tanks between shipments. The storage tank measurements were in turn verified by comparison with onboard measurements from a tanker load performed during a plant shutdown. There was good agreement in the shore tank to ship comparison (within +/-0.3%) but the small number of runs and the scatter in the comparison of the meters with the shore tanks gave rise to a greater statistical uncertainty in these results. Nevertheless there was still reasonable agreement between the three meters and the shore tanks, with the results coming within approximately +/- 0.5%, which was considered acceptable given the limitations of the test.

The main part of the test programme involved comparing the Caldon ultrasonic meter against both of the Coriolis meters in order to assess the reproducibility of the results. The philosophy behind this was that any lack of reproducibility in either technology would be apparent, given that the comparison was between two completely different technologies, including two variants of Coriolis design. The stated aim was that the day-to-day reproducibility should be better than +/- 0.25%.

In terms of reproducibility the comparisons were similar in the case of both Coriolis meters. In terms of the absolute values there was good agreement between the Caldon ultrasonic meter and one of the Coriolis meters, with a more significant bias existing between these two and the second Coriolis meter. Figure 17 below shows the comparison of the Caldon ultrasonic meter and one of the Coriolis meters, using the percentage deviation in 8-hour totals taken over a period of twelve days. The average agreement between the two meters was better than 0.1%, with a statistical uncertainty of less than +/- 0.15%.

These results were taken as a positive confirmation of the performance of both technologies.

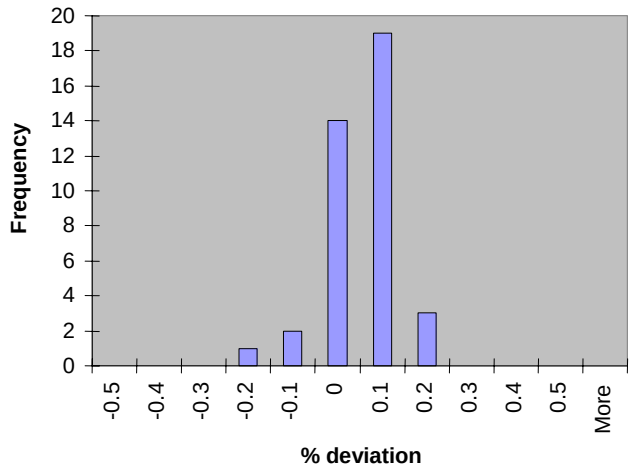

Figure 17 Comparison of Caldon USM and Coriolis meter totals on LNG [2]

4.2 LNG Density Measurement

In order to compare the ultrasonic meter with the Coriolis meters, a density input was required. Various methods of determining the density were compared. These included direct measurements from the Coriolis meters and a Solartron densitometer, calculations using equations of state (e.g. Klosek-McKinley), and density calculated by the Caldon meter. The differences between these different methods were generally less than 0.1%, as shown in Figure 18. The output from the ultrasonic meter was offset from the other results by approximately 0.4%, but tracked the changes in density closely. This result from the Caldon meter shows promise for further development either as a primary or check measurement of LNG density.

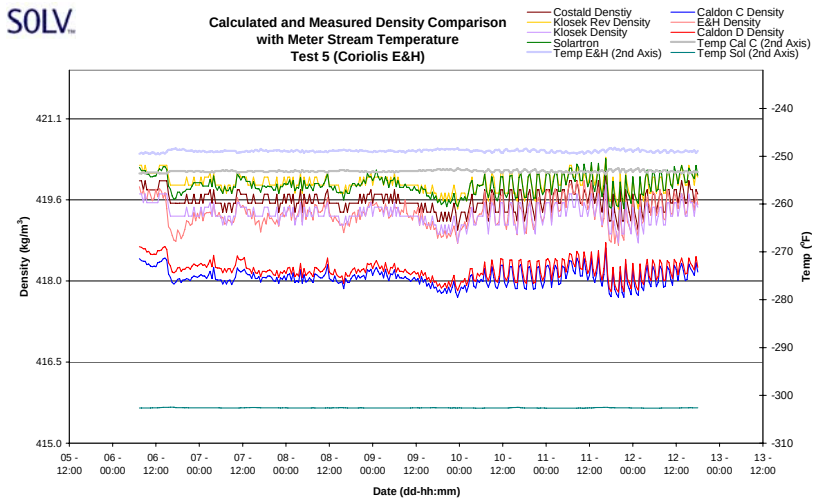

Figure 18 Comparison of calculated and measured densities [2]

4.3 8-Path Swirl Compensation in Action

As two outputs were logged from the Caldon meter, it was possible for the project team to evaluate the outputs from both plane A (i.e. paths 1 – 4) and plane B (paths 5 – 8) separately. When this was done it was found that, relative to the Coriolis meter, one plane was biased by approximately +0.4% and the other by approximately -0.4%, as illustrated in the results shown in Figure 19 below.

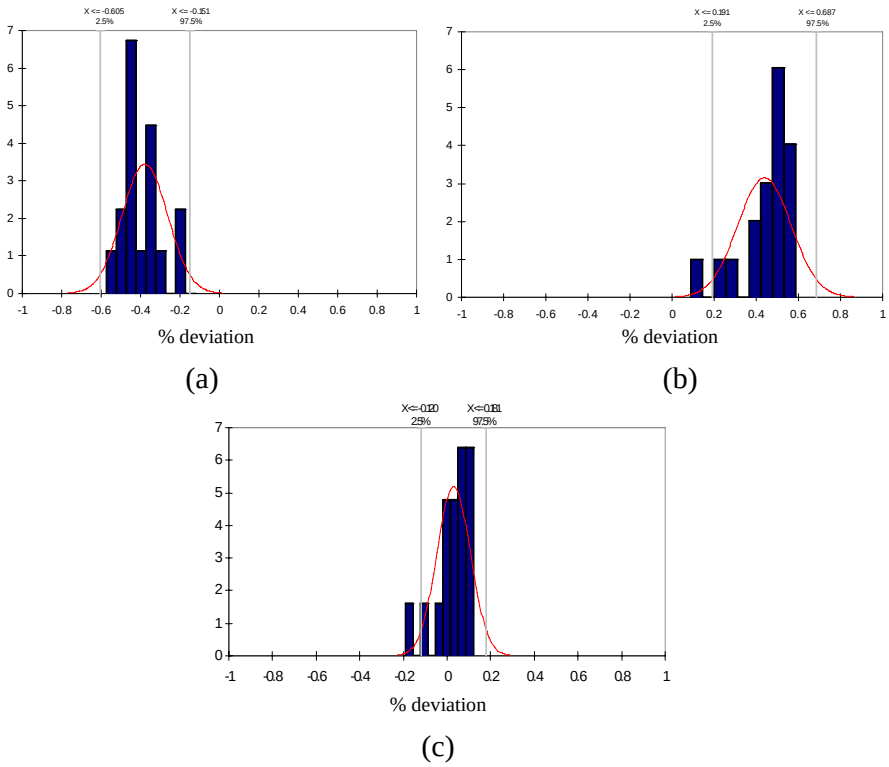

Figure 19 Eight-hour totals, compared with the Coriolis meter
(a) Plane A, paths 1-4, (b) Plane B, paths 5- 8, and (c) 8-path meter results[2]

A symmetrical bias of this magnitude between the two planes of an 8-path meter is normally indicative of strong asymmetric swirl. The Caldon meter was installed at Kenai with approximately 37 diameters of straight pipe upstream and no flow conditioning. This would normally be considered an acceptable installation condition. However, immediately upstream of the straight pipe there were three out-of-plane bends. This sort of configuration is notorious for producing swirl. Add to this the fact that low viscosity of LNG results in such high Reynolds numbers that swirl perpetuates for longer than is usual in liquid applications (see section 3.2.2) and it is perhaps not so surprising that there would be a significant level of swirl present at the location of the meter.

The presence of swirl was confirmed by logging the path velocities from the meter. Figure 20 shows the normalised path velocities obtained during logging at a flowrate of approximately 400 m^3/hr. Note the general similarity of the data in Figure 20 to that of Figure 15(c), typical of a swirling flow. The information in the graph below can be used to estimate the swirl magnitude. The pair of path velocities at each radial

position can be used to yield a transverse velocity, which can in turn be converted to an equivalent tangential velocity at the pipe wall. Performing this calculation for the data shown in Figure 20 results in an average equivalent tangential velocity that is 6.5% of the axial velocity. Similarly, the data can be used to estimate the maximum swirl angle, which is calculated to be approximately 5 degrees. Another way of interpreting the data is to say that the flow undergoes one complete rotation every 48 pipe diameters/every 1.2 seconds.

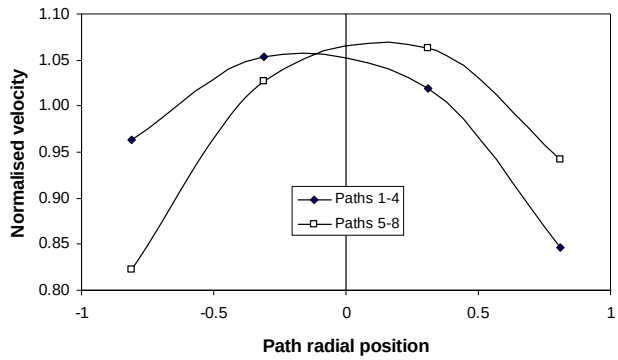

Figure 20 Path velocity information confirming the presence of swirl

The most important thing to note about this data is that despite the biases that are present in the results from each plane, the combined 8-path results shown in Figure 19(c) were within 0.1% of the Coriolis meter. This illustrates the benefits of the 8-path meter configuration with overlapping crossed paths at each chordal location. Similar performance can not be achieved with single-tilted-plane, or staggered criss-crossed path arrangements unless swirl-removing flow conditioners are used.

4.4 Final Meter Selection

The project team responsible for the trials at Kenai were satisfied with the flow measurement performance of the Caldon ultrasonic meter and the Coriolis meters. However, other factors proved to be important in the final selection.

Ensuring minimum pressure drop was the biggest factor in the final meter selection. The importance of this issue was increased further by the project requirement for check metering. Two Coriolis meters in series would have created too much pressure drop. On the other hand the Caldon 280C is non-intrusive. It also has two 4-path planes that operate independently and can be used in a duty and check arrangement. Furthermore, the 8-path, dual electronics design makes the meter extremely fault tolerant.

On this basis the Caldon meter was selected for the Qatar Common LNG Project, and has continued to be used in service at Kenai since the end of 2005.

5 SUMMARY AND CONCLUSIONS

A Caldon ultrasonic meter and two makes of Coriolis meter were evaluated by a joint venture project team in field trials at Kenai in Alaska. All three meters tested were found to have acceptable flow measurement performance for the final application. However, the Caldon ultrasonic meter was selected as it had much lower pressure drop than the Coriolis meters, particularly if two Coriolis meters were to be used in series to provide check metering. The built-in redundancy and diagnostic capabilities of the Caldon 8-path meter also featured in the decision.

The Caldon meter uses transducers that are housed behind a stainless steel pressure boundary in the meter body. It has been demonstrated, both in the lab and in field trials, that this design is suitable for robust and accurate measurement of cryogenic liquids. This includes the large temperature cycles that the meter will experience whenever the line is warmed up or cooled down.

The configuration of the Caldon 280C is such that there are two sets of fully redundant electronics, each operating a different 'plane' of four measurement paths. This results in a compact metering installation that can be used in a duty and check arrangement and is extremely fault tolerant.

The particular arrangement of paths used in the Caldon 8-path meter makes the meter very insensitive to velocity profile changes and swirl. As a result, this meter design can easily transfer its calibration from the lab to the field, without use of a flow conditioner, and still achieve better than +/- 0.22% uncertainty. As such this technology is suitable for allocation measurement and also has the potential to be used for tanker loading.

REFERENCES

[1] The Parliamentary Office of Science and Technology (2004) *The Future of UK Gas Supplies*, Postnote no. 230.

[2] Mullally, M, Stobie, G J, and Salavudheen, K H (2007) "In-line measurement of LNG for fiscal allocation", *15th International Conference & Exhibition on Liquified Natural Gas*, Poster #56 Handout, Barcelona, Spain, April 2007

[3] van Wijngaarden, H and van der Grinten, J G M (2006) *Evaluation of the Caldon scaling methodology to convert water calibrations of an ultrasonic meter, type LEFM, into an LNG meter curve*, NMi Report No. C-SP/606627-HvW/Rap

[4] Zagarola, M V and Smits, A J (1998) *Mean flow scaling of turbulent pipe flow*, J. Fluid Mech, 373, 33 - 79.

[5] McKeon, B J, Li, J, Jiang, W, Morrison, J F and Smits, A J (2004) *Further observations on the mean velocity in fully-developed pipe flow*, J. Fluid Mech. 501, 135 - 147.

[6] Brown, G J, Barton, N A, and Moore, P I (1999) "Installation effects on ultrasonic flowmeters", *Proceedings of the North Sea Flow Measurement Workshop*, Oslo, Norway, 25-28 October 1999.

[7] Moore, P I, Brown, G J and Stimpson, B P (2000) "Ultrasonic transit-time flowmeters modelled with theoretical velocity profiles: methodology", *Measurement Science and Technology*, Vol. 11, No. 12, pp 1802-1811.

[8] Brown, G J (1997) "Factors Affecting the Performance of Ultrasonic Flowmeters". *Proceedings of the North Sea Flow Measurement Workshop*, Kristiansand, Norway, 27 – 30 October 1997, Paper 33.

[9] Zanker, K J (1999) "The effects of Reynolds number, wall roughness, and profile asymmetry on single and multipath ultrasonic meters", *Proceedings of the North Sea Flow Measurement Workshop*, Oslo, Norway, October 1999, pp. 117-129.

[10] Brown, G J, Augenstein, D R and Cousins, T (2006) *The relative merits of ultrasonic meters employing between two and eight paths* Proceedings of the 5th South East Asia Hydrocarbon Flow Measurement Workshop, Kuala Lumpur, Malaysia.

[11] Halsey, D M (1987) *Flowmeters in swirling flows, J*. Phys. E: Sci. Instrum., 20, pp1036 – 1040.

[12] Hilgenstock, A and Heinz, M (1996) "Numerical flow simulation as a tool for developing and calibrating ultrasonic flowmeters", *Proceedings of FLOMEKO '96*, October 20-24, Beijing, China, pp. 156-161. 67.

[13] Duffell, C J, Brown, G J, Barton, N A and Stimpson, B P (2003) "A new family of ultrasonic flowmeters, with improved performance in asymmetric flows, produced by using optimization algorithms and CFD" *Proceedings of the International Conference on Hydrocarbon Flow Measurement*, Fluid Control Research Institute, Palakkad, India, September 2003.

[14] Brown, G J, Coull, C, and Barton, N A (2005) "Installation effect on ultrasonic flowmeters and evaluation of computational fluid dynamics prediction methods" *Proceedings of the South East Asia Hydrocarbon Flow Measurement Workshop*, 9 – 11 March 2005, Kuala Lumpur, Malaysia.

APPENDIX – VELOCITY PROFILE CONTOUR PLOTS

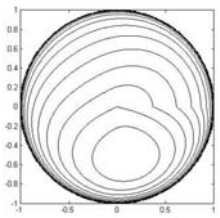

1

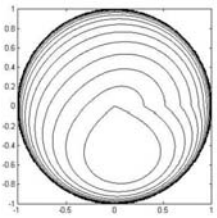

2

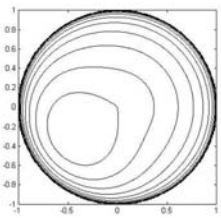

3

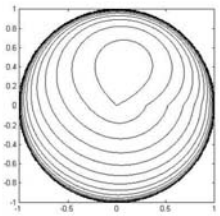

4

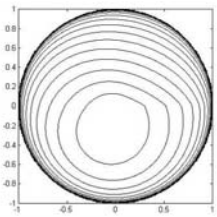

5

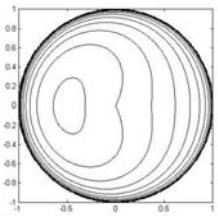

6

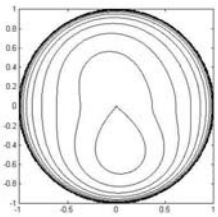

7

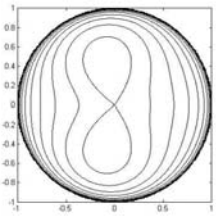

8

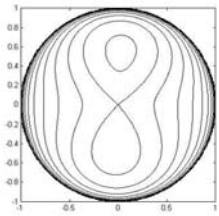

9

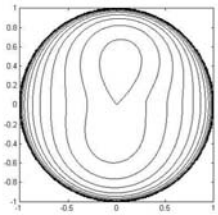

10

An Ultrasonic Flowmeter for Custody Transfer Measurement of LNG: A Challenge for Design and Calibration

Jankees Hogendoorn, André Boer and Helen Danen

KROHNE Altometer, The Netherlands.

---

1. INTRODUCTION

For the transport of natural gas, liquefying gas is becoming popular compared to for example transporting gas over large distance pipelines. Transport of gas is receiving much attention worldwide as for example gas is increasingly being found in remote areas and importing countries are looking for ways to diversify the resources of their gas supplies. Another trend is the increasing number of parties involved in the LNG market place. In addition, the costs of the liquefaction and re-gasification of gas and the transport of LNG are decreasing. An increase in the trade of LNG also means an increase in the custody transfer and fiscal metering points for gas in cryogenic conditions. Tank gauging has been a popular measurement method for LNG, but it has its limitations and increased demand for very accurate flow measurements can be observed.

For more than 20 years ultrasonic flowmeters have been used for the fiscal measurement of gas and for more than 10 years for the fiscal metering of liquid hydrocarbons [1],[2],[8],[9],[10]. Over the past years, much experience has been gained with hundreds of custody transfer ultrasonic flowmeters operating in the field. The application of highly accurate ultrasonic flowmeters have been very successful and can be considered as a proven technology in this field [3].
Next to successful applications at 'normal' operating conditions, the ultrasonic measurement principle in itself is also very suitable for high accuracy flow measurement at cryogenic conditions. The development, construction and calibration of an ultrasonic flowmeter for custody transfer of LNG is, however, not simple taking into account the very low temperatures and the limitations regarding the calibration under reference conditions.

This paper describes the development of an ultrasonic flowmeter for the fiscal measurement of LNG. The following items are discussed:

- Transducer design
- Flowmeter body design
- Calibration concept
- Tests results on liquefied nitrogen

This paper finishes with some conclusions and a discussion the steps to be taken in the next future.

2. TRANSDUCER DESIGN

2.1. Tests with piezo crystals at low temperatures

The behaviour of acoustic piezo crystals is one of the areas that have to be investigated for use of ultrasonic flowmeters at cryogenic conditions. The acoustic piezos form the basis of any ultrasonic flowmeter measurement. They generate the acoustic waves, which are sent up and

down the flow. The difference in transit times is directly proportional to the flow. When the piezos do not perform well, the ultrasonic flow measurement will suffer from it.

The investigation has been focussed on researching the electric, acoustic and mechanic properties of piezo ceramic material at cryogenic conditions [4].
As a first step we were interested in the performance of just the piezo i.e. in a situation whereby the piezo forms no part of the transducer construction. The behaviour of the piezo might be affected, when it is part of the transducer construction.
The construction that has been build for this test consists of a frame with two free positioned piezos in the middle (see Figure 1).

Figure 1 Set up for piezo tests at liquefied nitrogen (-196 [ºC]).
Left hand figure: Frame with piezo crystals hanging above the container with liquefied nitrogen.
Right hand figure: frame with piezo crystals submerged in the container with nitrogen.

In order to create a reference situation with respect to electric and acoustic properties, the construction first has been submerged in water at ambient conditions, and afterwards the same construction in liquefied Nitrogen at a temperature of -196 [ºC]. The electric and acoustic properties have been measured again.

It turns out that the electric impedance reduces with approximately 8 [dB] when compared to water at a temperature of 20 [ºC]. In addition, the acoustic bandwidth slightly decreases. This can be observed from **Fout! Verwijzingsbron niet gevonden.**. The effect is, however, not significant.

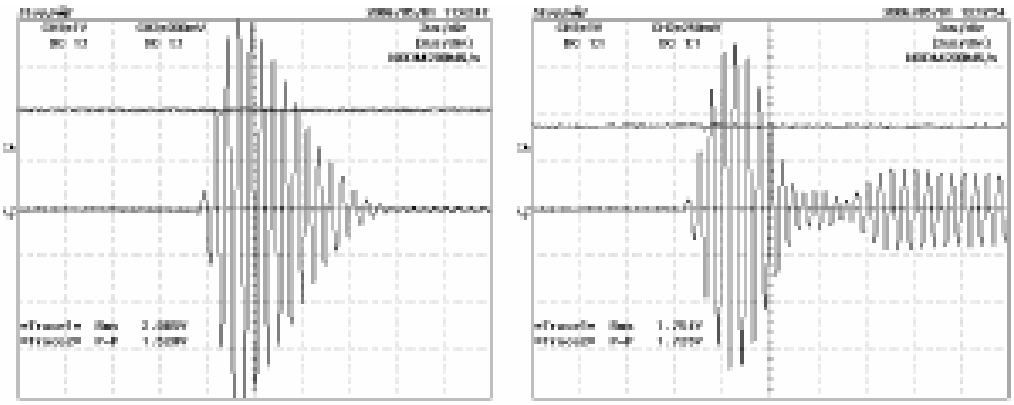

Figure 2 Acoustic signals of the piezo ceramic material.
Left figure: water at 20 [ºC],Right hand figure: liquefied nitrogen at -196 [ºC].

The same holds for the efficiency of the output signal. It turns out that thermo shocks can be handled without any problem. No damage to the construction, nor a reduced performance has been observed, when submerging the construction into the liquefied nitrogen several times.

With respect to the use of piezo ceramic material the conclusion can be drawn that it is suitable for cryogenic application down to temperatures of -196 [ºC].

2.2 Transducer performance at cryogenic conditions

The next step in our investigation concerned measurements whereby the piezo element forms part of a transducer construction. Several items have to be taken into consideration, of which the acoustical coupling between the piezo and the acoustic window is the most critical one (see Figure 3).

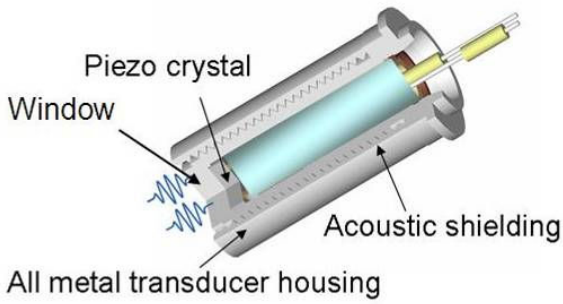

Figure 3 Basic design of an acoustic transducer

As soon as the acoustical contact between the piezo crystal and the acoustic window is lost, the transducer no longer functions. Therefore, it is important to have a reliable acoustical contact between piezo and window, even if considerable geometrical changes occur due to thermal expansion as a result of large temperature spans.

For most applications a standard coupling grease can be used to establish an efficient acoustical coupling between piezo and (sensor housing) window. However, for temperatures below e.g. -70 [ºC] normal coupling grease cannot be used. The grease becomes solid and its volume decreases as a result of shrinkage due to solidification. Consequently, the mechanical contact is lost and the acoustic signal disappears. For this reason a special cryogenic grease has been tested. According to its specifications it can be used for temperatures down to -200 [ºC]. This grease should have less shrinkage due to solidification.

A special test object has been built, consisting of two transducers with a wave guide in between to test the effect of low temperatures on the flowmeter (see Figure 4). The wave guide has been very useful for purposes of simulating the liquid in these tests and was not intended for precise flow measurements. It was also decided not to use the wave guide construction for the final design of the flow meter body. Reason for this is that the wave guide construction introduces an additional uncertainty in the transit time measurement. The transit time of the acoustic wave is affected by the speed of sound in the wave guide. The speed of sound varies with temperature changes. The temperature of the wave guide is not known accurately. This leads to an additional error in the transit time measurement and thus in the flow measurement. For this reason the wave guide has been left out and the wetted transducer design has been applied for the final design.

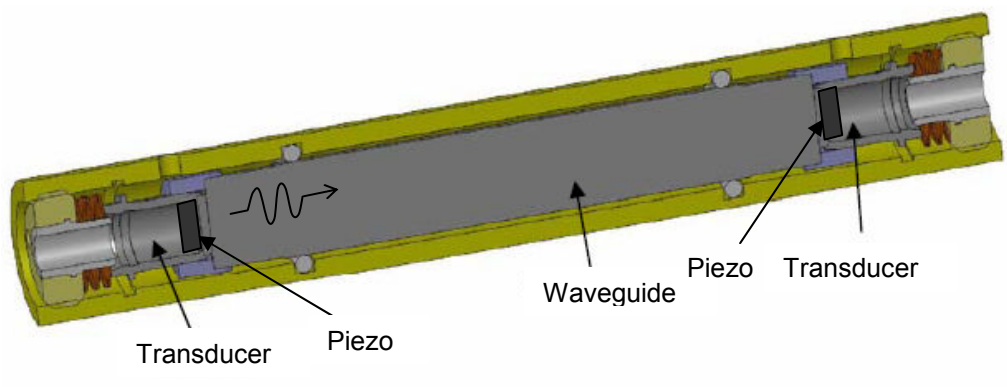

Figure 4 Test set up with two transducers at both ends and a waveguide in between simulating the liquid.

To test the acoustic contact, measurements have been carried out whereby the performance of the transducer construction has been studied over the entire temperature span. This test object has been installed in a refrigerator, which can be slowly cooled down to a temperature of -196 [ºC] (see left hand figure in Figure 5).

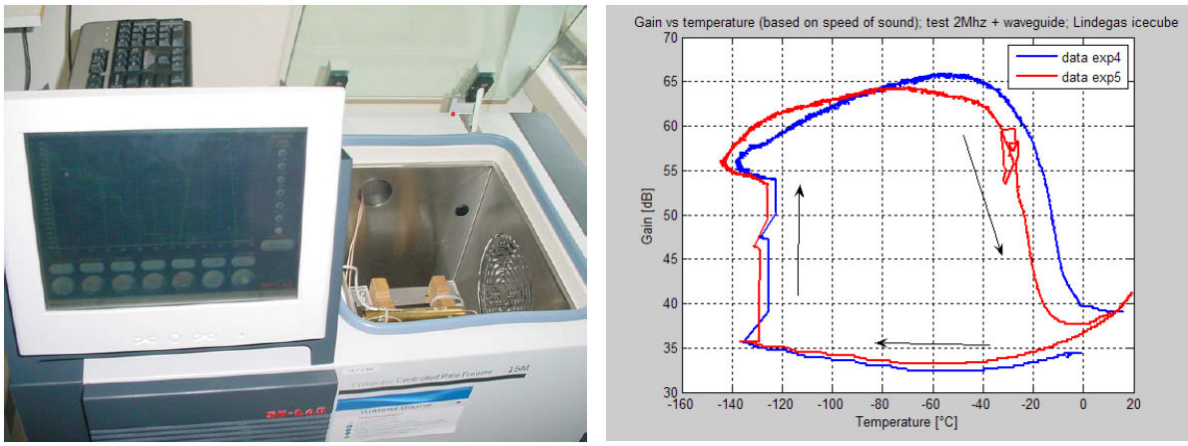

Figure 5 Left hand figure: Test set-up with test object in the refrigerator.
Right hand figure: Amplification factor (Gain) as function of temperature .

During the test, the electronic amplification factor (gain) of the signal has been monitored on-line. The gain is the amplification factor required to obtain a signal with a fixed amplitude. The test results are shown in the right hand figure (Figure 5).

The experiments started at the lower right hand corner of the graph with a temperature of about 0 [ºC] and a gain of ~35 [dB] (see the blue curve). The temperature in the refrigerator has been slowly decreased. Figure 5 shows that down to temperatures of approximately -130 [ºC] the gain stays more or less constant.
From this point a sudden increase in the gain up to a value of about 55 [dB] has been observed. It means that the signal is attenuated roughly with a factor 10. Increasing the temperature does not help. The gain has even increased up to a value of about 65 [dB] at temperatures of approximately -50 [ºC]. From that point the gain strongly dropped again until it reached more or less its original value of about 35-40 [dB] at temperatures between 0 and 20 [ºC]. Repeating the same test (see the red curve), resulted in a curve which reproduced fairly well.

The most likely explanation for the strong increase in attenuation at -130 [ºC] are small cavities that occur in the coupling grease as a result of the solidification of the grease. Solidification causes a decrease in volume of the grease, while at the same time the volume in between the

piezo crystal and the window, which is filled up by the grease, stays more or less constant. This leads to very small cavities in the grease. Which in its turn result in a strong additional acoustical attenuation. Consequently, the transducer gives a significantly weaker output signal.

This experiment has clearly demonstrated that the special cryogenic grease is not the right answer for applications with very low temperatures. Other methods are is required to guarantee a reliable acoustical coupling.

A solution has been found in the choice of another coupling technique. A thorough investigation has lead to a special design consisting of a combination of an acoustic coupling and a reliable transducer construction. To this extend the Finite Element Method has been used to simulate the mechanical properties into details. The patent for this solution is pending.

For the final design of the transducer construction we have been successful in maintaining an almost identical construction for cryogenic applications as for the standard construction. The advantage of using a standard construction is that it is well proven and reliable. The standard construction has already been used in thousands and thousands of applications with other ultrasonic flowmeters.

The final transducer construction has been tested according to the very similar test procedures as described above. In addition, tests have been carried out whereby the entire transducer construction was submerged instantaneously in liquefied nitrogen in order to realize a thermo shock (see Figure 6).

Figure 6 Test object with final transducer construction, submerged in liquefied Nitrogen at -196 [ºC].

During the submersion the acoustic signal has been monitored continuously. It turned out that even during the thermo shock the transducer kept on working. An example of the acoustic signals can be found in Figure 7.

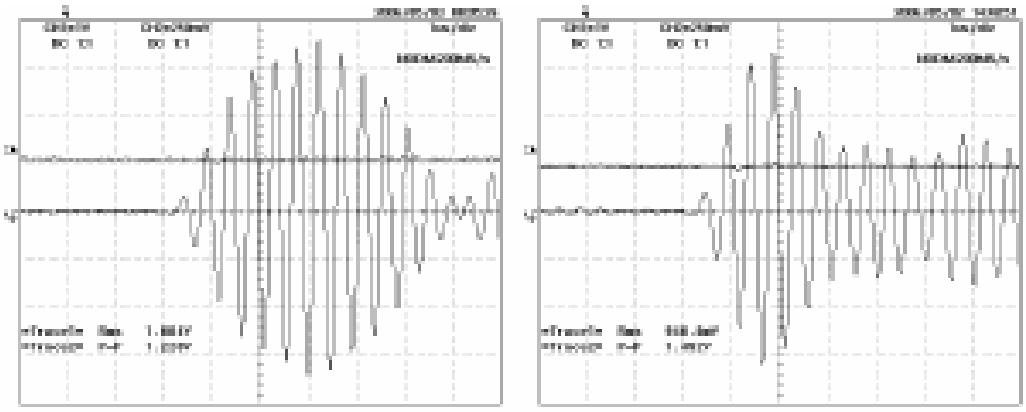

Figure 7 Acoustical signals with final transducer construction.
Left hand figure: signal in water at 20 [ºC].
Right hand figure: signal in liquefied Nitrogen at -196 [ºC].

The final additional attenuation obtained in liquefied nitrogen is about 6 [dB]. This is caused by the reduced electric capacitance of the acoustic piezo at -196 [ºC]. The signal shape is very well suited for a reliable signal detection required for a reliable flow measurement.

3. FLOWMETER DESIGN AND STATIC TESTS

The underlying concept for the development of the LNG flowmeter body design, was to keep it as close as possible to the standard design of a five beam ultrasonic flowmeter. The proven meter body design hardly needed any construction changes for the special cryogenic transducers as described in the previous chapter (see Figure 8).

Next to the special cryogenic transducers, another change in construction is the placement of an additional cap at the back side of the transducer, required to prevent the formation of ice on the inside of the transducer. Ice formation occurs due to water vapour in the air which freezes onto cold surfaces. In a worse case scenario, it might lead to malfunctioning of the transducers. A cap, closing off transducers completely, prevent ice formation inside the transducer.

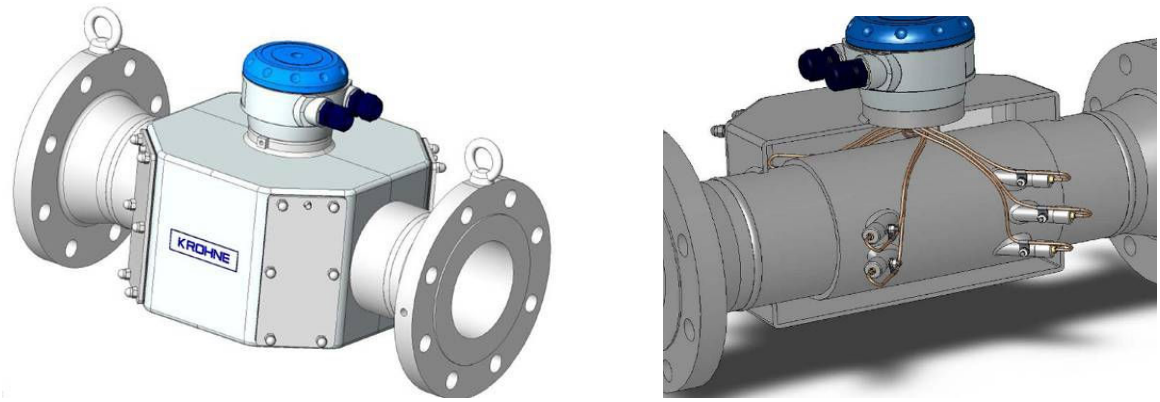

Figure 8 Five beam Ultrasonic flowmeter design for cryogenic applications (e.g. liquefied N_2 or LNG). Left hand figure: Exterior of the ALTOSONIC V. Right hand figure: housing partly removed.

The LNG flowmeter design has been used to carry out the next series of tests. These comprised of static tests whereby the flowmeter has been filled with liquefied nitrogen (see Figure 9). The results were very satisfying, as the flow meter design met all the pre-established requirements formulated by the development team. A strong acoustic signal has been obtained, as well as a

large acoustic bandwidth and a good signal-to-noise ratio. During cooling-down the flowmeter kept on working. Thermal cycles turned out to have no affect on the flowmeter at all.

Figure 9 Static flowmeter tests on liquefied Nitrogen. Left hand figure: set up. Right hand figure: Flowmeter filled with Nitrogen.

All tests demonstrated that the design of transducers and flowmeter body have been working according expectations regarding accuracy, stability and reliability.
The next phase in the development project concerned a full scale test after calibrating the flowmeter prototype on water.

4. CALIBRATION CONCEPT

There are two challenges regarding the calibration of any type of flowmeter for use in cryogenic applications. So far, there are no (laboratory) test facilities in the world where flowmeters, with a diameter larger than 4 inch, can be tested on LNG or on liquefied nitrogen against a reliable reference. And, secondly, in most applications it is not possible to calibrate flowmeters on site against a reliable reference.

This asked for the development of an alternative calibration method. In close cooperation with NMi, the Dutch Board of Weight and Measurement, a special calibration procedure has been developed for calibrating ultrasonic flowmeters for use of custody transfer of LNG.

A solution has been found in calibrating ultrasonic flowmeters with water at reference conditions and to use the water calibration as a basis for the application of the flowmeter at cryogenic conditions. Basically it is based on the concept of transferring a calibration at ambient conditions to an application at cryogenic conditions. The transfer or extrapolation of the flowmeter reading with a water calibration at ambient conditions to a reading at cryogenic conditions is, however, fairly complicated.

For a correct extrapolation the following phenomena have to be taken into account:

- Demonstrate that the flowmeter linearity is a function of Reynolds only
- Linearity curve gets horizontal at high Reynolds numbers
- Thermal expansion of the meter body
- Delay times

4.1 Linearity curve based on Reynolds calibration

Over a period of more than 10 years KROHNE has gained much experience and test data in the field of calibrating (five beam) ultrasonic flowmeters for fiscal metering and transferring the calibration results to other application areas.
A key advantage KROHNE has, is the large amount of experience gained in the field of calibration with the in house availability of certified and accredited facilities for the calibration of flowmeters on water. The calibration facilities operate by direct comparison and are traceable to

National Standards. Flowmeters of any size up to a diameter of 3.2 [m] can be calibrated at a large calibration tower. The best measurement capability (BMC), as certified by RvA, the Dutch Council for Accreditation, is 0,02% (k=1) over a flow range of 18 to 18.000 m3/hr.

Even at low flow rates the calibration rig allows for stable, accurate and reliable measurements. Developments in stable electronics enable high repeatabilities up to very low flow rates (for example 0,1 % accuracy down to 0,1 m/s) including for flowmeters with very small diameters.

Figure 10 Fisheye picture of the water calibration facility at KROHNE Altometer, The Netherlands. Maximum flow rate 3.10^4 [m^3/h], max. diameter 3.2 [m]

The above mentioned capabilities allow us to calibrate with water at low flow velocities for reaching low Reynolds numbers and applications can be simulated with higher viscous liquids at typical flow rate velocities in the field.

The Reynolds number is a function of the mean flow velocity (v), the internal pipe diameter (D), and the kinematic viscosity (ν):

$$Re = (v \times D) / \nu$$

This can be illustrated with a simple example. The Reynolds number with a

- a viscosity of 1 cSt, a diameter of 0,4 meter and a flow velocity of 10 m/s, is is $(0,4 \times 10) / (1 \times 10\text{-}6) = 4 \times 10^6$
- a viscosity of 0,2 cSt, a diameter of 0,4 meter and a flow velocity of 2 m/s, is $(0.4 \times 2) / (0.2 \times 10\text{-}6) = 4 \times 10^6$

This enables us to simulate low Reynolds numbers with the calibration of ultrasonic flowmeters on water (with a viscosity of 1 cSt), with a high accuracy and repeatability while calibration with other hydrocarbons are no longer required. The results of flowmeters calibrated on water can be transferred to other different types of mediums as long as they are in the same Reynolds number area.

See for example the calibration results in figure 11 whereby the same fiscal ultrasonic flowmeter has been tested on water and on naphtha. The flowmeter shows the same linearity curve with water as with naphtha.

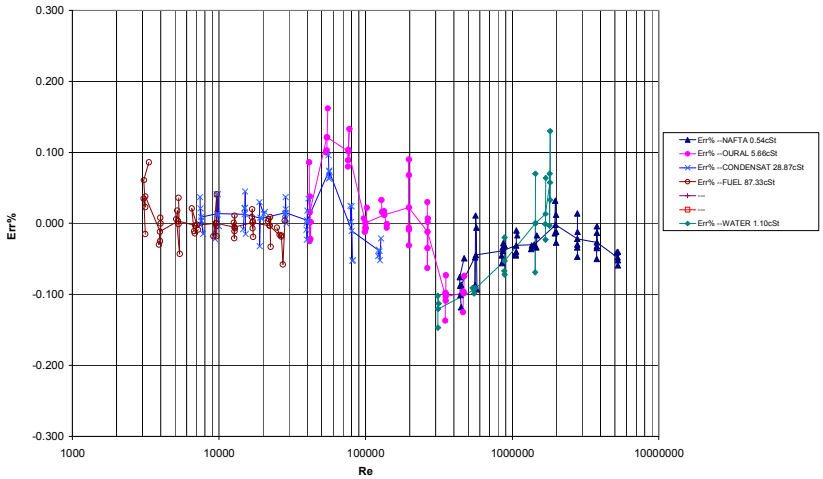

Figure 11: Linearization curves, expressed in Reynolds numbers, of the same five beam ultrasonic flowmeter tested on water, naphtha, oural, condensate and fuel oil.

LNG has a lower viscosity (approximately 0,2 cSt) than water and as a result an ultrasonic flowmeter used for LNG will be operating at higher Reynolds numbers. To transfer the calibration results from water to LNG, it will be necessary to extrapolate the linearity curve.

Based on our experience we know that for the five beam ultrasonic flowmeter the shape of linearity curves becomes more horizontal at higher Reynolds numbers. The physical explanation for this effect is that the shape of the velocity profile does not change much at larger Reynolds numbers.

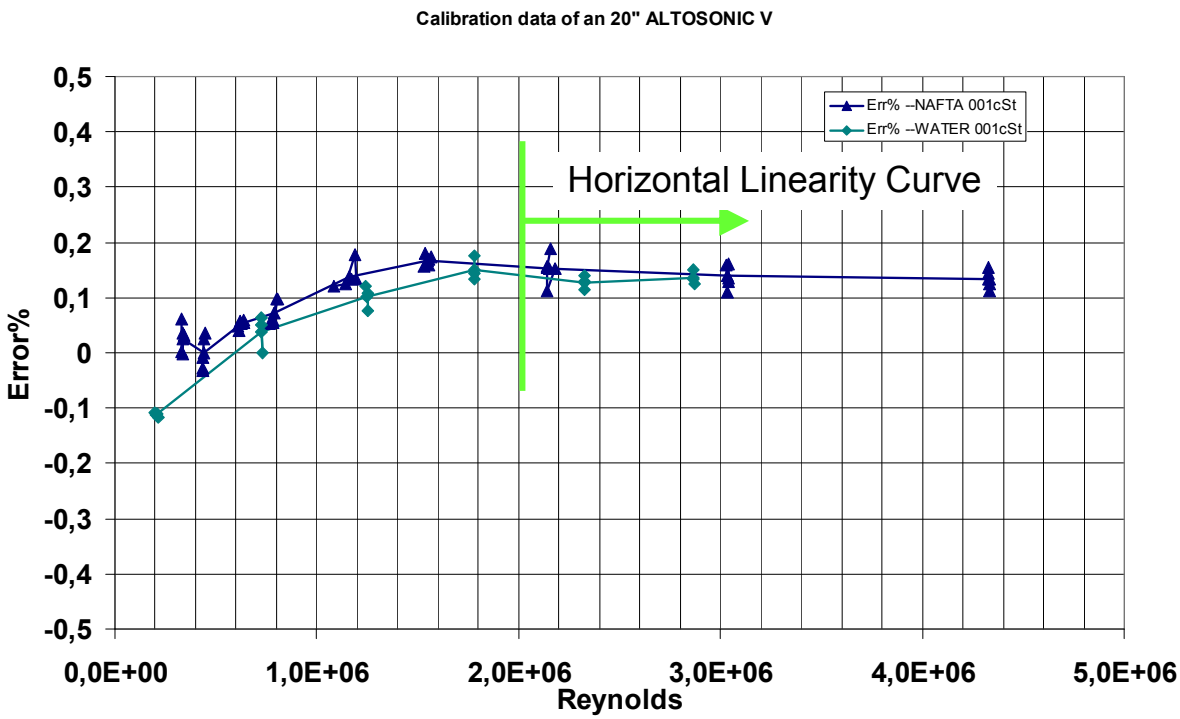

Figure 12: Calibration data of a 20" Five beam ultrasonic flowmeter for custody transfer calibrated on water and on naphtha. The linearity curve has a more horizontal shape at higher at higher Reynolds numbers

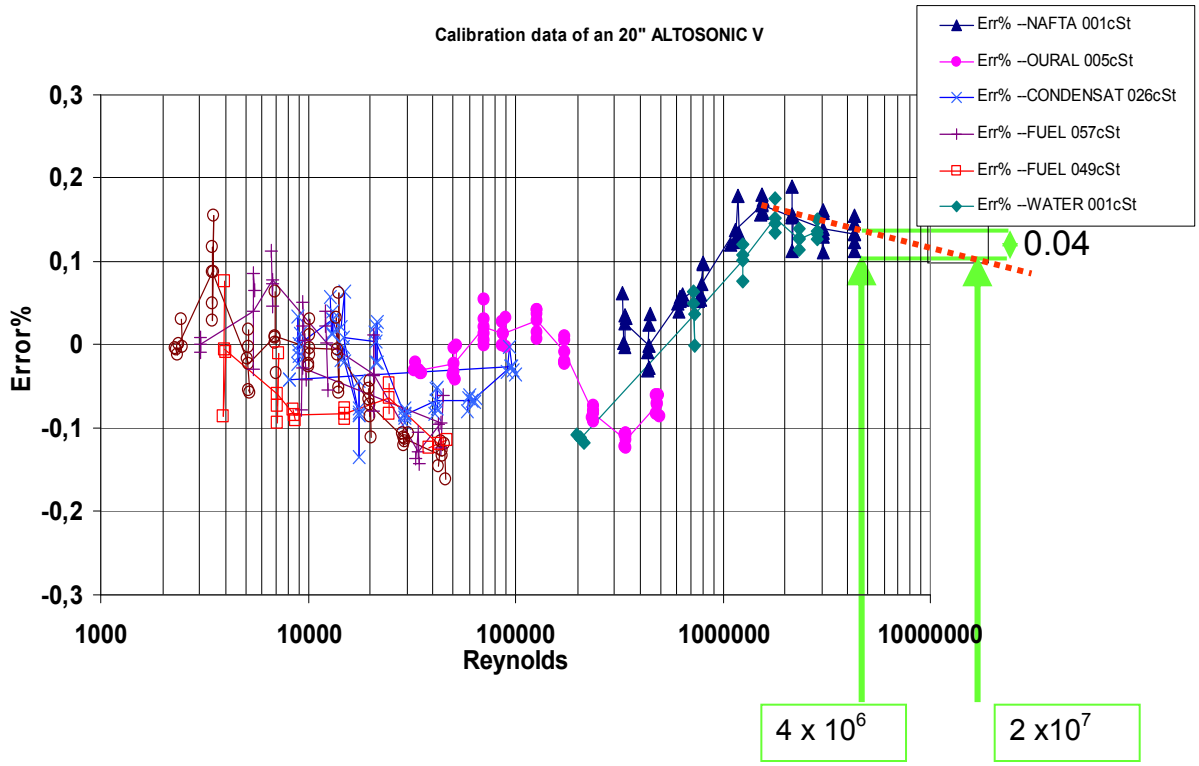

Figure 13: Calibration data of a 20" ultrasonic flowmeter for custody transfer calibrated on water and on naphtha

With water the high Reynolds numbers as required for LNG, cannot be reached to the full extend and therefore we need to add a relatively small extrapolation. This is the reason why the horizontal shape of the linearity curve with higher Reynolds numbers is of such importance. In order to make an estimation of the behaviour at higher Reynolds numbers, the linearity can be expressed as a logarithmic scale (see figure 13).
The calibration results, as shown in figure 13, illustrate that with higher Reynolds numbers the extrapolation even becomes more reliable.

See the following example:

- A ratio of [2 x 10^7 / 4 x 10^6] is a factor 5 (factor of 5 extrapolation in Reynolds numbers).
- The estimated error in this example is 0.04%.

The Dutch Board of Weight and Measures is, however, rather pre-cautionary and advises to use an additional uncertainty of 0,1% when extrapolating with a factor 1.7, and an additional uncertainty of 0,2% when extrapolating with a factor 2.2.

4.2 Thermal expansion of the meter body

There is one other key aspect that needs to be taken into consideration when measuring at very low temperatures. The geometric sizes of a flowmeter change, because of the large temperature changes.
For calculating the average flow velocity over a pipe section, the pipe diameter is assumed to be constant, but in case of very low temperatures the pipe diameter will change.

Flow = A (Area) x V (Flow velocity)

$$= [\pi D^3] / [4 \sin(2\beta)] * [(T_{B \rightarrow A}) - (T_{A \rightarrow B})] / [(T_{B \rightarrow A}) * (T_{A \rightarrow B})]$$

Whereby	D	=	Diameter [m]
	β	=	Angle of diameter with average flow velocity [º]
	$T_{B \rightarrow A}$	=	Upstream transit time from transducer B to A [s]
	$T_{A \rightarrow B}$	=	Downstream transit time from transducer A to B [s]

In other words the pipe diameter under calibration conditions does not equal to the pipe diameter under operating conditions. Compensation for this will be necessary. Question is how to correct for the diameter at the very low temperature conditions.

$$D_{oper} = D_{cal} * (1 + \alpha \Delta T)$$

whereby
α = Linear expansion coefficient of pipe wall material [K^{-1}]
ΔT = Temperature difference between operating and calibration conditions [K]

Using the meter factor (MF) as a function of D^3 gives:

$$MF_{oper} = MF_{cal} * (1 + 3 \alpha \Delta T)$$

whereby
$MF_{oper} < MF_{cal}$ at cryogenic conditions

Let us look at the following practical example for LNG:

- In case of a calibration at 20^0[C] and operation at - 160^0[C] (-256^0 [F])
- α = 12 ppm; ΔT = - 180^0[C] (-324^0 [F])
- $\alpha \Delta T$ = -2.16 e-3 = -0.216%

This gives a change in meter factor of (3 * $\alpha \Delta T$) of -0,648%. In other words the operating meter factor is 0,648% smaller than the calibrated meter factor.

Based on the above theoretical calculation example it is clear that a correction for the meter factor is required for receiving accurate performance data.

In addition the following requirements are necessary for an accurate calculation:

- Mechanical behaviour of the flowmeter must correspond with the expansion formula
- Reproducible behaviour of the flowmeter
- Linear expansion coefficient of pipe wall material must correspond with the specifications of the construction material

Together with for example PTB extensive and very accurate measurements with a three beam ultrasonic flowmeter have been done to experimentally verify the above mentioned calculated results. Similar tests have been done with the five beam meter, showing the same results.

The following figures show the:

1. Uncorrected results
2. Test results corrected for thermal expansion 3 $\alpha \Delta T$
3. Test results corrected for thermal expansion plotted as a function of the Reynolds number
4. Linearized test results corrected for thermal expansion plotted as a function of the Reynolds number

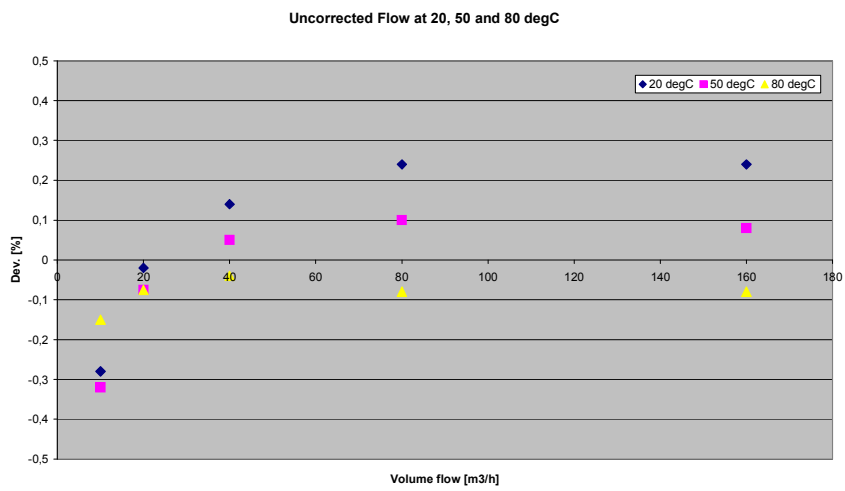

Figure 14 Uncorrected results

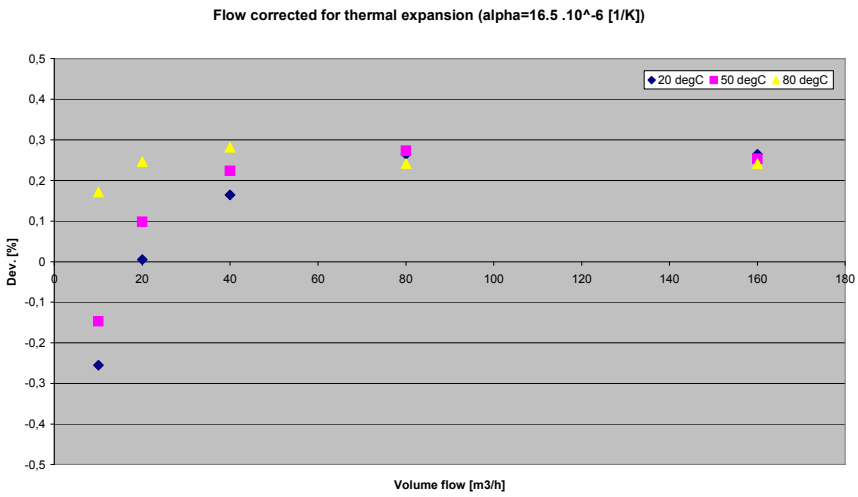

Figure 15 Test results corrected for thermal expansion 3 α ΔT

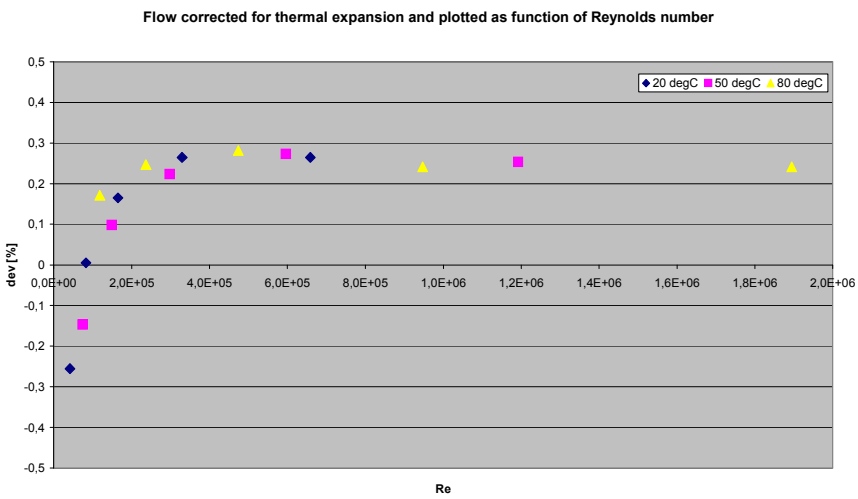

Figure 16 Test results corrected for thermal expansion plotted as a function of the Reynolds number

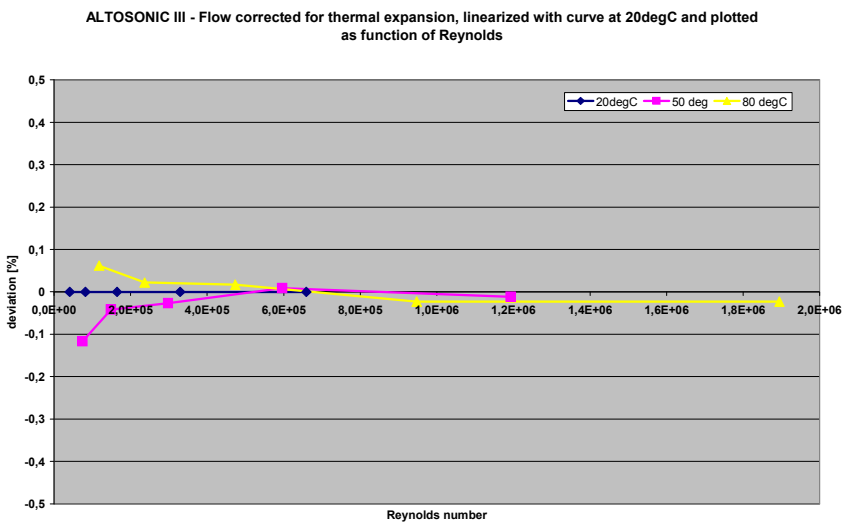

Figure 17 Linearized test results corrected for thermal expansion plotted as a function of the Reynolds number

Based on the above and other test results, the LNG project team decided that the formula (*3 α ΔT*) very well describes the effect of thermal expansion, and more importantly can be used for a reliable correction for the thermal expansion of the five beam ultrasonic flow meter body.

5. TESTS ON LIQUEFIED NITROGEN

Having developed a LNG ultrasonic flowmeter design in combination with the described calibration concept, the next step in the investigation has been to perform tests on liquefied nitrogen. NMi was invited to witness the tests.

5.1 Tests Done at the National Institute of Standards and Technology (NIST)

A flow calibration facility where it is possible to perform tests on cryogenic liquids is located at the National Institute of Standards and Technology (NIST) in Boulder, Colorado [6].
A dynamic weighing system is used to measure totalized mass flow and, with the use of NIST thermodynamic property data for density, volumetric flow. Calibrations are typically performed with liquid nitrogen in a flow range of 0.95 to 9.5 [kg/s], pressure range of 0.4 to 0.76 [MPa], and temperature range of 80 to 90 [K].

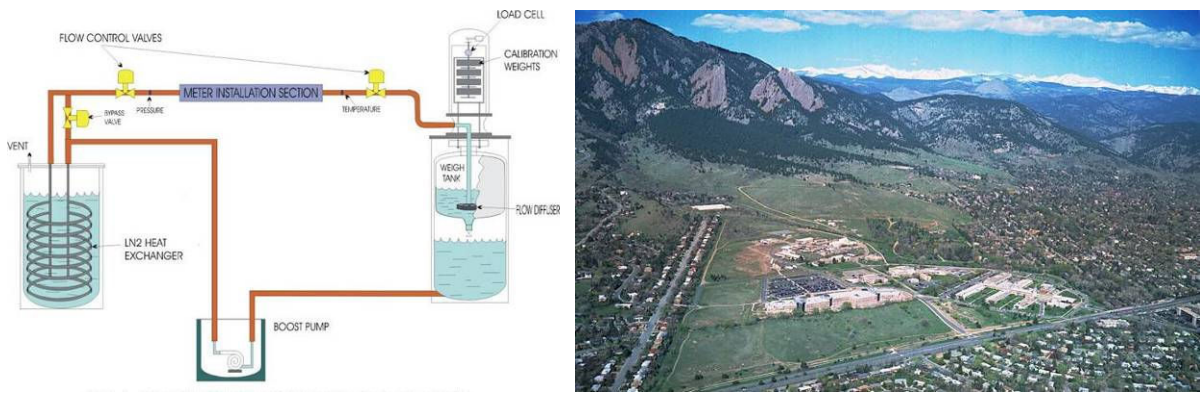

Figure 18 Left hand figure: Schematic overview of Calibration facility for Liquefied Nitrogen at NIST in Boulder. Right hand figure: NIST Location in Boulder, USA.

A schematic of the liquid flow facility is shown in figure 18. Liquid nitrogen is circulated throughout the closed loop by a variable-speed centrifugal pump. The liquid flows through the sub-cooler, a heat exchanger consisting of a finned tube submerged in a nitrogen bath where the thermal

energy due to pumping and ambient heat leak is removed. The temperature of the liquid nitrogen in the flow loop can be changed or controlled by adjusting the liquid level and the vapor pressure in the sub-cooler tank. Some of the test fluid also can be diverted around the subcooler, if necessary. After leaving the subcooler and bypass, the fluid passes through a vacuum-jacketed loop containing an in-line heater, through the test section, and into the weigh tank/catch tank system (described below) which represents the heart of the measurement system. The liquid flows into the bottom of the weigh tank through a pipe and diffuser. The diffuser removes the vertical component of the flow. The liquid then flows through the weigh tank valve and into the catch tank, and is drawn back into the circulation pump.The flow system is pressurized with helium gas to prevent the liquid nitrogen from boiling. The nitrogen is always subcooled by 10 to 15 [K].

The facility has an overall uncertainty of 0.17% (k=2) on totalized mass. The overall uncertainty for totalized volume flow is 0.18% (k=2). This uncertainty statement holds for flow rates in the range from 4.5 to 45 [m^3/h].

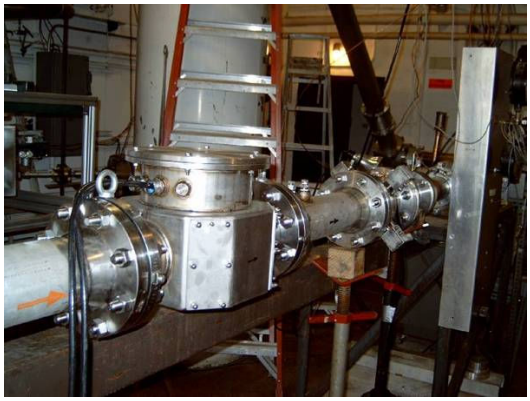

Figure 19 ALTOSONIC V on the calibration facility for liquefied Nitrogen at NIST.

The NIST test facility has been used to evaluate the five beam ultrasonic flowmeter on its sensitivity to pressure, temperature, flow rate and thermal cycling. The average temperature during the test was about 80 [K], the average pressure about 0.34 [MPa]. In addition, the repeatability, reproducibility and stability of the meter have been tested.

The flowmeter has been tested at several flow rates: 4.7, 12.6, 20.9, 29.2, 37.1 and 45.4 [m^3/h]. Single data points were taken at each of the individual flow rates mentioned, the next series of points was taken, followed by a third set of data. This provided three data points at each of the flow rates to be observed. There were also data points taken using small liquid nitrogen mass amounts to observe the meter performance with small sampling.

5.2 Test Results

- **Sensitivity to pressure and temperature**
  No sensitivity to pressure and temperature has been observed. The same holds for the effect of thermal cycling. The meter is still reproducing within the repeatability band after several thermal cycles.

- **Linearity**
  The linearity was well within expectations. The uncorrected linearity was considerably smaller than ±0.20% of M.V.. This corresponds to the experience with other applications at high Reynolds numbers. Since the Reynolds numbers are fairly high (due to low viscosity), a good linearity can be expected.

- **Repeatability and stability**
  The repeatability results have been very satisfactory. Despite the fact that the individual

calibration points have not been collected immediately after each other (a complete flow rate cycle has been run in between), a repeatability of ±0.07% has been obtained in the normal flow range. Even at very low flow rates (1.5% of F.S.) a very good and stable performance has been observed.

All results have been reported in a test report from NIST [7]).

6. NMi UNCERTAINTY STATEMENT

The test results described in chapter 4 and 5 have been used to further ground the calibration concept for ultrasonic flowmeters at cryogenic applications. NMi ('Netherlands Measurement Institute') has performed an overall uncertainty analysis for the 5 beam ultrasonic flowmeter for LNG, which resulted in an uncertainty of 0.26% to 0.33%, dependent on the range of application [5]).

Based on the analysis, NMi has released a written uncertainty statement (see figure 20). This uncertainty holds for the situation of a flowmeter calibration on water at ambient conditions and application on LNG at -163 [ºC].

Nederlands Meetinstituut

C-SP-06-WV-0178
Page 1 of 3

Date
23 June 2006

Your reference
Meeting 2 June '06

Our reference
C-SP-06-WV-0178

Subject
Estimated uncertainty Ultrasonic LNG Volume Measurement

Krohne Altometer
Attn. Mr. Jankees Hogendoorn
Kerkeplaat 12
3313 LC Dordrecht
The Netherlands

Dear Mr. Hogendoorn,

With reference to the meeting mentioned above, please allow me to inform you that we have carried out a preliminary study on the estimated measurement uncertainty in Volume Measurement of your ALTOSONIC V Ultrasonic flowmeter on LNG.
This preliminary study was based on:

- the test results presented by you
- our experience with the Altosonic V
- our experience with the Altosonic V on other media

Please note that in the absence of traceable, volumetric LNG standards, this is the best we could provide on such short notice. We strongly recommend to follow-up on this preliminary study by a more extensive study on Liquefied Nitrogen (-196 °C) in order to obtain more confidence in the Altosonic V for LNG applications.
Also note that broad international acceptance in the field of legal metrology requires all tests to be performed or witnessed by an independent third party such as ourselves, rather than relying on a manufacturer's own test results. Therefore some of the research tests you have performed and all future tests will need to be repeated / performed by, or in the presence of such a party.

With the above in mind, I would like to refer you to pages 2 and 3 of this letter, which summarised show that we expect the uncertainty in Volumetric measurement of LNG by the Altosonic V to be within a range of 0.26 to 0.33% of measured value.

I trust this informs you satisfactorily on this matter.

With kind regards,
NMi Certin B.V.

Wim Vlaskamp B.Sc.
Senior Product Manager, Liquid Measurement

NMi Certin B.V.
Hugo de Grootplein 1, 3314 EG Dordrecht
P.O. Box 394, 3300 AJ Dordrecht, NL
Phone +31 78 6332332
Fax +31 78 6332309
www.nmi.nl

NMi B.V., chamber of comm. no. 27235767
NMi Certin B.V., chamber of com. no. 27235748

NMi Certin B.V. is a subsidiary company of NMi B.V.

Figure 20 Uncertainty statement of NMi on ALTOSONIC V for LNG. Uncertainty 0.26% to 0.33% of M.V. on basis of water calibration at ambient conditions.

7. SUMMARY AND CONCLUSIONS

This paper describes the development project of the 5 beam ultrasonic flowmeter for measuring cryogenic liquids (e.g. LNG or Liquefied Nitrogen) with fiscal accuracy.

Tests have shown the importance of the acoustical coupling between the piezo ceramic element and the radiating window of the transducer. A thorough investigation has lead to a special design consisting of a combination of an acoustic coupling and a reliable transducer construction. The patent for this solution is pending. Extensive tests under isolated, static and dynamic conditions have shown that the transducer design is stable and generates reproducible and accurate results.

There are two challenges regarding the calibration of any type of flowmeter for use in cryogenic applications. There are no (laboratory) test facilities in the world where flowmeters, with a diameter larger than 4 inch, can be tested on LNG or on liquefied nitrogen against a reliable reference. And, secondly, in most applications it is not possible to calibrate flowmeters on site against a reliable reference. This asked for the development of an alternative calibration method.

The transfer of water calibration to application at cryogenic conditions forms the basis of the calibration concept. LNG and liquid nitrogen have a low viscosity, leading to fairly high Reynolds numbers, which, as confirmed by the tests, improves linearity of the 5 beam ultrasonic flowmeter.
The calibration procedure for calibrating ultrasonic flowmeters for use of custody transfer of LNG has been developed in close cooperation with NMi, the Dutch Board of Weight and Measurement,

This paper also describes tests done at the cryogenic calibration facility at NIST. The performance of the LNG ultrasonic flowmeter with regard to the reproducibility, repeatability and the linearity have been well within expectations and market requirements. The tests at NIST have been witnessed by NMi ('Netherlands Measurement Institute').

Based on this we can conclude that ultrasonic flowmeters form a reliable and highly accurate solution for the custody transfer of LNG. In addition, the developed calibration procedure based on a water calibration offer a good solution for proving the flowmeters.

8. REFERENCES

[1] Hogendoorn, J. and A. Boer, *Experience with Ultrasonic Flowmeters in Fiscal Applications for Oil (-products)*, 17th North Sea Flow Measurement Workshop, 1999.

[2] Dahlström, M.J., *Two Years of Fiscal Performance*, 17th North Sea Flow Measurement Workshop, 1999.

[3] Dahlström, M.J., *KROHNE ALTOSONIC V, with Master Meter Approach*, 21th North Sea Flow Measurement Workshop, 2003

[4] Klooster, J. van, *Sensorconstructie LNG toepassingen*, Internal report KROHNE, 2006.

[5] Volmer, W., *Uncertainty statement ALTOSONIC V on LNG*, Letter of NMi, 2006.

[6] Description of the *'Cryogenic Flow Facility at NIST'* given by NIST, undated.

[7] Lewis, M., *Test report of ALTOSONIC V – LT on liquefied Nitrogen*, NIST, 2007.

[8] J. Hogendoorn, H. Hofstede, H. Danen, ALTOSONIC III – A Dedicated Three-beam Ultrasonic Flowmeter for Custody Transfer of Liquid Hydrocarbons, NSFMW 2004.

[9] T. Folkestad, Proving a fiscal 5 path Ultrasonic Liquid Meter with a Small Volume Prover Norsk Hydro ASA Can it be done?, NSFMW 1999

[10] T. Folkestad, Testing a 12" KROHNE 5-path ALTOSONIC V ultrasonic liquid flowmeter on Oseberg crude oil and on heavy crude oil, NSFMW 2001

[11] Hofstede, H., Hogendoorn J., and Danen, H., *ALTOSONIC III – A Dedicated Three-beam Ultrasonic Flowmeter for Custody Transfer of Liquid Hydrocarbons, SEAHFMW 2005*

9. ACKNOWLEDGEMENTS

The authors like to thank all the colleagues from the KROHNE R&D team who contributed to this project. In particular we like to mention the names of Jeroen van Klooster, Jan van Bekkum, Peter van Brakel and Arie Huijzer.

Tekna
North Sea Flow Measuremement Workshop
16.-19. October 2007, Oslo

Abstract paper 20

Hammerfest LNG Plant – Fiscal metering system

Corresponding author: Erik Forgaard Andreassen
Company. StatoilHydro- Hammerfest LNG
Adress: Melkøya, PB 525, 9615 Hammerfest, Norway
Epost: efan@statoil.com
Telephone : 94877142

Abstract:
Hammerfest LNG Plant is the first LNG Plant in Norway and the first offshore development in the Barents Sea. New technology has been taken in use in many parts of the this LNG-plant. Most spoken of is the subsea installation located 143 km from shore, the LNG process design as well as the CO2 re-injection to the reservoir. When it comes to the fiscal metering system the design basis was to use well proven technology which in most cases was well known within the company. However, fiscal metering competence was challenged when LNG measurement concept for the plant had to be defined.
The knowledge within fiscal metering of LNG has developed both for the company and the authorities (Norwegian Petroleum Directorate /Norwegian Metrology and Accreditation Service standards department) during the project. As part of this the Norwegian Measurement regulations were amended in December 2004.

The presentation is a short introduction to the fiscal metering system at Hammerfest LNG Plant with most of the focus on the LNG fiscal metering. Following metering stations at Hammerfest LNG Plant are spoken of in the presentation.

- Condensate metering
- LPG metering
- LNG metering
- Vapour metering
- Fuel and Flare metering

Paper will not be submitted

25TH INTERNATIONAL NORTH SEA FLOW MEASUREMENT WORKSHOP
October 16-19, 2007, Oslo, Norway

Flare Metering with Optics

From Blue-Sky Technology to the Real World

Jody Parker, Gordon Stobie, ConocoPhillips Company
Ivan Melnyk, Photon Control
Chip Letton, Letton-Hall Group

Abstract

During a presentation at the 2006 North Sea Flow Measurement Workshop on new and current flare metering technologies, infrared and other optical methods of gas flow measurement were referred to as "blue-sky" technology. The inference was that these technologies, whilst they might have merit, probably would not be available for some time, if ever. In reality, this is far from true, as at least one vendor of such devices has developed its technology to the point that laboratory and field testing have been carried out, and more than twenty-five units have been sold and installed into operational plants.

The purpose of this paper is to review the development, testing and deployment of the Photon Control Optical Flow Meter. In particular, the following topics will be addressed:

1. Overview of the technology, its various embodiments, its advantages and shortcomings, with a synopsis of a Canadian JIP under which development was carried out.
2. Presentation of results:
   - Flow Laboratory testing for installation effects
   - A variety of general Canadian onshore retrofit installations
   - Specific examples from the eight ConocoPhillips Canada "Real World" installations
   - An example using optical flare metering technology in Statoil
3. Detailed conclusions on the JIP, the gradual implementation of the new technology into the industry, with feedback from both users and regulators on being able to manage flare gas discharges.

1. STATE OF OPTICAL FLOW METERING: A REVIEW

Historically, optics are less well known in the realm of gas flow measurement whereas analytical instrumentation – LIDAR*, gas analyzers, etc., use the inherent features of light such as specific absorption, fluorescence or scattering which cannot be realized by any other techniques.

Optical methods for measuring gas flow, or optical flow meters (OFM), use optical velocimetry, the measurement of gas flow velocity from which the volumetric flow rate can be derived. These methods can be subdivided into laser Doppler velocimeters (LDV) and optical transit time

* LIDAR (*Light Detection and Ranging*) is an optical remote sensing technology that measures properties of scattered light to find range and/or other information of a distant target. The prevalent method to determine distance to an object or surface is to use laser pulses. Like the similar radar technology, which uses radio waves instead of light, the range to an object is determined by measuring the time delay between transmission of a pulse and detection of the reflected signal.

velocimeters. The latter can be divided into laser-two-focus (L2F), scintillation-based and absorption-based transit time velocimeters.

1.1 Product History

Spectron Development Laboratories conducted a study for the Gas Research Institute to determine the possibility of developing a volumetric gas flow meter based on the L2F technique in 1989.[3] Although this study never resulted in a commercial device, it caught the attention of Nova Husky Research where optical methods were in use for particle sizing and monitoring the quality of filters. A project on the L2F volumetric flow meter was conducted for several years at Nova, and later at TransCanada Pipelines Ltd. (TCPL). The effort was continued in 1999 - 2000 as a joint development project with a major flow meter manufacturer.[4,5] The work focused on developing a high-accuracy Optical Flow Meter (OFM) which would be suitable for gas custody transfer measurement, and in particular for the replacement of orifice meters.

In 2002 Photon Control Inc., licensed this optical flow metering technology from TCPL for the purpose of its further development and commercialization in a variety of gas flow metering applications.

During 2003 Photon Controls proposed to the Canadian oil and gas industry a Joint Industry Project venture in order to mitigate the meter development costs and to gain access to 'real world' facilities. Unfortunately the take up on this venture was poor, and it was not until somewhat later at the 2004 Canadian School of Hydrocarbon Measurement in Calgary, Alberta, that ConocoPhillips Canada (COPC) became aware of what looked like an attractive option for flare metering. At this time COPC and Photon Control began to collaborate with the development of the meter systems for flare and vent gas applications.

COPC recognised that there was a 'hole' in the management of their plants and resources, and saw that local regulations would soon require them to report flare and vent quantities to a level which had been unachievable in the past. COPC were uncomfortable with their existing estimates of stack losses and wanted more accurate information in order to reduce or eliminate background gas to the flare systems. It was seen that flare/vent metering was the only way forward, and that the existing flare and vent meters at that time did not meet the Business Units' needs as either being fit for purpose or especially cost efficient. The collaboration process continued through 2006.

1.2 Laser Doppler Velocimetry

LDV is the oldest form of optical velocimeter, and was proposed soon after appearance of the first commercial lasers. However, LDV has found little industrial or commercial application because of its high cost and the need to particle-seed the flows due the very low signal-to noise ratio. In laboratories, LDV offers impressive accuracy and the ability to measure very high velocities. This, combined with the ability to measure complex 3D gas flows makes LDV an important tool in turbomachinery and avionics applications.

1.3. Optical Transit Time Velocimeters

1.3.1. Laser-Two-Focus (L2F) Meters

Thompson first described the possible implementation of the L2F method for flow measurement in 1968.[1] Schodl contributed significantly to the practical aspects of the L2F technique, but the method never went beyond flow laboratory implementation other than a few commercial L2F meters built by Polytec in the early 1980s.[2]

1.3.1.1. Principle Of Operation

The operational principle of the optical gas flow meter based on L2F velocimetry is explained in Figure 1. Small particles which accompany natural and industrial gases pass through two laser beams focused in a pipe by illuminating optics. Laser light is scattered when a particle crosses the first beam. The detecting optics collects scattered light on a photodetector P1, which then generates a pulse signal. If the same particle crosses the second beam, the detecting optics collect scattered light on a second photodetector P2, which converts the incoming light into a second electrical pulse. By measuring the time interval between these pulses, τ, the gas velocity is calculated as

$$V=S/\tau \tag{1}$$

where S is the distance between the laser beams.

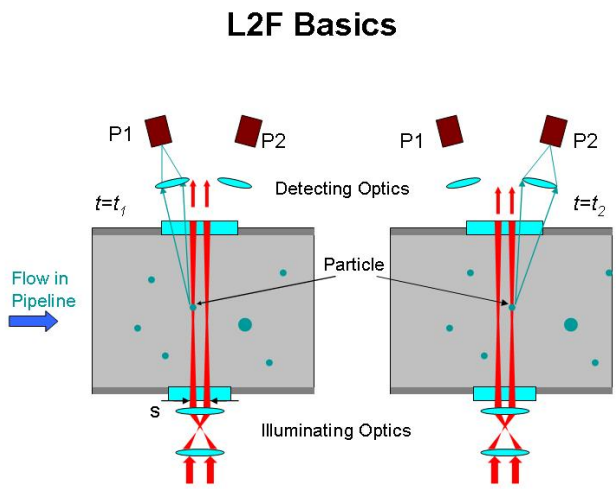

Figure 1. Operating principle of the L2F velocimetry

1.3.1.2. Accuracy Of The L2F Method

The linear gas velocity can be measured with high accuracy using the L2F method independent of pressure, temperature and gas composition. Using (1) above, the velocity uncertainty σ_v can be estimated as

$$\sigma_v = \sqrt{(\sigma_d^2 + \sigma_t^2)} \tag{2}$$

where σ_d and σ_t are the standard deviations in velocity due to errors in optical spacing and lapse time, respectively.

The uncertainty of the optical spacing is defined by the accuracy at which the beam spacing can be measured. For typical beam spacing d=1mm and positioning uncertainty of Δ_d=1 μm, the typical optical uncertainty would be around 0.1%. The lapse time uncertainty could be even smaller, as it is defined by the sampling frequency f_s. Smart, for example, reported a velocity uncertainty of less than 0.02% while using analog-to-digital conversion at a sample frequency of 100MHz.[6] The number of particles effectively crossing the two laser beams, N, contributes to

the velocity uncertainty as approximately $1/\sqrt{N}$. Conversion of the linear velocity measured at a single point to an average velocity, however, leads to a larger uncertainty due to the flow profile variations and turbulence. According to Schodl, the total error of the L2F velocimeter could be as low as 0.5% in a predictable profile, if the turbulence does not exceed 4%.[7]

The value *N* is determined by the following factors:

a) the meter itself which includes: the efficiency of the delivery and collecting optical systems, the detectability of the photodetectors , the laser power and the wavelength;

b) the purity of the gas moving in the pipe;

c) the gas velocity profile and turbulence level.

In contrast to LDV devices, L2F velocimeters usually do not require seeding because of their inherently high signal-to-noise ratio, SNR. High SNR in L2F velocimeters results from the concentration of laser light into two focal sheets. LDV signals, however, consist of multiple fringes occurring after the interference of two convergent laser beams. Photodetectors such as the avalanche photodiodes used in L2F gas velocimeters, register individual photons, which allows them to use relatively low power lasers. These mass-produced semiconductor lasers transmit from 1 to 5 milliwatts through single-mode fibers, and can be focused into narrow sheets measuring between 20 and 30 μm wide in a 2- to 6-inch pipe. The collecting optics must be designed to collect the scattered light within as large a solid angle as possible while blocking all direct light coming from the sheet. For 2-inch and 4-inch meters, the dark-field collecting optics must block the straight light from 0 to 2.5 degrees. Light scattering efficiency is determined by the size of the particles and the laser wavelength. L2F velocimeters operated at near-IR (850nm) can measure the velocity of air with a minimum particle diameter of approximately 0.3μm.[6] Shortening the laser wavelength reduces this minimum detectable particle size to less than 0.1 μm. During the early development of the L2F gas flow meter, particles found in a typical gas pipeline were shown to range from 1 to 10 μm.[3]

Lowering the gas velocity reduces the number of detectable particles. At a certain minimum velocity, V_{min}, the OFM cannot distinguish the organized flow from the stochastic movement of particles in the pipe due to 'thermal stratification and other external factors'. The value of V_{min} establishes the minimum measured flow rate, and thus the rangebility of the meter.

1.3.1.3. Turn-Down Ratio

The turn-down ratio, or rangebility, is probably the most important parameter of any flare gas meter that is proven to be repeatable. Some manufacturers of ultrasonic flare meters claim values of V_{min} of 0.03 m/s and V_{max} of 80 m/s, yielding a turn-down ratio in excess of 2500:1. The turn-down ratio of 100:1 recently claimed for a 12-inch flare meter from Instromet should perhaps be considered realistic for the class of ultrasonic flare meters.

In contrast to ultrasonic meters, L2F flare meters have virtually no limits for V_{max}. An extreme maximum velocity, up to V_{max}=720 m/s, was reported during the testing of the L2F velocimeter in a recent supersonic aircraft[8] test.

The minimum velocity for Photon Control's OFM is defined by presence of particles - the dirtier the gas, the lower V_{min} is possible. It has been shown that flow through the OFM can be measured down to V_{min} =0.1 m/s, as confirmed by testing in the flow loop at CEESI described below. Testing for a high V_{max} is limited in larger pipes by the limitations imposed by the

available flow testing facilities. L2F OFM have been tested up to V_{max}=100 m/s [9], which is used to define the L2F turn-down ratio as 1000:1.

1.3.2 Other Optical Meter Types

There are a number of other optical meter types using different principles, and these are listed briefly for completeness.

1.3.2.1 Optical Scintillation Meters

Ting-I Wang[14] described an OFM whose operational principle is based on a scintillation technique, or registration of variations in refraction of the light beam caused by local fluctuations of the refractive index produced by turbulence and heat exchange in the gas. The scintillation OFM is the only gas flow meter whose performance improves with turbulence.

An improved version of the scintillation OFM called the ”Laser-Two-Beam”, or L2B meter is offered by Photon Control for larger nominal bore pipes.

1.3.2.2 Optical Absorption-Based Meters

Liquid hydrocarbons and water absorb energy more than gases in the IR region. This effect was the basic operating principle of an absorption-based OFM originally proposed for non-gaseous flow applications, such as asphalt and cement production.[12]

The technique was attempted recently for flare gas measurement, although laboratory testing using simulation media of air and water droplets was able to reach only V_{min} = 0.4 m/s.[13]

The principle of the IR-absorption meter is illustrated in Figure 3. Two collimated beams from IR LEDs or IR lasers cross the pipe perpendicular to the gas flow. The presence of hydrocarbons or water droplets in the flow causes changes in the optical transmission, which is detected in each channel. A cross-correlation technique is used for calculation of transit time.

An absorption-based meter requires the presence of large water droplets that discretely cross the beams amid turbulent hydrocarbons. Uniformly distributed water vapour and/or methane lead to static changes of the absorption, which can make transit time measurement very difficult.

A fundamental drawback of the absorption method is that it actually does not provide averaging across the pipe. It is probably this effect which is responsible for an average of 15% error being recorded during the lab testing of the IR absorption meter reported by NEL[13] at the NSFMW in 2006.

1.3.2.3 OFM Based On Sagnac Effect

Similarly to ultrasound, light passing along and against the gas flow will have different phase velocities which are related to the gas flow velocity. This difference can be detected using the Sagnac effect; the method was first described and demonstrated by Blake.[14]

Although encouraging laboratory data has been demonstrated[15], the Sagnac OFM has never been fully investigated. The meter will be sensitive to vibration of the pipe and flow turbulence; also, one can expect significant beam deviation at a long optical distances due to the temperature gradient in the pipe.

2. FLARE METERING BY LASER TWO-FOCUS (L2F) METERS

L2F meters are at present the most intensively studied method of optical gas flow measurement. L2F meters were publicly introduced for flare measurement at the NEL Flare Gas Metering Seminar in 2005.[16]

2.1. Laser Two-Focus Design

The L2F consists of an optical head and a signal processing unit, which are connected by a fiber optic cable.

2.1.1. Optical Head.

The basic OFM head developed by Photon Control is designed to fit into a standard ANSI flange and is shown in Figure 5.

An insertion-style optical head as shown in Figure 6 was designed for use in larger pipes, from 6 to 32 inches nominal bore. The optical system is incorporated in a ¾in stainless steel sleeve, which is installed in the pipe in a similar manner as thermal dispersion mass flow meters. The stainless steel optical head incorporates the delivery and collecting optical system assemblies, which are positioned perpendicular to the flange bore and are insulated from the gas by optical windows.

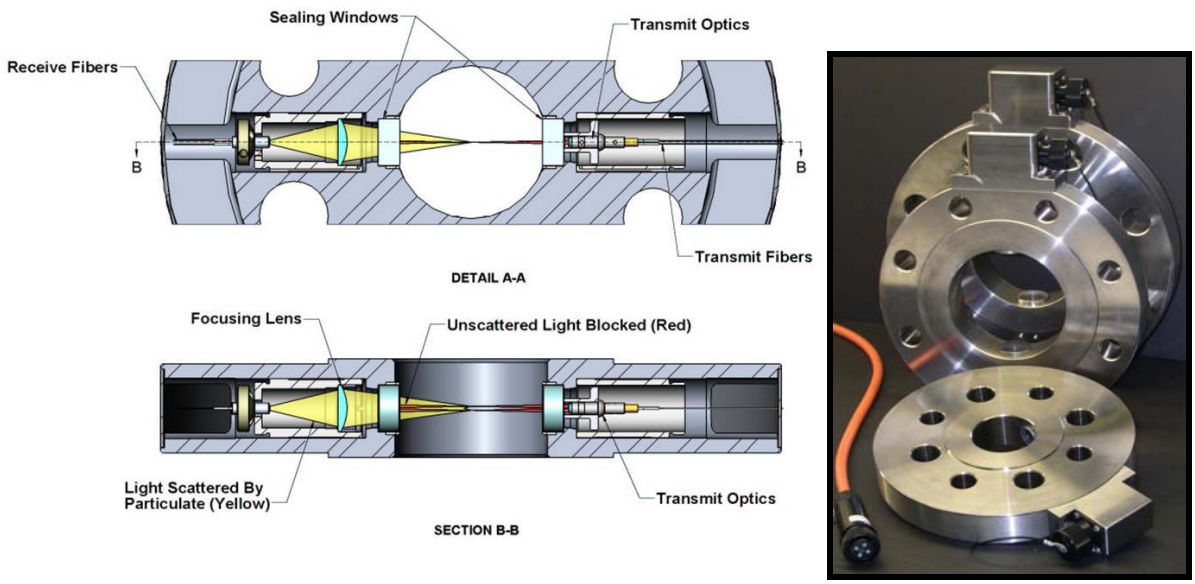

Figure 5. Flange 2-in and 4-in optical heads

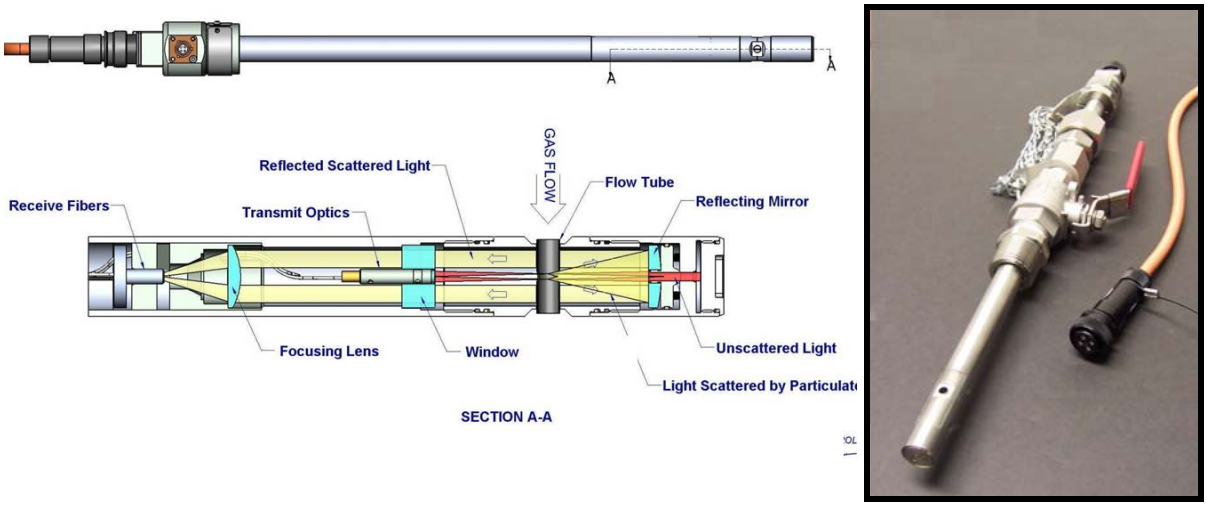

Figure 6. 3/4-in insertion optical head with a ball valve

The optical head is typically designed for single-point measurement which is located in the center of the pipe or at a quarter-radius from the pipe wall.

2.1.2. Signal Processing Unit.

The signal processing unit (or opto-electronic converter) is designed on one electronic board which fits into a normal NEMA or an explosion proof enclosure. These are is shown in Figure 7.

(a) (b)

Figure 7. Signal Processing Unit: (a) NEMA 4X and(b) explosion-proof

The board incorporates a digital signal processing (DSP) chip with internal analog-to-digital conversion at sample rates up to 12MHz. It has inputs for pressure and temperature transmitters,

so that various flow calculations can be performed. The unit provides typical flow meter outputs: 4-20 mA, frequency and pulse, and RS232 or RS485 digital. The board is powered from 24VDC, the average power consumption is 3 watts.

Signal pulses are collected over a fixed sampling interval, which is determined from the flow rate and number of particles in the gas. The raw flow velocity is calculated using a fast correlation technique (correlogram), the raw velocity data is then input to a post-processing calculation. The flow calculation is accomplished in three stages as is described by Figure 8. The post processing filters average the output and remove spurious readings based on previously calculated data. The flow profile correction is used to calculate the average flow velocity (bulk velocity) from the point velocity reading using a progarmmable look-up table specific to the piping and meter configuration. The standard volumetric flow rate is determined using AGA8-determined compressibility and the local pressure and temperature.

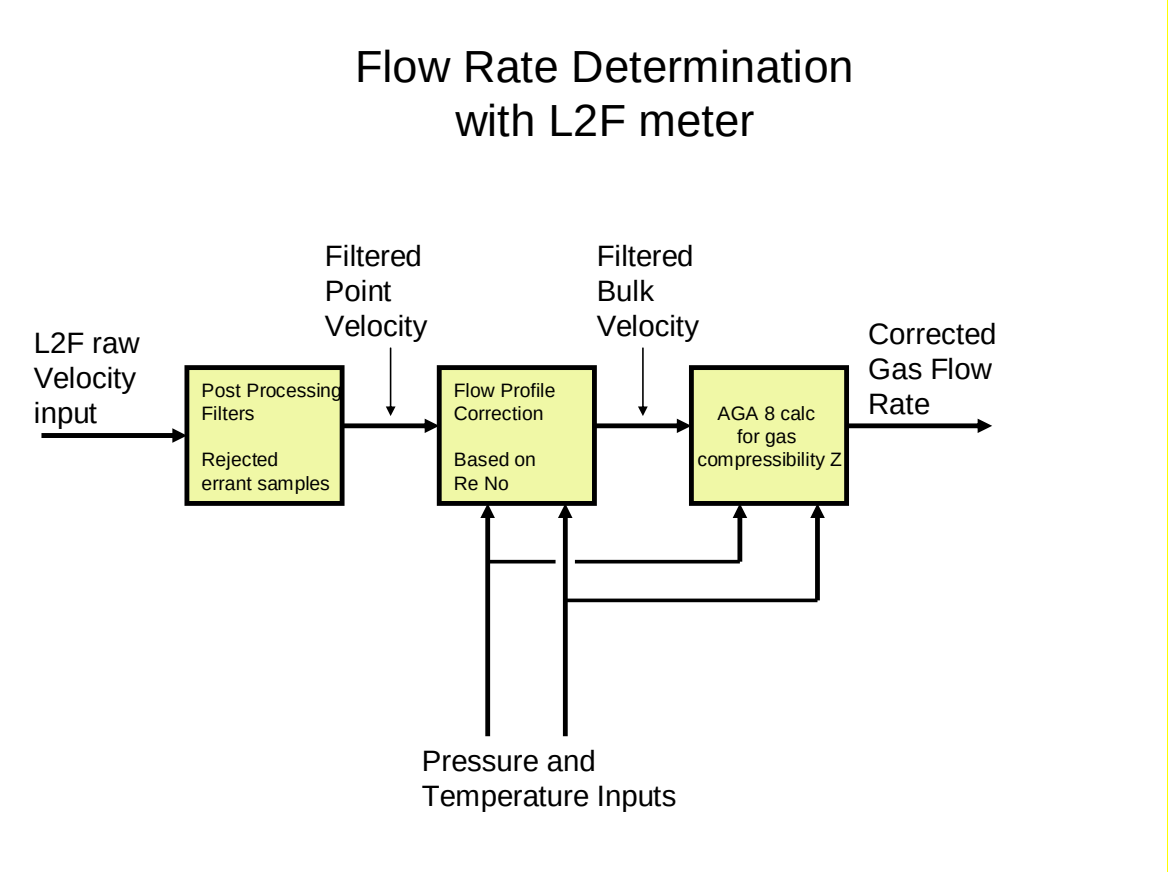

Figure 8. Flow calculation block diagram

2.1.3. Fiber Optic Cable.

The fiber optic cable accommodates a group of single-mode and multi-mode fibers protected by a flexible metal conduit and waterproof indoor/outdoor PVC jacket. The standard length of the cable is 20 meters, but the power budget of the system allows extension of the cable length far beyond 100m.

2.2. Testing the L2F meters

L2F meters have been extensively tested over a 36 month period at several facilities, including:

- Coanda Research, Burnaby, BC – testing to determine installation effects, particle size, and flow conditioning requirements;
- Didsbury TCPL Test Loop, Alberta – testing flanged OFMs in natural gas at high pressure;
- Southwest Research Institute, San Antonio, TX - testing in natural gas at low and high pressures;
- Colorado Engineering Experiment Station Inc (CEESI), Nunn, CO – final testing of the insertion OFM for accuracy and installation effects;
- Terasen Calibration Facility, Penticton, BC – testing and calibration against ultrasonic 4-path meter in air flows at low pressure.

2.2.1. Velocity Accuracy and Calibration

A set of *N* pulses from many scattering events are averaged to produce each data point. This reduces the variation in localized velocity measurement caused by flow turbulence by a factor of $\sqrt{N}$.

For example, the standard deviation of the fluid velocity in fully turbulent flow in the center of the pipe is typically 5% of reading. The number of correlated particles is usually within the range of 10 to 100 per sampling interval, therefore, the standard deviation of the velocity measurement is reduced to 0.5% to 1.5%.

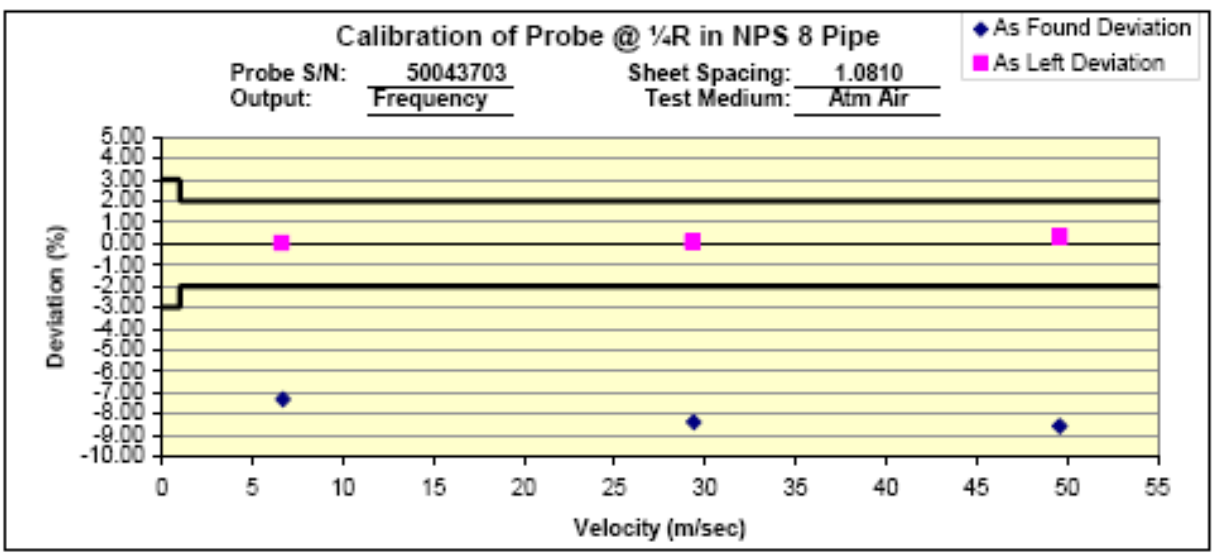

Figure 9. Example of a calibration result for the insertion L2F meter in an 8-inch pipe

An example of a calibration report is shown in Figure 9. The velocity uncertainly from unknown beam spacing can ordinarily be neglected since the beam spacing is controlled with an accuracy better than 1 µm and the base distance between the laser sheets is set at 1.0 mm. This feature underlines another important advantage of the L2F meter – once it is calibrated, there should be no need to recalibrate the unit in the field. In the same way that ultrasonic meter readings depend only on transducer spacing and difference in time-of-flight, the L2F depends on the fixed beam spacing and measured particle travel time. Absent changes in these two parameters, there should be no drift in the meter.

2.2.2. Flow Measurement Range and Accuracy

Detailed testing of the insertion OFM at CEESI was conducted in the summer of 2005.[17] In those tests, the Focus Probe OFM matched the reference within ±2.5% over the 1.0 to 100 m/s operating range, and within ±7% over the 0.1 to 1.0m/s operating range. Increased flow instability was observed by the Focus Probe meter in the 0.1 to 1.0m/s range. This is shown in Figure 10.

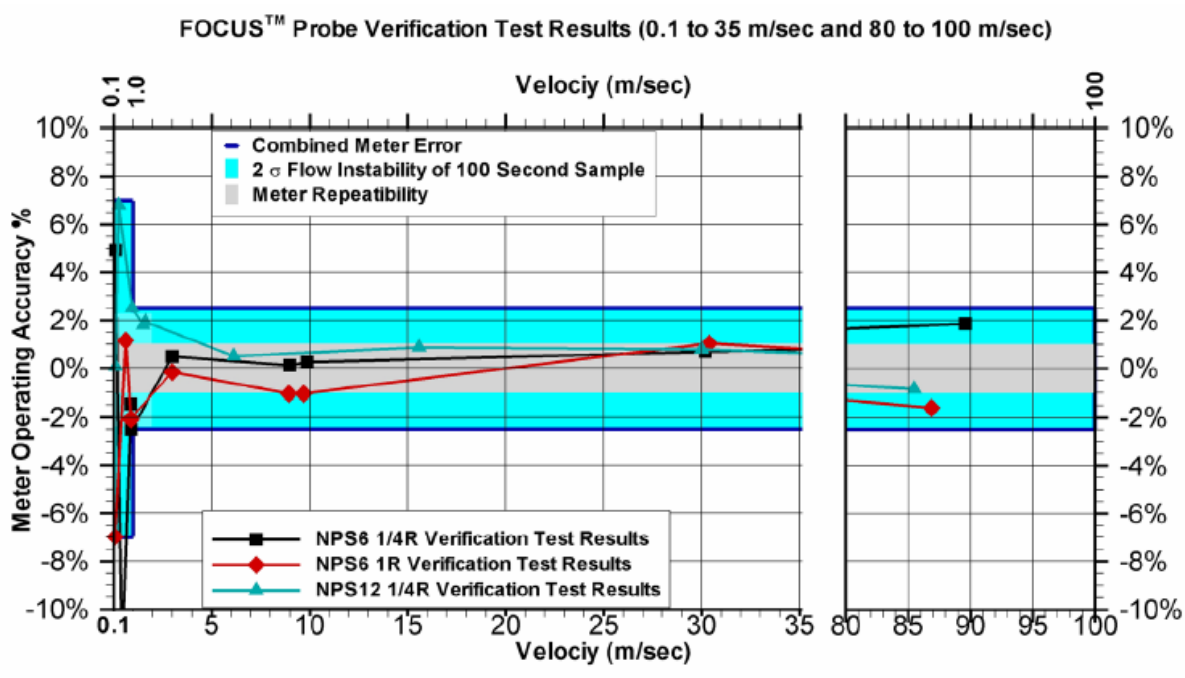

Figure 10. Verification results from testing the Insertion Focus™ Probe Meter in 6-inch and 12-inch pipes at CEESI, Nunn, CO.

2.2.3. Flow Meter Installation Effects

Practically all flow meters exhibit installation effects. Some of the flow testing earlier referred to concerned installation effect testing, which were recognized as an important factor when metering with a L2F flow meter.

Testing at CEESI in Colorado, included:

- 45 degree header installation
- 90 degree header
- Two elbows out of plane

for several line pipe sizes

The graphs shown below in figures 11A-C illustrate the installation bias effects recorded for some of the header configurations, sizes and gas velocities tested at CEESI. Further details are provided in Reference17.

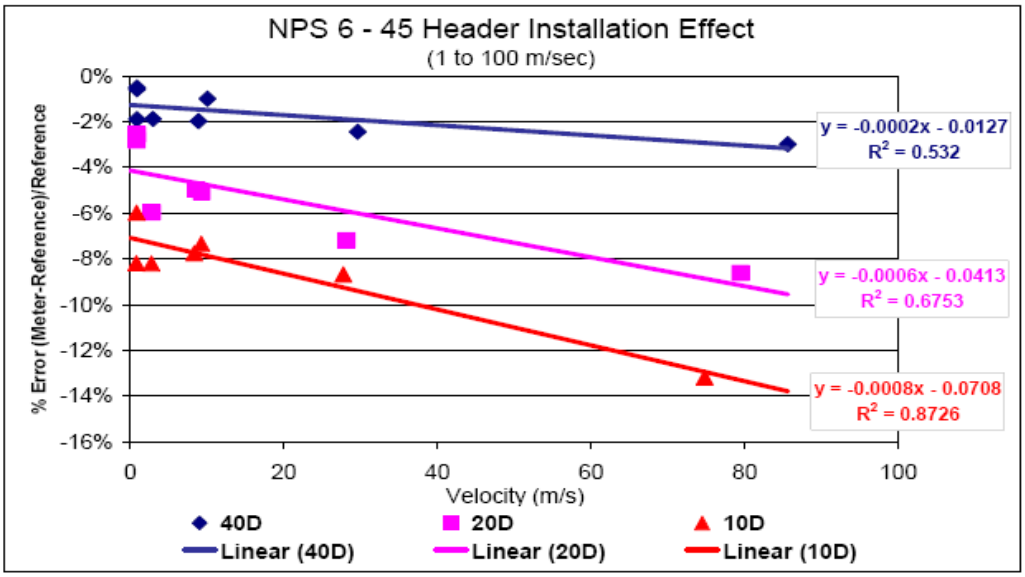

Figure 11A. 6-inch NB – 45 degree Header Installation Effect from CEESI

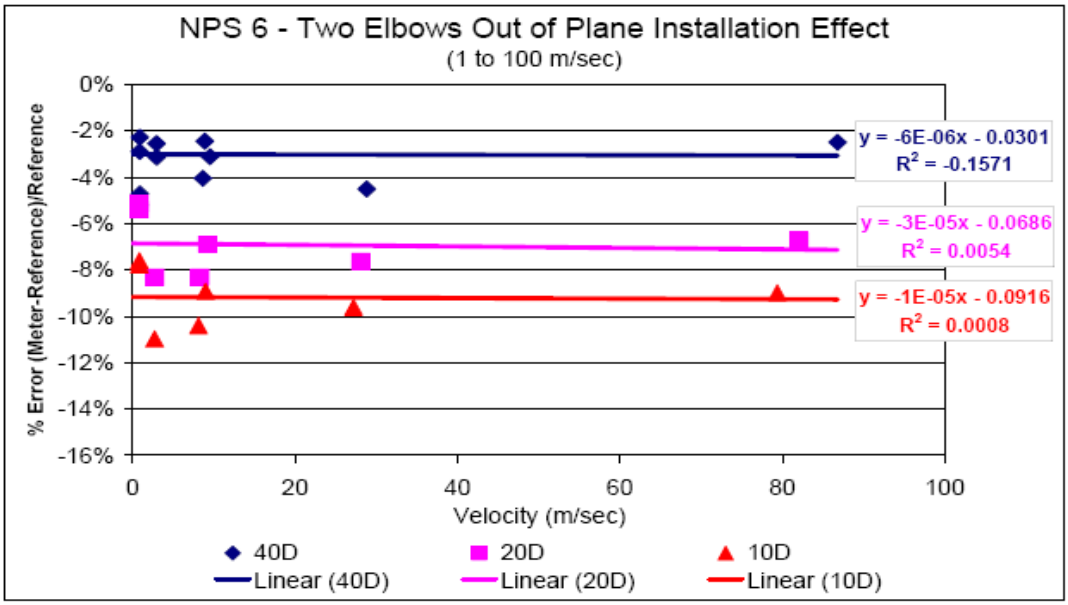

Figure 11B. 6-inch NB Two Elbows out of Plane Installation Effect from CEESI

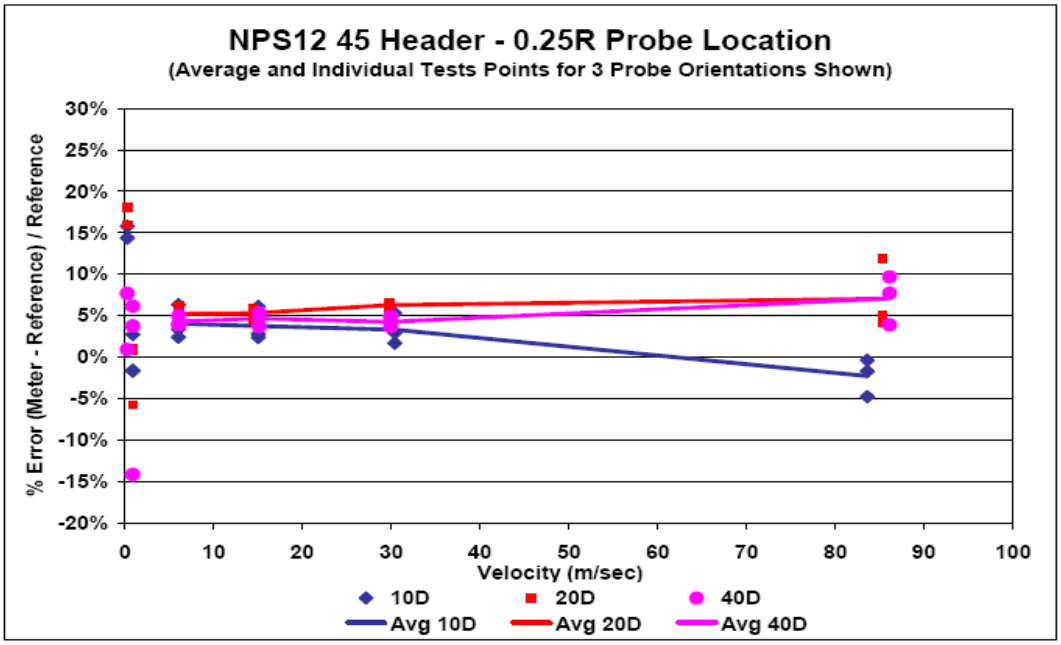

Figure 11C. 12-inch NB – 45 degree Header Installation Effect from CEESI

2.3. Practical Implementation of the L2F Meters

With any new technology, there are often numerous practical issues that a user may encounter in a Real-World installation. These will be addressed in the following sections.

2.3.1. Mitigation Of Fouling Effects

Contamination of optical components is an inevitable concern when contemplating a flow measurement system using optics in a flare gas environment. This is especially so with flare gas, which generally have a variable composition and liquid content. Photon Control addressed this issue at the beginning of its Focus Probe development by implementing a shroud design.[17] This solution dramatically improved the resistance of the device to concurrent liquid hydrocarbons, which are known to cause problems for other types of flare meters.

Another improvement aimed at liquids dropping out of the gas was the application of heated windows. In early commercial installations it was discovered that many flare and biogas facilities deal with wet gas. Keeping the windows warmer than the ambient gas prevents laser light from scattering due to foggy or wet window surfaces. Currently this is a standard feature for all L2F OFMs produced by Photon Control.

In Figure 12 the Focus Probe Meter is shown with heated window kit installed.

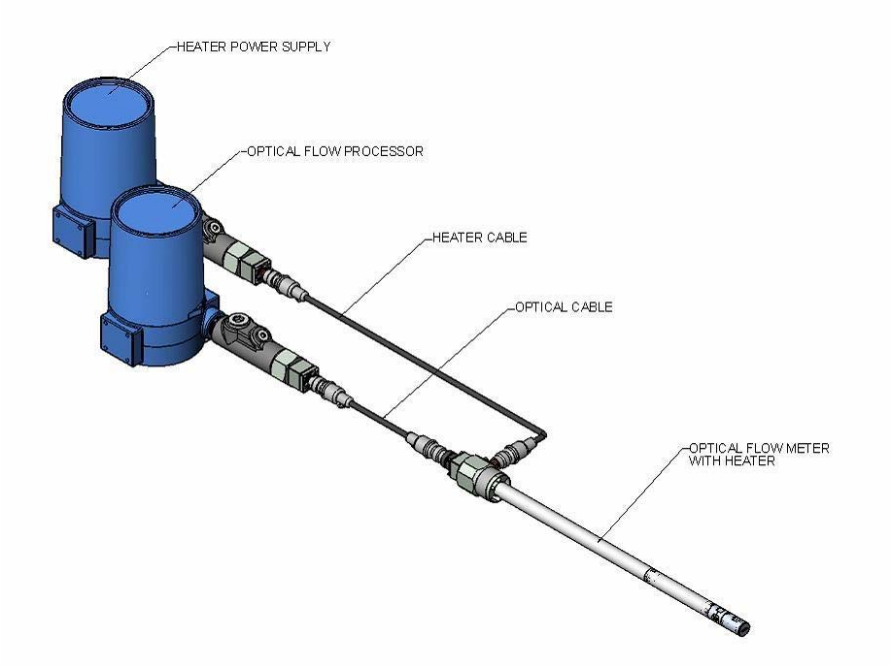

Figure 12. Insertion Focus™ Probe with heated windows to prevent condensation.

2.3.2. Installations In The Field

Over 25 laser-two-focus OFMs have been supplied and installed in the field since commercialization began in late 2005. Table 1 give the details of some of these installations. Applications include flare gas and associated gas flow measurement in pipe sizes from 2 inches to 24 inches, fuel gas measurement in natural gas pipelines, and biogas flow metering.

There have been a number of enquiries for larger wafer-type OFMs for separator offgas. However these will require substantial engineering, and proving.

A larger 42-inch NB pipe flare system has also been supplied for the Statoil operated Tjeldbergodden Methanol Plant, Norway. .

UPDATE	18-Sep-07								
DATE	***COMPANY***	***PLANT***	***PROV/STATE***	***QTY***	***METER***	***PIPE DIA***	***PLANT/***	***INSTALL***	***DAYS IN***
			COUNTRY		***TYPE***	***Inch***	***APPL.***	***DATE***	***SER***
24-Mar-06	**Blackrock Ventures**	**Peace River**	Alberta	1	Probe	8	Oil Battery	9-Aug-05	777
	now Shell Canada	**1-26-83-15w5**	Canada						
24-Mar-06	**Canetic Energy**	**Nottingham**	Saskatchewan	1	Wafer	2	Oil Battery	17-Nov-05	677
		2-34-5-2 W2	Canada						
3-May-06	**ConocoPhillips**	**Vulcan**	Alberta,	1	Probe	10	Flare Stack	28-Feb-05	939
			Canada	1	Probe	24	Flare Stack	28-Feb-05	939
30-Nov-05	**ConocoPhillips**	**Ghostpine**	Alberta	1	Probe	16	Flare Stack	27-Sep-05	728
			Canada	1	Wafer	2	Fuel Gas	13-Jun-05	834
23-Dec-05	**ConocoPhillips**	**Marengo**	Saskatchewan	1	Probe	6	Oil Battery	1-Aug-05	785
16-Aug-05	**EOG Resources**	**Grand Prarie**	Grande Prairie, Canada	1	Wafer	4		18-Aug-05	768
7-Apr-06	**ConocoPhillips**	**Wembley**	Alberta, Canada	1	Probe-XL	16	Flare Stack	10-May-06	92
11-Aug-06	**ConocoPhillips**	**Valhalla**	Alberta	1	Wafer	2	Separator Off Gas	10-Aug-06	411
		16-14-75-9 W6M	Canada						
25-Jul-06	**ConocoPhillips**	**Valhalla -**	Alberta	1	Wafer	2	Fuel Gas	12-Sep-06	378
		7-22-75-9-W6M	Canada						
26-Oct-06	**PetroCanada**	**Hanlan Robb**	Alberta, Canada	1	Probe	12	Flare Stack	7-Nov-06	322
26-Oct-06	**PetroCanada**	**Hanlon-Robb**	Alberta, Canada	1	Wafer	2	Flare Stack	18-Oct-06	342
26-Oct-06	**DPH/ ConocoPhillips**	**Cessford**	Alberta, Canada	1	Probe	14	Flare Stack	11-Oct-06	349
8-Aug-07	**Plains Marketing**	**High Prairie**	Alberta	1	Probe-HTR	10	Flare Stack	20-Feb-07	217
		(780) 523-4690	Canada	1	Wafer	4	Purge gas	4-Jul-07	83
18-Jun-06	**GVRD**	**Richmond**	B C, Canada	1	Probe-HTR	8	Biogas	28-Sep-06	362
15-Feb-07	**Evergreen Packing**	**Pine Bluff**	Arizona, USA	2	Probe-HTR		Fuel Gas	TBD	TBD
12-Jul-07	**ConocoPhillips**	**Saddle Hills**	Alberta, Canada	1	Probe	6	Flare Stack	8-Sep-07	17
10-May-07	**Innotech**		Russia	1	Probe	6	Associated Gas	10-Jun-07	
15-Sep-07	**GVRD**	**Lion's Gate**	B C, Canada	1	Probe - HTR	4	Flare Stack	TBD	TBD

Table 1 – Photon Controls OFM commercial installations

Figure13 shows a typical installation of the insertion OFM in a flare line. It has been found that horizontal orientation of the probe is preferable in order to avoid trapping liquids in the space around the shroud.

Figure 13. Insertion Focus™ Probe installed in a 12-inch pipe, gas processing plant, Alberta, Canada

Figure14 shows a flare event metered with a Focus™ Probe flowmeter. The device was measuring a base line of 1.1 m/sec when the velocity rapidly increased to about 28 m/sec, decreasing to and holding at 20 m/sec during the plant incident.

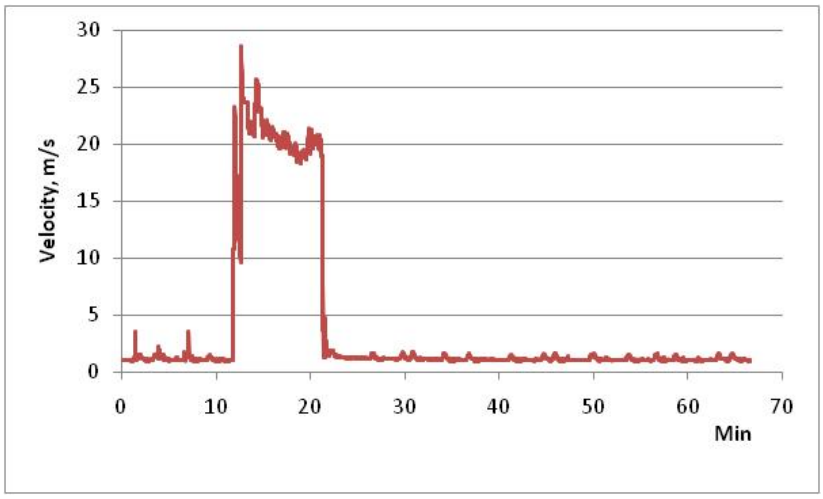

Figure 14. Flare event recorded by Focus™ Probe meter, base line 1.1m/sec

2.3.3. Performance Of The Flanged OFM

The flanged OFM (Figure 5) can operate at high pressures and temperatures, and creates no additional pressure drop in the pipe. Initially designed for pipeline gas measurement, the flanged OFM works perfectly well for fuel gas measurement and well monitoring.

Figure 15 shows an example of total energy recorded by a 2-inch OFM when compared with a vortex flow meter installed in the same fuel supply line at the Crowsnest TCPL facility gas compressor station. The total energy was calculated based on gas volume metered and the gas

energy derived from the gas composition measured by a local gas chromatograph. The data show that the OFM agrees with the Vortex meter previously approved by Measurement Canada. In general the discrepancy between the two meters is within ±1%.

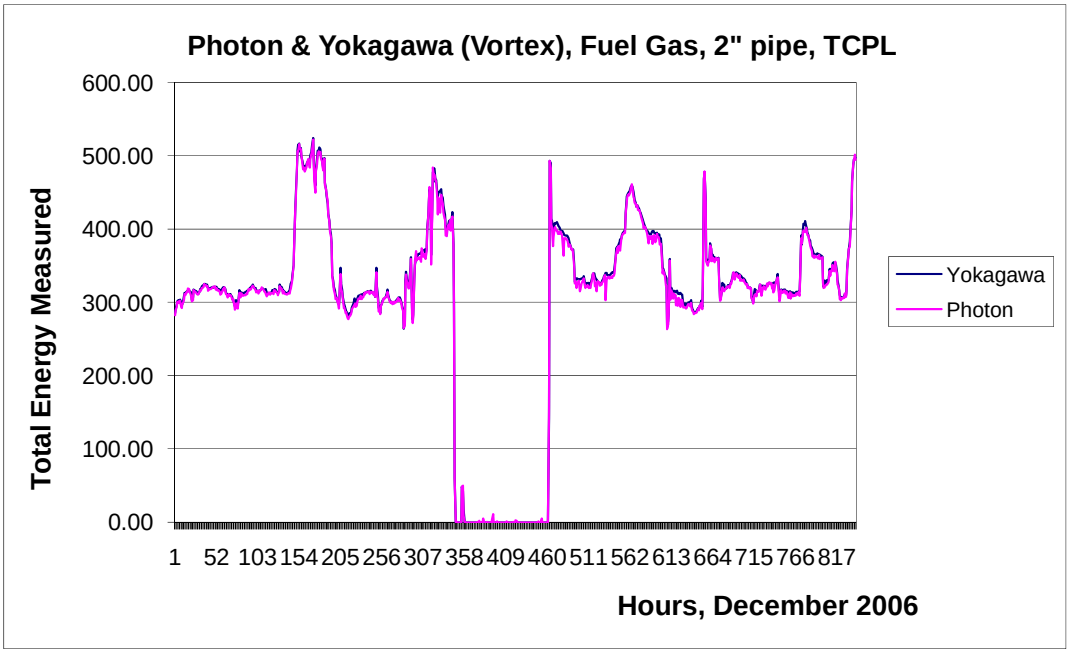

Figure 15. Comparison of a flanged L2F and a 2-inch Yokogawa vortex flow meter in a fuel gas line.

2.3.4. Wet Gas Flare Measurement

The majority of commercial OFM installations occur without the benefit of a comparison with other meters. OFMs are supplied calibrated from the Photon Control production facility.

A rare case of being able to compare the results between an OFM and a conventional meter is shown in Figure 16. Here, the flow data from an OFM and that from a thermal mass meter are presented, both measuring low pressure biogas at the Lulu Island waste treatment plant in Richmond, British Columbia.

The reason for installing the OFM was that the user had expressed concern about significant apparent over-readings by the thermal mass meter, especially in warm weather. Direct comparison with the OFM demonstrated a discrepancy between the two devices.

Whilst the OFM averaged about 1 m/sec almost continuously, the reading from the thermal mass meter steadily rose to as much as 65 m/sec after several days. The readings from the OFM matched the calculated flow rates based on the total amount of energy provided to the generator.

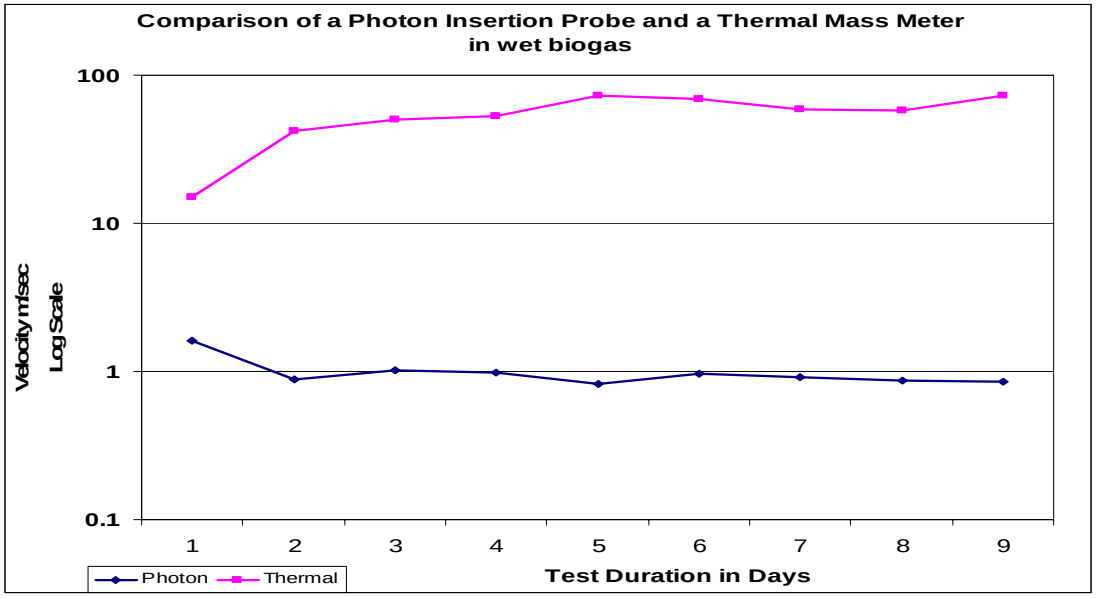

Figure 16. Insertion OFM against thermal mass meter in a 16-inch pipe, biogas plant

3. CONCLUSIONS

A recent editorial in The Wall Street Journal, it was reported that a World Bank-financed study valued the amount of flared gas in 2006 as being about $40 billion, and due to a variety of reasons this value had risen by 14% from 2004. It also noted that flaring had dropped significantly in two countries, Norway and Canada, due to implementation of measurement controls and a stiff 'carbon tax'. It is interesting that in both these countries home-based flare metering initiatives have been developed and continue to be enhanced.

The product related in this paper is a direct result of vision and partnership between an Optical sensor manufacturer with R&D capability and an Oil and Gas Operator.

Through many years of flare metering, the authors have come to the conclusion that there is no silver bullet when it comes to flare metering. The authors have direct experience with many applications and installations, both onshore and offshore, none of which have been 100% satisfactory.

These issues include:

- Limited accuracy in the low end of the meter range (±15% or more inaccuracy), where probably 95% of all flare and vent flows occur.
- High cost of installation and maintenance
- Limited rangeability, meaning for some regulators, there is a need for multiple meters to cover the full flow range of the flare
- Composition dependency
- Flow restrictions

By thinking "outside the box", and based on preliminary discussions and a full understanding of both COPC and the local regulatory requirements, COPC began to work with Photon Control to test their Optical meter at a sour gas facility. As with any new product there were issues to overcome. The testing revealed that the meter needed:

(1) more robust electronics,

(2) a protective shroud,

(3) a way of retrieving the probe without shutdown (retractable device), and

(4) a calibration curve to move to within an acceptable accuracy of +/- 5%.

The parties worked through these issues together, and COPC now have seven flare metering installations. These installations have now accumulated about 11 man-years of operation time and are functioning correctly.

These installations are now able to maintain a closer plant balance, which gives the impression that the meters are more accurate and dependable than any previous flare metering devices. The COPC Operations and Engineering personnel are comfortable making facility decisions based on the meter information.

The advantages of accurate flare metering include:

- meeting Regulatory and environmental requirements,
- understanding your facility process, and
- making decisions based on good data.

The return on capital employed to install these meters was minimal compared to the benefits, and it has, it is felt, been adequately repaid based on a reduction in the loss of background gas. In many facilities a large quantity of background gas goes up the stack unnoticed. Flare reduction is not just an environmental responsibility, it affects the facility's bottom line. Wasted gas is lost profit, and more importantly an unnecessary environmental load.

COPC are now in a position where there is trust in the flare measurments, following close to 11 man-years of operation, and using the axiom that you "cannot optimize what you have not measured", are now in a position to optimize and manage an area of the facility operations which heretofore had been unmanageable.

4. REFERENCES

(1) Thompson, D.H. (1968). A tracer-particle fluid velocity meter incorporating a laser. J. Sci. Intsr. S.2, v.1 pp.929-932.

(2) Schodl, R. (1976). On the extension of the range of applicability of LDA by means of the laser-dual-focus (L2F) technique. The Accuracy of Flow Measurement by Laser Doppler Methods, pp.480-489

(3) Azzazy, M. (1990). Development of an Optical Volumetric Flowmeter. Spectron Development Labs., Inc., Costa Mesa, CA. Final Report

(4) Kiel, D.E. and Williamson, I.D., (2000). Optical flow meter integrally mounted to a rigid plate with direct optical access to the interior of a pipe, US Patent No 6128072

(5) Williamson, I.D., Sharonov, S., Daniel P-J. and Kiel, D.E. (2002). Optical flow meter capable of operating with a variable refractive index, US Patent No.6429926

(6) Smart, A.E. and Abbiss, J.B, (1988). Discrimination techniques for a highly accurate laser-sheet anemometer", 7th Int. Conf. Photon Correlation Techniques and Applications Abbiss and Smart (eds) v. 1. OSA, pp.109-116

(7) Schodl, R. (1976). On the extension of the range of applicability of LDA by means of the laser-dual-focus (L2F) technique. The Accuracy of Flow Measurement by Laser Doppler Methods, pp.480-489.

(8) Smart, A.E. and Abbiss, J.B, (1992). On-board correlator-based measurements of particle properties and aircraft velocity in the upper atmosphere. Int. Conf. Photon Correlation Techniques and Applications Abbiss and Smart (eds). OSA

(9) Testing of Insertion Probe Flow meter, CEESI, report No: 05RN-CE01743, 2005

(10) Ting-I Wang, (2003). Optical flow sensor using a fast correlation algorithm, US Patent No. 6611319

(11) Report of special test of optical flow sensor (OFS) at NIST, April 2001. Available at www.opticalscientific.com

(12) Hyde J. (2002) Gas velocity measurement by infrared radiation absorption. WIPO 02/077578 A1.

(13) Gibson J. and Hyde J. (2006) A novel infrared absorption technique for measuring flare gas flow. 24th Int. North Sea Flow Measurement Workshop. NEL.

(14) Blake, J.N. and Tselikov A.A., (2003). Fiber optic alignment system and method. US Patent No. 6545261

(15) De Carvalho, R. and Blake,J.N., (1994) Slow-flow measurements and fluid dynamics analysis using the Fresnel drag effect, App. Opt.., vol. 33, pp. 6073-6077.

(16) Melnyk I. (2005). Novel technique for flare gas measurement – optical L2F gas flow meters, NEL Flare Gas Measurement and Reporting Seminar, Aberdeen, June 15.

(17) Rans R. (2006). Summary Report of the CEESI Tests of the FOCUS ™ Probe Optical Gas Flow Meter Sept 19-30 2005. Prepared by RanSolution, March 2006, available at www.photon-control.com

(18) Melnyk I. (2005). The theory and application of optical flow meters in the natural gas industry. WGMSC, Reno, Nevada.

Uncertainty analysis of emissions from the Statoil Mongstad oil refinery

Kjell-Eivind Frøysa[1], Anne Lise Hopland Vågenes[2], Bernhard Sørli[2] and Helge Jørgenvik[2]

[1]Christian Michelsen Research AS, Box 6031 Postterminalen, N-5892 Bergen, Norway.
[2]Statoil Mongstad, 5954 Mongstad, Norway

ABSTRACT

In new European and national legislations, there is increased focus on the reporting of the emmissions related to greenhouse gases from process plants. This includes reporting and documentation of uncertainty in the reported emmissions, in addition to specific uncertainty limits depending on the type of emission and type of measurement regime.

In a process plant like the Statoil Mongstad oil raffinery, there may be a huge number of measurement points for mass flow. These measured mass flow rates have to be added in order to obtain the total emission for a given source. Typically, orifice plates are used at many of the measurement points. These orifice plate meters are ususally not equipped with individual densitometers. In stead, they are pressure and temperature corrected from a common upstream densitometer. This will give correllations between the individual flow meters.

In the present paper, the flow meter set-up for Statoil Mongstad will be briefly addressed. thereafter, an uncertainty model suitable for the CO_2 emission from the Statoil Mongstad oil raffinery will be presented, included a practically method for handling the partial correllation between the uncertainty of the various flow meters. This model will comply with the ISO 5168 for measurement uncertainty. Various uncertainty contributions will be reviewed, in order to work out an uncertainty budget for the specific emission sources. From these results and the use of a specially developed calculation tool, improvements on the instrumentation have been suggested in order to reduce the uncertainty, both in a short and a long time range. In particular, it is necessary to plan the flow metering instrumentation so that the uncertainty is maintained also for the new gas flow regime that will appear when the new gas power plant at Statoil Mongstad is ready.

1. INTRODUCTION

The refinery at Mongstad, north of Bergen, Norway has a capacity of 12 million tons crude oil and condensate per year. It is a medium complex refinery, which is medium sized and with high upgrading capacity. It is the largest refinery in Norway. The largest production is petrol, diesel, aviation petrol and other light petroleum products. The production of petrol at Mongstad is about one and a half time the total Norwegian consumption. Most of the production from the refinery is exported, especially to Europe.

Fig. 1 Overview over the Statoil Mongstad oil refinery

National and European regulations requires report of the CO_2 emissions from e.g. Mongstad, within given uncertainties [MRG, 2007], [SFT, 2007]. The uncertainty of the reported CO_2 emissions has to be documented. If the uncertainty is not within the requirements, the authorities can give orders on specified improvements in order to reduce the uncertainty.

The uncertainty requirement is classified in Tiers. These put requirements to the uncertainty in the reported values of activity data (mass consumption of fuel gas) and in carbon factor (quantity

CO_2 produced when burning a given quantity if gas). Tier 4 is the highest tier-approach, and Tier 1 the lowest tier approach. For emissions larger than 500 000 ton/year, the highest Tier shall be used for all major source streams. The reporting to the authorities are typically pr energy carrier.

The fuel gas at Statoil Mongstad is under Tier 4. The uncertainty limits under Tier 4 are different depending on the type of gas. For fuel gas, Tier 4 gives an uncertainty limit of 1.5 % for activity data, and 0.5 % for carbon factor, both with 95 % confidence level. The flare gas at Statoil Mongstad is under Tier 3, which is the highest Tier for that gas type. Here the uncertainty limits are 7.5 % for activity data, and 2.5 % for carbon factor.

The main part of this paper discusses the uncertainty in the activity data (Section 3 and 4). Some considerations regarding the uncertainty of the carbon factor has also been given in Section 5.

2. INSTRUMENTATION AND REPORTING AT STATOIL MONGSTAD

The CO_2 emission at Statoil Mongstad originates from a variety of different sources. A variety of mass flow measurements of fuel gas are carried out throughout the refinery. The CO_2 emissions are calculated from the activity data and the carbon factor. For the reporting of the CO_2 emission, the various fuel gas flows are grouped together in some groups (for 2006: five groups), based mainly on energy carrier. The various sources thus have different gas composition in the fuel gas.

The various mass flows are measured by different flow metering principles. These include

- Orifice plates
- Venturi meters
- Annubar differential pressure meters
- Coriolis meters
- Ultrasonic flare gas meters

In addition, some small gas flows are estimated, and a fixed number is used. By far the most commonly used mass flow meter principle at Statoil Mongstad is the orifice plate. The density is typically measured far upstream the orifice plates, and calculations are carried out in order to compensate for the pressure and temperature differences from the densitometer to the orifice plate.

3. UNCERTAINTY MODEL

The uncertainty model for a given source (group of mass flows) consists of the uncertainty model for the various individual flow meters, and a model for the sum of the various flow meters. This includes the evaluation of correlated and uncorrelated contributions between the different flow meters. It should be mentioned that the final uncertainty model does not only depend on the type of flow meters, but also on the operation of the various flow meters. This will be illustrated below.

As an illustrating example, it is here chosen to show the uncertainty model for the sum of the flow through two orifice plates. It is assumed in the example that upstream the two orifice plates, the gas density is measured, in addition to the pressure and temperature. Downstream the densitometer, the gas is split into two pipes, and orifice plates measure the flow through each of them. The gas composition is thereby the same for the gas through both orifice plates. In order to find the gas density upstream each of the two orifice plates, the pressure and temperature upstream the two orifice plates is to be used. This is either measured or estimated by other means.

The uncertainty model should cover both cases. It should here be mentioned that in the calculation of density at upstream orifice conditions, ideal gas law is assumed. this is because of the low pressure at similar installations at Statoil Mongstad.

The uncertainty model can be further extended to several orifice plates and to combinations of various flow meter technologies, included correlations between some and not all the flow meters.

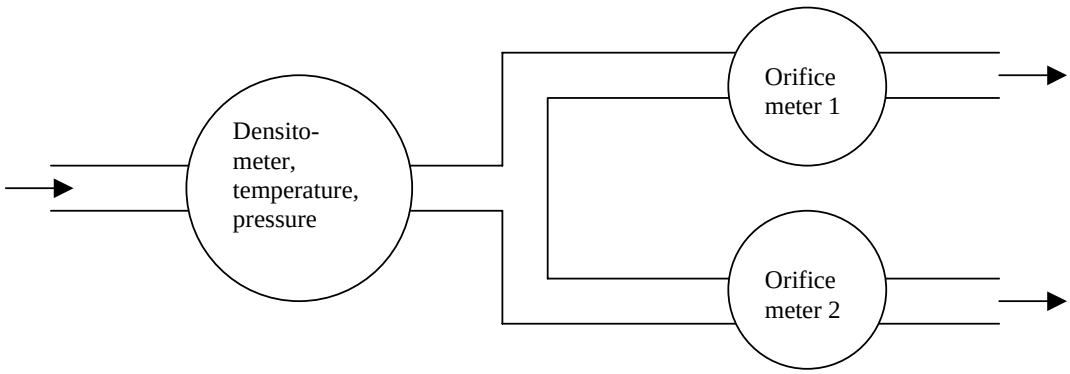

Fig. 2 Metering configuration for the illustrative example

3.1. Orifice plate uncertainty model

It is well known that in the flow-metering situation using orifice plates, measurement of differential pressure over the orifice plate is carried out. In addition, pipe and orifice diameter, discharge coefficient, expansibility factor and upstream gas density are needed. The functional relationship for the mass flow rate is in this case:

$$q_m = \frac{C}{\sqrt{1-(d/D)^4}}\,\varepsilon\,\frac{\pi}{4}\,d^2\sqrt{2\rho_M \Delta P} \qquad (1)$$

where

q_m	mass flow rate
C	discharge coeffisient
ε	expansibility coeffisient
d	orifice diameter, at line conditions
D	pipe diameter, at line conditions
ρ_M	density upstream the orifice plate
ΔP	differential pressure over the orifice plate

In the example to be discussed here, the density is determined from the measured density at densitometer conditions, and pressure and temperature corrections to the conditions upstream the orifice plate:

$$\rho_M = \rho_0 \frac{P_M T_0}{P_0 T_M} \qquad (2)$$

where

ρ_0	density at densitometer conditions
T_0	absolute temperature at densitometer conditions

P_0	pressure at densitometer conditions
T_M	absolute temperature upstream orifice plate
P_M	pressure upstream orifice plate

The relative standard uncertainty of the mass flow rate measured by an orifice plate, can now be found using [ISO 5167] in addition to the extra terms from the temperature and pressure calculations for the density from densitometer to orifice plate conditions:

$$\begin{aligned}\left(\frac{u(q_m)}{q_m}\right)^2 &= \left(\frac{u(C)}{C}\right)^2 + \left(\frac{u(\varepsilon)}{\varepsilon}\right)^2 + \left(\frac{2\beta^4}{1-\beta^4}\right)^2\left(\frac{u(D)}{D}\right)^2 \\ &+ \left(\frac{2}{1-\beta^4}\right)^2\left(\frac{u(d)}{d}\right)^2 + \frac{1}{4}\left(\frac{u(\Delta P)}{\Delta P}\right)^2 + \frac{1}{4}\left(\frac{u(\rho_0)}{\rho_0}\right)^2 \\ &+ \frac{1}{4}\left(\frac{u(P_0)}{P_0}\right)^2 + \frac{1}{4}\left(\frac{u(T_0)}{T_0}\right)^2 + \frac{1}{4}\left(\frac{u(P_M)}{P_M}\right)^2 + \frac{1}{4}\left(\frac{u(T_M)}{T_M}\right)^2\end{aligned} \tag{3}$$

It should be mentioned that it here is assumed that all uncertainty contributions (from discharge coefficient, expansibility coefficient, diameters, differential pressure, measured density, pressure and temperature) are here assumed to be mutually uncorrelated.

3.2. Correlations

A typical situation to be addressed when adding several mass flow rate measurements into a single number is the issue of correlation between the various measured flow quantities. This is briefly addressed in the EU guidelines [MRG, 2007], where the formulas for uncertainty for a sum and a product are given, when the various terms/factors are either uncorrelated or fully correlated. However, these models are too simple to be used in practice in a situation where partial correlation between two or more measured flow rates exist. Therefore, two more extensive methods that cover such situations will be presented here. These are the covariance method and the decomposition method.

The ***covariance method*** is the classical way of treating partial correllation between quantities. It is recommended in ”Guide to the expression of uncertainty in measurement” [ISO, 1995]. In short, it can be presented in the following way: Let

$$z = f(x, y) \tag{4}$$

The standard uncertainty in $u(z)$, is to be expressed by the standard uncertainties of x and y ($u(x)$ og $u(y)$). The classical approach is as follows

$$u(z)^2 = \left(\frac{\partial f}{\partial x}u(x)\right)^2 + \left(\frac{\partial f}{\partial y}u(y)\right)^2 + 2r(x,y)\frac{\partial f}{\partial x}\frac{\partial f}{\partial y}u(x)u(y) \tag{5}$$

where $r = 0$ if x and y are fully uncorrellated and $r = 1$ if x and y are fully correllated. In general, r is a number between –1 and 1. By partial correllation, the r – value has to be determined. It may be a challenging task to do this determination in an objective way.

The ***decomposition method*** is used in ISO 5168, Annex J. It is here assumed that the contributions to the standard uncertainty in x and y originate from different sources of uncertainty. Some of these contributions can be correllated (r = 1) and other can be uncorrellated (r = 0) between x and y. in this way, the standard uncertainty in x and y can be written as

$$\begin{aligned} u(x)^2 &= u(x_C)^2 + u(x_U)^2 \\ u(y)^2 &= u(y_C)^2 + u(y_U)^2 \end{aligned} \tag{6}$$

where the indexes C and U denote the correllated and the uncorrellated contributions, respectively. The correllated and the uncorrellated uncertainty contributions are treated separately, with r set to 1 and 0, respectively. Then, the following formula is obtaind for the standard uncertainty in z:

$$u(z)^2 = \left(\frac{\partial f}{\partial x} u(x_U)\right)^2 + \left(\frac{\partial f}{\partial y} u(y_U)\right)^2 + \left(\frac{\partial f}{\partial x} u(x_C) + \frac{\partial f}{\partial y} u(y_C)\right)^2 \tag{7}$$

The advantage of this formula is that it is not necessary to determine a value for r. However, the various uncertainty contributions for x and y have to be studied and classified as either correllated or uncorrellated between x and y.

In the NFOGM, NPD and CMR handbook for ultrasonic gas flow metering stations [Lunde and Frøysa, 2001] this formalism is derived from a formal decomposition:

$$\begin{aligned} x &= x_C + x_U \\ y &= y_C + y_U \end{aligned} \tag{8}$$

This decomposition is just formal, and does not represent a physical interpretation. The correllated contributions to the uncertainty are there associated with x_C and y_C, and the uncorrellated contributions with x_U and y_U. It can be showns that

$$\begin{aligned} \frac{\partial f}{\partial x_C} &= \frac{\partial f}{\partial x_U} = \frac{\partial f}{\partial x} \\ \frac{\partial f}{\partial y_C} &= \frac{\partial f}{\partial y_U} = \frac{\partial f}{\partial y} \end{aligned} \tag{9}$$

Now r = 1 is set for the correllation between x_C and y_C, and r = 0 between all the other variables. Then Eq. (7) is obtained.

It is possible to go do calculations from the decomposition method to the correlation method in the following way. Eq. (7) can be re-written as

$$\begin{aligned} u(z)^2 = &\left(\frac{\partial f}{\partial x}\right)^2 \left(u(x_U)^2 + u(x_C)^2\right) + \left(\frac{\partial f}{\partial y}\right)^2 \left(u(y_U)^2 + u(y_C)^2\right) \\ &+ 2\frac{\partial f}{\partial x}\frac{\partial f}{\partial y} u(x_C) u(y_C) \end{aligned} \tag{10}$$

By using Eq. (6), this can be written

$$u(z)^2 = \left(\frac{\partial f}{\partial x}\right)^2 u(x)^2 + \left(\frac{\partial f}{\partial y}\right)^2 u(y)^2 + 2\frac{\partial f}{\partial x}\frac{\partial f}{\partial y} u(x_C)u(y_C) \qquad (11)$$

This can further be written as

$$u(z)^2 = \left(\frac{\partial f}{\partial x}\right)^2 u(x)^2 + \left(\frac{\partial f}{\partial y}\right)^2 u(y)^2 + 2\frac{u(x_C)u(y_C)}{u(x)u(y)}\frac{\partial f}{\partial x}\frac{\partial f}{\partial y} u(x)u(y) \qquad (12)$$

which is Eq. (5) with the following expression for *r*:

$$r(x,y) = \frac{u(x_C)u(y_C)}{u(x)u(y)} = \frac{u(x_C)u(y_C)}{\sqrt{u(x_U)^2 + u(x_C)^2}\sqrt{u(y_U)^2 + u(y_C)^2}} \qquad (13)$$

It is thereby shown that these two methods are equivalent. In addition, the decomposition method provides a formula for calculation of *r*.

For the use in the example mentioned above with two orifice plates, each input uncertainty contribution has to be evaluated with respect to correllation or not between the two orifice plates in question. For this example, the following considerations have been made:

Discharge coefficient: Because the flow profiles are never quite the same in two independent installations, the uncertainty contributions from the discharge coefficients are uncorrelated between the two orifice plates.

Expansibility coefficient: Because flow profiles, pressure and temperatureare never the same in two independent installations, the uncertainty contributions from the expansibility factor are uncorrelated between the two orifice plates.

Pipe diameter: If the pipes at the two orifice plates are produced independently of each other (as when the pipe dimensions are different between the two orifice plate installations, the uncertainty contributions from the pipe diameter can be regarded as uncorrelated between the two orifice plates. However, if they are produced in the same batch of pipes, it may be more correct to regard them as being correlated. In the present work, they are considered to be uncorrellated.

Orifice diameter: The orifice plates are typically produced independently of each other. Often, the orifice plates are of different size, and they are measured by independent measurements. Therefore, they are regarded as uncorrelated between the two orifice plates. There may, however, be a small correlation between the two orifice plates when the same measurement system is used for measurement of the orifice diameter in the two plates. This is from the calibration of the measurement system. In the work reported here, this correlated contribution has been evaluated and found to be small enough to be neglected.

It should, however, be commented that there is a correlation between the pipe diameter and the orifice diameter on each orifice plate, from the common temperature expansion. This will be the case both if the temperature expansion is corrected for and if it is not. This is addressed in [Dahl

et al, 2003], where the covariance method is applied. In the present work, the equivalent decomposition method has been used.

Differential pressure: This quantity is measured by separate differential pressure transmitters for the two orifice plates. This uncertainty contribution is therefore considered to be uncorrelated between the orifice plates. However, due to common calibration facility for the two differential pressure transmitters, there will be a small correlation between the two orifice plates. In the work reported here, this correlated contribution has been evaluated and found to be small enough to be neglected.

Density at densitometer conditions: The density measured by the densitometer is used as input to both orifice metering stations. This uncertainty contribution is therefore correlated between the two orifice plates.

Pressure at densitometer conditions: This quantity is used as input to both orifice metering stations. This uncertainty contribution is therefore correlated between the two orifice plates.

Temperature at densitometer conditions: This quantity is used as input to both orifice metering stations. This uncertainty contribution is therefore correlated between the two orifice plates.

Pressure at upstream orifice conditions: If this is measured with separate dedicated pressure transmitters, they will be uncorrelated between the two orifice plates. However, due to common calibration facility for the two pressure transmitters, there will be a small correlation between the two orifice plates. In the work reported here, this correlated contribution has been evaluated and found to be small enough to be neglected. In the case where the pressure is not measured, but just estimated, the uncertainty may be correllated or uncorrelated between the two orifice plates, depending on the process in question. In the work presented here, the uncertainty contributions when the pressure is measured are considered as uncorrelated. This conclusion is supported by measurements campains at the plant.

Temperature at upstream orifice conditions: If this is measured with separate dedicated temperature transmitters, they will be uncorrelated between the two orifice plates. However, due to common calibration facility for the two temperature transmitters, there will be a small correlation between the two orifice plates. In the work reported here, this correlated contribution has been evaluated and found to be small enough to be neglected. In the case where the temperature is not measured, but just estimated, the uncertainty may be correllated or uncorrelated between the two orifice plates. In order to account for both these cases, the model will include both a correlated and an uncorrelated term for this quantity.

Based on the considerations above, the following uncertainty model can be specified for the uncertainty for the sum of the two mass flow rates measured by the two orifice plates, included correlations between the orifice plates:

$$
\begin{aligned}
\left(\frac{u(q_m)}{q_m}\right)^2 = \left(\frac{q_{m1}}{q_m}\right)^2 \Bigg\{ & \left(\frac{u(C_1)}{C_1}\right)^2 + \left(\frac{u(\varepsilon_1)}{\varepsilon_1}\right)^2 + \left(\frac{2\beta_1^{\,4}}{1-\beta_1^{\,4}}\right)^2 \left(\frac{u(D_1)}{D_1}\right)^2 \\
& + \left(\frac{2}{1-\beta_1^{\,4}}\right)^2 \left(\frac{u(d_1)}{d_1}\right)^2 + \frac{1}{4}\left(\frac{u(\Delta P_1)}{\Delta P_1}\right)^2 \\
& + \frac{1}{4}\left(\frac{u(P_{M1})}{P_{M1}}\right)^2 + \frac{1}{4}\left(\frac{u(T_{M,U1})}{T_{M,U1}}\right)^2 \Bigg\} \\
& + \left(\frac{q_{m2}}{q_m}\right)^2 \Bigg\{ \left(\frac{u(C_2)}{C_2}\right)^2 + \left(\frac{u(\varepsilon_2)}{\varepsilon_2}\right)^2 + \left(\frac{2\beta_2^{\,4}}{1-\beta_2^{\,4}}\right)^2 \left(\frac{u(D_2)}{D_2}\right)^2 \\
& + \left(\frac{2}{1-\beta_2^{\,4}}\right)^2 \left(\frac{u(d_2)}{d_2}\right)^2 + \frac{1}{4}\left(\frac{u(\Delta P_2)}{\Delta P_2}\right)^2 \\
& + \frac{1}{4}\left(\frac{u(P_{M2})}{P_{M2}}\right)^2 + \frac{1}{4}\left(\frac{u(T_{M,U2})}{T_{M,U2}}\right)^2 \Bigg\} \\
& + \frac{1}{4}\left(\frac{u(\rho_0)}{\rho_0}\right)^2 + \frac{1}{4}\left(\frac{u(P_0)}{P_0}\right)^2 + \frac{1}{4}\left(\frac{u(T_0)}{T_0}\right)^2 \\
& + \frac{1}{4}\left(\frac{q_{m1}}{q_m}\frac{u(T_{M,C1})}{T_{M,C1}} + \frac{q_{m2}}{q_m}\frac{u(T_{M,C2})}{T_{M,C2}}\right)^2
\end{aligned}
\tag{14}
$$

In this formula, the indexes U and C represent uncertainty contributions that are uncorrelated and correlated between the two orifice plates, respectively. Index 1 and 2 corresponds to the two orifice plates.

For simplicity, the terms handling the correlation between d and D due to temperature expansion are omitted. However, in the calculation example presented in Section 4, this effect is included.

3.3. Model for Source 1 at Statoil Mongstad

The total flow rate at each source at Statoil Mongstad is a sum of the measured flow rates at a variety of flow metering points. Here, one of these sources (here denoted as “Source 1”), with 16 orifice plates and one minor point where the flow rate is estimated, will be discussed. These 16 orifice plates have one common densitometer, similar to the situation discussed above. In Fig. 3, some details on this source are given, regarding densitometer position (marked with “D”), flow meter position (marked with “F”) and detailing of number of heaters and boilers.

A classification of correlated and uncorrelated contributions similar to the one carried out above, has been done for this source. The discussion is similar as above, but the more detailed and process plant specific details in the discussion will not be presented. Based on this discussion, a full uncertainty model for the whole source is established. This is similar to the model for two orifice plates discussed above, but extended to 16 orifice plates and one estimated point.

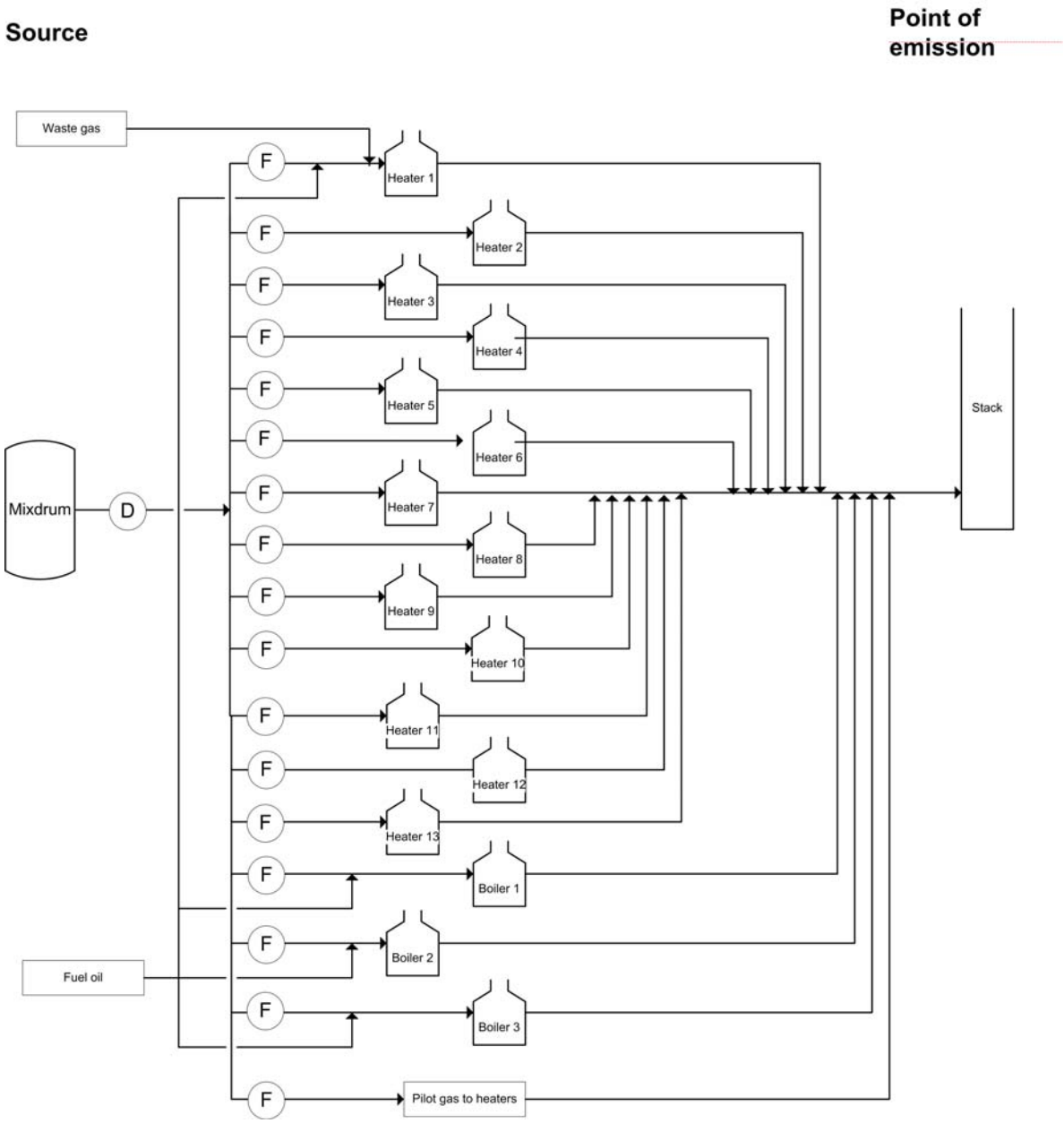

Fig. 3 Overview over Source 1. "D" denotes the location of the densitometer, and "F" denotes a mass flow meter.

4. CALCULATION EXAMPLE

4.1. Input uncertainties

An important issue in the uncertainty analysis, is the specification of the input uncertainties.

All the input uncertainty quantities should be documented based on vendor specifications or considerations based on the process in question. In cases where there may be doubt about the input specification, it is chosen to be on the conservative side, so that the uncertainty is not underestimated. The following considerations have been carried out:

Discharge coefficient: The orifice plates are installed according to ISO 5167. The quantity and the uncertainty of the discharge coefficient is therefore calculated according to ISO 5167.

Expansibility coefficient: The orifice plates are installed according to ISO 5167. The quantity and the uncertainty of the expansibility coefficient is therefore calculated according to ISO 5167. It should be mentioned that this quantity may be largely flow dependent, and should therefore be recalculated when the flow rate is changing.

Pipe diameter: Vendor specification.

Orifice diameter: Vendor specification.

Differential pressure: The uncertainty of the differential pressure measurement is calculated according to the Handbook [Dahl et al, 2003], with vendor specification and installation/calibration specifications for the differential pressure transmitter in question. Also this quantity may be largely flow dependent, and should therefore be recalculated when the flow rate is changing.

Density at densitometer conditions: The uncertainty of the density measurement is calculated according to the Handbook [Dahl et al, 2003], with vendor specifications for the densitometer in question. Velocity of sound correction is not carried out, and contributes therefore to increased uncertainty.

Pressure at densitometer conditions: This uncertainty is calculated according to the handbook [Dahl et al, 2003], with vendor specifications for the pressure transmitter in question.

Temperature at densitometer conditions: This uncertainty is calculated according to the handbook [Dahl et al, 2003], with vendor specifications for the temperature transmitter in question.

Pressure at upstream orifice conditions: For some orifice plates, the pressure is measured. In these cases, the uncertainty is calculated according to the Handbook [Dahl et al, 2003], with vendor specifications for the pressure transmitter in question. For the other orifice plates, the relative standard uncertainty is estimated to 5 % (10 % with 95 % confidence level), in order to be sure not to underestimate this quantity.

Temperature at upstream orifice conditions: For three of the orifice plates, there is a common temperature measurement. In this case, the correlated standard uncertainty of the temperature estimate is set to 0.5 °C, due to specifications of the temperature transmitter. The uncorrelated standard uncertainty is set to 1.5 °C in order to account for some uncorrected variation in temperature between the orifice plates. For the other orifice plates, the temperature is estimated. The standard uncertainty is here set to 5 °C correlated contribution and 5 °C uncorrelated contribution. This uncertainty specification is based on 3 measurement campains during 2006 at some orifice plates. The variation in temperature between the orifice plates, and over time give some input for estimating the uncertainty. In addition, there is accounted for some extra variation.

4.2. Results for 2006

The results for the uncertainty of source 1 have been calculated according to the model and input uncertainties described above. The results are shown in Fig. 4, where the uncertainty contribution

from each of the 16 orifice plates and the one estimated flow are shown, in addition to the relative expanded uncertainty for the source in total (for total flow measured from all the 17 measurement points). It can be seen that the relative expanded uncertainty is calculated to about 1.89 %. In Table 1, the *r* values for the correlation between the various flow meters are shown. Note that these values are not actively used in the calculations, but are calculated afterwards from the uncertainty results, using a generalised version of Eq. (13).

The calculated relative expanded uncertainty of 1.89 % is outside the requirement from the authorities that in this specific case is 1.5 %. Therefore, it has been looked for corrections to the instrumentation set-up in order to reduce the uncertainty. From Fig. 4, it is seen that orifice plate no. 1 contributes most to the uncertainty for the total source. This is not because of especially large uncertainty for the measured flow rate of that specific orifice plate. Instead it is because the flow through that orifice plate is by far the largest for that source. Therefore, that orifice plate is weighted more than the other orifice plates in the total uncertainty budget.

In Fig. 5, the various uncertainty contributions for the flow measurement using orifice plate 1 are shown. It can be seen there that by far the largest uncertainty contributions are from temperature at the orifice plate. This is because the temperature at the orifice plate is estimated, and not measured. It was therefore recommended to install a temperature measurement upstream this orifice plate. In August 2007, this new temperature measurement was set into operation. The uncertainty analysis was thereafter re-calculated with the reduced uncertainty contribution from the temperature upstream the orifice plate appearing after installation of the temperature measurement. The results from that calculation are shown in Fig. 6. It can be seen that the uncertainty contribution from orifice 1 to the uncertainty of the total flow in the source is significantly reduced compared to Fig. 4. The relative expanded uncertainty for the total flow in source 1 is now well within the requirement of 1.5 %. This illustrates how the uncertainty model and analysis can be used as a documentation of the uncertainty as per today and also as a tool for planning modifications of the instrumentation in order to reduce the uncertainty.

Finally it should be mentioned that it is not only new instrumentation that can change the uncertainty. Significant changes in flow rates, both in total and individually between the orifice plates will also affect the uncertainty results, even when the instrumentation is unchanged. There are several reasons for that, e.g. the following:

- The uncertainty of the differential pressure measurement is flow velocity dependent
- The uncertainty of the expansibility factor is flow velocity dependent
- The weighting of the uncertainty between the different orifice plates is changed when the flow rates are changed.

This means that when there are significant changes in the flow rates in a process plant, the uncertainty should be re-calculated. For Statoil Mongstad, this will be the case when the new energy plant (gas power plant) will be opened.

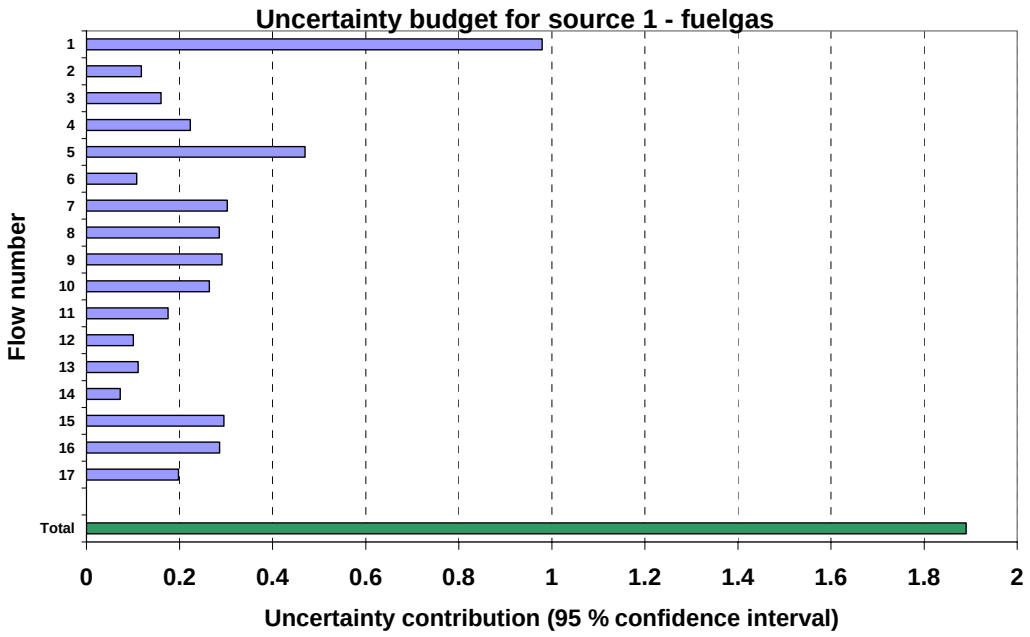

Fig. 4 Uncertainty budget for Source 1, 2006 results

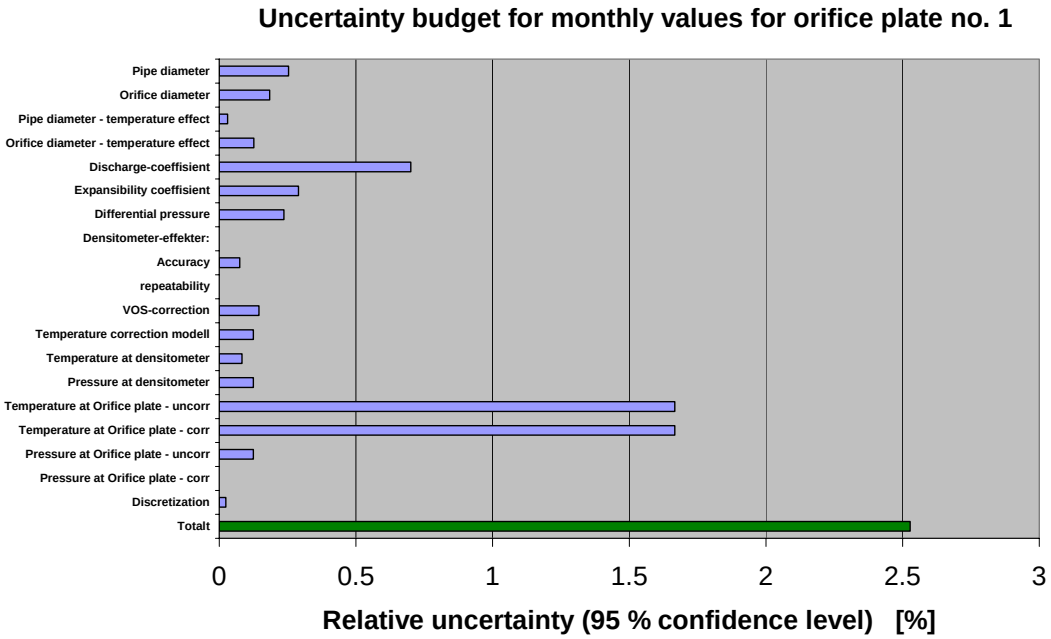

Fig. 5 Uncertainty budget for orifice plate no. 1 in Source 1, 2006 results.

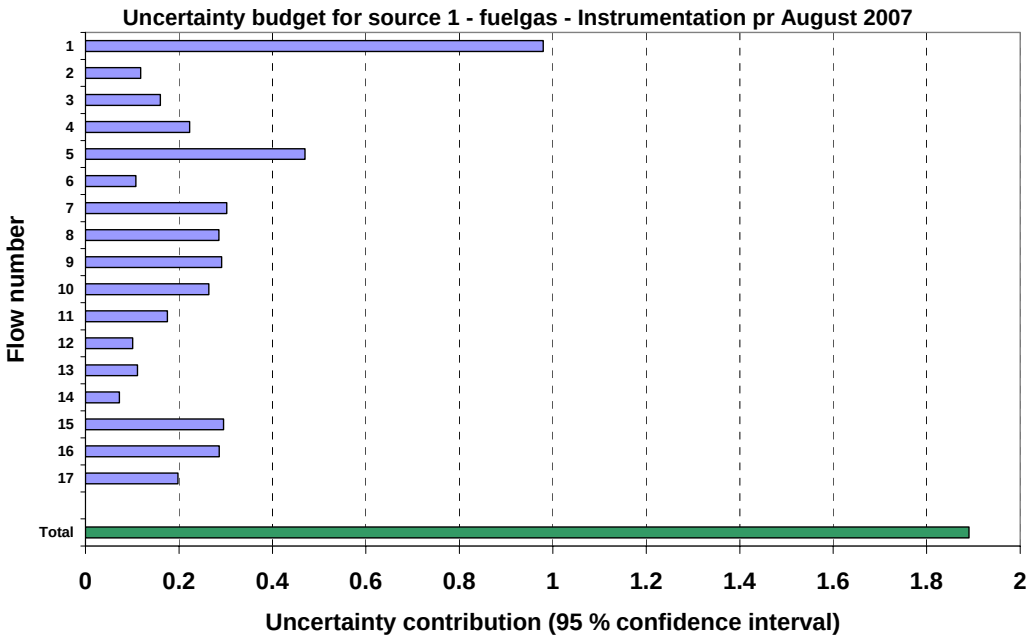

Fig. 6 Uncertainty budget for source 1, 2006 results, but with an extra temperature sensor installed at orifice plate no. 1.

Table 1 r-value implicitly used for the covariance between the uncertainty of the various flow measurements in Source 1.

	1	**2**	**3**	**4**	**5**	**6**	**7**	**8**	**9**	**10**	**11**	**12**	**13**	**14**	**15**	**16**	**17**
1		0.203	0.203	0.203	0.201	0.203	0.202	0.201	0.202	0.202	0.203	0.202	0.000	0.203	0.043	0.042	0.042
2			0.092	0.092	0.091	0.092	0.091	0.091	0.091	0.091	0.092	0.091	0.000	0.092	0.019	0.019	0.019
3				0.092	0.091	0.092	0.091	0.091	0.091	0.091	0.092	0.091	0.000	0.092	0.019	0.019	0.019
4					0.091	0.092	0.091	0.091	0.091	0.091	0.092	0.091	0.000	0.092	0.019	0.019	0.019
5						0.091	0.091	0.090	0.091	0.091	0.091	0.091	0.000	0.091	0.019	0.019	0.019
6							0.091	0.091	0.091	0.091	0.092	0.091	0.000	0.092	0.019	0.019	0.019
7								0.091	0.091	0.091	0.091	0.091	0.000	0.091	0.019	0.019	0.019
8									0.091	0.091	0.091	0.091	0.000	0.091	0.019	0.019	0.019
9										0.091	0.091	0.091	0.000	0.091	0.019	0.019	0.019
10											0.091	0.091	0.000	0.091	0.019	0.019	0.019
11												0.091	0.000	0.092	0.019	0.019	0.019
12													0.000	0.091	0.019	0.019	0.019
13														0.000	0.000	0.000	0.000
14															0.019	0.019	0.019
15																0.004	0.004
16																	0.004
17																	

5. CARBON FACTOR

The carbon factor is a factor that specifies the quantity of CO_2 that is obtained from burning a specified quantity of fuel gas. It can e.g. be given in kg CO_2 pr kg fuel gas. This carbon factor can be calculated from the fuel gas composition.

The carbon factor is determined in several ways depending on the actual situation at the process plant in question. Some examples are:

- Online GC for the fuel gas.
- Online GC for a fuel gas that is close to but not equal to the fuel gas in question.
- Regular sampling and laboratory analysis of the gas composition e.g. on a daily, weekly or monthly basis.
- Some few sampling and laboratory analyses for giving an indication of the carbon factor.
- In cases of mixing of various flows of various known gas qualities to a final gas: assumption of the mixing ratios in this mixing.

The uncertainty of the carbon factor depends heavily on the method chosen for determination of the carbon factor. The uncertainty study can thus include issues like the uncertainty of the GC-analysis, uncertainty due to GC measurements on a slightly different gas type, uncertainty due to sampling procedures, sampling period and laboratory analysis, and uncertainty due to unknown mixing. In the present work, details will not be given on procedures and uncertainty estimations for a specific installation.

6. SUMMARY AND CONCLUSIONS

In the present paper, a project regarding documentation of the uncertainty of the CO_2 emissions from the Statoil Mongstad oil refinery has been presented. The national and European regulations for this uncertainty reporting have been briefly described. Uncertainty limits have there been set for activity data (accumulated fuel gas mass) and carbon factor (number of kg CO_2 produced from the burning of one kg fuel gas). In this work, uncertainty of the activity data has been the main focus.

After description of the instrumentation at Statoil Mongstad, a simplified uncertainty model including the correlation between various measurements has been presented. Here, two approaches for treatment of correlation have been presented: the covariance method and the decomposition method.

The decomposition method has thereafter been used on uncertainty calculation for a specific source including 16 orifice meters and one estimation point, at Statoil Mongstad. It is shown that the uncertainty can be improved by suggesting new instrumentation based on the uncertainty budgets worked out in the present work. Based on these results, a new temperature measurement has been installed and is now in operation.

Finally, some considerations regarding the uncertainty of the carbon factor are given.

REFERENCES

Dahl, E. O, Frøysa, K.-E. and Lunde, P.: "Handbook of uncertainty calculations. Fiscal Orifice Gas and Turbine Oil Metering Stations," Issued by Norwegian Society of Oil and Gas Measurement, Norwegian Petroleum Directorate, Norwegian Society of Chartered Engineers and Christian Michelsen Research AS, Norway (free download available from www.nfogm.no) (March 2003).

Commission decision of 18 July 2007 establishing guidelines for the monitoring and reporting of greenhouse gas emissions pursuant to Directive 2003/87/EC of the European Parliament and of the Council. Document number C(2007) 3416 **(MRG 2007)**.

Forskrift om endring av forskrift av 23. desember 2004 nr 1851 om kvoteplikt og handel med kvoter for utslipp av klimagasser (klimakvoteforskriften). Fastsatt av Miljøverndepartementet 14. september 2007 (**SFT 2007**).

Frøysa, K.-E. and Hallanger, A.:"Usikkerhet til rapportert CO_2-utslipp ved Statoil Mongstad" (English: Uncertainty for reported CO_2 emissions at Statoil Mongstad), CMR report no. CMR-06-F10649-RA-01, CMR, Bergen, Norway, February 2007 (Confidential, in Norwegian).

ISO, "Guide to the expression of uncertainty in measurement" (GUM). First edition, 1993, corrected and reprinted 1995. International Organization for Standardization, Geneva, Switzerland (1995).

ISO 5167: "Measurement of fluid flow by means of pressure differential devices inserted in circular cross-section conduits running full – Part 1-4", ISO standard, 2003.

ISO 5168: "Measurement of fluid flow -- Procedures for the evaluation of uncertainties", ISO standard, 2005.

Lunde, P. and Frøysa, K.-E.: "Handbook of uncertainty calculations. Ultrasonic fiscal gas metering stations," Issued by Norwegian Society of Oil and Gas Measurement, Norwegian Petroleum Directorate and Christian Michelsen Research AS, Norway (free download available from www.nfogm.no) (December 2001).

25th International North Sea Flow Measurement Workshop
16th – 19th October 2007: Paper 22

Measurement of Produced Water Discharges – Regulatory Requirements and Recent Progress

Alick MacGillivray, Ming Yang and Richard Paton
TUV NEL Ltd

1 INTRODUCTION

Until recently, produced water was considered to be a waste stream for which metering was not a critical issue. As a result, little attention had been paid to the subject of metering this stream. However, in 2001 OSPAR (Oslo – Paris Commission) recommended a 15% reduction of oil discharged via produced water by 2006 [1], in relation to the year 2000. This meant that there was a need to accurately measure both the concentration of oil in produced water and the volume of water being discharged. In the UK, new Regulations, called OPPC (Offshore Pollution Prevention and Control) [2] were introduced in 2005, which require the measurement of produced water volume to an uncertainty of ± 10% [3].

This paper is divided into two parts. The first part (Part A) will provide a summary of the regulatory requirements related to the discharge of produced water in the North Sea and in UK in particular. It will examine the measurement issues raised by the introduction of the new legislation, including the best methods of achieving the performance targets. The second part (Part B) illustrates the importance of reporting produced water volumes at standard conditions of temperature and pressure (15°C and 1.01325 bar absolute). Equations that can be used to calculate the density, and hence the expansion factors of produced water are proposed. These apply across the wide range of temperatures and salinities found in practice.

PART A: REGULATORY REQUIREMENTS AND RECENT PROGRESS

2 REGULATORY REQUIREMENTS

International Law considers five main categories of discharges associated with the operations of offshore platforms. These are [4]:

- Platform drainage from machinery spaces, e.g. pumps and generator areas
- Contaminated sea water due to normal operations, e.g. storage tanks cleaning
- Offshore processing drainage, e.g. leaks collected from treatment installations and surface piping
- Production water, i.e. the water separated from production fluids
- Displacement water, i.e. water used to compensate the decreasing level of oil in storage tanks to assist offloading and to ensure stability and integrity of the platforms

The first two of these are regulated under the provision of the International Convention for the Prevention of Pollution from Ships 1973, as amended 1978 (MARPOL 73/78) [5]. Annex I of MARPOL 73/78 provides the full regulations for the prevention of pollution by oil, which entered into force on 2 October 1983. Here

one of the key points is that the water must be treated and can only be discharged if the concentration of the oil is less than 15 parts per million (volume/volume) or ppm.

The discharges associated with the other three categories are regulated through national and regional regulations.

As oil fields mature, increasing amounts of water are being produced. Worldwide it is estimated some 250 million barrels are produced daily [6], which is more than three times the amount of oil produced. In the North Sea, some 9 million barrels per day is produced of which some 15% is re-injected [7]. As a result, around 8547 tonnes of oil (OSPAR 2004 official figure) is discharged via the discharge of produced water in the North Sea. Produced water is by far the largest waste stream for oil production. Oil discharged via the discharge of produced water now accounts for over 90% of the total amount of oil discharged to the sea in the North Sea as figures shown in Table 1.

Table 1 Amount of oil discharged into the North Sea in 2004 [7]

Source of oil discharged	Produced & displacement water	Oil and organic fluids from drilling	Oil spillage	Total
Quantity (tonnes)	8547	425	199	9171
Percentage (%)	93.2	4.6	2.2	100

Produced water also contains components such as heavy metals, production chemicals and naturally occurring radioactive materials (NORM) in addition to the residual oil. Therefore its discharge is in general strictly regulated as these components can potentially cause damage to the marine environment.

2.1 Regulatory Framework in the North Sea

In the North Sea, OSPAR was created to look after the marine environment. It is a convention which is legally binding on its member states ("contracting parties") with an area that encompasses the North East Atlantic from Greenland down to the Straits of Gibraltar.

OSPAR was created when Oslo Convention and Paris Convention was merged in 1992. It came into force on 25 March 1998. The Oslo Convention was originally created for the prevention of marine pollution by dumping from ships and aircraft, which was signed in 1972 in Oslo. The Paris Convention was made for the prevention of marine pollution from land-based sources, which was signed in 1974 in Paris.

OSPAR takes three types of measures, termed decisions, recommendations and agreements. Decisions are formal and legally binding on the contracting parties. Recommendations are not legally binding, but still formal and usually most contracting parties implement these in the same way as the decisions. Decisions and recommendations from OSPAR are made to address specific issues that are essential to reach the objectives of OSPAR. Less important measures, which may be addressed

by less formal agreements, come under the category of "other agreements". Agreements are not legally binding.

Implementation of OSPAR measures can be made in three ways: enforcement by law, implementation by administrative action or by negotiated agreement between the competent authorities and industry.

One of the key measures undertaken by OSPAR recently is the OSPAR Recommendation 2001/1 for the Management of Produced Water from Offshore Installations [1], which was adopted in June 2001. The Recommendation has since been amended in 2006 [8]. Some of the key points included in the recommendation are:

- Any new or substantially modified existing installation after 1st January 2002 must take, as a point of departure, zero discharge of oil in produced water into the sea or at least the minimisation of discharges.
- Each contracting party has to make a complete review of existing installations, of Best Available Technology (BAT) and Best Environment Practical (BEP) used for the management of produced water, by the end of 2005.
- For each contracting party, the total quantity of oil in produced water discharged into the sea during the year 2006 from all installations must be reduced by a minimum of 15% compared to the equivalent discharge in the year of 2000.
- The performance standard for dispersed hydrocarbons in the discharged water is reduced from 40 mg/l to 30 mg/l by the end of 2006.
- The dispersed oil content in the produced water should be measured using an infrared method as adopted in 1988, as described by the Agreement 97-16 [9].

The update of the recommendation in 2006 reflects the changes made since the recommendation was originally produced. The main points are:

- No individual offshore installation should exceed a performance standard for dispersed oil of 30 mg/l from 1 January 2007.
- Contracting parties should report to the OSPAR Offshore Industry Committee (OIC) meeting in 2008 the offshore installations that fail to meet the performance standard of 30 mg/l.
- Contracting parties should continue to exchange information on dissolved oil in produced water on the basis of work in hand.
- The new reference method for the measurement of dispersed oil against which the performance standard is set is the method described in OSPAR Agreement 2005-15 [10].

Until the OSPAR Recommendation 2001/1, the only parameter, with which a performance standard was set, was the dispersed oil concentration. Presently, oil in produced water concentration is still the main parameter that is measured and compared to the performance standard for compliance.

However in the OSPAR Recommendation 2001/1, not only the performance standard was lowered from 40 mg/l to 30 mg/l, but also each contracting party was required to

make a minimum of 15% reduction in the amount of oil discharged into the sea via the discharge of produced water by the year 2006 compared to the year 2000 figure. As a result, accurate measurement of oil concentration was no longer the only thing that operators have to comply with. Accurate quantification of the discharge volume and meeting the overall 15% reduction had become equally important.

2.2 Regulatory Framework in UK

The discharge of produced water in the United Kingdom Continental Shelf (UKCS) is regulated by the Department of Business, Enterprise and Regulatory Reforms (BERR), formerly called the Department of Trade and Industry (DTI). In the past, the key piece of legislation was the Prevention of Oil Pollution Act 1971 (PoPA). However PoPA has now been replaced by OPPC Regulations 2005, which came into force in August 2005. The new Regulations have been designed to encourage offshore operators to continue to reduce the quantities of hydrocarbons discharged during the course of offshore operations. The Regulations updated the definition of oil, introduced a permitting system for oil discharges and strengthened BERR's powers to inspect and investigate oil discharges. The issue of permits under these new regulations has replaced the issue of exemptions under the previous Regulations and will be on a permanent basis for the duration of an activity covered. These new Regulations were made in line with the OSPAR Recommendation 2001/1.

To facilitate the attainment of the 15% reduction target in oil discharges from 2000, a Produced Water Trading Scheme has been set up in the UK. In this Scheme, which started on 1 January 2007, permits are issued to each installation in the UKCS that discharges produced water. The permits are issued according to an allocation plan, which gives details of discharge allowances for each installation. Discharge allowances allocated by BERR are the maximum amount of dispersed oil that is permitted to be discharged by an installation.

Allowances can then be traded to achieve compliance. The Trading Scheme in UK was designed to provide a mechanism in which the 15% reduction target could be achieved in a cost-effective way. It also provides the means to achieve further oil discharge reductions in the future.

2.2.1 Measurement of Dispersed Oil in Produced Water

(i) Performance standard

The OPPC Regulations prohibit the discharge of oil into the sea unless it is in accordance with the schedule conditions of a permit issued to cover the discharge. Many of the schedule conditions contained in an OPPC permit depend on the accurate measurement of oil. On 1 January 2006 the performance standard for dispersed hydrocarbons in the UKCS was reduced from 40 mg/l to 30 mg/l, which was a year earlier than the OSPAR Recommendation 2001/1 required.

(ii) Approved analysis methods

Until the end of 2006, the only oil-in-water analysis method approved by BERR was the infrared (IR) / tetrachloroethylene (TTCE) method (BERR IR method) [11]. Since 1 January 2007 the new OSPAR/(BERR) approved oil-in-water analysis reference method is the OSPAR GC-FID method [10].

(iii) Sampling

Details of oil in produced water sampling requirements can be found in the BERR Guidance notes [12]. A brief summary is provided here.

If an installation discharges more than 2 tonnes of dispersed oil per annum, for manned installations, a minimum of 2 samples should be taken at an approximately equal time intervals. For unmanned installations, three duplicate samples are taken each time the installation is visited, one is analysed and reported. Providing that the result obtained is satisfactory the other two are discarded. When the installation is temporally manned for more than 48 hours, one sample is taken every 48 hours.

If the installation discharges less than two tonnes per annum, for manned installations, three duplicate samples are taken once a month. One is analysed and reported; if the result is satisfactory the other two are discarded. If the installations are unmanned, then three duplicate samples are taken each time the installation is visited unless the visit is repeated in the calendar month. One is analysed and reported. Providing the result obtained is satisfactory the other two are discarded.

For installations that discharge produced water in batches, representative sample(s) of each batch must be taken and analysed.

2.2.2 Measurement of Produced Water Discharges

(i) Performance standard

An early version of the BERR guidance notes [13] issued in 2004 on OPPC Regulations stated that permit holders should monitor or calculate the volume of the produced water discharge to ± 10% uncertainty on volume. Although not stated explicitly, this refers to a 95% confidence level. It also stated that the discharge volume should be determined daily and the volume reported at standard conditions (15°C and 1.01325 bar).

The current permit schedule as shown on the BERR website [3] requires the following:

"Details of the method used to measure the volume discharged, or the method used to calculate (or estimate) the average daily production of the discharge stream (this should include an estimate of the uncertainty of the measurement or calculation, e.g. +/- 10% for this produced water discharges). It should be noted that the method of measurement may require to be independently verified, as a condition of the oil discharge permit"

There is currently no reference to the need to express the discharge volume at standard conditions.

(ii) Measurement methods

The most popular method employed to quantify produced water discharges is direct metering. This method has the lowest uncertainty and is most likely to attain the performance target stipulated in the previous section. Other methods employed include estimation of volume using well test data or inference of flow from pressure drops across hydrocyclones. In this area there are still several issues to be considered such as how the measurement methods should be verified or calibrated and whether current measurement methods could be used to derive reliable data for individual assets served by the same host discharging installation. However there is no standard or reference method for produced water volume determination.

2.2.3 Reporting of Produced Water Discharges

Permit holders are currently required to maintain detailed records of the sampling and analyses undertaken, and the quantities of produced water discharged. BERR has the legal right to view those records, but the normal method of accessing the dispersed oil in produced water discharge data is via the EEMS (Environmental Emissions Monitoring Service) database [14].

(i) Oil-in-Water discharge report

Submission of the EEMS database returns will continue to be a condition of permits issued under the OPPC Regulations, and permit holders will be required to submit the returns on a calendar monthly basis, supplemented by an annual summary return. These returns will continue to be used to assess compliance with legislative reporting requirements. BERR may additionally request access to the original records to check the EEMS data.

(ii) Operator report

This is a record that should be retained by the operator and, according to BERR OPPC guidance notes, should include the following:

- The date and time when the oil-in-water samples were collected
- The hydrocarbon concentration of each sample
- The volume of the daily discharge
- The daily hydrocarbon discharge
- The monthly hydrocarbon discharge
- The volume of the annual discharge
- The annual hydrocarbon discharge

(iii) New reporting requirements

In addition to the EEMS reporting requirements, since 1 January 2007 a new condition was included in the permits issued under the OPPC Regulations, requiring

permit holders to prepare a separate, annual, Dispersed Oil in Produced Water Trading Scheme Discharge Report, and to seek independent verification of that report to demonstrate compliance with the Rules of the Scheme.

This report should include the following information

- The analyses and measurements undertaken to quantify discharges of dispersed oil in produced water
- The methodologies employed for the analyses and measurements
- The uncertainties associated with the analyses and measurements
- The methodology used to calculate the quantity of dispersed oil in produced water during each calendar year

A new guidance (draft version) on how to prepare this report has recently been released by BERR [15].

2.2.4 Annual Discharge Report Verification

Permit holders must instruct accredited verifiers to audit and review the annual report and to verify the quantity of dispersed oil in produced water during each calendar year. The verification should be undertaken in accordance with the requirements specified by BERR, and the verified report must be submitted to BERR no later than 30 April of the year following the calendar year to which the report relates.

Verification must be carried out by an independent organisation which is UKAS (United Kingdom Accreditation Service) accredited. The objective of the verification exercise is to establish that clear evidence exists to demonstrate how the annual discharge oil in produced water figure is derived, and that this figure is accurate.

Verifiers will however in general not be required to go offshore in order to complete the verification.

At the previous North Sea Flow Measurement Workshop, Beecroft [18] provided a comprehensive review of the history of regulations related to the discharge of produced water from offshore installations with a particular emphasis on the United Kingdom sector.

3 RECENT PROGRESS

In anticipation of the implementation of the OSPAR Recommendation 2001/1, in particular regarding the introduction of a new oil-in-water analysis reference method, and the 15% discharge oil reduction target, two Joint Industry Projects (JIP) were subsequently launched by TUV NEL – Oil-in-water Analysis Method (OIWAM) and Produced Water Volume Determination (ProVol).

3.1 Oil-in-water Analysis Method (OIWAM)

Following the OSPAR 2001/1 Recommendation and subsequent agreement to adopt a new reference oil-in-water analysis method based on using gas chromatograph, it soon became clear that the offshore oil and gas industry would face some major challenges in implementing the new reference method. This is because the new method based on gas chromatography is inherently different from the previous reference method based on infrared quantification. More importantly, the new reference method is not ideally suited for offshore use for several reasons, e.g. it is complex to operate and uses pressurised and flammable gases.

TUV NEL launched the OIWAM JIP in 2004 with following objectives:

- To identify the best practical means to implement the new reference method
- To establish best practice guidelines for oil in produced water sample taking and handling
- To develop a realistic set of acceptance criteria for the use of alternative oil-in-water analysis methods offshore
- To advise on how to relate results from the new reference method to those of the old method

A total of 10 organisations including BERR, the State Supervision of Mines (The Netherlands), BG Group, BHP Billiton, CNR International, Chevron, Kerr-McGee (now Maersk Oil North Sea UK), Marathon Oil, Shell UK, and Talisman Energy supported the project. The project was completed in 2005 with the final report [16] issued in July 2005.

Following on the OIWAM JIP, two major documents were produced, both of which were primarily based on the OIWAM JIP report. One was the publication of the OSPAR Guidance entitled "Oil in Produced Water Analysis – Guideline on Criteria for Alternative Method Acceptance and General Guidelines on Sample Taking and Handling" [17] in year 2006. The other one was a UK Government Guidance Note entitled "The Sampling and Analysis of Produced Water and Other Hydrocarbon Discharges" [12], which was published in September 2006.

Both of these documents have since played an important role in the implementation of the new reference method across the North Sea countries since 1st January 2007.

3.2 Produced Water Volume Determination (ProVol)

Knowing that there would be a new requirement of ±10% for the uncertainty in produced water volume determination and a possible accompanying requirement for annual verification, and the possibility that there would be an UK wide produced water trading scheme, it was clear that measurement of produced water discharge volume was to become an increasingly important issue.

Unlike the measurement of oil in produced water, there was no specified or generally agreed method for produced water volume determination. Neither was there a mechanism by which the accuracy of the reported data can be verified. In addition a brief survey carried out by TUV NEL early in 2004 indicated that methods used for produced water volume determination varied significantly from operator to operator,

and installation to installation. It also became obvious that there would be large differences in terms of accuracy of the different methods used.

Produced Water Volume Determination (ProVol) was therefore initiated in 2005 by TUV NEL. The project had the following objectives:

- To conduct a survey to find out methods currently used in calculating the volume of produced water discharged into the sea
- To carry out case studies to estimate uncertainties associated with some of these methods identified
- To develop best practice guidance in achieving the required ±10% uncertainty
- To identify verification methods and to develop verification procedures
- To carry out field verification

The project was sponsored by BERR, CNR International, Marathon Oil, Maersk Oil North Sea UK, Shell UK and Talisman Energy. It was completed with a final report issued to the sponsors in June 2007. The main outputs from the project are summarised below.

3.2.1 Survey of Current Produced Water Measurement Methods

Since there is currently no recommended standard method of produced water discharge measurement, the first aim of ProVol was to survey operators to find out which methods were currently being used in the North Sea. The survey found that the most common method, accounting for nearly half of the operators, was to install a meter on the discharge line. Meters commonly used for this purpose included electromagnetic, ultrasonic, Coriolis and orifice plates. Another relatively popular method of measuring the produced water flow was to infer it from the performance curve of a hydrocyclone, which is commonly used for the separation of oil and produced water. Some operators used well test data as the primary method of produced water volume measurement while others used it to complement one of the more popular methods.

3.2.2 Compliance with the Uncertainty Performance Target

The next part of ProVol was to conduct a series of case studies, using data supplied by the participating operators, to evaluate the uncertainty of each typical measurement method and relate it to the ±10% uncertainty standard. Ways of reducing the overall uncertainty of each method were also suggested. The uncertainty of direct metering depends heavily on factors such as installation effects and the frequency and uncertainty of calibration or verification. By following good metering practice and by conducting regular calibrations or verifications this method will comply with the performance target and is recommended as the primary method of produced water volume measurement. The case studies undertaken in this project revealed that to comply with the uncertainty performance targets it is necessary to undertake regular maintenance to minimise the uncertainty in the other measurement methods. In the hydrocyclone method the major uncertainty source is the build up of fouling of the equipment caused by the passage of produced water. With regular cleaning to reduce this build up, this method can comply with the performance target. The use of well

test data can comply if the meters measuring the flow of oil and water from the test separator are both calibrated regularly and to an uncertainty of less than 5%.

3.2.3 The Requirement for Verification

The final outputs from ProVol were two best practice guides which were made available to sponsors. The first described best practice in using the methods of produced water measurement outlined previously. This includes ways of minimising uncertainty so that they comply with the ±10% overall uncertainty performance target. It is important to note that the uncertainty of all of the measurement methods will change with time (for example through instrument drift or fouling build-up). To ensure continued compliance with the uncertainty performance target it is necessary to conduct regular verification tests. ProVol has produced a best practice guide in conducting these tests. This guide was supported by a series of field trials conducted on sponsor installations and includes recommendations of suitable methods of verification, including the use of clamp-on ultrasonic meters and tracer injection techniques.

PART B: VOLUME CORRECTION FACTORS FOR PRODUCED WATER

4 VOLUME CORRECTION

The UK OPPC Regulations (2004) stated that the produced water discharge volume should be reported at standard conditions of temperature and pressure (15 °C and 1.01325 bar (a)). However, the current (2005) statement of these Regulations does not refer to standard conditions. The equivalent Regulations in USA (EPA Region 6 NPDES Permit System) also require produced water discharge volume to be reported but do not specify standard conditions.

A 1 m^3 volume of produced water measured at 80°C, a temperature commonly experienced in practice, will reduce by approximately 2.5% when cooled to 15°C. In the context of the OPPC target of ±10% uncertainty in measured produced water volume, this may be a significant factor in determining whether an operator complies or otherwise. To account for this effect it is recommended that the measured volume should be referred to standard conditions. To apply this volume adjustment, it is therefore necessary to be able to formulate an equation to accurately evaluate the density of produced water over a comprehensive range of temperatures.

4.1 Pure Water Volume Correction

The thermal expansion factor for water is defined as the ratio of the density at the measured condition to the density at standard conditions. Several different formulations expressing the density of water as a function of temperature and pressure can be found in the literature. Most however are only valid for temperatures up to 40°C and when reproduced many do not make this limitation clear. This gives rise to errors when extrapolating to higher values. The International Association for the Properties of Water and Steam (IAPWS) currently provides the most reliable formulation for water density in the form of equations of state for pure water. The best

of these is the IAPWS-95 formulation [19], which allows the calculation of water properties over a very wide range of temperatures and pressures, and includes density, compressibility, viscosity, speed of sound and other thermodynamic properties. Unfortunately the formulation is complex. However Jim Watson prepared a series of simplified curve fits to this formulation for use within TUV NEL and these give manageable equations for everyday use. The density formula produced is valid over a temperature range of 0°C to 95°C and agrees with the full formulation to within 0.001 kg/m^3. This formula, giving the density of air-free water in kg/m^3 at 1.01325 bar, is shown in equation (1)

$$\rho_{IAPWS} = c_0 \cdot \left(\frac{1 + c_1 t_n + c_2 t_n^2 + c_3 t_n^3}{1 + c_4 t_n + c_5 t_n} \right) \qquad (1)$$

where t is the temperature (°C), t_n is the normalised temperature = t/100. The constants c_0 to c_5 are given by

c_0 = 999.84382 c_3 = -0.0309777
c_1 = 1.4639386 c_4 = 1.4572099
c_2 = -0.015505 c_5 = 0.0648931.

4.2 Application to Produced Water

In contrast to pure water, produced water is a complex mixture of different salts and other chemicals. Typically, and in terms of the behaviour for expansion, produced water can be represented as having similar salt composition to sea water however the salinity levels can be very much higher. Salinities up to 140 g/kg are commonly experienced while sea water has a typical salinity of up to 35 g/kg. It is not possible to assume that salt water has the same thermal expansion factors as pure water.

Two formulations which provide density of saline water were identified. The first of these is a set of state equations for salt water, including density, compressibility and speed of sound in a technical standard from UNESCO for use in Oceanography [20-21], in which formulations are included which are valid up to temperatures of 40°C and salinities of 40g/kg. It is noted that this formulation produces significant errors when extrapolated to high temperatures. This in most part is due to the use of a pure water formulation limited to 40 °C. A modified UNESCO formulation was produced based on the IAPWS formulation and this was used as the basis for formulation development. The second formulation was published by Isdale and Morris [22-23] as part of NEL research into desalination processes and published in 1972. This formulation covers temperatures ranging from 5°C to 95°C and salinities of up to 140 g/kg. Extrapolation to temperatures below 5°C and salinities below 35 g/kg using this formulation is not recommended.

Since both formulations provide good source data within their relative range and have some degree of acceptable extrapolation it was considered possible to combine these two equations to give a formulation that may be applied across the range of conditions suitable for produced water. A data table combining values from both formulations was derived. Data from any one formulation was discarded where differences

exceeded 0.05% and the value was in the extrapolated region of one of the formulations. This process provided a data set covering all of the proposed range of salinities and temperatures. A surface fit was then carried out on the derived data set. The proposed equation for the density of salt or sea water is given by:

$$\rho_{saltwater} = \left(\frac{a + b \cdot t + c \cdot t^2 + d \cdot t^3 + e \cdot S}{1 + f \cdot t + g \cdot t^2 + h \cdot S} \right) \quad \text{kg/m}^3 \qquad (2)$$

t = temperature (°C), S = Salinity (g/kg) and :

$a = 1000.625267$ $\quad d = 1.31139\times10^{-5}$ $\quad g = -1.75832\times10^{-5}$
$b = 2.340698$ $\quad e = 0.611416$ $\quad h = -1.73344\times10^{-4}$
$c = -2.31026\times10^{-2}$ $\quad f = 2.36919\times10^{-3}$

When compared with the actual values in the table, this formulation agreed to within 0.03% for temperatures down to 5°C. Where the temperature is below 5 °C and the salinity is below 50 g/kg the agreement is not so good with the residuals rising to 0.07 %. This region corresponds to temperatures below the maximum density of water and shows the selected function is not adequately following this turning point. The level of agreement between the data and the surface fit gives sufficient confidence to propose an equation for the density of saline water across the temperature range 0 °C to 95 °C and salinities up to 140 g/kg.

No uncertainty was given within the UNESCO publication. Isdale and Morris suggest that density was measured with an uncertainty of 0.02 % at high salinities and temperatures, and an uncertainty of 0.01 % at low concentrations rising to 0.1 % at higher temperatures and concentrations (60 °C - 130 g/kg) depending on the data source. The densities predicted by the combined formulation were compared with the original NEL experimental data and are shown in Table 1.

Table 2: Comparison of NEL experimental data to the formulation

Temperature C	Salinity g/kg	Density Measured kg/m3	Density Calculated kg/m3	Difference %
20.00	10.0	1.0058	1.0056	0.021
20.00	70.0	1.0512	1.0514	-0.022
20.00	130.0	1.0982	1.0982	-0.002
20.00	10.0	0.9992	0.9994	-0.019
20.00	70.0	1.0438	1.0440	-0.022
20.00	130.0	1.0896	1.0896	0.003
20.00	10.0	0.9902	0.9905	-0.027
20.00	70.0	1.0345	1.0345	-0.002
20.00	130.0	1.0795	1.0794	0.006
20.00	63.1	1.0179	1.0181	-0.018
20.00	63.1	1.0056	1.0056	-0.002
20.00	92.7	1.0454	1.0458	-0.034

20.00	92.7	1.0332	1.0335	-0.031
20.00	121.0	1.0618	1.0620	-0.016
20.00	148.5	1.083	1.0834	-0.033

Given the agreement found between the two formulations, it can be assumed that the proposed equation can be used with an uncertainty within 0.1 % below 5 °C and 50 g/kg and 0.05 % across the remaining range.

Beecroft [18] presented measured densities for produced water across a reasonably wide temperature range. At the time it was not required to measure the salinity of the water. This data is reproduced in Fig 1. This shows the density measured from the different samples vary by around ± 0.1 %. If the salinity is assumed to be 131.5 g/kg the above equation can be overlaid on this data and shown to reproduce the correct functional form and curve shape. As the salinity value has been assumed no inference can be made on the absolute agreement.

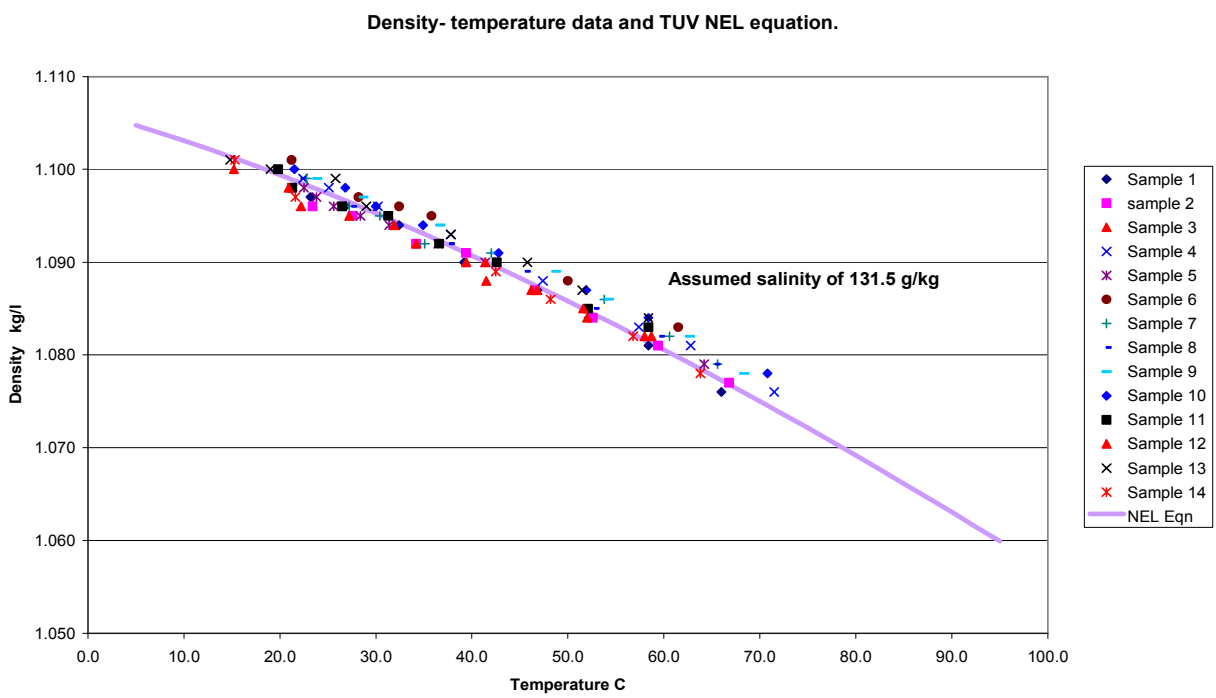

Fig 1: Comparison of produced water data and formulation.

4.3 Volume Correction Factor (Ctl)

Having derived a function for density, the volume correction factor (Ctl) can now be derived for the full range of conditions for which the density function is defined. The correction factor is calculated by evaluating the ratio of the density at measured and standard conditions. A reference temperature of 15 °C was chosen and Ctl values were calculated across the temperature range from 5 °C to 95 °C and salinities from 0 g/kg to 140 g/kg. The curves fitted to resultant data were restricted to relatively simple forms to provide a solution which could be easily applied in flow computers. This exercise showed that thermal expansion has a relatively weak dependence on

salinity and as such it was decided to provide a curve dependant on temperature only. The function below is the thermal expansion correction factor to adjust volumes to that at 15 °C.

$$ctl = a + b \cdot t^{1.5} + c \cdot \frac{1}{t^2} \tag{3}$$

Where t is temperature (°C)

a = 1.00246 b = -4.29 x10^{-5} c = 7.7713 x10^{-3}

Selecting a nominal volume and correcting it to standard conditions across the temperature and salinity range shows that this formula will provide correction to the volume (to 15 °C) agreeing with that derived from equation (2) to within ±0.2%. It is noted however that the differences are biased with respect to salinity within this ±0.2 % range.

4.4 Compressibility

The compressibility of salt water can be considered as being insignificant for most applications where produced water is discharged. The correction will amount to less than 0.02 % on volume when the pressure is 5 bar. Potentially in some applications, produced water may be measured in the high-pressure re-injection lines. This would require a volume correction of around 0.5 % at 100 bar pressure. A fit to data generated from the IAPWS-95 formulation provides an equation for the isothermal compressibility *Beta (B)* of pure water as given in equation (4):-

$$Beta = A_0 \cdot \left[\frac{(1 + A_1 t_n + A_2 t_n^{\ 2} + A_3 t_n^{\ 3})}{1 + A_4 t_n} \right] \tag{4}$$

where

t_n = normalised temperature = t/100
t is temperature (°C)
A_0=5.08821x10^{-10}
A_1=1.2639418
A_2=0.2660269
A_3=0.3734838
A_4=2.0205242

The compressibility is used to calculate the pressure correction factor (Cpl) and is given by:

$$Cpl = \frac{1}{1 - Beta \times P} \tag{5}$$

where P = pressure (barg)

A compressibility function is provided within the UNESCO equation of state. When compared with the pure water formula it is evident that the salinity has an effect on the compressibility which should not be discounted. The UNESCO equation was examined in more detail and again it shows a departure from the expected

compressibility when extrapolated above 40 °C and 35 g/kg. In assessing this effect, the potential error in compressibility is not expected to be significant in terms of produced water measurement; being estimated as being within 0.005 % on resultant volume. The UNESCO formulation is however complex and does not lend itself to a simple calculation procedure. A simplified formula was generated from the extrapolated UNESCO formula and including data for pure water from the IAPWS-95 formula. This gives the isothermal compressibility, *Beta (B)* as:

$$B_{Saltwater} = \left(a + b \cdot t + c \cdot S + d \cdot t^2 + e \cdot S^2 + f \cdot t \cdot S\right) \times 10^{-10} \quad \mathrm{Pa}^{-1} \qquad (6)$$

Where t = temperature (°C) , S = salinity (g/kg) and

$a = 5.0348$	$d = 2.513\times10^{-4}$
$b = -2.561\times10^{-2}$	$e = 1.593\times10^{-5}$
$c = -1.214\times10^{-2}$	$f = 8.368\times10^{-5}$

This formula is expected to provide an estimate of the compressibility to within 0.5 % except at the highest temperatures and salinity where the uncertainty is estimated to rise to 1 %. This will result in an uncertainty of 0.0001 and 0.0005 % in the resultant corrected volume.

4.5 Summary

The formulae presented have been developed by using data generated from other formulations rather than from raw experimental data. They provide a sound set of equations which may be used in practice when reporting the volume of saline produced water.

Clearly it would be advantageous to confirm these equations with sound laboratory based experimental data covering the density and compressibility functions. It should be stressed that experimental work should be carried out within an overall plan and in a controlled and thorough manner. Salinity, salt constituents and conductivity should be recorded when testing produced water and the results compared with the results from standard sea water constituents. It should also include examples of produced water compositions in addition to simulated sea water.

When taking samples of produced water for analyses, extreme care should be taken to ensure some of the salts do not precipitate out when the sample is cooled. Sodium chloride has a flat precipitation curve in relation to temperature and so little of this will precipitate. Other salts, although present in smaller quantities, will precipitate out hence changing the composition of the sample and also potentially damaging apparatus by precipitating out on the walls of containers valves and densitometer tubes.

References

1. "OSPAR Recommendations 2001/1 for the management of produced water from offshore installations". (www.ospar.org)
2. "Offshore Petroleum Activities (Oil Pollution Prevention and Control Regulations)", http://www.opsi.gov.uk/si/si2005/20052055.htm
3. "Oil Discharge Permit Application Form", http://www.og.dti.gov.uk/environment/OPPCAppform_0507.doc
4. MARPOL Amendments , 2005 edition
5. MARPOL 73/78 IMO Publication, Sale No: IMO-520E
6. S. Robertson and L. Jahnsen, "Worldwide survey on the amount of oils discharged via the discharges of produced water", TUV NEL's 4th Produced Water Workshop, 24-25 May 2006 Aberdeen, UK
7. "OSPAR report on discharge, spills and emissions from offshore oil and gas installations in 2004", OSPAR Commission 2006, www.ospar.org
8. OSPAR Recommendation 2006/4 Amending OSPAR Recommendation 2001/1 for the Management of Produced Water from Offshore Installations, OSPAR Commission Meeting, 26-30 June 2006, Stockholm
9. OSPAR Agreement 1997-16 on "Sampling and analysis procedure for the 40 mg/l target standards"
10. OSPAR Agreement 2005-15 – "Sampling and analysis procedure for the 40 mg/l target standard", www.ospar.org
11. DTI approved oil-in-water analysis method: "Methods of sampling and analysis of production and displacement water discharges for exemptions from Section 3 of the Prevention of Oil Pollution Act 1971 Issued by the Department of Trade and Industry for Offshore Installations"
12. "Guidance Notes for the Sampling and Analysis of Produced Water and Other Hydrocarbon Discharges, Part 1: Notes", Version 1 September 2006
13. "Guidance Notes on the Offshore Petroleum Activities (Oil Pollution Prevention and Control) Regulations 2004", October 2004 Version, 2004
14. http://www.eems-database.co.uk/
15. "Dispersed Oil in Produced Water Trading Scheme Annual Report and Verification Report: Part A: Preparation Instructions and Part B: Verification Guidance", Draft version 17th of August 2007
16. "Oil-in-water Analysis Method (OIWAM)", final report, TUV NEL Report 2005/96, July 2005
17. OSPAR Agreement 2006-6 "Oil in produced water analysis – guidance on criteria for alternative method acceptance and general guidelines on sample taking and handling", 2006
18. D. Beecroft et al, "There's oil that there water! – Impact of the OPPC 2005 Regulations; an operator's response, a paper presented at the 24th International North Sea Flow Measurement Workshop, 24 – 27 October 2006, Scotland
19. http://www.iapws.org
20. UNESCO technical paper in Marine Science, 1981, 36
21. Fofonoff, N. P., 1985, *Journal of Geophysical Research*, Vol 90 No. C2, pp 3332-3342.
22. Morris R and Isdale J., 1972, Desalination. Vol 10, pp 329 - 339

23. Engineering sciences data unit Item number 77024; Thermal conductivity, viscosity, heat capacity, density and Prandtl number of sea water and its concentrates, 1977, ISBN 0 85679 196 2.

THE RELEVANCE OF TWO DIFFERENT PATH LAYOUTS FOR DIAGNOSTIC PURPOSES IN ONE ULTRASONIC METER

MR. JOHN LANSING, SICK | MAIHAK, Houston, Texas
DR. VOLKER HERRMANN, SICK | MAIHAK, Dresden, Germany
MR. TORALF DIETZ, SICK | MAIHAK, Dresden, Germany

ABSTRACT

During the past several years the use of ultrasonic meters (USMs) has gained world-wide acceptance for fiscal applications. The many benefits of USMs have been documented in several papers at virtually every major conference. As the cost of gas continues to increase, the importance of knowing that the ultrasonic meter is operating accurately has never been more important. The use of diagnostics to help identify metering issues has been discussed in several papers over the past few years [Ref 1 & 2].

The traditional method of verifying whether the USM is operating accurately essentially requires using the USMs' diagnostic information to help understand the meter's health. This has often been referred to as Conditioned Based Maintenance, or CBM for short. Different USM meter designs require different analysis techniques, especially for the velocity profile analysis. For the field technician, it is often difficult to understand all the diagnostic features of each USM meter design. Through the years software has been developed to help determine if the meter is operating correctly or not. However, it is still very difficult to clearly define limits on some of the diagnostic parameters that translate into a quantifiable metering error.

This paper will discuss a new CBM concept to assist in understanding if the fiscal 4-path USM meter is operating accurately. Rather than relying entirely on the understanding and interpretation of the meter's diagnostics, a meter designed with an additional built-in diagnostic path has been developed. In this paper the meter design will be referred to as the CBM 4+1 meter.

1. INTRODUCTION

The CBM 4+1 meter design is a conventional fiscal 4-path chordal (Westinghouse path layout) ultrasonic meter that incorporates an additional, independent single-path and associated electronics incorporated into the same meter body. The purpose of the additional path is to continuously check the fiscal 4-path meter's measurement results.

The transducers for the independent single path are located in such a fashion as to traverse the meter in the center of the meter body. The transducers for the fiscal 4-path meter are located in the traditional Westinghouse configuration common to many 4-path chordal meters. The reason for locating the single-path in the middle is to put it in the most sensitive position of the meter. This will result in a difference between this single path and the fiscal 4-path when the velocity profile changes. That is, the single-path meter, with the sensors located in the middle of the flowing gas, is more sensitive to flow disturbances than the 4-path meter design.

These disturbances (velocity profile changes) can be caused by several external factors including partially blocked flow conditioners and pipeline contamination. All of these will cause a change in the velocity profile seen at the meter. This concept works because changes in profiles significantly impact the reading by the centrally located single path while having very little affect on the 4-path meter. Figure 1 is an artist drawing of this design.

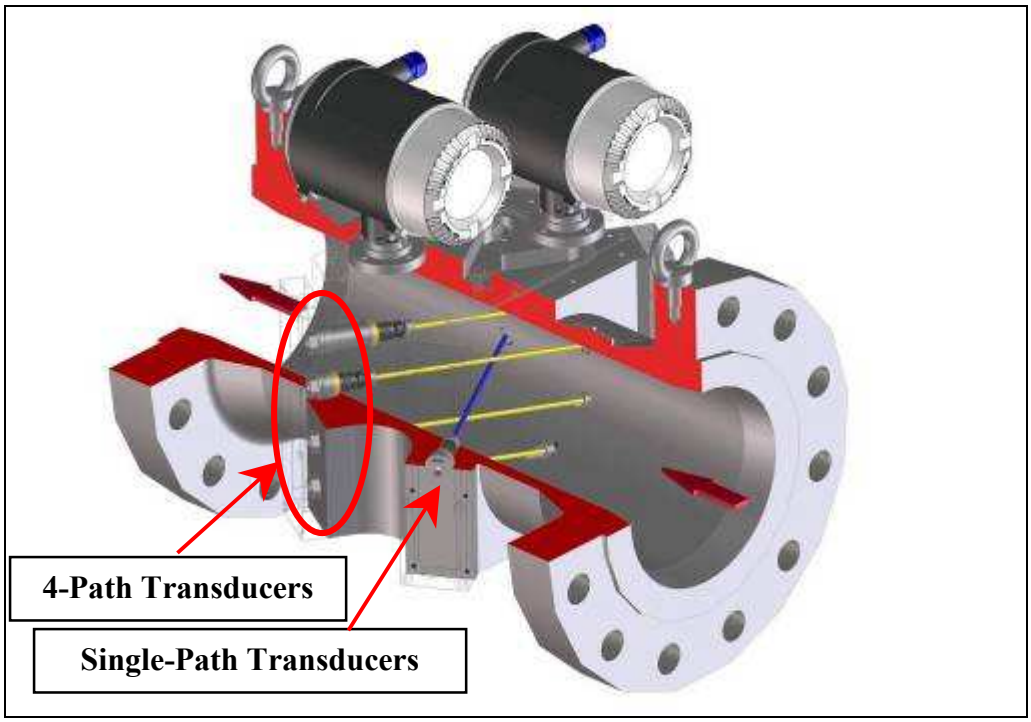

Figure 1: CBM 4+1 Meter Design

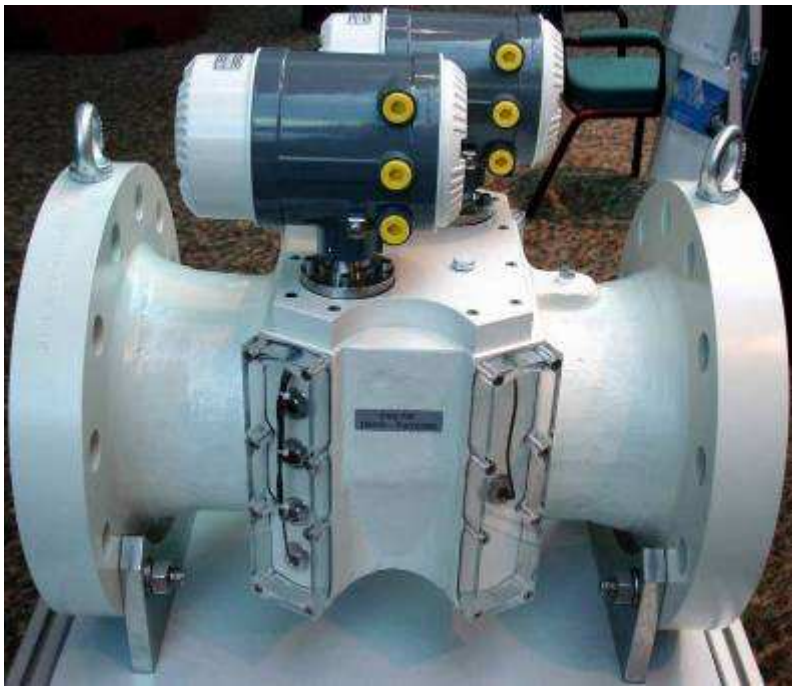

Figure 2: 8-inch CBM 4+1-Path Meter

Figure 2 shows an 8-inch 4+1 meter with plastic covers over the transducer mounting area. The plastic is simply for a better view and certainly would not be used in the field. Figures 3 and 4 show the transducer locations as well as the installation of the two electronics.

Figure 3: CBM 4+1 Transducers

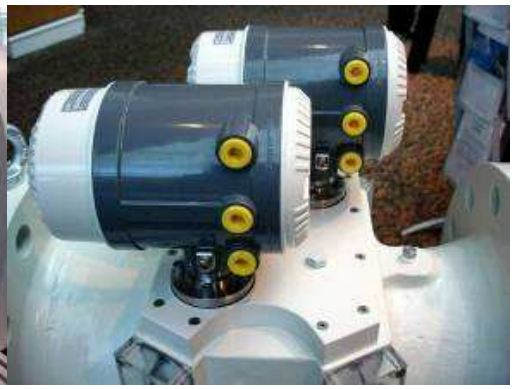

Figure 4: CBM 4+1 Dual Electronics

Figure 3 shows a close-up of the transducers in a demo model. The single-path transducers on the right of the meter are located in the center of the meter and do not bounce off of the meter body (direct path configuration). Figure 1 shows this direct path uses the traditional angle of 60 degrees. Thus the overall path length of this single-path pair of transducers is only slightly longer than the longest paths (paths 2 and 3) in a 4-path meter.

Two independent Signal Processing Units (SPU) are used, one for the 4-path configuration, and one for the single-path configuration. Both electronics energize their transducers independently of the other. There is also no communication between the electronics, and no interaction between the sound pulses from one "meter" to the other. Figure 4 shows the dual electronics and the mounting on the top of the meter.

The concept of comparing the flow determined by the 4-path to that of the single-path is not new. This technique has been used by TransCanada Pipelines for many years. In their installation configuration they often utilize a single-path center-line bounce meter installed approximately 5 nominal diameters downstream of a 4 path chordal custody transfer meter. The single path meter would be adjusted to agree with the calibrated 4-path at the time of commissioning. In other words, the single path meter would not be flow calibrated at a laboratory, but rather "in situ" calibrated after installation in the field. This would be performed at the time of commissioning when the meter station piping was clean and there were no measurement problems.

The theory behind this technique is relatively simple. The purpose of using 4 paths to measure gas volumes in fiscal applications is to reduce measurement uncertainty due to changes in the profile that can occur over time. As the profile may change due to operating conditions, it is desired that the accuracy of the fiscal meter not be affected. The TransCanada Pipeline installations, as well as most other North American designs, utilize a perforated plate style of flow conditioner, known as the CPA 50E, to reduce the effects of upstream piping disturbances. The flow conditioner produces a relatively symmetrical, non-swirling and repeatable velocity profile throughout the operational velocity range of the meter.

The comparison of the output of both meters is not on a real-time basis, but rather performed once per hour. That is, the uncorrected accumulated volume in the 4 path meter is compared to the single path meter at the hourly level. Hourly checks help eliminate the minor

differences that will occur on a real-time basis between the two meters due to their different velocity sampling techniques. This also permits using a tighter tolerance difference and increases the reliability of the testing.

Over time conditions can change in the piping system that can impact the accuracy of the meter, even when using a flow conditioner. These changes include blockage of the flow conditioner with a foreign object, contamination over time from oil and mill scale, unexpected or unanticipated pulsation of gas, and potential changes within the 4-path meter electronics and transducers. By incorporating a second independent electronics with an independent path, this design essentially provides a real-time flow check against the 4-path meter. But why use a single path design to check the 4-path meter instead of another 4-path design checking the fiscal 4-path meter?

During the past several years data has shown that single path meters, with the transducers located to send sound pulses through the middle of the meter body, are more sensitive to profile changes. These include asymmetry, swirl and other profile changes that occur due to contamination or anything that causes a different profile entering the meter.

In a paper published in 1998 by Terry Grimley [Ref 3], installation effects were measured on two multi-path meters, and on two single-path meters. A variety of installation effects were tested including two elbows in and out of plane upstream of the four meters. The multipath meters performed relatively well with errors attributed to the installation effects on the order of 0.5% or less. In the same piping configuration the single path meters had errors that were on the order of 2-5%. Clearly the multipath meters could deal with the asymmetrical and swirling profiles far better than the single-path meters.

Profile changes also occur when contamination develops on the inside of the piping and meter. As the buildup occurs, the wall friction increases causing the velocity profile in the center of the meter to be higher relative to the area along the pipe wall. A paper published at the North Sea Flow Measurement Workshop (NSFMW) in 2005 [Ref 1] discusses how the profile changed over time due to internal pipeline contamination. This paper shows examples of the meter's response when blockage occurs upstream at the flow conditioner. The velocity profile differences between the 4 path meter and the independent single path meter resulted in significantly different measurements between the two designs.

Placing the single-path pair of sensors in the center of the meter body was done intentionally as this is the most sensitive location for flow measurement. That is the center-line path will shift far more than if located at any other position within the meter. This makes it an excellent check against the 4-path which experiences much less shift when the profile changes.

The benefit of the chordal design and understanding the velocity profile has been discussed in several published papers [Ref 1, 4, 5 & 7]. When the meter is installed with a flow conditioner, the technician can identify problems by looking at the velocity profile. Some problems develop over time, some occur very quickly as in the case of a foreign object lodging itself against the flow conditioner. Other blockage conditions can occur due to hydrate formation when the gas may be cold, or encounters significant pressure change. This hydrate condition has been known to completely block the transducer ports and thus render the meter inoperative.

Through the use of meter diagnostics, and the associated manufacturer's software, many of the above problems can be identified. The problem with the conventional method of identifying potential measurement errors is that most users only check the meter's diagnostics on a monthly basis, and sometimes less often that that. When a problem occurs, it may be weeks before it is identified, and thus the impact on billing can be substantial.

By using the CBM 4+1 method of comparing the output of a single-path meter to that of the fiscal 4-path chordal meter, the performance of the two meters is validated every hour. This means if a problem occurs, a potential measurement error can be identified by the system within one hour. Once a problem has been identified, technicians can be dispatched to investigate or the meter can be monitored more closely for further action. In today's environment where the price of gas is ever increasing, errors in transportation, buying and selling of natural gas can lead to more significant financial risk than ever before. Knowing a meter has a potential problem within an hour will help reduce unaccounted for gas (UAF).

2. PROVING THE CONCEPT

Does this technique really work when it is contained within only one meter body? To answer this question, testing was conducted at the CEESI Iowa high flow calibration facility in Garner, Iowa. For this test a 12-inch 4+1 meter was installed with a CPA 50E flow conditioner upstream. This type of flow conditioner has been used in many USM applications around the world.

One of the issues with using a flow conditioner is that debris can collect in front of the flow conditioner. When this occurs there can be an affect on the USM accuracy. The effect has been documented in several presentations [Ref 1, 5 & 6].

To quantify the benefits of this design, testing with several blockage scenarios was conducted. Not only were the 40% blockage tests duplicated from previous tests [Ref 5 & 6], but additional testing was done with just 3 holes blocked on the CPA, and also with only 1 hole blocked. In order to identify whether location of the blockage was an influence, the 3 holes blockage test was performed with the blocked holes on the bottom, and then also with the blocked holes located 90 degrees from the bottom. Three velocities were used for all of these tests. These were approximately 7 m/s, 14 m/s and 21 m/s.

All testing was performed with a significant length of straight piping upstream of the metering package. This upstream length of straight pipe would present a very symmetrical and non-swirling profile to the CPA 50E flow conditioner.

Figure 5 shows the 12 inch meter installed at the CEESI facility for the testing..

Figure 5: 12-inch 4+1 CBM Meter CEESI

A CPA was installed 10D upstream for baseline testing. After the baseline testing was complete, and the adjusted output for both the 4 path meter and the single path meter were verified, the 12-inch CPA was partially covered with duct tape (40% blockage). Figure 6 shows the flow conditioner prior to testing.

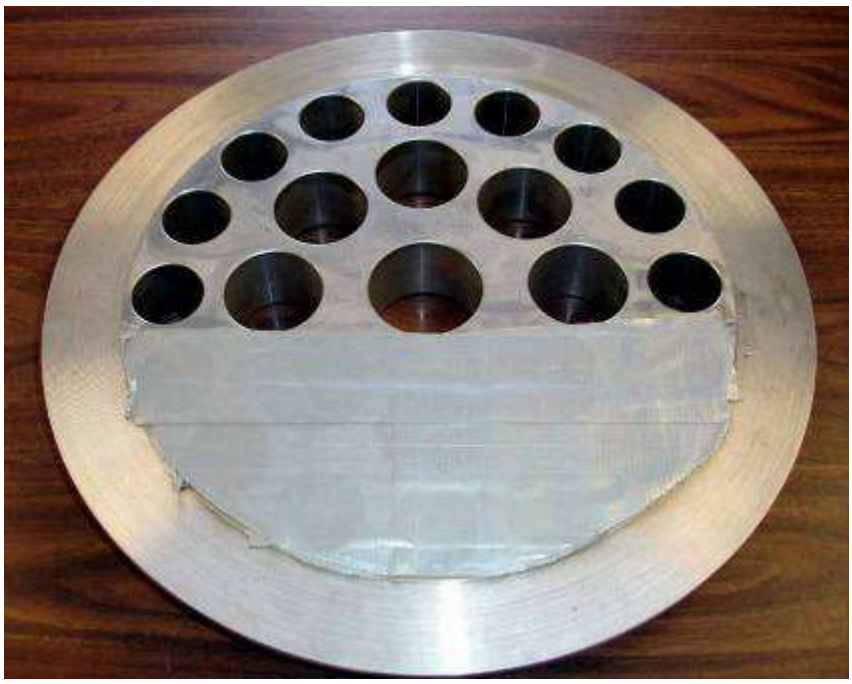

Figure 6: 12-inch CPA with 40% Blockage

Duct tape was used to block the holes as this provides a repeatable method of testing and can withstand the pressures created by the flow rates used.

Figure 7 shows the results of the 4-path meter after baseline calibration (piecewise linearization) and subsequent results with 40% blockage of the flow conditioner.

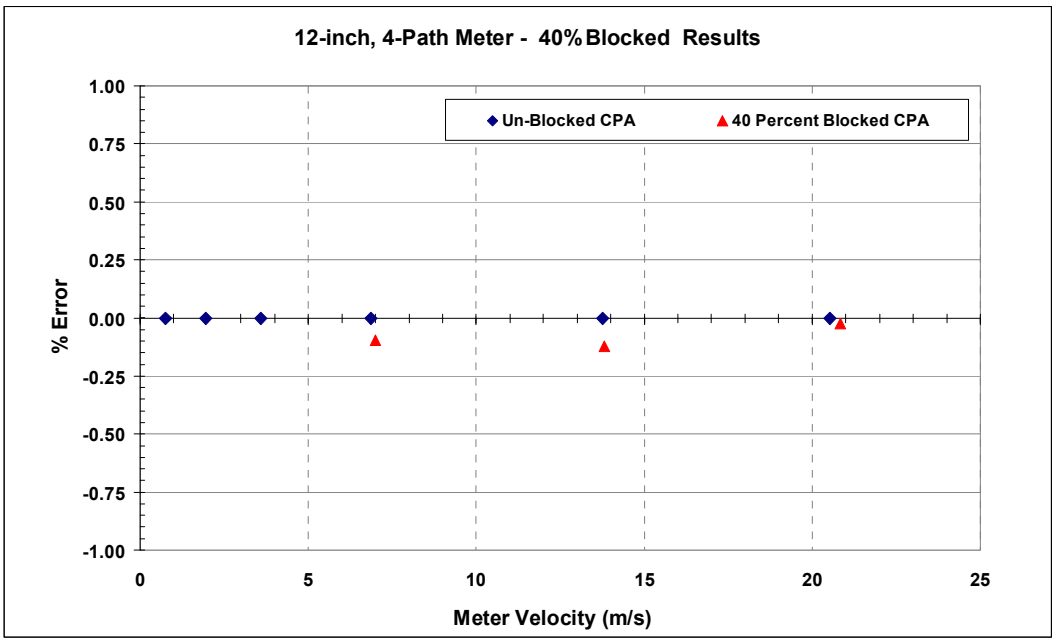

Figure 7: 12-inch, 4-Path Meter Results with 40% Blockage

Figure 7 shows that the 12-inch, 4-path meter shifted on the order of -0.15%, or less, for all three velocities tested. Figure 8 shows the results of the single-path during this same time.

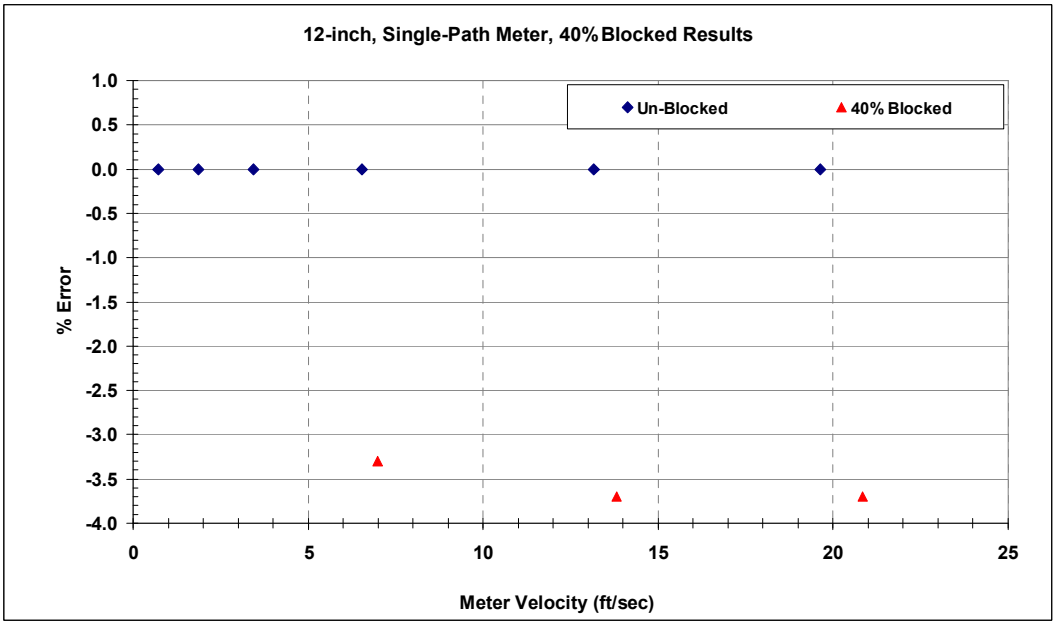

Figure 8: 12-inch, single-Path Meter Results with 40% Blockage

Figure 8 shows the impact on the single-path meter to be on the order of -3.5%. Thus for the same blockage the 12-inch meter, the single-path meter shifted more than 20 times as much as the 4-path meter.

The next test involved blocking only 3 holes at the bottom of the meter. Figure 9 shows the flow conditioner with these holes blocked.

Figure 9: 12-inch CPA with 3 Holes Blocked

The blockage of the three holes was developed by simply removing some of the duct tape that had been used to block 40% of the CPA. Thus there is some residual adhesive left on the face of the flow conditioner.

Figure 10 shows the results of the 4-path meter with blockage at the bottom, and then rotated to the side (90 degrees from the original location).

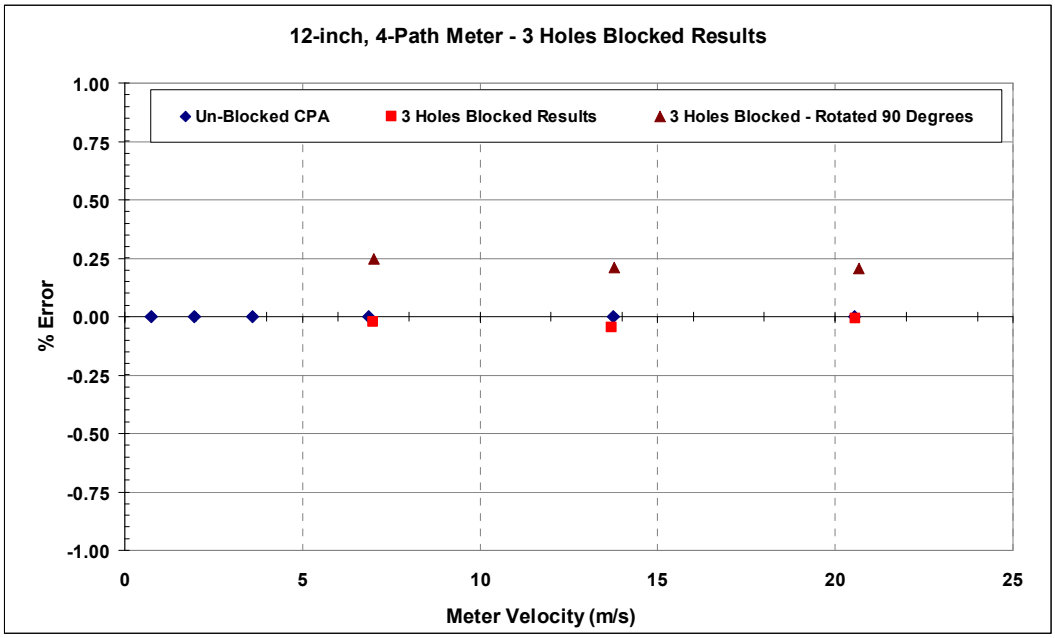

Figure 10: 12-inch, 4-Path Meter Results with 3 Holes Blocked

When the blockage was at the bottom of the meter run, there was very little impact on accuracy. When the blockage was rotated 90 degrees to the side, the meter responded with a shift of about +0.25%. All other blockage tests to date had shown the meter responded with a negative shift in error, but for the first time the meter now measured fast with this blockage.

Figure 11 shows the results of the single-path during these tests.

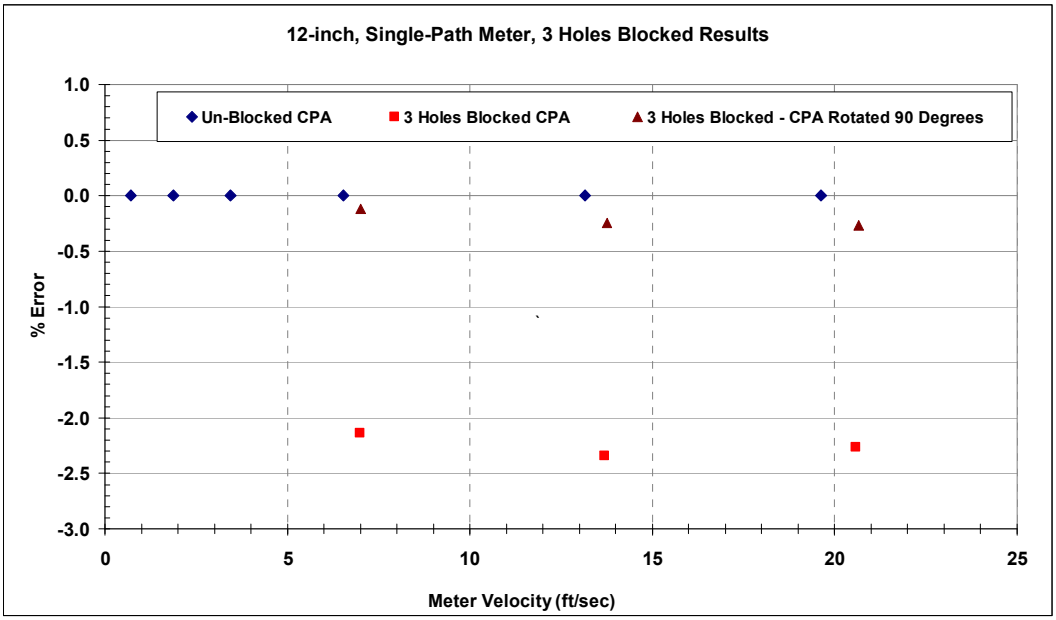

Figure 11: 12-inch, Single-Path Meter Results with 3 Holes Blocked

The single path meter shifted more than 2% slow when the blockage was at the bottom, and about 0.3% slow when the blockage was on the side. Even though the shift in the single-path meter was only 0.3% slow when the blockage was on the side, the difference between the 4-path and the single-path was still approximately 0.5%. The next step was to test the meter with only one blocked hole. Figure 12 is a picture of the CPA prior to the testing.

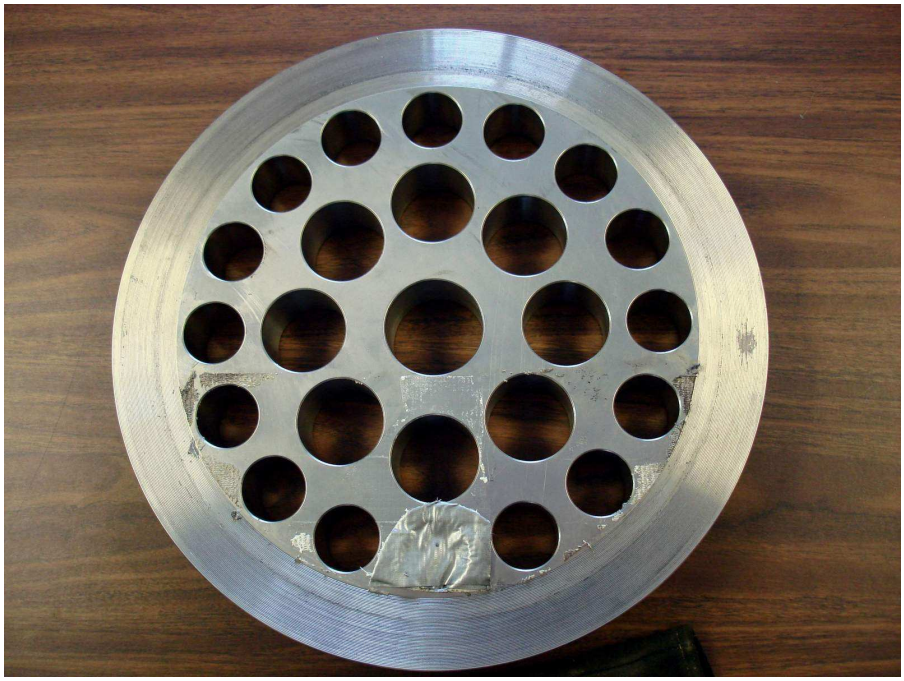

Figure 12: 12-inch CPA with 1 Hole Blocked

The single hole that was blocked was located on the bottom of the meter. This location was chosen as the most likely place for blockage to occur.

Figure 13 shows the results of the 12-inch, 4-path meter with this blockage and Figure 14 shows the results of the 12-inch, single-path meter.

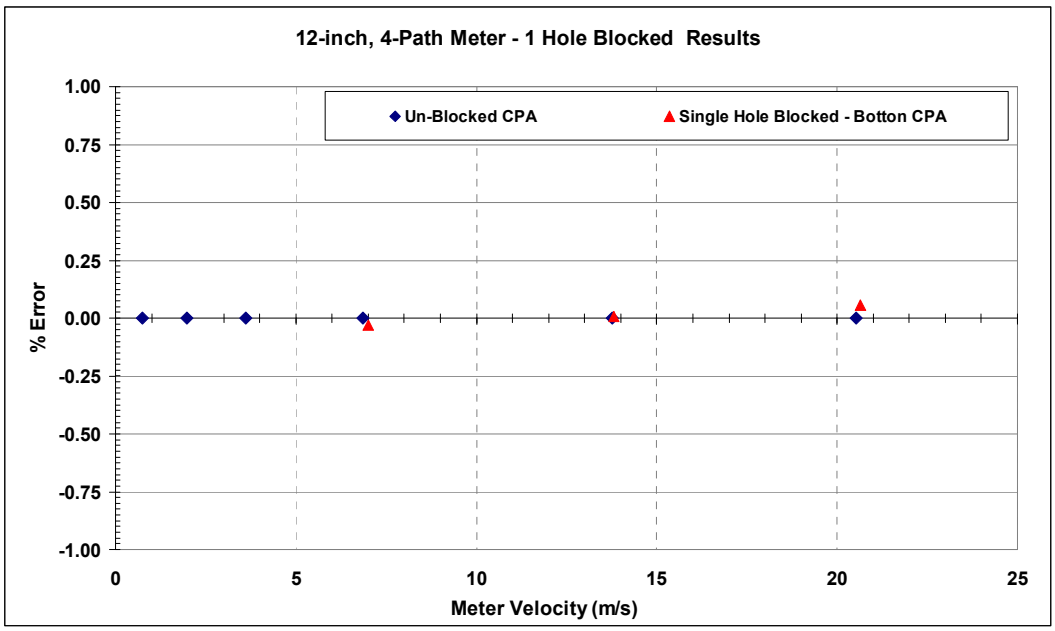

Figure 13: 12-inch, 4-Path Meter Results with 1 Hole Blocked

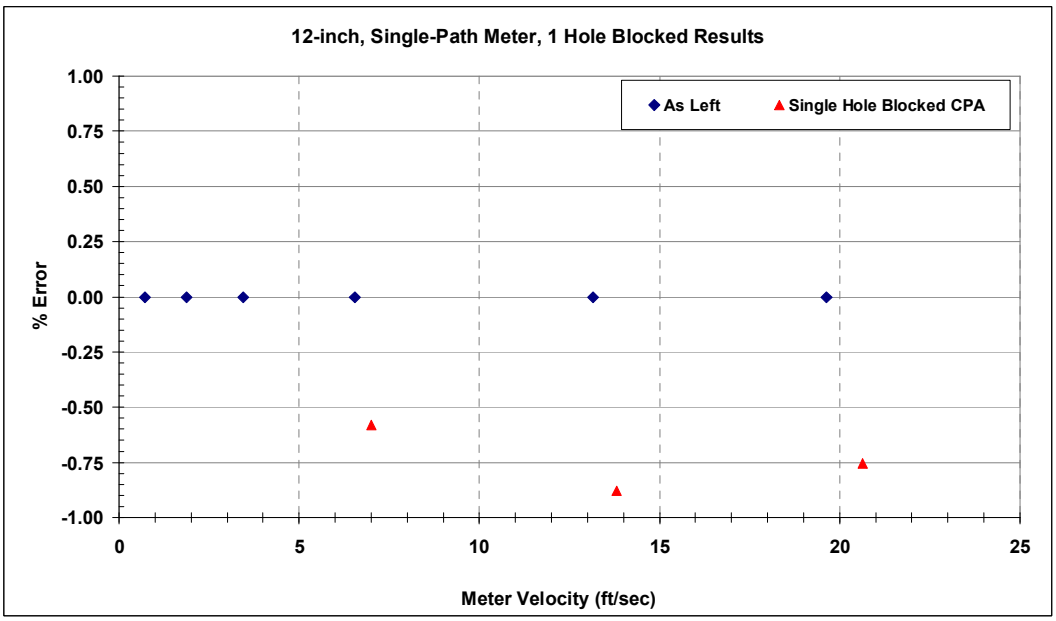

Figure 14: 12-inch, Single-Path Meter Results with 1 Hole Blocked

Figure 13 shows there is no impact on the 4-path meter's accuracy, while the single-path meter, shown in Figure 14, shifted between -0.6% and -0.85%. Thus, even with one hole blocked, the single-path meter shift was very significant, and thus the difference between the 4-path and single-path could be easily identified.

Pipeline contamination, especially over time, is a more challenging problem for the technician. Many pipelines have some minor amount of oil and mill scale that is being transported down the pipeline. Although this contamination is generally small, it can accumulate and have a significant impact on a meter's accuracy.

Several papers have been published over the past 10 years [Ref 4, 7, 8, 9 & 10] which discuss the impact on the meter's accuracy. Some meter designs tend to register fast when contamination coats the meter piping and meter body, while others tend to register slower. The challenge for all users of USMs is to identify this contamination and then to decide when it is time to clean the meter run.

The question is: "Can the 4+1 CBM meter design identify contamination in the piping?". To answer this question an existing 4-path meter was borrowed from a customer. This particular meter is an inter-company operational meter, in a bi-directional application. During the several years of service it has been cleaned numerous times due to contamination.

For this test the entire meter run (including all piping and flow conditioner) was removed, and sent to the CEESI Garner calibration facility. As the installed meter was not a 4+1 CBM design, only the piping was used for this testing to see if the contamination could be identified by the CBM meter.

As this meter was installed in the late 1990's, it used a 19-tube bundle. Figures 15 and 16 show this flow conditioner during disassembly at the CEESI facility.

Figure 15: 19-Tube Bundle

Figure 16: Close-up of 19-Tube Bundle

Unfortunately the meter run had been cleaned recently and the upstream piping was not as dirty as was expected. Figure 17 shows the "as-found" condition of the piping between the flow conditioner (19-tube bundle) and the meter.

Figure 17: 12-inch Dirty Piping

As Figure 17 shows, there was not a lot of contamination remaining due to the recent cleaning of the meter piping. This was a bit of a disappointment for the customer as they expected the piping to be a bit dirtier.

Figure 18 is a close up of one of the meter pipes prior to any cleaning.

Figure 18: 12-inch Dirty Piping Close Up

Today most designers do not use this type of flow conditioner but instead select a perforated plate like the CPA 50E. The customer chose to re-install the meter after testing and replace the 19-tube bundle with the CPA unit. For this reason all testing was conducted with a CPA flow conditioner. To simulate what the flow conditioner may look like had it been subjected

to normal pipeline contamination, "texture" paint was applied to the CPA flow conditioner. Figure 19 shows the flow conditioner just prior to being installed for the testing.

Figure 19: 12-inch CPA with "Texture Paint"

Although this coating might not represent the identical contamination to the piping, it was felt at the time that some type of contamination was needed to at least simulate surface buildup. The 19-tube bundle could have been used for this testing. The customer had previously decided to re-install the 4+1 CBM meter, after all testing was complete, for some long-term testing and wanted the CPA to be used during this time. In order to save some calibration time, rather than conduct testing with the 19-tube bundle, it was decided to contaminate the CPA for the "as found" dirty testing.

Figure 20 shows the results for the 4-path meter both dirty and clean.

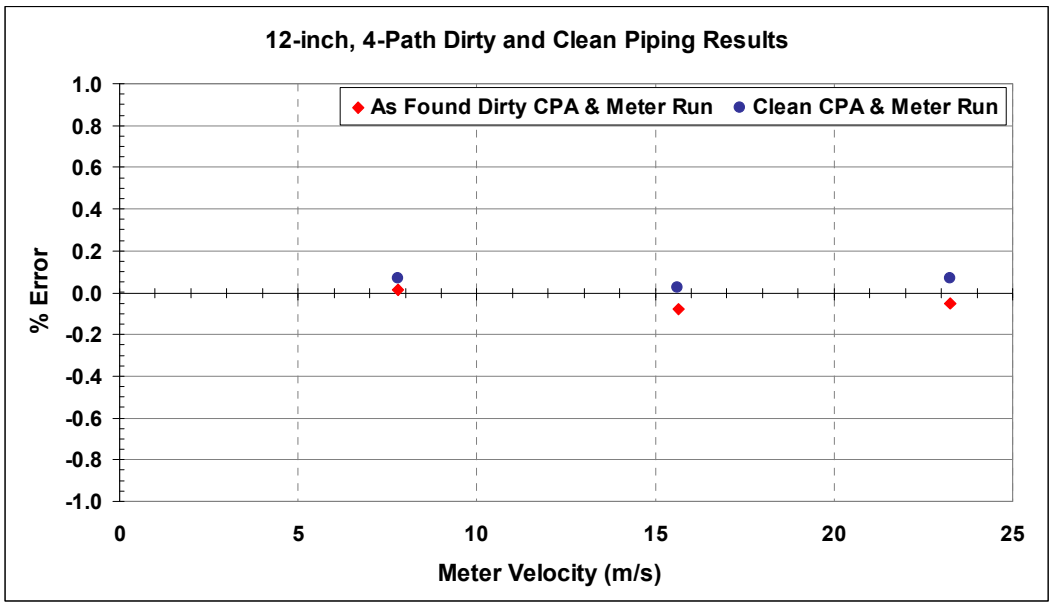

Figure 20: 12-inch, 4-path As-Found Dirty and As-Found Clean

The results of the 4-path meter as-found baseline are show with the blue dots after the piping was cleaned (meter was brand new and thus clean). The red dots represent the as-found results with the upstream piping and CPA dirty. The table in Figure 21 shows the difference between the two at each flow rate.

Velocity	% Diff.
23.3	-0.12
15.7	-0.10
7.8	-0.05

Figure 21: 4-path Dirty vs. Clean Differences

Figure 21 shows the meter registered slightly slower with the upstream piping being dirty compared to the clean piping. This is the expected results since a previous paper [Ref 4 & 7] had demonstrated that the upstream piping tends to cause the chordal meter to register slightly slower when dirty.

Figure 22 shows the results for the single-path during the same conditions.

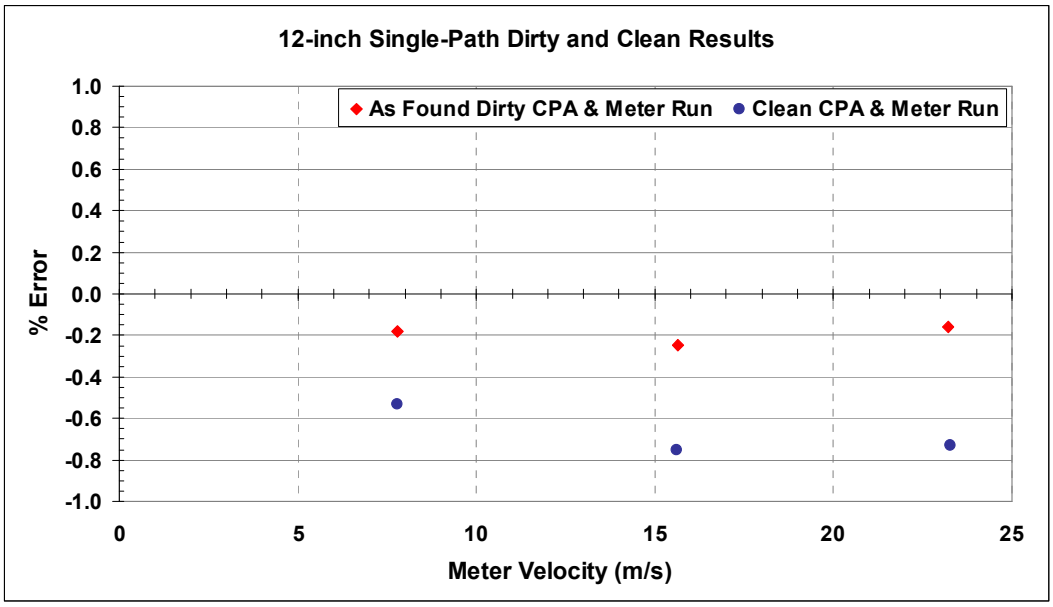

Figure 22: 12-inch, 4-path As-Found Dirty and As-Found Clean

In Figure 22 the single path meter registered faster (red dots) when the upstream piping was dirty compared to the clean upstream piping as shown with the blue dots. This difference is summarized in Figure 23.

Velocity	% Diff.
23.3	-1.30
15.7	-1.26
7.8	-0.88

Figure 23: Single-path Dirty vs. Clean Differences

As this table shows the single path meter registered faster when dirty and is just the opposite of what the 4-path meter showed. Although this isn't as thorough of a test as a uniformly dirty meter, it does show that the single-path meter behaves differently than the 4-path meter. With very little contamination on the upstream pipe wall, the single path meter's response was easily seen. In the near future this entire meter assembly will be removed and once again tested but this time all the components will have been contaminated uniformly. The results of this will be published in a future paper.

3. IMPLEMENTING THIS DESIGN

As discussed earlier in this paper, both electronics operate independently. The output of each meter needs only to be brought into the same flow computer and volumes stored for both as would normally be done for two separate meters. To take advantage of this feature, the hourly uncorrected volumes would then be compared and an adjustable tolerance set based upon some history established during commissioning. The tolerance may vary somewhat from site to site, and will depend slightly upon the upstream piping conditions and the symmetry of the profile downstream of the flow conditioner. However, the typical agreement that has been seen from some field data is on the order of ±0.5%.

The comparison test probably should not be conducted when meter velocities are below perhaps 3 m/s as the profile effects can become more significant. For this reason the flow computer should accumulate separate totals for comparison testing since the effective cutoff for the comparison would be perhaps 3 m/s. Thus it may not be practical to use the absolute uncorrected volumes through each meter if the flow rate is frequently below this velocity.

For most installations meter velocities are usually always above 3 m/s. This is common in mainline stations where there is always flow. For these cases a direct comparison of hourly uncorrected volumes would suffice. Many users already have this capability built in to their flow computers. They do comparisons of "run ratios" in order to spot potential problems. For these users they simply have to connect the meter to the flow computer, set the comparison ratio to a value, and start monitoring for the alarm. Thus taking full advantage of this meter design can be incorporated immediately without special flow computer programming.

The next phase of testing will be to determine how much the single-path meter will shift when installed in "real-world' conditions where contamination exists. Papers have been published [Ref 1 & 7] showing that the chordal design meter is relatively insensitive to contamination over time. It is expected the single-path meter will shift significantly during this period. The real question is "Can the use of the 4+1 CBM meter design be used to predict when the 4-path fiscal meter error exceeds a prescribed amount?"

Many users today know they have contamination in their metering systems. They periodically clean the meter in order to minimize the uncertainty effect due to contamination. If the amount of difference between the 4-path meter and the single-path meter can be used to determine the cleaning interval, these users will then benefit from extended inspection intervals and thus save significant O&M expenses.

4. CONCLUSIONS

Today the cost of energy is higher than it was several years ago, and it is not likely this trend will reverse itself. By implementing ultrasonic metering technology users have been able to improve their measurement and reduce their UAF during the past several years. One task always remains for the technician and that is to insure the meter is operating correctly and accurately. This applies to all measurement technologies, not just USMs. The significant benefit of the USM is the ability to provide diagnostic information for the user to help determine the meter's "health."

Today technicians have software to help understand the operation of their USM. Since each manufacturer of USMs uses a different velocity integration technique (different path configurations), it is often difficult for the technician to fully understand whether his USM is operating correctly or not. Additionally, since most only inspect the meter's operation once per month, problems can occur and go undetected for many days or weeks. This can significantly increase measurement uncertainty during this time.

The CBM 4+1 meter design relies on basically two principles. First, the fiscal meter is chosen to be the least sensitive to any flow profile changes that may occur in normal operation. And second, the "check" meter design is chosen to be one that is the most sensitive to any flow profile changes. Ideally any affect of profile changes would not only have a significantly different impact on accuracy, but the effect would be in opposite directions, making the difference much easier to detect.

The benefit of the CBM 4+1 meter design is that the flow computer is used to check the health of the fiscal 4-path chordal meter by simply comparing it to the single-path meter. If the velocity profile remains relatively constant, both meters will agree. Should some process condition upset the normal profile, the single-path meter will respond significantly different than the 4-path. These upsets can include the following:

- Blockage in front of the flow conditioner
- Contamination due to oil and mill scale buildup over time
- Pulsation in the pipeline due to compressors (sampling rate for the single-path exceeds 75 times per second, thus virtually making the single-path insensitive to pulsation)
- Potential problems with the fiscal meter including transducers and electronics problems
- Full redundancy should there be a failure of the electronics

Today the cost of accuracy has never been more important. There are many applications where the accuracy of the measurement must be maintained to the highest degree possible. This CBM 4+1 meter design provides a "real-time health check" on the custody transfer meter. This significantly reduces the overall uncertainty of the measurement, and also reduces the O&M costs attributable to the technician by providing a timely (almost immediate) warning when a problem occurs.

5. REFERENCES

1. John Lansing, *How Today's USM Diagnostics Solve Metering Problems*, North Sea Flow Measurement Conference, October 2005, Tonsberg, Norway
2. Klaus Zanker, *Diagnostic Ability of the Daniel Four-Path Ultrasonic Flow Meter*, Southeast Asia Flow Measurement Workshop, 2003, Kuala Lumpur, Malaysia
3. T. A. Grimley, *The Influence of Velocity Profile on ultrasonic Flow Meter Performance*, AGA Operations Conference, 1998
4. John Lansing, *Dirty vs. Clean Ultrasonic Flow Meter Performance*, North Sea Flow Measurement Conference, October 2004, St. Andrews, Scotland
5. Larry Garner & Joel Clancy, *Ultrasonic Meter Performance – Flow Calibration Results – CEESI Iowa – Inspection Tees vs. Elbows*, CEESI Ultrasonic Conference, June 2004, Estes Park, CO
6. John Lansing, *Features and Benefits of the SICK Maihak USM*, CEESI Ultrasonic Conference, June 2006, Estes Park, CO
7. John Lansing, *Dirty, vs. Clean Ultrasonic Gas Flow Meter Performance*, AGA Operations Conference, May 2002, Chicago, IL
8. L. Coughlan, A. Jamieson, R.A. Colley & J. Trail, *Operational Experience of Multipath Ultrasonic Meters in Fiscal Service*, North Sea Flow Measurement Conference, October 1998, St. Andrews, Scotland
9. John Stuart, Rick Wilsack, Re-Calibration of a 3-Year Old, Dirty, Ultrasonic Meter, AGA Operations Conference, 2001, Dallas, Texas
10. James N. Witte, *Ultrasonic Gas Meters from Flow Lab to Field: A Case Study*, AGA Operations Conference, 2002, Chicago, IL

Test of a 1 inch Roxar Watercut meter on light condensate with very low water content.

Georg Johnsen, Roxar
Rune Martinussen, co writer, Roxar

1 INTRODUCTION

The Oil industry is rapidly moving towards more difficult crude products, as more and more of the easy produce able crude oil will be finished. This leads to new challenges for the whole industry, finding better equipment to coupe with these challenges.

One such trend is in the oil business is moving towards lighter oils or condensates. These will have to be processed and transported under high pressure, to stay liquid. The residue water, more or less saline, in condensates can cause serious corrosion problems in the downstream process equipment and pipelines.

The Roxar Watercut meter have undergone a test on light condensate, with standard density of about 625 kg/m^3, to establish how good the meter is for measuring the very low water content in such products. The ordinary process conditions were 0-650 ppm volume water, while the maximum range was 0-1650 ppm. The test took place offshore on a real condensate line, and was conducted by a large oil company.

A standard Watercut meter was optimized during the installation process for optimization to these process conditions. Also the different contributions to the total measurement uncertainty from the different sensors (microwave, temperature and density) were evaluated, to see if such an installation was possible in the first place.

In-line calibration is crucial on such installations, because it basically will compensate for any biased uncertainty in the measurement system. Establishing the dry oil permittivity under such circumstances is crucial for correct determination of the water content in the meter. Also, sampling several times, then averaging the samples, gives a very good correspondence, better than 50ppm under fairly stable process conditions.

2 THE MEASUREMENT CHALLENGE

2.1. Measurement terms of Water content.

Water content is mostly usually measured in volume percent (%). But for very low water content, it is often wanted to measure the water content in ppm. Since this is rather seldom, the correspondence between these two is not obvious to everyone. To recollect, these are:

1 % = 10.000 ppm
0.1 % = 1.000 ppm
0.01 % = 100 ppm

2.2 The application.

As the easy accessible hydrocarbons more and more are been exploited, the industry will have to turn to more difficult reservoirs to fill the worlds need for hydrocarbons. One set of such more difficult reservoirs are light condensate reservoirs.

Some typical characteristics of a light condensate application are:

- High pressure
- Possibility of flashing
- Stable density
- Stable temperature
- Very low water content (easily separable phases)
- Generally very little problems with scaling

2.3 Permittivity measurement of the condensate and water mixture

The Roxar Watercut meter is designed to measure the permittivity of the content flowing through the meter. The permittivity measured in any resonance cavity is defined by.

$$\varepsilon_{mix} = \left(\frac{f_{vac}}{f_{mix}} \right)^2$$

The meter will then establish the expected permittivity of the dry hydrocarbon fraction in the meter, and the permittivity of the water in the mixture.

These numbers will then go into the famous Bruggeman equation, well established as the correct way of determining the content of one fluid entrained within another fluid with different permittivity. For a hydrocarbon continuous flow with entrained water, this formula will look like:

$$\beta = 1 - \frac{\varepsilon_{mix} - \varepsilon_{water}}{\varepsilon_{oil} - \varepsilon_{water}} \sqrt[3]{\frac{\varepsilon_{oil}}{\varepsilon_{mix}}}$$

In this equation, the establishment of ε_{mix} can be done with a very low degree of uncertainty, and high degree of repeatability.

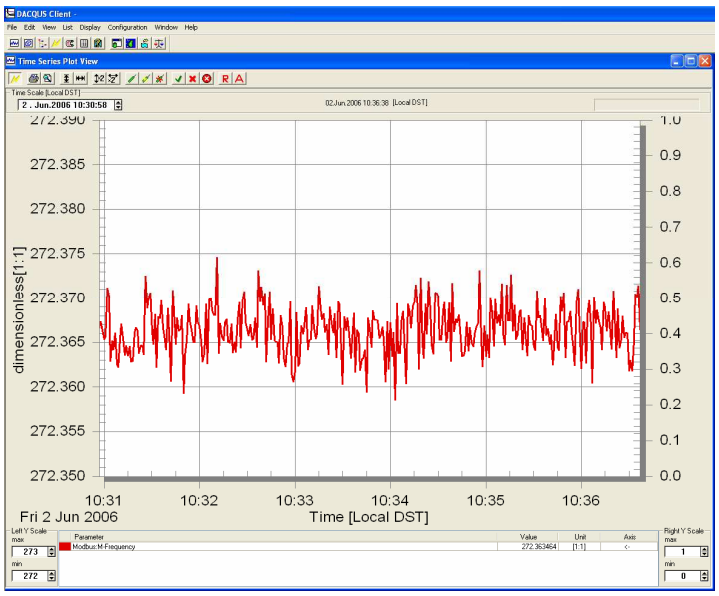

Fig. 1

The chart is logged with a fixed reference. Every point is independent measurements. As we see, the scatter band is maximum ±5 kHz at a measurement frequency of 272 MHz, or proximately ± 20 ppm.

It can be demonstrated with a sensitivity analysis of the Bruggeman equation that the ε_{water} has a non significant influence on the calculations of low water contents, and for this application just as well could be set to a typical number, e.g. 100.

It now remains to establish the permittivity of the pure hydrocarbon fraction. This is the main challenge in a light condensate application, which requires this degree of low measurement uncertainty.

Roxar have earlier done research on how to establish the hydrocarbon permittivity. The main single factor which contributes to the variation of the hydrocarbon permittivity is the hydrocarbon density. [1]

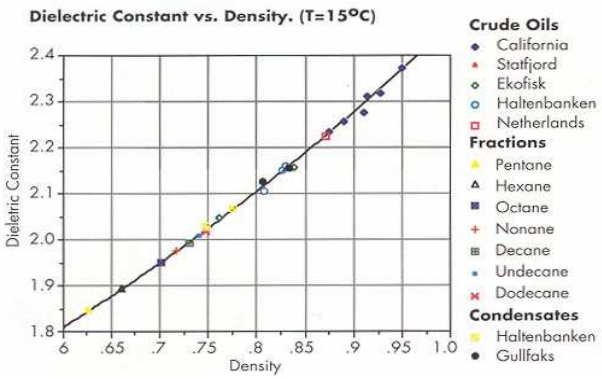

Fig. 2 :

Correlation between density and pure hydrocarbon permittivity (or Dielectric Constant).

Therefore, the most important input to meter, next to the microwave measurements, is a density signal. A reliable density signal is totally crucial for an application like this, and can not be skipped.

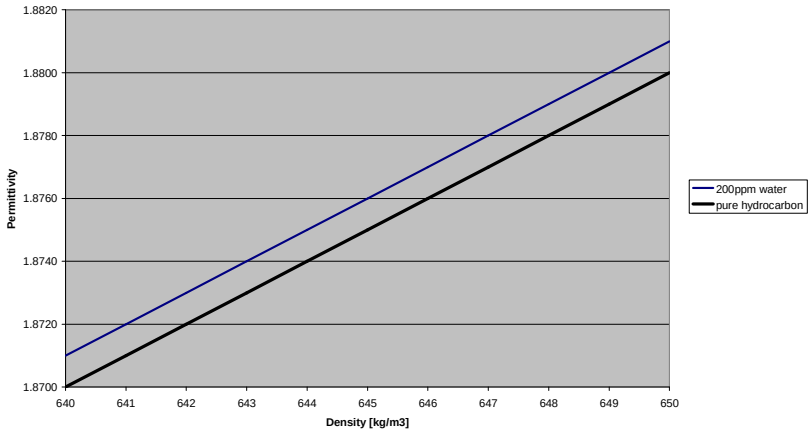

Fig. 3.

Difference in pure hydrocarbon permittivity and 200ppm water mix permittivity

However, there are more factors contributing to the hydrocarbon density. When measuring with the very low degree of measurement uncertainty needed in an application like this, the effects of these other uncertainty contributors must be taken into considerations. A temperature signal will standard be given as a input to the meter. (All Roxar Watercut meters are delivered with a temperature transmitter as a standard.)

Several other effects will also be present to a certain degree. These will have to be cancelled out somehow, and we will soon see how this can be done.

Also, the density signal will have some measurement uncertainty attached to itself. A density input of 1 kg/m^3 would in reality lead to a wrong calculation of the Watercut

of about 270 ppm to low, depending slightly on where in the measurement region the measurements are taken.

Looking into the datasheet of the different options for density measurement, reveal that they all will have some uncertainty attached to them. However, even if the density out of a coriolis meter has a slightly higher uncertainty attached to it, my experience with coriolis meters is that the measurement uncertainty of this figure, is mainly a biased figure, and that the repeatability of this is very good.

Since most applications will have a need for both a flow meter and a Watercut meter, combining a coriolis meter with a Roxar Watercut meter is a very good combination. In this application it will have three effects: Firstly the client will (obviously) have a flow meter. Secondly the density output from a coriolis meter can be used as an input to the watercut meter to establish the correction of hydrocarbon permittivity. And, thirdly, the biased part of the measurement uncertainty of the density, and most of the effect of all the other contributors to establishment of the hydrocarbon permittivity, will effectively cancel out with an inline calibration of the Watercut meter.

With the Watercut meter correctly inline calibrated, the meter was now ready to measure the water content in the condensate.

3 THE TEST

3.1 The test setup

The meter tested was a standard 1 inch Roxar Watercut meter, equipped with the standard Autozero option. The meter had especially short cables of one meter, and extra attenuators were added, to ensure that cable effects (antenna effects) were minimized. Extra attenuators could lead to very high watercuts that is more then volume % higher than 25% would not be measured, but this is way above all water contents applicable for any application like this.

During commissioning, also a special designed software was tested, but this did not improve the performance of the meter any, and was therefore abandoned. A full data logger (Daqcus) was also provided, to log all data during the test. This would reveal any correlations, and would give us the possibility to fully analyze any moment during the test where we suspect anything odd happening.

The standard commissioning procedure for commissioning Roxar Watercut meters was used as the setup basis of the meter, and a best fit offset value was established as the inline calibration of the meter.

The reference system for the test was a sampler system. The tester had made sure to have the best equipment and personnel available to take samples and analyze them.

3.2 The test results

The test stretched for about a week. Several different well-configurations were tested during this period, to check the meter reactions to these changes.
The results from analyzing the samples and from the Watercut meter, clearly indicates that there is two major clashes of test points, and in addition some scattered results.

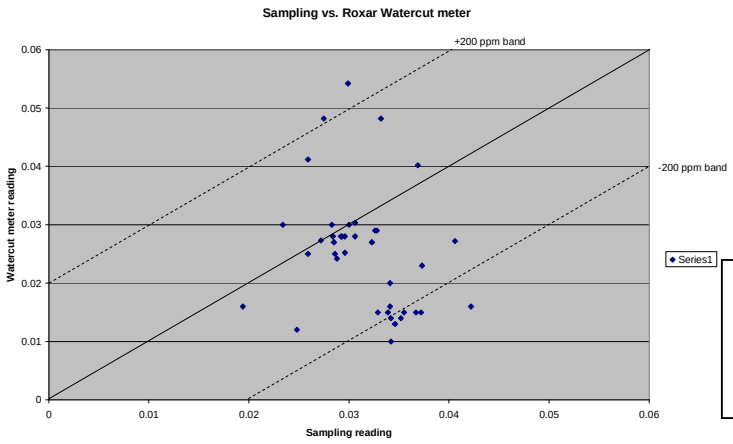

Fig. 4

Linearity of readings of watercut readings vs. sampling

Taking a look at the timeline of the project, vs. the difference in watercut reading, indicates a stable period in the start of the test, then a more scattered intermediate period, then a very stable period in the end of the test. The time the points makes a 'jump', corresponds very good to the tester changing well configurations.

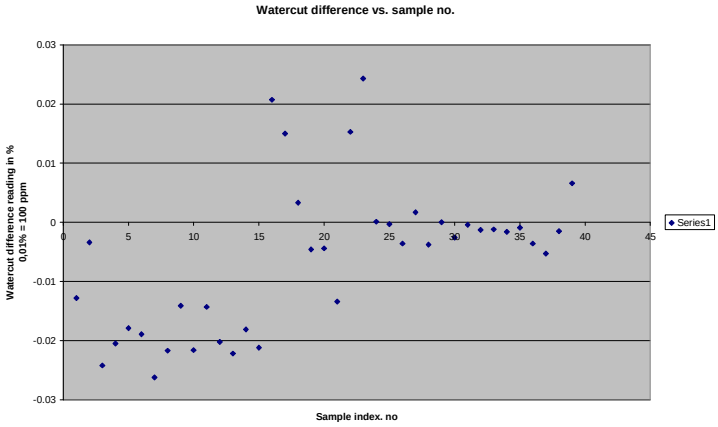

Fig. 5

Difference of watercut reading between the Watercut meter and sampling analyzis.

We would expect that the change of hydrocarbon composition should give a small different permittivity independent of the hydrocarbon density. This corresponds to the small scatter of points along the density vs. permittivity curve in chapter. 2.1.

Plotting the results as a function of densities measured at the test points, clearly demonstrates a correspondence between the density measured at the test point, and the watercut difference.

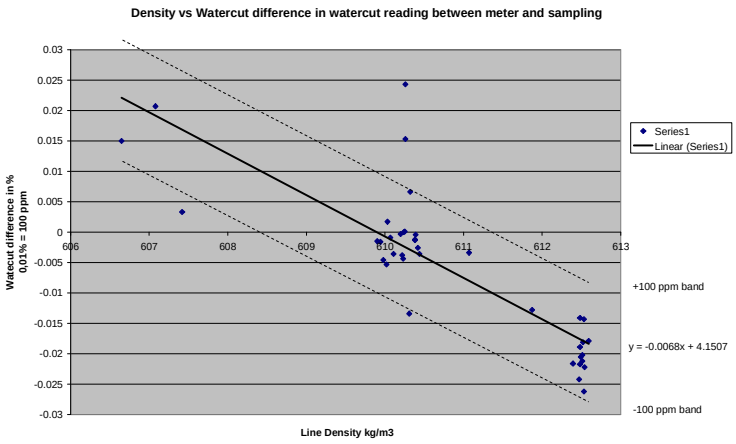

Fig. 6

Density vs. Watercut difference reading between Watercut meter and sampling analysis.

There are mainly two reasons for this:

1. The density correction in the meter is slightly inaccurate in this region for this particular application.

2. The different well configurations in this application will result in different hydrocarbon compositions, creates a pattern which is unique for this application.

The good correspondence between the sampler measurements and the Watercut meter measurements both clearly demonstrates that the sampling was done at very high degree of accuracy, and that the meter is very repeatable. However, in any systems doing repeatable operations (taking repeatable samples), with the possibility of many types of error (including human), it must be expected that one or some few of the sampling results are off. It is therefore impossible to determine if the reason for the few misreading is that the sample result is inaccurate, or the Watercut meter is inaccurate. The only conclusion we can make in such a case is that at least one of the measurements is inaccurate.

4 A PROPOSED SOLUTION FOR THIS MEASUREMENT CHALLENGE

Exploiting the correlation data between the density and the water content difference between the meter and reference indicates that it is possible to impose a correction for this. However, the data from this test exclusively is insufficient to make a general correction in the meter, valid for all applications. Also, improving the Watercut meter, based on data obtained from the meter itself, is not an independent way of improvement.

However, a local correction is possible to do. And, since every application is unique, a local correction method for these types of applications is probably the far best route to go.

A method of determining a correction for the meter has been developed and then implemented into the meter. We have called this method: Local Characterization. The following steps must be followed to implement this method fully into the meter:

1. First the meter must be installed, and measurements started. It should be possible to change well configuration and/or reservoir during this calibration.
2. Run a high number of samples over the full operation area of the meter, and note down the Watercut- and density reading corresponding to every sample.
3. Calculate the watercut difference between the samples and the watercut readings from the meter.
4. Plot the correlation between the density (x-axis) and the watercut difference (y-axis).
5. Find a best fit linear (ax+b) correlation between density and watercut difference.
6. Enter the coefficients ‘a’ and ‘b’ into the Watercut meter. This line will now be the watercut baseline in the meter for this application

The measurement uncertainty will now be the scatter around this line.

In appendix 2 is a numbered example of how to establish a linear correlation between density and permittivity.

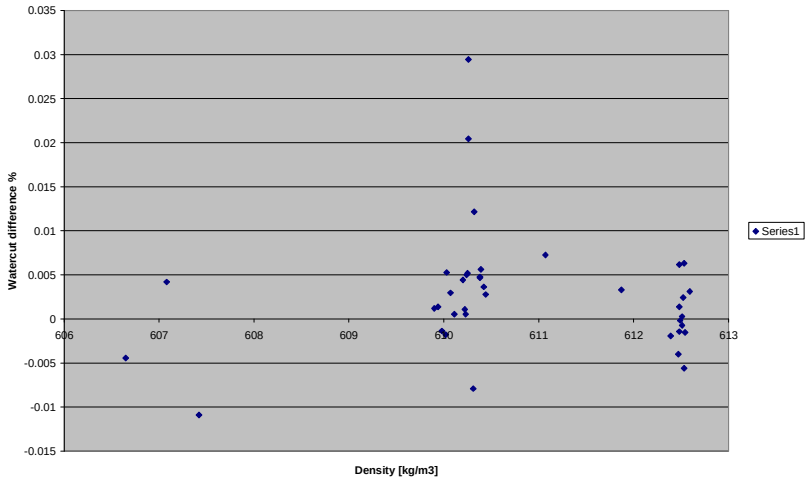

Figure 6

Watercut difference between sample analysis and Watercut meter reading, back-calculated from test results.

Roxar have now implemented this method into the Watercut meter software, and it is available as an option with a new meter. Further, since this method is implemented as a software change only, it is possible to upgrade existing meter with new software with this functionality included.

There is however some uncertainties attached to this method. If the application consists of three or more distinct hydrocarbon compositions, there is a possibility that these three can not be aligned to a line fit. A best fit approach will however reduce the measurement uncertainty greatly, but some additional uncertainty around this must be expected in cases where the different hydrocarbon does not fit linearly.

5 CONCLUSION

Condensate applications, close to a reservoir but after separation, are known to be very stable processes. The water content is generally very low, since water separates fairly easy from the condensate. Also, any process changes are generally slow, due to the fact that the condensate has had time to settle down and mix in the separator tank.

On an application of light condensate with very low water content, it is possible to achieve very low measurement uncertainty with the method ‘local characterization’ implemented into the Watercut meter. The method is basically an advanced way of inline calibrating a meter, and taking into considerations local effects of different hydrocarbon compositions.

The method will cancel out local effects on the special offset of the local hydrocarbon composition, as well as small local differences from the general correction of the density versus the hydrocarbon permittivity.

It is assumed that the hydrocarbon composition from one reservoir is stable throughout the lifetime of the reservoir. Therefore, the calibration will only have to be done once. Based on the foregoing assumption, it should be valid throughout the lifetime of the reservoir.

6 ABBREVIATIONS

ppm	parts per million	(No unit)
T	temperature	ºC
CCFR	Center Cylindrical Fin Resonator	
CFR	Cylindrical Fine Resonator	

7 NOTATION

β	Watercut (as a number between 0 and 1)
ε_{oil}	Permitivitty of pure hydrocarbon
ε_{mix}	Permitivitty of fluid through the meter
ε_{water}	Permitivitty of water
f_{vac}	Resonnance frequency in vacuum
f_{mix}	Resonnance frequency in mix

8 REFERENCES

[1] ROXAR, Roxar Watercut meter, Operation and Maintenance Manual.

[2] Klaus Kupfer & Ebbe Nyfors,Electromagnetic Aquametry, ISBN 3-540-22222-7

[3] Ebbe Nyfors, Cylindrical Microwave Sensor for Measuring Materials under Flow, ISBN 951-22-4983-9

APPENDIX 1

The Roxar Watercut meter used in the test, was a model called: Centre Cylindrical Fin Resonator (CCFR). This is a variant of the more general Cylindrical Fin Resonator (CFR). The only difference is that the CCFR will have a small cylinder on the top of the fin, which is in the centre of the pipe.

The fin has two functions in the meter:

1. It creates a resonance cavity in the measurement section of the meter.
2. It reduces the cut-off frequency of this pipe section by approximately 63%, enabling microwaves to travel freely in the pipe section with the fin, while the microwaves will have a to low frequency to escape up or down the pipe.

The fin resonator will have two antenna probes. One probe is placed exactly opposite the fin, the other exactly 90 degrees to the fin [2].

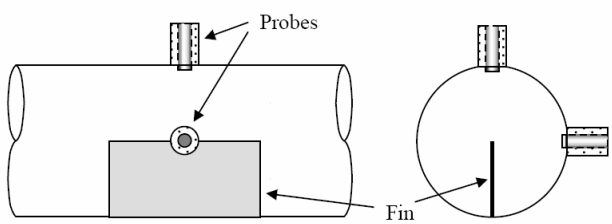

Fig. 7

Principal measurement sketch of a fin resonator.

The Microwaves will be transmitted into the pipe through one of the antennas. The microwaves will then form an electromagnetic wave pattern in the complete area of the pipe. The pattern is rather complex, but we can look at some microwave patterns of some simple microwave modes in the meter [3].

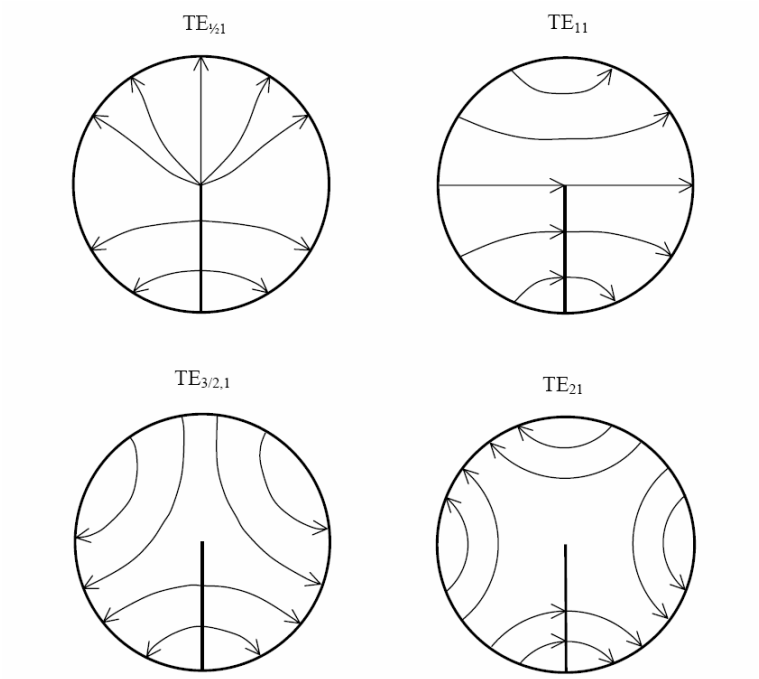

Fig. 8

Four different mode patterns of microwave patterns in the meter

The important thing to notice is that the microwaves will cover the full bore of the meter, thus all water passing through the meter will be measured. Also, the wave pattern is fairly uniform at resonance. Thus, a gradient of water content in the watercut will not influence the measurements particularly.

The Bruggeman equation, as implemented in the Watercut meter, is valid for oil continuous flow with water droplets which in size is less than 1/10 of the pipe diameter. Droplets sizes greater than this, could cause the measurement uncertainty to increase.

In case of full separation, the meter will still measure this water, but a higher degree of measurement uncertainty must be expected.

For the lowest degree of measurement uncertainty, a fairly good mix should exist in the meter. The meter should be vertically installed to ensure that no free water (water fully separated from the oil) can be present in the meter.

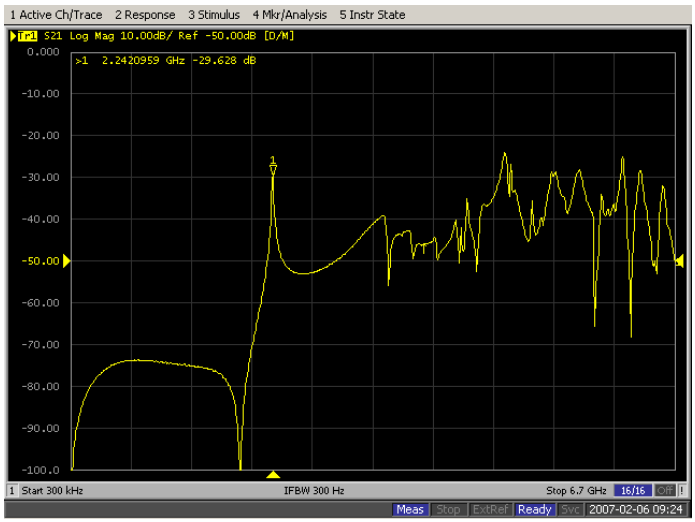

Fig. 9

Plot taken with a Network Analyzer of a 2 inch fin sensor filled with air. On the x-axis is frequency. On the y-axis is received power divided on transmitted power, including 20dB antenna attenuators.

APPENDIX 2

A numbered example of the implementation of the 'Local Characterization' method.

This example will follow the method in the 6 steps described in chapter 4.

1. We assume that the meter is installed, and production has started.
2. In this exampled 30 samples are done, varying the meter conditions over the full range of what is expected of this application. Data is filled in column 1 through 3 in the table.
3. Column four is calculated as the difference of column 1 and two.

Watercut meter	Sampling result	Density	Watercut difference
0.045	0.049	645.9	-0.004
0.053	0.055	642.4	-0.002
0.033	0.032	640.7	0.001
0.079	0.088	644.8	-0.009
0.021	0.017	642.9	0.004
0.048	0.073	649.9	-0.025
0.062	0.058	639.8	0.004
0.055	0.059	647.2	-0.004
0.064	0.053	640.7	0.011
0.094	0.075	640	0.019
0.086	0.067	641.1	0.019
0.061	0.083	649.2	-0.022
0.05	0.048	639.9	0.002
0.044	0.05	645.8	-0.006
0.049	0.055	644.1	-0.006
0.073	0.08	646	-0.007
0.085	0.081	645.7	0.004
0.099	0.104	646.3	-0.005
0.012	0.035	649.4	-0.023
0.054	0.042	639.8	0.012
0.077	0.067	641.2	0.01
0.072	0.063	642.4	0.009
0.083	0.078	642.3	0.005
0.031	0.045	648	-0.014
0.029	0.037	645.1	-0.008
0.076	0.069	642.2	0.007
0.084	0.092	645.3	-0.008
0.045	0.053	648.8	-0.008
0.067	0.056	641.9	0.011
0.092	0.088	643.2	0.004

4. Column three (density) vs. column four (watercut difference) is plotted in a plot.
5. A best fit line (ax+b) to the data is established.

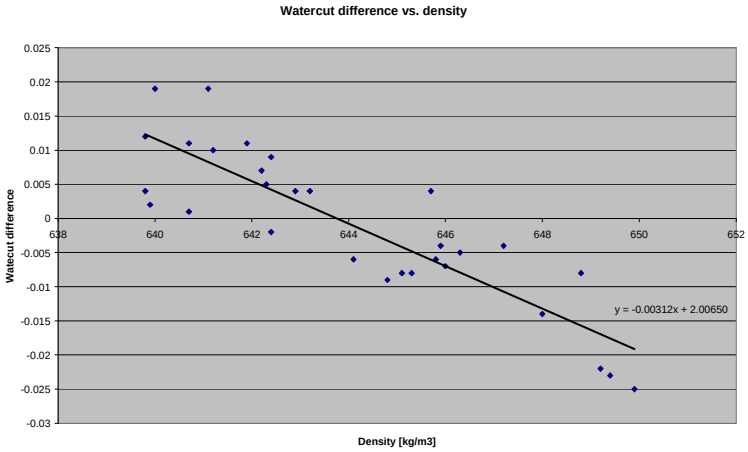

Fig. 10

Density vs Watercut difference between sample analysis and Watercut reading plot.

6. The coefficients ‘a’ and ‘b’ from the line are now entered into the Watercut meter.

The meter is now calibrated with the ‘local characterization’ method for the range of this application.